Improvement of Cementitious and Marble Structural Properties by Photoautotrophic and Heterotrophic Bacteria

A Thesis

Submitted in fulfilment of the requirements for the award of the degree of

DOCTOR OF PHILOSOPHY

by

Navneet Sidhu

(Roll No. 901700002)

Under the Guidance of

Dr. M. Sudhakara Reddy
Professor
Department of Biotechnology

Dr. Shweta Goyal
Professor
Department of Civil Engineering



Department of Biotechnology
Thapar Institute of Engineering and Technology, Patiala-147004
Punjab, India

March, 2024

Certificate

Certified that the thesis "**Improvement of Cementitious and Marble Structural Properties by Photoautotrophic and Heterotrophic Bacteria**" which is submitted by Ms. **Navneet Sidhu**, in fulfilment of the requirement for the award of the degree of **Doctor of Philosophy** in the Department of Biotechnology, Thapar Institute of Engineering & Technology, Patiala, is a record of the candidate's own independent and original research work carried out by her under my supervision and guidance. The matter embodied in this thesis has not been submitted in part or full to any other University or Institute for the award of any degree.



Dr. M. Sudhakara Reddy
Professor
Department of Biotechnology
Thapar Institute of Engineering & Technology, Patiala



Dr. Shweta Goyal
Professor
Department of Civil Engineering
Thapar Institute of Engineering & Technology, Patiala

Declaration

I hereby declare that the work presented in the thesis entitled "**Improvement of Cementitious and Marble Structural Properties by Photoautotrophic and Heterotrophic Bacteria**" in the fulfilment of the requirement for the award of the Degree of **Doctor of Philosophy** in the Department of Biotechnology, Thapar Institute of Engineering & Technology, Patiala, is an authentic record of my own work during the period July 2017 to March 2024, under the supervision of **Dr. M. Sudhakara Reddy**, Professor, Department of Biotechnology, Thapar Institute of Engineering & Technology, Patiala and **Dr Shweta Goyal**, Professor, Department of Civil Engineering, Thapar Institute of Engineering & Technology, Patiala. The material embodied in this thesis has not been submitted in parts or full in any other university or institute for the award of any degree in India or Abroad.



Place: Patiala
Date: 14.03.2024

Navneet Sidhu
Department of Biotechnology
Thapar Institute of Engineering
& Technology, Patiala

Acknowledgement

This thesis is the end of my journey in obtaining my PhD, probably the most stimulating activity of my life. It was a long and challenging yet very fulfilling journey that I completed. In pursuit of this academic endeavor, I have been exceptionally fortunate because inspiration, guidance, direction, cooperation, love and care came my way in abundance. I feel nostalgic when I look back on my journey and find it difficult to put into words the never-ending support and encouragement of everyone throughout these years.

First and foremost, I would like to bow to Almighty for blessing me so abundantly, far beyond what I deserve. With a deep gratitude, I acknowledge my PhD Supervisor, ***Professor M. Sudhakara Reddy****, Department of Biotechnology, TIET, Patiala for giving me this wonderful opportunity to be a part of his research team. His guidance, motivation, enthusiasm and dedication for research rendered to me during my work, without which the present endeavour would not have achieved the same status. His support and faith in my ability made me strive for excellence and nothing less.*

I reckon this opportunity to express my regards and gratitude to my PhD co-supervisor, ***Professor Shweta Goyal****, Department of Civil Engineering, TIET, Patiala. Her valuable suggestions, proficient guidance and advice helped me successfully accomplish this difficult task. Her constructive criticism and spirit of striving for excellence is commendable.*

I take this opportunity to express my gratitude for ***Professor Padmakumar Nair****, Director, TIET, Patiala, for providing all the amenities for the completion of my research work. I extend my heartfelt thanks to* ***Professor N. Tejo Prakash****, Dean (Research and Development cell), TIET, Patiala, for providing motivating research environment during my stay in the Institute. I would also like acknowledge DBT, Ministry of Science & Technology (Govt. of India) for providing research grant (BT/PR27190/BCE/8/1428/2017).*

I am privileged to thank ***Professor Prem Pal Bansal****, Professor & Head, Department of Civil Engineering and* ***Professor Anil Kumar****, Coordinator, TIFAC-CORE in Agro and Industrial Biotechnology, TIET, for providing facilities, and brilliant environment which is very conducive for research work. I am thankful to doctoral committee members* ***Professor Dinesh Goyal****,* ***Professor Moushumi Ghosh*** *of Department of biotechnology,* ***Professor Shruti Sharma****, Department of Civil Engineering for their constant support and constructive criticism*

*during my study. I profoundly thank **Dr. M Vasundhara**, Department of Biotechnology for her valuable support.*

*I express my unfathomable regards to my seniors **Dr. Sumit Joshi**, **Dr. Arkadeep Mukherjee**, **Dr. Bharti Thakur**, **Dr. Shikha Khullar** and **Mrs. Tanveer Kaur** for their great support and treasured suggestions during need of the hour. I express my profound regards to my friends **Anu Gupta, Eetika Chot, Anviksha** and **Anjali Chauhan** for their continuous support and fond memories. I would specially thank **Navneet Kaur Dhiman**, and **Dr. Kamal Anand** for unconditional support throughout these years and for many fruitful and refreshing discussions. I owe special thanks to my colleagues **Himanshu**, **Harvinder, Swati, Anuni, Bhavdeep, Nirmalya and Simarpreet, Ishtpreet and Parman** for stirring discussions and emotional support. I would also like to thank all the project students **Divyanshi**, **Nishtha**, **Manjot**, **Shelly**, **Tanya** who have worked in our Laboratory for their love and support.*

I would specially thank ***Mrs. Manjula Kamra*** for her unconditional support and motivation throughout these years. *I owe a word of thanks to **Mr. Soni Singh, Mr. Ram Newal (Babbanji)** and **Mr. Ram Simran**.*

*I find it difficult to express in words, my sincere sense of indebtedness towards my parents, brother and sister-in-law. My unquestionable gratitude is for the never-ending love and support of my father **Mr. Shingara Singh Sidhu** and mother **Mrs. Manjit Kaur Sidhu**. My father is my backbone and my mother is the pillar of my strength. I consider myself lucky to have such supportive and loving parents. I extend my respect to my younger brother **Mr. Karanvir Singh Sidhu** and sister-in-law **Mrs. Parneet Kaur Sidhu** for their unconditional love and support. I consider myself lucky to have such supportive family who always stood by my side and encouraged me during difficult times.*

Finally, I extend my heartfelt thanks to all those who directly or indirectly contributed to this endeavor. Your support, whether in the form of discussions, technical assistance, or moral support, has been indispensable.

This thesis is a testament to the collective efforts of many, and I am deeply appreciative of the contributions of each and every individual who has played a part in this academic journey.

Date: 14.03.2024



Place: Patiala (Navneet Sidhu)

List of Publications

The following publications in peer reviewed journals are the outcome of the present research work:

1. Sidhu, N., Goyal, S., & Reddy, M. S. (2022). Biomineralization of cyanobacteria *Synechocystis pevalekii* improves the durability properties of cement mortar. AMB Express, 12:59. https://doi.org/10.1186/s13568-022-01403-z.
2. Sidhu, N., Goyal, S., & Reddy, M. S. (2023). Healing of cracks in concrete by using bacterial spores immobilized in metakaolin. Structures, 55:1144-1158. https://doi.org/10.1016/j.istruc.2023.06.097.
3. Sidhu, N., Goyal, S., & Reddy, M. S. (2023). Self-healing by biocomposite containing metakaolin immobilized bacterial spores in concrete using low-cost corn steep liquor media. Journal of Sustainable Cement-Based Materials, 12:11, 1430-1446. https://doi.org/10.1080/21650373.2023.2224805
4. Sidhu, N., Goyal, S., & Reddy, M. S. (2023). Crack bioremediation in concrete by photoautotrophic cyanobacteria through fly ash based cementitious biogrout. Journal of Materials in Civil Engineering. 36: 04023567.
5. Sidhu, N., Goyal, S., & Reddy, M. S. (2023). Comparative study of heterotrophic and photoautotrophic bacteria on strength and permeability properties of concrete. Journal of Building Engineering, 82: 108190. https://doi.org/10.1016/j.jobe.2023.108190.

Book Chapter

1. Dhiman, Navneet K., Sidhu, Navneet, Agnihotri, Shekar, Mukherjee, Abhijit, and M. S. Reddy. (2022). Role of nanomaterials in protecting building materials from degradation and deterioration. *Biodegradation and Biodeterioration at the Nanoscale*. 405-475. https://doi.org/10.1016/B978-0-12-823970-4.00024-5.

Table of content

	Page No.
List of Figures	i - xiii
List of Tables	xiv - xvi
List of Abbreviations	xvii
List of Symbols	xviii
Abstract	xix - xxii
Chapter 1. Introduction	
1. General Introduction	1 - 6
1.1 Research Gap	6 - 7
1.2 Aim and Objectives	7
Chapter 2. Review of Literature	
2 General background	8
2.1 Factors responsible for the deterioration of the building materials	8 - 10
2.2 Conventional treatment	10 - 12
2.3 Biomineralization	12 - 14
2.4 Microbial induced calcium carbonate precipitation (MICCP)	14
2.4.1 Heterotrophic-mediated pathway	14 – 16
2.4.2 Autotrophic-mediated pathway	16 - 18
2.5 MICCP by ureolytic and non ureolytic bacteria	18
2.5.1 Urease activity	18 - 19
2.6 Isolation of heterotrophic bacteria	19 - 22
2.7 MICCP by cyanobacteria (Blue green algae)	23 - 26
2.8 Application of MICCP	26
2.8.1 Sand consolidation	26 - 28
2.8.2 Influence of MICCP on cementitious properties	28 – 31
2.8.3 Crack remediation	31 - 32
2.9 Crack remediation via immobilizing bacteria in carrier material	32 – 37
2.10 Efficiency of grout	35, 38 - 39
2.11 Role of MICCP in restoration of stones and monuments	40 - 42
2.12 Challenges faced by MICCP in bioconcrete and restoration of stones	42 - 43
2.13 Concluding remarks	43

Chapter 3. Materials and Methods

3(A) Heterotrophic bacteria

3.1 Isolation and screening of heterotrophic bacteria 44

3.1.1. Sample collection 44 - 45

3.1.2 Isolation of heterotrophic bacteria 46

3.1.3 Qualitative characterization 46

3.2 Molecular characterization

3.2.1 DNA extraction and electrophoresis of DNA on agarose gels 46

3.2.2 Quantification of DNA by Nanodrop spectrophotometer 47

3.2.3 Amplification of 16S rRNA and Purification of PCR products 47

3.2.4 Sequence analysis 47 - 48

3.2.5 Phylogenetic analysis 48

3.3 Quantitative analysis

3.3.1 Urease enzyme activity 48

3.3.2 Calcium carbonate precipitation 49

3.4 Sand consolidation 49 - 50

3.5 Selection of the highest calcifying heterotrophic bacteria 50

3.6 Influence of different temperature and pH conditions on the physiology of *B. paramycoides* MD6

3.6.1 Effect of temperature and pH variation on growth cycle 51

3.6.2 Effect of temperature and pH variation on urease activity 51

3.6.3 Effect of temperature and pH variation on $CaCO_3$ precipitation 51 - 52

3.6.4 Microstructural and XRD analysis 52

3.7 Sand consolidation by *B. paramycoides* MD6 52 - 53

3.7.1 Microstructural analysis 53

3.8 Enhancement of the overall properties of concrete by ureolytic bacteria

3.8.1 Construction materials 53

3.8.2 Concrete mix design 54

3.8.3 Strength and Permeability 54

3.8.3.1 Compressive strength 55
3.8.3.2 Sorptivity test 55 - 56
3.8.3.3 Rapid chloride permeability test (RCPT) 56 - 58
3.8.4 Microstructural analysis and XRD 58
3.9 Development of metakaolin based bacterial carrier material 58
3.9.1 Spore preparation 59
3.9.2 Development of metakaolin carrier material 60
3.9.3 Storage and viability test 61
3.9.4 Urease activity and $CaCO_3$ precipitation 61 – 62
3.9.5 Preparation of concrete specimens 62
3.9.6 Concrete testing 62 - 63
3.9.7 Crack remediation and monitoring 63 - 64
3.9.8 Visual monitoring of crack closure 64
3.9.9 Microstructural analysis 65
3(B) Photoautotrophic strains
3.10 Cultivation and cell preparation 66
3.10.1 Growth cycle 66
3.10.2 Microbial calcium carbonate precipitation experiment 67
3.10.2.1 Microstructural analysis 67 - 68
3.10.3 Selection of highest $CaCO_3$ precipitating strain 68
3.10.4 Influence of different initial pH on $CaCO_3$ precipitation 68
3.11 Influence of Live (LV) and UV-treatment (UVT) cells in sand consolidation and improvement of cementitious material
3.11.1 Pre-treatment of cells 68
3.11.2 Sand consolidation 69
3.11.3 Surface treatment of mortar by ponding 70
3.11.4 Preparation of mortar specimens 70 - 71
3.11.4.1 Testing of mortar specimens 71 - 72
3.11.4.2 Thermogravimetric analysis (TGA) 72
3.11.4.3 Microstructural analysis 72
3.12 Development of fly ash based cementitious biogrout incorporating cyanobacteria *Synechocystis pevalekii*

3.12.1 Materials 73
3.12.2 Grout Mixture Design 74
3.12.3 Preparation of the grout mixture 75 - 76
3.12.4 Fresh Properties of Grout Mixture
3.12.4.1 Marsh cone 76 - 77
3.12.4.2 Mini slump test 77
3.12.4.3 Grout bleeding 78
3.12.4.4 Selection of the w/b and c/b ratio 78
3.12.4.5 Slump flow retention 78
3.12.5 Hardened Properties of Grout Mixes
3.12.5.1 Setting time 79
3.12.5.2 Compressive strength of the grout 79 - 80
3.12.6 Crack-Embedded Concrete Specimens 80
3.12.7 Crack Remediation with Bio-Based Cement Grout 81
3.12.8 Testing of crack repaired specimens 81-83
3.12.8.1 Mechanical strength 81
3.12.8.2 Sorptivity test 83
3.12.8.3 Sealing efficiency 83
3.12.9 Microstructural Analysis 83
3(C) Comparison of strength and permeability properties of concrete by Photoautotrophic and heterotrophic bacteria
3.13 Biological culture 84
3.14 Materials 84
3.15 Calcium Carbonate Precipitation 84 – 85
3.15.1 Effect of initial pH on $CaCO_3$ precipitation 85
3.16 Strength and Permeability 85 - 86
3.16.1 Microstructural analysis 87
3(D) Evaluation of biomineralization on marble surface by heterotrophic and photoautotrophic bacteria
3.17 Carbonate stone 88
3.17.1 Calcification on the marble stone 88
3.18 Acid attack

3.18.1 Bioremediation using MICCP 89
3.18.2 Weight loss with ultrasonic treatment 89 - 90
3.18.3 Microstructural analysis (FESEM-EDS) 90 - 91
3.19 Statistical analysis 91

Chapter 4. Results and Discussion

4(A) Heterotrophic bacteria

4.1 Isolation and screening of heterotrophic bacteria 92 - 93
4.2 Molecular characterization 93
4.2.1 DNA extraction 93 - 94
4.2.2 Amplification of 16S rRNA and Purification of PCR products 94 – 96, 97 - 98
4.3 Quantitative characterization
4.3.1 Urease activity 96, 99
4.3.2 Calcium carbonate ($CaCO_3$) precipitation 100 - 101
4.4 Sand consolidation 101 - 102
4.5 Selection of highest ureolytic bacteria 102
4.6 Influence of different temperature and pH conditions on the physiology of *B. paramycoides* MD6.
4.6.1 Effect of temperature and pH variation on the growth cycle 103 - 104
4.6.2 Effect of temperature and pH variation on urease activity 104 - 107
4.6.3 Effect of temperature and pH variation on $CaCO_3$ precipitation 107 - 108
4.6.4 Calcium removal 108 - 110
4.6.5 pH dynamic 110 - 111
4.6.6 Microstructural analysis 111 - 112
4.7 Sand consolidation using different-sized sand grains 112 - 115
4.8 Enhancement of the overall properties of concrete by ureolytic bacteria
4.8.1 Compressive strength 116 - 117
4.8.2 Rapid chloride penetration test (RCPT) 117 - 118
4.8.3 Sorptivity test 118 - 119
4.8.4 Microstructural analysis 119 - 120
4.8.5 XRD 120 - 121

4.9 Development of metakaolin based biomaterial

4.9.1 Viability of spores 121 - 122

4.9.2 Urease activity of biomaterial 122 - 124

4.9.3 Calcium carbonate precipitation by biomaterial 124 - 126

4.9.4 Microstructural analysis of $CaCO_3$ precipitates 126 - 127

4.9.5 Strength properties of concrete 127 - 129

4.9.6 Sorptivity test 129 - 130

4.10 Crack remediation by CSL-4 bacterial inoculum 130 - 131

4.10.1 Regain in ultrasonic pulse velocity (UPV) 132 - 133

4.10.2 Water tightness 133 - 134

4.10.3 Microstructural characterization 134 - 136

4.11 Crack remediation by NB-4 bacterial inoculum 136 - 139

4.11.1 Water tightness 139 - 140

4.11.2 Ultrasonic pulse velocity (UPV) 140 - 141

4.11.3 Microstructural characterization 141 - 143

4.12 Conclusions 143

4(B)Photoautotrophic bacteria

4.13 Screening of the highest $CaCO_3$ precipitating cyanobacterial strain

4.13.1 Growth cycle 144

4.13.2 Calcium carbonate precipitation 145

4.13.3 pH dynamic 146

4.13.4 Microstructural analysis 147 - 148

4.13.5 Selection of highest $CaCO_3$ precipitating cyanobacteria 148

4.14 Influence of different pH on $CaCO_3$ precipitation by *S. pevalekii* 149 - 150

4.15 Influence of Live (LV) and UV-treatment (UVT) cells in sand consolidation and improvement of cementitious material 150

4.15.1 Sand consolidation 150 - 152

4.15.1.1 Microstructural analysis 152 - 154

4.15.2 Surface treatment by ponding 154 - 155

4.15.3 Compressive strength 154 – 156

4.15.4 Water absorption 156 - 157

4.15.5 Thermogravimetric (TGA) analysis 157

4.15.6 Microstructural analysis 158 - 160

4.16 Development of fly ash-based cementitious biogrout incorporating cyanobacteria *Synechocystis pevalekii*

4.16.1 Fresh properties of grout 161

4.16.1.1 Marsh cone test 161 - 162

4.16.1.2 Mini slump test 162 - 163

4.16.1.3 Grout bleeding 164 - 165

4.16.1.4 Selection of optimum w/b or c/b ratio for grout 164 - 166

4.16.1.5 Slump flow retention 166 - 167

4.16.2 Hardened properties of grout

4.16.2.1 Setting time 167 - 168

4.16.2.2 Effect of fly ash dosage on compressive strength of grouts 168 - 170

4.16.2.3 Selecting the best cement-based biogrout 169

4.16.3 Crack remediation and testing 170 - 171

4.16.3.1 Compressive strength 170 - 172

4.16.3.2 Flexural strength 172 - 173

4.16.3.3 Water tightness 173 - 174

4.16.3.4 Sealing efficiency 174 - 175

4.16.3.5 Microstructural analysis 175 - 178

4.16.3.6 X-ray powder diffraction (XRD) 176, 178

4.16.3.7 Thermogravimetric analysis 176, 179

4.17 Conclusions 179

4(C) Comparison of strength and permeability properties of concrete by photoautotrophic and heterotrophic bacteria

4.18 Microbial density and $CaCO_3$ precipitation 180 - 181

4.18.1 FESEM analysis 181 - 182

4.18.2 Effect of initial pH on the growth of cyanobacterial and bacterial cells 182 - 183

4.18.3 Effect of initial pH on $CaCO_3$ precipitation 184

4.19 Strength and permeability properties

4.19.1 Compressive strength 185 - 186

4.19.2 Relative strength index 186 - 187

4.19.3 Rapid chloride penetration test (RCPT) 187 - 188
4.19.4 Sorptivity test 188 - 189
4.19.5 Microstructural analysis
4.19.6 X-ray diffraction (XRD) 190 - 192
4.19.7 Cost analysis 192
4.20 Conclusions 193

4(D) Evaluation of biomineralization on marble surface by heterotrophic and photoautotrophic bacteria

4.21 Calcification on the marble surface 194
4.22 Effect of acid solution and biomineralization efficiency on the marble surface 194 - 195
4.22.1 Effect of acid spray on the stone 195 - 196
4.22.2 Restoration by *B. paramycoides* and *S. pevalekii* 196 - 199
4.22.3 Weight loss due to sonication 199 - 200
4.22.4 Roughness 201 - 205
4.22.5 Visual examination 205 - 207
4.22.6 FESEM analysis 207 - 210
4.22.7 Conclusions 207

Chapter 5 Summary

5.1 Heterotrophic bacteria 211 - 214
5.2 Photoautotrophic bacteria 214 - 216
5.3 Comparison of strength and permeability properties of concrete by photoautotrophic and heterotrophic bacteria 216
5.4 Evaluation of biomineralization on marble surface by heterotrophic and photoautotrophic bacteria 217
5.5 Conclusions and future scope 218

References 219 - 275

Appendix I 276 - 281

Publications

List of Publications

The following publications in peer reviewed journals are the outcome of the present research work:

1. Sidhu, N., Goyal, S., & Reddy, M. S. (2022). Biomineralization of cyanobacteria *Synechocystis pevalekii* improves the durability properties of cement mortar. AMB Express, 12:59. https://doi.org/10.1186/s13568-022-01403-z.
2. Sidhu, N., Goyal, S., & Reddy, M. S. (2023). Healing of cracks in concrete by using bacterial spores immobilized in metakaolin. Structures, 55:1144-1158. https://doi.org/10.1016/j.istruc.2023.06.097.
3. Sidhu, N., Goyal, S., & Reddy, M. S. (2023). Self-healing by biocomposite containing metakaolin immobilized bacterial spores in concrete using low-cost corn steep liquor media. Journal of Sustainable Cement-Based Materials, 12:11, 1430-1446. https://doi.org/10.1080/21650373.2023.2224805
4. Sidhu, N., Goyal, S., & Reddy, M. S. (2023). Crack bioremediation in concrete by photoautotrophic cyanobacteria through fly ash based cementitious biogrout. Journal of Materials in Civil Engineering. 36: 04023567. https://doi.org/10.1061/JMCEE7.MTENG-16301
5. Sidhu, N., Goyal, S., & Reddy, M. S. (2023). Comparative study of heterotrophic and photoautotrophic bacteria on strength and permeability properties of concrete. Journal of Building Engineering, 82: 108190. https://doi.org/10.1016/j.jobe.2023.108190.

Book Chapter

1. Dhiman, Navneet K., Sidhu, Navneet, Agnihotri, Shekar, Mukherjee, Abhijit, and M. S. Reddy. (2022). Role of nanomaterials in protecting building materials from degradation and deterioration. *Biodegradation and Biodeterioration at the Nanoscale*. 405-475. https://doi.org/10.1016/B978-0-12-823970-4.00024-5.

Table of content

	Page No.
List of Figures	i - xiii
List of Tables	xiv - xvi
List of Abbreviations	xvii
List of Symbols	xviii
Abstract	xix - xxii
Chapter 1. Introduction	
1. General Introduction	1 - 6
1.1 Research Gap	6 - 7
1.2 Aim and Objectives	7
Chapter 2. Review of Literature	
2 General background	8
2.1 Factors responsible for the deterioration of the building materials	8 - 10
2.2 Conventional treatment	10 - 12
2.3 Biomineralization	12 - 14
2.4 Microbial induced calcium carbonate precipitation (MICCP)	14
2.4.1 Heterotrophic-mediated pathway	14 – 16
2.4.2 Autotrophic-mediated pathway	16 - 18
2.5 MICCP by ureolytic and non ureolytic bacteria	18
2.5.1 Urease activity	18 - 19
2.6 Isolation of heterotrophic bacteria	19 - 22
2.7 MICCP by cyanobacteria (Blue green algae)	23 - 26
2.8 Application of MICCP	26
2.8.1 Sand consolidation	26 - 28
2.8.2 Influence of MICCP on cementitious properties	28 – 31
2.8.3 Crack remediation	31 - 32
2.9 Crack remediation via immobilizing bacteria in carrier material	32 – 37
2.10 Efficiency of grout	35, 38 - 39
2.11 Role of MICCP in restoration of stones and monuments	40 - 42
2.12 Challenges faced by MICCP in bioconcrete and restoration of stones	42 - 43
2.13 Concluding remarks	43

Chapter 3. Materials and Methods

3(A) Heterotrophic bacteria

3.1 Isolation and screening of heterotrophic bacteria 44

3.1.1. Sample collection 44 - 45

3.1.2 Isolation of heterotrophic bacteria 46

3.1.3 Qualitative characterization 46

3.2 Molecular characterization

3.2.1 DNA extraction and electrophoresis of DNA on agarose gels 46

3.2.2 Quantification of DNA by Nanodrop spectrophotometer 47

3.2.3 Amplification of 16S rRNA and Purification of PCR products 47

3.2.4 Sequence analysis 47 - 48

3.2.5 Phylogenetic analysis 48

3.3 Quantitative analysis

3.3.1 Urease enzyme activity 48

3.3.2 Calcium carbonate precipitation 49

3.4 Sand consolidation 49 - 50

3.5 Selection of the highest calcifying heterotrophic bacteria 50

3.6 Influence of different temperature and pH conditions on the physiology of *B. paramycoides* MD6

3.6.1 Effect of temperature and pH variation on growth cycle 51

3.6.2 Effect of temperature and pH variation on urease activity 51

3.6.3 Effect of temperature and pH variation on $CaCO_3$ precipitation 51 - 52

3.6.4 Microstructural and XRD analysis 52

3.7 Sand consolidation by *B. paramycoides* MD6 52 - 53

3.7.1 Microstructural analysis 53

3.8 Enhancement of the overall properties of concrete by ureolytic bacteria

3.8.1 Construction materials 53

3.8.2 Concrete mix design 54

3.8.3 Strength and Permeability 54

3.8.3.1 Compressive strength 55
3.8.3.2 Sorptivity test 55 - 56
3.8.3.3 Rapid chloride permeability test (RCPT) 56 - 58
3.8.4 Microstructural analysis and XRD 58
3.9 Development of metakaolin based bacterial carrier material 58
3.9.1 Spore preparation 59
3.9.2 Development of metakaolin carrier material 60
3.9.3 Storage and viability test 61
3.9.4 Urease activity and $CaCO_3$ precipitation 61 – 62
3.9.5 Preparation of concrete specimens 62
3.9.6 Concrete testing 62 - 63
3.9.7 Crack remediation and monitoring 63 - 64
3.9.8 Visual monitoring of crack closure 64
3.9.9 Microstructural analysis 65
3(B) Photoautotrophic strains
3.10 Cultivation and cell preparation 66
3.10.1 Growth cycle 66
3.10.2 Microbial calcium carbonate precipitation experiment 67
3.10.2.1 Microstructural analysis 67 - 68
3.10.3 Selection of highest $CaCO_3$ precipitating strain 68
3.10.4 Influence of different initial pH on $CaCO_3$ precipitation 68
3.11 Influence of Live (LV) and UV-treatment (UVT) cells in sand consolidation and improvement of cementitious material
3.11.1 Pre-treatment of cells 68
3.11.2 Sand consolidation 69
3.11.3 Surface treatment of mortar by ponding 70
3.11.4 Preparation of mortar specimens 70 - 71
3.11.4.1 Testing of mortar specimens 71 - 72
3.11.4.2 Thermogravimetric analysis (TGA) 72
3.11.4.3 Microstructural analysis 72
3.12 Development of fly ash based cementitious biogrout incorporating cyanobacteria *Synechocystis pevalekii*

3.12.1 Materials 73
3.12.2 Grout Mixture Design 74
3.12.3 Preparation of the grout mixture 75 - 76
3.12.4 Fresh Properties of Grout Mixture
3.12.4.1 Marsh cone 76 - 77
3.12.4.2 Mini slump test 77
3.12.4.3 Grout bleeding 78
3.12.4.4 Selection of the w/b and c/b ratio 78
3.12.4.5 Slump flow retention 78
3.12.5 Hardened Properties of Grout Mixes
3.12.5.1 Setting time 79
3.12.5.2 Compressive strength of the grout 79 - 80
3.12.6 Crack-Embedded Concrete Specimens 80
3.12.7 Crack Remediation with Bio-Based Cement Grout 81
3.12.8 Testing of crack repaired specimens 81-83
3.12.8.1 Mechanical strength 81
3.12.8.2 Sorptivity test 83
3.12.8.3 Sealing efficiency 83
3.12.9 Microstructural Analysis 83
3(C) Comparison of strength and permeability properties of concrete by Photoautotrophic and heterotrophic bacteria
3.13 Biological culture 84
3.14 Materials 84
3.15 Calcium Carbonate Precipitation 84 – 85
3.15.1 Effect of initial pH on $CaCO_3$ precipitation 85
3.16 Strength and Permeability 85 - 86
3.16.1 Microstructural analysis 87
3(D) Evaluation of biomineralization on marble surface by heterotrophic and photoautotrophic bacteria
3.17 Carbonate stone 88
3.17.1 Calcification on the marble stone 88
3.18 Acid attack

3.18.1 Bioremediation using MICCP 89
3.18.2 Weight loss with ultrasonic treatment 89 - 90
3.18.3 Microstructural analysis (FESEM-EDS) 90 - 91
3.19 Statistical analysis 91

Chapter 4. Results and Discussion

4(A) Heterotrophic bacteria

4.1 Isolation and screening of heterotrophic bacteria 92 - 93
4.2 Molecular characterization 93
4.2.1 DNA extraction 93 - 94
4.2.2 Amplification of 16S rRNA and Purification of PCR products 94 – 96, 97 - 98
4.3 Quantitative characterization
4.3.1 Urease activity 96, 99
4.3.2 Calcium carbonate ($CaCO_3$) precipitation 100 - 101
4.4 Sand consolidation 101 - 102
4.5 Selection of highest ureolytic bacteria 102
4.6 Influence of different temperature and pH conditions on the physiology of *B. paramycoides* MD6.
4.6.1 Effect of temperature and pH variation on the growth cycle 103 - 104
4.6.2 Effect of temperature and pH variation on urease activity 104 - 107
4.6.3 Effect of temperature and pH variation on $CaCO_3$ precipitation 107 - 108
4.6.4 Calcium removal 108 - 110
4.6.5 pH dynamic 110 - 111
4.6.6 Microstructural analysis 111 - 112
4.7 Sand consolidation using different-sized sand grains 112 - 115
4.8 Enhancement of the overall properties of concrete by ureolytic bacteria
4.8.1 Compressive strength 116 - 117
4.8.2 Rapid chloride penetration test (RCPT) 117 - 118
4.8.3 Sorptivity test 118 - 119
4.8.4 Microstructural analysis 119 - 120
4.8.5 XRD 120 - 121

4.9 Development of metakaolin based biomaterial

4.9.1 Viability of spores 121 - 122

4.9.2 Urease activity of biomaterial 122 - 124

4.9.3 Calcium carbonate precipitation by biomaterial 124 - 126

4.9.4 Microstructural analysis of $CaCO_3$ precipitates 126 - 127

4.9.5 Strength properties of concrete 127 - 129

4.9.6 Sorptivity test 129 - 130

4.10 Crack remediation by CSL-4 bacterial inoculum 130 - 131

4.10.1 Regain in ultrasonic pulse velocity (UPV) 132 - 133

4.10.2 Water tightness 133 - 134

4.10.3 Microstructural characterization 134 - 136

4.11 Crack remediation by NB-4 bacterial inoculum 136 - 139

4.11.1 Water tightness 139 - 140

4.11.2 Ultrasonic pulse velocity (UPV) 140 - 141

4.11.3 Microstructural characterization 141 - 143

4.12 Conclusions 143

4(B)Photoautotrophic bacteria

4.13 Screening of the highest $CaCO_3$ precipitating cyanobacterial strain

4.13.1 Growth cycle 144

4.13.2 Calcium carbonate precipitation 145

4.13.3 pH dynamic 146

4.13.4 Microstructural analysis 147 - 148

4.13.5 Selection of highest $CaCO_3$ precipitating cyanobacteria 148

4.14 Influence of different pH on $CaCO_3$ precipitation by *S. pevalekii* 149 - 150

4.15 Influence of Live (LV) and UV-treatment (UVT) cells in sand consolidation and improvement of cementitious material 150

4.15.1 Sand consolidation 150 - 152

4.15.1.1 Microstructural analysis 152 - 154

4.15.2 Surface treatment by ponding 154 - 155

4.15.3 Compressive strength 154 – 156

4.15.4 Water absorption 156 - 157

4.15.5 Thermogravimetric (TGA) analysis 157

4.15.6 Microstructural analysis 158 - 160

4.16 Development of fly ash-based cementitious biogrout incorporating cyanobacteria *Synechocystis pevalekii*

4.16.1 Fresh properties of grout 161

4.16.1.1 Marsh cone test 161 - 162

4.16.1.2 Mini slump test 162 - 163

4.16.1.3 Grout bleeding 164 - 165

4.16.1.4 Selection of optimum w/b or c/b ratio for grout 164 - 166

4.16.1.5 Slump flow retention 166 - 167

4.16.2 Hardened properties of grout

4.16.2.1 Setting time 167 - 168

4.16.2.2 Effect of fly ash dosage on compressive strength of grouts 168 - 170

4.16.2.3 Selecting the best cement-based biogrout 169

4.16.3 Crack remediation and testing 170 - 171

4.16.3.1 Compressive strength 170 - 172

4.16.3.2 Flexural strength 172 - 173

4.16.3.3 Water tightness 173 - 174

4.16.3.4 Sealing efficiency 174 - 175

4.16.3.5 Microstructural analysis 175 - 178

4.16.3.6 X-ray powder diffraction (XRD) 176, 178

4.16.3.7 Thermogravimetric analysis 176, 179

4.17 Conclusions 179

4(C) Comparison of strength and permeability properties of concrete by photoautotrophic and heterotrophic bacteria

4.18 Microbial density and $CaCO_3$ precipitation 180 - 181

4.18.1 FESEM analysis 181 - 182

4.18.2 Effect of initial pH on the growth of cyanobacterial and bacterial cells 182 - 183

4.18.3 Effect of initial pH on $CaCO_3$ precipitation 184

4.19 Strength and permeability properties

4.19.1 Compressive strength 185 - 186

4.19.2 Relative strength index 186 - 187

4.19.3 Rapid chloride penetration test (RCPT) 187 - 188
4.19.4 Sorptivity test 188 - 189
4.19.5 Microstructural analysis
4.19.6 X-ray diffraction (XRD) 190 - 192
4.19.7 Cost analysis 192
4.20 Conclusions 193

4(D) Evaluation of biomineralization on marble surface by heterotrophic and photoautotrophic bacteria

4.21 Calcification on the marble surface 194
4.22 Effect of acid solution and biomineralization efficiency on the marble surface 194 - 195
4.22.1 Effect of acid spray on the stone 195 - 196
4.22.2 Restoration by *B. paramycoides* and *S. pevalekii* 196 - 199
4.22.3 Weight loss due to sonication 199 - 200
4.22.4 Roughness 201 - 205
4.22.5 Visual examination 205 - 207
4.22.6 FESEM analysis 207 - 210
4.22.7 Conclusions 207

Chapter 5 Summary

5.1 Heterotrophic bacteria 211 - 214
5.2 Photoautotrophic bacteria 214 - 216
5.3 Comparison of strength and permeability properties of concrete by photoautotrophic and heterotrophic bacteria 216
5.4 Evaluation of biomineralization on marble surface by heterotrophic and photoautotrophic bacteria 217
5.5 Conclusions and future scope 218

References 219 - 275

Appendix I 276 - 281

Publications

List of Figures

Figure No.	Description	Page No.
Fig. 2.1	Illustration of BIM mechanism, representing the interaction between metabolic products of microorganisms and inorganic compounds present in environment to induce biominerals precipitation.	13
Fig. 2.2	Illustration of Biologically Controlled Mineralization (BCM). (A) in extracellular BCM, mineral nucleation take place within the organic matrix through passive diffusion (B) in intercellular BCM surface of cells that line other cells (epithelial surfaces) acts like a natural substrate for mineralization, guiding and shaping the deposit of biominerals around the cell surface (C) intracellular BCM, minerals are precipitated within a specific vesicle in the cells and is then released.	13
Fig. 2.3	The microbial agents and processes involved in the formation of $CaCO_3$ deposits. The bacterial groups were categorized into two pathways: autotrophic (marked in orange) and heterotrophic (marked in black). Additionally, potentially hazardous compounds were highlighted with a red frame	17
Fig. 2.4	Pictorial illustration of surface improvement at different bacterial concentrations in concrete	31
Fig. 2.5	Different techniques of cell immobilization	35
Fig. 2.6	Flow properties and compressive strength of different dosage of capsule in grout	40
Fig. 3.1	Overview of thesis outline adopted to address the objectives of the study	44
Fig. 3.2	Marble dumping yard, site at Kishangarh, Jaipur, Rajasthan, India where the samples were collected for isolation of bacteria	45
Fig. 3.3	Experiment set-up of sand consolidation experiment using different bacteria	50
Fig. 3.4	Schematic representation of the sorptivity test	56

Fig. 3.5	Setup for rapid chloride permeability test (RCPT)	58
Fig. 3.6	*Bacillus paramycoides* MD6 spores	59
Fig. 3.7	Schematic illustration of *Bacillus paramycoides*- MD6 spores' development and storage after the immobilization in metakaolin (MK) material by lyophilization technique	60
Fig. 3.8	Schematic representation of the serial dilution technique and nutrient agar plates showing spore viability after 24 h of incubation at 37 °C	61
Fig. 3.9	(a) Four-point bending failure to generate the controlled crack (b) crack remediation and monitoring (c) water tightness test; top view of the specimen marked with three different locations of the water flow test on the specimens and side view of the setup of the water flow test with measuring cylinder adhesively attached to the specimen	64
Fig. 3.10	Photoautotrophic strains *Aphanocapsa montana* BDU21001, *Aphanothece* species BDHKU 40501, *Gleocapsa* species BDU 40111, *Synechococcus elongatus* BDU14174, and *Synechocystios pevalekii* BDHKU 35101 grown in BG11 broth	67
Fig. 3.11	Surface ponding by *S. pevalekii* calcifying solution on the cement mortar	70
Fig. 3.12	Hobart-type laboratory mixer (AIMIL India Ltd, New Delhi)	75
Fig. 3.13	Outline of different techniques used in the development of biogrout incorporating fly ash (0% – 50%) and w/b or c/b (0.45, 0.47, and 0.50) for vertical and horizontal oriented crack remediation	76
Fig. 3.14	Marsh cone test (a) V-funnel apparatus (b) dimensions of V-funnel	77
Fig. 3.15	(a) Mini slump cone (b) dimensions of slump cone	77
Fig. 3.16	(a) Grout bleeding test at 0-hour (b) Grout bleeding test at 6 hours; (c) square shape shows enlarged image grout bleed at 6 hours	78

Fig. 3.17	Compression testing machine for compressive testing of grout	80
Fig. 3.18	Graphical representation of the vertical and horizontal oriented crack remediation using *Synechocystis pevalekii* cell culture supplemented with calcifying solution ($CaCl_2$ + $NaHCO_3$)	82
Fig. 3.19	The experimental setup for photoautotrophic bacteria *Synechocystis pevalekii* and heterotrophic bacteria *Bacillus paramycoides* for strength and permeability improvement in concrete	86
Fig. 3.20	Graphical representation of the experimental set-up of MICCP treatment on acid damaged marble surface	90
Fig. 4.1	Enrichment and isolation of different strains of ureolytic bacteria from marble dust	93
Fig. 4.2	Visualization of DNA bands of different bacterial isolates on 0.8% agarose gel	94
Fig. 4.3	16S rDNA amplification of bacterial isolates using polymerase chain reaction	95
Fig. 4.4	Multiple sequence alignment of *Bacillus paranthracis* MD2 and *Bacillus paranthracis* MD2	97
Fig. 4.5	Multiple sequence alignment of *Bacillus paramycoides* MD4, MD5, MD6, and MD7	97
Fig. 4.6	Maximum parsimony tree based on bacterial 16S rRNA sequence analysis data of different bacterial isolates along with accession numbers available in the GenBank database. Numerical values represent bootstrap values from 1000 replicates. *Escherichia coli* was used as the outgroup	98
Fig. 4.7	Urease activity of different bacterial isolates at different incubation times. Values bearing different letters at each time interval are significant at $p<0.05$. Error bars represent the standard deviation (n=3).	99
Fig. 4.8	Calcium carbonate precipitation by bacterial isolates at different incubation times. Values bearing different letters at each time	100

interval are significant at $p<0.05$. Error bars represent the standard deviation (n=3)

Fig. 4.9 (a) Flow rate of calcifying solution through the sand column at an interval of 48 h for 20 consecutive days (b) $CaCO_3$ precipitation at the upper, middle, and lower layer of the sand column after 20 days. Values bearing different letters within the treatment (layers) are significant at $p<0.05$. Error bars represent the standard deviation (n=3) 102

Fig. 4.10 Growth cycle of *B. paramycoides* at different (a) temperatures (25 °C, 28 °C, 37 °C, 45 °C, and 55 °C) and (b) pH (6-12) conditions 104

Fig. 4.11 Urease activity at different temperature conditions. Values bearing different letters at each time interval are significant at $p<0.05$. Values are mean ± SD (n=3) 105

Fig. 4.12 Urease activity at different pH (6 -12). Values bearing different letters at each time interval are significant at $p<0.05$. Values are mean ± SD (n=3) 106

Fig. 4.13 (a) $CaCO_3$ precipitation at different temperature conditions (25 - 55 °C), (b) $CaCO_3$ precipitation at varied pH (6 – 12). Values bearing different letters are significant at $p<0.05$. Values are mean ± SD (n=3) 108

Fig. 4.14 Calcium removal percentage (%) at different temperatures (25 – 55 °C) at 24, 48, 72, 96 and 120 h. Values bearing different letters at each time interval are significant at $p<0.05$. Values are mean ± SD (n=3) 109

Fig. 4.15 Calcium removal percentage (%) at different pH (6 – 12) conditions at 24, 48, 72, 96 and 120 h. Values bearing different letters at each time interval are significant at $p<0.05$. Values are mean ± SD (n=3) 110

Fig. 4.16 pH dynamic during $CaCO_3$ precipitation experiment at different (a) temperatures (25 – 55 °C) and (b) pH (6 – 12) conditions at different time intervals (2, 4, 6, 24, 48, 72, 96 and 120 h) in nutrient broth supplemented with the calcifying solution (2% urea and 25 mM $CaCl_2$ 111

Fig. 4.17	(a) SEM analysis of powdered $CaCO_3$ precipitates, '□' symbol represent spot analyzed for EDS (b) EDS showing elemental composition of carbon (C), calcium (Ca) and oxygen (O) in precipitates (c) XRD analysis of powdered $CaCO_3$ precipitates depicting the presence of calcite as predominant crystalline	112
Fig. 4.18	(a, b) Consolidated sand columns using different-sized sand grains	114
Fig. 4.19	(a) Flow rate of nutrient broth supplemented with calcifying solution (2% urea and 25 mM $CaCl_2$) during 20 days (b) $CaCO_3$ precipitation in the upper, middle, and bottom part of sand columns. Values bearing different letters within the treatment are significant at $p<0.05$. Values are mean ± SD (n=3)	114
Fig. 4.20	(a-c) FESEM of bacterial treated sand column (d) EDS showing elemental composition of $CaCO_3$	115
Fig. 4.21	Bacterial admixed sand column (BC) and control specimen (CL) (Q: Quartz and C: Calcite)	115
Fig. 4.22	Compressive strength of *B. paramycoides* treated (BPC) and control at 3, 7, and 28 days of curing. The asterisk (*) sign indicates values are significant at $p<0.05$ using t-test. Values are mean ± SD (n=3)	117
Fig. 4.23	Rapid chloride permeability test (RCPT) at 7 and 28 days of curing. The asterisk (*) sign indicates values are significant at $p<0.05$ using t-test. Values are mean ± SD (n=3)	118
Fig. 4.24	Water absorption concrete specimens treated with *B. paramycoides* (BPC) and control at (a) 7 days and (b) 28 days of curing	119
Fig. 4.25	FESEM-EDS analysis of (a) control (b) BPC specimens after 28 days of curing	120
Fig. 4.26	XRD of BPC and control concrete specimens after 28 days of curing	121
Fig. 4.27	Bacterial cell count (log cfu/g) of developed biomaterial (a) NB-4 and NB-25 (b) CSL-4 and CSL-25 stored at 4 °C and 25 °C in the petri plate. The values are significant at $p<0.05$ using t-test	123

Fig. 4.28	Nutrient agar (NA) plates showing spore viability of developed biomaterial stored at 4 °C and 25 °C for 180 days (26 weeks)	123
Fig. 4.29	Corn steep liquor (CSL) agar plates showing spore viability of developed biomaterial stored at 4 °C and 25 °C for 180 days (26 weeks)	124
Fig. 4.30	Urease activity of developed biomaterial stored at 4 °C and 25 °C for 180 days. Values bearing different letters within the treatment at each time interval are significant at $p<0.05$. Values are mean ± SD (n=3)	125
Fig. 4.31	$CaCO_3$ precipitation of developed biomaterial stored at 4 °C and 25 °C for 180 days. Values are mean ± SD (n=3). Values bearing different letters within the treatment at each time interval are significant at $p<0.05$. Values are mean ± SD (n=3)	126
Fig. 4.32	FESEM-EDS of $CaCO_3$ precipitates (a, b) CSL-4 (c, d) NB-4 showing rhombohedral $CaCO_3$ crystal (CC) along with the presence of rod-shaped bacterial cells (BC). EDS spectrum marked square '□' shows elemental deposition of the $CaCO_3$	127
Fig. 4.33	(a) Flexural and (b) compressive strength of control, CSL-4 and NB-4 specimens at the age of 7 and 28 days. Values bearing different letters within the treatment at each time interval are significant at $p<0.05$. Values are mean ± SD (n=3)	129
Fig. 4.34	Water absorption by CSL-4 and control specimen at the age of (a) 7 and (b) 28 days	130
Fig. 4.35	Water absorption by NB-4 and control specimen at the age of (a) 7 and (b) 28 days	130
Fig. 4.36	Self-healing of crack by CSL-4 in concrete specimens at different healing percentage taken using DinoLite microscope	132
Fig.4.37	(a) Measurement of crack width at different intervals of time (0 – 50 days) (b) healing efficiency (%) based on the reduction of crack width at 0, 7, 14, 21, 28, 35, 42 and 50 days.	133
Fig. 4.38	Ultrasonic pulse velocity (UPV) of CSL-4 concrete crack specimens at different healing percentages of crack (0, 9, 32.5, 63, and 100%)	133

Fig. 4.39	(a)Water tightness and (b) crack sealing efficiency of bacterial treated CSL-4 concrete crack specimens at 0-, 14-, 28, 35- and 50 days curing time	134
Fig. 4.40	XRD pattern of CSL-4 and control specimens	135
Fig. 4.41	FESEM of the (a, b) crack healed CSL-4 concrete specimens (c, d) control (e, f) EDS spectrum marked '□' represents elemental deposition of the calcium carbonate	136
Fig. 4.42	Self-healing by biomaterials in concrete specimens at 0, 7, 14, 21, 28, 34- and 40-days of crack healing	138
Fig. 4.43	Self-healing of crack by metakaolin immobilized bacterial (*B. paramycoides*) spores in concrete specimens taken using DinoLite microscope	138
Fig. 4.44	(a) Evaluation of crack width due to self-healing application by *B. paramycoides* spores immobilized in metakaolin incorporated concrete crack specimens (b) sealing efficiency (%) based on the reduction of crack width at 0, 7, 14, 21, 28, 35, 40 days	139
Fig. 4.45	Water tightness and crack sealing efficiency of bacterial treated (*B. paramycoides*) Concrete crack specimens at 0-, 12-, 24, and 40-days curing time	140
Fig. 4.46	UPV of NB-4 added and control concrete specimens at different healing time	141
Fig. 4.47	(a, b) FESEM of the NB-4 added concrete specimens depicting rhombohedral crystal precipitation in healed crack region (c, d) control specimen (e) EDS showing elemental deposition of the $CaCO_3$ in healed crack region (f) EDS of the control specimen The '□' marked depicts the spot of EDS analysis	142
Fig. 4.48	XRD pattern of NB-4 and control specimens	143
Fig. 4.49	Growth cycle of cyanobacterial cultures incubated for 40 days in BG11 medium	144
Fig. 4.50	$CaCO_3$ precipitation by *A. montana*, *Aphanothece* sp., *Gleocapsa* sp., *S. elongatus* and *S. pevalekii* cells in BG11 broth supplemented with 100 mM $CaCl_2$ and 50 M $NaHCO_3$ calcifying solution during 120 hours incubation at 25 ± 2 °C. Values	145

bearing different letters within the same time interval are significant at $p<0.05$. Error bars represents standard deviation (n = 3)

Fig. 4.51 pH variation during $CaCO_3$ precipitation experiment 146

Fig. 4.52 SEM analysis of $CaCO_3$ precipitates by (a) *Aphanocapsa montana*, (b) *Aphanothece* sp., (c) *Gleocapsa* sp., (d) *Synechococcus elongatus* and (d) *Synechocystis pevalekii* 147

Fig. 4.53 EDS analysis of $CaCO_3$ precipitates by (a) *Aphanocapsa montana*, (b) *Aphanothece* sp., (c) *Gleocapsa* sp., (d) *Synechococcus elongatus* and (d) *Synechocystis pevalekii* 148

Fig. 4.54 XRD analysis of (a) *Aphanocapsa montana* BDU21001, (b) *Synechocystis pevalekii* BDHKU 35101 148

Fig. 4.55 Fig. 4.55 $CaCO_3$ precipitation by *S. pevalekii* at different pH (6 - 12) conditions. Values bearing different letters within the treatment at each time interval are significant at $p<0.05$. Error bars represent the standard deviation (n=3) 149

Fig. 4.56 Calcium removal percentage (%) during $CaCO_3$ precipitation at different pH (6 -12) conditions. Values bearing different letters within the treatment at each time interval are significant at $p<0.05$. Error bars represent the standard deviation (n=3) 150

Fig. 4.57 Estimation of (a) the flow rate of the calcifying solution (b) pH of the solution effluent injected through sand columns till 14 days. Values are mean ± SD (n=3) 151

Fig. 4.58 Sand columns (a) live (LT), (b) UV-treated (UVT) and (c) control 152

Fig. 4.59 Calcium carbonate precipitation in three different layers of sand columns by live *S. pevalekii* and UV-treated *S. pevalekii* cells. The asterisk (*) sign indicates values are significant at $p<0.05$ using t-test. Values are mean ± SD (n=3) 153

Fig. 4.60 SEM-EDX analysis of sand column treated with (a, b, c) live *S. pevalekii* cells, (d, e, f) UV-treated *S. pevalekii* cells, and (g, h, i) control 153

Fig. 4.61 SEM-EDX images representing the $CaCO_3$ crystals (CC) formation on mortar surfaces treated with *S. pevalekii* (a) live cells (b) UV-treated cells 155

Fig. 4.62 Compressive strength of mortar specimens cured with live and UV-treated *S. pevalekii* cells at 3, 7, and 28 days. Values bearing different letters within the treatment at each time interval are significant at $p<0.05$. Values are mean ± SD (n=3) 156

Fig. 4.63 Water absorption of mortar specimens treated with live and UV treated *Synechocystis pevalekii* at (a) 7 days (b) 28 days of curing time. Values are mean ± SD (n=3) 157

Fig. 4.64 (a) TGA analysis of mortar specimens treated with live and UV-treated *S. pevalekii* cells at 28 days (b) weight loss percentage (%) 158

Fig. 4.65 X-ray-diffraction pattern of mortar treated with live treated and UV treated *S. pevalekii* at 28 days 159

Fig. 4.66 SEM-EDX images represent $CaCO_3$ crystals (CC) in mortar specimens treated with live *S. pevalekii* (B.C.) cells (a, b); UV treated *S. pevalekii* cells (c, d), and control (e, f). The square '□' sign indicates the spot of EDX analysis. 160

Fig. 4.67 Marsh cone test analysis for fluidity of grout mixtures incorporated with different dosages of fly ash (FA); water/binder (w/b) ratio and culture/binder (c/b) ratio. The dotted line differentiates high and low fluidity for marsh cone test. Values bearing different letters within the same treatment are significant at $p<0.05$. Values are mean ± SD (n=3) 162

Fig. 4.68 Mini cone test analysis for fluidity of grout mixtures incorporated with different dosages of fly ash (FA); water/binder (w/b) ratio and culture/binder (c/b) ratio. Values bearing different letters within the same treatment are significant at $p<0.05$. Values are mean ± SD (n=3). 163

Fig. 4.69 Grout bleeding of grout mixtures incorporated with different dosages of fly ash (FA); water/binder (w/b) ratio and culture/binder (c/b) ratio. The dotted line differentiates low (stable) and high (unstable) grout bleed percentages. Values 165

bearing different letters within the same treatment are significant at $p<0.05$. Values are mean ± SD (n=3)

Fig. 4.70 Flow retention diameter of (a) plain grout and (b) biogrout partially replaced with different concentrations of fly ash at different time intervals. Values are mean ± SD (n=3) 167

Fig. 4.71 (a) Initial and (b) final setting time of FA (0% – 50%) incorporated plain and biogrout at w/b and c/b ratio 0.47. The asterisk (*) sign indicates values are significant at $p<0.05$ using t-test. Values are mean ± SD (n=3) 169

Fig. 4.72 Compressive strength of FA (0% – 50%) incorporated plain and biogrout at w/b and c/b ratio 0.47 after 28 days of curing. The asterisk (*) sign indicates values are significant at $p<0.05$ using t-test. Values are mean ± SD (n=3). 170

Fig. 4.73 Crack remediation using plain and biogrout (a) cracked specimen (b) injecting grout using 20 ml syringe (c, d) $CaCO_3$ precipitation after 7- and 28-days curing, (e) crack healed area after removal of additional carbonate precipitates 171

Fig. 4.74 Pictorial representation of curing treatment (spray and ponding) 171

Fig. 4.75 (a) Compressive strength and (b) flexural strength of REF: reference concrete specimen; UTC: untreated concrete; CST: plain (control) grout spray treatment; CPT: Plain (control) grout ponding treatment, BST: biogrout with spray treatment; BPT: biogrout with ponding treatment at 28 days of curing. Values bearing different letters within the treatment are significant at $p<0.05$. Error bars represent standard deviation (n=3) 173

Fig. 4.76 Water sorptivity of concrete specimen after cracks repaired treatment with grouting. UTC: untreated concrete; CST: plain (control) grout spray treatment; CPT: Plain (control) grout ponding treatment, BST: biogrout with spray treatment; BPT: biogrout with ponding; REF: reference concrete specimen at 28 days of curing. All experiments were carried out in triplicate (n=3) 174

Fig. 4.77 Sealing efficiency of the concrete specimen after cracks repaired treatment with grouting. REF: without crack concrete; CST: plain (control) grout spray treatment; CPT: Plain (control) grout 175

ponding treatment, BST: biogrout with spray treatment; BPT: biogrout with ponding treatment at 28 days of curing. Values bearing the different letters within the treatment

Fig. 4.78 FESEM imaging represents cubic shaped calcite and spherical shaped vaterite (V) $CaCO_3$ (CC) crystals formed in (a, b) biogrout ponding treatment: BPT, (c, d); biogrout spray treatment: BST specimens 177

Fig. 4.79 FESEM imaging of (a) Plain ponding grout treatment: CPT, (b) plain spray grout treatment: CST and (c) EDS of control plain grout 177

Fig. 4.80 EDS imaging and mapping of (a, b, c) biogrout ponding treatment: BPT, (e, f, g); biogrout spray treatment: BST 178

Fig. 4.81 XRD plot of plain and biogrout samples at 28 days of curing 178

Fig. 4.82 (a) Thermogravimetric analysis (TGA) and (b) weight loss (%) of the of plain and biogrout samples at 28 days of curing 179

Fig. 4.83 Cell density of microbes and $CaCO_3$ precipitation by (a) *S. pevalekii* and (b) *B. paramycoides* cells during 120 hours incubation 180

Fig. 4.84 Dissolved calcium (Ca^+) ions in the BG11 and NB broth during $CaCO_3$ precipitation experiment. The asterisk (*) sign indicates values are significant at $p<0.05$ using t-test. Values are mean ± SD (n=3) 182

Fig. 4.85 FESEM analysis of $CaCO_3$ (CC) crystals formed by (a, b) *S. pevalekii* and (c, d) *B. paramycoides* after 120 hours 183

Fig. 4.86 Effect of initial pH (6 – 12) on growth of *B. paramycoides* and *S. pevalekii* cell culture at different time interval 183

Fig. 4.87 $CaCO_3$ precipitation by *S. pevalekii* and *B. paramycoides* at varied initial pH of BG11 and nutrient broth after 120 hours. The asterisk (*) sign indicates values are significant at $p<0.05$ using t-test. Values are mean ± SD (n=3) 184

Fig. 4.88 (a) compressive strength (b) percentage change in compressive strength of concrete specimens at 3, 7, 28 days of curing. Values bearing different letters within the treatment at each time interval 186

	are significant at $p<0.05$. Error bars represent standard deviation (n=3)	
Fig. 4.89	Relative strength index of SPC and BPC specimens at 3, 7 and 28 days of curing	187
Fig. 4.90	(a) Rapid chloride permeability test (RCPT) (b) percentage change in RCPT at 7, 28 days of curing. Values bearing different letters within the treatment at each time interval are significant at $p<0.05$. Error bars represent standard deviation (n=3)	188
Fig. 4.91	Water absorption concrete specimens treated with *S. pevalekii* (SPC), *B. paramycoides* (BPC) along with the control at (a) 7 days (b) 28 days of curing	189
Fig. 4.92	FESEM-EDS of (a) control (b) SPC (c) BPC specimen showing $CaCO_3$ (CC) Crystallization . The square '□' sign indicates the spot for EDS analysis	191
Fig. 4.93	XRD of control, SPC, and BPC concrete specimen	192
Fig. 4.94	Weight gain of the marble surface due to $CaCO_3$ deposition on the surface by metabolic activity of (a) *B. paramycoides* and (b) *S. pevalekii*. Values bearing different letters within the treatment at each time interval are significant at $p<0.05$. Error bars represents standard deviation (n = 3)	195
Fig. 4.95	(Weight loss of marble stone due to the detrimental effect of acid spray. Values bearing different letters within the treatment at each time interval are significant at $p<0.05$. Error bars represents standard deviation (n = 3)	196
Fig. 4.96	Incubation of acid affected marble samples in (a) heterotrophic and (b) photoautotrophic bacteria	198
Fig. 4.97	Weight gain due to $CaCO_3$ deposition in (a) BP samples treated by *B. paramycoides* (b) BSP samples treated by *S. pevalekii*. Values bearing different letters within the treatment at each time interval are significant at $p<0.05$. Error bars represents standard deviation (n = 3)	198
Fig. 4.98	The improvement of colour and texture of marble stones after the MICCP treatment (a) *B. paramycoides* (b) *S. pevalekii*	199

Fig. 4.99	Weight loss of marble samples after sonication treated by (a) *B. paramycoides* and (b) *S. pevalekii*. Values bearing different letters within the treatment at each time interval are significant at $p<0.05$. Error bars represents standard deviation (n = 3)	200
Fig. 4.100	Roughness of the control marble surface without any deterioration and treatment	202
Fig. 4.101	Roughness of marble surface affected by artificial acid rain constituting (a) Test 1 (HNO_3), (b) Test 2 ($HNO_3 > H_2SO_4$), (c) Test 3 (H_2SO_4) and (d) Test 4 ($H_2SO_4 > HNO_3$)	203
Fig. 4.102	Roughness of marble surface treated by *B. paramycoides* culture (a) Test 1 (HNO_3), (b) Test 2 ($HNO_3 > H_2SO_4$), (c) Test 3 (H_2SO_4) and (d) Test 4 ($H_2SO_4 > HNO_3$) using MICCP technique.	203
Fig. 4.103	Roughness of marble surface treated by *S. pevalekii* culture (a) Test 1 (HNO_3), (b) Test 2 ($HNO_3 > H_2SO_4$), (c) Test 3 (H_2SO_4) and (d) Test 4 ($H_2SO_4 > HNO_3$) using MICCP technique	205
Fig. 4.104	Microscopic observation of marble surface (a) Control; before deterioration (b) marble surface after the different test group of acid attack (analogous to acid rain) (c) microbial (BP) treated surface showing $CaCO_3$ deposition	206
Fig. 4.105	Microscopic observation of marble surface (a) Control; before deterioration (b) marble surface after the different test group of acid attack (analogous to acid rain) (c) microbial (BSP) treated surface showing $CaCO_3$ deposition	206
Fig. 4.106	FESEM analysis of the acid affected marble surface (a) Test 1, (b) Test 2, (c) Test 3, (d) Test 4	208
Fig. 4.107	FESEM analysis *B. paramycoides* treated marble surface (a) BP-1, (b) BP-2, (c) BP-3, (d) BP-4	209
Fig. 4.108	FESEM analysis of the *S. pevalekii* treated marble surface (a) BSP-1, (b) BSP-2, (c) BSP-3, (d) BSP-4	210

List of Tables

Table No.	Description	Page No.
Table 2.1	Summary of different environmental sources and microorganisms isolated	21 - 22
Table 2.2	Overview of different cyanobacterial species, growth media, calcite precipitated and properties studies by the researchers	24 - 25
Table 2.3	Overview of different bacteria, concentration, carriers, methodologies adopted by the researchers to study the self-healing mechanism of cracks	36 - 37
Table 3.1	Chemical constituents of marble dust	45
Table 3.2	Chemical composition of the Metakaolin and the OPC - 43 grade	54
Table 3.3	Outline of the different mix designs for the experiment and curing treatment	54
Table 3.4	Rating of chloride penetrability of concrete	57
Table 3.5	Mix proportion of the concrete specimens	63
Table 3.6	Sand consolidation experiment set-up with different calcifying media	69
Table 3.7	Outline of different sets of mortar specimens and mechanism of curing treatment	71
Table 3.8	Chemical composition and specific gravity of ordinary portland cement (grade 43) and fly ash (FA)	73
Table 3.9	Outline of composition used in the development of 1200g plain (water) and biogrout (*Synechocystis pevalekii* culture) containing a different dosage of FA and cement	74
Table 3.10	Outline of different sets of repairing techniques using FA amalgamated cement-based grout specimens and mechanism of curing	82

Table 3.11	Outline of the different mix design of the experiment and curing treatment	86
Table 3.12	Concentration of different acid solution used in experimental damage of marble stones	89
Table 4.1	Enumeration of bacteria on nutrient agar	92
Table 4.2	Quantification of DNA templates using nanodrop spectrophotometer	94
Table 4.3	Quantification of purified PCR product using nanodrop spectrophotometer	95
Table 4.4	Molecular identification based on 16S rRNA sequencing data using NCBI nucleotide BLAST database	96
Table 4.5	The factorial ANOVA results indicate the effects of different bacterial isolates and time on urease activity, and $CaCO_3$ precipitation	101
Table 4.6	The factorial ANOVA results indicate the effects of different bacterial isolates and time on $CaCO_3$ precipitation in sand consolidation	102
Table 4.7	The factorial ANOVA results indicate the effect of different temperature, pH conditions on urease activity	107
Table 4.8	The factorial ANOVA results indicate the effects of different treatments and time of curing on cementitious properties	116
Table 4.9	The factorial ANOVA results indicate the effects of different treatments (*B. paramycoides* and control) and curing time on water absorption for concrete specimens	119
Table 4.10	The factorial ANOVA results indicate the effect of different storage temperatures and time on urease activity and $CaCO_3$ precipitation	126
Table 4.11	The factorial ANOVA results indicate the effect of different cyanobacterial culture and time interval on $CaCO_3$ precipitation	146
Table 4.12	Sorptivity coefficient different treatments at the age of 7 and 28 days	157

Table 4.13	The factorial ANOVA results indicating the effects of different concentrations (0% - 50%) of fly ash (FA) and water/binder (w/b) or culture/binder (c/b) ratio on injectable grout in a crack. The P values < 0.001 indicates the values are highly significant	165
Table 4.14	Fresh properties (a) Marsh cone, (b) mini-slump cone, and (c) grout bleeding of grout mixtures incorporated with different dosages of fly ash (FA); water/binder (w/b) ratio and culture/binder (c/b) ratio	166
Table 4.15	The ANOVA results indicate the effects of different treatments (*S. pevalekii*, *B. paramycoides*, and control) and time of curing for concrete specimens	186
Table 4.16	The ANOVA results indicate the effects of different treatments (*S. pevalekii*, *B. paramycoides*, and control) and time of curing on sorptivity for concrete specimens	189
Table 4.17	The factorial ANOVA analysis indicates the effects of different treatments and curing times for marble samples	200
Table 4.18	Roughness analysis of acid affected, bacterial and cyanobacterial treated marble samples	202

List of abbreviations

MICCP	Microbially induced calcium carbonate precipitation
NB	Nutrient broth
CSL	Corn steep liquor
DNA	Deoxyribonucleic acid
RNA	Ribonucleic acid
ASTM	American Society of Testing and Materials
IS	Indian standard
RCPT	Rapid chloride penetrability test
SEM	Scanning electron microscopy
EDS/EDX	Energy dispersive X-ray spectroscopy
FESEM	Field emission scanning electron microscopy
XRD	X-ray diffraction
TGA	Thermogravimetric analysis
MK	Metakaolin
FA	Fly ash
UPV	Ultrasonic pulse velocity

List of Symbols

%	Percentage
mg	Milligram
g	Gram
ml	millilitre
L	Litre
mm	Millimetre
cm	centimetre
v/v	Volume by volume
w/v	Weight by volume
mM	Millimolar
mol	Moles
N	Normality
h	Hours
s	Seconds
°C	Degree Celsius
V	Voltage
C	Coulomb
MPa	Megapascal
w/b	Water to binder
c/b	Culture to binder

Abstract

Microbially induced calcium carbonate precipitation (MICCP) is a novel and eco-friendly technique to enhance the consolidation properties of building materials. In this study, the MICCP was carried out by heterotrophic and photoautotrophic bacteria to improve the structural properties of cementitious and stone material. The research focuses on isolating and characterizing urease-producing bacteria from marble dust and their efficiency in calcium carbonate precipitation. Seven isolates of ureolytic bacteria were isolated and identified as *Bacillus cereus* MD1, *Bacillus paranthracis* MD2, *Bacillus paranthracis* MD3, *Bacillus paramycoides* MD4, *Bacillus paramycoides* MD5, *Bacillus paramycoides* MD6 and *Bacillus paramycoides* MD7 using 16S rRNA sequence analysis. These bacterial isolates were screened based on their urease activity, calcium carbonate ($CaCO_3$) precipitation, and sand consolidation properties. *B. paramycoides* MD6 observed the best results with urease activity of 1512 U/ml and $CaCO_3$ precipitation of 1232 mg/100 ml. The sand column treated by *B. paramycoides* MD6 was more compact and showed a reduction in the flow rate. The amount of $CaCO_3$ precipitated in the sand column's upper, middle and lower layers was 42.96 mg/g, 31.56 mg/g, and 21.13 mg/g, respectively. Different temperatures and pH conditions significantly influenced the growth cycle, urease activity, and $CaCO_3$ precipitation. The optimum temperature for growth of *B. paramycoides* MD6 was 37 °C with a pH range of 7-10. The sand consolidation experiment was performed for three diverse grain sizes (150 µm, 300 µm, and 600 µm) to examine the efficacy of consolidation in the presence of various-sized voids within the sand particles. A sand column with a 150 µm grain size had the highest precipitation rate with solid consolidation. *B. paramycoides* MD6 was also incorporated into the concrete mix and tested for strength and permeability properties after 7 and 28 days of curing. The strength was observed to be significantly reduced in bacterial admixed specimens than in the control. The sorptivity coefficient and amount of charge passed through the concrete during the rapid chloride penetrability test (RCPT) experiment were reduced significantly. The results were confirmed using Field emission electron microscopy (FESEM). Energy Dispersive (X-ray) spectroscopy (EDX/EDS) and X-ray Diffraction (XRD).

The biomaterial was developed by immobilizing *B. paramycoides* MD6 spores in metakaolin (MK). The immobilized bacteria in MK was used as carrier material in concrete to improve the

cementitious and self-healing properties. The nutrient broth (NB) and corn steep liquor (CSL) were used as nutrient media for self-healing. The biomaterial stored at 4 °C and 25 °C were tested for bacterial viability for 180 days. At the end of storage, after 180 days, the biomaterial stored at 4 °C showed better results in viability, urease activity, and $CaCO_3$ precipitation. The biomaterial NB-4 and CSL-4 showed significant improvement in concrete compressive and flexural strength at 7 and 28 days. The sorptivity coefficients of NB-4 and CSL-4 were 0.006 and 0.002 at 7 and 28 days, respectively, which were comparatively lower than the control. The self-healing capability of biomaterial was investigated for approximately 0.5 mm crack in 400 × 100 × 100 mm prismatic specimens. The crack was completely healed with 99.14% and 98.2% crack healing efficiency in CSL-4 and NB-4 biomaterial-incorporated specimens, respectively. During the healing of the crack, the water tightness of the repaired surface was 88.9% and 92.8% in CSL-4 and NB-4 specimens, verifying a reduction in water flow upon complete healing. During the crack healing period, the ultrasonic pulse velocity (UPV) was observed to improve and get closer to the reference specimens, proving the complete healing of the crack. At the end of testing, the precipitated mineral was assessed by FESEM-EDS and XRD. The developed metakaolin-based biomaterial can be used as self-healing supplementary cementitious material.

Most of the studies have emphasized using ureolytic bacteria to improve the durability properties of building structures. The present investigation examined the role of photoautotrophic bacteria in enhancing cementitious properties and crack remediation. Five photoautotrophic cyanobacteria, *Aphanocapsa montana* BDU21001, *Aphanothece* species BDHKU 40501, *Gleocapsa* species BDU 40111, *Synechococcus elongatus* BDU14174 and *Synechocystis pevalekii* BDHKU 35101 were procured from National Facility of Marine Cyanobacteria (NFMC), Bharathidasan University, Tamil Nadu, India and were tested for $CaCO_3$ precipitation. *S. pevalekii* showed maximum $CaCO_3$ precipitation (695 mg/100 ml) in BG11 broth, followed by *S. elongatus* and *Gleocapsa* species. Based upon the highest calcification potential, the photoautotrophic cyanobacteria *S. pevalekii* was selected to study the consolidation effect of carbonate precipitation. The sand consolidation experiment used live (LT) and UV-treated (UVT) cells. The LT sand column was more compact and solid than the UVT sand column. The *S. pevalekii* (LT and UVT) was also incorporated in the mortar mix and tested for mechanical and permeability efficiency. The compressive strength of mortar

specimens was significantly enhanced by 25.54% and 15.84% compared to control with live- and UV-treated *S. pevalekii* cells at 28 days of curing. Water absorption levels were reduced considerably in bacterial-treated mortar specimens compared to control at 7 and 28 days of curing. $CaCO_3$ precipitation was higher in live-treated cells than in UV-treated *S. pevalekii* cells. $CaCO_3$ precipitation by *S. pevalekii* cells was confirmed with SEM-EDS, XRD, and TGA analysis. These results suggest that using *S. pevalekii* bacteria can serve as a low-cost and environment-friendly MICCP technology to improve the durability properties of cement mortar. An eco-friendly and sustainable biogrout was developed using *S. pevalekii* for crack remediation in concrete. To improve the fluidity characteristics of the grout, fly ash (FA) was incorporated as a partial cement replacement in the cementitious grout. The cementitious grouts were tested for fresh properties at different dosages of FA (0%-50%) by keeping water (or bacterial culture) to binder ratios of 0.45, 0.47, and 0.50. Based on flowability results, a 0.47 culture/binder ratio was selected to examine different FA dosages for hardened properties. A 40% FA substituted cementitious biogrout was selected for repairing cracks at the lab scale. Different cracked concrete specimens were repaired and cured using ponding and spray treatment for 28 days. At the end of the experiment, a significant improvement in strength and permeability was recorded in biogrout-remediated cracked specimens. The sample was collected from the healed cracked region to confirm the $CaCO_3$ precipitation using FESEM-EDS, XRD, and thermogravimetric analysis (TGA). The developed FA-incorporated biogrout serves as an economical and eco-friendly MICCP technology for the remediation of existing cracks in concrete structures.

A comparative analysis was performed between photoautotrophic and heterotrophic bacteria to enhance concrete's mechanical and permeability properties. The specimens were cast using live *S. pevalekii* (SPC) and *B. paramycoides* (BPC) cells. The microbes incorporated concrete specimens showed significantly improved compressive strength compared to the control specimens prepared using tap water. However, a marginal difference (1.8%) was observed between the SPC and BPC specimens. The charge passed through SPC and BPC specimens during the rapid chloride permeability test was 1901 and 1440 coulombs, respectively, after 28 days of curing. The water absorption reduced after 28 days with 0.007 and 0.005 sorptivity coefficients for SPC and BPC specimens, respectively. The $CaCO_3$ crystallization in SPC and

BPC specimens was confirmed using a FESEM-EDS. The peaks of calcite and vaterite were observed in XRD.

Calcification potential and consolidation properties were studied to evaluate the efficacy of *S. pevalekii* and *B. paramycoides* to precipitate $CaCO_3$ on the marble stone. The bound $CaCO_3$ on the surface was analyzed by weight gain on the sample. Maximum weight gain was observed in marble samples treated with 6×10^{-7} cells with 1.40 g and 1.94 g in *B. paramycoides* and *S. pevalekii*-treated samples, respectively. The marble stones were tested for acid rain attack by performing lab-scale artificial acid rain spray using four different solutions. The four solutions comprise nitric acid (HNO_3), sulphuric acid (H_2SO_4), and a mixture of two solutions at different concentrations. The changes on the surface were assessed by weight change, roughness, microscopic visualization, and atomic force microscopic (AFM) observation. Exposure to acid rain affected the marble and resulted in weight loss due to granular disintegration. The alteration in colour was observed only in marble samples treated with H_2SO_4. The MICCP treatment was performed by immersing the acid-affected marble samples in bacteria and cyanobacteria culture for 28 days. The surface was improved significantly by the gain in lost carbonate at each consecutive interval by heterotrophic bacteria and photoautotrophic cyanobacteria. The outcomes demonstrated notable enhancements in roughness measurement and a negligible reduction of precipitated calcite on the surface due to sonication.

This study affirms that both *B. paramycoides* and *S. pevalekii* significantly improved concrete's strength and permeability properties. The microbes also considerably enhanced the aesthetic properties of marble stone. These results suggest that heterotrophic and photoautotrophic bacteria play an important role in enhancing cementitious materials and marble stone

Chapter 1 Introduction

1. General Introduction

Global urbanization has increased the demand for resilient and innovative civil infrastructure. It plays a significant role in the nation's economic expansion and ranking worldwide. The swift advancement of ready-mixed concrete represents an essential indicator of technological progress and overall quality improvement in the concrete industry. However, with continuous growth, the construction business also encounters problems related to the sustainability of concrete structures because of its low tensile strength and poor cracking resistance (Wang et al. 2019). Cracks are almost inevitable and can occur at any stage during its service life (Gupta et al. 2017). It allows the penetration of moisture, harmful agents like carbon dioxide (CO_2), sulphate (SO_4^{2-}), and chloride (Cl^-) into concrete crack, compromising its durability. Conventionally, cracks are repaired using chemical-based sealants (synthetic epoxides, polyurethane, epoxy resins, acrylics, and waxes). These sealants actively control undesirable infiltration but limit the application due to low heat resistivity and unsustainability (Dhiman et al. 2022). It also requires manual application which is undesirable due to the difficulty detecting cracks and the associated high maintenance and repair costs (Lee and Park 2018). Therefore, researchers and engineers are looking for low-cost and eco-friendly repair mechanism. One such innovative example is microbial concrete which has served as a potential solution for improving sustainability and enhancing cementitious properties. This involves the research on Microbially Induced Calcium Carbonate Precipitation (MICCP) that has attracted considerable interest on account of its eco-efficiency, sustainability, and potential as a practical solution (De Belie et al. 2018; Kan et al. 2019; Seifan and Berenjian 2019a).

MICCP is a biomineralization process in which microorganisms, primarily bacteria, play a crucial role in forming calcium carbonate ($CaCO_3$). This mechanism has garnered significant interest in various scientific and engineering disciplines, particularly biotechnology, environmental science, and civil engineering. Collaboration between the construction industry and microbiology has led to innovation and smart infrastructure development. MICCP requires less mechanical energy and has a low or zero carbon footprint, contributing to developing cost-

effective processes with environmental benefits (Muhammed et al. 2021). A variety of microorganisms (photoautotrophic, heterotrophic, and sulfate-reducing bacteria) are capable of $CaCO_3$ precipitation (Zhu and Dittrich 2016; Ali et al. 2023). Ureolysis is a renowned MICCP phenomenon in concrete by heterotrophic bacteria because of its high $CaCO_3$ precipitating property (Toncheva-Panova et al. 2010; Dhami et al. 2013b). Ureolytic bacteria can induce the formation of $CaCO_3$ by the accumulation of a urease enzyme. The enzyme utilizes urea as substrate and calcium as a source for mineralization. Knowledge of this technology dates back to the early 1990s and has fascinated researchers from various disciplines, mainly for its workability as a pioneering and effective approach for soil and concrete improvement. Microorganisms such as *Bacillus subtilis* (Nain et al. 2019; Feng et al. 2021a), *B. megaterium* (Dhami et al. 2013b), *B. pseudofirmus* (Lors et al. 2017; González et al. 2020), *B. pasteurii* (Nasser et al. 2022; Sohail et al. 2022), *B. sphaericus* (Pungrasmi et al. 2019a), *Escherichia coli* (Islam et al. 2022), *B. cohnii* (Rauf et al. 2020) are reported for their $CaCO_3$ efficiency. The $CaCO_3$ precipitation by ureolytic bacteria is the straightforward and simplest mechanism of urea hydrolysis to form carbonic acid and ammonia (Cuccurullo et al. 2022). From time to time, isolation and screening of calcifying microorganisms from various natural habitat have been done in laboratory condition (Achal et al. 2010b). However, numerous other microorganisms have yet to be recognized for their ability to precipitate $CaCO_3$ and its functionality. The major drawback of ureolytic bacteria is the release of ammonia (foul-smelling pollutant), which results in nitrogen oxide (NO_x) emission into the atmosphere, causing health and environmental concerns (Ramakrishnan VV 2015; Justo-Reinoso et al. 2021). Moreover, excessive ammonium in the concrete matrix increases the risk of salt damage by conversion to nitric acid (Seifan et al. 2016a).

An alternative approach involving photoautotrophic bacteria instead of ureolytic bacteria in MICCP has recently drawn the attention of many researchers toward more eco-friendly techniques in concrete environments. Photoautotrophic bacteria have the property to induce carbonate precipitation in aquatic as well as terrestrial environments (Douglas and Beveridge 1998; Altermann et al. 2006; Obst et al. 2006; Dittrich and Sibler 2010; Kranz et al. 2010). Microorganisms such as cyanobacteria have the natural ability to precipitate cement sand and sequestrate CO_2. The photosynthetic capability of photoautotrophic cyanobacteria has been outlined as a prime source in building the course of ecological and evolutionary changes

throughout the past centuries. Its ability to harness solar energy and assimilate CO_2 to organic compounds (Jansson and Northen 2010). Cyanobacteria are widespread aerobic (photosynthetic) photoautotrophic prokaryotes that originated 1.8-2.32 billion years ago (Golubic and Seong-Joo 1999). Many cyanobacteria fossils have been discovered in the microbially induced carbonate rocks. Cyanobacteria are phylogenetically diverse Gram-negative bacteria found in moist soil, marine or fresh water, and extreme habitats like hot springs, hypersaline water, and deserts. The most distinctive characteristic of cyanobacteria is that it can survive on a minimum requirement of light, CO_2, and water, which is inexpensive and at minimal cost nutrients (Castenholz et al. 2001; Singh et al. 2016). Cyanobacteria fix the atmospheric CO_2, HCO_3^- /OH^- exchange process occurs across the cell membrane, which increases pH, thus creating an alkaline microenvironment (Zhu and Dittrich 2016). Many Cyanobacterial species viz. *Synechococcus* (Obst et al. 2009; Paulo et al. 2018; Williams et al. 2019), *Synechocystis* (Han et al. 2017b), *and Oscillatoria* (Uma et al. 2014) have been reported to precipitate $CaCO_3$. Unlike ureolytic bacteria, photoautotrophs form carbonates with an environment-friendly technique, utilizing carbon dioxide and sunlight as energy and producing oxygen during their growth. The *Synechocystis* can favorably grow in an alkaline medium and in various unfavorable conditions like low temperature, hyperosmotic stress, and salt stress (Kamennaya et al. 2012; Yu et al. 2013).

Historically, MICCP has played a significant role in the cementation of the earth's natural systems, such as caves, soils, sediments, etc. MICCP has contributed to improving the constructional parameters and played a considerable role in various applications, such as strength enhancement, porosity reduction, crack remediation, corrosion prevention, etc. Self-healing is a practical crack-repair approach that incorporates bacteria when preparing fresh concrete. It is a sustainable and promising technique that utilizes bacterial ability to precipitate stable crystal polymorphs of $CaCO_3$ (Dhami et al. 2013b; Mutitu et al. 2019). The MICCP can operate independently and seal the cracks regardless of its location. Most studies reported the self-healing capabilities of freshly prepared bacterial carrier materials in concrete (Dinarvand and Rashno 2021). There is an extensive need to develop a higher shelf-life bacterial product for upscaling the MICCP technique. The viability of the bacteria is of paramount importance and is greatly influenced by factors such as the toxicity of immobilized carrier materials to bacterial cells, the cell entrapping properties of the material, and the availability of bio-agents

to bacterial cells (De Belie and Wang 2015; Wang et al. 2018a; Zhang et al. 2023). The bacterial survival determination inside the protective carrier is crucial to understand the metabolic behavior of bacteria (Zhu et al. 2021b; Sharma et al. 2022).

Moreover, alkaliphilic/alkali-tolerant spore-forming strains should be utilized because of the alkaline environment inside the concrete and the need for long-lasting healing agents (Wang et al. 2014; Liu et al. 2020a). Spores are more resistant to heat, radiation, and other chemicals (Kennedy et al. 1994; Xu and Wang 2018). This makes spores a better bioagent for MICCP than freshly prepared cultures. Spores become active when cracks appear, owing to the ingress of moisture and oxygen in the cracked area (Sharma et al. 2017; Lee and Park 2018). The bacterial endospores have ability to withstand the highly alkaline pH of the concrete mix during the casting and drying of concrete. Spores can endure high mechanical compressive stresses during concrete curing (Jonkers et al. 2010). Bacterial spores are made up of dehydrated spore cores, peptidoglycan cortex, Ca^{2+} ions, and dipicolinic acid (DPA) (Abel-santos 2015). The spores are able to induce growth as soon as they receive favorable conditions of growth (desired temperature, moisture, and nutrients) that can stimulate germination and overcome the dormancy period of spores. The germination rate of bacterial spores can range from a few minutes to several hours depending on the specific conditions provided. Nutrients (amino acids, sugar) binds to the inner membrane and rehydrates the spore core. Ca^{2+} - DPA (dipicolinic acid) is released from the spore core stimulating germination (Setlow 2003; Setlow and Johnson 2019). When spores germinate and vegetative cells start actively growing, they can produce extracellular enzymes, such as urease and carbonic anhydrase due to the metabolic activity of bacteria (Pungrasmi et al. 2019b; Christie and Setlow 2020).

Various techniques, including encapsulation and immobilization, serve to safeguard bacteria during the mixing process of concrete, as the bacteria become denser as a result of the hydration reactions of the cement (Silva et al. 2015; Zamani et al. 2020; Justo-Reinoso et al. 2022). Previously, researchers have reported various carrier materials such as hydrogels (Wang et al. 2014; Gao et al. 2020a; Zhu et al. 2021b), polyurea microcapsules (Zamani et al. 2020), alginate (Wang et al. 2016), biochar (Gupta et al. 2018), nanoplates (Khaliq and Ehsan 2016), low-weight aggregates (Alghamri et al. 2016; Wang et al. 2022a), and silica gel (Wang et al. 2012a; Oliveira et al. 2021; Gulin et al. 2021) as potential carrier materials for MICCP. However, these

carrier materials are considered to have poor compatibility with concrete. Carrier materials without bacterial inoculum can have a negative or zero impact on the mechanical properties of concrete because of their low density and hardness (Yuan et al. 2022). Researchers recommended that an ideal carrier material should be non-toxic (safe for the environment and the immobilized element), stable, affordable, and readily available (Dzionek et al. 2016). Also, it is best to use a carrier material synergistic with concrete. The high-water absorption capacity of the carrier material can affect the hydration of the cement. Gel-based carrier materials involve a difficult preparation process with increased production cost (Zhang et al. 2017; Zheng and Qian 2020). In addition, the shelf-life of bacteria-based carrier materials for longer durations is not well-defined. The freshly prepared bacterial culture was used for developing carrier-based self-healing materials, which limits the application of MICCP in the field owing to the availability of resources. Therefore, it is crucial to explore concrete-compatible carrier materials with high mineralization capabilities that can easily bond with bacteria and improve the self-healing properties of concrete.

In recent studies, metakaolin (MK) and fly ash (FA) have shown remarkable results as supplementary cementitious materials in construction industries (Bishnoi 2020; Rais and Khan 2021; Singh and Murugan 2022). MK and FA are industrial by-products containing siliceous aluminous resources exhibiting high pozzolanic activity (Li et al. 2022b). Worldwide FA production is estimated to exceed 900 million tons annually (Heidrich et al. 2013; Delić et al. 2022; Onyelowe et al. 2022). Of these, only 53.5% of the FA is utilized as replacement material in cement, brick production, and road construction (Kotelnikova et al. 2022; Onyelowe et al. 2022). Concerning the environmental issues related to FA and other additives, it is essential to understand that they provide no risk in utilizing it as carrier material or grout preparation (Celik and Canakci 2015). The micronized size distribution of MK in the concrete mixture improved the cement matrix's pore structure (Singh and Siddique, 2022). It can react with the free lime (calcium hydroxide) produced by cement hydration to form additional calcium silicate hydrates, making it an efficient carrier material for MICCP (El-Diadamony et al. 2018). Metakaolin decreases fluidity through the material, thus enhancing durability and reducing chloride ion diffusion (Badogiannis et al. 2015). The immobilization of spores using a porous adsorption material will ensure the viability of the biomaterial for a longer duration (Bhaskar et al. 2017). Many studies are available in the literature for the partial replacement of cement

with FA (Sha et al. 2018; Zhang et al. 2020; Bai et al. 2022; Mohamed and Khallaf 2022), but limited studies are available for crack repair using FA-substituted grout.

Concrete, marble, and limestone have been centuries' most robust and used construction materials. Most historical buildings and monuments were carved from limestone and marble. Despite its impeccable strength, these materials are highly porous and hydrophilic, making them highly susceptible to water (such as acid rain) and environmental pollutants (Wakefield and Jones 1998; Tiano et al. 1999; Rodriguez-Navarro et al. 2003). The primary environmental pollutants that significantly impact stonework are sulfur, carbon, nitrogen oxides, and aerosol particulate matter, such as smoke, which are the primary cause of pollution. Human activity has significantly augmented the concentrations of sulfur oxides (SO_2), nitrogen oxides (NO_x), and carbon dioxide (CO_2) in urban environments, leading to an increase in pollution levels in both urban and rural regions. These gases are inherently present in the atmosphere and can dissolve in water, producing acidic solutions and reacting with calcareous substances, ultimately resulting in acidic rainfall (Cappelletti and Fermo 2016; Kumar 2017).

Numerous conservation treatments have been implemented to safeguard and reinforce stone before extensive granular disintegration leads to irreversible harm by causing the loss of surface material. Protection measures are taken to prevent water or other weathering agents from penetrating the core of the stone by waterproofing and/or fortifying the stone surfaces (Siegesmund and Snethlage 2014; Artesani et al. 2020). On the contrary, consolidation involves employing cementing or hardening agents to strengthen and impregnate decayed, porous stones that are prone to crumbling. (Cappelletti and Fermo 2016). As an alternative, MICCP utilizing ureolytic and photosynthetic bacteria are recognized as a safe ecological source for restoration of the aesthetic properties of marble and limestone (Jimenez-Lopez et al. 2008).

1.1 Research Gap

Despite the numerous benefits associated with using MICCP, some challenges need to be addressed. The understanding of bacterial viability and enzyme activity at different temperature and alkaline condition is crucial for implementing the MICCP technique at field scale. Among the initial microorganisms to be examined for MICCP were ureolytic bacteria from the genus

Bacillus (Castanier et al. 2000; Joshi et al. 2017; Mazzoli et al. 2018). The presence of microorganisms from this particular genus has been constantly studied particularly in $CaCO_3$ biomineralization-inducing media. The investigation of other microorganisms that produce carbonates in cementitious and stone environments remains of paramount importance in order to gain a deeper understanding of their dynamics and functioning. There is lack of work on the efficacy of photoautotrophic bacteria in cementitious environment.

Various methods for self-healing through encapsulation and immobilization exist, and the effectiveness of these approaches can be assessed in terms of cell viability and the efficiency of $CaCO_3$ production. It is clear that the majority of research conducted in this field has not delved into the complexities of bacterial metabolic processes. Previous studies have reported various carrier materials to immobilize bacteria in the concrete and have proven to be productive for self-healing of concrete. But the shelf life of existing carrier materials is not defined prior to its application. Also, the high cost associated with these existing carriers limits its application. Hence a, thorough research is required to develop cost effective suitable carrier material of high and defined shelf life for the construction industry.

Although the protection of marble surfaces from the environmental weathering and dissolution caused by acid rain has been widely investigated, there is currently no completely satisfactory treatment available, as all existing methods have limitations that prevent them from being entirely effective. A thorough investigation is required to develop an effective MICCP treatment to restore the lost aesthetic and structural properties of marble stone.

1.2 Aim and Objectives

The aim of this investigation is to use photoautotrophic and heterotrophic bacteria to improve durability characteristics and repair the cracks through the application of carrier materials. To minimize the cost of self-healing approach, the corn steep liquor was used as alternative to nutrient broth. The following objectives were designed.

1. Isolation and characterization of potential calcifying bacteria from alkaline environmental sources

2. Evaluation of calcification process of selected bacteria in marble and concrete environment
3. Enhancement of the overall properties of marble and concrete specimens by isolated calcifying bacteria

Chapter 2 Review of Literature

2. General background

Concrete and marble are the most extensively used construction materials. Concrete is an artificially created hard composite material of cement, sand, aggregates, and water. Marble is a metamorphic rock formed from the transformation of pure limestone. It primarily comprises minerals such as calcite, dolomite, and serpentine (Vardhan et al. 2015; Minto et al. 2018). The global construction of concrete infrastructure has led to an unparalleled global demand for cement. The annual production of concrete is 10 billion tons which is estimated to reach 18 billion tons by 2050, with a projected growth of two-fold (Hasan et al. 2023). The properties of concrete, such as its mechanical strength and durability, make it an ideal hardening agent for various infrastructures, including buildings, bridges, dams, runways, and tunnels. Regular maintenance and repair of concrete structures are crucial to ensure their longevity, strength, and stability, as various factors can cause concrete deterioration (Wang et al. 2016). Concrete has low tensile strength and poor ductility, which causes it to resurface years after construction. Once a crack forms, the deterioration process can be initiated by many factors; however, it typically continues as a combination of different mechanisms. A single factor can cause the initiation of deterioration; however, once it has begun, it tends to involve various mechanisms. Concrete damage can occur when materials are exposed to adverse conditions such as weather, water, or chemicals over an extended period. Similarly, structural monuments and building made of marble or other limestones are vulnerable to the pollution and varying environmental conditions, leading to the deterioration of the stones. Different types of concrete and stone damage can be categorized according to the cause, type of damage, mechanisms of attack, types of deficient structures, financial loss due to defects, and the amount and extent of repair measures (Lee and Park 2018).

2.1 Factors responsible for the deterioration of the building materials

Structural defects often arise from inadequate design, specification, execution, and the use of low-grade materials. Several authors have diversified the causes of constructional damage into three broad categories. Concrete, marble, and other building materials may experience physical

damage due to mechanical weakening and fatigue stress, primarily caused by freeze/thaw, shrinkage, salt accumulation, crystallization, thermal effects, and fire. The repetitive freeze-thaw process can form a hydrophobic layer, which may cause expansion and cracking, scaling, and crumbling of the material. If left unaddressed, this can lead to significant structural damage (Villa et al. 2020). Freeze–thaw undermines the structure of the building and creates internal tension. Heidari et al. (2017) observed the degradation of the Anahita Temple Stone in Kangavar, West of Iran, caused by continuous free-thaw cycles. Concrete structures are also vulnerable to deformation over time, even without external loads. This phenomenon, known as shrinkage, can occur in two forms: plastic and dry shrinkage, resulting from both inherent and extensive factors. Intrinsic factors, such as the design strength, concrete mix, and aggregate size, are the material characteristics of concrete. Comprehensive factors that may vary after casting include temperature, pore water content, age at loading, and curing period (Lei et al. 2018). Concrete structures are susceptible to cracking or failure when subjected to loads exceeding their strength, which can result from overloading or an explosion (Larosche 2009). Despite the strengths of concrete and other building materials, poor construction practices can prevent them from reaching their desired design strengths. Earthquakes are typical examples of overloading that can cause significant damage (Clifton 1988). Additionally, the loss of support or soil movement beneath a building can lead to cracking and structural failure.

Concrete deterioration can also cause by various chemical processes, including hydrolysis, dissolution, and oxidation of the constituents or reactions between aggressive fluids and concrete (Woodson 2009). It can result in the formation of expansive products, including ettringite in the event of sulfate attack, alkali-aggregate attack, and iron hydroxide in the corrosion of reinforcing steel in concrete (Anisuddin and Khaleeq 2005). Reddy et al. (2020) conducted a study to quantify the impact of corrosive conditions caused by acid exposure, including hydrochloric acid (HCl), sulphuric acid (H_2SO_4), sodium chloride (NaCl), and magnesium sulphate ($MgSO_4$) at a concentration of 5%, on material for periods of 3, 7, 14, and 28 days. They found that exposure to different acids resulted in mass loss, with H_2SO_4 being the most aggressive, followed by HCl, NaCl, and $MgSO_4$. Permeable materials, such as stone, mortar, and concrete, may be susceptible to damage when salt crystals form within their pores from a supersaturated solution (Scherer 2004). This occurs when the solution becomes supersaturated, leading to surface scaling caused by physical sulfate attacks. Unlike chemical

sulfate attacks, which involve the interaction of sulfate ions and concrete hydration products, physical sulfate attacks do not include chemical reactions (Haynes et al. 2008; Nehdi et al. 2014). Concrete is also susceptible to damage from exposure to acids, as the acids can react with calcium hydroxide in hydrated Portland cement, causing erosion of the concrete surface by dissolving the hydraulic binders and some aggregates. Industrial waste and the combustion of fuels that contain sulfurous gases can form sulfuric acid, which can significantly degrade the surfaces of concrete and marble stone structures (Huber et al. 2017). Alkali aggregates within the concrete are chemically inert. Nevertheless, these aggregates can undergo a chemical reaction with the hydroxyl ions (OH^-) present in the pore solution, leading to expansion and cracking over an extended period (Thomas 2011).

Biodeterioration refers to the degradation of materials resulting from the metabolic activities of microorganisms, which can cause a variety of unwanted physical, chemical, and aesthetic changes and damage to the materials (Hueck 2001). Concrete buildings may have a high pH, which makes them resistant to microbial growth. However, microorganisms such as bacteria, algae, lichens, fungi, and cyanobacteria can still thrive on concrete and stone surfaces under favorable conditions (Wei et al. 2015). This can lead to the growth of a wide diversity of microorganisms on buildings, stone monuments, and other surfaces, which are constantly exposed to severe weather conditions and environmental factors, such as temperature, rainfall, relative humidity, pollution, and biological colonization (Webster and May 2006; Biswas et al. 2013). These factors can accelerate the growth of microorganisms and lead to deterioration of these structures over time. Carbonation and neutralization of hydrogen sulfide in concrete structures can lower the alkaline surface pH, thereby creating an environment conducive to microbial growth (Roger et al. 2008). Microbial aggregation on the surface of building structures, stone monuments, and works of art can cause direct physical and chemical degradation (Gaylarde et al. 2011).

2.2 Conventional treatment

In buildings, degradation phenomena, such as crack formation, are unlikely to be prevented through exposure to harsh environmental conditions. In the early stages of decay, the concrete structure and strength are not significantly compromised. However, they can seriously impact building materials in the long term. Implementing preventative strategies at an early stage is

imperative to prevent and repair crack formation. The two primary methods for treating surface cracks and pores in concrete are passive and active. Surface cracks can be repaired through passive treatments, whereas active techniques effectively heal internal and external cracks (Seifan and Berenjian, 2019). Conventional treatment includes application of chemical mixtures such as polyurethane, epoxy resins, acrylics, waxes, and siloxane, among others (Sisomphon et al. 2012). These sealants enhance the durability of the structures and prevent the infiltration of aggressive substances, making them suitable for use in a wide range of existing building structures (Seifan et al. 2016b). Pan et al. (2017) reported many challenges associated with the failure of polymeric sealers. These include blistering, cracking, holes, and peeling of the coating. Thus, a suitable alternative is required for effective repair of concrete structures. Researchers have reported various surface treatment methods to protect concrete structures against the penetration of aggressive ions by forming a barrier layer. Based on their chemical nature, surface-treatment materials can be classified into organic and inorganic protective agents. Organic materials are protective agents that do not react with the concrete substrate when applied on the repair surface. The inorganic surface materials are mainly aqueous solutions of sodium silicate. Many studies have reported positive results for these organic and inorganic materials in protecting the surface from aggressive ion penetration (Jiang et al. 2015; Pan et al. 2016). However, many challenges related to the synthesis, service life, and application cost need to be addressed, limiting its implementation at the field scale. By contrast, active treatment techniques are independent and can be immediately activated upon crack formation, thereby sealing the crack regardless of its position. This treatment includes techniques such as autogenous healing, polymeric encapsulation, and the microbial production of $CaCO_3$ (Wu et al. 2012; Seifan and Berenjian 2019b). Autogenous healing can effectively fill cracks by hydrating previously unhydrated cement particles or carbonating dissolved calcium hydroxide (De Belie et al. 2018). Calcium hydroxide reacts with atmospheric carbon dioxide (CO_2) to form $CaCO_3$. It is one of the most valuable and versatile fillers for plugging concrete voids, pores, and cracks (Barbhuiya et al. 2015). However, the presence of humidity in the surrounding environment, concrete matrix composition, and the amount of unhydrated cement are significant for autogenous healing. Autogenous healing can heal cracks that range from 0.1 to 0.3 millimeters in width as a result of cement hydration and the carbonation of hydrated products (Rajczakowska et al. 2019; Amer Algaifi et al. 2020; Althoey et al. 2023). An alternate form of active treatment entails encapsulating polymeric material, which

undergoes conversion into foam when exposed to moisture, effectively restoring cracks (Araújo et al. 2018). This method may lead to the expansion of existing damages caused by disparities in the chemical composition of the hardening agent and cement/concrete substrate. Furthermore, this technique requires the use of capsules, which can affect the workability and mechanical properties of concrete. Constraints of conventional approaches have generated significant interest in novel, innovative, passive, and active methods.

Similarly, many organic and inorganic treatments are applied for restoration of marble and other limestones structures and monuments (Minto et al. 2018). The utilization of hydrophobizing material such as copolymers, polymeric resins, organosilicone compounds, vinyl polymers, acrylic polymers and fluorinated materials have been applied as protective coatings to surfaces (Wu et al. 2005; Fermo et al. 2014; Cappelletti et al. 2015). Surface treatment of marble with polymers is a widely utilized technique due to its ability to provide a protective coating on the monument surface, as well as to regulate the movement of various fluids from the surface to the internal pores (Cappelletti et al. 2015). However, these treatments for restoration have certain limitations. Organic (hydrophobizing) materials may deteriorate rapidly, while inorganic materials, such as cement mortar, can fill surface cracks but ultimately lead to accelerated structural degradation due to the expansion of dissolvable crystalline minerals with varying expansion coefficients (Mosquera et al. 2003; Baglioni et al. 2013). with the aim of preserving the natural aesthetics of the stone structures, it is important to develop novel protection and restoration strategies that do not compromise their original characteristics.

2.3 Biomineralization

Biomineralization is a biogeochemical process that occurs in nature because of the activities of prokaryotic microorganisms, which adjust their metabolic rates in response to the surrounding environment, ultimately forming inorganic matter (Dhami et al. 2013b). This has emerged as a sustainable and eco-friendly approach for safeguarding and restoring building materials. It is currently known that more than 60 biominerals exist, including $CaCO_3$, silicates, and iron oxides or sulfides (Bazylinski 2003). Biominerals exhibit marked diversity in terms of shape, size, crystallinity, isotopic composition, and trace element content (Weiner, 2003). Mineral precipitation by prokaryotes can be categorized into three main categories based on their biomineralization methods: biologically induced mineralization (BIM), biologically controlled

mineralization (BCM), and biologically influenced mineralization (Lowenstam, 1981; Mann, 1993). The latter is also called organic-matrix-mediated mineralization or, occasionally, passive biomineralization. In BIM, biominerals are formed due to the interaction between microbial activity and the surrounding environment. Biominerals are formed by the metabolic processes of bacteria and fluctuations in the chemical equilibrium of the surrounding environment (Knoll 2003) (Fig. 2.1). In contrast, BCM, that is, biologically controlled mineralization, microorganisms controls the rate of nucleation, growth, and location of precipitates formed (Bazylinski 2003; Phillips et al. 2013). Weiner et al. (2003) classified mineral precipitates into inter-, intracellularly, and extracellularly formed. Bacteria control the composition, size, form, and location of minerals produced. BCM is solely dependent on bacteria and insensitive to external environmental factors that may influence mineral precipitation (Estroff et al. 2008; Krajewska 2018) (Fig. 2.2).

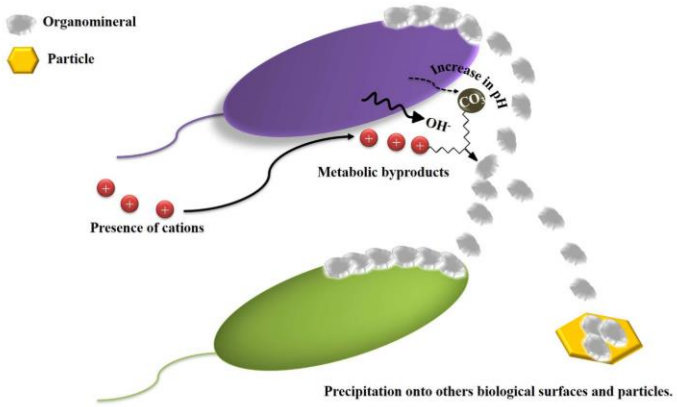


Fig. 2.1 Illustration of BIM mechanism, representing the interaction between metabolic products of microorganisms and inorganic compounds present in environment to induce biominerals precipitation. Adapted from Castro-Alonso et al. (2019)

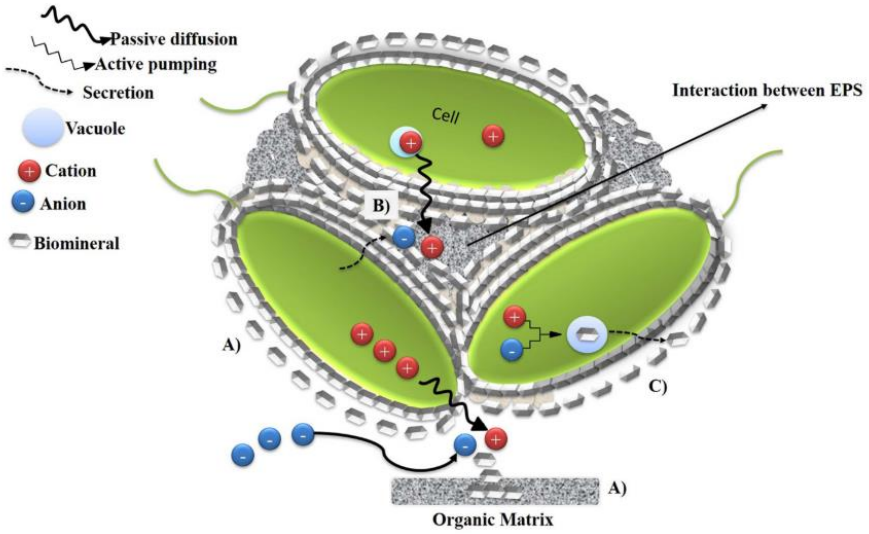


Fig. 2.2 Illustration of Biologically Controlled Mineralization (BCM). (A) in extracellular BCM, mineral nucleation take place within the organic matrix through passive diffusion (B) in intercellular BCM surface of cells that line other cells (epithelial surfaces) acts like a natural substrate for mineralization, guiding and shaping the deposit of biominerals around the cell surface (C) intracellular BCM, minerals are precipitated within a specific vesicle in the cells and is then released. Adapted from Castro-Alonso et al. (2019)

$CaCO_3$ precipitation by bacteria is a process that has been extensively studied in the field of biomineralization, and is commonly associated with the BIM approach. The deposition of $CaCO_3$ crystals by microorganisms is referred to as microbially induced calcium carbonate precipitation (MICCP). The metabolic ability of microorganisms has motivated researchers to explore the benefits of biomineralization for bioengineering applications. Calcium has a stronger affinity for bonding with carbonate than with other minerals. Carbonate is a polymorph that consists of three anhydrous crystalline phases: calcite, aragonite, and vaterite. A crystal's shape, structure, and size are primarily determined by the environmental factors in which it is discovered. The most stable form of $CaCO_3$ is a rhombohedral (calcite) induced by calcium chloride (Hu et al. 2022).

2.4 Microbial induced calcium carbonate precipitation (MICCP)

The MICCP process involves the formation of $CaCO_3$ crystals through a reaction between CO_3^{2-}, and Ca^{2+} ions present in the surrounding environment. Ehrlich (1999) reported that

various bacterial species in natural habitats precipitate carbonates in alkaline environments rich in Ca^{2+} ions using different mechanisms. The primary microbial metabolic processes involved in MICCP are urea breakdown, ammonification of amino acids, denitrification, dissimilatory sulfate reduction, and photosynthesis (Ali et al. 2023). Compared to other metabolic pathways, urea hydrolysis is relatively simpler and has been found to result in a higher calcite precipitation (between 20%-80%), making it the most commonly studied process in MICCP (Achal et al. 2011a). Heterotrophic (ureolytic) and autotrophic bacterial cells have various functional groups, such as sulfhydryl (-SH), amino ($-NH_2$), carboxyl (-COOH), and hydroxyl (-OH) groups, which serve as nucleation sites for binding with Ca^{2+} ions in solution and increase the $CaCO_3$ precipitation presumably in the EPS or S layer surrounding the cell (Zhu and Dittrich 2016). MICCP has been used in various biotechnological applications, such as the remediation of contaminated soil and water with heavy metals, metalloids, and cations (Ca^{2+}), soil bioconsolidation, CO_2 bio-sequestration, and self-healing concrete (bioconcrete) (Dzionek et al. 2016; Krajewska 2018; Sharma et al. 2020a; Kaur and Kaur 2021; Jarwar et al. 2023).

2.4.1 Heterotrophic-mediated pathway

The heterotrophic bacteria are the organism that derive energy from the organic compounds. They are abundant and widely distributed, existing either in anaerobic or aerobic environments. They can be found in soil, water, and food, and are omnipresent. The four broad categories of bacteria that establish these pathways are, sulphate reduction, denitrification, ureolysis, and carbon dioxide conversion (Kim et al. 2021).

Sulphate reducing bacteria (SRB) carried out heterotrophic pathway through the dissimilatory reduction of sulphate (Joshi et al. 2017). During this process, $CaCO_3$ is produced in an anaerobic environment when the medium contains high levels of organic matter, calcium, and sulphate (Seifan et al. 2016b; Tyagi et al. 2023). As the organic matter is metabolized by SRB, it results in the production of bicarbonate ions and hydrogen sulfide by the reduction of sulphates. The raise of pH in the surrounding environment, coupled with the presence of H_2S and Ca^{2+}, results in the precipitation of $CaCO_3$ (Troiano et al. 2013). Some of the examples of SRB are *Sulfovibrio desulfuricans* and *Desulfovibrio desulfuricans* (Kaushal et al. 2020).

In denitrification mediated heterotrophic pathway, precipitation of $CaCO_3$ involves nitrogen cycle and is further categorized into three different mechanisms: (1) The ammonification of amino acids, which involves the presence of organic matter and calcium in aerobic conditions, is a process that is essential for the breakdown of organic matter in soil. (2) The dissimilatory reduction of nitrate, which involves the presence of organic matter, calcium, and nitrate in anaerobic conditions, is a process that is essential for the conversion of nitrate to nitrogen gas in soil. (3) The urea degradation, which involves the presence of organic matter, calcium, and urea in aerobic conditions, is a process that is essential for the breakdown of urea in soil (Le Métayer-Levrel et al. 1999). This mechanism involves the reduction of nitrate (NO_3^-) to Nitrite (NO_2^-), nitric Oxide (NO), nitrous oxide (N_2O) and nitrogen gas (N_2) (Sidiq et al. 2019). The production of carbonate and bicarbonate ions, as well as ammonia (NH_3), serves as a metabolic end product. The formation of NH_3 leads to an elevated alkaline pH in the microenvironment of the bacterial cell and a decrease in the H^+ concentration, subsequently shifting the carbonate-bicarbonate equilibria toward the production of CO_3^{2-} ions. Furthermore, the presence of Ca^{2+} ions in the vicinity of the bacterial cell results in the formation of $CaCO_3$ precipitate. Some of denitrifying microorganism are *Diaphorobacter nitroreducens*, *Pseudomonas aeruginosa*, *Micrococcus*, *Achromobacter*, *Alcaligenes*, *Thiobacillus*, *Pseudomonas denitrificans*, and *Castellaniella denitrificans* (Erşan et al. 2016; Ali et al. 2023).

In the ureolysis pathway, the urease enzyme catalyzes the breakdown of urea into NH_3 and CO_2. Urease is a nickel containing metalloenzyme (EC 3.5.1.5) with molecular weight of ~550-kDa. The urease catalyzed $CaCO_3$ precipitation has been widely adopted in various fields, including construction and materials, geotechnical engineering, and environmental applications (Phang et al. 2018). As shown in Fig. 2.3 $CaCO_3$ precipitation by heterotrophic bacteria involves the degradation of urea to form carbonic acid (H_2CO_3) and NH_3 (Cuccurullo et al. 2022). The H_2CO_3 further equilibrates in water to form ammonium (NH_4^+), carbonate (CO_3^{2-}), and hydroxide ions (OH^-). Hydroxide ions lead to the alkalinization of the solutions. In the presence of calcium ions, one mole of carbonate precipitates to form one mole of $CaCO_3$ as shown in Equation 2.1 to 2.4.

$$CO(NH_2)_2 + H_2O \rightarrow NH_2COOH + NH_3 \qquad 2.1$$

$$NH_2COOH + H_2O \rightarrow NH_3 + H_2CO_3 \quad 2.2$$

$$2NH_3 + 2H_2O \rightarrow 2NH_4^+ + 2OH^- \quad 2.3$$

$$2OH^- + H_2CO_3 \rightarrow CO_3^{2-} + 2H_2O \quad 2.4$$

$$CO_3^{2-} + Ca^{2+} \rightarrow CaCO_3 \quad 2.5$$

While some researchers have suggested a CO_2 conversion mechanism through bacteria as a potential alternative for producing carbonate ions. It is noteworthy that this approach is promising as an eco-friendly method of CO_2 storage, as it involves converting CO_2, a major contributor to global warming, into carbonate minerals through a bio-chemical reaction utilizing the enzyme carbonic anhydrase that is inherent in bacteria. One of the most dominant examples of such bacteria is *Bacillus mucilaginous* (Qian et al. 2015).

2.4.2 Autotrophic-mediated pathway

The process of autotrophic pathway takes place when in the presence of CO_2, during which microorganisms transform CO_2 into carbonate through three distinct ways (Fig. 2.3). The first pathway is non-methylotrophic methanogenesis (by methanogenic archaea), second pathway is oxygenic photosynthesis (by Cyanobacteria) and third is anoxygenic photosynthesis (by purple bacteria) (Seifan et al. 2016a). In the non-methylotrophic methanogenesis pathway, microbes convert CO_2 and hydrogen to methane (Equation 2.6). The anaerobic oxidation of methane by electron acceptors like sulphate leads to the formation of bicarbonate as demonstrated by Equation 2.7 (Zhu and Dittrich 2016). The carbonate then precipitates as $CaCO_3$ in the presence of calcium ions, as shown by Equation 2.8. This mechanism is more prevalent in marine sediments.

$$CO_2 + 4H_2 \rightarrow CH_4 + 2H_2O \quad 2.6$$

$$CH_4 + SO_4^{2-} \rightarrow HCO_3^- + HS^- + H_2O \quad 2.7$$

$$Ca^{2+} + 2HCO_3^- \leftrightarrow CaCO_3 + CO_2 + H_2O \quad 2.8$$

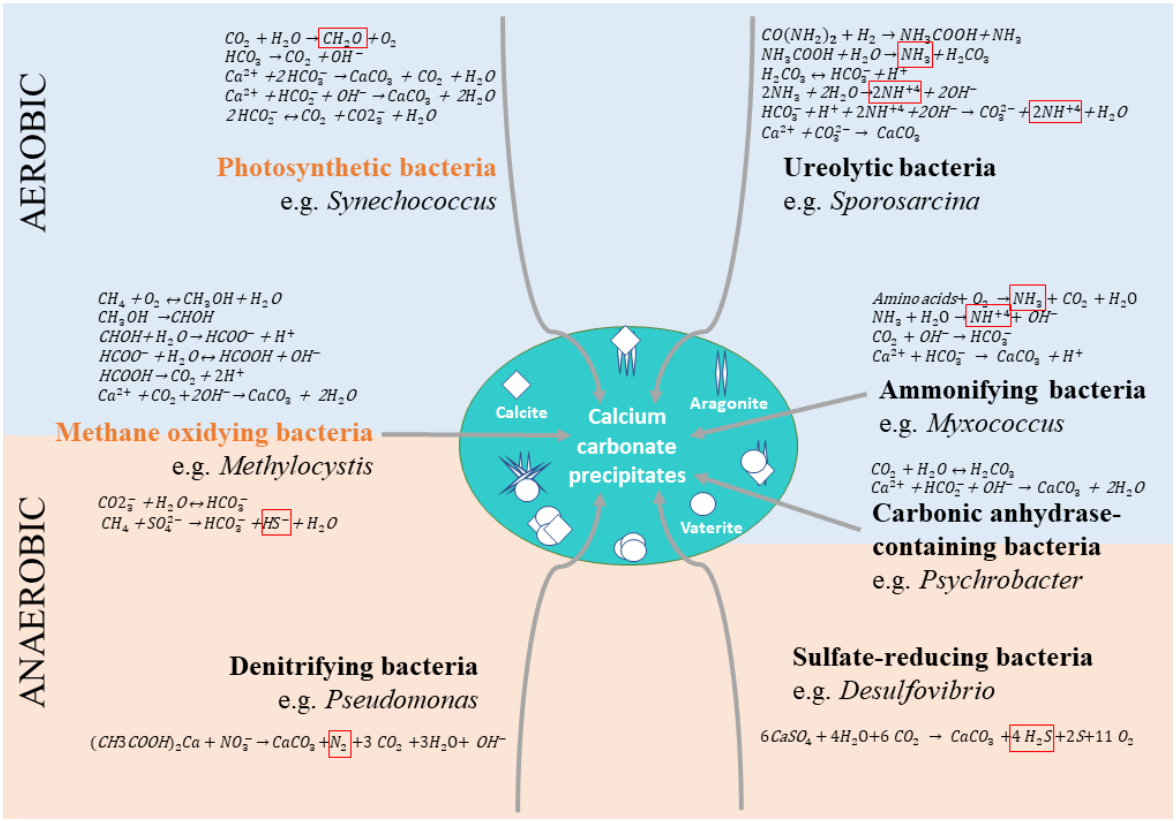


Fig. 2.3 The microbial agents and processes involved in the formation of $CaCO_3$ deposits. The bacterial groups were categorized into two pathways: autotrophic (marked in orange) and heterotrophic (marked in black). Additionally, potentially hazardous compounds were highlighted with a red frame. Adopted from Fronczyk et al. (2023)

Another autotrophic pathway is photosynthesis in which $CaCO_3$ is produced in the presence of calcium ions. There are two categories of photosynthetic bacteria: oxygenic and anoxygenic, which uses different types of electron donors to produce methanal by utilizing CO_2. According to Equation 2.9, water plays an important role of an electron donor in oxygenic photosynthesis. On the other hand, in anoxygenic photosynthesis, hydrogen sulfide (H_2S) is the electron donor in the redox reaction as shown in Equation 2.10, consequently oxygen is not produced (Ali et al. 2023).

$$CO_2 + H_2O \rightarrow CH_2O + O_2 \quad \text{(Oxygenic photosynthesis)} \qquad 2.9$$

$$CO_2 + 2H_2S + H_2O \rightarrow CH_2O + 2S + 2H_2O \quad \text{(anoxygenic photosynthesis)} \qquad 2.10$$

Further removal of CO_2 from surrounding environment during photosynthesis results in increase in the pH leading to formation of $CaCO_3$ in the presence of Ca^{2+} ions as shown in Equation 2.11 and 2.12.

$$2HCO_3^{2-} \leftrightarrow CO_2 + CO_3^{2-} + H_2O \quad 2.11$$

$$CO_3^{2-} + H_2O \leftrightarrow HCO_3^{-} + OH^{-} \quad 2.12$$

2.5 MICCP by ureolytic and non-ureolytic bacteria

Previous studies demonstrated improved cementitious properties by using different ureolytic and non-ureolytic strains of bacteria. Many ureolytic strains such as *B. sphaericus* (Wang et al. 2017; Jongvivatsakul et al. 2019; Nasser et al. 2022) *B. pasteurii* (Achal et al. 2010a; Omoregie et al. 2019; Kaur et al. 2021; Zhang et al. 2022), *B. megaterium* (Dhami et al. 2013a; Nain et al. 2019; Sun et al. 2019b; Anand et al. 2022a), *B. alkalinitrilicus* (Wiktor and Jonkers 2011), *B. subtilis* (Karimi and Mostofinejad 2020; Feng et al. 2021b), and *B. pseudofirmus* (González et al. 2020; Zamani et al. 2020) improve the durability and permeability properties of concrete. The major drawback is the release of NH_3 (foul-smelling pollutant) which results in nitrogen oxide (NO_x) emission into the atmosphere, causing health and environmental concerns (Ramakrishnan 2015; Justo-Reinoso et al. 2021). Many *Bacillus* species precipitate $CaCO_3$ mineralization by non-ureolytic pathways. Tziviloglou et al. (2017) isolated alkali-resistant *B. cohnii* and *B. alkalinitrilicus* from alkaline natural lakes and reported improvement in the cementitious properties of mortar. Jang et al. reported reduced sorptivity and $CaCO_3$ precipitation by non-ureolytic alkali-tolerant (*L. boronitolerans* YS11) and alkaliphilic (*B. alkaliphilus* AK13) bacteria in mortar (Jang et al. 2020).

2.5.1 Urease activity

Urease is a macromolecular catalyst that is highly sensitive to several key factors, including urea concentration, temperature, and pH. Omoregie et al. (2016) conducted an investigation and reported the urease activity of three bacterial isolates, LPB19, TSB12, and TSB31, which were isolated from samples collected from Sarawak limestone caves. The results revealed that the urease activity of LPB19, TSB12, and TSB31 was 16.14 mM,12.45 mM and 11.41 mM

urea hydrolyzed/min. Similarly, Nathan et al. (2020) reported urease activity of *B. halodurans* isolated from the sediments was 28 U/ml. Imran et al. (2019), investigated the effect of different pH and temperature conditions on the urease activity and found optimum conditions for the urease activity are pH 7 and temperature ranging between 25 °C – 40 °C. Earlier, Dhami et al. (2014) reported maximum urease activity at 35 °C which declined by 47% at temperature 55 °C. Similar, Fujita et al. (2017) reported increased cell concentration of *Pararhodobacter* sp. for 2 days and increase in urease activity until day 15. Urease activity was evaluated at different temperature and pH conditions suggesting maximum activity at temperature 60 °C and pH 8. Singh et al. (2017) reported maximum urease activity by *B. sphaericus* at 37 °C and pH 7. Phang et al. (2018) isolated bacteria from an acidic peat environment that exhibited urease activity at lower pH levels (maximum at pH 4), indicating compatibility with acidic environment. Hu et al. (2022) reported highest urease activity of 12.37 mM by *B. pasteurii*. Xie et al. (2023) reported temperature range of 10 – 50 °C and pH 8 -11 as the optimum range for urease activity. Urease activity increased from 0.59 mM at 10 °C to 25.53 mM urea hydrolyzed/min at 50 °C. In another research carried out by Maleki-Kakelar et al. (2022) the effect of increasing urea concentration and utilization of cheap nutrient media such as corn steep liquor (CSL) media was also studied. Their findings proved that urease activity of *S. pasteurii* increased with increase in urea concentration from 0 to 3 g/L, after which it declines. The urease activity of *S. pasteurii* cells was found to be significantly higher in a CSL – urea medium, as compared to other standard laboratory grade media.

2.6 Isolation of heterotrophic bacteria

Microorganisms play an essential role in inducing biomineralization, and the selection of the best bacteria for MICCP depends on their ability to produce carbonate minerals under different environmental condition. Microorganisms are found to inhabit extreme environments and are categorized into various classes based on their environmental niche (acidophiles, alkaliphiles, halophiles, thermophiles, psychrotolerant, metallotolerant, oligotrophs). It is important to conduct scientific research on the diversity of essential microbes found in different regions. Bacteria isolated from various ecosystems, including soils, freshwater, and saline environments, have the ability to precipitate $CaCO_3$ under both natural and laboratory conditions (Castro-Alonso et al. 2019). This phenomenon has been linked to the formation of

marine calcareous skeletons, carbonate sediments, and soil carbonate deposits (Dhami et al. 2013b). The potential of bacteria to form carbonates is a versatile tool that can be employed for various purposes, including the restoration of historic buildings and monuments made of limestone, heavy metal removal, and improvement of concrete structures and repairing of cracks (Chuo et al. 2020). The structural and chemical adaptations of microorganisms enable them to thrive in extreme environmental conditions (Skinner and Jahren 2007). To ensure the utilization of carbonate producing bacteria in the bio-cementation of building materials, it is necessary to select microorganisms that can survive in high pH environments like that of concrete (pH ~ 13). Literature documents the isolation of bacteria from naturally occurring carbonate-rich environments such as calcareous stones (Rodriguez-Navarro et al. 2012), calcareous sludge (Al-Thawadi and Cord-Ruwisch 2012), and calcareous soil (Bibi et al. 2018). The calcareous stones in the caves are natural geological structures that have harsh conditions that are not favorable for microbial growth due to the severe abiotic factors present. These conditions only allow microbial species that have adapted to low levels of nutrients to survive (Wu et al. 2015). Some of these cave microorganisms have the capability to deposit $CaCO_3$ on their cell surfaces, which has played a crucial role in the creation of various cave formations (Omoregie et al. 2019). Most of the carbonate producing bacteria can induce $CaCO_3$ at optimum temperature range of 28 - 55 °C. However, in regions where a protracted period of low temperatures is expected, adequate isolation from harsh conditions is necessary. Kumari et al. (2014) found that a psychrotolerant *Exiguobacterium undae* YR10 strain grow and precipitate $CaCO_3$ at 10ºC. Similarly, Li et al. (2022) also isolated psychrotolerant bacterium, *Glutamicibacter* DC1, from the tailing area of China which showed good growth, high urease activity at 10 °C and can even grow in high concentrations of heavy metals. Vincent et al. (2022a) isolated 14 strains from mineral rich alkaline seawater at the surface of steel grids. All the 14 strains produced carbonic anhydrase, and six were found to be urease positive. Shaheen et al. (2023) isolated spore forming (*Bacillus safensis* MUGA 156, *Bacillus pumilus* SH-B9) and non-spore forming (*Arthrobacter luteolus* LNR3, *Chryseomicrobium imtechense* HTHB4 and *Corynebacterium efficiens* YS-314 ns) bacteria from soil which were able to survive in harsh alkaline environment. Table 2.1 summarizes the exploration of the novel diversity of microorganisms belonging to varied genera for its potential in inducing $CaCO_3$. However, many more microbes are yet to be discovered.

Table 2.1 Summary of different environmental sources and microorganisms isolated

Source of isolation	**Microorganism isolated**	**Reference**
Cement samples	*Bacillus* sp.	Achal et al. (2010b)
Decayed calcarenite, San Jeronimo Monastery, Granada, Spain	*B. fusiformis, Acinetobacter sp., A. baumannii, and Arthrobacter crystallopoietes*	Jroundi et al. (2012); Jroundi et al. (2017)
Activated sludge, wastewater treatment plant, Perth, Australia	*Bacillus* species, *B. aqamarinus*, and *B. pasteurii*	Al-Thawadi and Cord-Ruwisch (2012)
Soil, Willipa Bay, Washington, USA	*Sporosarcina, Bacillus, Lysinibacillus, Arthrobacter and Brevibacterium*	Burbank et al. (2012)
Sludge and freshly cut concrete, Gaza, Palestine	*B. mycoides*	Abdelraouf and Mohammed (2013)
Deteriorated ignimbrites, siliceous acidic rocks, Morelia, Mexico	*Enterobacter cancerogenus* 22e, *Bacillus* sp. 32a and *B. subtilis* (52g)	López-Moreno et al. (2014)
Soil, Coimbatore, Tamil Nadu, India	*B. megaterium BSKAU, B. licheniformis BSKNAU, B. flexus BSKNAU*	Krishnapriya et al. (2015)
Concrete walls, Jingyo and Seoul, South Korea	*Bacillus* sp. JH3, *Bacillus.* sp. JH7*, and Sporosarcina* sp. HYO08	Kim et al. (2015)
Beidaihe marine sediment, China	*B. diminuta* CP16, *S. soli* CP23 and *B. lentus* CP28	Wei et al. (2015)
Soil from an abandoned mine, South Korea	*Viridibacillus arenosi* B-21, *S. soli* B-22, *Enterobacter cloacae* KJ-46, *E. cloacae* KJ-47, *L. sphaericus* KJ-64 *and S.pasteurii* WJ-2	Kang and So (2016)
Sea water samples, Nellore, Andhra Pradesh, India	*Exiguobacterium mexicanum*	Bansal et al. (2016)

Rice leaves of Agulha variety, Brazil	*B. subtilis* AP91	Schwantes-Cezario et al. (2017)
Soil, Qatar	*B. cereus, B. subtilis, B. licheniformis*	Bibi et al. (2018)
Peat soil, Miri, Sarawak, Malaysia	*Bacillus cereus*	Phang et al. (2018)
Source of isolation	**Microorganism isolated**	**Reference**
Livestock barn soil, Iraq	*B. atrophaeus, B. subtilis, B. aryabhattai and B. amyloliquefaciens*	Khadhim et al. (2019)
Salabat Khan Tomb, Westren India	*Bacillus sp., Arthobacter sp., Agromyces indicus and Aquamicrobium sp.*	Singh (2019)
Fairy Cave and wind cave nature reserve, Malaysia	*S. pasteurii, Pseudogracilibacillus auburnensis, B. lentus and B. fortis*	Omoregie et al. (2019)
Natural seawater and calcareous deposits, Atlantic coast, France	*Pseudoalteromonas,*	Vincent et al. (2022b); Vincent et al. (2022a)
Seawater and mud, Atlantic coast in Angoulins, France	*Pseudidiomarina, Epibacterium, Virgibacillus, Planococcus, and Bhargavaea.*	
Soil, Soda lake shores of Ethiopia	*B. paramycoides, Citrobacter sedlakii, and Enterobacter bugandensis*	Mekonnen et al. (2021)
Kashmir Smast (cave), Pakistan	*Paracoccus Limosus, Brevundimonas diminuta, B. toyonensis*	Jan et al. (2022)
Historical earth structures and desert soils in Yazd, Isfahan provinces of Iran	*Bacillus sp.*AF1	Farajnia et al. (2022)
Dung-rich soil, Gujarat, India	*Quasibacillus thermotolerans* and *B. zanthoxyli*	Khambholja et al. (2022)
Soil, Jilin Province, China	*Glutamicibacter soli SYB2, Paeniglutamicibacter psychrophenolicus AG31*	Li et al. (2022a)
Soil, Qatar	*Bacillus cereus* Q3.3	Sohail et al. 2022

Agricultural soil, Gilan, Iran	*B. licheniformis*	Nezafat et al. (2023)
Cultural Heritage artifacts	*Lysinibacillus fusiformis* 3.20, *Psychrobacillus psychro- durans* 7Mo and *Lederbergia lenta Vetro1*	Benedetti et al. (2023)

2.7 MICCP by cyanobacteria (Blue green algae)

Cyanobacteria are unicellular or filamentous photosynthetic bacteria precipitating $CaCO_3$ as the byproduct of oxygenic photosynthesis. The calcification by cyanobacterial species is of great ecological significance. Merz (1992) stated that cyanobacterial species traps sediment among the filaments and play crucial role in the foundation of stromatolites in both sea water and freshwater. Cyanobacteria generally prefer low-light intensities. Pentecost, (1984) determined the optimal intensity of light for photosynthetic reactions in *Oscillatoriaceans*, which is around 3000 lux in a natural environment. However, they exhibit photophobic responses when the irradiance exceeds 10,000 lux. Cox et al. (1989), observed calcite lamina in Nettle Cave and recurring recolonization of cyanobacteria cells after deposition of calcite for the 5 months. Thompson and Ferris (1990) reported formation of gypsum and calcite by *Synechococcus* sp., in aquatic environments. Merz-Preiß and Riding (1999) studied $CaCO_3$ precipitation in freshwater stream with dominant *Phormidium* (*Lyngbya*) *incrustatum* species. Researchers reported dense, thick and uneven encrustation around the sheath, creating calcareous tubes measuring 10–20 µm in thickness, which encased the cyanobacterial filaments. Cyanobacterial stromatolite, a calcareous fossil, has been discovered in various settings, including freshwater, marine, and terrestrial areas (Altermann et al. 2006). Moreover, turning of the entire water body milky, demonstrate the high potential of calcification by picocyanobacterial species (Cox et al. 1989). Dittrich and Sibler (2010) reported extracellular polysaccharides from cyanobacteria possess a capability to exchange protons with the surrounding environment which results in precipitation of $CaCO_3$. Three different strains of cyanobacteria *Synechococcus* PCC 7942, *Syn.* Green and *Syn.* Red were studied. Major species studied for $CaCO_3$ precipitation are *Synechococcus, Phormidium, Synechocystis, Gloeocapsa* species (Han et al. 2017a; Zhu et al. 2017; Heveran et al. 2020). Iijima et al. (2015) quantified the protein content of freshwater unicellular cyanobacterium *Synechocystis*. Researchers are continuously investigating for the calcification potential of cyanobacterial species in laboratory and field scale. Diverse studies are presented in Table 2.2.

Recently, Zhu et al. (2017) studied the calcification potential of live and UV-killed cells on the mortar surface and concluded that UV-killed cells were more efficient in improving the strength and water absorption ability of mortar cubes. The cyanobacterial cells were able to

produce EPS and biofilm layer which has strong bonding with the $CaCO_3$ crystallization as viewed by SEM analysis.

Table 2.2 Overview of different cyanobacterial species, growth media, calcite precipitated and properties studies by the researchers

Microbes	**Culture media**	**Properties studied**	**Calcification**	**Reference**
Synechococcus leopoliensis	Z⁄10 culture medium	Nucleation, AFM, Zeta potential, TEM	Calcite	Obst et al. (2006)
Planktothrix sp. and Synechococcus sp.	BG-11	Surface charge and zeta potential	-	Martinez et al. (2008)
S. leopoliensis	Z⁄10 culture medium	Saturation index, nucleation kinetics,	Rhombohedral calcite	Obst et al. (2009)
Synechococcus	Modified Z/10 medium	EPS content, SEM, EDS, FTIR	$CaCO_3$ spherical crystals	Dittrich and Sibler (2010)
Fresh and marine *Synechococcus*	ASN III	$CaCO_3$ biomineralization, AFM, SEM, XRD, pH dynamic	Rhombohedra calcite, needle-shaped crystals	Liang et al. (2013)
Synechococcus sp, *Thermosynechococcus elongatus*	BG-11, ASN-III	STXM, SEM, intracellular carbonate precipitation	Ca-carbonate within the cell cytoplasm and poles	Benzerara et al. (2014)
Oscillatoria willei and Phormidium valderianum	ASN-III	Total dissolved solids, dissolved oxygen (DO), FTIR, EDS	Rhombohedral calcite	Uma et al. (2014)
Gloeocapsa sp.	BG-11	Ca adsorption & uptake, Raman spectroscopy, SEM, TEM	Rhombohedral calcite	Bundeleva et al. (2014)
Synechococcus	ASN-III	Water absorption, pH dynamic, calcium (Ca) removal, XRD, Raman spectroscopy, surface study on mortar cubes	Rhombohedral calcite	Zhu et al. (2015)

Candidatus Gloeomargarita lithophora C7 and Ca. S. calcipolaris G9	BG-11 and MS-2	TEM, STXM	Spherical Amorphous calcium carbonates	Li et al. (2016)
Microbes	**Culture media**	**Properties studied**	**Calcification**	**Reference**
Synechocystis sp.	BG11	Kinetic analysis, TGA, SEM, EDS	Rhombohedral calcite	Han et al. (2017b)
Synechocystis, Synechococcus	Z medium and ASN-III medium	Ca concentration, SEM, raman spectroscopy, MICCP on mortar	Rhombohedral calcite	Zhu et al. (2018)
Synechococcus sp. *Cyanothece* sp., *Chroococcidiopsis* sp. *Gloeomargarita* sp. *Gloeocapsa* sp.	BG-11	Assessment of the Ca uptake by cyanobacterial strains	Amorphous calcium carbonates	De Wever et al. (2019)
Synechococcus sp.	modified F/2 media	Virus induced carbonate precipitation, SEM, XRD	Amorphous calcium carbonate and aragonite	Xu et al. (2019b)
Synechococcus	Medium A	FTIR, SEM, Raman spectroscopy, XRD, TEM, fluorescence spectroscopy, EPS, Ca adsorption	Amorphous calcium carbonate	Ludwig and Bryant (2011); Yu et al. (2020)
Phormidium alkaliphum	BG-11	Growth at high and alkaline condition		Paquette et al. (2022)
Phormidium sp.	BG11, BOLD 3N, modified BOLD 3N (MBOLD 3N)	EPS content, Strength, crack healing, FTIR, SEM,	Amorphous calcium carbonate	Chandra et al. (2023)

SEM: scanning electron microscopy, EDX: energy dispersive spectroscopy, XRD: x-ray diffraction, TGA: thermo-gravimetric analysis, FTIR: Fourier-transform infrared spectroscopy, STXM: scanning transmission X-ray microscopy, TEM: transmission electron microscopy, EPS: extracellular polymeric substances

Similar work was carried out by Srinivas et al. (2021) using two species, *Spirulina platensis* and *Synechococcus* elongatus. Research reported the efficient crack healing with 35% and 12% increase in compressive strength of the mortar cubes by *S.* elongatus and *S. platensis*, respectively.

Heveran et al. (2020) engineered a living building material by developing hydrogel scaffold with *Synechococcus* sp. In this investigation, the viability of *Synechococcus* within the sand-hydrogel composite was found to be significantly higher than that of other reported microorganisms in cementitious materials. Furthermore, calcite precipitation by cyanobacterial strain resulted in enhanced fracture toughness of the LBM. The results were confirmed by SEM analysis. Chandra et al. (2023) screened three cyanobacterial species (*Lyngbya* sp., *Phormidium* sp., and *Chlorella vulgaris*) for the EPS production and calcification potential. The best results were obtained by *Phormidium* sp. with 29.7% gain in strength and 2.2% gain in the weight of concrete cube which is considered as weight gain due to $CaCO_3$ crystallization.

2.8 Application of MICCP

The following sections discuss literature related to application of MICCP in various fields such as, soil consolidation, restoration of monuments, improvement of cementitious properties and cracks remediation.

2.8.1 Sand consolidation

Loose granular soil that undergoes seismic generation of excess pore water pressure, a sudden decrease in strength is observed, which is known as liquefaction. This leads to the phenomenon of lateral spreading and deformation, resulting in significant damage to buildings and structures located on the ground (Do et al. 2023). Different methods involved in soil improvement in which series of materials are injected into the soil or rock structure to change the physical properties of the structure. The injection can be employed for the purpose of repairing the cracks within the stone, bridging the gap between the sand particles and increasing the physical properties of loose soil to enhance its strength, density, and uniformity while reducing its permeability (Kalantary et al. 2022). Due to growing environmental concerns surrounding the injection of various types of grouts into soil, such as cement grout, micro fine cement grouts,

and chemical solutions, engineers have been diligently researching the use of slurries that are more compatible with the natural soil structure and composition. Moreover, the cost of new injection treatment should be less than the existing slurries mainly consisting of silica grout and resins. Therefore, utilization of the biological method to improve the sand can be considered as crucial aspect. The sandy soil, characterized by its good permeability, is highly suitable for research on the MICCP in sand consolidation. Another application of this method is to mitigate soil erosion, particularly in areas with high susceptibility to wind erosion. The research conducted by Aletayeb et al. (2021) demonstrated that biological stabilization can enhance the soil's resistance to erosion and prevent the formation of dust particles. Whiffin (2004) was instrumental in utilizing MICCP technology to enhance the mechanical properties of sand by cementing loose particles, resulting in improved strength and stiffness. Several other researchers have documented the utilization of MICCP in the stabilization and consolidation of sand and soil through $CaCO_3$ precipitation in between the particles (Cardoso et al. 2020). This method involves injecting bacterial cells along with a cementation solution (consisting of nutrient supplements, calcium sources, and urea) vertically into soil or sand columns.

Kantzas et al. (1992) reported reduction of porosity by 50% and permeability by 90% when *B. pasteurii* resulted in a cementation of the sand. Bang et al. (2011) demonstrated the feasibility of utilizing ureolytic bacteria for the suppression of dust through MICCP. Burbank et al. (2012) reported that the application of ureolytic microbes to soils on the shore of the Snake River in the United States resulted in the formation of approximately 1% $CaCO_3$ in the upper surface layer and 1.8% to 2.4% calcite below a depth of 90 cm. Similarly, Stabnikov et al. (2011) and Chu et al. (2012) have also reported a prominent decrease in flow rate using *Bacillus* sp. VS1 with urea and calcium salt solution. The application of MICCP increased stiffness of sand with tremendous decline in the permeability and enhancement of shear strength of soil due to the development of impermeable microbial carbonate crusts. Dhami et al. (2016) reported decrease in flow rate after the complete consolidation of the sand columns prepared using different sized sand grains. Choi et al. (2016) reported 138% and 186% an increase in the unconfined compressive and splitting tensile strength of the bio cemented fibre reinforced sand, respectively. Due to $CaCO_3$ precipitation the pores between the sand particles are obstructed. This leads to reduction in the permeability by 126% and the brittleness compared to untreated sand. Gomez et al. (2015) conducted a field experiment on the surface sand and reported a 2.5-

cm-thick hard cemented layer of sand. later, conducted a large-scale bio cementation test by utilizing a 1.7-meter diameter tank containing 0.7 cubic meters of a poorly-graded natural sand which was equipped with three wells arranged in a triangular configuration at a well-to-well spacing of 1.2 meters. Following the MICCP treatment, the shear wave velocities of 970 m/s, the calcite contents greater than 5.0%, and the increases in penetration resistances approaching 545% was reported. Sharma et al. (2020b) confirmed increase in strength and permeability reduction after the biotreatment with the consortium of *B. sphaericus* and Algae *Nostoc* commune. Kalantary et al. (2022) reported increase in mechanical strength and soil resistance post MICCP treatment with 4 to 9% precipitation of $CaCO_3$ up to a depth of 80 cm. Duo et al. (2018) reported increase in unconfined compressive strength, sand density, calcite content with increase in the concentration of solidification solution (0.5, 1.0, 1.5, 2.0 and 2.5 mol/L urea and $CaCl_2$).

Liu et al. (2021) evaluated the optimum physiological conditions; temperature (25, 30, 35 °C), pH of the media (7, 8, 9), and the inoculation ratio (1, 2, 3, 5%) of *Sporosarcina pasteurii* for sand consolidation. The best results were obtained at pH 9 and temperature of 30 °C. MICCP-cemented soil exhibits evident fragility, which serves as a significant hindrance to the utilization of MICCP technology in geotechnical engineering. However, the implementation of plastic bond between the matrix along with the $CaCO_3$ binding can improve the brittleness of sand column. Wang et al. (2022) reported significant improvement in strength by highly efficient strain named XR1$^{\#}$ with capability of uniform distribution of $CaCO_3$ crystallization and extracellular polysaccharide bonding. The enzyme activity increased with increase in the inoculation ratio.

2.8.2 Influence of MICCP on cementitious properties

The major benefit of microbial biomineralization is MICCP due to its efficient bonding capacity and compatibility with concrete compositions. It is considered the noblest, environment friendly and economical material for engineering applications. In other words, it is described as bioconcrete in which concrete is prepared by admixing bacteria with the capability of bacteria for precipitation of carbonate that aids in improving the overall properties of concrete and crack remediation (Wiktor and Jonkers 2011). Many microorganisms can precipitate $CaCO_3$ through different mechanisms or pathways such as photosynthesis,

ureolysis, ammonification, denitrification, sulphate reduction, anaerobic sulfide oxidation, and methane oxidation, by increasing pH or dissolved inorganic carbon (DIC) (Joshi et al. 2017). Both autotrophic and heterotrophic pathways are involved in forming an alkaline environment for bacterial-induced precipitation. The cell wall of the bacteria acts as a nucleation site for precipitation having Ca^{2+} ions attached to the surface (Dhami et al., 2013). Different diversity of microbes such as *Bacillus sphaericus, B. licheniformis, B pasteurii, B. pseudofirmus, B. magaterium, B. cohnii* utilizes organic compound such as urea and calcium source to proliferate the carbonate precipitation (Jonkers and Schlangen 2007; Wang et al. 2012b; Joshi et al. 2018a; Justo-Reinoso et al. 2021; Skevi et al. 2021). Some halophilic and halotolerant bacteria in particularly *Exiguobacterium mexicanum, Halomonas, Flavobacterium,* and *Acinetobacter* are reported to show carbonate precipitation (Rivadeneyra et al. 2000; Stabnikov et al. 2013; Bansal et al. 2016; Khan et al. 2021).

The potential of employing MICCP in cementitious composites to improve early as well as later strength properties have been widely reported by researchers in past two decades. Initially, Ramachandran et al., (2001) reported that using *B. pasteurii* positively influences the performance of Portland cement mortar. De Muynck et al., (2008) reported the mortar specimens made with *B. sphaericus* found less permeable than control specimens due to precipitation of $CaCO_3$ resulted in pore refinement. Achal et al., (2011a) reported improved compressive strength and water absorption of cement mortar by using *B. megaterium* ATCC 14581, which was grown in the nutrient broth media containing urea. Achal et al., (2011b) reported fly ash concrete containing *B. megaterium* cells absorbed nearly 3.5 times less water than the control concrete. Pei et al., (2013) used *B. subtilis* in the concrete specimens and concluded that the concrete specimen prepared with *B. subtilis* precipitated $CaCO_3$, thereby increasing the compressive strength by 15% and reduced the porosity by 1.64%. Pei et al. (2013) further reported that whether the *B. subtilis* cells are dead or live it does not significant effect on the compressive strengths of the mortar specimens. Dhami et al., (2013) reported 40% reduction in water absorption and 31% reduction in porosity due to bio-deposition of $CaCO_3$ on surface of specimens in comparison to control. This biogenic deposition of $CaCO_3$ acts as pore blocker and restrict the penetration of aggressive ions inside the concrete. Krishnapriya et al., (2015) used *B. megaterium* MTCC 1684 in the concrete specimens and reported an improvement in compressive strength of 12.1% compared to control specimens. Nosouhian et

al., (2016) reported that the incorporation of *S. pasteurii* and *B. subtilis* improved the resistance of concrete to chloride permeation and improve the strength of concrete. Indeed, the average number of coulombs passed through the bacteria-containing concrete was 11.7% less than that of control concrete. In another research, Siddique et al., (2016) found that 10^5 cells/ml of *B. aerius* improved 22% of the chloride permeation and 13.4% compressive strength of concrete on 10% replacement of cement by rice husk ash. Joshi et al., (2018) investigated the efficiency of curing treatments (admixed and spray) in improving mechanical properties of concrete using the ureolytic bacterial strain *Bacillus sp.* CT5 and found an average increase of 29% and 8% in bacterial admixed and spray treated specimens compared to control specimens at 28 days of testing. Mondal and Ghosh (2018) fabricated concrete specimens with *B. subtilis* having bacterial cell concentration of 10^3, 10^5 and 10^7 cells/ml and noticed a 15%, 27% and 19% improvement in compressive strength at 28 days of testing. Further tested the specimens for water absorption which was reduced by 13%, 23% and 27% for cell concentrations 10^3, 10^5 and 10^7 cells/ml respectively, compared to control specimens. Fig. 2.4 shows improvement of the surface and pore filling by different concentration of bacteria. Nain et al., (2019) tested concrete specimens prepared with *B. subtilis* and *B. megaterium* and found compressive strength improvement of 14.36% and 22.58% at 28 days of testing. A similar trend of improvement in split tensile strength was noticed in bacterial specimens. Recently researchers reported the effect of non-ureolytic bacteria on the mechanical properties of mortar and concrete (Kumari et al. 2017; Nguyen et al. 2019; Su et al. 2019). Kumari et al., (2017) reported 49% increase in compressive strength by using non-ureolytic bacteria *B. cohnii* at the age of 28 days. Saxena and Tembhurkar (2020) reported 28.3% increase in strength and 12% reduction in water absorption of mortar. Bhutange et al. (2020) also reported approximately 28% increase in compressive strength and 23% reduction in water absorption of mortar. Charpe et al. (2021) incorporated two ureolytic bacteria *B. cereus* and *Enterobacter cloacae* along with lentil seed powder, meat extract and table sugar as nutrient solution and reported 26.82% increase and 19.16% reduction in compressive strength and water absorption of mortar. Beside ureolytic and non-ureolytic bacteria, photosynthetic microbes also showed significant improvement in strength and reduction in water absorption. Hernández et al. (2016) reported increase in compressive strength by *Macrocystis pyrifera* (Marine brown algae). Zhu et al. (2017) reported improvement in compressive strength upon utilizing the UV-killed and live *Gloeocapsa* PCC73106 cells. However, Heveran et al. (2020) reported negligible difference in

compressive strength using *Synechococcus* sp. PCC 7002. Overall, it can be inferred that most of the reported studies used *Bacillus* species to precipitate $CaCO_3$ inside the concrete matrix and found significant improvement in the strength properties of concrete.

2.8.3 Crack remediation

Cracks are an unwanted feature in numerous structures that develop due to the effects of aging, construction or design flaws. The safety and sustainability of cementitious structures is driving the demand for the invention of smart self-healing materials and proactive repair strategies. The emergence of small crack (less than 300 µm) in concrete structures is an unfortunate yet

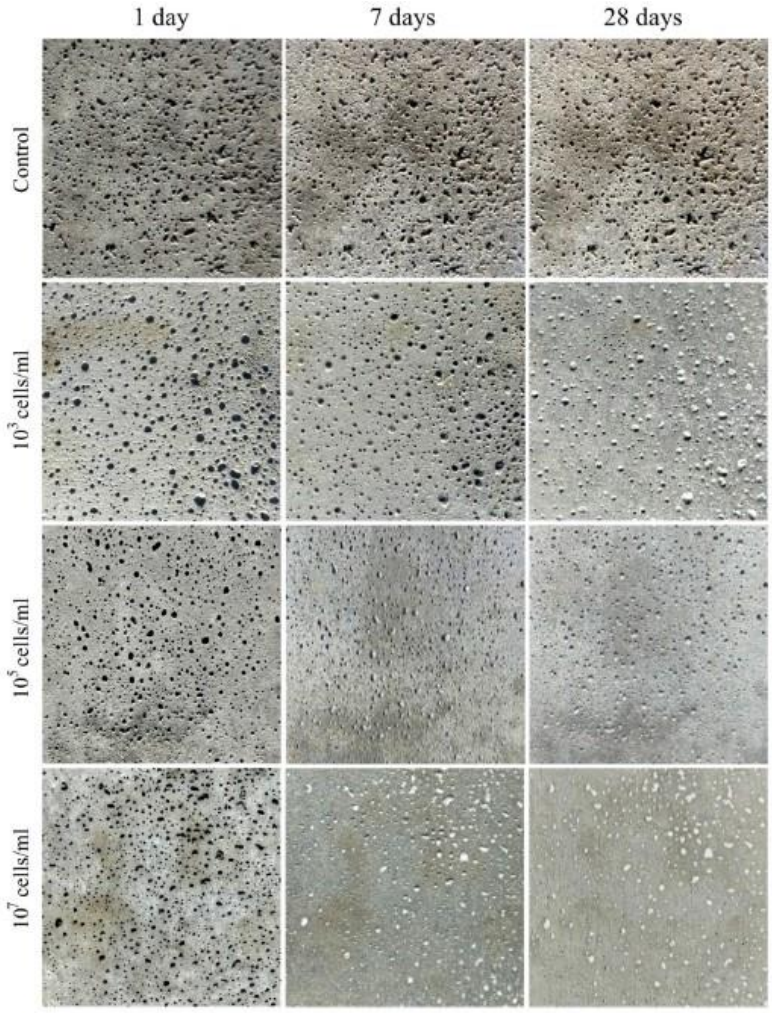


Fig. 2.4 Pictorial illustration of surface improvement of concrete treated with different bacterial concentrations. Adopted from Mondal and Ghosh (2018)

common occurrence. It weakens the concrete matrix, accelerating the degradation process, reducing the service life and sustainability of the structure, although it may not pose a risk of collapsing (De Belie et al. 2018). Self-healing concrete, an innovative technology designed to repair damaged concrete, is becoming an increasingly significant topic of interest. This type of concrete is created by incorporating bacterial spores along with a calcium source within the mixture. When water penetrates the cracks, it causes the pellets to open, resulting in the bacteria's germination and the production of calcite (Tziviloglou et al. 2017). *Bacillus* is the most commonly utilized bacterium in bioconcrete research due to its exceptional tolerance to alkaline conditions, making it an ideal bio-agent for carbonate precipitation. Moreover, it has the ability to form spores upon unfavorable conditions and is harmless to man which makes it suitable to use as self-healing agent in concrete (Gupta et al. 2017). Several investigators have used bacteria as a measure of crack healing in the last decade (Nguyen et al. 2019; Bergh et al. 2020; Jiang et al. 2020; Zamani et al. 2020; Khushnood et al. 2022). Initially, the application of bacteria to remediate the cracks in cement mortar specimens was reported by Ramachandran et al., (2001). Crack was artificially generated of 3.125 mm width and depth of 25.4 mm. Authors reported the mineralization process was effective in shallow cracks than in deeper ones because the bacteria grow more actively in presence of oxygen. Wiktor and Jonkers (2011) generated crack of varying width from 0.05 to 1 mm in prismatic specimens of 40 × 40 × 160 mm. *Bacillus alkalinitrilicus* showed promising result in crack filling at the curing age of 40 days. Achal et al. (2013) investigated the calcite precipitation by *Bacillus* sp. CT5 bacteria for enhancing the durability and heal crack of 27.2 mm depth in cement structures. Luo et al., (2015) simulated cracks in mortar specimen using embedded nail method of different crack with varying from 0.1 to 1 mm. Spore-forming alkali-resistant bacteria healed specimen with crack width up to 0.8 mm. Algaifi et al., (2020) generated artificial crack using copper plate in mortar specimen of 30 mm (dia) and 50 mm (height) and they reported the complete healing of a 0.4 mm crack width after 70 days. Vaezi et al., (2020) reported the optimum concentration of the crack healing mixture comprises of nutrients, 1% calcium lactate and 10^5 cells/ml in mortar. Jafarnia et al. (2020) found *Sporosarcina pasteurii* bacteria were able to heal crack of 0.58 mm width completely at 30 days by using bacteria in curing environment, while cracks up to 0.16 mm width were completely healed if bacteria were admixed in concrete samples. Researchers also reported increase of 23% compressive strength and 64% in electrical resistivity of concrete treated with bacteria containing 10% percentage zeolite.

2.9 Crack remediation via immobilizing bacteria in carrier material

Bacteria and other nutrient source are either directly incorporated in concrete mix, or carrier material is used for immobilization of bacteria. Literature reports utilization of different types of carrier materials e.g., silica gel (Wang et al. 2012a), graphene nano-platelet (Khaliq and Ehsan 2016), hydrogel (Wang et al. 2015), zeolite (Bhaskar et al. 2017), polyurea microcapsules (Zamani et al. 2020), alginate (Wang et al. 2016), biochar (Gupta et al. 2018), nanoplates (Khaliq and Ehsan 2016), low-weight aggregates (Alghamri et al. 2016; Wang et al. 2022b), and polyurea capsules (Zamani et al. 2020). Immobilization of bacterial strain safeguards the bacteria from harsh concrete conditions such as a high pH (~12 - 13), low nutrient and water access, thus enhancing the performance of bacterial admixed or bacterial treated concrete. Wang et al. (2014b) reported successful application of the hydrogel in healing a crack width of 0.5 mm. Due to the hydrophilic nature of the hydrogel, it can store sufficient water to foster bacterial growth and $CaCO_3$ precipitation. Bhaskar et al. (2017) used zeolite as a carrier material for immobilizing bacteria. Chen et al. (2016) used ceramsite as carrier material to immobilize bacteria *Bacillus mucilaginous* and Brewer's yeast. As a result of the $CaCO_3$ precipitation, the flexural strength of the specimens was effectively increased from 56% to 87.5%. Additionally, the self-healing properties of the specimens repaired cracks that were up to 0.3 - 0.4 mm in width and resulted in a reduction of water penetration. Singh and Gupta (2020) utilized cellulose fiber as a carrier material for immobilization of *B. subtilis*. The cellulose fibers were subjected to immobilization by soaking in a bacterial solution for a period of 24 hours. This resulted in an absorption capacity of 85% by weight, resulting in 9.3×10^5 bacteria immobilized/cm^3 of mortar. Amjad et al. (2023) immobilized *B. subtilis* in sisal fibre and reported successful healing of 0.48 mm crack width. Risdanareni et al. (2023) reported complete healing of cracks after the 30 days by using *B. sphaericus* cells encapsulated into alkali activated lightweight aggregate (LWA) which was prepared by agglomeration of fly ash and sidoarjo volcanic mud (Lusi-based). Researchers have employed various bacterial strains, carriers, and methodologies to investigate the self-healing mechanism of cracks in an autonomous manner. These examples are presented in Table 2.3. Various loading technologies have been developed to prolong the survival time of bacteria and spores. These technologies are primarily classified into porous and core-shell structures, based on the incorporation of the carrier (Zhang et al. 2021b). Porous materials, such as diatomaceous earth, expanded perlite,

expanded clay particles, biochar, and ceramic, are commonly used for porous loading in a self-healing system (Van Tittelboom et al. 2012; Amiri et al. 2018; Liu et al. 2020a; Tezer and Bundur 2020). However, the loading efficiency of these methods is relatively low, and the carriers can potentially weaken the strength of the concrete (Xu et al. 2019a). On the other hand, the core-shell structure (also known as capsules) is a more designable loading form with a higher loading rate. Microcapsules and macrocapsules are the two main categories of core-shell structures. The most commonly used materials for microcapsules are urea-formaldehyde, polyurethane, and melamine-formaldehyde. Macrocapsules, particularly spherical macrocapsules and hollow tubes, including glass tubes, ceramic tubes, and polymeric tubes are the most widely utilized (Wang et al. 2014; Araújo et al. 2018). It is imperative to assess the compatibility of microbes with carrier materials prior to their utilization. A suitable carrier material should be insoluble, non-toxic to both the immobilized material and the environment, easily accessible, affordable, and stable (Anand et al. 2022b). The porosity of the carrier material must be uniform, facilitating the free exchange of substrates and nutrients (Kourkoutas et al. 2004). The primary methods of microbial immobilization are adsorption, covalent binding, encapsulation, and flocculation as illustrated in Fig. 2.5 demonstrating the principles of these methods. Adsorption is a widely utilized physical procedure for the immobilization of microbial cells through various interactive forces, including van der Waals forces, hydrogen bonding, and ionic bonding between microorganisms and the carrier surface (Ehrlich 1999; Rouf et al. 2017; Seifan et al. 2018). Covalent binding is a method of immobilization that involves the use of a binding agent to form firm covalent bonds between the functional groups on the surface of the carrier and the groups on the microbial cell membrane, such as amino and carboxyl groups (Dzionek et al. 2016; Zhong et al. 2020). This method is considered an irreversible immobilization treatment and is rarely used for the immobilization due to the potential for adverse effects on cell activity. Instead, it is primarily used for enzyme immobilization. Encapsulation is an irreversible technique of immobilization that involves enclosing microorganisms within a restrictive, semi-permeable membrane (Van Tittelboom and De Belie 2013; Lee and Park 2018). This membrane allows the flow of nutrients into the membrane but restricts the movement of the microorganisms within the capsule (Kourkoutas et al. 2004; Górecka and Jastrzębska 2011). Encapsulation protects the microorganisms from the harsh internal environment of the cement-based material and maintains a high level of activity (Rouf et al. 2017). The precise control of the pore size of the membrane is crucial for

the success of this technology. An oversized pore size can lead to microbial leakage, while a too-small pore size can hinder nutrient flow. Another method of immobilization is flocculation that can be categorized as either natural or artificial (Vandamme et al. 2012; Bouabidi et al. 2019). Natural flocculation involves the use of self-flocculating microorganisms, which aggregate to form a group. Artificial flocculation, on the other hand, involves the use of cross-linking agents to cause bacterial cells to associate with one another and form a network. While flocculation can increase concentration of microorganism and facilitate microbial metabolism. Natural flocculation is time-consuming and can be easily disrupted by the environment. Moreover, the intense chemical reaction involved in artificial flocculation can damage microorganisms. Therefore, there is a need for improvement in the flocculation process (Datta et al. 2013; Feng et al. 2022).

2.10 Efficiency of grout

Grouting is the most extensively used technique in civil and geotechnical engineering involving injection of fluidized material for remediation of distresses of various forms (soil grouting, crack injection, and hole filling in concrete buildings) (Vasumithran et al. 2020). When

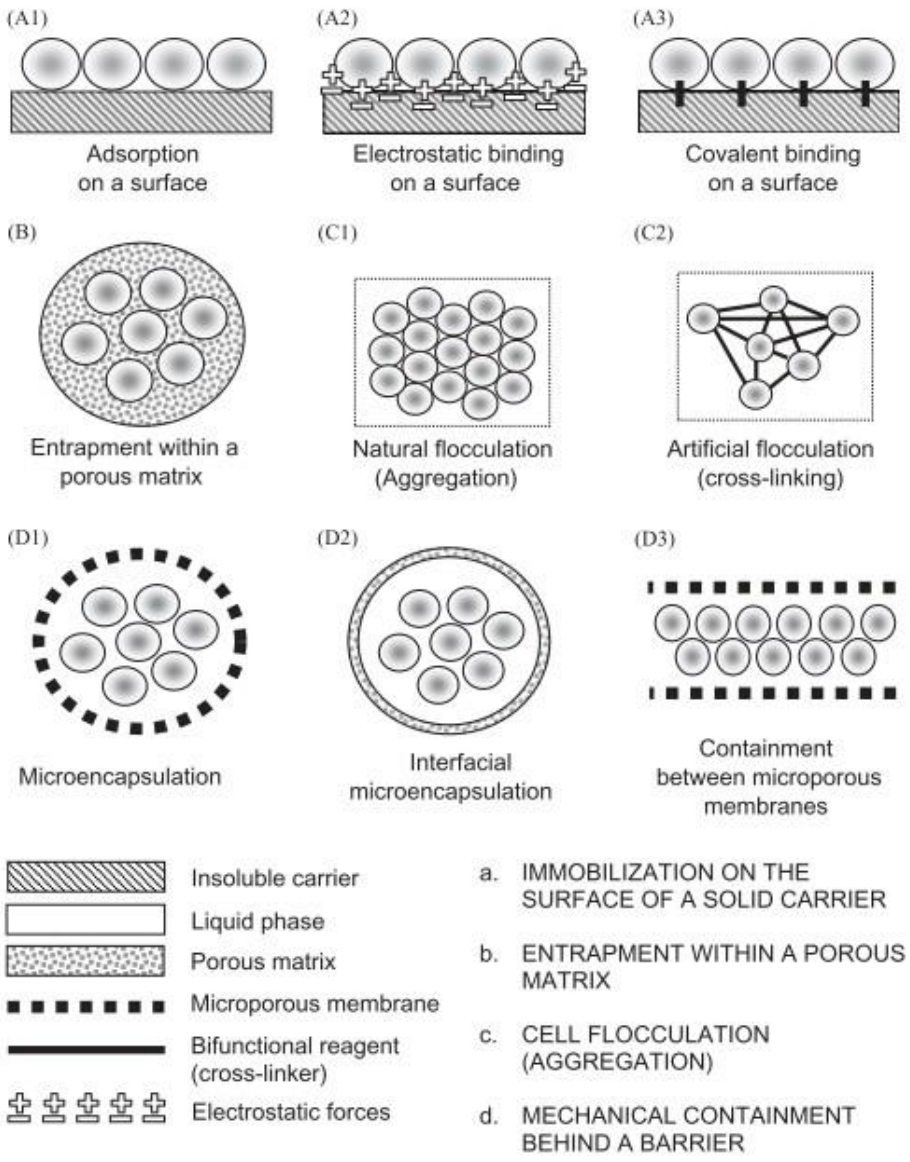


Fig. 2.5 Different techniques of cell immobilization. Adopted from Kourkoutas et al. (2004)

choosing grout, it's important to consider factors including adhesion, mechanical strengths, water retention, shrinkage, porosity, chemical and mineral composition, and durability (Bras and Henriques 2009). Primarily, the grout needs to be injectable and stable for a specific duration. The rheological behavior of the grout must be thoroughly understood and effectively managed in order to ensure proper pumping and flow within the porous medium, which is necessary for the filling of voids (Achal and Kawasaki 2016; Ivanov et al. 2019). It involves the consideration of various rheological attributes, such as stability, flow time bleeding, expansion, viscosity, and yield stress are essential for the characterization of the grout's flow

behavior (Shannag 2002; Li et al. 2015; Najjar et al. 2017). Gleaton et al. (2019) differentiated biogrout into two diverse mechanisms; injection biogrout and premixed biogrout. In injection

Table 2.3 Overview of different bacteria, concentration, carriers, methodologies adopted by the researchers to study the self-healing mechanism of cracks

Material	Bacteria	Concentration (cells/ml)	Carrier material	Immobilization method	Crack healed	Application	Reference
Concrete	*B. cohnii*	3.6×10^9 cell/ml	Expanded perlite	vacuum impregnation	0.79 mm	SEM, EDS, XRD	Zhang et al. (2017)
Mortar	*S. ureae and S. pasteurii*	-	Zeolite	Adsorption	0.70 mm	strength, water absorption, RCPT, SEM, EDS, XRD	Bhaskar et al. (2017)
Mortar	*S. pasteurii*	O.D – 1.3	Direct	--	0.15 to 1.64 mm	Tensile strength, Permeability, SEM	Choi et al. (2017)
Mortar	*B. pseudofirmus*	8.2×10^8 spores/g	Expanded perlite	Vacuum impregnation and adsorption	-	Water absorption, visual examination	Alazhari et al. (2018)
Mortar	*S. pasteurii*	4×10^8 CFU/ g	Direct	-	0.3–0.35 mm	Water absorption, visual examination, FTIR	Amiri et al. (2018)
Mortar	*S. pasteurii*	10^9 cells/mL	Calcium sulphoaluminate	Encapsulation	0.417 mm	Water absorption, visual examination, SEM, XRD	Xu and Wang (2018)
Concrete	*B. cereus*	3.52×10^7 cells/ml	Direct	-	0.1 to 0.8 mm	water absorption, water permeability, RCPT, FTIR, SEM, XRD, DSC	Wu et al. (2019)
Concrete	*B. subtilis*	~10^8 cells/L	Direct	-	0.4 mm	Strength, water absorption and permeability, Raman spectroscopy, RCPT, FTIR, SEM, XRD	Nguyen et al. (2019)
Mortar	*Lysinibacillus sp.*	1.8×10^9 cells/ml	Direct	Spores	0.4 -0.5 mm	Strength, TGA, SEM, XRD	Su et al. (2019)
Mortar	*B. sphaericus*	1.8×10^{12} cells/ml	Direct	-	85 % of 0.53 mm	Strength, water absorption and permeability, UPV, SEM, EDS	Jongvivatsakul et al. (2019)
Concrete	*B. cohnii*	1.1×10^9 cell/ml	Expanded perlite	Adsorption	upto 1.24 mm	Water permeability, SEM, XRD	Jiang et al. (2020)
Mortar	*B. pseudofirmus*		Polyurea	Microcapsules	Crack healing	Raman, FTIR, TGA, SEM, EDX	Zamani et al. (2020)
Concrete	*B. Subtilis*	6×10^8 cells/mL	Recycled coarse aggregates, fine aggregates	Vacuum impregnation and adsorption	1.1mm	Strength, UPV, SEM, EDS, XRD,	Khushnood et al. (2020)

Concrete	*Bacillus pseudofirmus, Diaphorobacter nitroreducens*	10^7 cells/ml	Calcium Alginate hydrogel beads	Encapsulation	0.12 – 0.17 mm	Slump and air tests, strength, Modulus of elasticity testing, self-healing, Stiffness recovery	Soysal et al. (2020)
Material	**Bacteria**	**Concentration (cells/ml)**	**Carrier material**	**Immobilization method**	**Crack healed**	**Application**	**Reference**
Concrete	*Bacillus pseudofirmus*	$1.85–2.24 \times 10^7$ spores/g	Calcium alginate beads, calcium alginate-chitosan beads	Encapsulation	1 mm	Strength, swelling properties, visual inspection, SEM	Gao et al. (2020)
Concrete	*B. cohnii*	Log 7.2 CFU/g	Magnesia cement	Unprotected bacterial spores	0.2 mm	Optical analysis, viability, SEM, XRD	Xiao et al. (2022)
Mortar	*B. cereus*	10^7 cells/ml	Zeolite	Adsorption	91.65 % crack healing	Strength, water absorption, Water permeability, air permeability, SEM, EDS, XRD	Yuan et al. (2022)
Concrete	*S. pasteurii spores*	10^7 CFU/ml	Ground granulated blast furnace slag	Vacuum impregnation and adsorption	Upto 0.10 – 0.14 mm	Strength, capillary water absorption, MIP, Visual examination, SEM-EDX, Raman spectroscopy	Zhang et al. (2022)
Concrete	*B. megaterium*	2.625×10^8 cells/m	Expanded perlite	Encapsulation	Upto 0.154 mm to 0.626 mm	UPV, water permeability, visual imaging, SEM-EDX	Ranjan et al. (2022)
Concrete	*B. megaterium*	1.62×10^9 cells/g	Expanded vermiculite	Coating	0.92 mm	Strength, UPV, water permeability, visual imaging, SEM-EDX	Ranjan et al. (2023)
Concrete	*S. pasteurii* and *B. sphaericus*		Direct			Recovery in compressive strength, water absorption, SEM, XRD	Nimafar et al. (2023)
Concrete	*B. cohnii*	1.02×10^{11} CFU/ml	Magnesia cement	Direct	Upto 0.250 mm	Water permeability, crack closure, SEM-EDX	Xiao et al. (2023)
Concrete	*Bacillus cereus MG708176*	1.3×10^7 spore/cm^3	Wood ash	Vacuum impregnation and adsorption	0.1 mm	Strength, SEM, Visual examination	Reyad and Mokhtar (2023)

Concrete	*Bacillus cohnii* (DSM 6307)	1.2×10^9	Expanded perlite Geopolymer	Vacuum impregnation and adsorption	0.376 mm - 0.340 mm	Crack healing at different temperature, visual examination	Jiang et al. (2023)

SEM: scanning electron microscopy, EDX: energy dispersive spectroscopy, XRD: x-ray diffraction, TGA: thermo-gravimetric analysis, FTIR: Fourier-transform infrared spectroscopy, DSC: differential scanning calorimetry, FESEM: field emission scanning electron microscopy, UPV: ultrasonic pulse velocity

based biogrout, the microbial calcifying culture is supplemented through ponding or spray after repairing the crack with the normal grout, whereas in the premixed, the microorganisms are added in the grout itself. Adding different types of mineral additives like rice husk ash, fly ash, silica fume, metakaolin, and cement kiln dust into cement admixed grout at different concentrations changes the fresh properties of grout significantly (Joshi et al. 2021). The incorporation of mineral additives in preparation of the cement grout reduces the overall cost and improves the fluidity and long-lasting capacity. Mirza et al. (2002) reported reduction in flow time, drying shrinkage and compressive strength. It has been observed that higher compressive strengths were obtained with cement grouts that incorporated Class C fly ash as compared to those that utilized Class F fly ash.

Bras et al. (2010) studied different percentage of fly ash (0%, 5% and 15%), w/b ratios (0.60, 0.70 and 0.80) and temperatures (5 °C, 20 °C and 35 °C) conditions. Based on the yield stress, plastic viscosity, consistency, the best results were obtained at w/b 0.80, temperature 20 °C, and fly ash 15%. Li et al. (2015) developed biogrout using *B. megaterium* bacterial strain to evaluate the comparison of urease-based bio-grouts and asparaginase-based MICCP process for sand bio-grout. The levels of NH_3 production were less in asparaginase activity than urease activity. The unconfined compressive strength of the asparaginase-based bio-grout and urease-based consolidation was 980 kPa and 1002 kPa. The asparaginase-based bio-grout failed to produce a cohesive mass due to absence of calcite precipitation. The permeability of the asparaginase-based bio-grout was recorded at 2.3×10^{-7} ms^{-1}, whereas the permeability of bio-grout produced from urease activity was measured to be 2.0×10^{-7} ms^{-1}. Najjar et al. (2017) used three different types of supplementary cementitious material; silica fume (SF), fly ash (FA), and metakaolin (MK) as a partial replacement of cement for grout. The best results were obtained with 0.45 w/b ratio with efflux time of $35 – 40 \pm 2$ s. Comparing the partial substitution of SF or MK with OPC by 10% showed 30 and 54% improvement in compressive strength compared to control at 7 days, respectively. The FA improved the flowability properties but increased bleeding time with reduction in compressive strength at 56 days.

Sha et al. (2018) conducted experiments with different dosage of fly ash (0%–40%,) bentonite (0%–15%) and superplasticizers (0.7%) and demonstrated that the addition of bentonite was found to enhance the stability of the grouts. Different cement and water glass (by volume) suspensions 1:1, 2:1 and 3:1were tested. The influence of varying contents of FA, bentonite, superplasticizers, and water glass on the flexural strength of hardened grouts is diverse. The

optimal range of FA contents for enhancing the flexural strength of grouts without supplementary cementitious materials (SCMs) is 20%-30%. On the contrary, the incorporation of 0.7% superplasticizer (SP) with increasing FA content in grouts decreases the flexural strength. The best grout was obtained with improved flexural and compressive strength with 0.7% SP, 20%–30% FA, 0%–5% bentonite, and water glass volume ratios of 2:1–3:1 with respect to cement.

Liu et al. (2018) developed a capsule of 173 μm using urea- formaldehyde as a shell material and epoxy resin as a core material. The flowability properties and compressive strength of the grout mixture was assessed for different concentrations of capsules (0%, 1%, 3%, 5%, and 8%) by the mass of grout, with a water-to-grout ratio of 0.13 (Fig. 2.6). Following the incorporation of an excessive percentage of capsules into the grouting materials, the porosity of the matrix was found to increase. It should be noted that the grout material with a capsule concentration of less than 3% met the initial and 30-minute acceptance criteria for flowability. The application of an excessive quantity of capsules within the grouting materials led to an elevated level of porosity in the matrix. The grout with >3% capsules integration was able to achieve the best results within acceptance criteria.

Microbial-facilitated bioremediation is considered as an eco-efficient and cost-effective technique that significantly increases strength and dilatancy and reduces hydraulic conductivity (Stabnikov et al. 2015; Xiao et al. 2020). Van Paassen et al. (2009) conducted an experiment to demonstrate the large-scale functionality of Biogrout, which resulted in significant cementation at a distance from the injection points, thereby verifying the technical feasibility of biogrout for ground reinforcement. The investigation of MICCP for the purposes of soil-stabilization and building-material is currently under extensive research. Marín et al. (2021) conducted research into the bio cementation properties of native urease producing *Sporosarcina* sp. and achieved unconfined compressive strength (UCS) that was 461% higher and $CaCO_3$ content that was 120% higher than those produced by *S. pasteurii* DSMZ 33.

Joshi et al. (2021) tested the flowability properties (march cone, mini slump) of biogrout developed with partial replacement of FA (0%-50%) with cement at different (0.45 and 0.50) w/b ratio. The flowability results were obtained best at 0.50 w/b ratio with maximum strength at 40% replacement of cement when *Bacillus* sp. CT5 was used as culture instead of water. Similar work was presented by Anand et al. (2023) using FA as the partial replacement of cement. Anand and his colleagues tested the flowability, shrinkage and strength of grout at

different dosage of FA and selected 40% replacement as optimum crack healing biogrout. The study included the monitoring of MICCP activity on the crack repaired surfaces by EMI technique signifying improvement in stiffness.

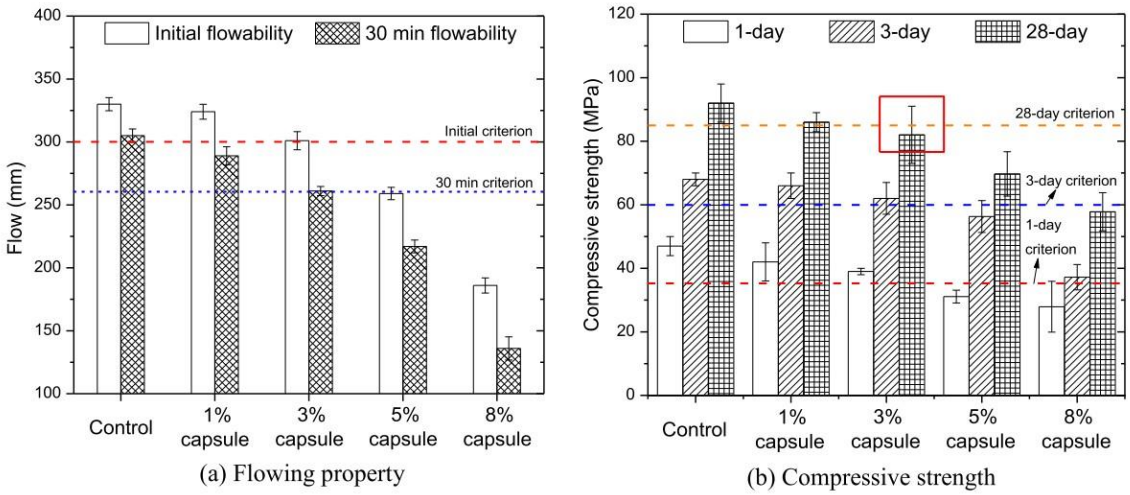


Fig. 2.6 Flow properties and compressive strength of different dosage of capsule in grout. Adopted from Liu et al. (2018)

2.11 Role of MICCP in restoration of stones and monuments

MICCP was proposed as a method for the restoration of calcareous stones with the help of calcifying bacterial strains through biomineralization. $CaCO_3$ precipitation by bacteria on the surface forming a protective coating was patented by Adolphe (1990) which has expired in 2010. This $CaCO_3$ layer formation by urease-producing bacteria in the presence of a Ca^{2+} ions and aerobic conditions plays a key role in the restoration process through biological healing (Anbu et al. 2016; Seifan et al. 2016a). The effectiveness of this methodology has been demonstrated through its ability to decrease stone porosity, leading to more solidified structures (Castanier et al. 2000). MICCP is a method of carbonate formation that is both eco-friendly and energy efficient. It is employed to fill gaps or cracks in rock or cement matrices, with the aim of preventing the penetration of water and thereby increasing strength and resistance (Perito et al. 2014). Various methods of MICCP treatment for stone conservation have been reported at the laboratory scale (Arun 1989; Jroundi et al. 2012; Minto et al. 2018).

Tiano et al. (1999) reported significant reduction in water absorption upon brushing the *Micrococcus* sp. and *Bacillus subtilis* on limestone samples. Rodriguez-Navarro et al. (2003)

reported that the calcite on ornamental stone provides better resistance to stress compared to the calcite grains present in the original stone. Rodriguez-Navarro et al. (2015) further conducted in situ experiment using *Myxococcus xanthus* bacterial culture on stone monuments of Granada, Spain in various areas of Renaissance (16^{th} century). This area was severely damaged due to granular disintegration and cracking. The deposition of calcite and vaterite was confirmed by SEM and XRD analysis. However, the major concern during in-situ research was pigmentation of freshly precipitated calcite on the surface due to sun exposure which was fortunately discovered to be within the threshold limits.

Li and Qu (2010) conducted biomineralization experiment to study the effectiveness of *Sporosarcina pasteurii* to promote carbonate mineralization in marble and concrete samples. It was reported that mineralization process did not significantly impact the pore size distribution, but resulted in a decrease in porosity. Similar work was carried out by De Muynck et al. (2010) using *B sphaericus* strain for consolidation of calcite layer on the Euville limestone which resulted in a 63% less weight loss as compared to untreated specimens during sonication. Further, 50% decrease in water absorption was reported upon increasing the concentration of calcium from 17g Ca^{2+} m^{-2} to 67g Ca^{2+} m^{-2}. Another study conducted by Jroundi et al. (2012) suggested *Acinetobacter* as potential inoculants for bioconsolidation treatments, both when utilized individually and in combination with *Myxococcus xanthus* bacterium. Similarly, Zhu et al. (2015b) found that the immersion method was more effective than the coating method in treating sandstone surfaces. The study showed that both methods were able to induce calcite precipitation with the formation of dense layer about 50 to 100 μm thick on the surface. The $CaCO_3$ crystals were 1 to 10 μm in size which formed a strong adhesive force between the stone surface and calcite layer. Mineralization provided resistance against the acid rain, light ageing, frosting and temperature changes.

Daskalakis et al. (2014) reported increase in weight of the marble samples due to crystal deposition on the surface by bacterium *Cupriavidus metallidurans*. Daskalakis et al. (2015) \ investigated the biomineralization efficiency by *B. pumilus* isolated from a cave stone under different temperature conditions and nutrient media concentration. The results suggested $CaCO_3$ formation at 25 and 30 °C which was confirmed of vaterite peak by XRD and FTIR analysis. It has been observed that the initiation of calcium removal occurred after 48 hours in both temperature conditions, with the rate of immobilization being faster at 30 °C than at 25

°C. Moreover, the carbonate layer formed a strong adhesive bond with the surface leading to less weight loss during ultrasonication experiment.

Minto et al. (2018) carried out MICCP treatment in a column filled with 1904.3 g marble grains of 0.5–1.4 mm particle size with the injection of 60 ml of *S. pasteurii* (strain DSM-33) culture followed by 400 ml cementation solution (urea and calcium source) for six days. The intact formation of sand column with strong bonding inward to a depth of 150 mm and loosely bound grains at the outlet was reported. Erşan et al. (2020) reported consolidation of Maastricht limestone surface by *B. sphaericus* culture with addition of 1.11 M urea, and 1.11 M calcium formate as calcifying solution. It improved 100% drilling resistance of the specimen to a depth of 35 mm from the surface.

2.12 Challenges faced by MICCP in bioconcrete and restoration of stones

Incorporating fresh bacterial culture in a liquid medium while preparing fresh concrete has significantly improved the mechanical and durability properties of concrete. However, in the long term, the primary concern regarding the utilization of MICCP in concrete has been the survival of bacteria in the highly alkaline concrete environment. Secondly, low survival rate of microorganisms due to shear stresses to the bacteria during the concrete mixing process and the dry condition of hardened concrete (Seifan et al. 2020). Moreover, the size of pores in most of the cases is smaller than 0.5 µm, while the size of bacteria is in the range of 1–3 µm. It is challenging for bacteria to endure such harsh conditions. MICCP presents some challenges regarding production of toxic by-products (NH^{4+}), requirement of bacterial concentration and nutrient, and provision of specific growth condition for bacteria are some of the difficulties for upscaling the application at field scale (Naveed et al. 2020a). Jonkers and Schlangen (2007) observed a decrease in the concentration of bacteria from 10^9 spores/cm^3 to 1.15×10^6 spores/cm^3 (0.12% of the original inoculums) of *B. cohnii* spores, 0.01% *B. halodurans* spores (10^9 spores/cm^3 to 1.07×10^5 spores/cm^3 of the original inoculum) and 0.06% *B. pseudofirmus* spores (10^9 spores/cm^3 to 5.62×10^5 spores/cm^3 of the original inoculum) survived 10 days after inoculation to cement paste. Similarly, Achal et al. (2011) reported a rapid decline in the concentration of *B. megaterium* from 10^7 to 10^5 cfu/mL after 3 days, and 10^4 cfu/mL after 28 days in mortar specimens (survival rate 0.1%). Basaran (2013) outlined 9×10^3 MPN/mL (0.4% of the original inoculums) viable cells after 28 days curing period. Out of all the viable cells, about 50% were observed to be spores. Principally, unprotected bacterial cells and spores have poor survival ability inside the cementitious matrix. Dzionek et al. (2016) reported various

protective carrier materials to immobilize bacteria and increase bacterial cell viability in concrete. However, the major concern is the dosage of carrier material to be used in the preparation of concrete. De Belie (2016) reported these carrier materials will have detrimental influence on the compressive strength, especially if these are added in dosages exceeding 1% weight of cement. Moreover, use of supplementary cementitious materials (SCM) as carrier materials are encouraged, as they can be immobilized in high dosage. Other reason is SCM has positive influence on strength due to pozzolanic action (Khaliq and Ehsan 2016). Another limitation of MICCP is that microbial methods are typically slower and more intricate than chemical processes. This is because microbial activity is significantly affected by different environmental variables such as pH, temperature, electron donors and acceptors, and availability of nutrient and metabolite concentrations and their diffusion rates (Ivanov and Chu 2008). As a result, the application of MICCP at a commercial scale is challenging.

2.13 Concluding remarks

The application of MICCP has given rise to a new field known as "microbial concrete" which has attracted researchers from all over the world due to its potential to enhance the durability properties of concrete structures. In the past decade, numerous studies have been conducted at the laboratory scale that highlight the significance of MICCP. However, despite these efforts, a comprehensive quantitative and qualitative assessment of microbial concrete is still limited to laboratory conditions. The literature available is based on application of the heterotrophic bacteria especially ureolytic bacteria on microbial concrete. However, literature on the autotrophic mediated pathway including photosynthetic microbes is limited. There are reports showing significant $CaCO_3$ precipitation by cyanobacteria. However, its role in enhancement of cementitious properties is not studied. Furthermore, there is a lack of research on the performance of microbial treated concrete under diverse environmental conditions beyond the laboratory setting. In long term, the survival of bacteria in high alkaline environment is of major concern. To address the survivability issue, isolation of alkaline resistance microbes and suitable carrier materials have shown satisfactory results in improving cementitious properties and crack remediation. The shelf-life carrier material immobilizing the bacteria is of major concern. Longer shelf life of bacterial product is desired for upscaling MICCP application to engineering application. The goal of present work is to develop a better understanding in MICCP technique, which will facilitate the practical implementation of microbial concrete in construction sector in the near future.

Chapter 3 Materials and methods

The current study is divided into three sections (Fig. 3.1). The first two sections includes the influence of heterotrophic and photoautotrophic bacteria in enhancing the cementitious properties and crack remediation. The third section elaborates the comparison of heterotrophic and phototrophic bacteria in enhancing the concrete structural properties and marble aesthetic properties.

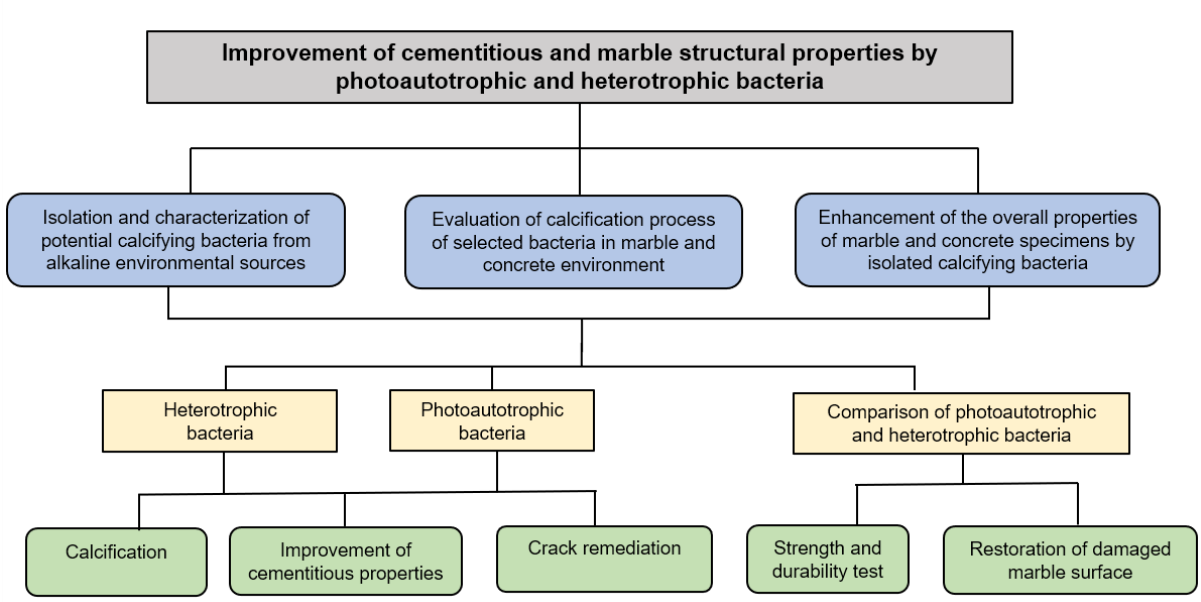


Fig. 3.1 Overview of thesis outline adopted to address the objectives of the study

3(A) Heterotrophic bacteria

3.1 Isolation and screening of heterotrophic bacteria

3.1.1. Sample collection

Marble dust was collected from different locations in the marble dumping yard (26°35'18.7008"N and 74°52'21.0468"E), Kishangarh, Jaipur, Rajasthan, India (Fig. 3.2). The tons of marble waste slurry dumped in the area results in the formation of plateaus as a result of biomineralization that binds the particles together. Sampling was performed from six different sites at a depth of 10 ± 2 cm using sterile ethanol equipment and containers. The samples were maintained in an ice box at a temperature of 4 °C, and were subsequently brought to the laboratory. The chemical composition of marble dust is given in Table 3.1

Table 3.1 Chemical constituents of marble dust

Constituents (%)	Marble dust
CaO	28.67
SiO_2	4.98
Al_2O_3	0.48
Fe_2O_3	0.41
MgO	20.32
K_2O	0.05
Na_2O	0.06
LOI	43.7



Fig. 3.2 Marble dumping yard, site at Kishangarh, Jaipur, Rajasthan, India where the samples were collected for isolation of bacteria

3.1.2 Isolation of heterotrophic bacteria

Marble dust was enriched for enumeration of heterotrophic bacteria by suspending 10 g of the sample in 90 ml of nutrient broth (NB) (Hi Media, India). The NB was supplemented with 2% syringe filter-sterilized urea under aseptic conditions and incubated at 37 °C for 72 h with shaking at 130 rpm (Achal et al. 2010b). Saline was prepared in 0.85% (w/v) sodium chloride (NaCl). One milliliter of the enriched medium was inoculated in 9 ml saline, which was further serially diluted and plated on nutrient agar plates. After 24 – 48 h of incubation, colonies were randomly selected and sub-cultured on nutrient agar plates. Colonies were assessed for their shape, colony count.

3.1.3 Qualitative characterization

Urease enzyme-producing bacteria were selected by streaking the colonies on urea agar base (UAB) plates (Hi Media, India). The UAB plates were incubated at 37 °C and a change in color from brownish yellow to pink was noted as a qualitative indicator of urease enzyme activity within 24 h. *Escherichia coli* was used as a negative control, and *Bacillus* sp. CT5 (Achal et al., 2010) were used as standards the for ureolytic activity.

3.2 Molecular characterization

3.2.1 DNA extraction and electrophoresis of DNA on agarose gels

Isolation of genomic DNA typically involves disrupting cells using chemical or enzymatic methods, followed by detergent lysis and organic solvent extraction using the alkaline lysis method described by Krishna et al. (2008). A bacterial colony of each isolate was inoculated into NB and incubated at 37 °C with shaking at 130 rpm. Following 14-16 hours of incubation, 2 milliliters of the liquid culture were centrifuged at 8,000 rpm for 1 minute. The resulting pellets were resuspended in 800 µl of saline-EDTA (0.1 M, pH 8.0) and 10 µl of freshly prepared lysozyme along with 2 µL DNase-free RNase solution (1 mg/100 µL). The mixture was incubated at 37 °C for 30 minutes, followed by the addition of 200 µl of 10% SDS, which was then incubated at 65 °C for 15 minutes. Following exposure of genomic constituents to the solution, organic solvents were used to eliminate cell debris and protein content, resulting in the desired genome. An equal volume of a mixture consisting of 25 parts phenol, 24 parts chloroform, and 1-part isoamyl alcohol (25:24:1) was added to the cell suspension and then centrifuged at 12,000 rpm for 10 min at 4 °C. The upper aqueous phase was then extracted in

another microfuge tube, and 0.7 volume of isopropanol was added. The mixture was then maintained at room temperature for 30 min. Nucleic material was extracted by centrifuging the mixture at 12000 rpm for 10 min, followed by washing with 70% ethanol. The resulting precipitated nucleic acids were resuspended in 40 µl of TE buffer and stored at 4 °C.

A standard agarose gel (0.8% w/v) was prepared with ethidium bromide (EtBr) and poured into an electrophoresis tray with a comb inserted at one end. After solidification, the comb is removed. The gel was then kept in an electrophoretic chamber containing 0.5X TBE, pH 8.0. DNA was loaded into the wells using a 6X loading dye and then electrophoresed for 55 min. The DNA was observed using a UV transilluminator.

3.2.2 Quantification of DNA by Nanodrop spectrophotometer

The DNA concentration in the suspension was determined by measuring the absorbance at A_{260} using a spectrophotometry. The purity of the DNA was calculated by comparing its absorbance at A_{260} and A_{280}, and the A_{260}/A_{280} ratio should be between 1.8 and 2.0. Additionally, the A_{230}/A_{260} ratio should be between 0.3 and 0.9. If the A_{260}/A_{280} ratio exceeds 2.0, it indicates RNA contamination, while a ratio less than 1.8 suggests protein or phenol contamination.

3.2.3 Amplification of 16S rRNA and Purification of PCR products

Polymerase chain reaction (PCR) amplification of the 16S rRNA gene was performed using the Gene Amp PCR system (Applied Biosystems, USA) with the following thermal cycling settings: denaturation of the DNA at 95 °C for 300s, followed by 35 cycles of 95 °C for 60s, annealing at 50 °C for 40s and extension at 72 °C for 120s and a final extension step at 72 °C for 420s. The PCR reaction mixture comprised 10X PCR buffer, 2 mM dNTPs, 50 mM $MgCl_2$, 0.1 µM (forward and reverse) primer and 2.5 U Taq DNA polymerase in a final volume of 25 µl. The forward primer 5'-AGAGTTTGATCCTGGCTCAG-3' and reverse primer 5'-AAGGAGGTGATCCAGCCGCA-3' of 16S rDNA were used for amplification (Weisburg et al., 1991). The amplified PCR products were purified using a Thermo Scientific Gene Jet PCR purification kit and sequenced from First Base Laboratories, Malaysia.

3.2.4 Sequence analysis

The DNA chromatogram sequences were analyzed and edited using Bio Edit Programme, and the sequences were saved in FASTA format (Hall 1999). The forward and reverse primer

sequences were removed before the sequences were compared to existing ones in the National Centre for Biotechnological Information (NCBI) GenBank database. Using the Basic Local Alignment Search Tool (BLAST) the sequences were compared to find the closest match. The matched sequences of the bacterial strains were analyzed using mult Align tool.

3.2.5 Phylogenetic analysis

The DNA sequences of each isolate were compared to those in the existing database in EzBioCloud and deposited in NCBI GenBank. For phylogenetic analysis, molecular evolutionary genetic analysis was done using the MEGA (version 11). The indefinite sequences at both ends were removed by adjusting gaps to improve the alignment. A consensus tree was constructed using the neighbor-joining method with 1000 bootstrap replicates to represent the evolutionary history. The evolutionary distances were then calculated using the maximum composite likelihood method.

3.3 Quantitative analysis

3.3.1 Urease enzyme activity

Urease activity is defined as the ability of the enzyme to convert urea to ammonia and form hydroxide ions, resulting in an increase in the pH of the medium and creating an alkaline environment surrounding the bacterial cell. As a result of urease activity, calcium ions present around the bacterial cell wall combine with carbonate ions to form $CaCO_3$ around the bacterial cell. The bacterial isolates labeled as MD1, MD2, MD3, MD4, MD5, MD6, and MD7 were tested for urease enzyme activity using phenol-hypochlorite (Natarajan 1995). One percent of overnight grown bacterial culture was reinoculated with an optical density ($0D_{600}$) of 0.5 in 100 ml NB (pH 7.0 ± 0.2). NB was supplemented with filter-sterilized 2% urea and incubated at 37 °C with shaking at 130 rpm (Achal et al. 2010). Ammonium chloride (0 – 1000 µM) was chosen as the standard to calculate the urease enzyme activity. Following a 24-h period, one milliliter of the bacterial culture was carefully isolated under sterile conditions and transferred into microfuge tubes. The supernatant was then extracted by centrifugation at 8000 rpm for five minutes. A total of 250 µL was added to test tubes containing one milliliter of potassium phosphate buffer (0.1 M) and 2.5 milliliters of urea (0.1 M). The mixture was incubated at 37 °C for a period of 5 min followed by addition of 1 ml of sodium nitroprusside and phenol hypochlorite. The mixture was then incubated at 37 °C for 25 min. The optical density was determined through the use of a UV spectrophotometer (Shimadzu, UV-1800) at a wavelength

of 626 nm. The experiments were performed in triplicate. The urease activity was calculated by standardizing the attained value using the ammonium chloride standard curve. One unit of urease is equivalent to the amount of urease degrading one µM urea per minute (Li et al. 2022a).

3.3.2 Calcium carbonate precipitation

The bacterial isolates were inoculated in autoclaved NB augmented with 2% urea and 25 mM $CaCl_2$. The cultural flask was incubated at 37 °C for 144 hours. At each 24-hour interval, the solution was filtered using a vacuum membrane filtration technique (0.45 micrometer). The $CaCO_3$ precipitate was collected on a membrane filter paper. The precipitate was washed with 95% ethanol and dried at room temperature. The weight of the crystals deposited on the filter paper was taken as the amount of $CaCO_3$ precipitated at each interval.

3.4 Sand consolidation

Microbiological sand consolidation experiment was performed using locally available natural river sand with 300 µm grain size. The sand was autoclaved twice at 121 °C for 15 min to remove the indigenous microflora. The heterotrophic strains MD1, MD2, MD3, MD4, MD5, MD6 and MD7 were grown in NB medium at 37 °C with agitation at 130 rpm for 16 hours. The bacterial cell pellet was harvested by centrifuging at 5000 rpm for 10 min, followed by washing with saline solution (0.85% NaCl). The cell pellet was resuspended in nutrient broth to achieve a final optical density (OD_{600}) of 0.5. Nutrient broth was supplemented with a calcifying solution (2% urea and 25 mM $CaCl_2$). The sand slurry for each column was prepared while maintaining a constant moisture content of 25%. Autoclaved river sand (100 g) was mixed with a 25 ml of MD1, MD2, MD3, MD4, MD5, MD6 and MD7 bacterial culture (OD_{600} = 0.5) under sterile conditions. The plastic column (height 7.6 cm; diameter 3.8 cm) was cut vertically into two pieces and joined using tape. The bottom of the plastic column was covered with scotch brite and Whatman paper as shown in Fig. 3.3. The column was filled with sand slurry. The air bubbles were removed by tapping a glass rod within the column and filling it with slurry. To prepare the control, sand was mixed with 25% NB instead of the bacterial culture and filled into a plastic column. All bacteria admixed columns were continuously supplied with calcifying solution (NB, 2% urea and 25 mM $CaCl_2$) every 12 h and bacterial culture every 48 h. The control column was supplied with NB only. The entire procedure was conducted for a time span of 20 days to study the flow rate. The flow rate of calcifying solution through the sand column per minute was noted. The effluent was collected in the beaker and

tested for the pH. At the end of experiment, once the flow rate of the sand column had decreased and stabilized, sand columns were then opened. The plugged sand column was split into three portions (upper, middle, and lower layers). Calcite precipitation was checked for each layer. The precipitated calcite from all three layers was measured using the EDTA titration method (AHPA 1989). One gram of the sand column sample was crushed, and subsequently, a few drops of 3N hydrochloric acid were added. The four ml of sodium hydroxide (NaOH) solution was added to the solution to obtain the final pH of 12 -13. A pinch of Eriochrome Black T was added and mixture was titrated against 0.05 M EDTA. The end point is noted as change in color from pink to blue. One ml of EDTA used for titration is equivalent to 5.004 mg of $CaCO_3$.

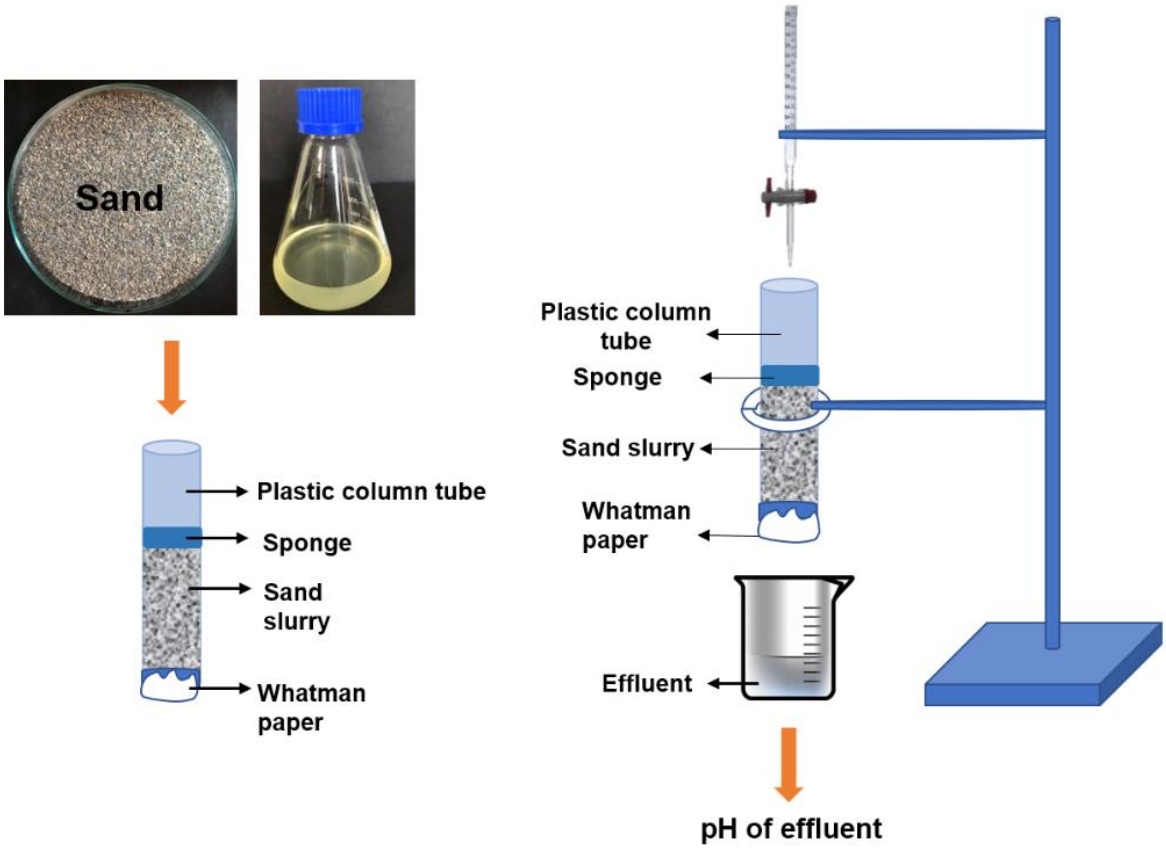


Fig. 3.3 Experiment set-up of sand consolidation experiment using different bacteria

3.5 Selection of the highest calcifying heterotrophic bacteria

The highest calcifying bacteria was selected based on the urease activity, $CaCO_3$ precipitation and sand consolidation experiment by heterotrophic strains, MD1, MD2, MD3, MD4, MD5, MD6 and MD7. The heterotrophic bacteria, MD6 was selected for further work. The MD6 was identified as *Bacillus paramycoides* using EzBioCloud.

3.6 Influence of different temperature and pH conditions on the physiology of *B. paramycoides* MD6

The effect of variation in the temperature and pH on the metabolic activity of bacteria, urease activity and $CaCO_3$ precipitation was studied at different time intervals.

3.6.1 Effect of temperature and pH variation on growth cycle

This study was carried out to investigate growth profile of *B. paramycoides* MD6 at various incubation temperatures (25 °C, 37 °C, 45 °C, and 55 °C) and pH values (6, 7, 8, 9, 10, 11, and 12). To evaluate growth cycle under various pH conditions, the pH of the nutrient broth was adjusted before autoclaving. The *B. paramycoides* MD6 bacterial strain was inoculated in a triplicate flask at an optical density (OD_{600}) of 0.5.

3.6.2 Effect of temperature and pH variation on urease activity

This study was carried out to investigate urease enzyme activity at various incubation temperatures (25 °C, 37 °C, 45 °C, and 55 °C) and pH values (6, 7, 8, 9, 10, 11, and 12). To evaluate urease activity under various pH conditions, the pH of the nutrient broth was adjusted before autoclaving. NB was autoclaved and supplemented with a filter sterilized 2% urea. The *B. paramycoides* MD6 bacterial strain was inoculated in a triplicate flask at an optical density (OD_{600}) of 0.5. The flasks were incubated at different temperatures in an orbital shaker for 120 h (Achal et al., 2010). After 24 h of regular intervals, 1 ml of culture aliquot was taken from the flask to monitor urease enzyme activity. The urease activity by bacteria was calculated by evaluating the amount of ammonia released from urea during phenol hypochlorite assay (Natarajan 1995).

3.6.3 Effect of temperature and pH variation on $CaCO_3$ precipitation

The experiment was conducted in two parts. In the first set of experiments, the overnight grown culture of *B. paramycoides* MD6 culture was reinoculated in NB (OD_{600} - 0.5) supplemented with calcifying solution (2% urea and 25 mM $CaCl_2$). NB flasks were incubated at different temperatures (25, 37, 45, and 55 °C) for 120 h. Similarly, NB were prepared at various pH values (6, 7, 8, 9, 10, 11, and 12) and supplemented with calcifying solutions. Upon completion of the incubation period (120 h), the $CaCO_3$ precipitated in the flask was collected on Whatman filter paper. The precipitate from each flask was washed with 95% ethanol and room-dried for

6 h. The amount of powdered $CaCO_3$ collected on Whatman filter paper was weighed. In the second set of experiments, one ml of aliquot was taken from the flask at 24, 48, 72, 96, and 120 h and centrifuged to measure the amount of soluble calcium content in the supernatant after the centrifugation using the EDTA titration method (Stocks-Fischer et al. 1999). Five ml of supernatant solution was mixed with 3N hydrochloride (HCl) acid. The four ml of sodium hydroxide (NaOH) solution was added to the solution to obtain the final pH of 12 -13. A pinch of Eriochrome Black T was added and mixture was titrated against 0.05 M EDTA. The end point is noted as change in color from pink to blue. One ml of EDTA used for titration is equivalent to 5.004 mg of $CaCO_3$. The calcium removal percentage (%) was evaluated based on soluble calcium (Ca^{2+}) ions. Change in pH were measured at 24, 48, 72, 96, and 120 h using a pH meter (Eutech Instruments).

3.6.4 Microstructural and XRD analysis

The crystal formation and elemental composition of the powdered samples were analyzed using SEM-EDS, which involved Energy-dispersive X-ray spectroscopy (EDX), to determine the elements present in the microstructural crystals. Samples were prepared by careful polishing and sputter-coating with gold. A Bruker D8 X-ray diffractometer was used to conduct X-ray diffraction (XRD) with a scan from 20° to 60° at a two-theta angle using a Cu anode (40 kV and 30 mA).

3.7 Sand consolidation by *B. paramycoides* MD6

Microbiological sand consolidation experiments were performed using locally available natural river sand with different grain sizes (150 µm, 300 µm, and 600 µm). The sand was autoclaved twice at 121 °C for 15 min to remove the indigenous microflora. *B. paramycoides* was grown in NB medium at 37 °C with agitation at 130 rpm for 16 hours. The bacterial cell pellet was harvested by centrifuging at 5000 rpm for 10 min, followed by washing with saline solution (0.85% NaCl). The cell pellet was resuspended in nutrient broth to achieve a final optical density (OD_{600}) of 0.5. Nutrient broth was supplemented with a calcifying solution (2% urea and 25 mM $CaCl_2$). The slurry for each column was prepared while maintaining a constant moisture content of 25%. Autoclaved sand (200 g) was mixed with a 25% *B. paramycoides* culture (OD_{600} = 0.5) under sterile conditions. The plastic column (diameter (dia) = 3 cm, height (ht) = 15 cm) was cut vertically into two pieces and joined using tape. The bottom of the plastic column was covered with scotch brite and Whatman paper. The column was filled with 200 g

sand slurry. The air bubbles were removed by tapping a glass rod within the column and filling it with slurry. To prepare the control, sand was mixed with 25% NB instead of the bacterial culture and filled into a plastic column. All columns, except for the control, were continuously supplied with NB every 12 h and bacterial culture every 48 h. The entire procedure was conducted for a time span of 20 d to study the flow rate. The plugged sand column was split into three portions (upper, middle, and lower layers). Calcite precipitation was checked for each layer. The precipitated calcite from all three layers was measured using the EDTA titration method (AHPA 1989).

3.7.1 Microstructural analysis

A chunk of the upper layer of the sand-plugged column was used for the microstructural analysis. The samples were then polished and sputter-coated with gold. A thin layer of carbon was placed on the polished surface to neutralize any excess charge on the sample. The microstructural crystals were analyzed using energy-dispersive X-ray spectroscopy (EDX) to determine their elemental compositions.

X-ray diffraction (XRD) was performed on the powdered samples obtained from the upper layer of the column, and A Bruker D8 X-ray diffractometer was used to conduct X-ray diffraction (XRD), which involved scanning from 20°to 60°at a two-theta angle with a Cu anode (40 kV and 30 mA). The data obtained was compared with the standards set by the International Center for Diffraction.

3.8 Enhancement of the overall properties of concrete by ureolytic bacteria

3.8.1 Construction materials

Commercially available ordinary Portland cement (OPC) - 43 grade, as per the Indian standard, was used (IS:8112, 2013). Locally sourced natural well-graded river sand was used as fine aggregates, meeting the requirements of Zone II according to the Indian standard. The specific gravity of the fine aggregate was 2.62 and a water absorption rate of 1.3%. Coarse aggregates with particle sizes of 20 mm and 10 mm were used, with specific gravities of 2.61 and 2.63, and water absorption rates of 1.38% and 1.42%, respectively. The fine and coarse aggregates used in the casting process complied with the Indian standards (IS 383 2016). For spore immobilization, Metakaolin (MK) was obtained from a private vendor. The chemical properties of MK and OPC - 43 used in the experiments are listed in Table 3.2.

3.8.2 Concrete mix design

Control concrete mix was prepared using cement: fine aggregate: coarse aggregate in a proportion of 1:1.82:3.24 (by weight), maintaining a water-to-cement ratio (w/c) of 0.47 (IS 10262 2019). To make the bacterial treated specimens, *B. paramycoides* (OD – 0.5) culture supplemented with 2% urea (w/v) and 25 mM calcium chloride solution (w/v) was used instead of water was used. The specimens were cured in bacterial and nutrient media. A control sample was prepared and cured in tap water. A detailed summary of the experimental setup is presented in Table 3.3.

Table 3.2 Chemical composition of the Metakaolin and the OPC - 43 grade

Composition (%)	Metakaolin	Cement
SiO_2	52.2	21.3
CaO	0.21	63.2
Fe_2O_3	1.53	2.5
Al_2O_3	44.5	7.3
MgO	0.32	1.52
K_2O	0.45	0.54
Na_2O	0.16	0.27
SO_3	0.05	2.42
TiO_2	1.48	0.37

Table 3.3. Outline of the different mix designs for the experiment and curing treatment

Specimens	Material used	Curing
Control	Cement: sand: coarse aggregates Water/cement = 0.47	Water curing
BPC*	Cement: sand: coarse aggregates culture/cement = 0.47 2 % urea + 25 mM $CaCl_2$	Submersion in *B. paramycoides* culture supplemented with 2% urea and 25 mM $CaCl_2$

*The curing medium was replenished every seven days with the respective media and inoculated with freshly prepared culture.

3.8.3 Strength and Permeability

Different specimens were prepared to test the strength and permeability of the concrete. The 150 × 150 × 150 mm cubes were cast and tested for compressive strength, as per the Indian standards (IS 516 2021). Test specimens with dimensions of 100 (dia) × 200 (ht) mm were cast for rapid chloride permeability and sorptivity coefficient. The 100 × 200 mm specimens were

sliced into 100 (dia) × 50 (ht) mm size for the rapid chloride permeability test (RCPT) (ASTM C1202 2012) and sorptivity experiments (ASTM C1585, 2013).

3.8.3.1 Compressive strength

The influence of the inclusion of vegetative bacterial cells and their nutrient medium (NB) supplemented with 2% urea and 25 mM $CaCl_2$ on the mechanical property of concrete mix was investigated at an age of 7 and 28 days of curing, as per the Indian standard IS 516 2021. The compression test was carried out using the COMPTEST 3000 automatic compression testing machine (AIMIL India Ltd, New Delhi). The results were obtained by taking the average of three specimens as the compressive strength of the mix. The compressive strength was evaluated according to Equation 3.1:

$$\text{Compressive strength} = \frac{\text{Load in newton}}{\text{area of cube in mm}^2} \qquad 3.1$$

3.8.3.2 Sorptivity test

The sorptivity test measures the unidirectional absorption of water by a concrete specimen due to capillary rise and is used to determine the transport of water through the pore system of the specimen. Standard test samples, with dimensions of 100 (dia) × 50 (ht) mm, were utilized after 7- and 28-days curing. The samples were subjected to saturation in a vacuum desiccator for 3 hours. After the saturation, the specimens were placed in an environmental chamber for three days. The environment chamber's temperature and relative humidity were 50 ± 2 °C and 80 ± 3%, respectively. Subsequently, the samples were stored in a sealable container at a temperature of 23 ± 2 °C for a minimum of 15 days before the absorption test. The specimens' side surface was hermetically sealed with an epoxy, while one face was covered with a plastic sheet and the other was made accessible to the water such that only 2 ± 1 mm of the height is exposed as shown in Fig. 3.4. The weight change was recorded at various intervals, including 60 seconds, 5, 10, 20, 30, 60 minutes, and every hour up to a maximum of 6 hours. Using the recorded mass changes, the volume of water absorbed per unit cross-sectional area was calculated for each time interval. A plot was then created to show the relationship between the square root of time and the volume of water absorbed. The rate of mass absorption, which is denoted by "I," is calculated by dividing the change in mass by the product of the cross-sectional area of the test specimen and the density of water.

$$I = \frac{m_t}{a \times d} \qquad 3.2$$

Where,

I = the absorption by specimen (mm)
mt = change in mass of specimen in grams (g) at time interval 't'
a = exposed cross-sectional area of specimen, (mm^2)
d= density of water, (g/mm^3)

The rate at which water is absorbed ($mm/s^{1/2}$) is calculated by finding the slope of the line that best fits a plot of 'I' versus the square root of time ($s^{1/2}$). The slope is determined by least squares, linear regression analysis of the plot of I against $time^{1/2}$.

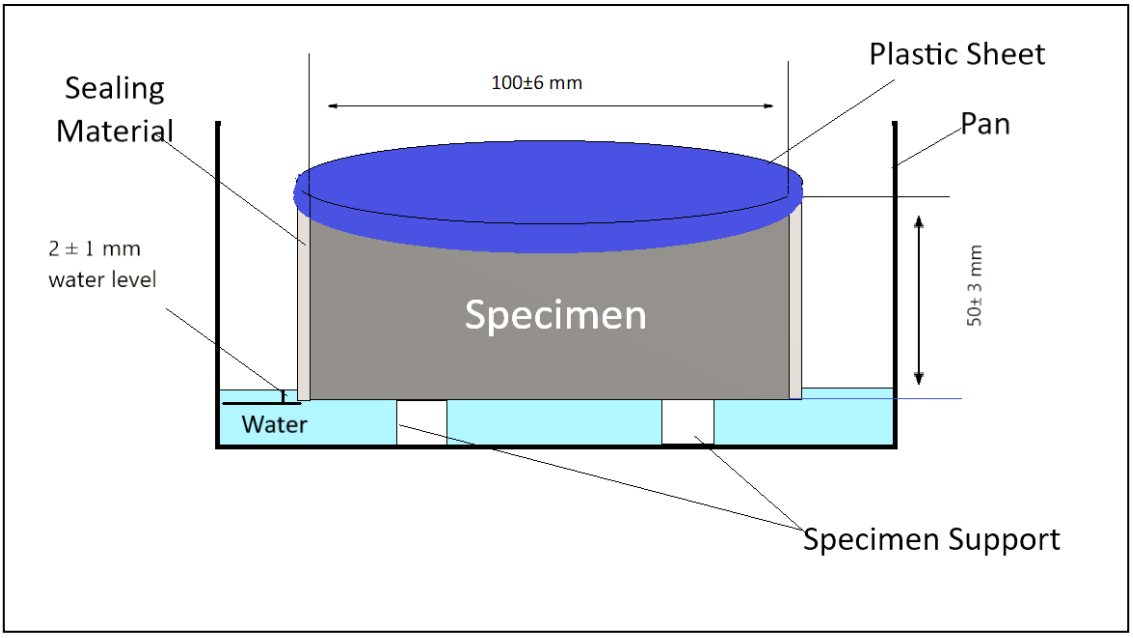


Fig. 3.4 Schematic representation of the sorptivity test

3.8.3.3 Rapid chloride permeability test (RCPT)

The RCPT test was performed to determine its resistance to chloride ion penetration. This test method involves saturating the concrete specimens and monitoring the amount of electrical current that passed through a concrete sample over a period of 6 hours measured using an LCD connected to the cell. A 60 V DC potential difference was sustained across the specimen, with one end submerged in a sodium chloride (3.0%) solution and the other in a sodium hydroxide (0.3 N) solution. The total charge passed (in terms of coulombs) is directly proportional to the electrical conductance of the concrete and a measure of its chloride penetrability.

Conditioning of concrete specimen:

To prepare de-aerated water, tap water was boiled in a large, sealable container and then it was cooled at room temperature. Next, a rapid setting sealant was applied to the side surfaces of concrete disc samples using a brush, and the samples were allowed to cure until the sealant was no longer sticky to the touch. The coated samples were then placed in a vacuum desiccator with both end faces exposed, and the desiccator was sealed with a cover after being filled with the previously prepared de-aerated water. The vacuum pump was started, and the pressure was decreased to less than 50 mm Hg within a few minutes. The vacuum was maintained for 3 hours, after which the vacuum line stopcock was closed and the pump was turned off. The test samples were then soaked in water in a beaker for 18 ± 2 hours.

Test procedure

The conditioned samples were carefully removed from the water and the excess moisture was wiped away with a damp paper towel. Samples were installed into the voltage cell and rubber gaskets were used to make it water tight. One side of the cell was connected to the negative terminal of the power supply and filled with 3.0% NaCl solution. The second side of the cell was filled with 0.3 N NaOH solution and connected to the positive terminal of the power supply. Power supply was turned on. The concrete disc sample was placed inside the voltage test cell and was subjected to a potential difference of 60 V for a duration of 6 hours. The voltage of the apparatus was monitored every 30 minutes while the current was recorded automatically by the data acquisition device (Fig. 3.5). The test was concluded after 6 hours, and the concrete samples were removed. During the test, automated data processing machinery performed the integration and exhibited the coulomb value. The electrical conductance of the concrete during the 6-hour period of the test serves as a measure of the total charge passed. The test result rates the chloride ion penetrability of concrete as shown in Table 3.4.

Table 3.4 Rating of chloride penetrability of concrete

Charge passed (coulombs)	Chloride ion penetrability
>4000	High
2000 – 4000	Moderate
1000 – 2000	Low
100 - 1000	Very low
<100	negligible



Fig. 3.5 Setup for rapid chloride permeability test (RCPT)

3.8.4 Microstructural analysis and XRD

To determine the crystallization in concrete by bacterial treatment, a small chunk of the concrete sample was taken for microstructural investigation. The samples were sputter-coated with gold after careful polishing. FESEM-EDS was performed to determine the elements constituting the microstructural crystals. X-ray diffraction (XRD) was performed to identify minerals and crystal formation in the samples. A Bruker D8 X-ray diffractometer was used to conduct X-ray diffraction (XRD), which involved scanning from 20°to 60° at a two-theta angle with a Cu anode (40 kV and 30 mA).

3.9 Development of metakaolin based bacterial carrier material

MICCP have shown promising results in strength enhancement and reduction in permeability. For crack remediation, the bacterial immobilized carrier material was developed by incorporating the carrier material in concrete mix during the cast. Moreover, using spores instead of freshly inoculated culture using a porous adsorption material will ensure the viability of the biomaterial for a longer duration.

3.9.1 Spore preparation

The current study was further extended to develop metakaolin as a sustainable carrier material for immobilizing bacterial spores using an adsorption technique. To prepare spores of the bacterial strain *B. paramycoides*, commercial nutrient broth (NB) media and industrial waste corn steep liquor (CSL) media were used. Nutrient-deficient nutrient broth media (NB 3 g/L, $NaHCO_3$ 2.12 g/L, urea, 10 g/L) and corn steep liquor media (CSL 3 ml/L, $NaHCO_3$ 2.12 g/L, urea, 10 g/L) were prepared as reported by Pungrmi et al. (2019). The medium flask was incubated at 28 °C ± 2 °C in an incubator shaker at 100 rpm for seven days. After the incubation period, the spores were exposed to heat shock in a water bath at 80 °C for 10 min to stimulate spore formation for any remaining vegetative cells. Following heat shock, the spores were subjected to cold shock for ten minutes by placing the flask in chilled or crushed ice. The bacterial spores were collected after centrifugation at 5000 rpm for 10 min. The pellet was washed with 0.85% saline to remove any additional NB or CSL medium and was suspended in distilled water. The spore concentration was evaluated using the colony-forming unit (CFU) count. The intactness of the spores was tested by subjecting the cells to endospore staining with by Schaeffer-Fulton endospore staining method (Hussey 2013). The spores were visualized using a compound microscope. As shown in Fig. 3.6, the spores exhibited a circular morphology and dark blue-purple staining of the outer coating, which is expected for integral cell walls. The spore concentration was evaluated using the colony-forming unit (CFU) count.

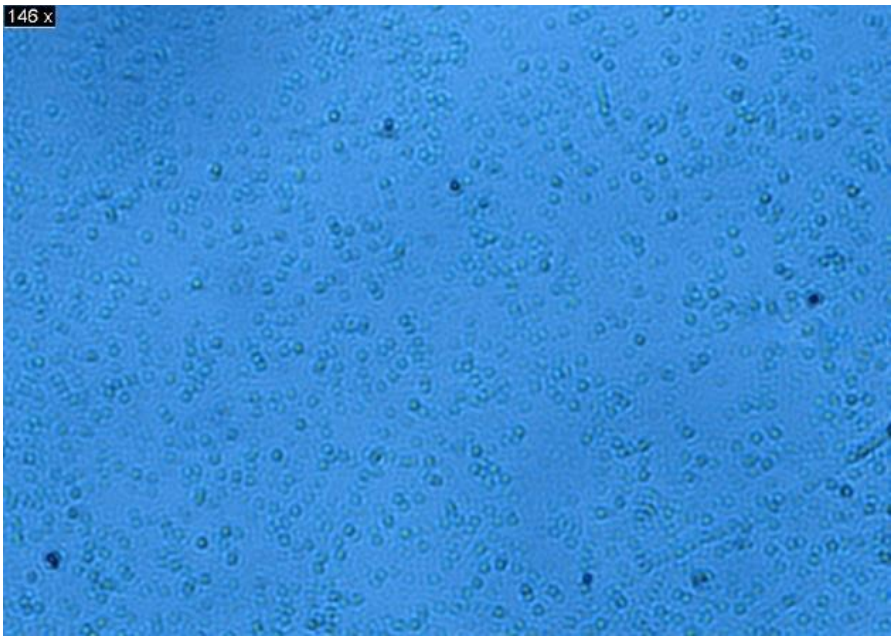


Fig. 3.6 *Bacillus paramycoides* MD6 spores

3.9.2 Development of metakaolin carrier material

To immobilize the bacterial spores in MK, it is important to mix the spore suspension gently and maintain a longer contact time between the spores and metakaolin during the mixing time. A concentration of 5.2×10^{-5} spores was uniformly mixed in the MK powder under aseptic conditions. MK powder was used as a carrier material to immobilize the spores. A moisture content of 20% was maintained in the MK material to mix the spores in the biomaterial uniformly (Anand et al. 2022b). The moisture content should be sufficient for the spores to adhere to the metakaolin particles. To immobilize spores with MK, the mixture was allowed to remain for a few hours. This period allows the spores to interact with the metakaolin particles and establish an immobilization matrix by forming a strong interlinking bond with the metakaolin particles. After development, the mixture can be dried under controlled conditions, such as a lyophilizer to remove excess moisture. Drying ensures the stability and viability of spores for a longer duration. The spore-infused biomaterial was freeze-dried at -20 °C, followed by lyophilization at -55 °C to remove moisture and immobilize the spores in metakaolin powder. A schematic representation of bacterial spore formation and immobilization in MK for the development of biomaterials is shown in Fig. 3.7.

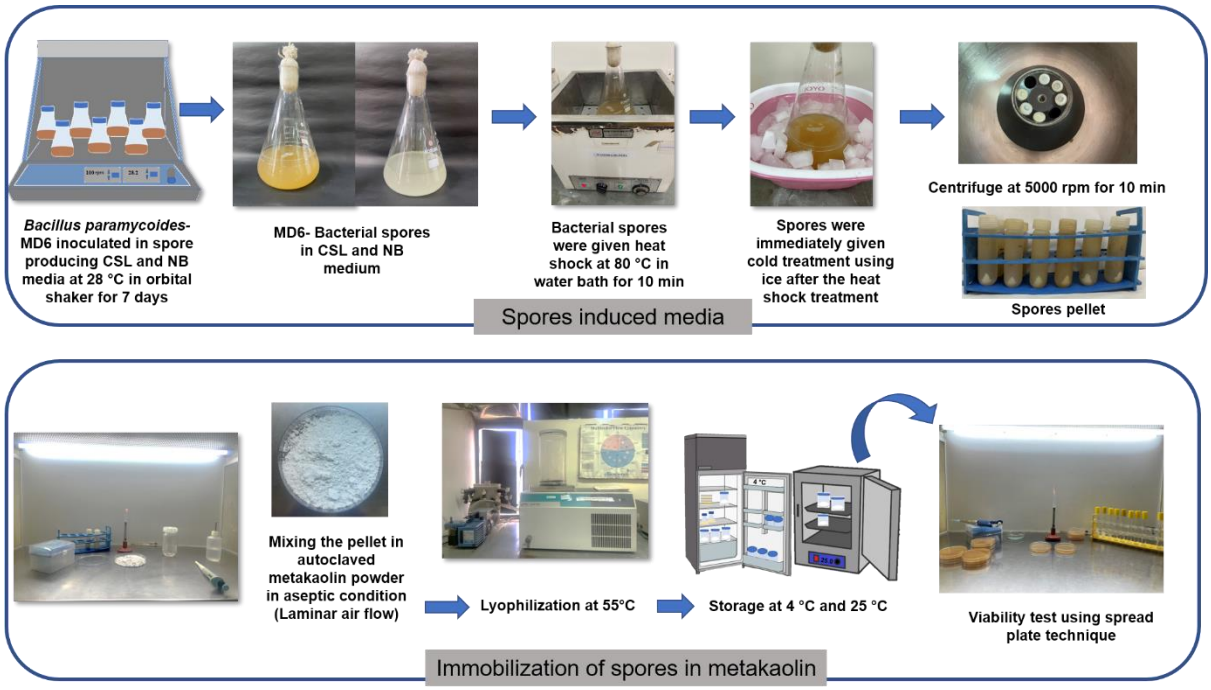


Fig. 3.7 Schematic illustration of *Bacillus paramycoides*- MD6 spores' development and storage after the immobilization in metakaolin (MK) material by lyophilization technique

3.9.3 Storage and viability test

The spore-immobilized MK material, labeled as a biomaterial, was stored in sterile petri dishes at 25 °C and 4 °C. Viability tests were conducted at regular intervals of seven days during storage. The biomaterials stored at 25 °C were labeled as NB-25 and CSL-25, and those stored at 4 °C were labeled as NB-4 and CSL-4. One gram of the sample was weighed from each stored petri plate and suspended in 9 ml of a 0.85% saline test tube. Dilutions were made to 10^{-8} by transferring 1 ml of the dilution to each test tube (Fig. 3.8). The efficiency of immobilized spores in the MK carrier material was determined using the CFU count. One hundred microliters of the aliquot were spread on nutrient agar plates using a sterilized spreader. The nutrient agar plates were incubated at 37 °C for 24 – 48 h. The colony forming units per gram were expressed by determining the log value of the colonies that appeared on nutrient agar plates.

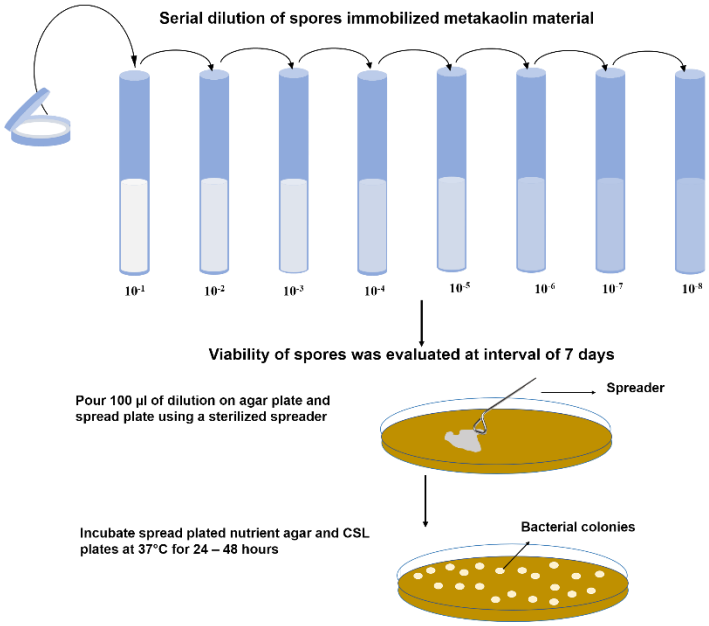


Fig. 3.8 Schematic representation of the serial dilution technique and nutrient agar plates showing spore viability after 24 h of incubation at 37 °C

3.9.4 Urease activity and $CaCO_3$ precipitation

The biomaterial was stored for 180 d at 25 °C and 4 °C. The efficiency of the biomaterial was tested by quantifying the urease activity and $CaCO_3$ precipitation after 180 days of storage. To evaluate urease activity, 1% of the biomaterial inoculum (NB-25, CSL-25, NB-4, and CSL-4) was incubated in NB and CSL broth supplemented with 2% urea. The experiment was

performed in triplicate and the flasks were incubated at 37 °C for 120 h. Urease activity was measured every 24 h using a phenol-hypochlorite assay as described by Natarajan (1995). The urease activity was calculated by standardizing the attained value using the ammonium chloride standard curve (Fig. 3.9). One unit of urease is equivalent to the amount of urease degrading one µM urea per minute (Li et al. 2022a).

For $CaCO_3$ precipitation, NB and CSL broths were inoculated with 1% biomaterial inoculum (NB-25, CSL-25, NB-4, and CSL-4) and supplemented with 2% urea and 25 mM $CaCl_2$. The broth was then incubated at 37 °C for 144 h. At each 24 h interval, the solution was filtered using a vacuum membrane filtration technique (0.45 micrometer). The $CaCO_3$ precipitate was collected on a membrane filter paper. The precipitate was then washed with 95% ethanol and dried at room temperature. The weight of the crystals deposited on the filter paper was taken as the amount of $CaCO_3$ precipitated at each interval. The stored biomaterial that performed the best in the viability test, urease assay, and $CaCO_3$ precipitation was used as a potential self-healing biomaterial for concrete testing.

3.9.5 Preparation of concrete specimens

To investigate the effect of the biomaterial on the concrete properties, the specimens were cast using biomaterial stored at 4 °C (selected based on viability and urease activity tests). Prismatic specimens of 500 × 100 × 100 mm, 150 mm cubes, and 100 mm (dia) × 200 mm (ht) cylindrical concrete specimens were cast using cement, sand, and coarse aggregate in the proportion of 1:1.82:3.24 (by wt.) and 0.47 water-to-cement ratio (w/c), as listed in Table 3.5. The 2% biomaterial stored at 4 °C was added as supplementary material during the mixing of the concrete constituents. The specimens were divided into three categories; control, CSL-4, and NB-4. Similarly, for crack remediation, prismatic specimens were cast using the same mix proportions mentioned above. Reinforced concrete (RC) specimens with dimensions of 400 mm × 100 mm × 100 mm were prepared by embedding a 12 mm rebar at the center and curing for 28 days. To generate cracks, the prepared RC specimens were subjected to a four-point bending failure (IS 516 2021) to attain a crack width of approximately 0.5 mm (Fig. 3.9a). Trials were conducted to achieve crack width of 0.5 mm.

3.9.6 Concrete testing

Prismatic specimens with dimensions of 500 × 100 × 100 mm and 150 mm cubes were tested for flexural and compressive strengths after 7 and 28 d of curing (IS 516 2021). Cylindrical

specimens of 100 × 50 mm were tested for water absorption (ASTM C1585 2013) after 7 and 28 d of curing. All experiments were performed in triplicates. The protocol for the same was mentioned in section 3.8.3.1 and 3.8.3.2.

Table 3.5 Mix proportion of the concrete specimens

	Mix proportion (kg/m^3)					
Specimens	Cement	Sand	Metakaolin bio-composite	Coarse aggregate		Water/nutrient growth medium
				10 mm	20 mm	
Control	396	722	--	770	513	186
Biomaterial	396	722	7.94**	770	513	186*

*CSL growth medium composed of CSL broth (1.3% w/v), urea (2% w/v), and 25 mM $CaCl_2$
*NB growth medium composed of NB broth (1.3% w/v), urea (2% w/v), and 25 mM $CaCl_2$
**metakaolin biomaterial stored at 4 °C & 180 days storage age

3.9.7 Crack remediation and monitoring

The cracked prism specimen consisting of the biomaterial inoculum (NB-4 and CSL-4) was subjected to self-healing treatment at room temperature. Initially, the cracked region was injected with CSL and NB growth media supplemented with 2% urea and 25 mM calcium chloride ($CaCl_2$) so that nutrients could reach the depth of the crack. The $CaCl_2$ used in the present investigation was 25 mM (3.67 g/L), which is within permissible limits and does not affect the rebar (Paine 2016). CSL and NB growth media were injected using a syringe four times a day to activate the spores immobilized in the biomaterial. Subsequently, the spray treatment was repeated daily until complete healing of the cracked region was achieved. The ultrasonic pulse velocity (UPV) was measured at different crack healing percentages to determine the efficiency of the MICCP (ASTM C 597 2016). The UPV value was estimated by placing the transducer and receiver 100 mm from the crack, as shown in Fig. 3.9b. Measurements were taken at different time intervals.

The water tightness was examined until complete crack healing was achieved (Pal et al. 2020). For this experiment, three different regions were marked A, B, and C on the crack region to determine the amount of water flowing through the crack (Fig. 3.9c). The flow rate was estimated based on the amount of water flowing through the crack within 20 s. A 50 ml measuring cylinder was adhesively attached with the help of clay to the surface to avoid water leakage. Experiments were conducted until the cracks were completely closed. Crack-sealing

efficiency was evaluated based on the amount of water flowing through the defined crack region. Crack-sealing efficiency was evaluated using Equation 3.3 (Liu et al. 2020b).

$$\text{Sealing efficiency } (\%) = \frac{\text{WF.}_i\text{-WF.}_t}{\text{WF.}_i} \times 100 \qquad 3.3$$

where WF_i is the initial water flow and WF_t is the final water flow in the crack at different time intervals.

3.9.8 Visual monitoring of crack closure

During the crack remediation process, the reduction in the crack width was periodically monitored using a DinoLite microscope. To better understand the crack closure using MICCP, the crack width along the defined length was measured during the healing process. The average of the multiple readings for a particular duration was recorded. The crack-healing efficiency was evaluated according to Equation 3.4 (González et al. 2020).

$$\text{Crack healing efficiency } (\%) = \frac{\text{CW.}_i\text{-CW.}_t}{\text{CW.}_i} \times 100 \qquad 3.4$$

CW_i is the initial crack width and CW_t is the crack width at different time intervals.

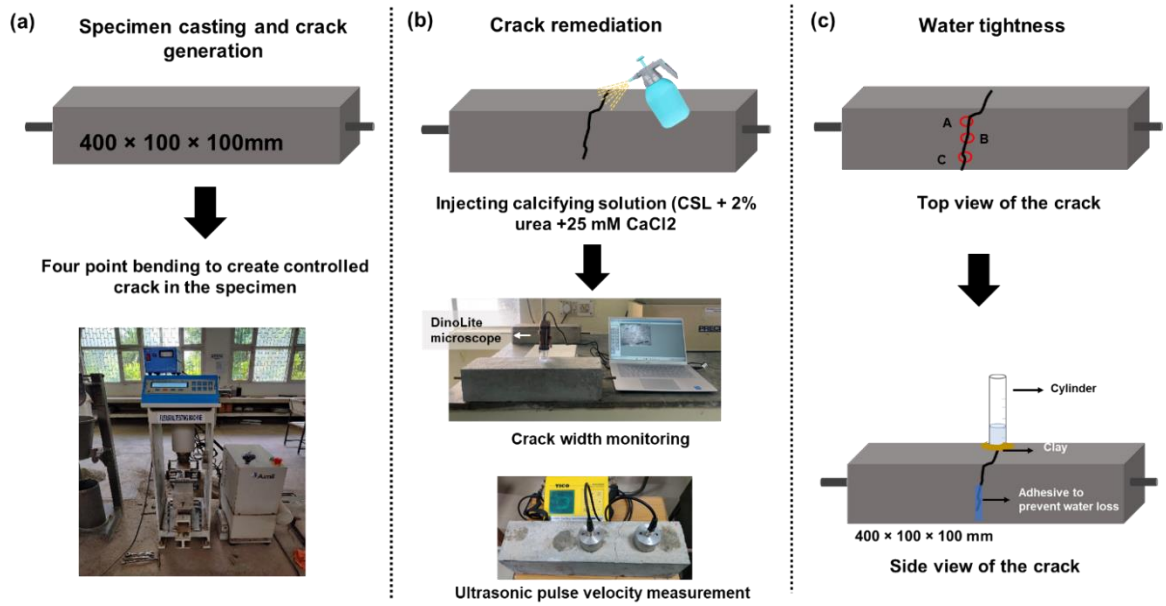


Fig. 3.9 (a) Four-point bending failure to generate the controlled crack (b) crack remediation and monitoring (c) water tightness test; top view of the specimen marked with three different locations of the water flow test on the specimens and side view of the setup of the water flow test with measuring cylinder adhesively attached to the specimen

3.9.9 Microstructural analysis

To determine the $CaCO_3$ precipitation in the bacterial-cured specimens after 28 days of curing, the samples were examined using field emission scanning electron microscopy (FESEM). Energy dispersive spectroscopy (EDS) was performed to confirm the elemental composition of the precipitate in the concrete. The samples were gold-coated, polished, and coated with carbon to disperse extra charges. X-ray diffraction (XRD) scanning was performed on the powdered concrete samples from 20° to 60° at 2θ angles with a Cu anode (40 kV and 30 mA) using a Bruker D8 X-ray diffractometer.

3(B) Photoautotrophic Bacteria

Unicellular marine cyanobacterial strains *Aphanocapsa montana* BDU21001, *Aphanothece* species BDHKU 40501, *Gleocapsa* species BDU 40111, *Synechococcus elongatus* BDU14174, and *Synechocystios pevalekii* BDHKU 35101 were obtained from the National Facility of Marine Cyanobacteria, Bharathidasan University, Tiruchirappalli, Tamil Nadu, India.

3.10 Cultivation and cell preparation

All the strains were grown in BG 11 medium: $NaNO_3$ 1.5 g, K_2HPO4 0.04 g, $MgSO_4 \cdot 7H_2O$ 0.075 g, $CaCl_2 \cdot 2H_2O$ 0.036 g, Citric acid 0.006 g, Ferric ammonium citrate 0.006 g, EDTA (disodium salt) 0.001 g, Na_2CO_3 0.02 g, Trace metal mix A5 1.0 ml. trace metal mix A5: H_3BO_3 2.86 g, $MnCl_2.4H_2O$ 1.81g, $ZnSO_4.7H_2O$ 0.222 g, $NaMoO_4.2H_2O$ 0.39 g, $CuSO_4.5H_2O$ 0.079 g, $Co(NO_3)_2.H_2O$ 49.4 mg and Distilled water 1.0 L (Rippka et al. 1979). The batch cultures of each strain were maintained in 250 ml Erlenmeyer flasks containing 100 ml of medium, which was constantly shaken at 110 rpm at temperature of 25 ± 2 °C (Fig. 3.10). Illumination was provided at an intensity of 1200 lux, with a photoperiod of 12 hours of light followed by 12 hours of dark. After reaching the stationary growth phase, cyanobacterial cells were collected by centrifuging the culture at 5000 rpm for 15 min. The cells were then washed in a sterilized 0.1 M sodium nitrate ($NaNO_3$) solution through three cycles of centrifugation, discarding the supernatant, and resuspending in 0.1 M $NaNO_3$ solution. After the final wash, the cells were washed again in 0.1 M NaCl solution and resuspended in BG11 broth.

3.10.1 Growth cycle

The cyanobacterial strains *Aphanocapsa montana* BDU21001, *Aphanothece* species BDHKU 40501, *Gleocapsa* species BDU 40111, *Synechococcus elongatus* BDU14174, and *Synechocystios pevalekii* BDHKU 35101 was inoculated in autoclaved BG11 broth. The initial O.D was kept constant in the broth 0.01 and incubated at 25 ± 2 °C and constantly shaken at 110 rpm under an illumination photoperiod of 12:12 h (light: dark). The growth was analyzed by measuring the O.D. at 680 nm at regular interval of time.

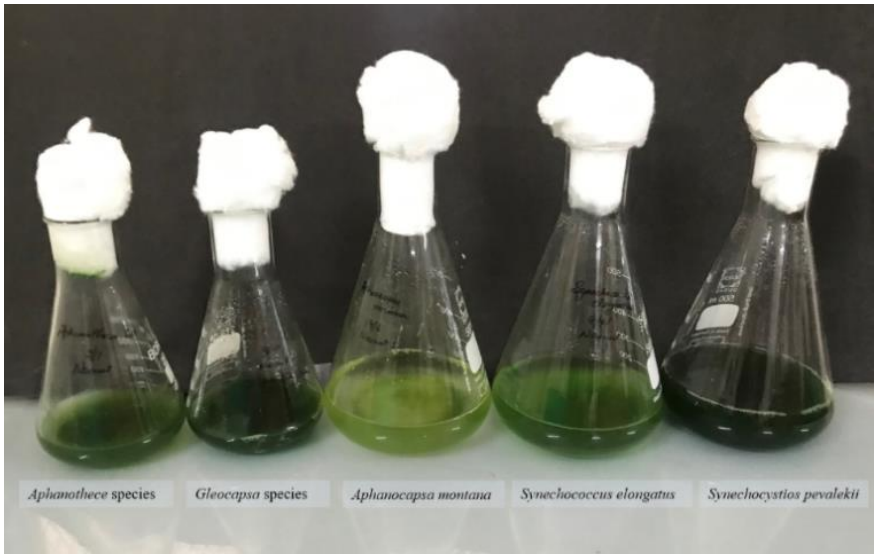


Fig. 3.10 Photoautotrophic strains *Aphanocapsa montana* BDU21001, *Aphanothece* species BDHKU 40501, *Gleocapsa* species BDU 40111, *Synechococcus elongatus* BDU14174, and *Synechocystios pevalekii* BDHKU 35101 grown in BG11 broth

3.10.2 Microbial calcium carbonate precipitation experiment

Cyanobacterial cells of each strain with an optical density (O.D. – 1.0) were inoculated into 250 ml Erlenmeyer flasks containing 90 ml of BG11 medium supplemented with 50 mM sodium bicarbonate ($NaHCO_3$) and 100 mM calcium chloride ($CaCl_2$), incubated at temperature (25 ± 2 °C), and constantly shaken at 110 rpm under an illumination photoperiod of 12:12 h (light: dark). The concentration of $CaCl_2$ used is within the range of concentrations employed in other studies on MICCP (Zhu et al. 2017). All samples were prepared in triplicate. At each 24 h interval, the solution was filtered using a vacuum membrane filtration technique (0.45 micrometer). The $CaCO_3$ precipitate was collected on a membrane filter paper. The precipitate was then washed with 95% ethanol and dried at room temperature. The weight of the $CaCO_3$ precipitates collected of the filter paper was measured.

3.10.2.1 Microstructural analysis

The $CaCO_3$ crystals precipitated by photoautotrophic strains were analyzed using SEM-EDX for their morphology. The elemental composition of the precipitates was determined by XRD analysis. At each 24 h interval, the solution was filtered using a vacuum membrane filtration technique (0.45 micrometer). The $CaCO_3$ precipitate was collected on a membrane filter paper. The precipitate was then washed with 95% ethanol and dried at room temperature. The $CaCO_3$

crystals were examined by SEM (Zeiss EVO50) at accelerating voltages ranging from 15 to 35 kV, equipped with an energy dispersive X-ray analyzer (Bruker-AXS, QuanTax 200) for elemental analysis. Samples were gold-coated with a sputter coating Emitech K575 before the examination.

3.10.3 Selection of highest $CaCO_3$ precipitating strain

Based on the experiment explained in section 3.11.2, microbial calcium carbonate precipitation experiments the cyanobacterial strain with highest $CaCO_3$ precipitation was selected for the further testing.

3.10.4 Influence of different initial pH on $CaCO_3$ precipitation

The BG11 broth with varied initial pH (6, 7, 8, 9, 10, 11, and 12) was supplemented with calcifying solutions. The cell culture was inoculated with an optical density (O.D. – 1.0) in BG11 broth and incubated at (25 ± 2 °C) as mentioned in section 3.11.2. The experiment was conducted for 120 h in two experiment set. In first set of experiment, the $CaCO_3$ precipitated in the flask was collected on Whatman filter paper at 24 h intervals. The precipitate from each flask was washed with 95% ethanol and room-dried for 6 h. The amount of powdered $CaCO_3$ collected on Whatman filter paper was weighed. In the second set of experiments, one ml of aliquot was taken from the flask at 24, 48, 72, 96, and 120 h and centrifuged to measure the amount of soluble Ca^{2+} content in the supernatant after the centrifugation using the EDTA titration method (Stocks-Fischer et al. 1999). The protocol is described in section 3.7.3. The calcium removal percentage (%) was evaluated based on soluble calcium (Ca^{2+}) ions.

3.11 Influence of Live (LV) and UV-treatment (UVT) cells in sand consolidation and improvement of cementitious material

3.11.1 Pre-treatment of cells

Cells were harvested after reaching the logarithmic growth stage and collected by centrifugation at 5000 rpm for 15 min. Cells were washed by three cycles of centrifugation, disposing of the supernatant, resuspension of cells in sterilized 0.1 M $NaNO_3$ solution, and finally in 0.1 M NaCl solution prior to the experiments. The cyanobacterial cell suspension was resuspended in BG 11 broth after washing with NaCl solution. Two different treatments, "live treated (LT) cells and ultraviolet treated cells (UVT) were selected for the experiment. To kill

the cells, one-half of the cell suspension was exposed to UV light for 1 h, and the remaining live-cell suspension was kept for the live treatment experiment.

3.11.2 Sand consolidation

To determine the binding property of crystals the sand consolidation experiment was performed using live and UV treated cells. For UV treatment, *S. pevalekii* cell suspension was exposed to UV light for 1 hour. For the sand column, locally available clean, dry, well-graded, natural river sand was used. The sand was sieved through 300 μm mesh and autoclaved to remove the indigenous microflora (Hamamura et al. 2006). To prepare a sand slurry, the moisture content of 25% was maintained in sand column. The live (LT) and UV treated (UVT) cells were taken and resuspended in 25 ml sterilized calcifying media. The bacterial suspension was further mixed with 100g sand to make sand slurry under aseptic conditions. Sand slurry was filled into a plastic tube (height 7.6 cm; diameter 3.8 cm). The bottom portion of each column was wrapped with Whatman filter paper. A burette was attached at the top of the plastic column so that calcification media could be dropped at a constant amount through the column. The control sets were made similar way without the bacterial cells, while other specimens had the bacterial inoculum mixed. Outline for the experimental setup and calcifying solution used are presented in as shown in Table 3.6. All the columns were fed with 25 ml calcification media twice with a 12-hour duration at room temperature for 14 days. From the bottom of the sand columns, the effluent was collected in the beaker at regular intervals of 0, 2, 4, 6, 8, 10, 12, and 14 days to estimate the flow rate and pH to assess the activity of cyanobacterial cells within the sand columns. The sand column was opened on day-15, and the consolidated sand column was dried in an oven at 70 °C for 24 h. Samples were digested in 1.0 M hydrochloric acid at 40 °C under continuous stirring and were divided into three layers to estimate the amount of precipitation in each layer using the EDTA titration method (Stocks-Fischer et al. 1999). A protocol of EDTA titration is explained in section 3.5 A small sample piece of upper consolidated sand layer was taken further for microstructural analysis (SEM-EDS).

Table 3.6 Sand consolidation experiment set-up with different calcifying media

Groups	**Composition of sand column**	**Calcifying media**
Live cells (LT)	Sand (300 μm) + cyanobacterial cells + $CaCl_2$ + $NaHCO_3$	cyanobacterial cells + $CaCl_2$ (100mM) + $NaHCO_3$ (50 mM)
UV treated cells (UVT)	Sand (300 μm) + cyanobacterial cells + $CaCl_2$ + $NaHCO_3$	cyanobacterial cells + $CaCl_2$ (100mM) + $NaHCO_3$ (50 mM)
Control	Sand (300 μm) + Deionized water	Deionized water

3.11.3 Surface treatment of mortar by ponding

Mortar cubes of 50 × 50 × 50 mm were prepared and cured for 28 days in water. For the mortar mixture, the cement: sand mass ratio was kept as 1:3 (w/w) with a water to cement ratio (w/c) of 0.47. After curing, a reservoir of 50 × 50 × 50 mm was made with the help of an acrylic sheet to expose the single face of the mortar cube (Fig. 3.11). The pool was filled with the solution of calcium chloride (100 mM), and sodium bicarbonate (25 mM) along with live (LT) and UV treated (UVT) *S. pevalekii* cells. The curing of cubes was done for 7 days. The SEM. analysis was performed to identify the crystal structure.

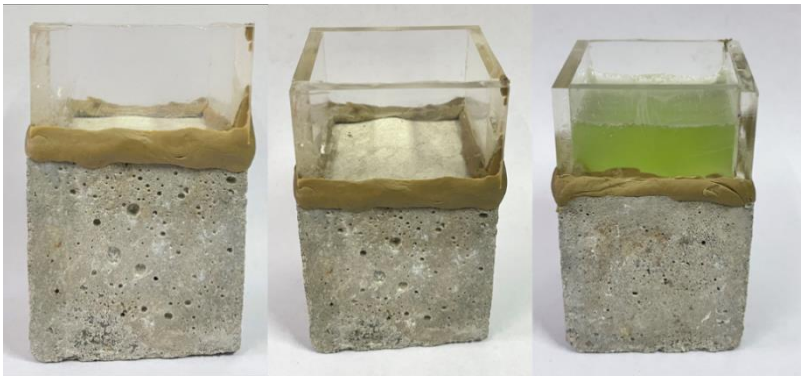


Fig. 3.11 Surface ponding by *S. pevalekii* calcifying solution on the cement mortar

3.11.4 Preparation of mortar specimens

Mortar cubes of 70.6 × 70.6 × 70.6 mm were cast using an ordinary Portland cement (43 Grade) according to the IS: 8112 (2013). Locally available natural river sand was used as fine aggregate corroborative to Zone II as per Indian standard (IS 383 2016). Cement mortar mix was prepared by using cement: sand in the ratio of 1:3 (w/w) and water to cement ratio (w/c) of 0.47 as per IS: 4031 (2005). To cast cyanobacterial-treated mortars, both live and UV-treated *S. pevalleikii* (4×10^8 cells/ml) culture was used instead of water. The bacterial culture to cement ratio was also maintained at 0.47. Freshly mixed ingredients at the plastic stage were immediately transferred into iron moulds in the casting room at room temperature of 27 ± 2 °C. After 24 h, the specimens were demolded and cured till the testing age. Different treatments, materials used, and the method of curing are mentioned in Table 3.7. The mortar specimens were divided into three groups. The first group was subjected to live *S. pevalleikii* cells, the second group with UV treated culture, and the third group without bacterial treatment. All the mortar specimens were cured for 3-day, 7-day, and 28-day with their respective medium

as mentioned in Table 3.6. Cyanobacterial-treated specimens were initially submerged in live, and UV killed culture for 24 hours and then in BG11 medium with 50 mM $NaHCO_3$ and 100 mM $CaCl_2$ in a plastic container at room temperature of 30 ± 2 °C for different curing periods. All specimens were exposed to a light intensity of 1200 lux for 12 h and kept under darkness for 12 h. For 28-day curing specimens, the cubes were incubated in culture for 24 hrs at the beginning of every week and then transferred to BG11 medium with 50 mM $NaHCO_3$ and 100 mM $CaCl_2$. At the end of the experiment, mortar specimens were dried in an oven at 72˚C for 24 hrs, and analyzed for various parameters.

Table 3.7 Outline of different sets of mortar specimens and mechanism of curing treatment

Specimens	Material used	Mechanism of curing
Control	Cement: Sand: 1:3 Water/cement ratio 0.47	Water curing for 3,7 and 28 days
LT	Cement: Sand: 1:3; Live *S. pevalekii* culture/cement ratio 0.47	Curing for 3,7 and 28* days in BG11 medium supplied with 100 mM $CaCl_2$, 50 mM $NaHCO_3$.
UVT	Cement: Sand: 1:3; UV-treated *S. pevalekii* culture/cement ratio 0.47	Curing for 3,7 and 28* days in BG11 medium supplied with 100 mM $CaCl_2$, 50 mM $NaHCO_3$

*Mortar cubes were incubated in culture for 24 hrs. at the beginning of every week and then transferred to medium

3.11.4.1 Testing of mortar specimens

Compressive strength

The compressive strength was measured at 3, 7 and 28 days of curing as per the Indian standard IS 516 2021. The compression test was carried out using the COMPTEST 3000 automatic compression testing machine (AIMIL India Ltd, New Delhi). The protocol has been explained in section 3.8.3.1

Water absorption test

A water absorption test was performed based on the RILEM 25 P.E.M. (II-6) as described in Achal et al. (2011). The mortar specimens were cured for 7 and 28 days. After which the samples were dried at 45 °C in a ventilated oven until the result in a mass balance of less than 0.1% between two measurements taken 24 hours apart. The four sides of the cube specimens were coated with the epoxy to avoid evaporation and dried at room temperature. The upper

surface of the cube was covered with plastic sheet which was secured with rubber band. The other surface was exposed to the water 10 ± 1 mm at room temperature of 25 ± 2 °C. The specimens were removed at regular time intervals (15 min, 30min, 1h, 1.5 h, 3h, 5 h, 8h, 24h, 72h, 96h, 120 h, and 144h) and weighed after drying the surface with a wet towel. The test specimens were immediately submerged again after being measured. The sorptivity coefficient, k (g.cm $s^{-1/2}$.$h^{-1/2}$) was evaluated as:

$$Q = k\sqrt{t} \qquad 3.5$$

where

Q = amount of water absorbed
A = area of the cross section of the specimen in contact with water (cm^2)
t = the time (h)

Q/A was plotted against the square root of time, then k was calculated from the slope of the linear relation between the former.

3.11.4.2 Thermogravimetric analysis (TGA)

Thermogravimetric analysis (TGA) was performed to determine $CaCO_3$ precipitation in mortar specimens. Briefly, the sample was broken, crushed, and powdered into homogenous particle sizes and 20 mg of mortar powder was taken in a TGA holder and increased the temperature constantly up to 850 °C with a heating rate of 10 °C/min. Nitrogen (10 ml/min) was used as a purge gas, and the loss of weight (%) of the sample during heating was plotted against temperature (°C). The weight loss in the temperature range of 550 -750 °C corresponds to $CaCO_3$ decomposition.

3.11.4.3 Microstructural analysis

Scanning electron microscopy (SEM) (ZEISS EVO 50) was performed for the samples at 28-day, and the elemental composition of microstructural crystals was identified with energy-dispersive X-ray spectroscopy (EDX.). Samples were finely polished and gold-coated with a sputter coating. X-ray diffraction (XRD) was performed using Bruker D8 X-ray diffractometer with a Cu anode (40 kV and 30 mA) and scanning from 20 - 60 degrees at a 2θ angle.

3.12 Development of fly ash based cementitious biogrout incorporating cyanobacteria *Synechocystis pevalekii*

The early onset of cracking in concrete structures significantly effects the service life of cementitious structures, resulting in increased maintenance costs. In addition to conventional repair methods, a microbial approach to strengthen and reduce the permeability of the cementitious materials has shown promising results. Therefore, the study was further conducted to develop cyanobacteria incorporated cementitious grouts to repair cracks in existing concrete structures.

3.12.1 Materials

The commercially available ordinary portland cement (OPC, 43 grade) corroborative to Indian standard (IS: 8112 2013) was used. For the cement replacement, fly ash of class F obtained from Rajpura Thermal Plant, Punjab, India, was used. The chemical composition and specific gravity of OPC and FA are presented in Table 3.8. It can be inferred from table that the alumina percentage is 40.3%. It is a bituminous coal that has generally high content of alumina (Yao et al. 2014). As per ASTM C618 (2019) and IS 3812 (2013) standard Class F fly ash has silicon dioxide (SiO_2), aluminum oxide (Al_2O_3), iron oxide (Fe_2O_3) more than 70% of total amount. Many studies are available in literature that reports utilization of fly ash rich in alumina (Achal et al. 2011c; Yu et al. 2020a). Recently, Yu et al. (2023) reported 53.5% of Al_2O_3 is fly ash obtained from thermal power station in central Inner Mongolia of China.

Table 3.8. Chemical composition and specific gravity of ordinary portland cement (grade 43) and fly ash (FA)

Chemical composition (%)	**OPC**	**FA (Class F)**
Calcium oxide (CaO)	65.9	0.5
Silicon dioxide (SiO_2)	21.5	57.2
Aluminum oxide (Al_2O_3)	5.3	40.3
Iron oxide (Fe_2O_3)	3.1	1.0
Sulfur trioxide (SO_3)	1.6	-
Potassium oxide (K_2O)	0.9	0.3
Magnesium oxide (MgO)	0.6	0.1
Sodium oxide (Na_2O)	0.5	0.3
Loss of ignition (LOI)	-	0.7
Specific gravity	3.18	2.33

3.12.2 Grout Mixture Design

The cement grout mixture consists of different ratios of fly ash (0% – 50%) by the total cement mass. The water/binder (w/b) and culture/binder (c/b) are important parameters that have a notable outcome on the fresh and hardened properties of the grout mixtures. Therefore, three different w/b and c/b ratio (0.45, 0.47 and 0.50) were used. In total, 36 grout mixtures were designed to study the impact of different fly ash dosages (0% -50%), w/b, and c/b ratios on the properties of cement grout. The 36-grout mixture dosages with respective c/b and w/b ratios were prepared as mentioned in Table 3.9. The *S. pevalekii* cell suspension was prepared by growing the cell culture at 25 ± 2 °C till it obtained the optical density (OD_{680}) of 1.0. To prepare the biogrout mixture, the water was replaced with *S. pevalekii* cell suspension supplemented with calcium chloride (100 mM) and sodium bicarbonate (25 mM) to the grout mixture. Water-based cement grout, designated as plain grout, and bio-based cement grout, denoted as biogrout, were prepared. The grout mixes containing cement without any FA incorporation are designated as control grout.

Table 3.9 Outline of composition used in the development of 1200g plain (water) and biogrout (*Synechocystis pevalekii* culture) containing a different dosage of FA and cement

S.no.	Cement (g)	Fly ash (g)	*S. pevalekii* culture/water (g)	w/b or c/b	FA (%)
1	1200	0	540	0.45	0
2	1080	120	540	0.45	10
3	960	240	540	0.45	20
4	840	360	540	0.45	30
5	720	480	540	0.45	40
6	600	600	540	0.45	50
7	1200	0	564	0.47	0
8	1080	120	564	0.47	10
9	960	240	564	0.47	20
10	840	360	564	0.47	30
11	720	480	564	0.47	40
12	600	600	564	0.47	50
13	1200	0	600	0.50	0
14	1080	120	600	0.50	10
15	960	240	600	0.50	20
16	840	360	600	0.50	30
17	720	480	600	0.50	40
18	600	600	600	0.50	50

3.12.3 Preparation of the grout mixture

The Hobart-type laboratory mixer (AIMIL India Ltd, New Delhi) was used to prepare the cement-based fly ash grout (Fig. 3.11). As described by Joshi et al. (2021) a standard procedure was followed for mixing the grout. First, cement and fly ash were dry mixed for 60 seconds at slow speed (140 ± 5 rpm) in the mixer. The water was subsequently mixed into the cement and fly ash composite in the mixer, with the mixer operating at a slow speed for the next minute. The speed was then increased immediately for the next 30 seconds. For preparing cyanobacterial cementitious grout, microbial culture (O.D - 0.5) was added into the mixer instead of water. The mixer was stopped for 90 seconds, and during that time, the cementitious grout was properly mixed by hand. Afterwards, the mixer was operated at high speed (285±5 rpm) for the final minute of the mixing process. Thirty-six grout mixtures were prepared to study the fresh properties of the grout to select the best w/b and c/b ratio. All the tests were conducted within 5 to 10 minutes after the preparation of grout to select the best grout for crack remediation with different orientation (Fig. 3.13).

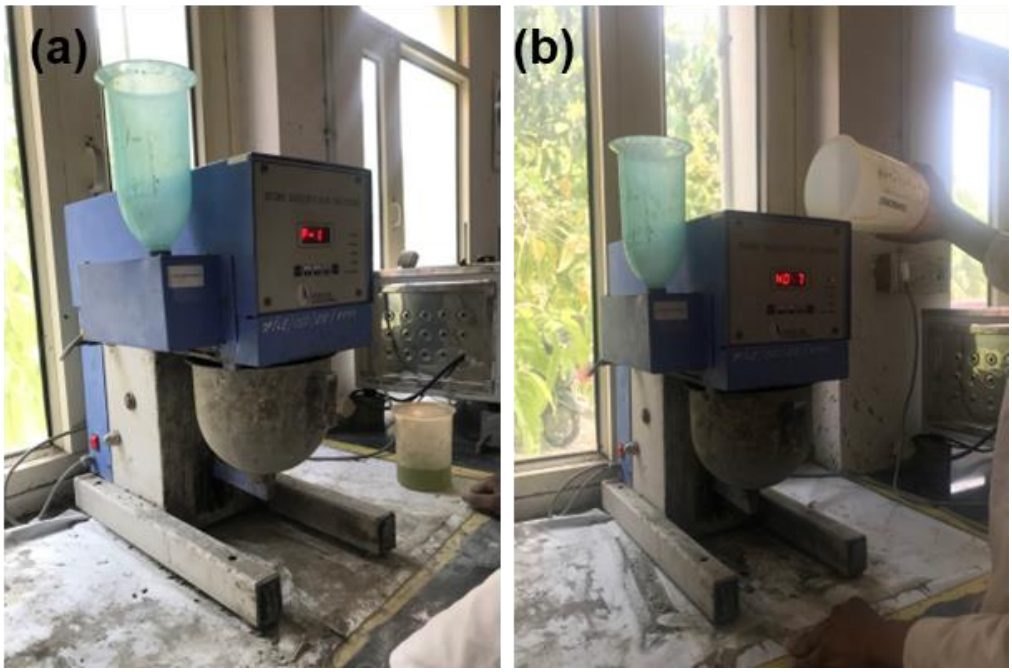


Fig. 3.12 Hobart-type laboratory mixer (AIMIL India Ltd, New Delhi)

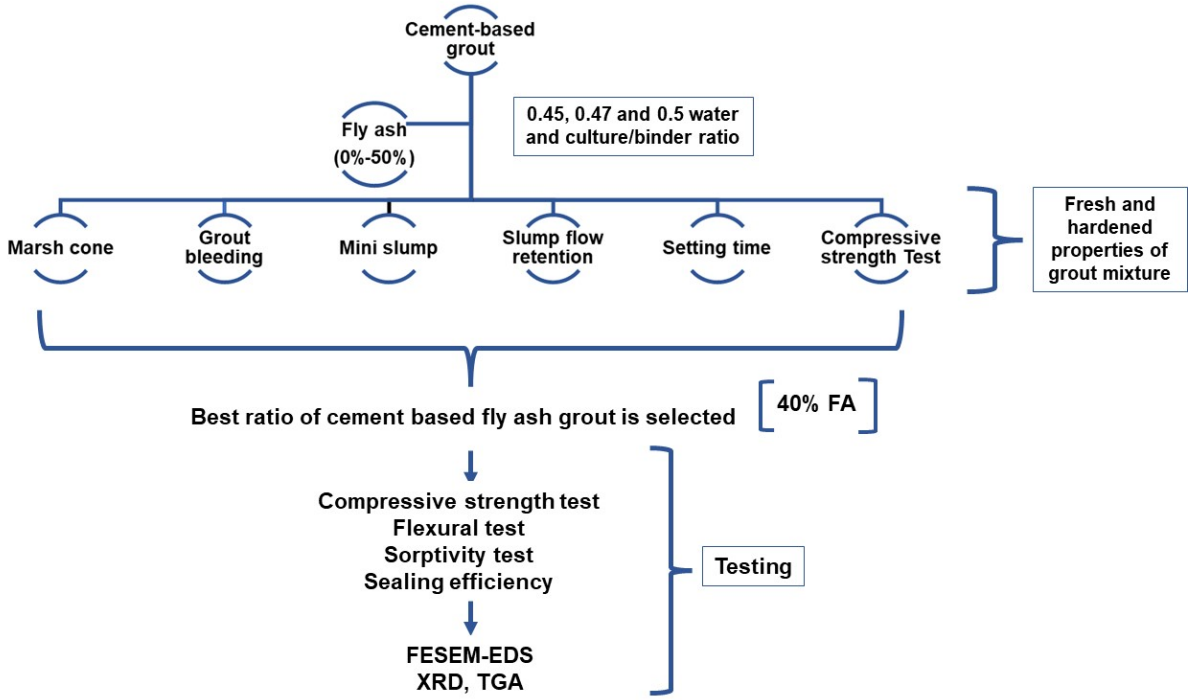


Fig. 3.13 Outline of different techniques used in the development of biogrout incorporating fly ash (0% – 50%) and w/b or c/b (0.45, 0.47, and 0.50) for vertical and horizontal oriented crack remediation

3.12.4 Fresh Properties of Grout Mixture

The cementitious slurry prepared in the laboratory mixture for grout was immediately used within 5 – 10 minutes for different flowability tests. To study the workability and fluidity of cement grout mixture, the marsh cone's flow time, the mini-slump test, grout bleeding, and slump flow retention were tested (Fig. 3.13).

3.12.4.1 Marsh cone

The marsh cone flow test was performed to test the grout mixture's flow characteristics as per ASTM C939 (2010). As shown in Fig. 3.14. the cementitious grout mix was poured into a metallic V-shaped funnel (capacity of 1,500 cm^3) with a secure vent at the end of the funnel, which is 50 mm long by 4.7 mm in diameter. The outflow time required for 800 ml of grout mix to drift out through the orifice was noted as the flow time.

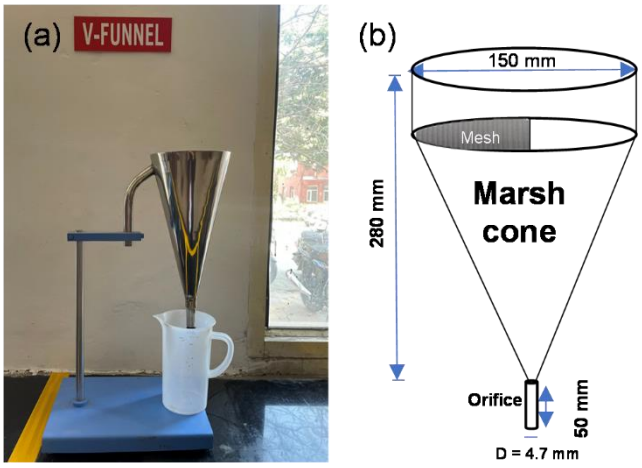


Fig. 3.14 Marsh cone test (a) V-funnel apparatus (b) dimensions of V-funnel

3.12.4.2 Mini slump test

The miniature slump test was done to evaluate the bio-based cement grout's working efficiency by measuring the grout's flow diameter upon lifting the mini-slump cone. The dimensions of the slump cone were similar to those suggested by Kantro (1980). The top and bottom diameter of the cone was 19 mm and 38 mm with 57 mm height (Fig. 3.15). This experiment involved pouring freshly prepared cementitious grout into a mini slump cone that was positioned on a flat surface. The cone was filled completely, and a small spatula was used to remove any air bubbles that were entrapped in the grout by moving it laterally and vertically. The slump cone was lifted, thereby allowing the grout mix to spread. The mini slump area was determined by subtracting the initial area at the base of the mini slump cone from the total spread area. Several diameters of the spread grout were recorded, and the average flow diameter was calculated.

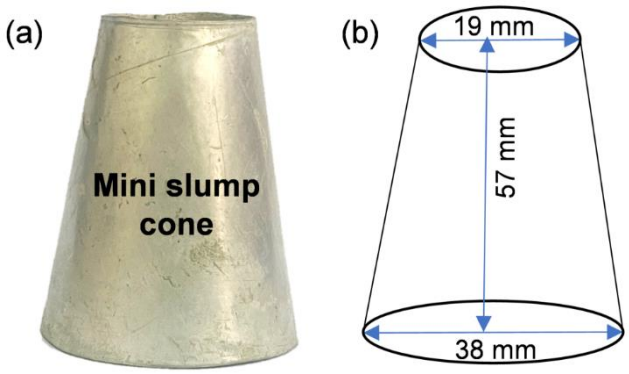


Fig. 3.15 (a) Mini slump cone (b) dimensions of slump cone

3.12.4.3 Grout bleeding

The accumulation of water above the grout surface is called grout bleeding. Excessive bleeding can devitalize the grout strength by increasing porosity and compromising its durability. The bleeding test was conducted according to the ASTM:C940-10a (2010). Following the completion of mixing, introduce the grout into a 1000-mL cylinder until the volume of the sample is 800 mL. Place the cylinder on a level surface free of vibration and cover it to prevent evaporation of the bleed water. The bleed value was noted at an interval of 1 hr for 6 hr (Fig. 3.16).

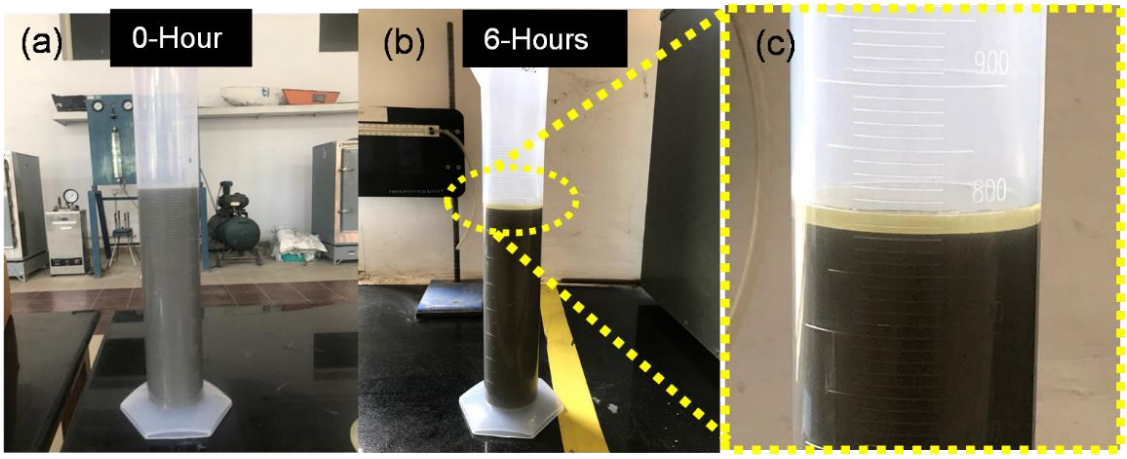


Fig. 3.16 (a) Grout bleeding test at 0-hour (b) Grout bleeding test at 6 hours; (c) square shape shows enlarged image grout bleed at 6 hours

3.12.4.4 Selection of the w/b and c/b ratio

Based on the flowability test, grout mixes with low workability or unmanageable segregation were not selected for further testing.

3.12.4.5 Slump flow retention

To determine the effect of $CaCl_2$ and FA, flow retention time was tested as per ASTM-C1437 (2015) method described by Kaladharan and Rajabipour (2022) for the grout mixes with maximum workability. The flow diameter using mini slump cone was determined at a 20-minute gap of up to 120 minutes after the grout mix first come in contact with water. The mixtures were kept in a closed container after the preparation to prevent loss of water due to evaporation. The mixture was remixed for 2 minutes at 120 rpm before each test. Flow diameter of bio grout at each interval was measured by lifting the cone.

3.12.5 Hardened Properties of Grout Mixes

For measurement of setting time and compressive strength, the grout mix of different ratios of FA (0 – 50) % were used as replacement of cement using 0.47 of c/b and w/b ratio.

3.12.5.1 Setting time

The initial and final setting time for selected biogrout and plain grout was measured by conducting Vicat needle tests (IS: 4031 (Part 6) 2005). Cementitious fly ash-based grout was prepared in the Hobart mixer and filled in the vicat mould within the 3 to 5 minutes of preparation. After smoothing the surface of the grout mixture with a trowel and making it level with the top of the mould, the mould was placed on a resting plate. The Vicat plunger, which confirmed to (IS : 5513, 1996) standards, was then allowed to touch the surface of the mould and was quickly released to sink into the grout mixture.

To determine the initial setting time, a needle attached to a rod was gently lowered into a Vicat apparatus until it made contact with the grout in the mold. The needle was then quickly released and repeatedly pushed against the grout until it could no longer penetrate the paste by more than 5.0 ± 0.5 mm from the bottom of the mold. The time when the water was added to the cement and the time when the needle failed to penetrate the cement paste to this depth is considered the initial setting time. To find the final setting time of the cement, an annular attachment was used instead of the needle in the Vicat apparatus. The grout is considered to have reached final set time when the needle, when gently pressed onto the surface of the paste, creates an impression. The time when water is added to the cementitious grout and the time when the needle creates an impression on the surface of the grout paste is the final setting time.

3.12.5.2 Compressive strength of the grout

The cube specimens 50 × 50 ×50 mm was cast and demolded after 24 hours according to ASTM standard (ASTM:C942, 2010). The grout mixture was prepared using fly ash (0% – 50%) partial replacement of cement with w/b and c/b ratio of 0.47 as selected from the section 3.9.4. Cube specimens prepared with water grout mixes were designated as plain grout and were cured in water. The cubes prepared with cyanobacterial grout mixes were cured in *S. pevalekii* cell suspension containing 100 mM $CaCl_2$ (w/v) and 25 mM $NaHCO_3$. The cube specimens were cured for 28 days and the tested for strength using compression testing machine (AIMIL India Ltd, New Delhi) (Fig. 3.17). The results were evaluated as explained in section 3.7.3.1.



Fig. 3.17 Compression testing machine for compressive testing of grout

3.13 Crack-Embedded Concrete Specimens

To investigate the crack remediation in concrete specimens, prismatic specimens of 500 × 100 × 100 mm for flexural strength, concrete cubes of 150 × 150 × 150 mm (for compressive strength testing) and Cylindrical specimens (for water tightness testing) 100 mm (dia) × 50 mm (ht) were cast with 0.5 mm width embedded crack. Prismatic and cube specimens were prepared using iron mould of specific dimensions whereas, for cylindrical specimens' polyvinyl chloride (PVC) mould of 100 (dia) × 50 (ht) mm was used. The lower part of mould was closed with hard board sheet cut with 102 mm diameter to completely cover the lower part of the mould. The mould before adding concrete mix was wrapped with tape to prevent leakage of the mix. Similar protocol was adopted by Joshi et al. (2021) and Anand et al. (2023). The concrete mix was prepared using cement: sand: coarse aggregate in 1: 1.82: 3.24 (w/w), and the water-to-cement ratio was kept at 0.5. In order to create an artificial crack, 0.5 mm steel plate was inserted in the concrete specimen, penetrating up to 20 mm immediately after pouring the concrete mix. The specimens were monitored until the initial setting of concrete, after which the steel plate was removed carefully such that the concrete surrounding the crack remained uninterrupted and unbroken. All the specimens were kept at room temperature of 27 ± 2 °C for 24 hours till de-moulding. Later all the specimens were cured in water for up to 28 days.

3.14 Crack Remediation with Bio-Based Cement Grout

After curing, crack-damaged concrete specimens were restored using 40% FA amended biogrout. The crack repair technique was divided into two different approaches; horizontal and vertical oriented healing (Fig. 3.18). In the first approach, the specimens were placed such that crack was in a horizontal position, whereas in another approach, the specimens were positioned vertically. The orientation has been selected on the basis of lab-scale study and field requirement. Though at lab scale, both treatment; horizontal (ponding) and vertical (spray) are feasible. However, in certain circumstances specifically in field, vertical injection treatment would be more applicable than the horizontal treatment. In both methods, the biogrout and plain grout were injected using a 20 ml syringe. Before injection, the cracked surface was thoroughly wetted to mitigate the moisture absorption during grouting. The direction of injection was from one direction to other. In vertical orientation, the crack was filled from bottom to top to uniformly fill the grout in cracked region. Once the biogrout and plain grout were injected horizontally and vertically, the specimens were left uninterrupted for 24 hours to harden. Biogrout repaired specimens were cured by *S. pevalekii* cells suspended in calcifying solution (100 Mm $CaCl_2$ and 25 Mm $NaHCO_3$) by ponding (horizontal healing) and spray treatment (vertical healing). Control specimens were cured using water both by ponding and spray treatment. The specimens were divided into three different categories. Firstly, as control uncracked concrete specimen, secondly, plain grout without any cyanobacterial suspension both placed horizontally and vertically. Third, biogrout repaired specimens with horizontal and vertical healing, as presented in Table 3.10. All the specimens were placed under the artificial light source of 1200 lux for a photoperiod of 12:12 h (light: dark). In the present investigation, atmospheric CO_2 was taken into account for the experiment. As per NOAA (2022) concentration of atmospheric carbon dioxide (CO_2) in air is in range of 410 - 421 ppm.

3.15 Testing of crack repaired specimens

3.15.1 Mechanical strength

The compressive and flexural strength of reference (REF), untreated (UTC), control (CPT and CST) and cyanobacterial grout repaired concrete specimens (BPT and BST) was tested. The influence of cyanobacterial grouts and curing methods on the mechanical properties of concrete was examined using the COMPTEST 3000 machine, at an age of 28 days of curing. Concrete specimens 500 × 100 × 100 mm and 150 × 150 × 150 mm cube was tested for flexural and compressive strength as per the Indian standards (IS 516 2021), respectively.

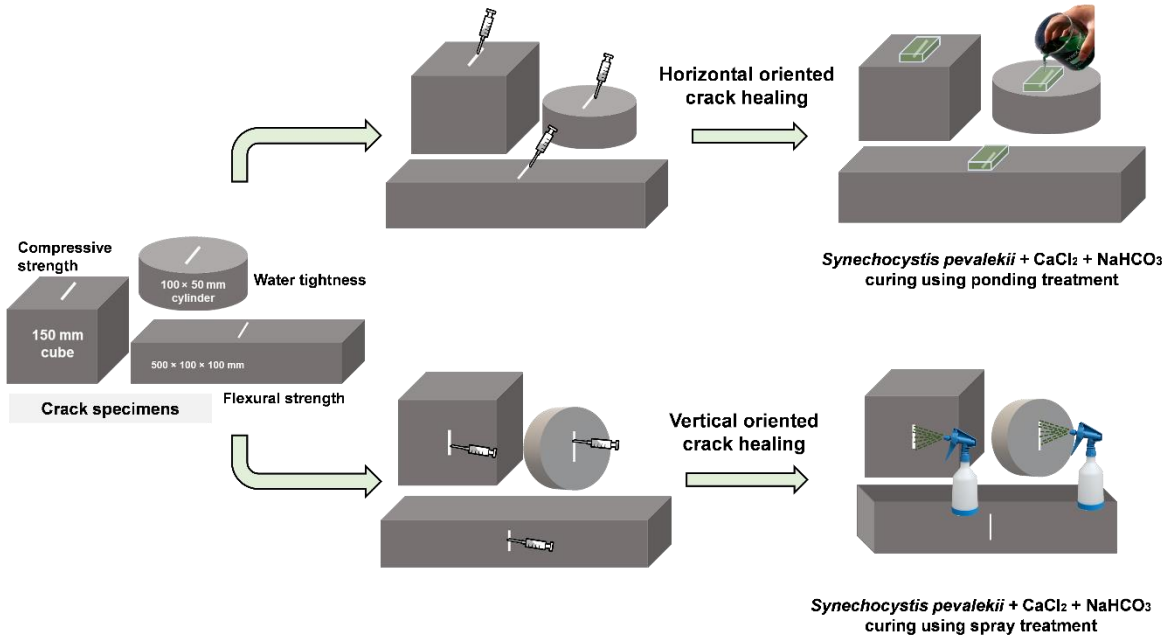


Fig. 3.18 Graphical representation of the vertical and horizontal oriented crack remediation using *Synechocystis pevalekii* cell culture supplemented with calcifying solution ($CaCl_2$ + $NaHCO_3$)

Table 3.10 Outline of different sets of repairing techniques using FA amalgamated cement-based grout specimens and mechanism of curing

Label	Specimens	Grouting material	W/b or C/b ratio	Curing method (28 days)
UTC	Untreated cracked concrete	Without grouting	Without grouting	Water curing
REF	Uncracked concrete	Without grouting	Without grouting	Water curing
CST	Plain grout -control Spray treatment	FA (40%) Cement (60%)	W/b ratio = 0.47	Water curing (spray-on repaired crack thrice a day)
CPT	Plain grout -control Ponding treatment	FA (40%) Cement (60%)	W/b ratio = 0.47	Water curing of the repaired area with ponding
BST	Biogrout- spray treatment	FA (40%) Cement (60%)	C/b ratio = 0.47	*S. pevalekii* culture (BG11 medium + 100 mM $CaCl_2$ + 25 mM $NaHCO_3$) spray curing thrice a day
BPT	Biogrout- ponding treatment	FA (40%) Cement (60%)	C/b ratio = 0.47	Ponding with *S. pevalekii* culture (BG11 medium + 100 mM $CaCl_2$ + 25 mM $NaHCO_3$)

3.15.2 Sorptivity test

Concrete cylindrical specimen 100 (dia) × 50 (ht) mm was tested for evaluating the water tightness ASTM C1585 (2013). However, the modification was done for testing the water tightness, only crack repaired (70 × 30) mm region of the 100 (dia) × 50 (ht) mm cylindrical specimen was exposed for water absorption test. The rest of the area was covered with the epoxy sealant. The protocol for the performance of the test is explained in the section 3.7.3.2.

3.15.3 Sealing efficiency

The sealing efficiency of the crack-healed specimens using plain and biogrout was evaluated for 70 (length)× 30 (width) mm area cylinder specimens by calculating the water absorption at six hours using the equation (Equation 1) as described by (Liu et al. 2020b).

$$SE\ (\%) = \frac{(Qo - Qg)}{Qo} \times 100 \qquad 3.6$$

Where SE represents the sealing efficiency of grout, Q_0 is designated as initial water absorption before grouting, and Q_g is water absorption after grouting.

3.15.4 Microstructural Analysis

The crystals' morphology, characterization, and size were identified using a field emission scanning electron microscope (FESEM). To further elaborate on the elemental composition of the crystals, the energy dispersive spectroscopy (EDS) was done at 28 days, for which a small piece of the sample was collected from the biogrout and plain grout specimens after curing the crack-healed grouted specimens at 28 days. To analyses the crystal composition and identification, the XRD was performed using powdered samples collected from the biogrout and plain grout samples.

3(C) Comparison of strength and permeability properties of concrete by Photoautotrophic and heterotrophic bacteria

The efficiency of $CaCO_3$ precipitation by photoautotrophic and heterotrophic bacteria and its impact on concrete's strength and permeability properties was tested. The results were compared to elucidate the efficiency of photoautotrophic and heterotrophic pathway in concrete environment.

3.16 Biological culture

The study used two strains, photoautotrophic bacteria, *S. pevalekii* BDHKU 35101 and the other ureolytic bacteria, *B. paramycoides* MD6, with different modes of nutrition. This strain was cultivated and maintained in blue-green algae (BG11) broth under controlled conditions of 25 ± 2 °C, with the illumination of 1200 lux for 12 hours of light followed by 12 hours of dark under shaking conditions at 110 rpm. *B. paramycoides*, a heterotrophic strain, was grown in nutrient broth (Hi media, India) and incubated at 37 °C under shaking conditions at 120 rpm.

3.17 Materials

The study used commercially available ordinary Portland cement (OPC) - 43 grade, as per the Indian standard (IS: 8112 2013). As fine aggregates, locally sourced natural well-graded river sand was used, meeting the requirements of Zone II according to the Indian standard (IS 383 2016). The fine aggregate had a specific gravity of 2.62 and a water absorption rate of 1.3%. Coarse aggregates with particle sizes of 20 mm and 10 mm were used, having specific gravities of 2.61 and 2.63, and water absorption rates of 1.38% and 1.42%, respectively. The fine and coarse aggregates used in the casting process complied with Indian standards (IS 383 2016).

3.18 Calcium Carbonate Precipitation

The *S. pevalekii* cells with an optical density of 0.5 at 650 nm were introduced in BG11 broth supplemented with 50 mM sodium bicarbonate ($NaHCO_3$) and 100 mM calcium chloride ($CaCl_2$). The solutions were prepared from analytical-grade reagents (Hi media, India). The media flasks were then placed on a rotating shaker in a temperature-controlled incubator at 25 ± 2 °C under the constant shaking of 110 rpm. Illumination was provided at an intensity of 1200 lux, with a photoperiod of 12 hours of light followed by 12 hours of dark. The concentration of $CaCl_2$ used is within the range of concentrations employed in other studies on MICCP (Paine 2016; Zhu et al. 2017). At the same time, overnight grown *B. paramycoides*

with an optical density of 0.5 was inoculated in the nutrient broth supplemented with 2% urea and 25 mM $CaCl_2$. Triplicate flasks were prepared for each sample. At specific time intervals (24, 48, 72, 96, and 120 hours), the sample was collected and filtered through a 0.45 µm cellulose nitrate membrane to measure the quantity of $CaCO_3$ precipitated. The precipitates were washes twice with deionized water and lyophilized for FESEM analysis. The filtered solution was analyzed for dissolved calcium (Ca^{2+}) ions using atomic absorption spectroscopy (AAS) experiment.

3.18.1 Effect of initial pH on $CaCO_3$ precipitation

The $CaCO_3$ precipitation was noted at different pH (6, 7, 8, 9, 10, 11 and 12) conditions by inoculating the *S. pevalekii* and *B. paramycoides* culture in BG11 broth and nutrient broth, respectively. The pH of the BG11 broth and nutrient broth were adjusted before autoclaving by sodium hydroxide (NaOH) and hydrochloride acid (HCl). The BG11 broth was supplemented with 50 mM $NaHCO_3$ and 100 mM $CaCl_2$. Whereas the nutrient broth was supplemented with 2% urea and 25 mM $CaCl_2$. After 120 hours, the broth was collected and filtered through a 0.45 µm cellulose nitrate membrane. The precipitates were dried in lyophilizer and weight of $CaCO_3$ precipitates was measured.

3.19 Strength and Permeability

The concrete mix was prepared using cement: fine aggregate: coarse aggregate in the proportion of 1:1.82:3.24, keeping the water-to-cement ratio (w/c) of 0.47. The culture of *B. paramycoides* (OD – 0.5) and *S. pevalekii* (OD – 0.5) was incorporated in the concrete mix along with the respective nutrients during the cast. The nutrition media used for *B. paramycoides* was nutrient broth (NB) along with 2% urea and 25 mM $CaCl_2$. Whereas for *S. pevalekii* culture, blue-green algae 11 (BG11) broth with 100 mM $CaCl_2$ and 50 mM $NaHCO_3$. The specimens were cured with respective bacterial culture and nutrient media as shown in Fig. 3.19. The control was prepared and cured in tap water. A detailed summary of the experimental set up is mentioned in Table 3.11. Different specimens were prepared to test the concrete's strength and permeability properties. The 150 × 150 × 150 mm cubes were cast and tested for compressive strength, as per the Indian standards (IS 516 2021). Test specimens of 100 (dia) × 200 (ht) mm dimensions were cast for rapid chloride permeability and sorptivity coefficient. The 100 × 200 mm specimens were sliced into 100 (dia) × 50 (ht) mm size for testing the rapid chloride permeability test (RCPT) (ASTM C1202 2012) and sorptivity experiment (ASTM

C1585 2013) as per the ASTM standard. The detailed description of the procedure for compressive strength, sorptivity test and RCPT is mentioned in section 3.8.3.

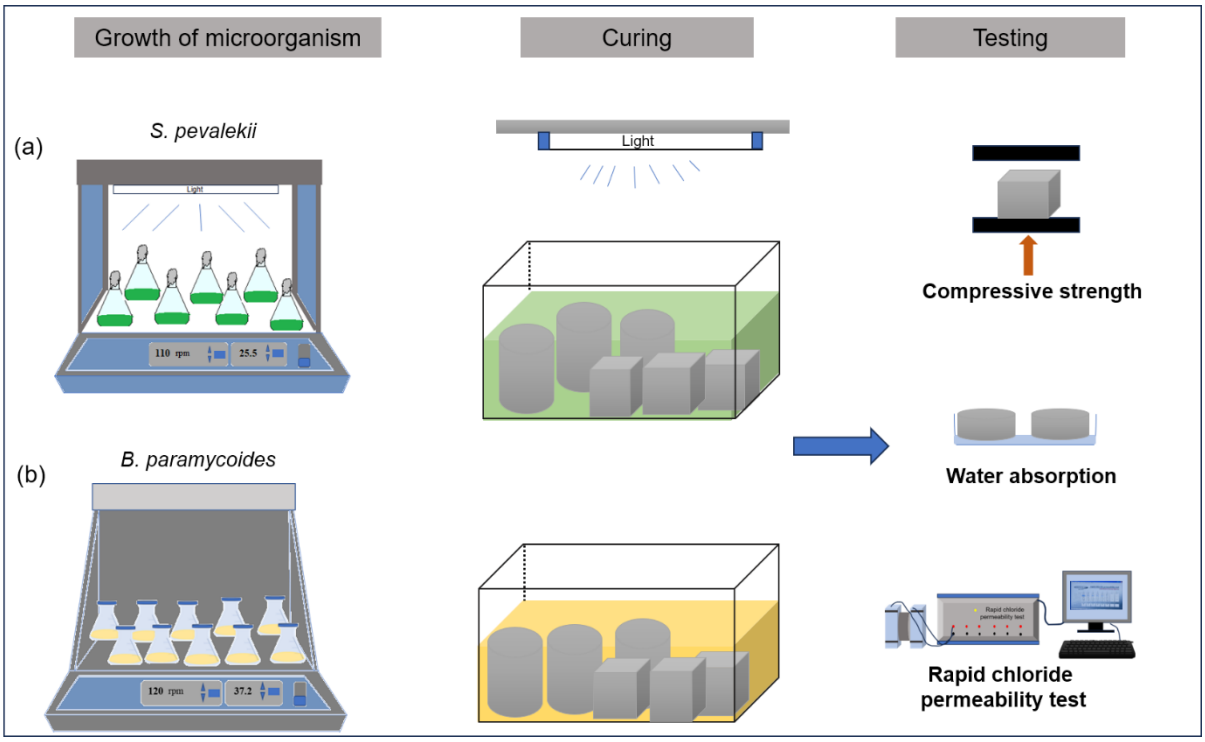


Fig. 3.19 The experimental setup for photoautotrophic bacteria *Synechocystis pevalekii* and heterotrophic bacteria *Bacillus paramycoides* for strength and permeability improvement in concrete

Table 3.11. Outline of the different mix design of the experiment and curing treatment

Specimens	Material used	Curing
Control	Cement: sand: coarse aggregates Water/cement = 0.47	Water curing
BPC*	Cement: sand: coarse aggregates culture/cement = 0.47 2 % urea + 25 mM $CaCl_2$	Submersion in *B. paramycoides* culture supplemented with 2% urea and 25 mM $CaCl_2$
SPC*	Cement: sand: coarse aggregates culture/ cement = 0.47 50 mM $NaHCO_3$ + 100 mM $CaCl_2$	Submersion in *S. pevalekii* culture supplemented with 50 mM $NaHCO_3$ and 100 mM $CaCl_2$

*The curing medium was replenished every seven days with respective media and inoculated with the freshly prepared culture

3.19.1 Microstructural analysis

To determine the crystallization in concrete by bacterial treatment, the small chunk of concrete sample was taken for the microstructural investigation. Samples were sputter-coated with gold after being carefully polished. The FESEM-EDS was performed to determine the elements that make up microstructural crystals. X-ray diffraction (XRD) was carried out to identify the minerals and crystal formation in the sample. The Bruker D8 X-ray diffractometer was used to conduct the X-ray diffraction (XRD), which involved scanning from 20 to 60 degrees at a two-theta angle with Cu anode (40 kV and 30 mA).

3(D) Evaluation of biomineralization on marble surface by heterotrophic and photoautotrophic bacteria

Marble stones are commonly used in the construction of buildings and monuments, and are susceptible to chemical weathering when exposed to atmospheric pollutants such as SO_4 and NO_X (Vazquez et al. 2016; Ni et al. 2020). The calcification potential of heterotrophic bacteria *B. paramycoides* MD6 and *S. pevalekii* was studied on the marble surface.

3.20 Carbonate stone

The calcareous marble stone used in the present study was dungri, which is one of the most delicate marble stones from makrana-based mines used in building flooring and walls (Garg et al. 2019). All carbonate stones were cut to a size of 4 cm × 4 cm × 2 cm and sterilized by three cycles of autoclaving at a pressure of 15 psi and 121 °C for 20 min to remove indigenous flora.

3.20.1 Calcification on the marble stone

The heterotrophic bacteria *B. paramycoides* MD6 and photoautotrophic bacteria *S. pevalekii* was observed for biomineralization on the unpolished calcareous surface (marble stone). The culture isolate *B. paramycoides* MD6 was inoculated in nutrient broth and maintained at 37 °C for 12 - 24 hours under shaking conditions. Similarly, the photoautotrophic strain *S. pevalekii* was inoculated in autoclaved BG11 broth and incubated at 25 ± 2 °C and constantly shaken at 110 rpm under an illumination photoperiod of 12:12 h (light: dark). The calcification experiment was carried out by submerging the marble stones samples in microbial culture with different cell concentration of 6×10^{-3}, 6×10^{-5} and 6×10^{-7} supplemented with the calcifying media. The calcifying media used in NB was 2% urea and 25 mM $CaCl_2$ whereas in BG11 the 100 mM $CaCl_2$ and 50 mM $NaHCO_3$ was used. The incubation was done at room temperature 25 ± 2 °C. The marble stone sample submerged in BG11 broth inoculated with photoautotrophic bacteria *S. pevalekii* was incubated under the artificial light source of 1200 lux. To analyze the $CaCO_3$ precipitation induced by photoautotrophic and heterotrophic bacteria in the presence of calcifying media, the weight increase in the sample was noted for each sample after 7, 14, 21, and 28 days. The percentage of $CaCO_3$ produced by *B. paramycoides* MD6 bacteria was evaluated using Equation 3.7.

$$Percentage\ of\ calcium\ carbonate\ precipitation\ = \frac{W_1 - W_2}{W_1} \times 100 \qquad (3.7)$$

Where, W_1 is the weight of the marble stone slab before the biomineralization experiment, and W_2 is the weight of the marble stone slab at consecutive days of the biomineralization experiment.

3.21 Acid attack

To investigate the influence of acid on marble stones, the slabs were categorized into four experimental groups consisting of five marble stones with dimensions of 4 cm × 4 cm × 2 cm. The four groups involved four different concentrations of acid solutions (analogous to acid rain) of sulfuric and nitric acids, as shown in Table 3.12 (Vazquez et al. 2016). The marble stones were exposed to an acidic solution as spray for three weeks (Fig. 3.20). The concentration and volume of the spray was maintained similar in each group. The weights of all the marble stone samples exposed to an acidic environment were measured before and after the experiment. The surface roughness of the samples was evaluated using atomic force microscopy.

Table 3.12 Concentration of different acid solution used in experimental damage of marble stones

Experimental groups	Conc. of HNO_3	Conc. of H_2SO_4
Test 1 (mol $^{-1}$)	10.1	-
Test 2 (mol $^{-1}$)	7.1	1.61
Test 3 (mol $^{-1}$)	3.0	3.7
Test 4 (mol $^{-1}$)	-	5.3

3.21.1 Bioremediation using MICCP

The acid-affected specimens were dipped in deionized water for 48-72 hours to remove excess acid from the surface and pores of the stones. The marble stone slabs were then exposed to alkaline water (pH 9) to reduce the pH of the stone, which was affected by the acid attack. Furthermore, marble stones were biotreated with heterotrophic bacteria *B. paramycoides* MD6 and photoautotrophic bacteria *S. pevalekii* strain using the MICCP technique as follow:

(a) Acid-affected marble stones were dipped in NB medium inoculated with *B. paramycoides* MD6 bacterial culture supplemented with 2% urea and 25 mM $CaCl_2$.

(b) Acid-affected marble stones were dipped in BG11 medium inoculated with *S. pevalekii* culture supplemented with 50 mM $NaHCO_3$ and 100 mM $CaCl_2$.

Weight gain due to the MICCP treatment of the acid-affected marble stone was noted at 7 days intervals for 28 days.

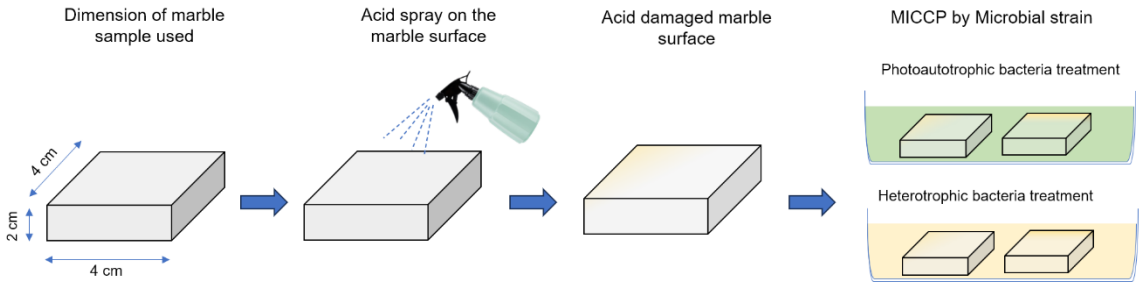


Fig. 3.20 Graphical representation of the experimental set-up of MICCP treatment on acid damaged marble surface

3.21.2 Weight loss with ultrasonic treatment

To examine the adhesion property of $CaCO_3$ precipitation induced by bacteria on marble stone, an ultrasonication test was carried out (Rodriguez-Navarro et al. 2003). It is a lab-scale study equivalent to wind erosion occurring in nature. Biomineralized marble stone slabs were dipped in distilled water and subjected to four cycles of sonication for 5 min. The samples were oven-dried at 40 °C for 24 h after sonication. Sonication removes loosely attached $CaCO_3$ grains from the surface. Therefore, the weight loss percentage of the specimens was calculated using Equation 3.8.

$$Percentage\ of\ weight\ loss\ = \frac{W_1 - W_2}{W_1} \times 100 \qquad 3.8$$

Where, W_1 is weight of the marble stone slab before the sonication experiment, W_2 is the weight of the marble stone slab after the sonication experiment.

3.21.3 Microstructural analysis (FESEM-EDS)

The effects of acid and bacterial treatment on marble stones affected by acid (Tests 1–4) and biomineralization were visualized using a DinoLite microscope. Microscopic images were obtained before and after the acidic effect on the marble surface after 21 days. The images were taken after 28 days of MICCP treatment. To analyze the $CaCO_3$ precipitation in the bacterial-

cured specimen after 28 days of treatment, the samples were analyzed for FESEM (field emission electron microscopy (FESEM). EDS was performed to confirm the elemental composition of the precipitates in the concrete. The samples were gold-coated, polished, and coated with carbon to disperse the extra charge on them.

3.22 Statistical analysis

All the experiments were performed in triplicates. Data were analyzed by analysis of variance, and the means were compared using Tukey's test or t-test at $p < 0.05$. using the GraphPad Prism 8.0.1 software.

Chapter 4 Results and discussion

4(A) Heterotrophic bacteria

4.1 Isolation and screening of heterotrophic bacteria

Heterotrophic bacteria induce $CaCO_3$ precipitation by catalyzing urea degradation. In the current study, ureolytic bacteria were isolated from marble dust collected from a marble dumping yard, Kishangarh, Rajasthan, India. The marble dumping yard was chosen because of the formation of small marble dust plateaus at the site, which might be due to the formation of a binding agent ($CaCO_3$) by microorganisms in the dust. The results of the enumeration of bacteria are shown in Table 4.1.

Table 4.1 Enumeration of bacteria on nutrient agar

Incubation days ↓	Dilution →	10^3 Log CFU/g	10^4 Log CFU/g	10^5 Log CFU/g	10^6 Log CFU/g
24 h		2.04	1.98	1.73	1.67
48 h		2.30	2.26	2.07	1.73
72 h		Not countable	2.32	2.30	1.94

Colonies with different shapes, sizes, and colors were selected and streaked on nutrient agar plates. Primary screening of ureolytic bacteria involves qualitative testing. In total, 45 colonies were selected and streaked onto a urea agar base to screen ureolytic bacteria qualitatively. Morphologically, all the selected colonies differed in color and texture. Most colonies were brownish-white with a smooth surface. Out of the 45 colonies streaked onto the urea agar base, only seven bacterial colonies were selected based on the color change from orange to pink (Fig. 4.1). Urea agar contains urea and phenol, which degrade to form ammonia, giving a pink color due to the increased pH (Burbank et al. 2012; Omoregie et al. 2019). The selected colonies were circular, creamy, mucoid, opaque, and slightly rough at their corners. The seven bacterial colonies were further streaked onto nutrient agar medium and maintained in a 40% glycerol stock at − 80 °C. The pink color indicates urease enzyme production, converting urea to ammonia, as shown in Fig. 4.1. Ammonium formation changes the alkalinity of the medium by changing its pH. The selected colonies were labeled as MD1, MD2, MD3, MD4, MD5, MD6, and MD7. A literature review reports the isolation and utilization of different ureolytic

bacteria for $CaCO_3$ precipitation. Omoregie et al. (2017) isolated *Sporosarcina pasteurii* from limestone samples collected from the cave. Similarly, *B. megaterium*, *B. licheniformis*, and *B. flexus* were isolated from alkaline soil samples of a cement factory (Krishnapriya et al. 2015). Khambholja et al. (2022) isolated *Quasibacillus* Sp. and *Bacillus* sp. from livestock dung-rich soil samples. Nezafat Tabalvandani et al. (2023) recently isolated *B. licheniformis*, and Elmi et al. (2023) isolated *Bhargavaea cecembensis* from soil.

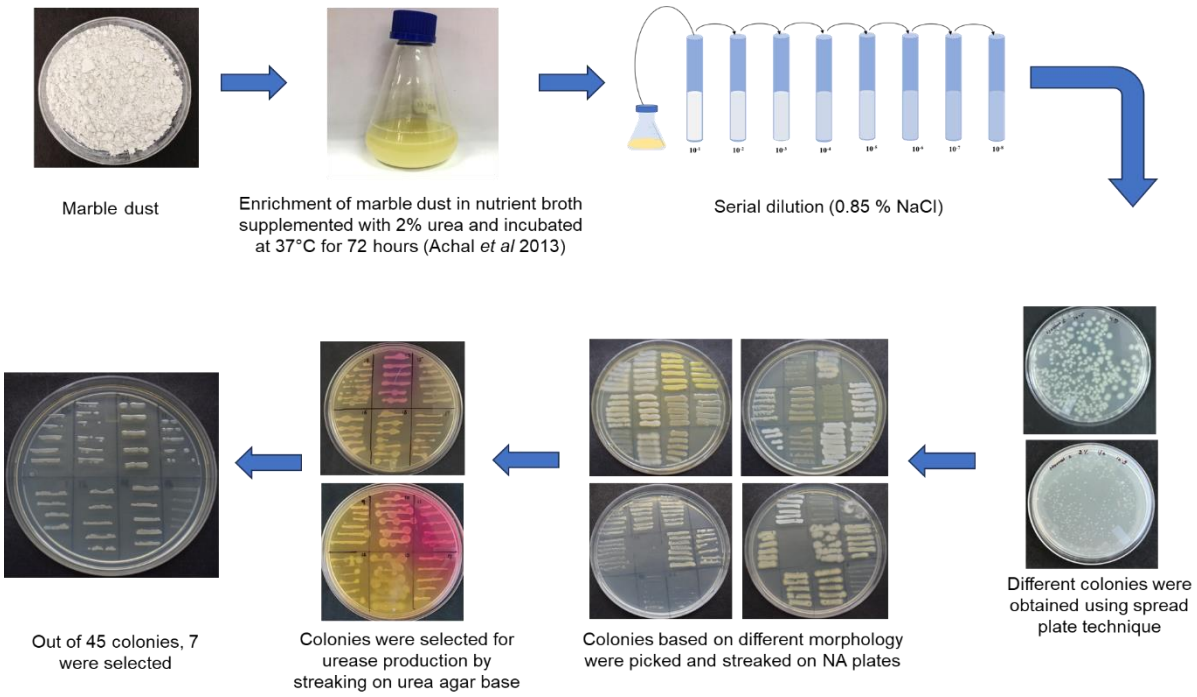


Fig. 4.1 Enrichment and isolation of different strains of ureolytic bacteria from marble dust

4.2 Molecular characterization

After qualitative screening, seven urease-positive isolates were characterized based on their molecular identities.

4.2.1 DNA extraction

The DNA templates were successfully isolated using the alkaline lysis method described by Krishna et al. (2008). As shown in Fig. 4.2, the bands were visualized on a 0.8% agarose gel containing ethidium bromide (EtBr) after electrophoresis in a gel documentation system under UV light. DNA was quantified by measuring the purity of the DNA template suspended in the TE buffer using a nanodrop. As shown in Table 4.2, the absorbance of the DNA template was measured at 260/280 nm because nucleic acids, such as DNA and RNA, absorb in this region,

whereas protein absorption is noted at 280 nm. A ratio of ~1.8 is generally considered "pure" for DNA, while a ratio of ~ 2.0 is considered "pure" for RNA. If the ratio is significantly lower in either case, it may indicate the presence of contaminants such as proteins, phenols, or other compounds that strongly absorb at or near 280 nm. The absorbance ratios at 260 and 230 nm can be used as supplementary criteria for evaluating the purity of DNA or RNA. A ratio within the range of 2.0 - 2.2 is indicative of a pure sample, while a ratio lower than this expected range may suggest the presence of interfering substances in the sample that can absorb at 230 nm.

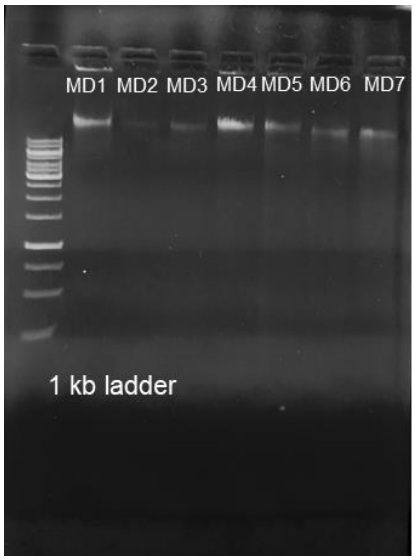


Fig. 4.2 Visualization of DNA bands of different bacterial isolates on 0.8% agarose gel

Table 4.2 Quantification of DNA templates using nanodrop spectrophotometer

Sample	Absorbance (260/230)	Absorbance (260/280)	Concentration(ng/µl)
MD1	0.71	1.92	215.2
MD2	0.51	1.79	156.3
MD3	0.21	2.02	81.2
MD4	0.60	2.03	112.7
MD5	0.45	2.10	159.3
MD6	0.62	2.10	61.7
MD7	0.14	1.92	27.9

4.2.2 Amplification of 16S rRNA and Purification of PCR products

The 16S rRNA gene was amplified by PCR to generate fragments of approximately 1500 base pairs (Fig. 4.3). The PCR product was purified and quantified by measuring its purity using a Nanodrop (Table 4.3). The resulting PCR products were sequenced and saved in FASTA

format. The resulting sequences of the seven bacterial strains are listed below. The sequences were compared to those in the EzBioCloud database.

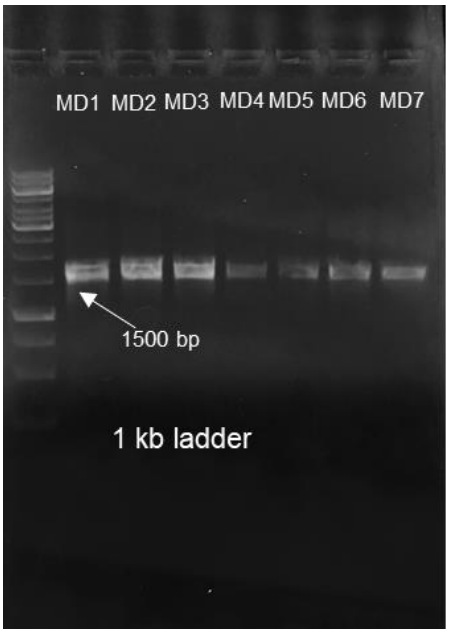


Fig. 4.3 16S rDNA amplification of bacterial isolates using polymerase chain reaction

Table 4.3 Quantification of purified PCR product using nanodrop spectrophotometer

Sample	Absorbance (260/230)	Absorbance (260/280)	Concentration(ng/µl)
MD1	1.18	1.83	187.4
MD2	1.90	1.87	154.7
MD3	1.23	1.78	190.3
MD4	1.99	1.88	266.4
MD5	1.92	1.87	215.1
MD6	1.45	1.83	142.1
MD7	1.71	1.93	104.3

The sequences were analyzed using multiple sequence alignment to check for similarities between sequences. A maximum similarity of 99.73% was found between MD2 and MD3. A maximum similarity of 99.78% was found between MD4, MD5, MD6, and MD7 (Fig. 4.4, and 4.5). According to the BLAST analysis, most ureolytic bacteria displayed significant levels of similarity (98%–99%) with bacterial sequences in the EzBioCloud database (Table 4.4). The correlation level of the 16S rRNA region of BLAST analysis results was found to be reasonable, particularly concerning the morphological descriptions of the species within the genus, and this correlation was found to be especially strong with respect to physiological

characterization (Achal et al., 2010). Based on partial 16S rRNA gene sequencing, the obtained 16S rRNA gene sequences were identified as *Bacillus cereus* MD1, *Bacillus paranthracis* MD2, *Bacillus paranthracis* MD3, *Bacillus paramycoides* MD4, *Bacillus paramycoides* MD5, *Bacillus paramycoides* MD6, and *Bacillus paramycoides* MD7. The isolates showed good-quality sequences, with an average length of approximately 1450 bp. The 16S rRNA sequence for MD1, MD2, MD3, MD4, MD5, MD6 and MD7 were deposited in NCBI GenBank under accession numbers OR673981, OR673982, OR673983, OR673984, OR673985, OR673986 and OR673986, respectively (Appendix I). Based on the phylogenetic analysis, all strains belonged to the Bacilli class, as shown in Fig. 4.6. Studies have reported that *Bacillus* species have the highest urease activity (Achal et al. 2010b; Dhami et al. 2013a; Khambholja et al. 2022; Rathakrishnan and Gopalan 2022).

Table 4.4 Molecular identification based on 16S rRNA sequencing data using NCBI nucleotide BLAST analysis

Isolate ID	**GenBank Accession No.**	**Bacterial species closest match**	**Base pair (bp)**	**Query cover (%)**	**Similarity (%)**
MD1	OR673981	*Bacillus cereus*	1452	98.6	98.76
MD2	OR673982	*Bacillus paranthracis*	1471	99.0	98.38
MD3	OR673983	*Bacillus paranthracis*	1468	99.5	98.57
MD4	OR673984	*Bacillus paramycoides*	1460	99.1	98.86
MD5	OR673985	*Bacillus paramycoides*	1456	99.0	98.97
MD6	OR673986	*Bacillus paramycoides*	1440	97.7	99.65
MD7	OR673986	*Bacillus paramycoides*	1450	99.8	99.86

4.3 Quantitative characterization

Based on the qualitative urease test, 7 out of 45 bacterial isolates were selected for quantitative analysis of urease activity and $CaCO_3$ precipitation.

4.3.1 Urease activity

The urease activity of the bacterial isolates was quantitatively tested. After 24 hours (h) of incubation at 37 °C, MD6 showed the highest urease activity, followed by MD4 and MD5. MD2 bacterial isolate showed the lowest urease activity. The maximum urease activity

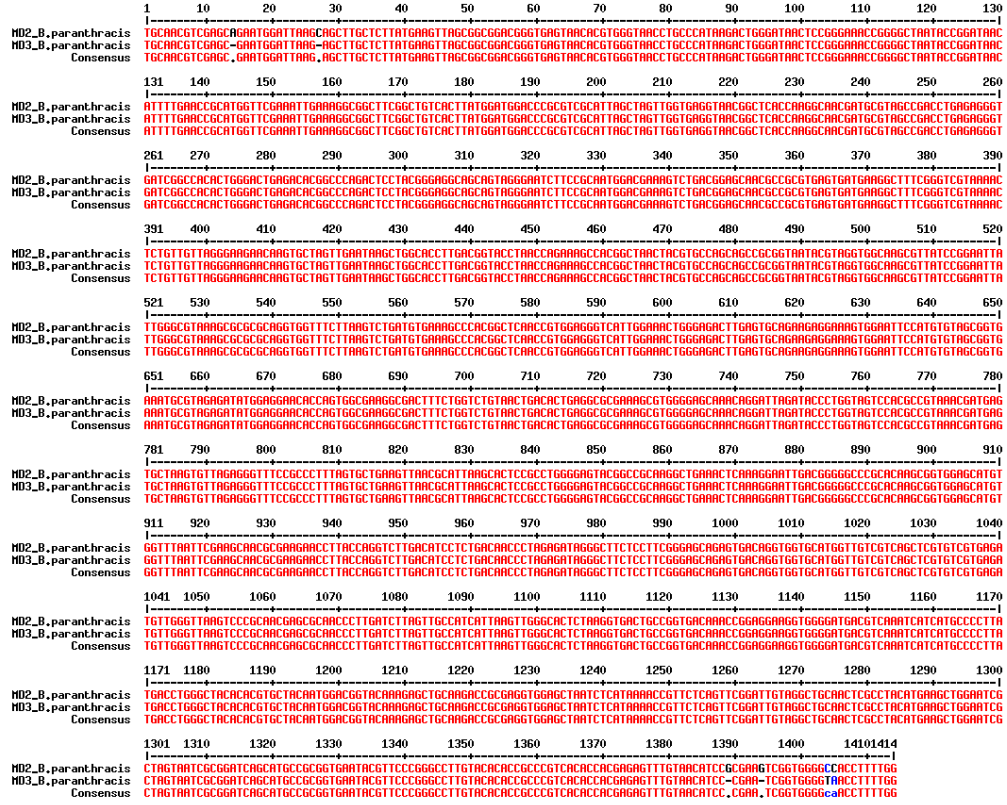


Fig. 4.4 Multiple sequence alignment of *Bacillus paranthracis* MD2 and *Bacillus paranthracis* MD3

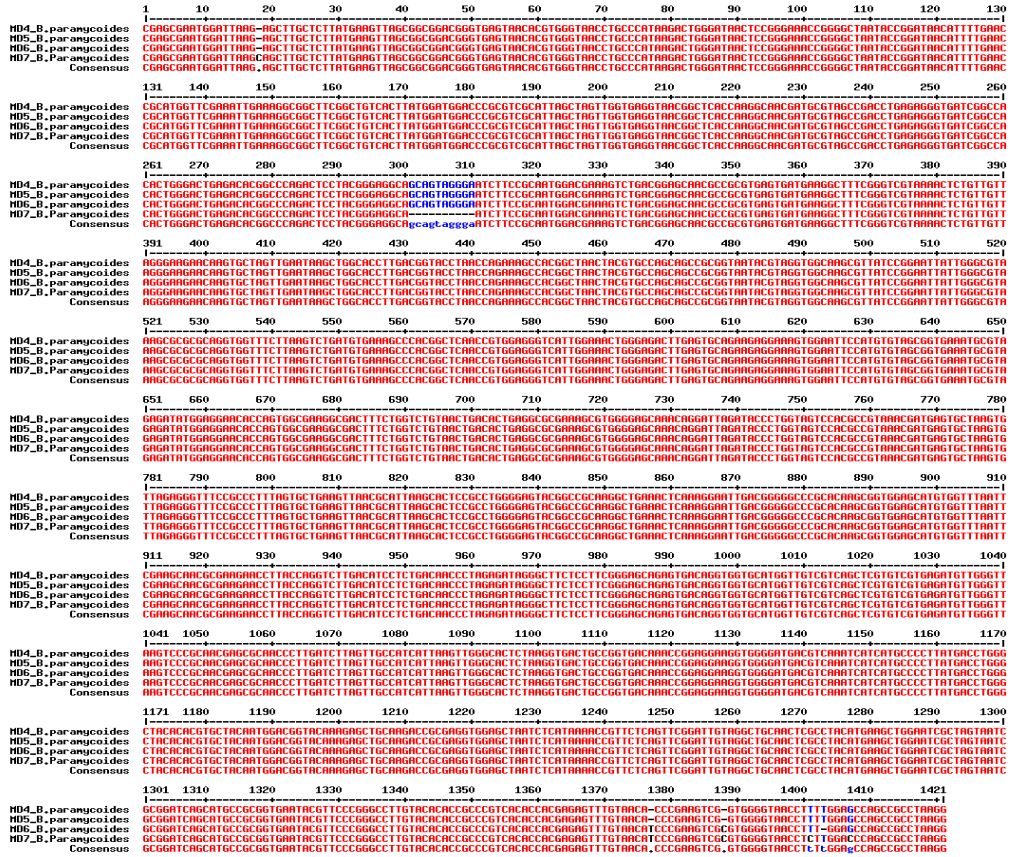


Fig. 4.5 Multiple sequence alignment of *Bacillus paramycoides* MD4, MD5, MD6, and MD7

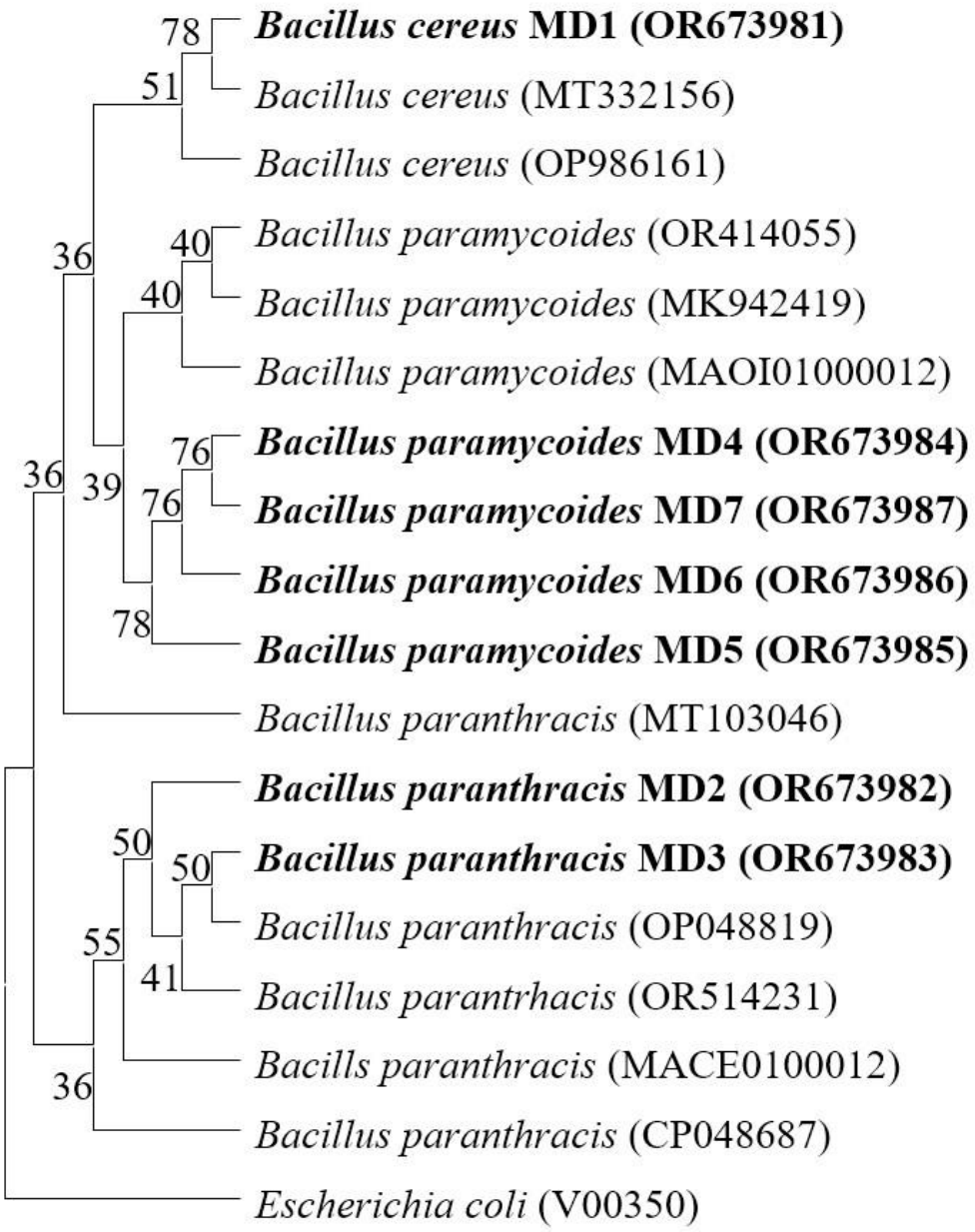


Fig. 4.6 Maximum parsimony tree based on bacterial 16S rRNA sequence analysis data of different bacterial isolates along with their accession numbers of NCBI database. Numerical values represent bootstrap values from 1000 replicates. *Escherichia coli* was used as an outgroup

Was observed by MD6 was 1512 U/ml after 96 h of incubation. The other isolates MD1, MD2, MD3, MD4, MD5, and MD7 showed urease activity of 904.5, 552.2, 936.5, 1380.8, 1449.4, and 581.3 U/ml at 96 h of incubation (Fig. 4.7). Urease activity declined upon further incubation for up to 120 h. The urease activity increased with the metabolic activity of the

bacteria and decreased upon complete exhaustion of nutrients. The urease activity results were compared to previously isolated bacteria *Bacillus* sp. CT5 (Achal et al., 2010). The urease activity of MD6 was 54.8% higher than that of *Bacillus* sp. CT5. *B. paramycoides* produced the highest urease enzyme activity compared with *B. cereus* and *B. paranthracis*. It might be because the metabolism and level of urease expression in *B. paramycoides* were higher than those in the other strains (Bibi et al. 2018). It was observed that *B. paramycoides* showed 602.4 U/ml of urease activity after 24 h and 1512 U/ml after 96 h of incubation at 37 °C. At 120 h, *B. paramycoides* showed 1168.44 U/ml of urease activity. This decline in urease activity may be due to the depletion of nutrients, insufficient sugar content in the medium, and bacterial death (Amiri et al. 2016). Therefore, this study focuses only on 120 h. In addition to *B. paramycoides, B. cereus and B. paranthracis* were equally proficient in producing urease until 120 h of incubation. These results are consistent with the findings of Omoregie et al. (2017), Leeprasert et al. (2022), and Fitri et al. (2023). Statistical analysis showed that the incubation time and bacterial isolates significantly affected urease enzyme activity at a 5% significance level (Table 4.5).

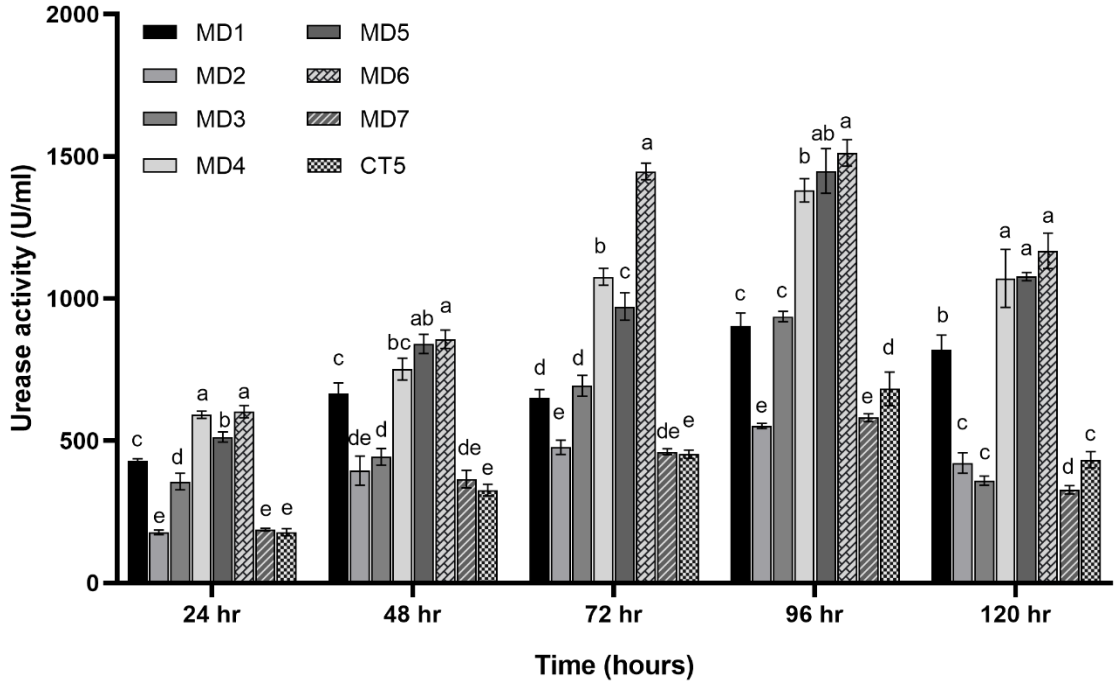


Fig. 4.7 Urease activity of different bacterial isolates at different incubation times. Values bearing different letters at each time interval are significant at $p<0.05$. Error bars represent the standard deviation (n=3)

4.3.2 Calcium carbonate ($CaCO_3$) precipitation

The amount of $CaCO_3$ precipitated in the nutrient broth supplemented with 2% urea and 25 mM $CaCl_2$ was evaluated at different time intervals (24, 72, 120, and 168 h). $CaCO_3$ precipitated by all isolates was weighed and measured in grams. $CaCO_3$ precipitation increased with increase of incubation period. There was not significant difference after 24 hours incubation therefore the results were analyzed at 48 hours interval. *B. paramycoides* MD6 showed the highest precipitation of $CaCO_3$, followed by MD5 and MD4. The $CaCO_3$ was collected in powdered form on Whatman paper. As shown in Fig. 4.8, the $CaCO_3$ precipitated by strains MD1, MD2, MD3, MD4, MD5, MD6, MD7, and CT5 were 1.14, 0.70, 1.11, 1.17, 1.17, 1.23, 0.53, 0.71 g/100 ml after 168 h incubation at 37 °C under shaking conditions. There was no further increase in precipitation upon further incubation because of the lack of available nutrients. Of all the isolates, *the B. paramycoides* showed maximum precipitation of $CaCO_3$. Similar results have been reported for *Bacillus* sp. (Farajnia et al. 2022), *Citrobacter* sp. (Wei et al. 2022), *Lysinibacillus fusiformis* and *Lysinibacillus xylanilyticus* (Leeprasert et al. 2022). The $CaCO_3$ precipitation by different isolates at consecutive time interval were observed to be statistically significant at the 5% significance level (Table 4.5).

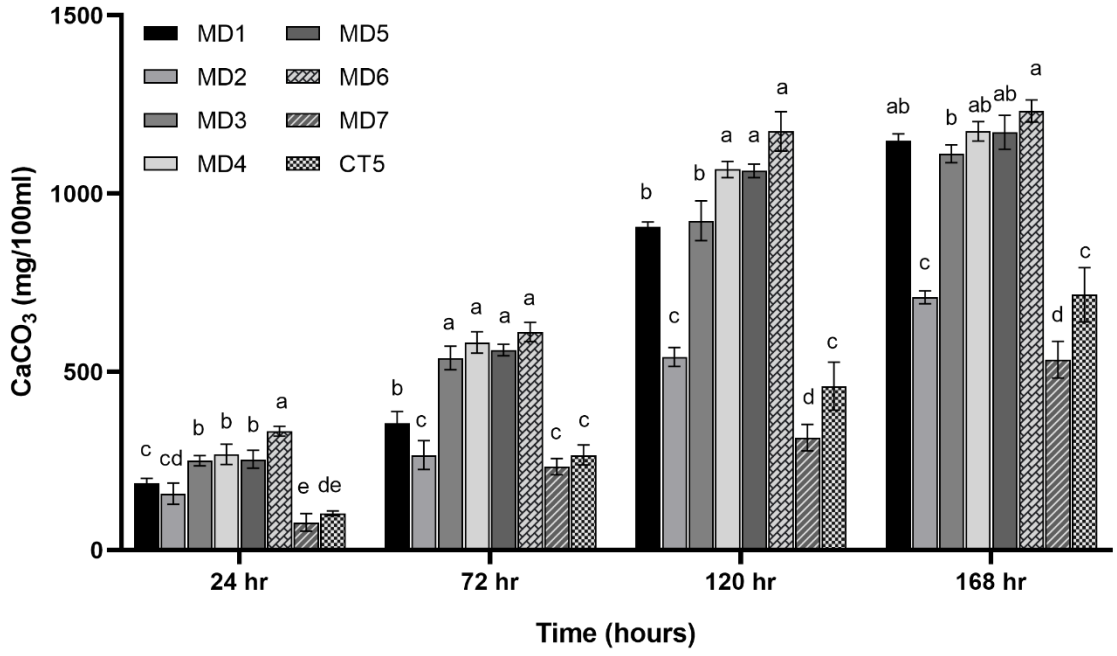


Fig. 4.8 Calcium carbonate precipitation by bacterial isolates at different incubation times. Values bearing different letters at each time interval are significant at $p<0.05$. Error bars represent the standard deviation (n=3)

Table 4.5 The factorial ANOVA results indicate the effects of different bacterial isolates and time on urease activity, and $CaCO_3$ precipitation

Variables	Degree of freedom	Isolates	Time	Interaction (Isolates × Time)
Urease activity	df	7,56	4,42	4,18
		P < 0.0001	P < 0.0001	P = 0.0004
$CaCO_3$ precipitation	df	7,56	3,42	2,12
		P < 0.0001	P < 0.0001	P= 0.0016

The P values < 0.001 indicates the values are highly significant

4.4 Sand consolidation

The bacterial isolates (MD1, MD2, MD3, MD4, MD5, MD6, and MD7) were tested for consolidation. The flow rate and amount of calcite precipitated in each sand column were measured at the end of the experiment. Initially, the flow rate of the calcifying medium in each bacterial admixed columns and control was same. However, a significant decrease in the amount of medium flowing through the column was observed as shown in Fig. 4.9a. In comparison to the initial flow rate, it decreased by 71.6%, 70.6%, 71.9%, 71.97%,70.5%, 73.3%,72.8% for MD1, MD2, MD3, MD4, MD5, MD6, and MD7 admixed sand columns, respectively, on the 20^{th} day. The flow rate decreased by 39.6% for the control (CL) specimen. Maximum flow rate reduction was seen in the MD6 admixed sand column in which the flow rate decreased from 14.92 ml/min to 3.99 ml/min, respectively. It could be attributed to the fact that $CaCO_3$ precipitated in the bacterial sand columns filled the voids between the sand particles, obstructing the flow of the calcifying solution through the column. The carbonate precipitates reduce the pore size between the sand particles. Subsequently, the sand columns were broken into three layers, and each layer was tested for calcite precipitation. Sand columns treated with bacterial cells were more compact and firmer than control columns. The upper layer was sturdier than the middle and lower layers. The sand grains exhibited partial binding between the sand grains in the lower layer in almost every sand column. The maximum amount of $CaCO_3$ was precipitated in the upper layer of the MD6 bacterial admixed sand column, followed by MD5, MD4, and MD7. The $CaCO_3$ precipitated in the MD6 upper, middle, and lower layers were 42.96, 31.56, and 24.13 mg/g, respectively (Fig. 4.9b). Whereas the $CaCO_3$ precipitated in the upper layer of other sand columns, i.e., MD1, MD2, MD3, MD4, MD5, and MD7 was 27.86, 26.5, 25.36, 36.06, 36.9 and 30.86 mg/g, respectively. The sand column's flow rate and calcite content proved that the bacterial strain MD6, followed by MD5, which has been

identified as *B. paramycoides*, showed the best-consolidating property. The $CaCO_3$ precipitation in the different layers of the column was in agreement with previous studies (Jie and Zhiming 2019; Sharma et al. 2020a). Similar results were reported by Achal et al. (2011), who observed a decrease in the flow rate and 33% calcite content in the top layer of a sand column. The statistically analyzed data showed significant differences in flow rate analysis and calcite precipitation in the bacteria-treated and control columns at the end of the experiment (Table 4.6).

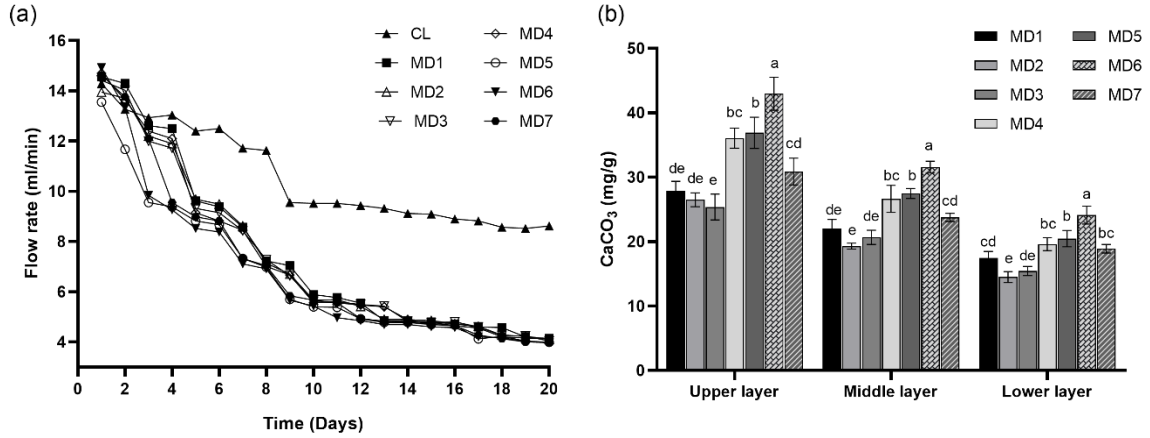


Fig. 4.9 (a) Flow rate of calcifying solution through the sand column at an interval of 48 h for 20 consecutive days (b) $CaCO_3$ precipitation at the upper, middle, and lower layer of the sand column after 20 days. Values bearing different letters within the treatment (layers) are significant at $p<0.05$. Error bars represent the standard deviation (n=3)

Table 4.6 The factorial ANOVA results indicate the effects of different bacterial isolates and time on $CaCO_3$ precipitation in sand consolidation

Variables		**Isolates**	**Factors**	**Interaction (Isolates × Factors)**
$CaCO_3$ precipitation	df	6, 12	2, 4	12, 24
		P < 0.0001	P < 0.0001	P=0.0009

The P values < 0.001 indicates the values are highly significant

4.5 Selection of highest ureolytic bacteria

Based on the highest urease activity and $CaCO_3$ precipitation of the different isolates, the *B. paramycoides* MD6 strain was selected for further quantitative characterization. The effect of

temperature and pH on *B. paramycoides* MD6 growth cycle, urease activity, and $CaCO_3$ precipitation was tested at different intervals.

4.6 Influence of different temperature and pH conditions on the physiology of *B. paramycoides* MD6

Physical parameters such as pH and temperature affect bacterial cell cycle, urease activity, and calcite precipitation (Ferris et al. 2004; Nemati et al. 2005). Therefore, it becomes imperative to study the growth cycle of bacteria at varied pH conditions as the pH of the concrete environment is highly alkaline, with a pH value up to 11, which can rise to 13 (Seifan et al. 2016a; Algaifi et al. 2020).

4.6.1 Effect of temperature and pH variation on the growth cycle

Fig. 4.10 showed variation in the growth cycle of bacterial isolates *B. paramycoides* MD6 at different temperature and pH conditions. The cell density in the NB was determined by measuring the optical density of the culture. The lag phase of the bacterial growth cycle lasts for 4 h at incubation temperatures of 28 °C, 37 °C, and 45 °C, 2 h at 55 °C, and 6 h at temperature 25 °C. The log phase of the *B. paramycoides* growth continues till 8 h at 55 °C, 12 h at 28 °C, 37 °C and 45 °C and 18 h at 25 °C. After the log phase, the bacterial cell cycle gradually enters the stationary phase. The lag phase of the growth kinetics corresponds to a low concentration of bacterial cells (~10^1 cells/ml), whereas the initial log phase of the growth cycle corresponds to a concentration of ~10^3 cells/ml. The optical density of the culture increased from 0.253 at 4 h to 0.792 at 6 h at 37 °C. The concentration increases with the increase in the incubation time corresponding to the concentration of ~10^8 cells/ml. The optimum range of bacterial growth was observed at 28 °C - 45 °C. At high temperatures, the metabolic activity of the bacteria quickly leads to the utilization of the nutrients and reaches the stationary phase earlier than in lower temperature conditions. On the contrary, at low temperatures, the cells remain in the lag phase for longer periods because of less affinity for nutrient uptake (Membré et al. 2005). At temperatures lower than optimum growth temperature, the cell membrane becomes stiff, decreasing the transport of nutrients across the membrane (Nedwell 1999). Similarly, the growth of bacteria was measured at different pH (6 - 12) conditions. The optimum range at which bacterial growth was observed to maximum was between pH 7 and 10. The concentration of cells during the lag phase was approximately 10^1 cells/ml, which increases gradually to ~10^3 cells/ml during the initial-log phase after 6 h incubation at 37 °C in

nutrient broth media with an optimum pH range 7 -10. Higher and lower pH levels than this range can alter the bacterial growth cycle, slowing the activation energy to increase the cell yield in the solution or surrounding environment. Meanwhile, the lag phase at pH 11-12 is continuous for 6 – 8 hours and then enters the log phase until 18 hours of incubation. Similar results were reported by Kadapure et al. (2020) at temperatures 24 °C, 30 °C, 37 °C, 40 °C and 45 °C and reported optimum growth of *B. sphaericus* at 37 °C. Another researcher, Membré et al. (2005), also studied the growth cycle of *B. cereus* at temperatures 15 °C, 25 °C, 35 °C and 45 °C. Feng et al. (2021) reported pH 10 best for *B. subtilis*, M9 growth.

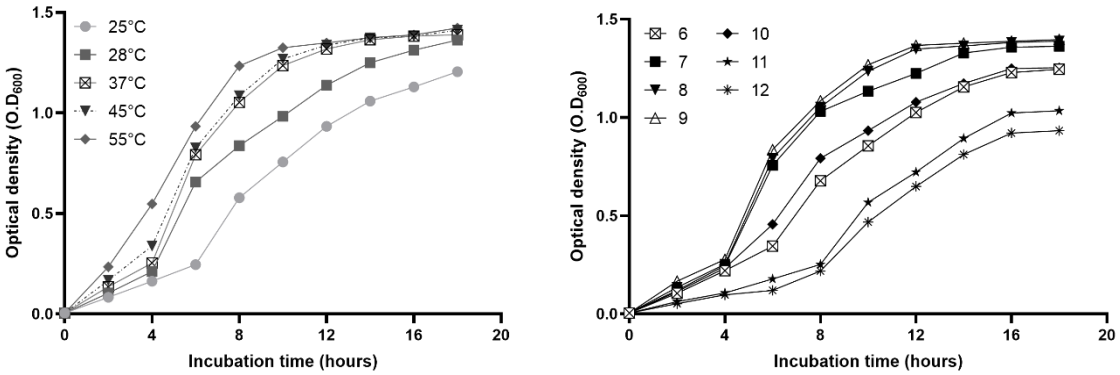


Fig. 4.10 Growth cycle of *B. paramycoides* at different (a) temperatures (25 °C, 28 °C, 37 °C, 45 °C, and 55 °C) and (b) pH (6-12) conditions

4.6.2 Effect of temperature and pH variation on urease activity

The *B. paramycoides* was tested for urease activity at different temperatures. As shown in Fig. 4.11, temperature significantly affected urease activity at 24, 48, 72, 96, and 120 h of incubation. Enzyme activity was evaluated in the temperature range of 25 – 55 °C. The bacteria exhibited the highest urease activity in the temperature range of 28 – 45 °C with maximum activity at 37 °C. After 24 h of incubation, the urease activity increased by 41.8% when the temperature was increased from 25 to 37 °C. However, compared to 37 °C, enzyme activity reduced by 13.8% and 37.9% at 45 °C and 55 °C, respectively. The highest urease activity was recorded after 96 h of incubation at 37 °C (1126.55 U/ml), followed by 28 °C (931.28 U/ml). The urease activity evaluated at a high temperature of 55 °C was 439.98 U/ml after 96 h of incubation. During the initial incubation phase, urease activity was higher at 45 °C than at 25 °C and 28 °C. However, a significant drop-in urease activity was observed after 96 h of

incubation, possibly because of the immediate utilization of the substrate (urea) and nutrients provided. Due to the high metabolic activity of bacteria at high temperatures, they soon enter a declining growth phase and show a decrease in urease activity. Microbes are said to have a suitable temperature range in which the metabolic activity of bacteria is highest, at which enzyme activity is also maximum. Temperature increases beyond this range would decrease enzyme activity due to protein denaturation and loss of bacterial metabolic activity (Xie et al. 2023). Urease tends to degrade at higher temperatures (Sun et al. 2019) and weaken at low temperatures (Whiffin et al. 2007). In the current study, bacteria efficiently exhibited urease activity in the 25 °C to 55 °C range. Moreover, the study correlated with the scope of the field study where temperature does not exceed 50 °C. Temperature below 25 °C slows bacterial metabolism and inhibits growth (Sun et al. 2019a). Similarly, Omoregie et al. (2017) studied urease activity in the temperature range of 20 – 45 °C and reported maximum urease activity by bacteria at 30 °C. Sun et al. (2019) showed a rise in urease activity of *B. megaterium* and *Sporosarcina pasteurii* with an increase in temperature from 15 to 30 °C. Unlike this, Whiffin (2004) reported a 70 °C optimum temperature for the enzyme activity of *S. pasteurii*.

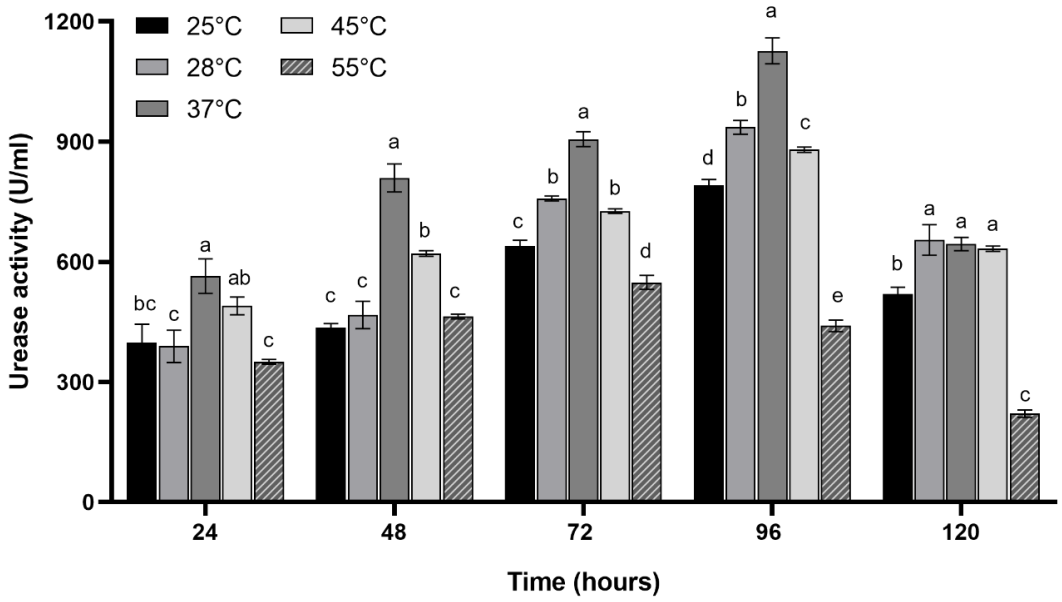


Fig. 4.11 Urease activity at different temperature conditions. Values bearing different letters at each time interval are significant at $p<0.05$. Values are mean ± SD (n=3)

Likewise, urease activity by *B. paramycoides* was evaluated at different pH (6 -12) conditions to investigate the efficiency of the metabolic activity of bacteria. The optimum pH range was 7 – 10, with the highest urease activity at pH 9. The highest urease activity of 1547.8 U/ml was

recorded at pH 9 (Fig. 4.12). At pH 9, the urease activity decreased by 38.7% and 60.1% after 96 h of incubation at pH 11 and 12, respectively. In all flasks, enzyme activity decreased after 120 h of incubation. At pH 9, the enzyme activity decreased 41% after 120 h of incubation. Therefore, urease activity was not observed after 120 h owing to a sudden decrease in enzyme activity, possibly because of nutrient depletion and cell death. The optimization results were consistent with the findings of Singh et al. (2017) and Oualha et al. (2020). pH significantly affects bacterial metabolism, affecting the ability of bacteria to break down urea. A high pH can slow the growth cycle by extending the lag phase (Yi et al. 2021). Moreover, a significant change in pH can alter the enzyme's structural integrity, which may further impact the binding ability of the enzyme to the substrate (Piumetti 2022). Other studies have reported similar results. Wang et al. (2017) discovered the highest urease activity at pH 8.5 and a sharp decline at pH 11.5. Lors et al. (2017) found maximum urease activity in the pH range of 8 – 10 and claimed that alkaliphilic bacteria could endure neutral to basic pH levels of up to 11. Nathan et al. (2020) reported maximum urease activity at pH 7. The optimal pH of two *Aspergillus* fungal isolates was between 8.0 and 8.5 (Kappaun et al. 2018). In contrast, a study by Phang et al. (2018) reported higher urease activity at pH four than at pH 7, suggesting acidic urease compatibility. The data were analyzed using Tukey's test, which showed that temperature and pH variation significantly affected urease activity at 5% significance (Table 4.7).

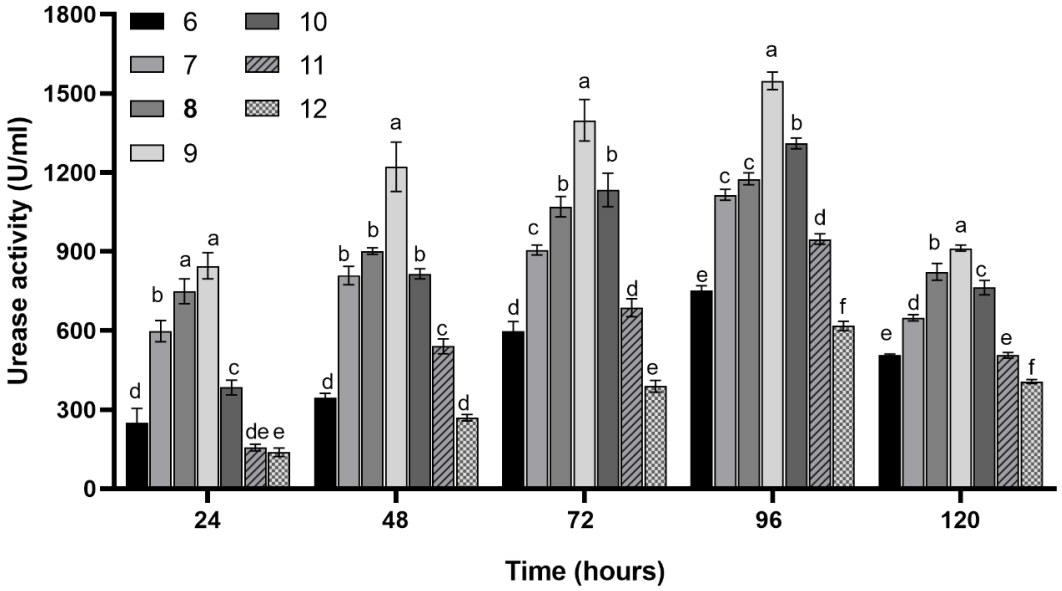


Fig. 4.12 Urease activity at different pH (6 -12). Values bearing different letters at each time interval are significant at $p<0.05$. Values are mean ± SD (n=3)

Table 4.7 The factorial ANOVA results indicate the effect of different temperature, pH conditions on urease activity

Variables			Treatment	Time	Interaction (Treatment× Time)
Urease activity	Temperature	df	4,8	4,8	16,32
			P < 0.0001	P < 0.0001	P < 0.0001
	pH	df	6,12	4,8	24,48
			P < 0.0001	P < 0.0001	P < 0.0001

4.6.3 Effect of temperature and pH variation on $CaCO_3$ precipitation

Fig. 4.13 (a) and (b). showed the amount of $CaCO_3$ precipitated by *B. paramycoides* in nutrient broth supplemented with 2% urea and 25 mM $CaCl_2$ incubated at different temperatures (25 – 55 °C) and pH values (6 – 12). The amounts of $CaCO_3$ precipitation recorded at different temperature conditions, that is, 25 °C, 28 °C, 37 °C, 45 °C, and 55 °C after 120 h incubation was 604, 699, 806, 799, and 720 mg per 100 ml, respectively. $CaCO_3$ precipitation was not observed in flasks incubated without urea or calcium chloride addition. Maximum $CaCO_3$ precipitation was achieved at 37 °C. The highest $CaCO_3$ formation by *B. paramycoides* was found in the 28 – 55 °C range, indicating that *B. paramycoides* bacteria are capable of high-temperature conditions. The $CaCO_3$ precipitation is highly dependent on the ureolytic reaction provided nutrients, calcium sources, and urea are available for the metabolism of bacteria. $CaCO_3$ precipitation was observed to increase with the increase in the temperature. It is reasonable from the urease activity results that the higher the temperature, the faster the metabolic reaction and the urea hydrolysis to form $CaCO_3$. Unlike urease activity, high temperature does not have a significant effect on $CaCO_3$ deposition except when comparing low temperature (25 °C) to moderate (37 °C) and to high (45 °C) temperature, which shows a significant difference in $CaCO_3$ precipitation. Temperature range might affect the rate of reaction and urea hydrolysis, but overall, $CaCO_3$ precipitation is dependent on amount of substrate and enzyme available for the reaction. However, the rate of Ca^{2+} removal may vary depending on conditions provided at different times. Similar work was carried out by Korchef and Touaibi (2020).

Similarly, the amount of $CaCO_3$ precipitated under different pH conditions indicated that *B. paramycoides* was metabolically active in alkaline environments (Fig. 4.12b). The maximum precipitation was recorded at pH 9, after which $CaCO_3$ precipitation decreased upon further

increasing the pH of the medium. The amounts of $CaCO_3$ precipitated in the controlled laboratory conditions recorded after 120 h of incubation at pH 9, 10, 11, and 12 were 975, 952, and 897 mg/100 ml. Compared to pH 12, the $CaCO_3$ precipitated at pH 7 was 806 mg/100ml, 10% less than pH 12. Therefore, it can be concluded that an alkaline environment promotes $CaCO_3$ precipitation. In the current experiment, the temperature was kept constant at 37 °C. $CaCO_3$ precipitation was observed to be increasing with an increase in pH till pH nine, after which it shows a decreasing trend, which might be attributed to the low metabolic rate. The slow activity of the urease enzyme resulted in a lower consumption of calcium ions (Xie et al. 2023). The highest $CaCO_3$ precipitation was observed at pH 9. The results were analyzed statistically at a 5% level of significance. pH affects the ureolytic reaction, resulting in the amount of NH_3, NH_4^+, CO_3^{2+}, and HCO_3^- present in the pore solution, influencing the $CaCO_3$ precipitation rate and output. If pH is in the optimum range, the metabolism of the bacteria is fast, and Ca^{2+}, CO_3^{2-}, and HCO_3^- ions are in saturation state. This leads to faster mineralization and the formation of smaller $CaCO_3$ crystals (Tang et al. 2020). Similar results were also reported by Seifan et al. (2017); Sun et al. (2019); Yi et al. (2021); Elmi et al. (2023). Another researcher, Helmi et al. (2016), reported $CaCO_3$ precipitation by *B. licheniformis* at optimum pH of 8 and temperature 35 °C with no precipitation at 50 °C.

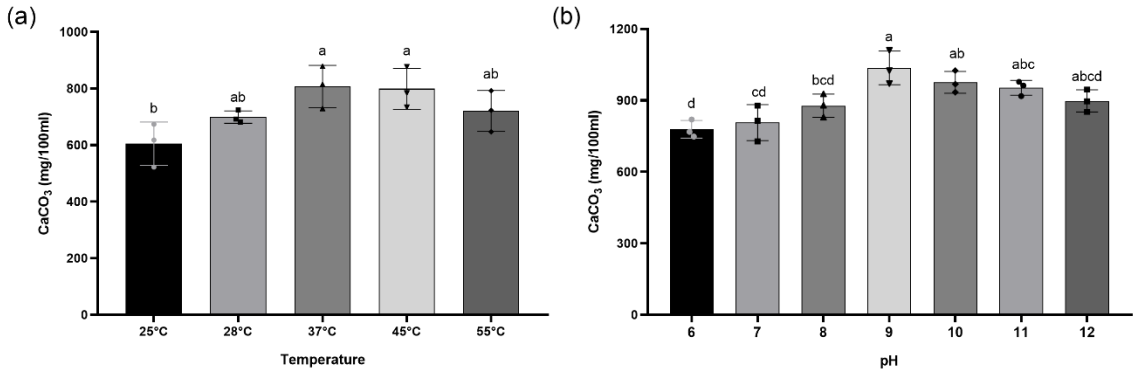


Fig. 4.13 (a) $CaCO_3$ precipitation at different temperature conditions (25 - 55 °C), (b) $CaCO_3$ precipitation at varied pH (6 – 12). Values bearing different letters are significant at $p<0.05$. Values are mean ± SD (n=3)

4.6.4 Calcium removal

Fig. 4.14 and 4.15 shows the percentage removal of calcium ions at different temperature conditions during the $CaCO_3$ precipitation experiment. Calcium (Ca^{2+}) removal percentage was

evaluated based on the presence of soluble Ca^{2+} ions in the supernatant collected at each time interval. The investigation was carried out at different temperature (25 – 55 °C) and pH (6 – 12) conditions. The quantity of soluble calcium in the media decreased continuously with an increase in the incubation period. Ca^{2+} removal was estimated at different incubation temperatures. Maximum Ca^{2+} removal was observed at 37 °C followed by 45 °C, 55 °C, 28 °C and 25 °C with 96, 89, 84, 66 and 64% calcium removal, respectively (Fig. 4.14). Percentage removal variation at different temperatures could be because bacterial growth varies at each temperature conditions. During the bacterial lag phase, calcium removal was slow and started increasing as soon as the bacterial cycle entered the log phase of growth. The statistical analysis showed that temperature and time interval significantly affect calcium removal percentage from the calcifying solution. Similarly, Ca^{2+} removal was evaluated at varied pH (6 – 12) conditions (Fig. 4.15). After 120 h of incubation, minimum (76%) calcium removal was observed at pH 6, and maximum (96%) removal at pH 9. Whereas, at highly alkaline conditions, i.e., pH 12, 80% of calcium removal was evaluated. The statistically analyzed data showed that pH and time interval significantly affect $CaCO_3$ precipitation. Similar work was carried out by Zhu et al. (2017) by live and UV-killed biofilm-forming cyanobacterial *Gloeocapsa* PCC73106.

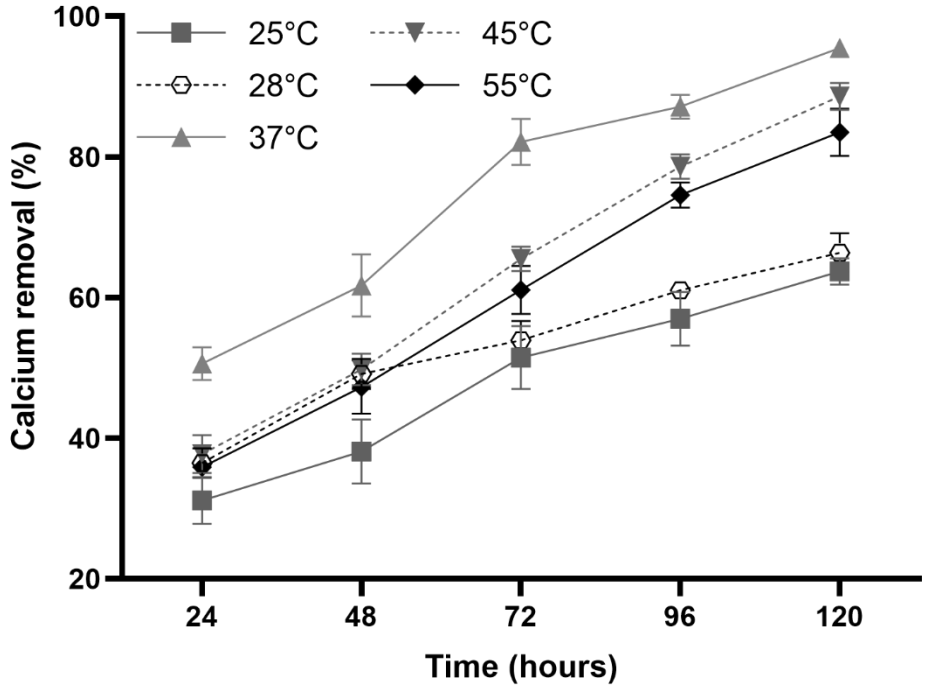


Fig. 4.14 Calcium removal percentage (%) at different temperatures (25 – 55 °C) at 24, 48, 72, 96 and 120 h. Values bearing different letters at each time interval are significant at $p<0.05$. Values are mean ± SD (n=3)

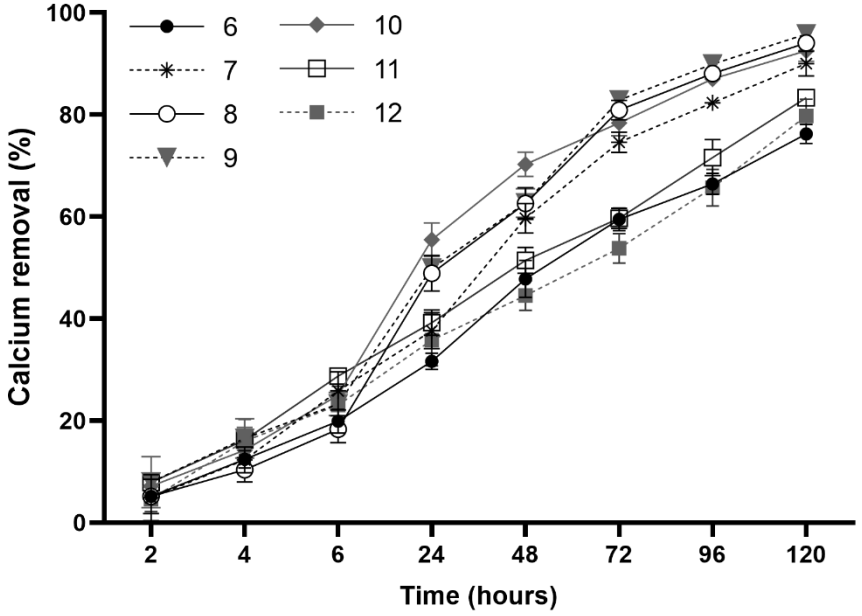


Fig. 4.15 Calcium removal percentage (%) at different pH (6 – 12) conditions at 24, 48, 72, 96 and 120 h. Values bearing the different letters at each time interval are significant at $p<0.05$. Values are mean ± SD (n=3)

4.6.5 pH dynamic

The pH of the solution was monitored during the $CaCO_3$ precipitation experiment at varied temperature and pH conditions. Initially, pH was monitored for 2-, 4-, and 6- h at 24-hour incubation intervals. The pH of the nutrient broth dropped after adding calcifying solution (2% urea and 25 mM $CaCl_2$) but was recovered within a few h of incubation. It might be due to a urease enzyme reaction increasing the pH of the media. The flask inoculated at 37 °C showed a drop in pH from 7 to 5.78 as urea and $CaCl_2$ were added, which further dropped down to 5.26 till the 4 h of incubation (Fig.4.16a). However, the pH of the nutrient broth medium increased to 7.24 at 24 h and 7.62 at 120 h. The pH of the media increased after 24 h of incubation at every temperature condition. It can be attributed to the fact that the soluble Ca^{2+} ions in the medium were decreasing at each time interval, proving calcium binds with bicarbonates (HCO_3^-) in the media to form $CaCO_3$.

At the same time, the pH of the solution was also examined at varied pH (6 - 12) conditions to determine the physiological changes in the nutrient broth during calcification. The experiment was carried out in triplicate. Initially, the broth's pH was adjusted as per the experiment's requirement. It suddenly decreased after adding calcium chloride to 5.34, 5.78, 6.94, 7.95, 8.9, 9.53, and 11.64 at pH 6, 7, 8, 9, 10, 11 and 12, respectively (Fig. 4.16b). When added in the

media, calcium chloride absorbs hydroxide and leaves free protons behind. This lowers the pH of the media. After six h of incubation, an increase in the pH was observed, showing $CaCO_3$ precipitation in the solution. The statistically analyzed data proved time significantly affects pH variation during $CaCO_3$ precipitation. Liang et al. (2013) and Zhu et al. (2017) reported variations in pH during $CaCO_3$ precipitation. Similar results were documented by Obst et al. (2009); Han et al. (2017).

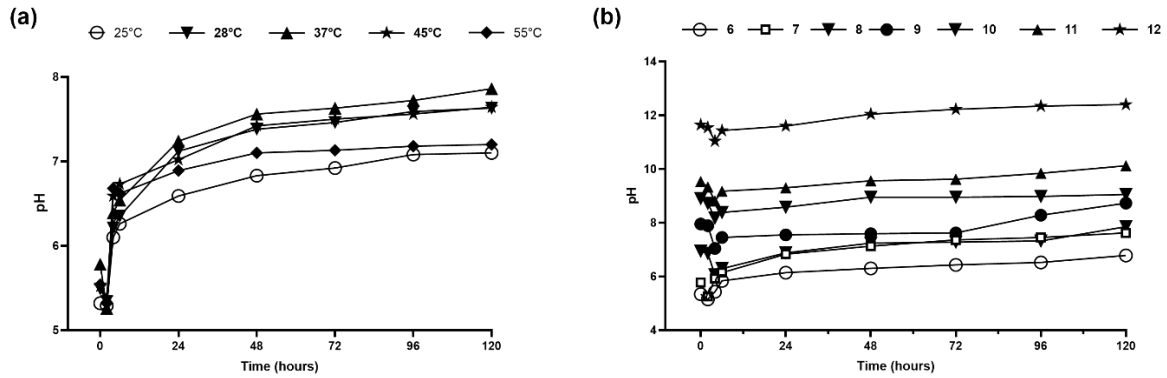


Fig. 4.16 pH dynamic during $CaCO_3$ precipitation experiment at different (a) temperatures (25 – 55 °C) and (b) pH (6 – 12) conditions at different time intervals (2, 4, 6, 24, 48, 72, 96 and 120 h) in nutrient broth supplemented with the calcifying solution (2% urea and 25 mM $CaCl_2$)

4.6.6 Microstructural analysis

Fig. 4.17 shows crystallization formed due to ureolysis in NB using SEM-EDS. The crystal lattice was identified to be a rhombohedral structure assembled over each other in triangular layer form. The crystallization was recognized as $CaCO_3$. The chemical composition of the crystals formed was analyzed using EDS. The amount of calcium, oxygen, and carbon in a sample collected was 14.9, 63.4, and 21.2%, respectively (Fig. 4.17c, d). The X-ray powder diffraction (XRD) results confirmed the presence of calcite crystals with a high-intensity peak at 29.2° (Fig. 4.17c). The other peaks of calcite were observed at 39.36, 43.11, 47.44, and 48.45, corresponding to 104, 113, 202, 018, and 116 planes of calcite. The powdered crystal powder was observed to be ~100% pure calcite. The results were in correspondence with other researchers (Qian et al. 2021; Rui and Qian 2021). These diffractograms are consistent with those reported in the literature for pure calcite

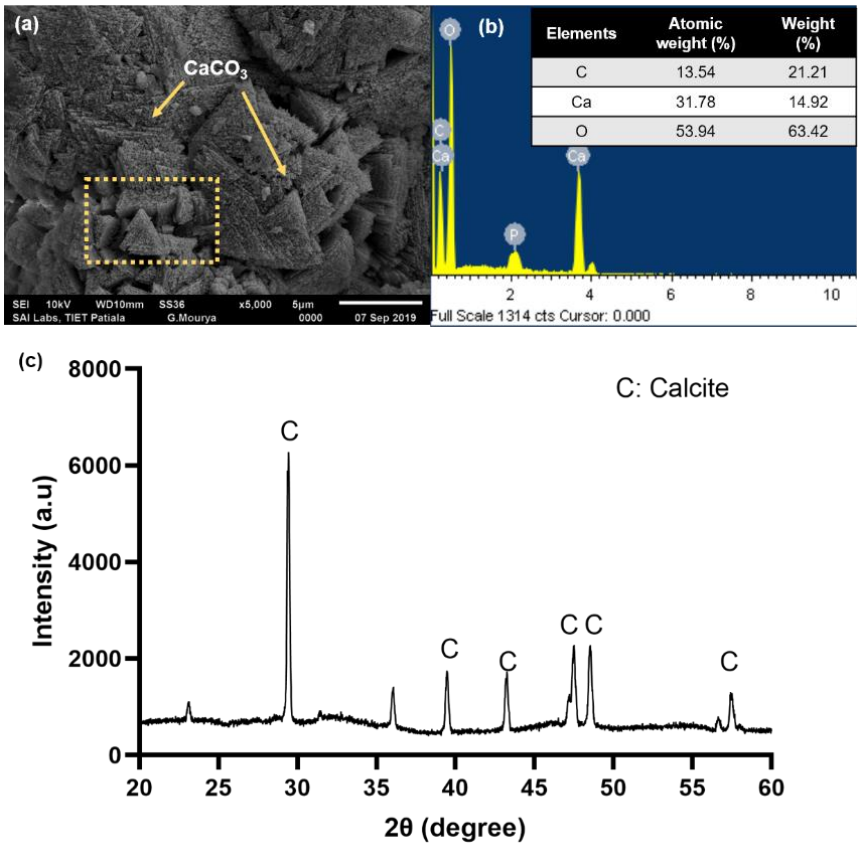


Fig. 4.17 (a) SEM analysis of powdered $CaCO_3$ precipitates, '□' symbol represent spot analyzed for EDS (b) EDS showing elemental composition of carbon (C), calcium (Ca) and oxygen (O) in precipitates (c) XRD analysis of powdered $CaCO_3$ precipitates depicting the presence of calcite as predominant crystalline

4.7 Sand consolidation using different-sized sand grains

The binding property of the $CaCO_3$ precipitated by *B. paramycoides* was studied using the sand consolidation experiment. The bacteria admixed and control sand column was continuously fed with NB at 12 h intervals. The sand columns were opened, and a solid cylindrical consolidated sand column was observed in bacterial admixed columns (Fig. 4.18). The flow rate of the calcifying medium was measured at regular intervals till 20 days of consolidation. The flow rates of the bacterial cell treated and the control columns were almost the same initially. As shown in Fig. 4.19 (a), there was a 32.6%, 32.8%, and 25% reduction in the flow rate of control columns after 20 days. However, the flow rate declined significantly in the bacterial admixed sand columns, indicating that MICCP is causing gradual restriction of the flow channels. The flow rate was almost obstructed at the end of the 20th day. Initially, on the 0-day, the flow rate was estimated to be 7.71, 7.46, and 8.65 ml/min in the experiment set—

BC-150, BC-300, and BC-600, which declined to 2.34, 2.56, and 2.63 ml/min, respectively at 20th day. The reduction in the flow rate in BC-150, BC-300, and BC-600 treated columns is primarily because of the deposition of bounded carbonates. The carbonate biominerals reduce the pore size between the sand particles, clogging the flow of the calcifying solution. Dhami et al. (2016) studied sand consolidation using different grain sizes (0.2, 0.5, and 1.0 mm) and reported an 88% decrease in the flow rate in all bacterial columns and a 5% reduction in the control column. Achal et al. (2011) also reported a decline in the flow rate and 33% calcite content in the top layer of a sand column. The statistically analyzed data shows a significant difference in the flow rate analysis of the bacterial treated and control columns at the end of the experiment.

The bacterial admixed sand column after complete consolidation was compared to the control without bacteria. Sand columns treated with bacterial cells were more compact and solider than control columns. Partial binding was formed in sand columns BC-300 and BC-600 (Fig. 4.19b). Small clumps were shaped on the bottom of BC-300 and BC-600, which were not completely bound together during the 20 days. However, the upper part of the sand column was consolidated entirely. On the other hand, the control sand column (NB-150, NB-300, and NB-600) showed negligible binding of the sand grains. The consolidated sand column was further divided into three parts to estimate the $CaCO_3$ content. The upper part of the column in BC-150, BC-300, and BC-600 was dense and more rigid than the bottom parts. Fig. 3.21 shows the decreasing trend of $CaCO_3$ formation in the three layers of the sand column in BC-150, BC-300, and BC-600 columns. The maximum $CaCO_3$ precipitation recorded in the upper layer of BC-150 was 42.5 mg/g. The $CaCO_3$ precipitation in the upper layer of BC-300 and BC-600 columns was 32.3 and 31.1 mg/g, respectively. The $CaCO_3$ precipitation in the middle part of the sand columns was 31.6 mg/g, 26.6 mg/g, and 21.6 mg/g, respectively, in BC-150, BC-300, and BC-600 columns. Statistically analyzed data showed significant differences in calcite precipitation in different parts of the columns. The $CaCO_3$ precipitation in the different layers of the column was in agreement with previous studies (Mahawish et al. 2019; Sharma et al. 2020a; Sharma et al. 2021; Jin et al. 2022).

A chunk of the upper layer of the sand column was taken and analyzed using FESEM-EDS to confirm the $CaCO_3$ precipitation. Fig. 4.20 gives explicit confirmation of calcite formation in the BC-150 sand column. The precipitation was observed to be dense and bonded to form an

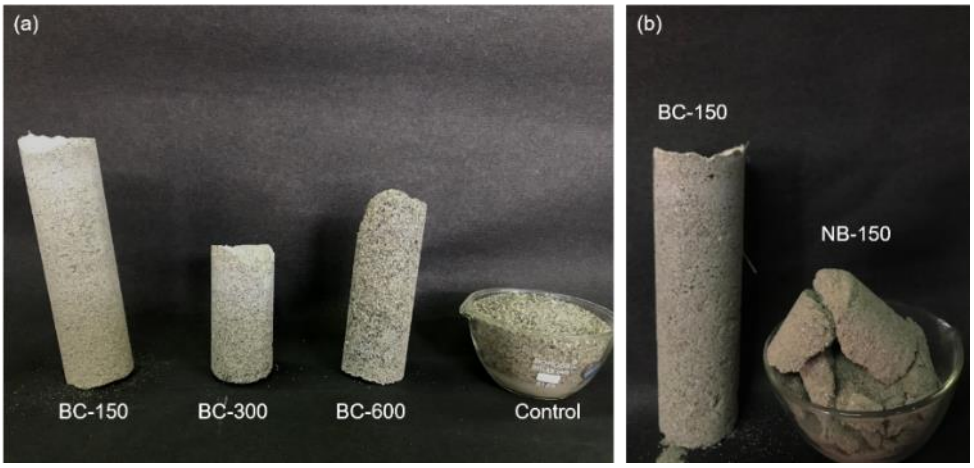


Fig. 4.18 (a, b) Consolidated sand columns using different-sized sand grains by *B. paramycoides* MD6

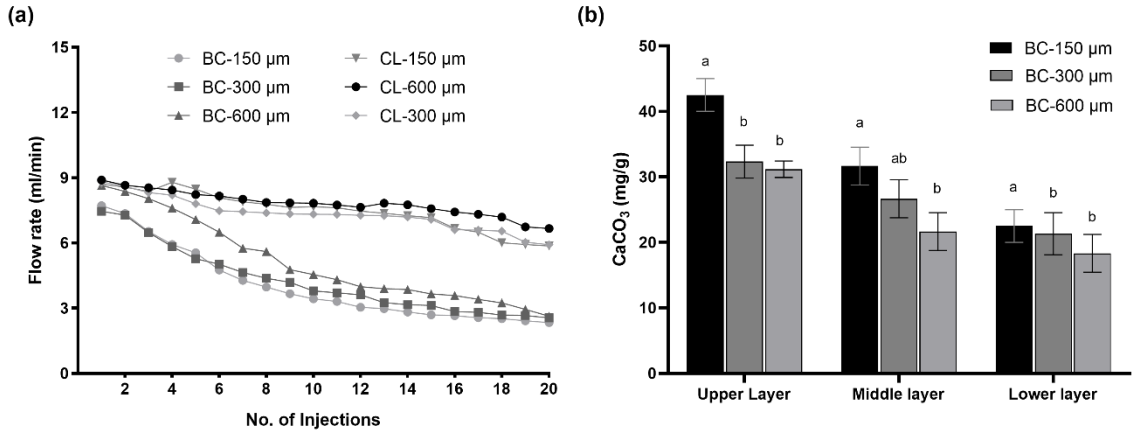


Fig. 4.19 (a) Flow rate of nutrient broth supplemented with calcifying solution (2% urea and 25 mM $CaCl_2$) during 20 days (b) $CaCO_3$ precipitation in the upper, middle, and bottom part of sand columns. Values bearing the different letters within the treatment are significant at $p<0.05$. Values are mean ± SD (n=3)

aggregation of crystals. The crystals were rhombohedral in shape with a size of 5 - 10 µm. The precipitated crystal was established to be a $CaCO_3$ polymorph by the elemental analysis of the whole area using energy dispersive spectroscopy (EDS). Fig. 4.20 (d) confirms the chemical composition of calcite to be carbon, oxygen, calcium, and silica, which shows the presence of sand particles. These results suggest that *B. paramycoides* cells can precipitate $CaCO_3$ crystals within the voids of the sand column. The X-ray diffraction analysis confirmed calcite precipitation in the consolidated sand column after 20 days. XRD spectrums of bacterial

admixed and control samples are presented in Fig. 4.21. The prominent peaks observed in the powdered sand sample are quartz (Q), and calcite (C). The high-intensity peak of calcite was observed at 29.2° in bacterial treated sand column. However, no peak was seen in control, indicating the precipitation of $CaCO_3$ in bacteria-incorporated sand columns. Similar results were reported by (Phua and Røyne 2018; Park et al. 2022a).

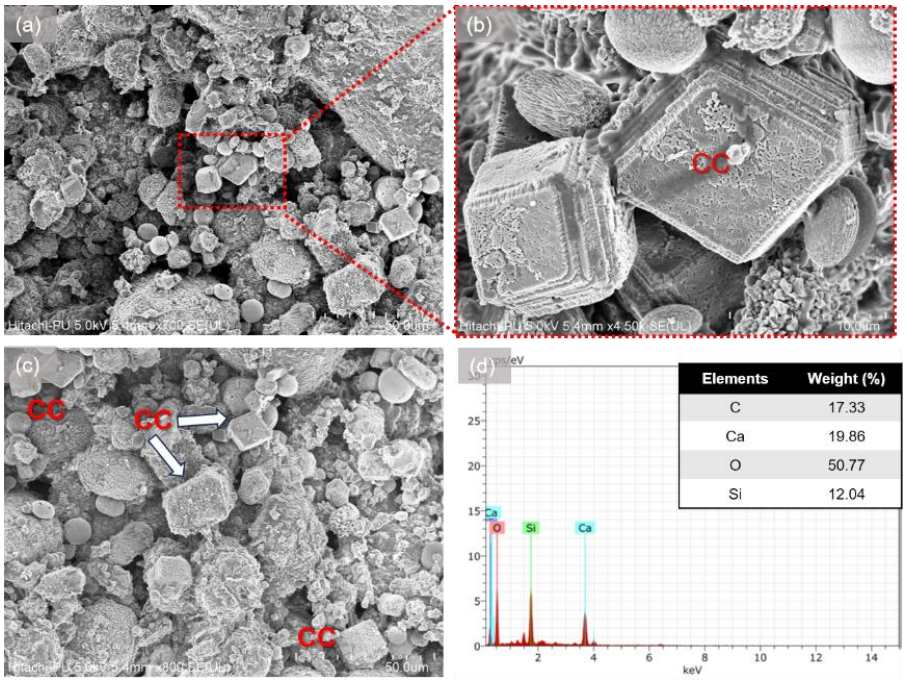


Fig. 4.20 (a-c) FESEM of bacterial treated sand column (d) EDS showing elemental composition of $CaCO_3$

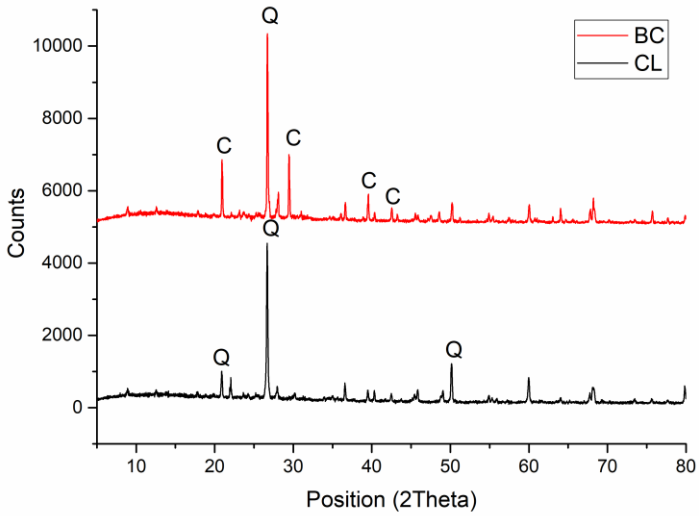


Fig. 4.21 Bacterial admixed sand column (BC) and control specimen (CL) (Q: Quartz and C: Calcite)

4.8 Enhancement of the overall properties of concrete by ureolytic bacteria

The effect of ureolytic bacteria on mechanical strength and permeability of concrete specimens was tested at different curing times. The *B. paramycoides* culture was incorporated in the concrete mix and added during curing treatment. The results were compared with the conventional concrete mix, i.e., concrete specimens prepared with tap water, which was taken as control in the present investigation.

4.8.1 Compressive strength

The strength properties of concrete specimens were tested at 3, 7, and 28 days of curing. Fig. 4.22 showed a significant improvement in the compressive strength of specimens cast and cured using *B. paramycoides* (BPC) compared to the control. After 28 days of curing, the compressive strength of BPC specimens was 44.5 MPa. At the same time, the control specimens showed 34.5 MPa of compressive strength. Compared to the control, BPC specimens showed a 28.9% improvement in the strength properties of concrete. The ureolytic reaction by heterotrophic bacteria utilizes the urease enzyme as a catalyst and initiates the $CaCO_3$ precipitation as bacterial growth enters the log phase. If urea and calcium sources are available, the biomass of bacteria produces the carbonate precipitation that fills up the pores in the concrete (Krishnapriya et al. 2015). The analysis of variance inferred that the incorporation of different bacterial treatments and curing periods (3, 7, and 28 days) had a significant effect on the strength properties of concrete (Table. 4.8). Similar results were reported by other researchers (Basaran Bundur et al. 2015; Skevi et al. 2021; Dhivakar Karthick et al. 2022).

Table 4.8 The factorial ANOVA results indicate the effects of different treatments and time of curing on cementitious properties

Variables		3 days	7 days	28 days
Compressive strength	df	4	4	4
		P = 0.0033	P = 0.0030	P < 0.0001
RCPT	df	-	4	4
		-	P = 0.0003	P = 0.0002

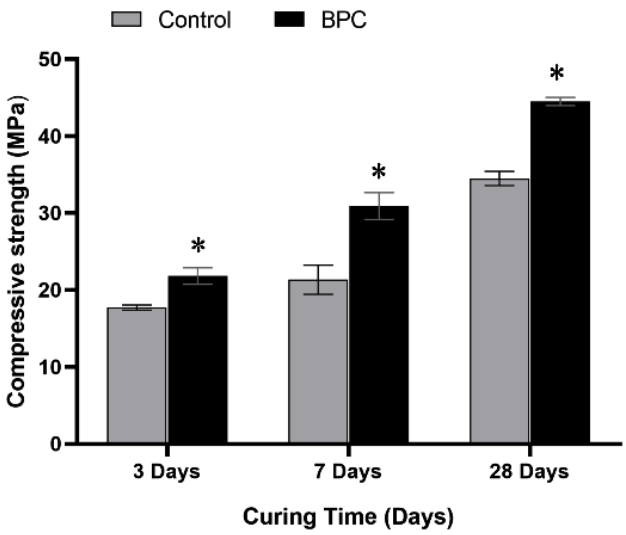


Fig. 4.22 Compressive strength of *B. paramycoides* treated (BPC) and control at 3, 7, and 28 days of curing. The asterisk (*) sign indicates values are significant compared to control at $p<0.05$ using t-test. Values are mean ± SD (n=3)

4.8.2 Rapid chloride penetration test (RCPT)

The RCPT of the concrete specimen was tested at 7 and 28 days of curing. The chloride penetration in the concrete samples treated by *B. paramycoides* bacterial culture decreased significantly with an increased curing period. The results were expressed in the coulombs, measuring the amount of current passed at 30-minute intervals for six hours. Compared to the control, the BPC specimens treated by heterotrophic strain *B. paramycoides* showed minimum penetration among all the groups. Fig. 4.23 represents the current passed through BPC specimens during the RCPT experiment, which was 1440 coulombs (C). The test results for BPC specimens showed 27.2% and 57.8% reduction after 7 and 28 days of curing by decreasing chloride ingression during the RCPT experiment, respectively. As per the ASTM standard C1202, the penetrability of chloride ions after 28 days of curing was moderate based on the charge passed through the specimens (ASTM C1202 2012). This might be due to $CaCO_3$ particles that seal the pores in concrete, making it difficult for water and other particles to infiltrate through concrete pores. However, the charge passed through the control specimen was higher than BPC specimens. The statistical analysis showed that different curing treatments (*B. paramycoides*, and control) and curing time (7 and 28 days) have a significant

effect on the chloride penetration in the cylindrical specimen (Table 4.8). Similar findings were reported by other researchers (Nosouhian et al. 2016; Wu et al. 2019; Soda and Mini 2022).

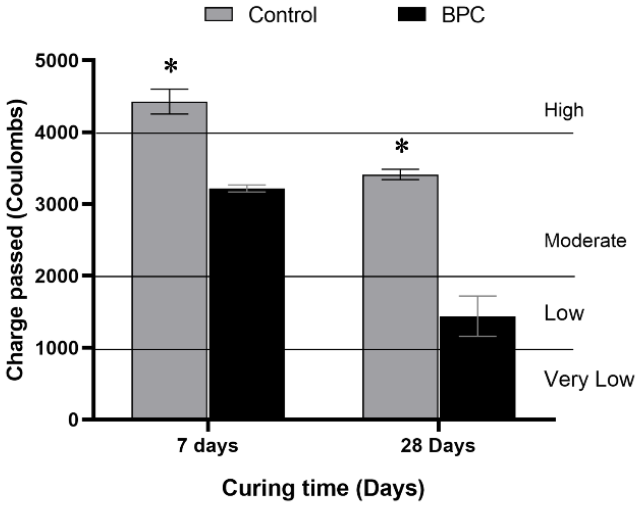


Fig. 4.23 Rapid chloride permeability test (RCPT) at 7 and 28 days of curing. The asterisk (*) sign indicates values are significant at $p<0.05$ using t-test. Values are mean ± SD (n=3)

4.8.3 Sorptivity test

The water absorption test was carried out at 7 and 28 days of curing. The results were analysed during the rapid absorption phase for initial 6 h. The results are illustrated in Fig. 4.24a and 4.24b as the average water absorption by 100 mm × 50 mm cylindrical specimens against square root mean of time. The seven days cured BPC specimens showed cumulative water absorption of 1.2 mm of water after 6 h of the experiment, respectively (Fig. 4.24a). Compared to which control specimen showed water absorption of 2 mm. It clearly indicates that bacterial treatment significantly affects the water absorption rate compared to the control. After seven days, the sorptivity coefficient '*k*' of BPC, and control specimens was observed to be 0.007, and 0.011, respectively. After 28 days of curing, the control specimens showed higher water absorption of 1.7 mm, which might be due to the rise of water through capillary pores. However, bacterial curing showed a significant reduction in BPC specimens. BPC specimens showed 0.94 mm of average water absorption at the end of the experiment. It might be due to the activity of bacteria that precipitates the $CaCO_3$ particles in the pores of the concrete. As a result, the interconnected capillary pores were blocked, reducing the water's capillary rise in concrete. The sorptivity coefficient '*k*' evaluated for the BPC and control specimens was 0.005

and 0.01, respectively (Table 4.9). The lower sorptivity coefficient '*k*' for the BPC specimens proved that ureolytic action reduces the specimens' capillary pores. Similar results were reported by Xu et al. (2018), Anand et al. (2022a), and Vaezi et al. (2020) in ureolytic bacteria-based concrete.

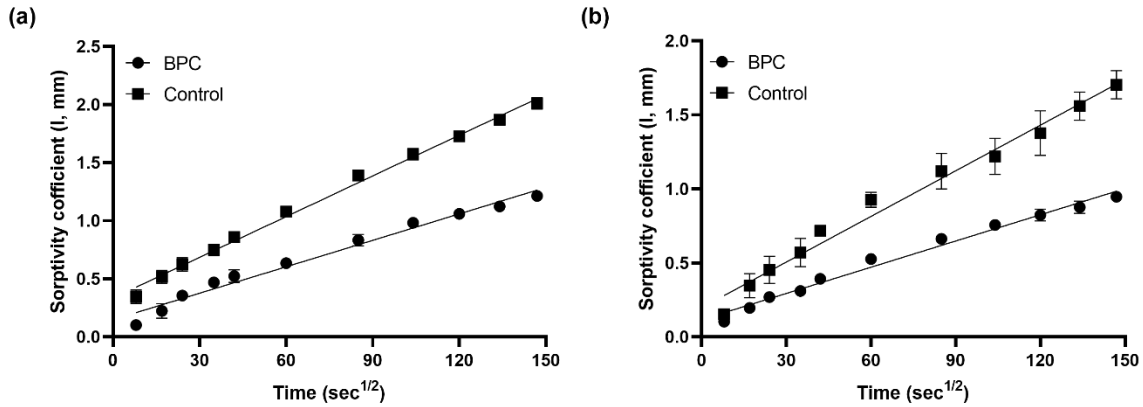


Fig. 4.24. Water absorption concrete specimens treated with *B. paramycoides* (BPC) and control at (a) 7 days and (b) 28 days of curing

Table 4.9 The factorial ANOVA results indicate the effect of different treatments (*B. paramycoides* and control) and curing time on water absorption for concrete specimens

	Sorptivity coefficient '*k*'		**R^2**			
Variables	7 days	28 days	7 days	28 days	P value	Significant
Control	0.01168	0.01027	0.9906	0.9592	P<0.0001	Yes
BPC	0.00759	0.005902	0.9715	0.9792	P<0.0001	Yes

4.8.4 Microstructural analysis

Fig. 4.25. shows the structural analysis of $CaCO_3$ precipitation in the concrete sample. The crystals were tightly packed and formed a perfect rhombohedral crystal lattice in a 5 – 10 μm size range in BPC specimens. $CaCO_3$ crystals were identified as calcite, further confirmed by EDX analysis. The mineral constituents characterized by EDX analysis indicate high-intensity Ca, O, and C peaks formed in BPC specimens compared to the control. The carbon, oxygen, and calcium percentages in the BPC sample were 18.15%, 58.02%, and 22.50%, respectively (Fig. 4.25b). In control, the carbon, oxygen, and calcium percentages were 34.49%, 46.90%, and 12.58%, respectively (Fig. 4.25a). The calcite precipitation by heterotrophic bacteria was

also reported by Park et al. (2022b), Qian et al. (2022), and Qin et al. (2021). Anand et al. (2022b) reported calcite crystallization by *Bacillus megaterium* SS3 in concrete.

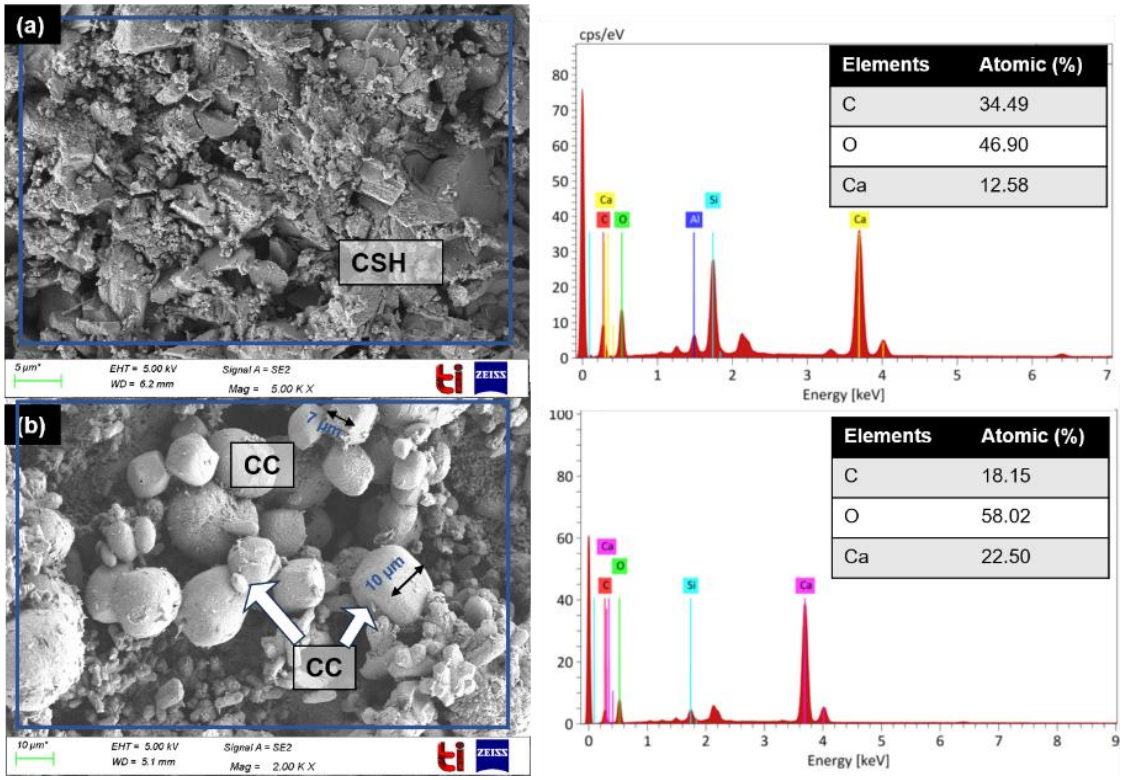


Fig. 4.25 FESEM-EDS analysis of (a) control (b) BPC specimens after 28 days of curing

4.8.5 XRD

The X-ray diffraction analysis confirmed calcite precipitation in the hardened concrete cured using microbial cultures (*B. paramycoides*) at 28 days. XRD spectrums of BPC, and control sample are presented in Fig. 4.26. The prominent peaks observed in the powdered concrete sample are quartz (Q), calcium silicate hydrate (CSH), calcite (C), and vaterite (V). The intensity peak of calcite observed at 29.2° was higher in BPC specimens than in the control. Calcite is the most stable crystalline form (Xiao et al. 2010). It indicates that microbial activity occurring in concrete precipitates $CaCO_3$. Moreover, the weak diffraction peak of vaterite, which is a thermodynamically unstable crystal form with a high nucleation rate, was also seen in the BPC specimens. The slow diffusion of carbonates (CO_3^{2-}) and calcium ions (Ca^{2+}) can lead to calcite formation (Weiner and Patricia M. Dove 2003). Both microbial cultures efficiently induced the calcite precipitation in the concrete. It is unclear why different polymorphs of $CaCO_3$ are formed during microbial $CaCO_3$ mineralization in concrete. Stuckrath et al. inferred the presence of functional groups, such as sulfhydryl (-SH), amino (-

NH_2), carboxyl (-COOH), and hydroxyl (-OH) groups, that serve as nucleation sites for binding with Ca^{2+} ions can control the crystal deposition (Stuckrath et al. 2014). Other factors affecting $CaCO_3$ precipitation are calcium ion concentration, dissolved inorganic carbon (DIC) concentration, pH, and the availability of nucleation sites (Tripathi et al. 2019).

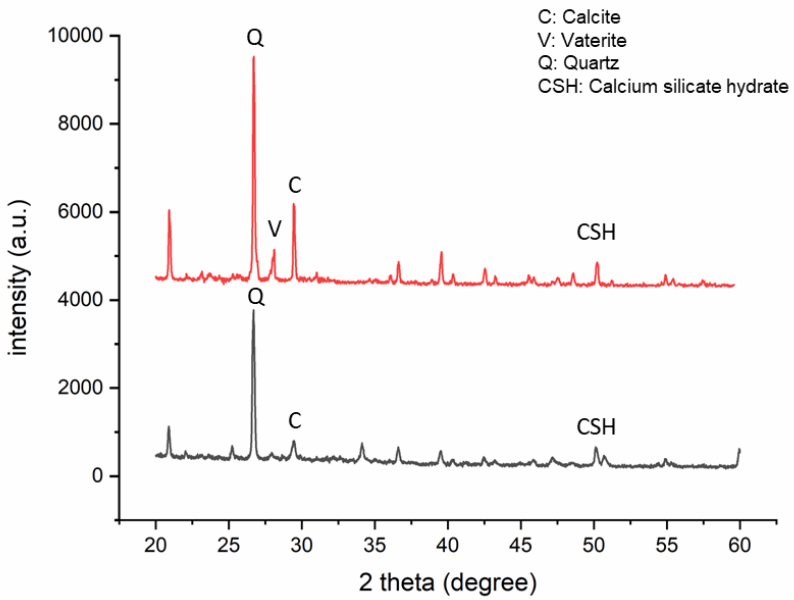


Fig. 4.26 XRD of BPC and control concrete specimens after 28 days of curing

4.9 Development of metakaolin based biomaterial

The current study was further extended to develop metakaolin as a sustainable carrier material for immobilizing bacterial spores using adsorption. To prepare the spores of the bacterial strain *B. paramycoides*, commercial nutrient broth (NB) media, and industrial waste corn steep liquor (CSL) media was used. MK powder was used as a carrier material to immobilize the spores. To prepare a carrier material a concentration of 5.2×10^{-5} spores was uniformly mixed in the MK powder under aseptic conditions. A moisture content of 20% was maintained in the MK material. The spore-immobilized MK biomaterial was stored in sterile petri dishes. The biomaterial stored at 25 °C was labeled as NB-25, CSL-25, and at 4 °C was labeled as NB-4 and CSL-4.

4.9.1 Viability of spores

Bacterial spores are dormant and have a hard shell known as spore coat around the cell wall, which helps them to endure harsh environmental conditions such as high temperatures, freezing, and desiccation (Checinska et al. 2015). The spore-immobilized MK biomaterial was

stored in sterile petri dishes. The survival of spores immobilized in metakaolin carrier material was evaluated every 7 days for up to 180 days of storage using the plate count method. The carrier material stored at 25 °C was labeled as NB-25 and CSL-25; at 4 °C, it was labeled as NB-4 and CSL-4. Fig. 4.27 shows the viability results evaluated in terms of log colony-forming units per gram (CFU/g). Initial cell viability before storage for NB and CSL immobilized bacterial spore is 7.7 log cfu/g. When NB was used as a nutrient source, the developed biomaterial exhibited a cell count of 7.7 and 7.6 log cfu/g after 91 days, which declined to 7.6 and 7.5 log cfu/g after 180 days at 4 °C and 25 °C, respectively. Whereas, when CSL was used as nutrient source, the cell viability of the biomaterial was 7.6 and 7.5 log cfu/g after 91 days, which declined to 7.4 and 7.3 log cfu/g after 180 days of storage at 4 °C and 25 °C, respectively. It was observed that the biomaterial stored at 4 °C proved to be more efficient than 25 °C for maintaining the dormant stage's spores for a long time. However, it is important to note here that the biomaterial stored at 25 °C was also successful in the maintenance of the immobilized spores during storage with a cell concentration of 7.5 and 7.3 log cfu/g in NB-25 and CSL-25 after 180 days, respectively. Therefore, it can be inferred that spores stored at different temperatures (25 °C and 4 °C) could break the dormant stage and activate the vegetative stage as moisture and nutrients were provided. Figs. 4. 28 and 4.29 represent colony formation on the solid agar plates, depicting the viability of the biomaterial for a storage period of 180 days. The immobilization approach enables bacteria to adhere to the carrier substance, protecting it within the concrete environment for an extended amount of time without losing viability. These results were in agreement with those reported by other researchers (Zhu et al. 2021b; Yang et al. 2022). Anand et al. reported the effective survivability of freshly incorporated bacterial cells in fly ash and silica fume after 180 d of storage (Anand et al. 2022c; Anand et al. 2022b). Son et al. reported an initial concentration of $2.0 \pm 0.5 \times 10^6$ cfu spores in microcrystalline cellulose tablets (Son et al. 2022). Xiao et al. reported a decline in the concentration of viable spores stored in an alkaline solution at 25 °C for 30 days (Maleki-Kakelar et al. 2022). Joshi et al. also reported the utilization of CSL as an alternative nutritional source as efficient as commercial nutrient growth media for the growth of ureolytic bacteria (Joshi et al. 2018b).

4.9.2 Urease activity of biomaterial

The urease activity was evaluated for the spores immobilized in metakaolin biomaterial stored at 4 °C and 25 °C before and after 180 days of storage. It was noted that biomaterial, when inoculated in nutrient broth (NB – 4 and NB - 25) and CSL broth (CSL - 4 and CSL - 25) the

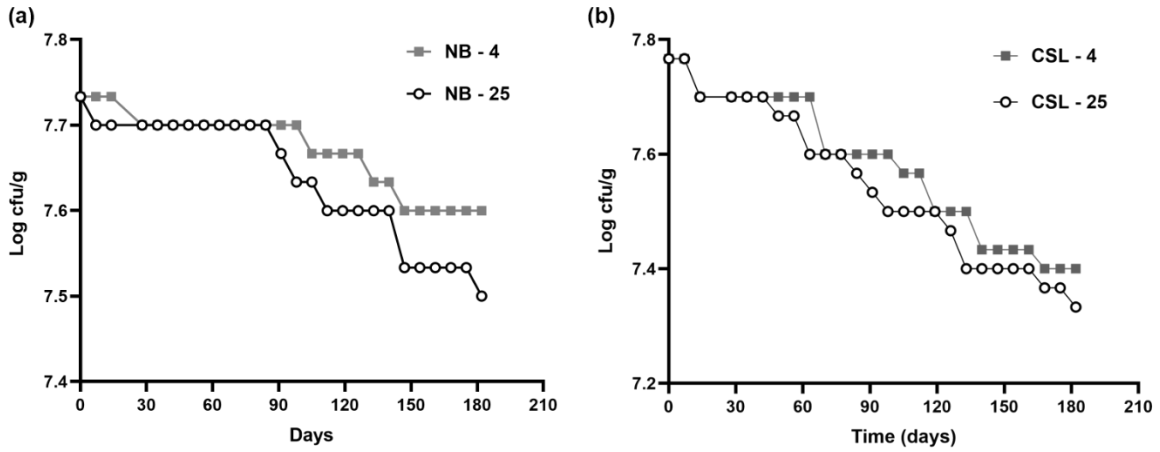


Fig. 4.27. Bacterial cell count (log cfu/g) of developed biomaterial (a) NB-4 and NB-25 (b) CSL-4 and CSL-25 stored at 4 °C and 25 °C in the petri plate. The values are significant at $p<0.05$ using t-test

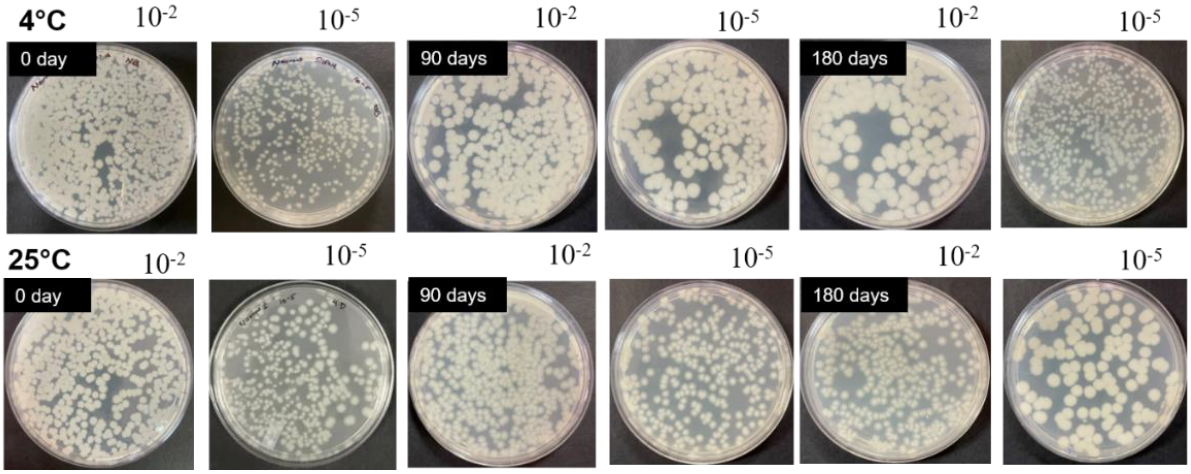


Fig. 4.28 Nutrient agar (NA) plates showing spore viability of developed biomaterial stored at 4 °C and 25 °C for 180 days (26 weeks)

spores were able to germinate and increase the concentration of bacteria in the nutrient broth due to the availability of the nutrients and oxygen. As shown in Fig. 4.30, the urease activity of biomaterial before storage was 554.48 U/ml after 24-h incubation in NBU at 37 °C. The biomaterial exhibited the highest urease activity of 989.07 U/ml after 96-h incubation. However, after 120-h incubation, the urease activity starts to decline. Therefore, the experiment was conducted till 120 h of incubation. The urease activity of the biomaterial before storage after 120-h incubation was 714.6 U/ml. The CSL – 4, NB – 4, CSL – 25, and NB – 25 efficiently

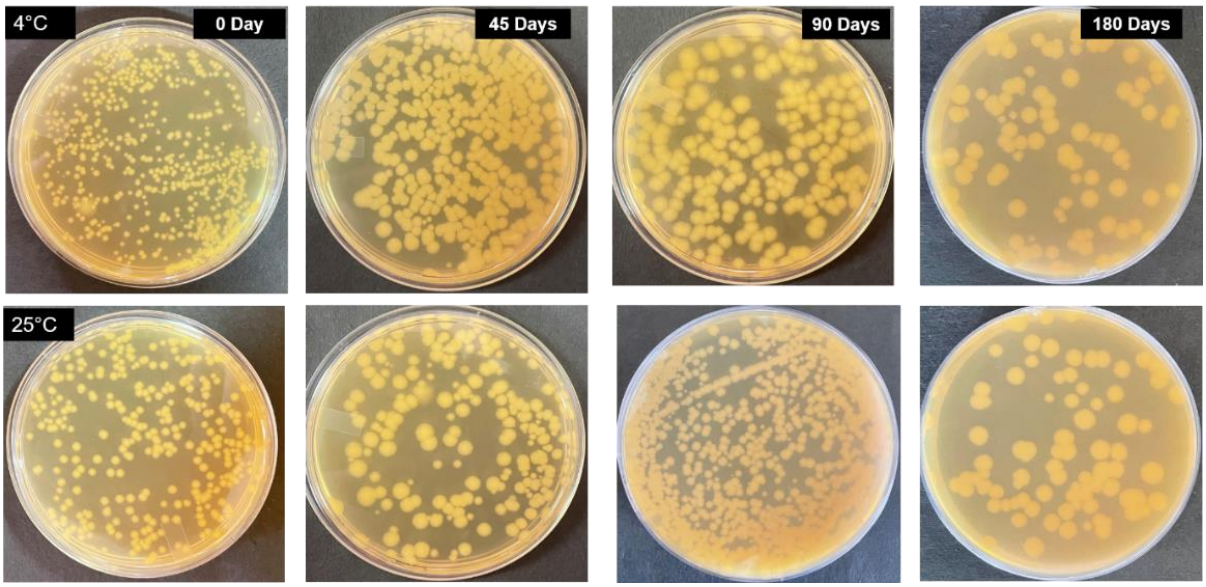


Fig. 4.29 Corn steep liquor (CSL) agar plates showing spore viability of developed biomaterial stored at 4 °C and 25 °C for 180 days (26 weeks)

exhibited urease activity even after 180 d of storage. However, the urease activity of biomaterials NB – 4 and CSL–4 was comparatively higher than that of NB – 25 and CSL–25. The urease activity of NB-4 and CSL-4 was 942.93 U/ml and 951.75 U/ml after 96 h incubation at 37 °C. Similarly, the urease activity for NB-25 and CSL-25 was 874.8 U/ml and 880.44 U/ml after 96 h incubation at 37 °C. The ability of the spores to show metabolic activity after 180 days of storage proved metakaolin is an efficient carrier material for spore immobilization. The data was analyzed statistically at 5% level of significance (Table 4.10). Similar results were reported by Maleki-Kakelar et al. (2022). Achal et al. (2010a) and Babakhani et al. (2020) used CSL as a nutrient growth medium.

4.9.3 Calcium carbonate precipitation by biomaterial

Fig. 4.31 shows the amount of $CaCO_3$ precipitated by the spore-based biomaterial (NB-4, CSL-4, NB-25, and CSL-25) incubated at 37 °C before and after 180 days of storage. The experiment was carried out in triplicates, and at each 24-h interval, a 100 ml flask was used to measure the amount of $CaCO_3$ precipitated. Before storage, $CaCO_3$ precipitation by biomaterial (0-D) was 139.6, 223.6, 416.6, 550.8, and 640.4 mg/100 ml at 24, 48, 72, 96, and 120 h, respectively. $CaCO_3$ precipitation by CSL-4 was 135.77, 233.79, 441.25, 580.67, and 652.43 mg/100 ml at 24, 48, 72, 96, and 120 h, respectively. Similarly, the $CaCO_3$ precipitation by CSL-25 was 136.7, 235.67, 416.60, 545.92, and 636.42 mg/ml at 24, 48, 72, 96, and 120 h, respectively.

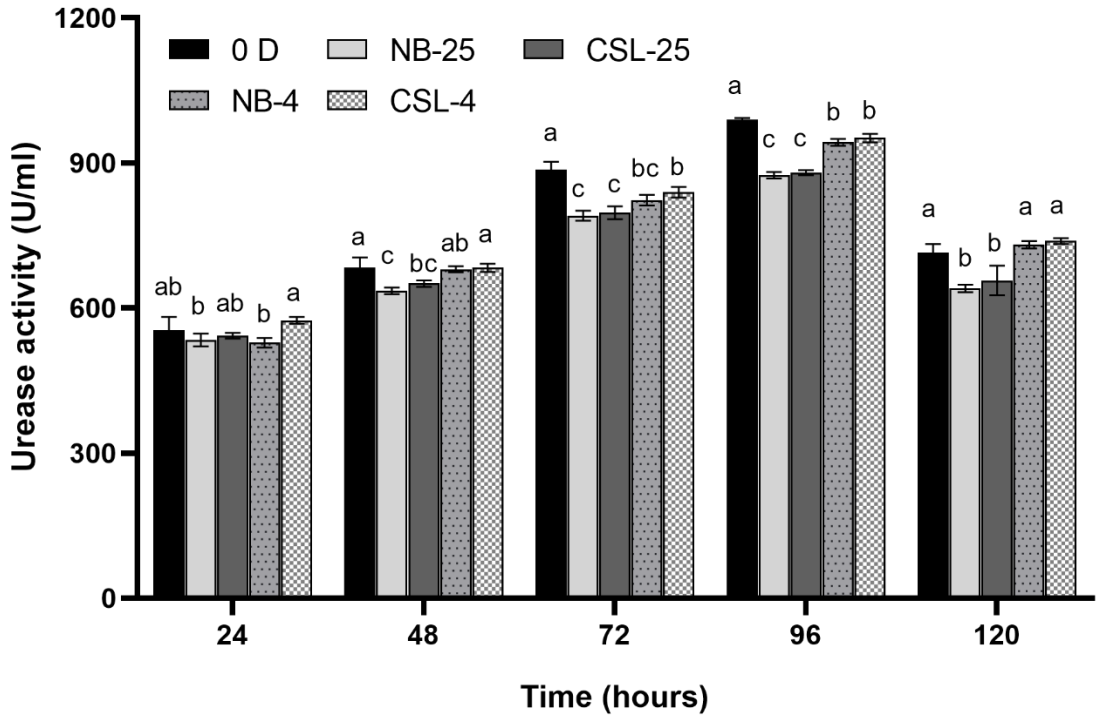


Fig. 4.30 Urease activity of developed biomaterial stored at 4 °C and 25 °C for 180 days. Values bearing different letters within the treatment at each time interval are significant at $p<0.05$. Values are mean ± SD (n=3)

The precipitation ability of the biomaterial proved that the spores were able to maintain their shelf life during storage to induce MICCP in the CSL solution. After storage of 180 days, $CaCO_3$ precipitation recorded by NB-4 was 134.4, 229.8, 427.2, 566.5, 642.4 mg/100 ml at 24, 48, 72, 96, and 120 h, respectively. Similarly, $CaCO_3$ precipitation at NB-25 was 138.12, 223.7, 407.64, 533.9 and 633.03 mg/100ml at 24, 48, 72, 96, and 120 h, respectively. The protective shells of endospores prevent bacterial cells from dying during nutrient deficiency, allowing them to preserve their long shelf lives. The highest urease activity was recorded by biomaterial CSL-4, followed by NB-4 and 0-D. Spores strongly resist dryness and severe conditions in their surroundings (Zhu et al. 2022). Zamani et al. confirmed the germination of bacterial spores encapsulated in a polyurea polymer and precipitation of $CaCO_3$ using FESEM (Zamani et al. 2020). Other researchers have reported MICCP using spores immobilized on different carrier materials (Wang et al. 2016; Wang et al. 2017; Xiao et al. 2022b). During urease activity, the pH of the medium increases, creating an alkaline environment adjacent to the bacterial cells for $CaCO_3$ precipitation (Achal et al. 2010b). The urease enzyme breaks down urea, producing carbonate ions as byproducts. These carbonate ions then interact with the

calcium around the bacterial cell to produce $CaCO_3$ precipitates in the medium (Dhami et al. 2013b). The $CaCO_3$ precipitated by biomaterial stored at different temperature conditions was analyzed statistically at 5% significance level (Table 4.10).

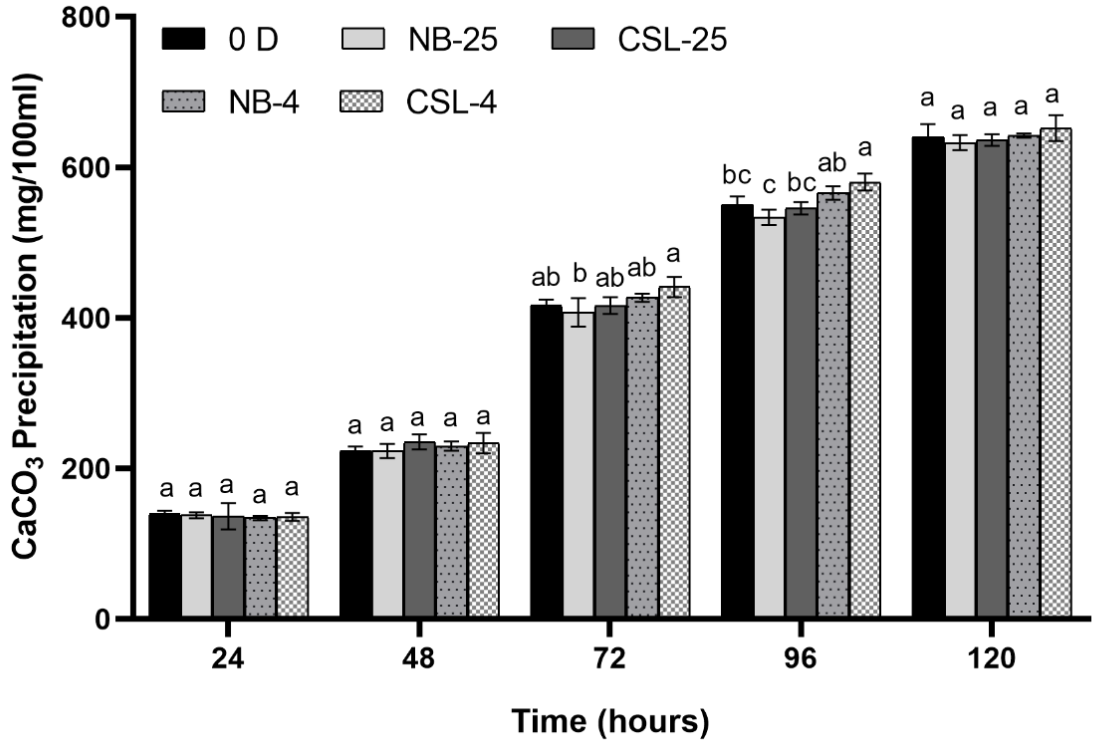


Fig. 4.31 $CaCO_3$ precipitation of developed biomaterial stored at 4 °C and 25 °C for 180 days. Values are mean ± SD (n=3). Values bearing different letters within the treatment at each time interval are significant at $p<0.05$. Values are mean ± SD (n=3)

Table 4.10 The factorial ANOVA results indicate the effect of different storage temperatures and time on urease activity and $CaCO_3$ precipitation

Variables		Treatment	Time	Interaction (Treatment× Time)
Urease activity	df	4,8	4,8	16,32
		P < 0.0001	P < 0.0001	P < 0.0001
$CaCO_3$ precipitation	df	4, 8	4, 8	16, 32
		P=0.0011	P < 0.0001	P=0.1267

4.9.4 Microstructural analysis of $CaCO_3$ precipitates

Fig. 4.32 shows the microstructural analysis of the $CaCO_3$ crystals (CC) in the powdered sample collected from the CSL broth and NB using SEM-EDS. The $CaCO_3$ precipitated in

CSL-4 broth showed staircase layers over one another, depicting the abundance of calcite precipitation by the bacteria immobilized in the biomaterial. The presence of bacterial cells was also detected along with the $CaCO_3$ precipitates. Similarly, in NB-4 filtrate, the $CaCO_3$ crystals were observed to be 3–4 µm and the bacterial cells were 1 µm. The EDS analysis confirmed the deposition of $CaCO_3$ in the form of carbon, oxygen, and calcium, as shown in Fig. 3.33 (b, d). The elemental analysis using EDS proved the presence of weight percentage of calcium, carbon, and oxygen 28.84%, 16.29%, and 47.75% in CSL-4 and 14.89%, 20.11%, 66% in NB-4 precipitated calcite powder, respectively. Similar results have been reported by Joshi et al. (Joshi et al. 2018b) by using CSL as a nutritional source for $CaCO_3$ precipitation.

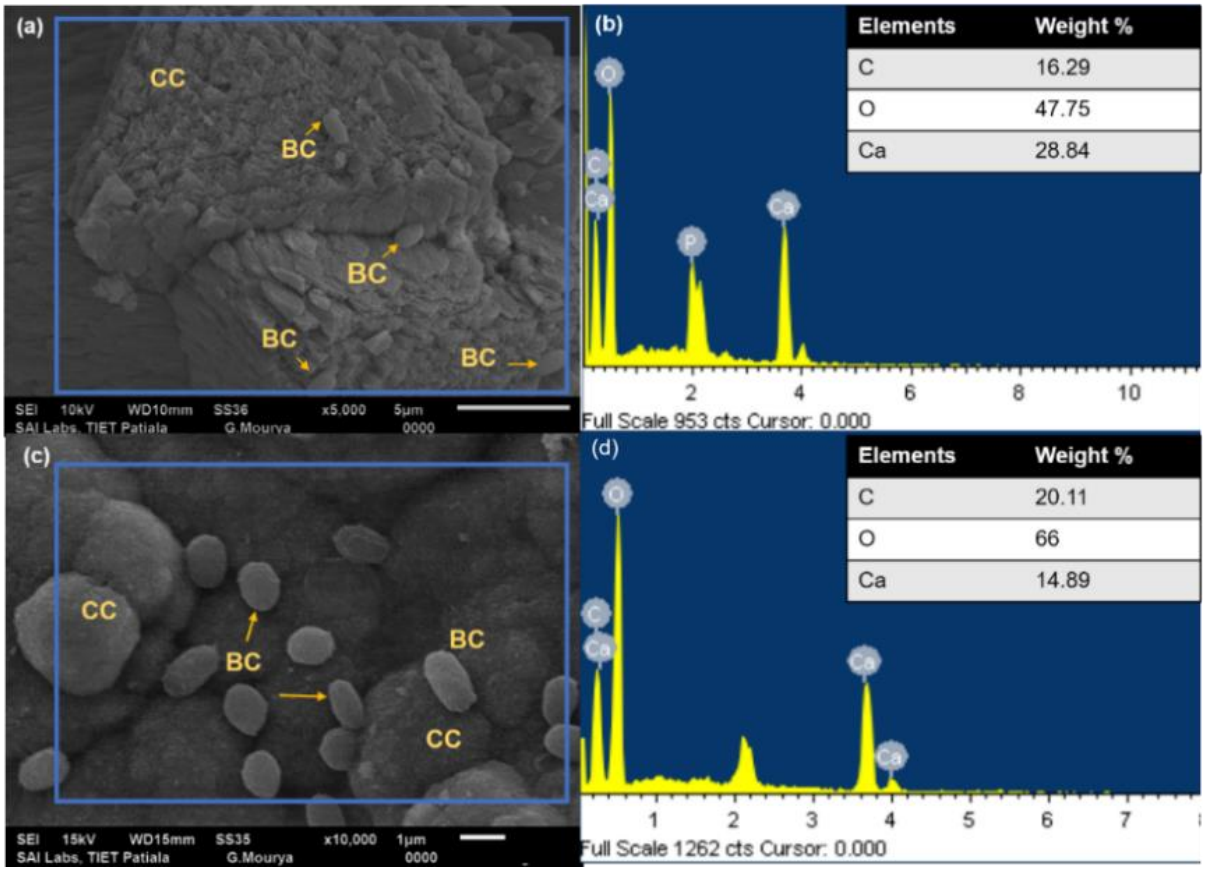


Fig. 4.32 FESEM-EDS of $CaCO_3$ precipitates (a, b) CSL-4 (c, d) NB-4 showing rhombohedral $CaCO_3$ crystal (CC) along with the presence of rod-shaped bacterial cells (BC). EDS spectrum marked square '□' shows elemental deposition of the $CaCO_3$

4.9.5 Strength properties of concrete

Fig. 4.33. shows the (a) flexural and (b) compressive strength results of the concrete specimens incorporated with 2% biomaterial after 7 and 28 days. The specimens were cured in growth

media consisting of CSL broth and NB supplemented with 2% urea and 25 mM $CaCl_2$, and control specimens were cured in tap water. The flexural strength of the biomaterial-incorporated specimens CSL-4 and NB-4 increased by 19.1% and 17.7% after the specimens were cured in the growth (CSL and NB) media, respectively. Similarly, at 28 days, the compressive strength of the CSL-4 and NB-4 specimens improved by 27.3% and 28.3%. This proves that the biomaterial actively increased the strength of the concrete. Spores immobilized in the biomaterial survive the harsh conditions of the concrete environment and lead to the densification of the concrete matrix by precipitating $CaCO_3$ in the pores of the specimens. The flexural and compressive strength of control is 4.18 MPa and 37.62 MPa after 28 days curing. Whereas the flexural strength of CSL-4 and NB-4 is 4.98 and 4.92 MPa, respectively. The compressive strength of CSL-4 and NB-4 is 47.90 and 48.27 MPa, respectively. The addition of biomaterials significantly improves the strength properties. Notably, no additional bacterial culture was inoculated into the curing medium during curing. The direct incorporation of urea and $CaCl_2$ without bacteria in cementitious material has retarding effect on the hydration process of concrete (Erşan et al. 2015; Başaran Bundur et al. 2017; Joshi et al. 2018a; Anand et al. 2023). However, in this study, the spores immobilized in MK served as an inoculum for bacterial growth, and the bacteria grew when they were provided with nutrients and moisture. In addition, the use of yeast extract (as a medium) without any bacterial inoculum decelerates the strength of the concrete (Amiri and Bundur 2018). However, when bacteria are added together with urea and calcium chloride, it forms $CaCO_3$ and enhances the strength of concrete (Yazici et al. 2023). Researchers have reported an improvement in flexural and compressive strength by immobilizing bacterial spores in different carrier materials such as zeolite (Bhaskar et al. 2017), metakaolin-based geopolymers (Yılmazer Polat and Uysal 2021), and calcium alginate beads (Soysal et al. 2020). Gao et al. reported a 10.28% increase in compressive strength and a 13.79% increase in flexural strength with the addition of hydrogel beads containing immobilized bacterial spores. In addition, metakaolin is considered a good supplementary cementitious material because it has a high silica content and is reported to increase the strength properties of concrete owing to the early stage of hydration (Barbhuiya et al. 2015; Pillay et al. 2022). Moreover, utilization of the CSL as nutrient medium does not changes the chemical characteristics of concrete (Joshi et al. 2018b). The improvement in strength properties of mortar was observed on addition of CSL as nutrient growth media (Achal et al. 2010a; Amiri and Bundur 2018).

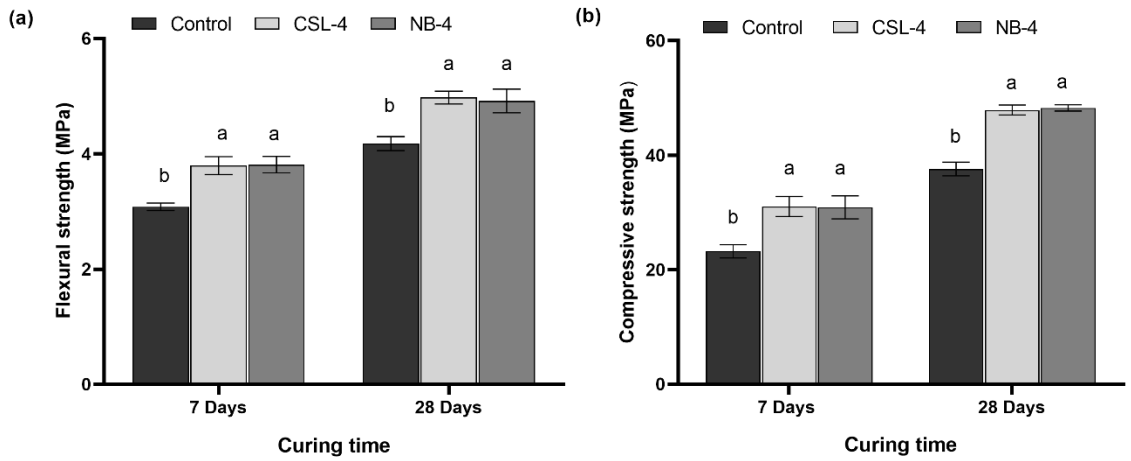


Fig. 4.33 (a) Flexural and (b) compressive strength of control, CSL-4 and NB-4 specimens at the age of 7 and 28 days. Values bearing different letters within the treatment at each time interval are significant at $p<0.05$. Values are mean ± SD (n=3)

4.9.6 Sorptivity test

Fig. 4.34 and Fig. 4.35 shows the amount of water absorbed per unit cross-sectional area of the CSL-4, NB-4, and control concrete specimen at 7 and 28 days. The bioconcrete specimens prepared using biomaterial (labeled as CSL-4 and NB-4) were more efficient in controlling the water absorption than the control specimens. The experiment was conducted for 6 h. The cumulative water absorbed at the end of the investigation by 7 days and 28 days cured control cylindrical specimens was 2.18 and 1.22 mm, respectively. However, CSL-4 specimens showed reduced cumulative water absorption after 7 and 28 d. The water absorption by the CSL-4 was 1.22 and 0.41 mm, respectively (Fig. 4.34). The water absorbed by NB-4 specimens was 1.23 and 0.41 mm at 7 and 28 days, respectively (Fig. 4.35). This low water absorption rate in CSL-4 and NB-4 concrete proves that bacteria precipitate in the pores of the concrete matrix. The outcome can be evaluated based on the biotreated specimen's sorptivity coefficient '*k*.' The sorptivity coefficients of the CSL-4 specimens were 0.006 and 0.002 at 7 and 28 days, respectively. The sorptivity coefficients of the NB-4 specimens were 0.006 and 0.002 at 7 and 28 days, respectively. However, the control specimens showed sorptivity coefficients of 0.01 and 0.007 at 7 and 28 days of curing, respectively, which were comparatively higher than those of the CSL-4 specimens. The CSL-4 specimens' low '*k*' values confirmed that incorporating bacterial spores could significantly improve the permeation properties. According to the literature, adding metakaolin to a specimen improves the permeation properties of concrete

(Abouhussien and Hassan 2015; TANYILDIZI et al. 2022). Similar results were also reported by Pillay et al. (2022) on the partial replacement of metakaolin in concrete.

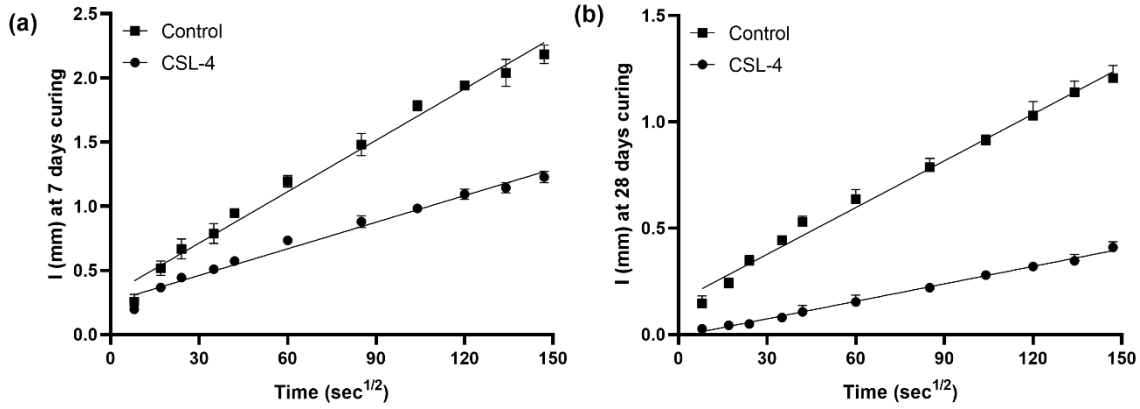


Fig. 4.34 Water absorption by CSL-4 and control specimen at the age of (a) 7 and (b) 28 days

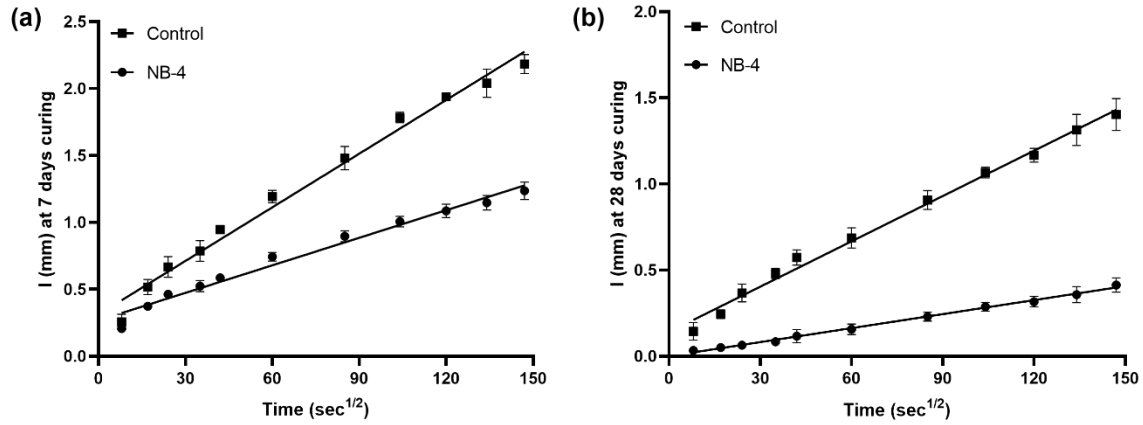


Fig. 4.35 Water absorption by NB-4 and control specimen at the age of (a) 7 and (b) 28 days

4.10 Crack remediation by CSL-4 bacterial inoculum

Two groups of specimens, CSL-4 and control were monitored for the complete duration of crack healing. The control specimens were sprayed with water without adding calcifying solution (2% urea and 25 mM $CaCl_2$). CSL-4 samples were initially subjected to an injection-based treatment of growth media supplemented with calcifying solution (2% urea and 25 mM $CaCl_2$) for five days to activate the endospores and their biomineralization activity at adjacent boundaries of the crack. After which, the spray curing with CSL and the calcifying solution

was employed up to the complete healing. $CaCO_3$ precipitation was not seen in the control specimen. The visual examination of crack healing was monitored, and the crack width was measured. The UPV and water tightness were studied at different healing durations. Upon complete healing, the healing particles inside the crack were identified using FESEM-EDX and XRD.

Initially, the precipitation was only visible on the crack edges in the CSL-4 specimen. A microscopic image was taken using a DinoLite microscope, showing the deposition of $CaCO_3$ crystals at the depth of the cracked area (Fig. 4.36). The presence of urea and $CaCl_2$ in the growth medium facilitated ureolytic biochemical reactions in the cracked region, promoting the bio-mediated $CaCO_3$ precipitation. Crack closure was monitored by measuring the reduction in the crack width at five different locations in the concrete specimens. Measurements were taken using a DinoLite microscope. Initially, crack widths of 0.538 mm, 0.468 mm, 0.532 mm, 0.514 mm, and 0.483 mm were measured at five locations in the crack region. After continuous treatment using the CSL medium in the crack region, white carbonate precipitates were observed on the walls of the cracked region after seven days. On the 14^{th} day, visible detection of $CaCO_3$ was observed, with a reduction in the crack width to 0.502 mm, 0.428 mm, 0.497 mm, 0.472 mm and 0.439 mm. Over a period of 50 days curing, the crack width at location 'A' decreased from 0.538 to 0. 007 mm, with a crack-healing efficiency of 98.7% (Fig. 4.37 a, b). Similarly, at location 'B', the crack width decreased from 0.468 mm to 0.009 mm, exhibiting a crack-healing efficiency of 97%. At the same time, locations 'C, D, and E' showed healing efficiencies of 100% (Fig. 4.37b). Statistical analysis using one-way ANOVA proved that the crack width was significantly reduced in the 50-day duration at a 5% significance level. No precipitation was seen in control specimens. Specimens incorporated with biomaterial showed autonomous healing of crack width in the 0.450 mm and 0.550 mm range. Similar results were corroborated using bacteria immobilized on different carrier materials, such as expanded glass granules (Zhang et al. 2022), hydrogels (Gao et al. 2020b), and rubber particles (Xu et al. 2019a). Xu et al. reported 100% crack healing with 417 μm crack closure using a low-alkali cementitious material (Xu and Wang 2018). Anand et al. (2022b) reported 0.5 mm crack healing in 45 days using bacteria immobilized in silica fume as a carrier material. Previously reported studies have shown that carrier materials have significantly maintained microbial mineralization activity and improved the crack self-healing efficiency (Borg et al. 2017; Feng et al. 2022). Even the CSL has been proven to be an effective nutrient growth medium for crack healing by Amiri et al. (2016) and Amiri et al. (2018).

4.10.1 Regain in ultrasonic pulse velocity (UPV)

Fig. 4.38 shows the UPV was measured for a reference specimen (REF) without any cracks, specimens after cracking (AC), and specimens with healed cracks (HC). The UPV was found to be 4018 m/s in the REF specimen. Also, the UPV was acquired on the cracked prismatic specimen (AC) and was recorded to be 3276 m/s. To monitor the healing process, UPV was acquired till the complete healing. The regain in UPV measurement ensured the in-depth healing of cracks due to $CaCO_3$ precipitation by the bacteria. At 9%, 32.5%, and 63% of crack healing, the UPV values were observed to be 3474.7, 3584.3, and 3726.3 m/s. Upon complete crack closure, the UPV value was observed closer to the reference specimens, which is 3986.4 m/s. The crack was 100% healed, and restoration of the crack region was successful. Moreover, this increase in pulse velocity confirmed the deposition of $CaCO_3$ at the depth of the crack. Meanwhile, a 3.1% regain in UPV was seen in control, which clearly depicts negligible healing. The Statistical analysis confirmed a significant improvement at the 5% significance level. Other researchers have also reported the recovery of UPV during the healing process (Kanwal et al. 2022; Soda et al. 2022; TANYILDIZI et al. 2022).

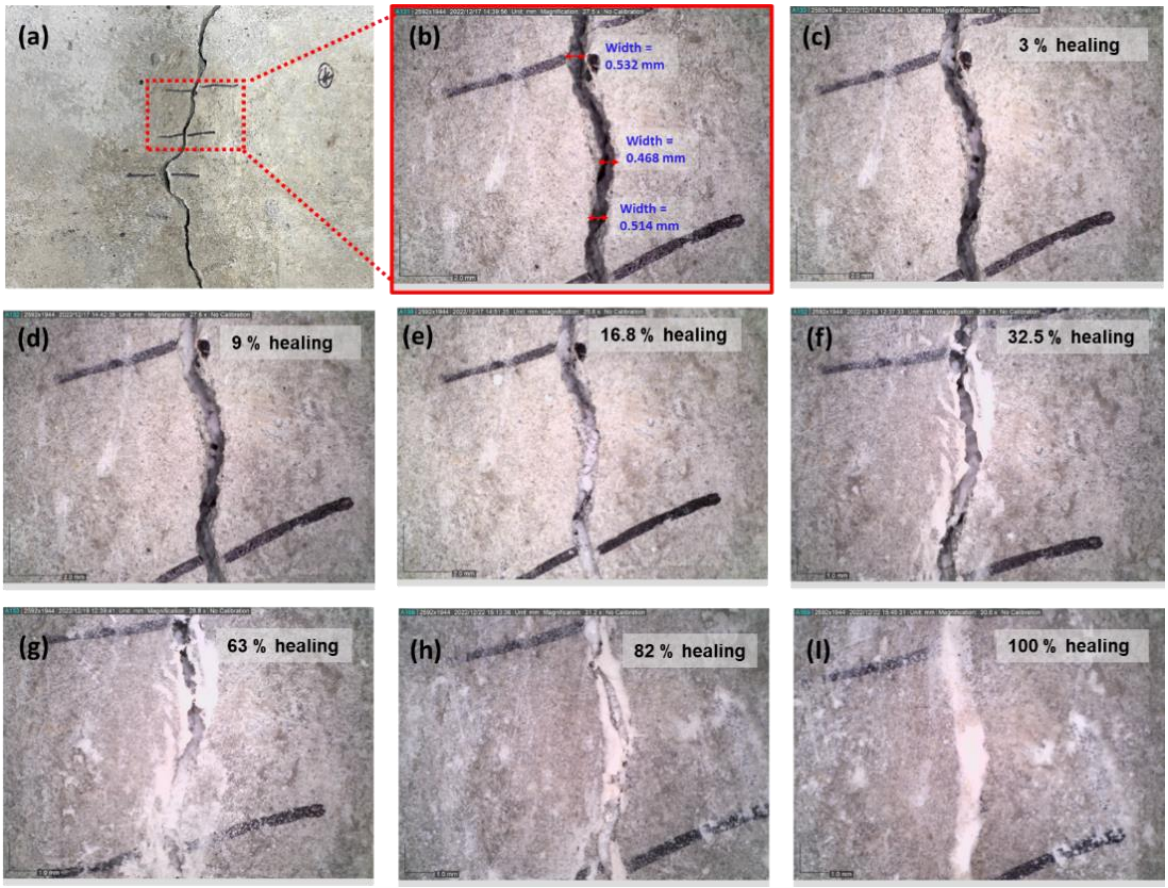


Fig. 4.36 Self-healing of crack by CSL-4 in concrete specimens at different healing percentage taken using DinoLite microscope

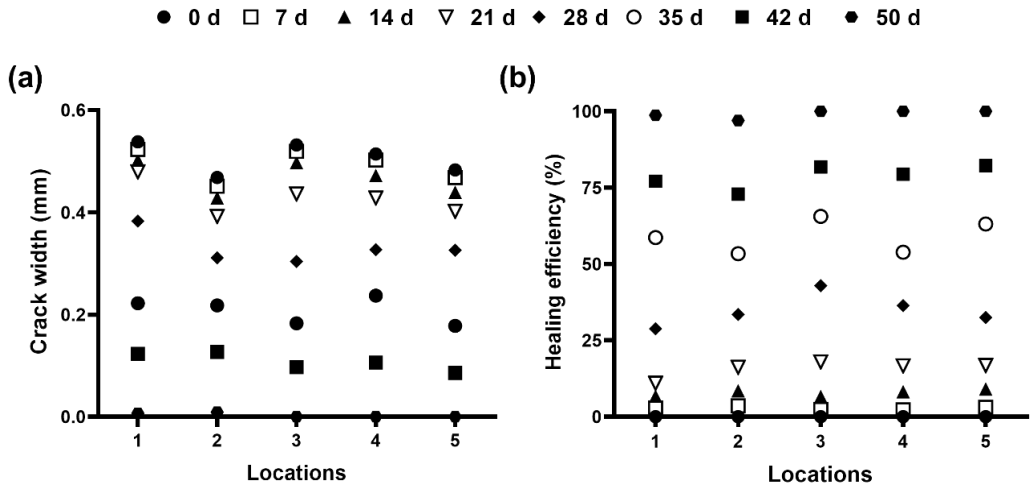


Fig.4.37 (a) Measurement of crack width at different intervals of time (0 – 50 days) (b) healing efficiency (%) based on the reduction of crack width at 0, 7, 14, 21, 28, 35, 42 and 50 days

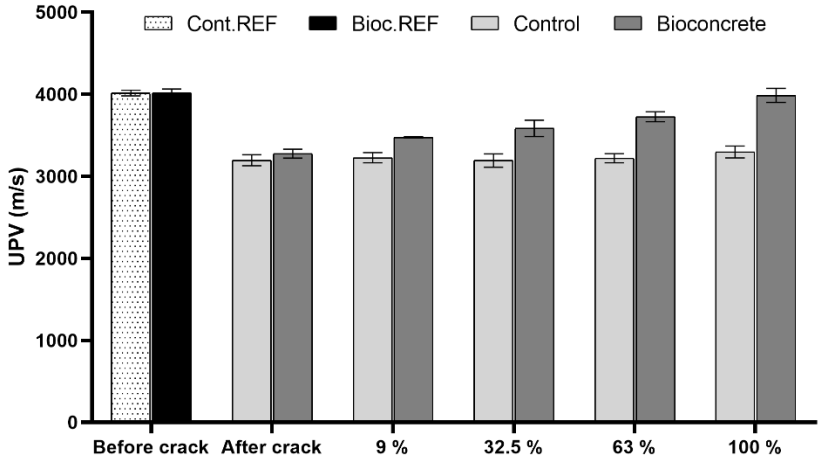


Fig. 4.38 Ultrasonic pulse velocity (UPV) of CSL-4 concrete crack specimens at different healing percentages of crack (0, 9, 32.5, 63, and 100%)

4.10.2 Water tightness

Water tightness was evaluated based on the water flowing through the crack zone in 20 seconds until complete crack closure. Different locations were marked as 'A, B, and C' on the specimens to determine the amount of water flowing through the different regions of the crack. The crack widths and depths varied at these locations. The amount of water flowing through the cylinder fixed at these locations was measured at regular intervals, as described by Kaur et al. (2020). The amounts of water flowing through the crack region initially and during the healing period are shown in Fig. 4.39a. It was observed that initially, 7 ml/20 sec of water flowed through the cracked location 'A,' which declined from 5.9 ml/20 sec to 0.8 ml/20 sec

at 14 and 50 days, respectively. Similarly, at other locations 'B', the amount of water flowing through the crack region decreased from 6.2 ml/20 sec to 0.4 ml/20 sec at 50 days. As the $CaCO_3$ precipitates healed the crack, the free water flowing through the crack decreased. The water flow varied at each location, which might be due to variations in crack depth and width. The crack sealing efficiency percentage was calculated as the amount of free water flowing through the crack zone initially and during the crack healing period. As shown in Fig. 4.39b, the crack-sealing efficiency at location A increased from 15.7% on day 14^{th} to 88.57% on day 50^{th}. Similarly, in locations B and C, 87.09% and 91.3% of sealing efficiency based on the water flow test was estimated at the end of the experiment. Similar results were also reported by Kaur et al. (2020). Likewise, (Wang et al. 2018a) reported an 81%–90% water flow reduction in hydrogel-incorporated concrete specimens.

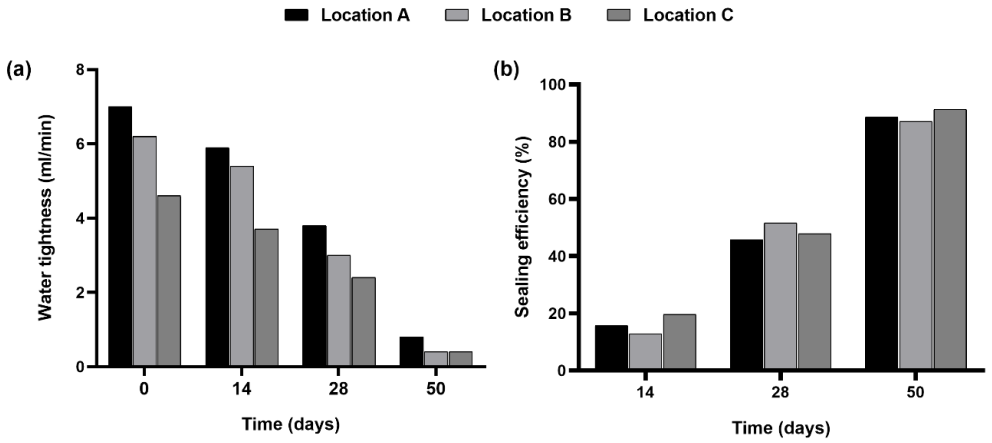


Fig. 4.39 (a) Water tightness and (b) crack sealing efficiency of bacterial treated CSL-4 concrete crack specimens at 0-, 14-, 28, 35- and 50 days curing time

4.10.3 Microstructural characterization

The sample collected from a depth of 10 mm in the healed region was assessed using XRD, FESEM and EDS for the biomineralization application of the bacteria. The crystalline morphology was verified using X-ray diffraction (XRD). As shown in Fig. 4.40, high-intensity calcite peaks were observed at 29.2°, 39.5° corresponding to crystallography planes of 104 and 113 calcite. Another X-ray diffraction peak located at (2θ) = 27.5° corresponds to the 101 planes of the vaterite crystals. The presence of calcite and vaterite peaks confirms that the healed material is $CaCO_3$ precipitates induced by the immobilized spores in the metakaolin material. Other peaks of quartz (Q), calcium hydroxide (CH), and calcium silicate hydrates (CSH) were also observed in the sample. These peaks were also observed in the control

concrete specimens. The intensity of the calcite peak in the CSL-4 specimen was high as compared to control. Other researchers have reported similar results by introducing bacterial interactions into the cementitious environment (Qin et al. 2020; Ahmad et al. 2022).

As shown in Fig. 4.41a, a uniform distribution of rhombohedral and vaterite crystals was observed in the sample. The crystals were stacked to form a calcite layer. The rhombohedral crystals were in the range of 3 - 8 µm, whereas the vaterite crystals were in the range of 5 – 7 µm. In control, the concrete sample from the cracked area was broken and taken for FESEM-EDS analysis. As seen in Fig. 4.41 (c, d), no calcite crystal deposition was seen. Both samples were also analyzed for EDS to confirm the elemental deposit. The elemental analysis of the healed precipitates in CSL-4 showed that the crystals formed were composed of $CaCO_3$. Elemental examination revealed that the healed bio cementitious material consisted of four essential elements: carbon (C), oxygen (O), and calcium (Ca) at 7.98, 59.55, and 32.47 weight percentage ratio (Fig. 4.41e). At the same time, silicon (Si), oxygen (O), and calcium (Ca) at 23.26, 58.57, and 18.17 weight percentage ratios were observed in the control (Fig. 4.41f). The percentage formation of calcium was observed to be higher in CSL-4, which marks the fact that there is some bacterial activity in CSL-4 specimens that leads to calcite formation. Anand et al. (2022c) corroborated similar $CaCO_3$ deposition results from a healed region. Different literature studies have reported $CaCO_3$ crystals with such diverse forms and structures (Ben Chekroun et al. 2004; Xiao et al. 2010). The results were also in agreement with Achal et al. (2010a) and Babakhani et al. (2020).

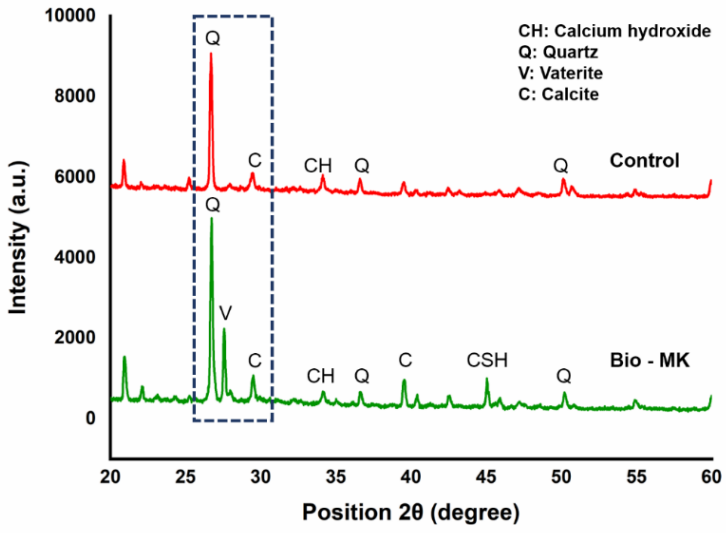


Fig. 4.40 XRD pattern of CSL-4 and control specimens

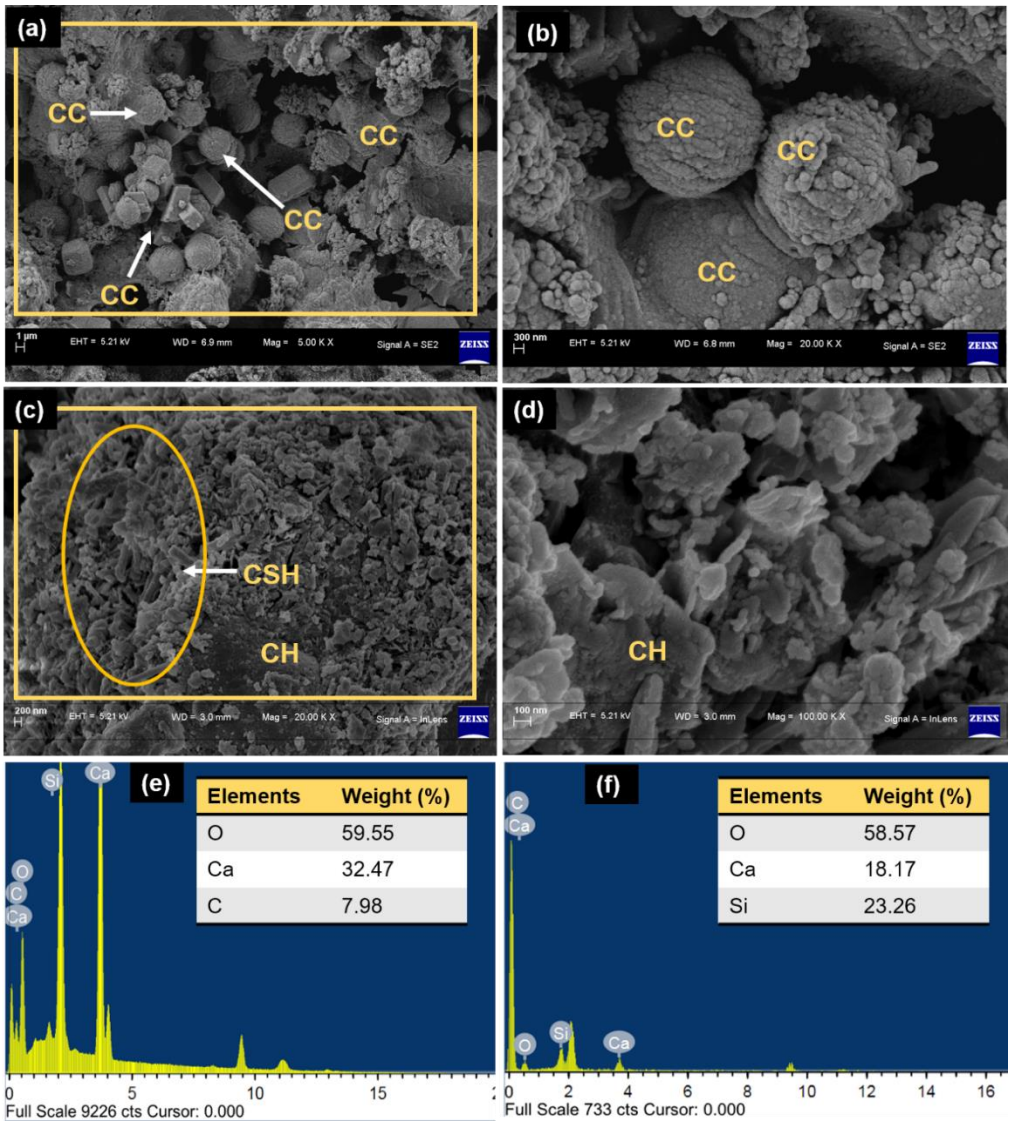


Fig. 4.41 FESEM of the (a, b) crack healed CSL-4 concrete specimens (c, d) control (e, f) EDS spectrum marked '□' represents elemental deposition of the calcium carbonate

4.11 Crack remediation by NB-4 bacterial inoculum

Besides CSL-4 bacterial inoculum, another bacterial inoculum developed using nutrient broth grown bacterial culture (NB-4) was monitored for crack remediation in concrete specimens. In this study, two groups NB-4 and control, were closely observed for crack healing at regular intervals using a DinoLite microscope. The 400 × 100 × 100 mm bioconcrete (NB-4) specimen was observed for the $CaCO_3$ deposition in the cracked region. The crack width was measured at different intervals, and images were obtained for visual monitoring. In the control specimens, no reduction in crack width was observed. There was no visual detection of any calcification

in the control specimens, which explains why the presence of $CaCO_3$ in the NB-4 specimens was due to the metabolic function of the spores immobilized in metakaolin. In the NB-4 specimens, the cracks completely healed after 40 days (Fig. 4.42). It can be stated that the bacterial spores were able to break the dormant endospore stage and become active owing to the availability of moisture and nutrients. The presence of urea and $CaCl_2$ in the nutrient growth medium facilitated bio-mediated $CaCO_3$ precipitation because of the ureolytic biochemical reactions in the cracked region. Therefore, voids were filled in the concrete specimens. The crack width was monitored for crack closure until the crack was completely healed, and the crack-healing efficiency was calculated based on the crack-width reduction. Water tightness and sealing efficiency were calculated using a water flow test.

Crack closure was monitored by measuring the reduction in the crack width at five different locations in the concrete specimens. Measurements were taken using a DinoLite microscope (Fig. 4.43). Initially, crack widths of 0.543 mm, 0.558 mm, 0.533 mm, 0.516 mm, and 0.537 mm were measured at five locations in the crack region. After the continuous injection of the NBUC medium into the crack region, slight white carbonate precipitates were observed on the walls of the cracked region after eight days. On the 14^{th} day, visible detection of $CaCO_3$ was observed, with a reduction in the crack width to 0.428, 0.425, 0.434, 0.442, and 0.419 mm. It is worth mentioning here that no additional bacterial culture was inoculated in the nutrient growth medium used for spray treatment. Over a period of 40 days, the crack width at location 'A' decreased from 0.543 to 0. 008 mm, with a crack-healing efficiency of 98.5% (Fig. 4.44a and 4.44b). Similarly, at location 'B', the crack width decreased from 0.558 mm to 0.005 mm, exhibiting a crack-healing efficiency of 99.1%. At the same time, locations 'C, D, and E' showed healing efficiencies of 97.05, 97.76 and 98.88%, respectively (Fig. 4.44 b). Statistical analysis using two-way ANOVA proved that the crack width was significantly reduced in the 40-d duration at a 5% level of significance. Whereas in the control specimen water was sprayed and no noticeable $CaCO_3$ precipitation was seen. The crack width of 0.52 mm was wider for autogenous healing to occur. Specimens incorporated with NB-4 bacterial inoculum showed autonomous healing with a 0.53 mm crack width. Anand et al. (2022b) reported 0.5 mm crack healing in 45 days using bacteria immobilized in silica fume as a carrier material. Authors further documented no sign of healing in control specimen by using nutrients, urea and $CaCl_2$ on the control cracked specimen. Similar results were corroborated using bacteria immobilized on different carrier materials, such as expanded glass granules (Zhang et al. 2022), hydrogels (Gao et al. 2020a), and rubber particles (Xu et al. 2019a). Kanwal et al. (2022) documented

crack healing of 500 µm and 800 µm widths with 100% and 68% crack-sealing efficiency, respectively. Wang et al. (2022) reported 84% crack healing ratio with 99% recovery of the compressive strength and water tightness in concrete specimens incorporated with bacteria immobilized recycled concrete aggregates. Xu and Wang (2018) reported 100% crack healing with 417 µm crack closure using a low-alkali cementitious material. Previously reported studies have showed that carrier materials have significantly maintained microbial mineralization activity and improved the crack self-healing efficiency (Feng et al. 2022).

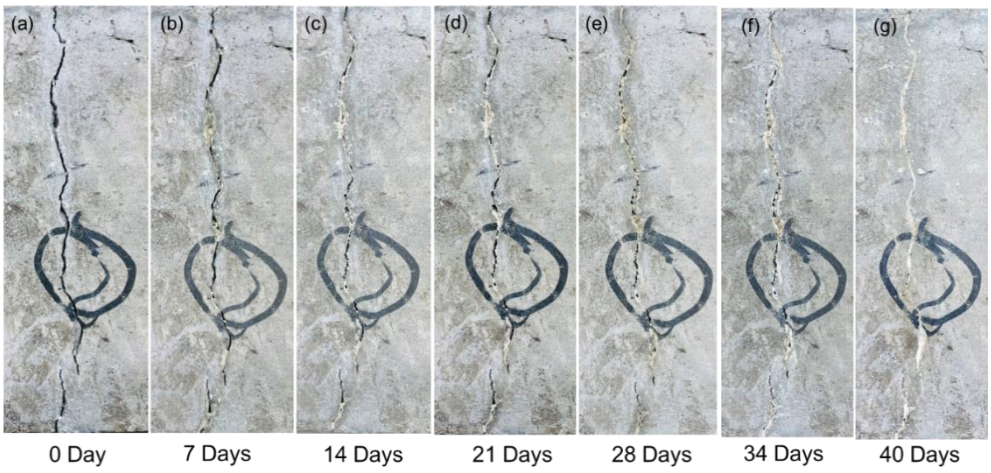


Fig. 4.42 Self-healing by biomaterials in concrete specimens at 0, 7, 14, 21, 28, 34- and 40-days of crack healing

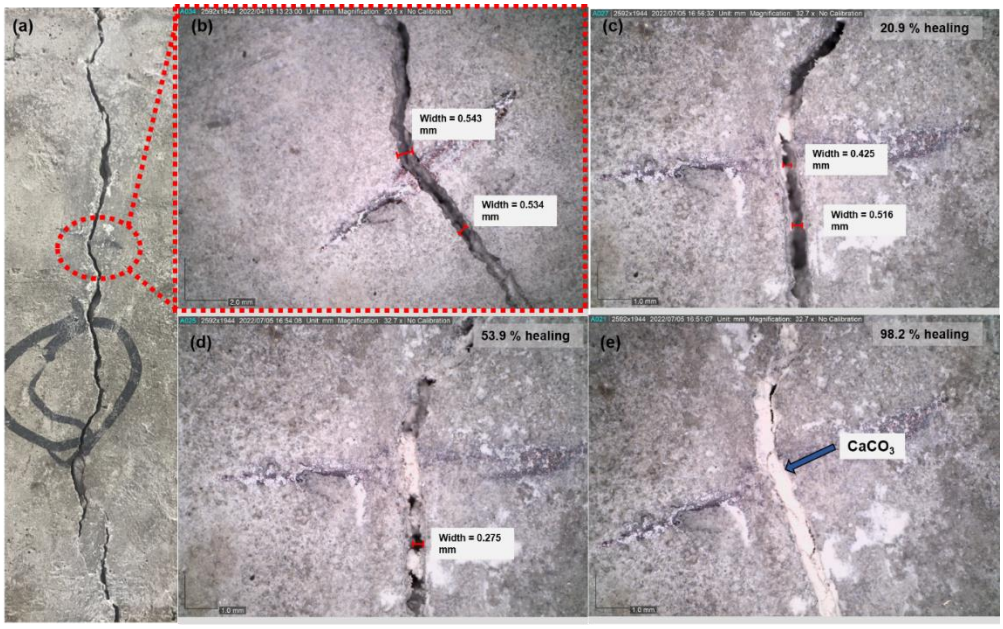


Fig. 4.43 Self-healing of crack by metakaolin immobilized bacterial (*B. paramycoides*) spores in concrete specimens taken using DinoLite microscope

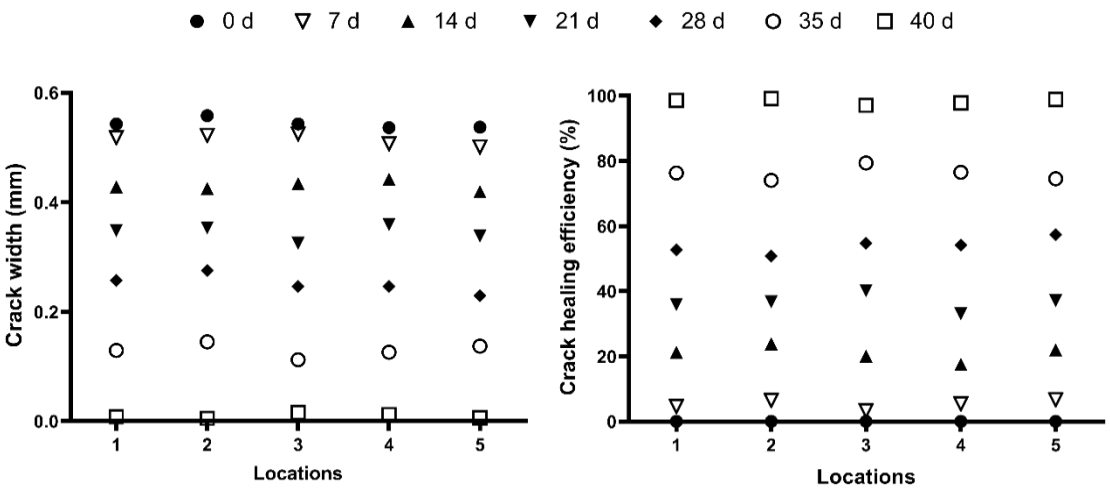


Fig. 4.44 (a) Evaluation of crack width due to self-healing application by *B. paramycoides* spores immobilized in metakaolin incorporated concrete crack specimens (b) sealing efficiency (%) based on the reduction of crack width at 0, 7, 14, 21, 28, 35, 40 days

4.11.1 Water tightness

Water tightness was evaluated based on the amount of water flowing through the crack zone in 20 s until complete crack closure. Different locations were marked as A, B, and C on the specimens to determine the amount of water flowing through the different regions of the crack. The crack widths and depths varied at these locations. At regular intervals, the amount of water flowing through the cylinder fixed at these locations was measured, as described by Kaur et al. (2020). The amounts of water flowing through the crack region initially and during the healing period are shown in Fig. 4.45. It was observed that initially, 6 ml/20 sec of water flowed through the cracked location 'A' which declined to 4.5 ml/20 sec to 0.4 ml/20 sec at 14 and 40 days, respectively. Similarly, at other locations 'B' the amount of water flowing through the crack region decreased from 4.8 ml/20 sec to 0.3 ml/20 sec at 40 days. As the $CaCO_3$ precipitates filled the empty space in the crack region, the amount of free water flowing through the crack decreased, indicating that the crack area healed because of bacterial biomineralization. The water flow varied at each location, which might be due to variations in crack depth and width. Similarly, in control specimen the rate of water flow remained constant during the experiment. Initially, the amount of water flowing through the cracked locations A, B, and C was 4.6 ml/20 sec, 5.4 ml/20 sec and 3.2 ml/20 sec. There was a negligible difference each time. The average water flow rate was 4.4 ml/20 sec after 40 days of the experiment. The crack-sealing efficiency percentage was calculated as the amount of water flowing through the

crack zone initially and after crack closure. As shown in Fig. 4.45, the crack-sealing efficiency at location A increased from 25% to 93.34% on day 40. Compared to location A, 93.75 and 91.3% of healing was noted at locations B and C. On average, 92.8% of the area was healed by bacterial spores immobilized in the metakaolin incorporated into the concrete. Similar work was carried out by Wang et al. (2018b), who reported an 81%–90% water flow reduction in hydrogel-incorporated concrete specimens.

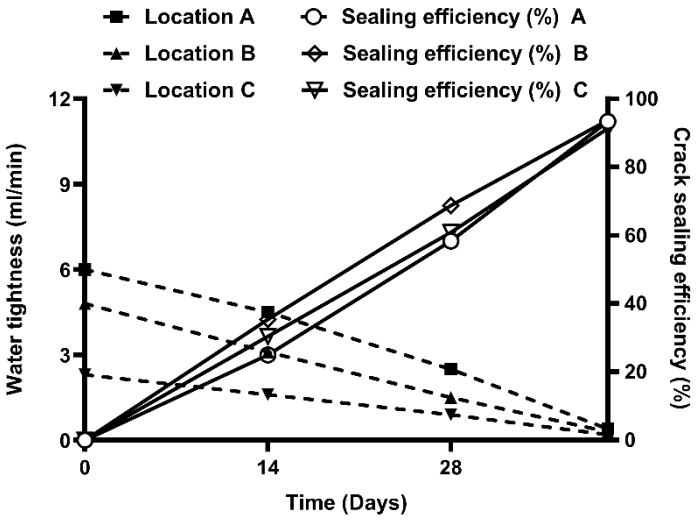


Fig. 4.45 Water tightness and crack sealing efficiency of bacterial treated (*B. paramycoides*) concrete crack specimens at 0-, 12-, 24, and 40-days curing time

4.11.2 Ultrasonic pulse velocity (UPV)

The UPV was measured for a reference specimen without a crack in NB-4 bioconcrete (Bioc.REF) specimens and in control (Cont.REF) specimens. The UPV was noted after crack (AC) formation and until the complete closure of the crack by healing. A maximum pulse velocity of 4049 m/s was observed in the Bioc.REF specimens, which decreased by 19.14% after cracking of the specimens. The UPV value showed a regain in pulse velocity after the plugging of cracks by $CaCO_3$ precipitation, formed as a result of bacterial metabolic activity in the bioconcrete specimen. The healing of the crack for 40 days led to 98.2% closure of the crack width, which eventually resulted in the recovery of the pulse velocity. The UPV was evaluated at intervals of 14, 28, and 40 days of crack healing, as shown in Fig. 4.46. The increase in pulse velocity confirmed the deposition of $CaCO_3$ at the depth of the crack. On 14^{th}, 28^{th}, and 40^{th} days of crack healing, the UPV values was observed to be increase by 6.4%, 11.5%, and 21.7% compared to the after-cracking in bioconcrete specimens, respectively. The UPV value envaulted at complete healing of the crack was observed to be 3982 m/s. The

Statistical analysis confirmed a significant improvement in UPV upon crack healing in biomaterial added concrete at the 5% significance level. At the same time, the UPV for Cont.REF without biomaterial incorporation was 3159 ± 36 m/s before cracking which showed 0.7% increase in the pulse velocity after 40 days of the healing period. Therefore, autogenous healing of 0.5 mm crack width was excluded. Other researchers have also reported the recovery of UPV during the autonomous healing process (Kanwal et al. 2022; Ranjan et al. 2022a; TANYILDIZI et al. 2022).

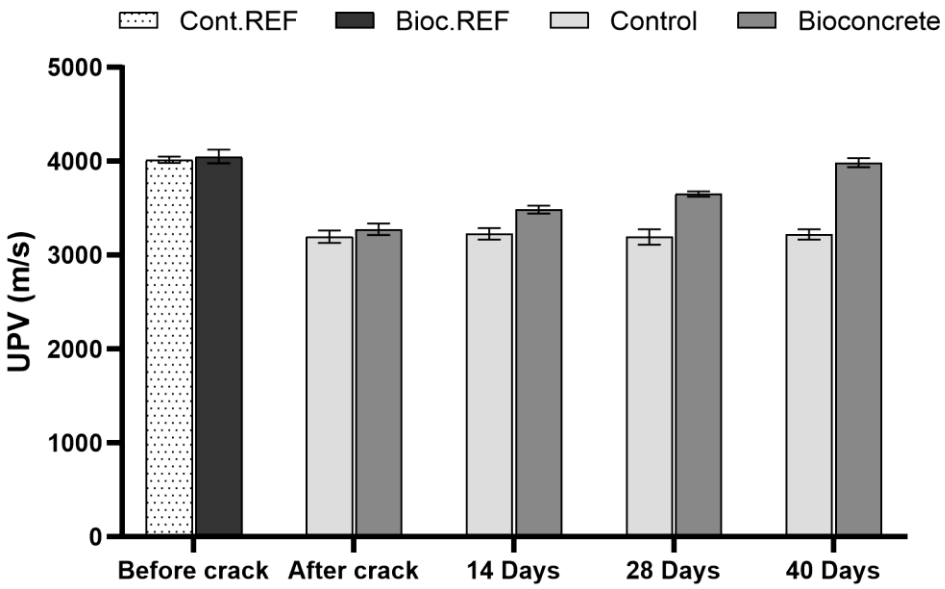


Fig. 4.46 UPV of NB-4 added and control concrete specimens at different healing time

4.11.3 Microstructural characterization

The sample collected from a depth of 10 mm in the healed region was visualized using FESEM and EDS for the biomineralization application of the bacteria. As shown in Fig. 4.47a, b uniform distribution of rhombohedral and vaterite crystals was observed in the sample. The crystals were stacked to form a calcite layer. The rhombohedral crystals were 10-12 µM in size, whereas the vaterite crystals were 5 – 8 µM in size. Elemental analysis of the healed precipitates showed that the crystals formed were composed of $CaCO_3$. In contrast, calcite deposition was not observed in the control specimens (Fig. 4.47c, d). Elemental examination revealed that the healed $CaCO_3$ precipitates consisted of four essential elements: carbon (C), oxygen (O), calcium (Ca), at 8.25, 49.34, and 42.41 weight percentage ratio. The elemental composition of C, O, Ca and quartz or silica (Si) in control was 21.19, 44.95, 12.80 and 6.32%, respectively

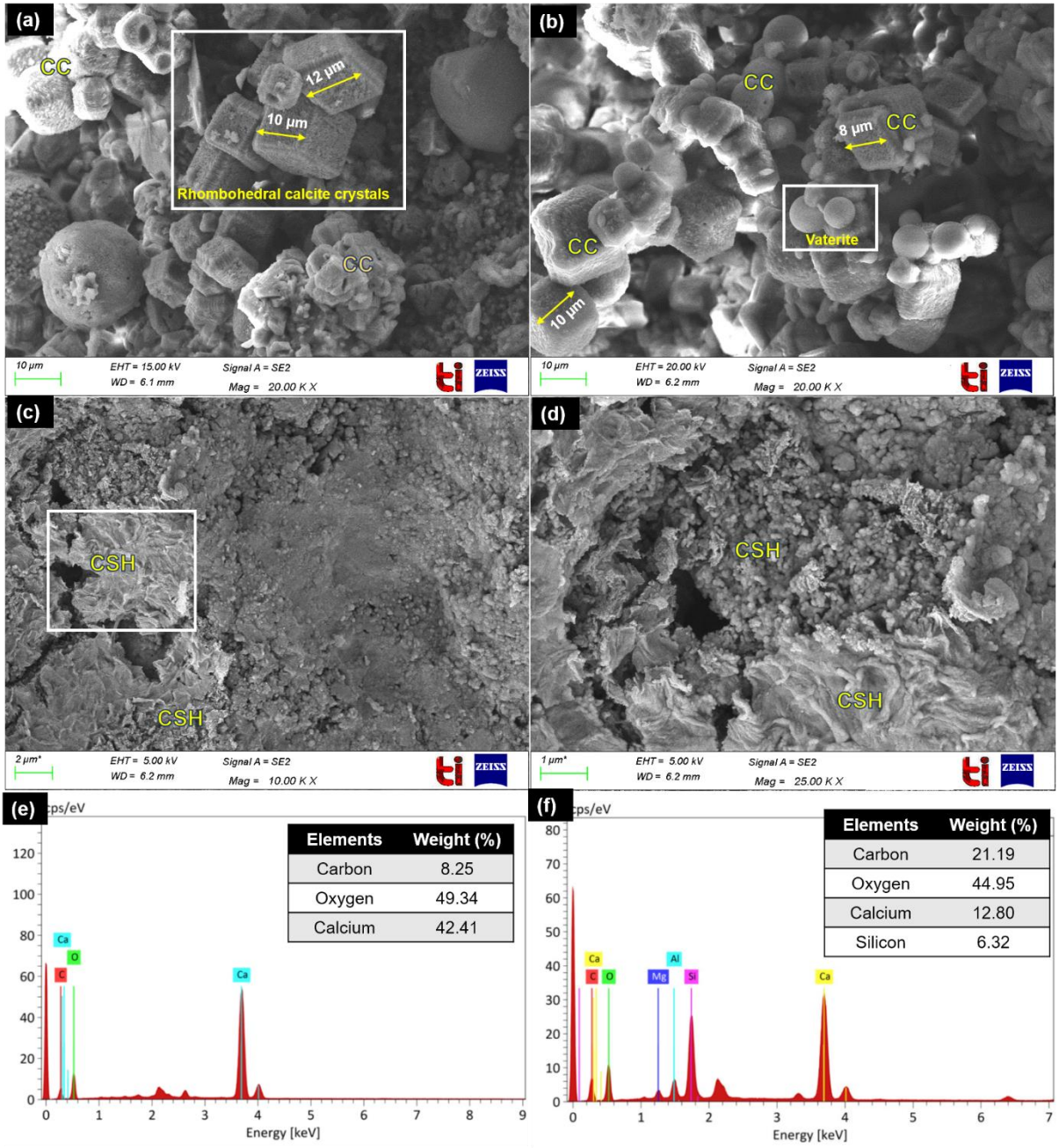


Fig. 4.47 (a, b) FESEM of the NB-4 added concrete specimens depicting rhombohedral crystal precipitation in healed crack region (c, d) control specimen (e) EDS showing elemental deposition of the $CaCO_3$ in healed crack region (f) EDS of the control specimen The '□' marked depicts the spot of EDS analysis

(Fig. 4.47 e, f). Kua et al. (2019) and Rauf et al. (2020) also reported $CaCO_3$ deposition from a healed cracked region. Furthermore, the interaction between the cementitious material and biomineralization components was analyzed using X-ray diffraction (XRD). An XRD analysis was performed to verify the presence of calcite in the bioconcrete specimens. As shown in Fig.

4.48, a high-intensity calcite peak was observed at 29.2°, corresponding to 104 planes of calcite. Another X-ray diffraction peak located at (2θ) = 27.1° corresponds to the 101 planes of the vaterite crystals. The presence of calcite peaks confirms that the healed material is a $CaCO_3$ precipitate induced by the immobilized spores in the metakaolin material. Other peaks of quartz (Q) and calcium silicate hydrates (CSH) were also observed in the sample. These peaks were also observed in the control concrete specimens. Similar results were reported Gao et al. (2020b).

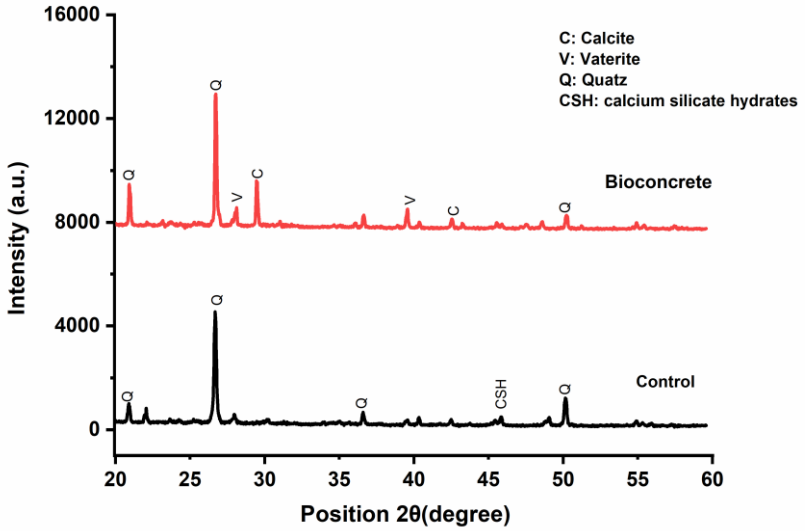


Fig. 4.48 XRD pattern of NB-4 and control specimens

4.12 Conclusions

The *B. paramycoides* was an efficient ureolytic bacteria that can induce $CaCO_3$ precipitation under favorable conditions. The optimum temperature conditions for MICCP were 28 – 45 °C and a pH range of 7 – 10. The *B. paramycoides* exhibited a notable sand consolidation property, characterized by solid compaction and binding. The study results indicated that the bacterial admixed specimens demonstrated superior performance in enhancing the strength and permeability properties compared to the control group. The carrier material developed by immobilizing bacteria in metakaolin showed a sustainable shelf-life of 180 days. The carrier material enhanced the strength and self-healing properties of the concrete. The crack was remediated successfully with improved UPV and water absorption properties. The results were verified by FESEM-EDS and XRD, proving the precipitation of rhombohedral calcite precipitation.

4(B) Photoautotrophic bacteria

4.13 Screening of the highest $CaCO_3$ precipitating cyanobacterial strain

The cyanobacterial cultures *Aphanocapsa montana* BDU21001, *Aphanothece* species BDHKU 40501, *Gleocapsa species* BDU 40111, *Synechococcus elongatus* BDU14174, *Synechocystis pevalekii* BDHKU 35101 were procured and screened for the highest $CaCO_3$ precipitation. The growth cycle, $CaCO_3$ precipitation, and pH variation were tested during the screening process.

4.13.1 Growth cycle

The cyanobacterial cultures, *A. montana, Aphanothece* sp., *Gleocapsa sp*., *S. elongatus*, and *S. pevalekii* were inoculated in BG 11 broth with the initial O.D. of 0.01. The growth pattern was monitored for over 40 days by measuring the optical absorption at 680nm (Fig. 4.49). There was no significant difference in the optical density for the initial 48 hours of incubation (during the lag phase of the growth cycle). The growth cycle was different for all the strains. After the lag phase, log (exponential) growth phase was observed in *S. elongatus* and *S. pevalekii* after 4 days, whereas in *A. montana, Aphanothece* sp., *Gleocapsa* sp. was observed after 6 days. The exponential phase was faster between the 6^{th} and 27^{th} days of inoculation. After that, the growth of *S. pevalekii* and *S. elongatus* was steady and entered the stationary phase. However, cell growth of *A. montana Aphanothece* sp. and *Gleocapsa* sp. enters the stationary phase after 32 days. *S. pevalekii*, followed by *S. elongatus,* showed the maximum cell growth. At the same time, the other three strains showed slighter lower growth compared to *S. elongatus, S. pevalekii*. Minimum cell growth was observed in *Gleocapsa* sp. Other researchers reported similar results (Cui et al. 2020; Naveed et al. 2020b; Yu et al. 2020b).

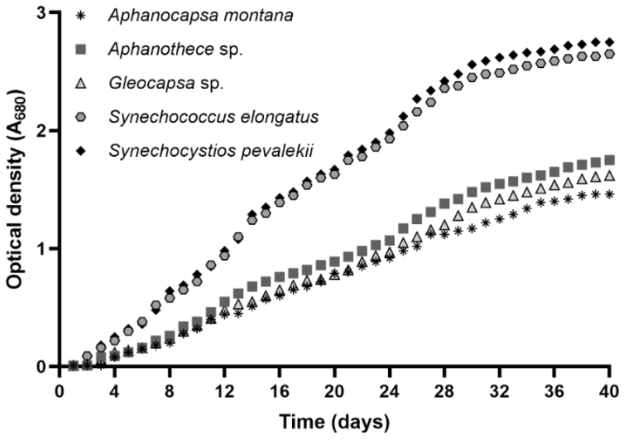


Fig. 4.49 Growth cycle of cyanobacterial cultures incubated for 40 days in BG11 medium

4.13.2 Calcium carbonate precipitation

The calcification potential of all the procured cyanobacteria culture "*A. montana*, *Aphanothece* sp., *Gleocapsa* sp., *S. elongatus*, and *S. pevalekii*" was evaluated to select the best strain for the estimation of calcification in alkaline environmental conditions. The $CaCO_3$ precipitation is formed as a result of photosynthetic activity of bacteria in the presence of CO_2 and light. The amount of $CaCO_3$ formed in the calcifying solution was estimated by measuring the weight of precipitates collected on the Whatman paper. The cyanobacterial cultures exhibited an increasing trend of carbonate precipitation during 120 hours of incubation (Fig. 4.50). The highest $CaCO_3$ (695 mg/100 ml) was precipitated by *S. pevalekii* cells in the BG11 broth supplemented with calcifying solution. Other cyanobacteria strains i.e., *A. montana*, *Aphanothece* sp., *Gleocapsa* sp., *S. elongatus* precipitated 475, 439, 524, and 604 mg/100 ml after 120 hours incubation at 25 ± 2 °C, respectively. Cyanobacteria used the $CaCl_2$ provided as the source of calcium in the medium and form the carbonate ions. The statistically analyzed data showed significant variation in $CaCO_3$ precipitation by all strains at a 5% level of significance (Table 4.11). Similar results were corroborated by Liang et al. (2013); Zhu et al. (2018) using three *Synechococcus* strains.

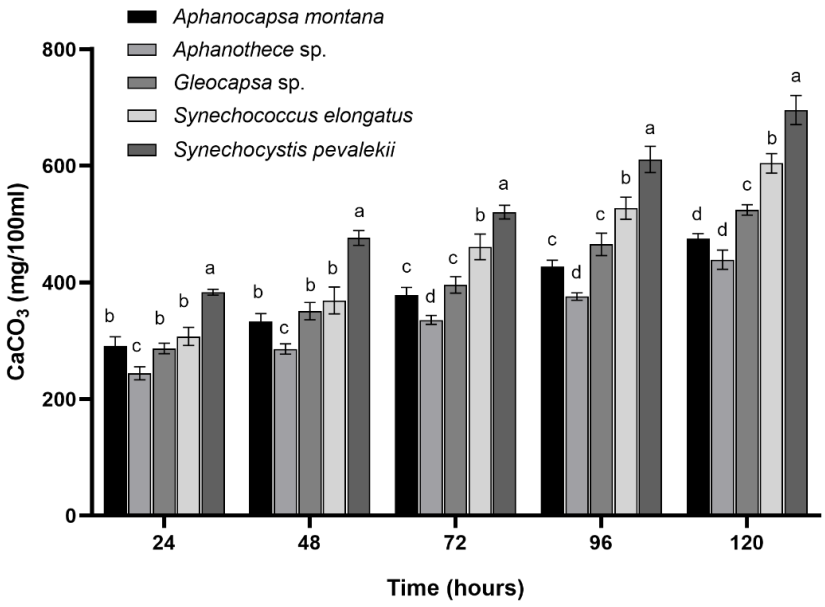


Fig. 4.50 $CaCO_3$ precipitation by *A. montana*, *Aphanothece* sp., *Gleocapsa* sp., *S. elongatus* and *S. pevalekii* cells in BG11 broth supplemented with 100 mM $CaCl_2$ and 50 M $NaHCO_3$ calcifying solution during 120 hours incubation at 25 ± 2 °C. Values bearing different letters within the same time interval are significant at $p<0.05$. Error bars represents standard deviation (n = 3)

Table 4.11 The factorial ANOVA results indicate the effect of different cyanobacteria and time interval on $CaCO_3$ precipitation

Variables		Culture	Time	Interaction (Culture × Time)
$CaCO_3$ precipitation	df	4, 8 P < 0.0001	4, 8 P < 0.0001	16, 32 P < 0.0001

4.13.3 pH dynamic

Calcification in the flask under illumination directly concurred with a slight increase in pH that occurred after 8 hours of the sampling period. Initially, pH was 7.5 ± 0.2, which dropped to 5.85, 6.10, 5.56, 5.86, and 5.78 after injecting $CaCl_2$ in *A. montana*, *Aphanothece* sp., *Gleocapsa* sp., *S. elongatus* and *S. pevalekii* inoculated flask respectively (Fig. 4.51). It may be due to the change of speciation in the solution. When added to the media, calcium chloride absorbs hydroxide and leaves free protons behind. This lowers the pH of the media. The photosynthetic metabolism of the cyanobacterial strains was directly responsible for the alkalinization of the experimental microenvironment because the pH did not increase in any of the control samples. pH of the medium was monitored for 72 hours. A slight increase in pH of the medium was observed from 5.50, 5.70, 5.65, 5.67, and 5.50 after 6 hours to 5.89, 6.20, 6.37, 6.10, and 6.10 after 8 hours, in *A. montana*, *Aphanothece* sp., *Gleocapsa* sp., *S. elongatus*, and *S. pevalekii* respectively. pH increased in all the cultural flasks under laboratory conditions, with white color precipitation observable in all the flasks. The data were analyzed using Tukey's test, which showed that pH variation was significantly affected at a 5% level of significance during the $CaCO_3$ precipitation experiment.

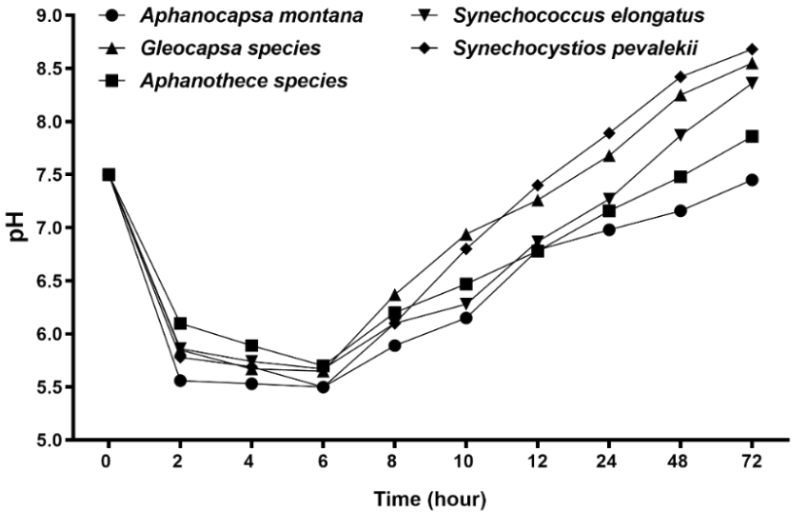


Fig. 4.51 pH variation during $CaCO_3$ precipitation experiment

4.13.4 Microstructural analysis

The $CaCO_3$ precipitated by these bacteria was analyzed by SEM for their morphology. The elemental composition of the carbonate crystals formed were analyzed by energy dispersive spectroscopy (EDS) coupled to SEM. The elemental analysis of the precipitate was determined by XRD analysis. Rod and coccus-shaped bacteria were observed attached to the carbonate precipitates and also embedded in big calcite crystals (Fig. 4.52). Cyanobacteria have a layer of extracellular polymeric substances (EPS) which can form biofilms in the surrounding environment. It was observed that some of the calcite precipitates were closely associated with each other, forming layer of crystallization, while the remaining ones were randomly distributed throughout the biofilm. The EDX spectrum (Fig. 4.53) showed that the elemental composition of the crystals corresponds to calcite with Ca, O, and C. The presence of a higher amount of calcium in all the filtrate supports the precipitation by bacteria in the form of $CaCO_3$. Zhu et al. (2015), Paulo et al. (2018), and Zhu et al. (2021a) also reported calcite precipitation by *Synechococcus* PCC8806 under varied ecological conditions. The elemental analysis of the precipitates formed by *A. montana* and *S. pevalekii* was determined by XRD analysis. XRD spectra were obtained by using an X'Pert PRO diffractometer with Cu anode (40 kV and 30 mA) and scanning from 20 to 90˚ 2θ. XRD results revealed the formation of rhombohedral crystal formation. A high intense peak was observed at 29.2°, which corresponds to the 104 planes of calcite (Fig. 4.54). Similar results were reported by Bundeleva et al. (2014) and Chandra et al. (2023).

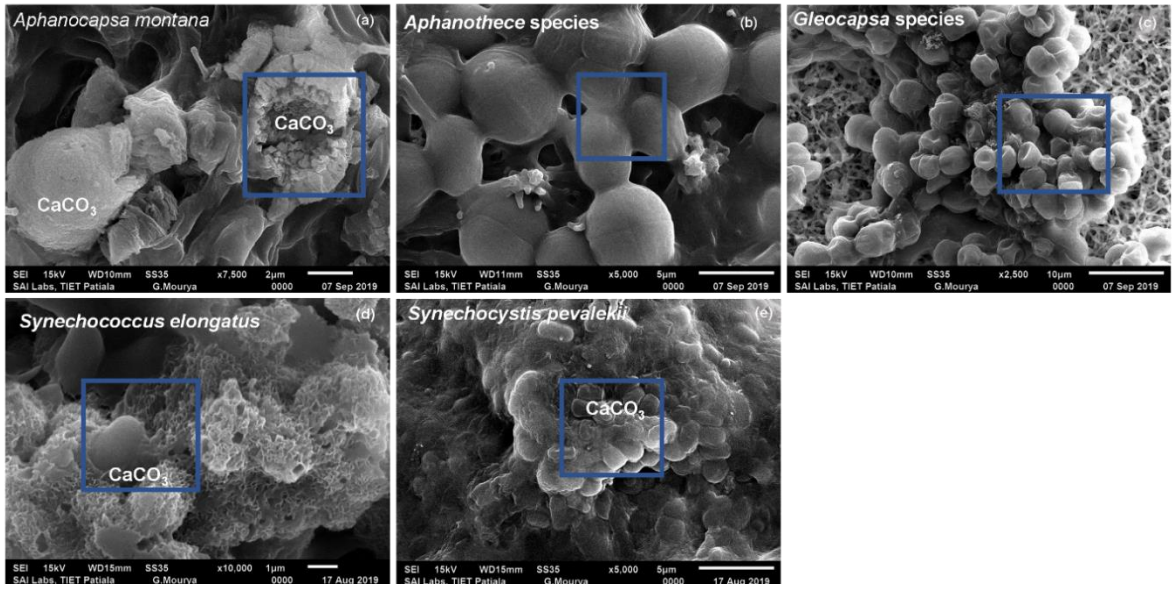


Fig. 4.52 SEM analysis of $CaCO_3$ precipitates by (a) *Aphanocapsa montana*, (b) *Aphanothece* sp., (c) *Gleocapsa* sp., (d) *Synechococcus elongatus* and (d) *Synechocystis pevalekii*

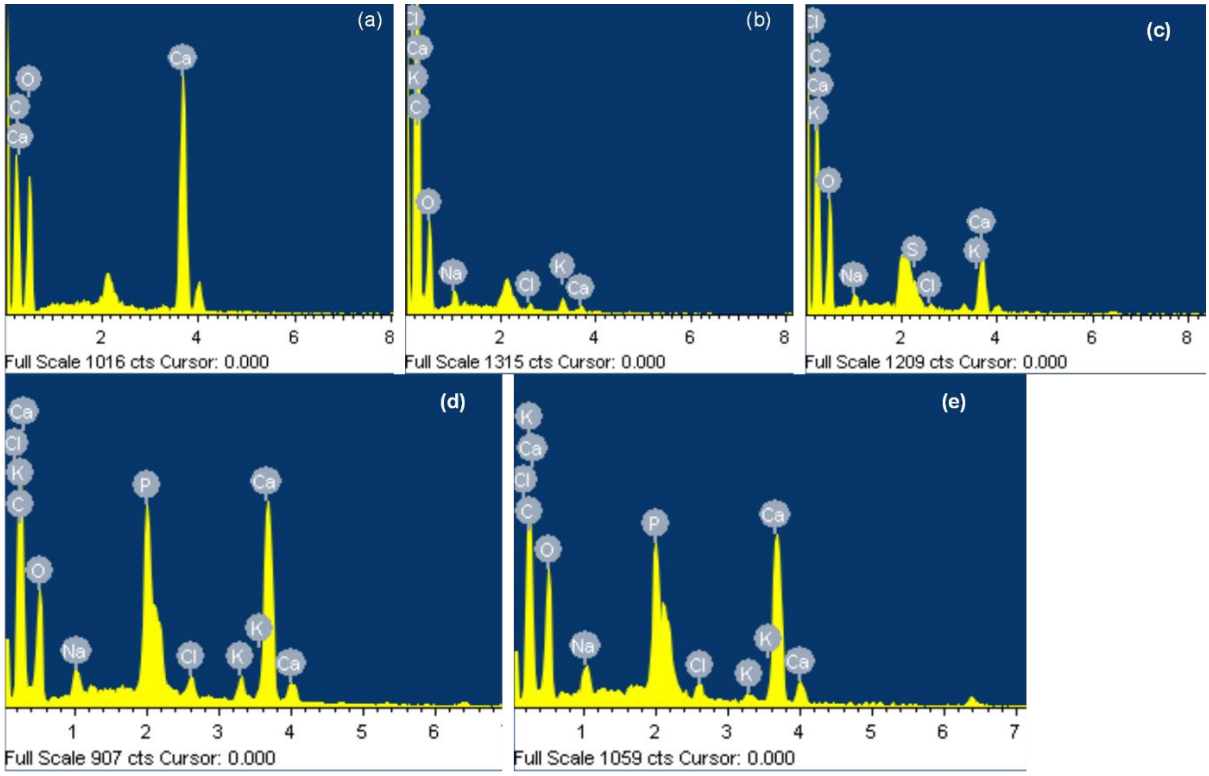


Fig. 4.53 EDS analysis of $CaCO_3$ precipitates by (a) *Aphanocapsa montana*, (b) *Aphanothece* sp., (c) *Gleocapsa* sp., (d) *Synechococcus elongatus* and (d) *Synechocystis pevalekii*

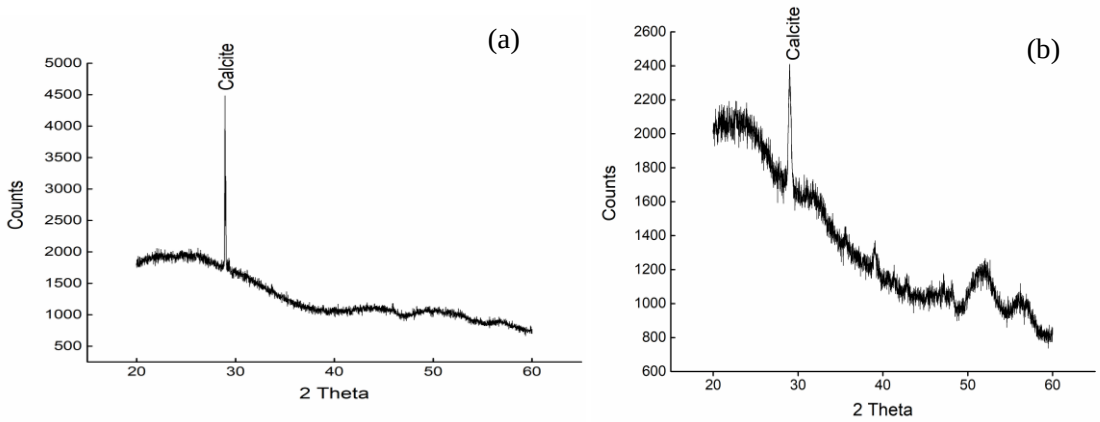


Fig. 4.54 XRD analysis of (a) *Aphanocapsa montana* BDU21001, (b) *Synechocystis pevalekii* BDHKU 35101

4.13.5 Selection of highest $CaCO_3$ precipitating cyanobacteria

S. pevalekii was selected based on the highest $CaCO_3$ precipitated than other cyanobacteria. *S. pevalekii* precipitated 695 mg/100 ml of $CaCO_3$ in the BG11 broth.

4.14 Influence of different pH on $CaCO_3$ precipitation by *S. pevalekii*

Fig. 4.55 shows the amount of $CaCO_3$ precipitated by *S. pevalekii* at different pH conditions. The maximum precipitation was recorded at pH 9, after which $CaCO_3$ precipitation decreased upon further increasing the pH of the medium. The amounts of $CaCO_3$ precipitated after 120 h of incubation at pH 6, 7, 8, 9, 10, 11, and 12 were 434, 695, 756, 858, 799, 668 and 594 mg/100 ml, respectively. $CaCO_3$ precipitation was observed to be increasing with an increase in pH till pH 9, after which it shows a decreasing trend, which might be attributed to the low metabolic rate at high pH. The highest $CaCO_3$ precipitation was observed at pH 9 and optimum range of $CaCO_3$ precipitation was 7 - 9. The results were analyzed statistically at a 5% level of significance. Similarly, Ca^{2+} removal was evaluated at varied pH (6 – 12) conditions (Fig. 4.56). After 120 h of incubation, 33.5%, 44.5%, 48.5%, 53.1%, 48.2%, 38.4% and 36.2% calcium removal was observed at pH 6, 7, 8, 9, 10, 11 and 12, respectively. The statistically analyzed data showed that pH and time interval significantly affect $CaCO_3$ precipitation. Similar work was carried out by Zhu et al. (2017) by live and UV-killed biofilm-forming cyanobacterial *Gloeocapsa* PCC73106.

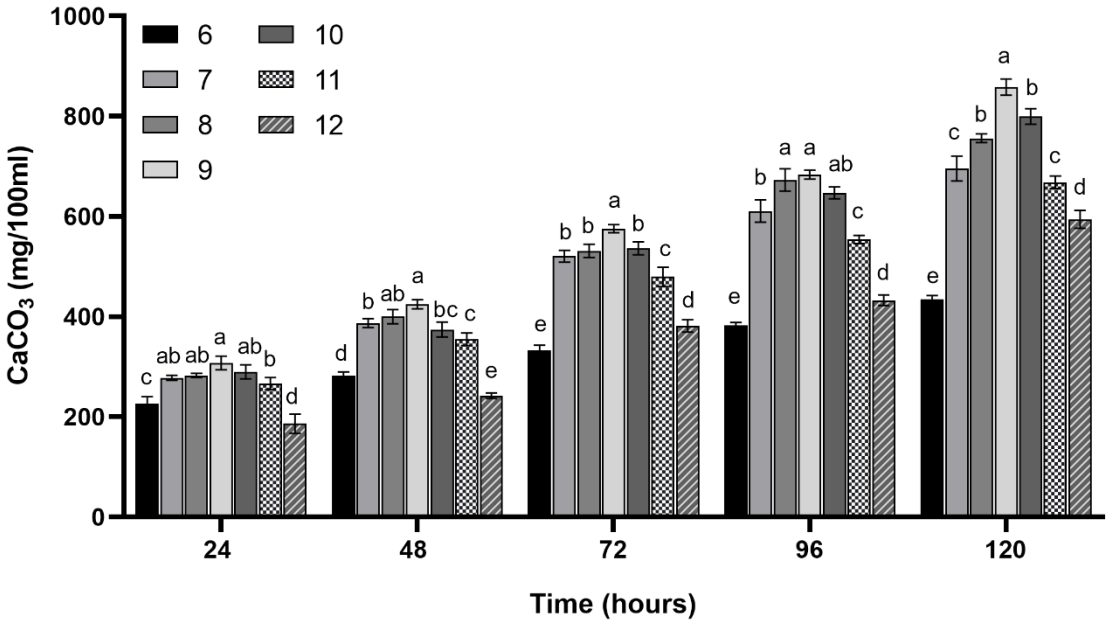


Fig. 4.55 $CaCO_3$ precipitation by *S. pevalekii* at different pH (6 -12) conditions. Values bearing different letters within the treatment at each time interval are significant at $p<0.05$. Error bars represent the standard deviation (n=3)

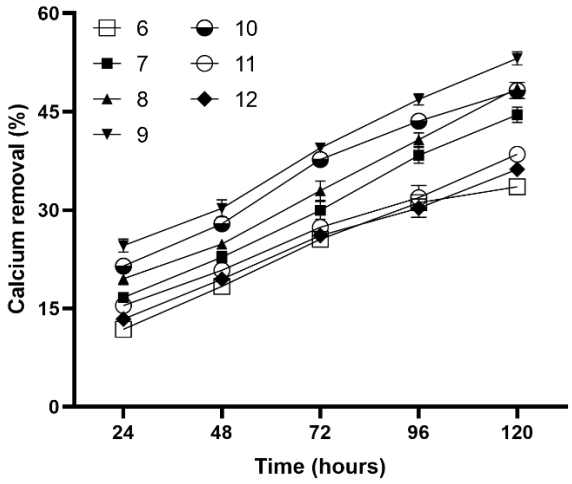


Fig. 4.56 Calcium removal percentage (%) during $CaCO_3$ precipitation at different pH (6 -12) conditions. Values bearing different letters within the treatment at each time interval are significant at $p<0.05$. Error bars represent the standard deviation (n=3)

4.15 Influence of Live (LV) and UV-treatment (UVT) cells in sand consolidation and improvement of cementitious material

4.15.1 Sand consolidation

To study the binding property of the $CaCO_3$ precipitated by *S. pevalekii* cells, the sand consolidation experiment was performed with both live (LT) and UV-treated (UVT) cells of *S. pevalekii*. After 14 days, the sand columns were opened, and a solid cylindrical consolidated sand column was observed in cyanobacterial injected columns. The flow rate of the calcifying medium was measured at regular intervals till 14 days of consolidation. The flow rates of *S. pevalekii* treated columns and the control columns were almost the same initially. There was a 12.9% reduction in the control column's flow rate after 14 days, which shows a marginal change in the control column's structures due to the flow. However, in the LT and UVT columns, the flow rate declined progressively, indicating that MICCP is causing gradual constraints of the flow channels. The flow rate was almost obstructed at the end of the 12^{th} day. Initially, on the 0-day, the flow rate was estimated to be 16.38, 17.44, and 18.52 ml/min in the experiment set – LT, UVT, and C (control). The flow rate on the 14^{th} day of the investigation set LT and UVT at 4.10 and 6.23 ml/min, respectively. Bacterial columns showed a maximum 40.2% reduction in the flow rate on the 4^{th} day of the study, increasing to 74.90% on the 14^{th} day (Fig. 4.57a). $CaCO_3$ precipitation by *S. pevalekii* cells plug the pores between the sand particles. The reduction in the flow rate in LT and UVT-treated columns is primarily because of the enclosed

biomass and carbonate deposition. The carbonate biominerals reduce the pore size between the sand particles, clogging the flow of calcifying material.

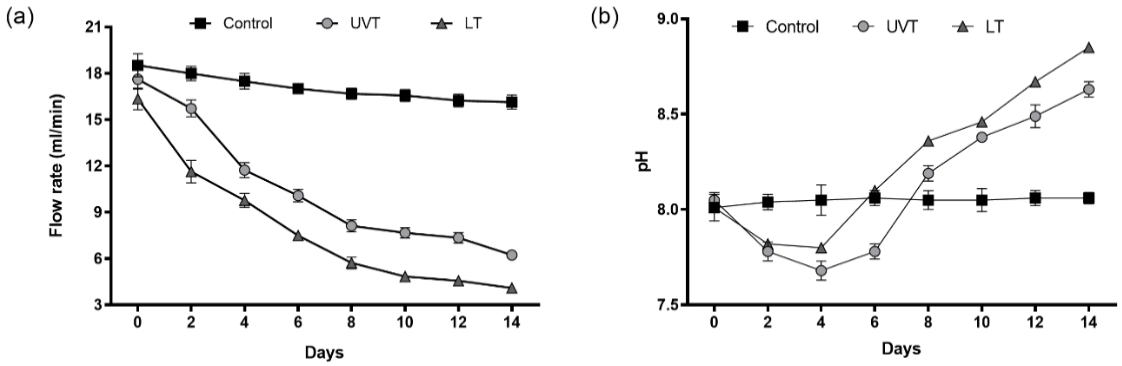


Fig. 4.57 Estimation of (a) the flow rate of the calcifying solution (b) pH of the solution effluent injected through sand columns till 14 days. Values are mean ± SD (n=3)

The change in pH of the effluent collected at the bottom of the injected calcifying medium was monitored at 0, 2, 4, 6, 8, 10, 12, and 14 days of the experiment. The effluent's pH was 7.3 to 7.5 for LT and 7.6 to 7.8 for UVT at the end of the 14 days (Fig. 4.57b). Conversely, the pH of the effluent from control columns remained the same throughout the experiment, i.e., pH 8.1. In every treatment, the pH decreased eventually. The pH of the effluent from the control and the bacterial-treated columns showed significant variance, so it can be considered an indicator of the activity of MICCP. Therefore, it can be assumed that the most functional element in the calcifying solution is calcium chloride and sodium bicarbonate, which act as a catalyst for precipitation. DeJong et al. (2010) have reiterated that $CaCO_3$ precipitation is imperative in distributing crystals between the sand voids to form bonds between the particles. Sodium bicarbonate used in these columns acts as a catalyst to initiate the formation of $CaCO_3$ by bacterial cells. LT column resulted in complete consolidation of sand compared to control without bacteria. Sand columns treated with live cells were more compact and firm than UV-treated columns. Partial binding formed in the UVT experimental setup, where about two-thirds of the sand was consolidated. There were clumps of sand on the top in UVT, whereas in control, the sand came out without consolidation (Fig. 4.58). The consolidated sand column was further divided into three parts to estimate the $CaCO_3$ content. The upper part of the column in LT and UVT was dense and more rigid than the bottom parts.

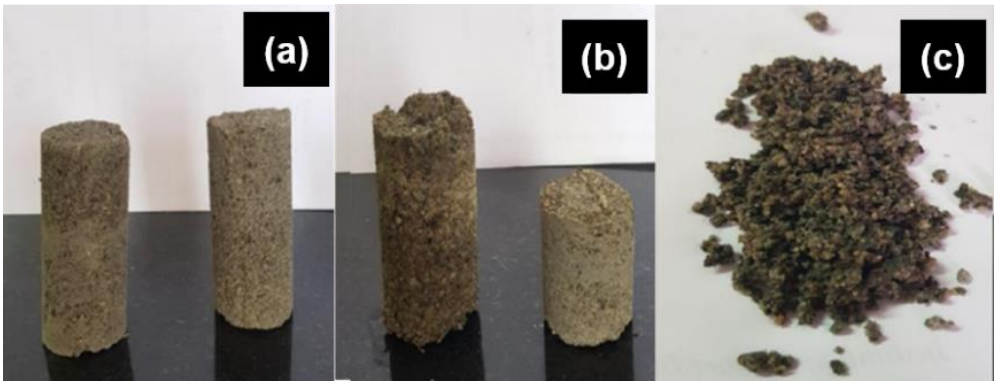


Fig. 4.58 Sand columns (a) live (LT), (b) UV-treated (UVT) and (c) control

Fig. 4.59 depicts the decreasing trend of $CaCO_3$ formation in the three layers of the sand column in LT and UV-treated columns. The upper layer's maximum $CaCO_3$ content was observed (8.67 mg/g) in LT treated column. At the same time, 6.67 mg/g of $CaCO_3$ deposition was recorded in the upper part of the UVT column. The $CaCO_3$ precipitation in the middle part of the sand columns were recoded to be 6.43 mg/g, and 5.43 mg/g, respectively. Comparatively, minimum calcite content was observed in the bottom part of the columns, indicating that the growth of *S. pevalekii* cells was promoted in the upper layer of the column due to exposure to the light source and aeration. The results correlated with those of Dhami et al. (2016), who studied sand consolidation using different grain sizes (0.2, 0.5, and 1.0 mm). They reported an 88% decrease in the flow rate in all bacterial inoculated columns and only a 5% reduction in the control. The effluent pH of bacterial columns was reported to be in the range of 8.5–8.9, whereas the control columns had a pH below 8.1. A similar trend was reported by Achal et al. (2011b), whereas decrease in the flow rate and 33% calcite content in the top layer of a sand column. Yang et al. (2020) also reported sand consolidation using urease-producing bacteria. The percentage of calcite precipitated in different column layers was concordant with previous studies (Mahawish et al. 2019; Sharma et al. 2020a; Sharma et al. 2021).

4.15.1.1 Microstructural analysis

The upper layer of the sand column was analyzed using SEM-EDS to confirm the $CaCO_3$ precipitation. Fig. 4.60a and 4.60b explicitly confirm calcite formation in LT sand column. The precipitation was observed to be dense and bonded to form an aggregation of crystals. Similarly, in Fig. 4.60d, the staircase of crystals is formed in the UVT sand column, which might be formed due to the accumulation of thick layers of calcite precipitates. The crystals were identified to be a rhombohedral of size 5-7 µm (Fig.4.60e). In comparison, no calcite

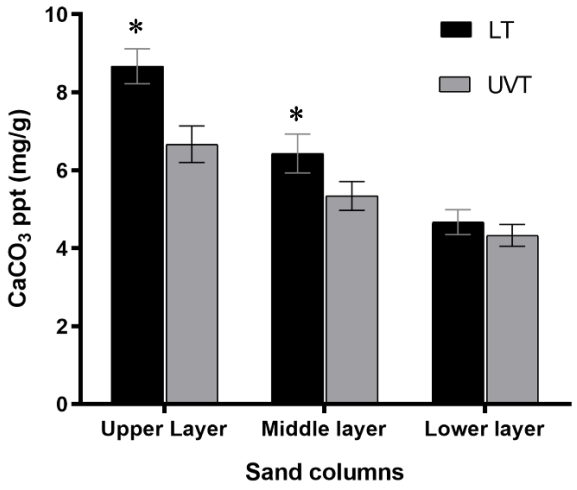


Fig. 4.59 Calcium carbonate precipitation in three different layers of sand columns by live *S. pevalekii* and UV-treated *S. pevalekii* cells. The asterisk (*) sign indicates values are significant at $p<0.05$ using t-test. Values are mean ± SD (n=3)

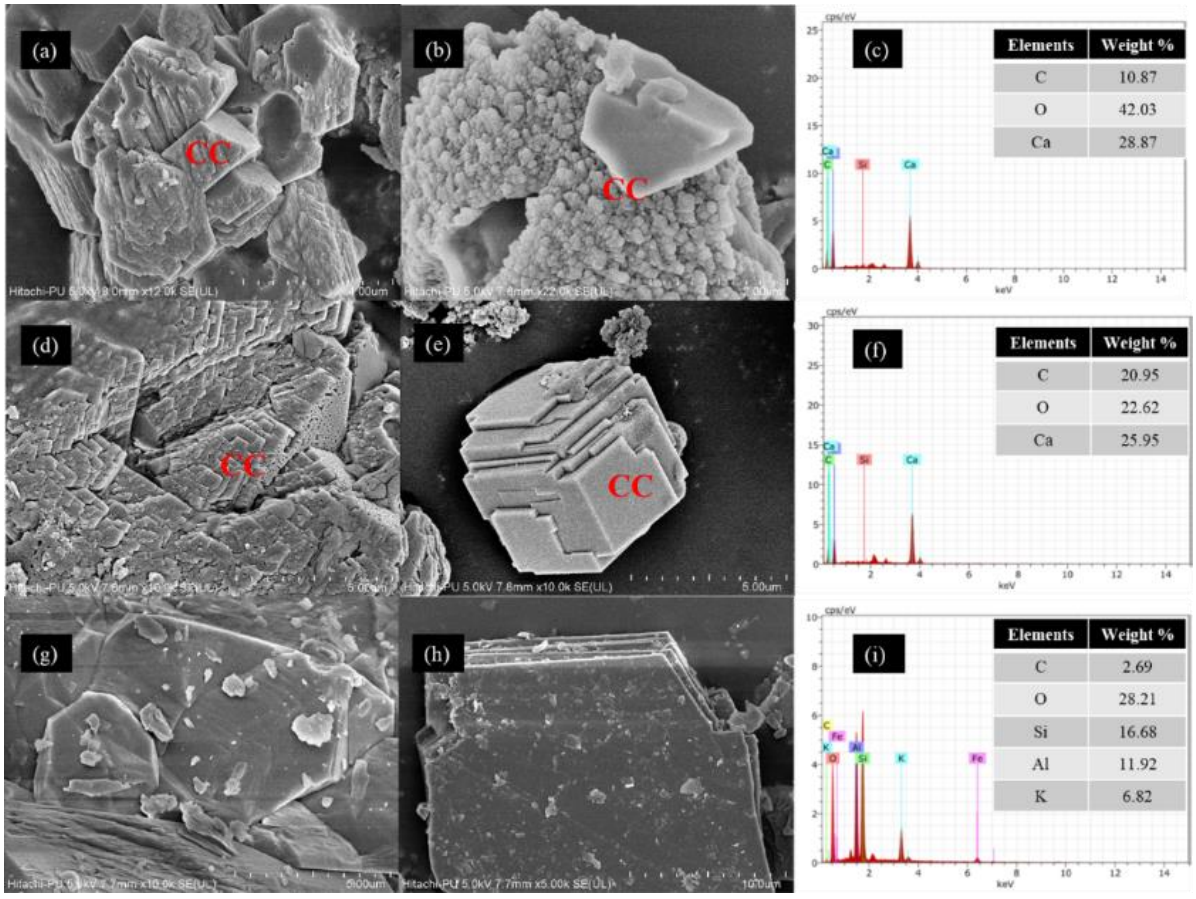


Fig. 4.60 SEM-EDX analysis of sand column treated with (a, b, c) live *S. pevalekii* cells, (d, e, f) UV-treated *S. pevalekii* cells, and (g, h, i) control

deposition was observed in the control after 14 days of treatments. The precipitated crystal was established to be a $CaCO_3$ polymorph by the elemental analysis of the whole area using energy dispersive spectroscopy (EDS). Fig. 4.60c and 4.60f prove the chemical composition of calcite to be carbon, oxygen, calcium, and silica. Hence, there was no uncertainty to finally validate that *S. pevalekii* cells can precipitate $CaCO_3$ crystals within the voids of sand to consolidate sand columns.

4.15.2 Surface treatment by ponding

S. pevalekii was capable of precipitating $CaCO_3$ on the surface of cement mortar. SEM analysis revealed a thick layer of precipitates on the surface of the mortar cube treated with both LT and UVT cells. The rhombohedral calcite mineral formation was observed in the LT mortar cube. Calcite crystals were able to adhere to the surface of the mortar cube. Uniform distribution of precipitates was observed in LT and UVT-treated cells (Fig. 4.61). The results were confirmed by EDX analysis, which showed the presence of Ca, O, C, and Si peaks in both samples. Our study suggests that incorporating live and UV-treated cyanobacterial cells successfully induced $CaCO_3$ precipitation in the cementitious environment. It is important to consider here that UV-treated cells retain the cellular membrane as UV radiations are observed only by purines and pyrimidines of nucleic acid. In heat-killed or autoclaved cultures, cell lysis occurs, thus destroying the organic framework of the cell membrane (Malke 1982). Therefore, it is conceivable that besides the slow metabolism of the cell, heterogenous nucleation is promoted by a negative charge on the cell wall, which leads to calcite precipitation in UV-treated cells. Zhu et al. (2017) reported that UV-treated cells are linked to form more vital adherence to the mortar surface than live cells. Live cells actively utilize nutritional media and grow within the medium.

4.15.3 Compressive strength

The compressive strength of the mortar specimens was done at different testing ages to study the influence of LT and UVT cells on the cement matrix. The LT and UVT specimens showed improvement in compressive strength, which is attributed to the deposition of $CaCO_3$ within the pores of the cement-sand matrix. As evident from Fig. 4.62, the compressive strength of LT specimens increased from 26.28 MPa at 7 days to 48.11 MPa at 28 days. A similar trend was recorded with UVT specimens, where the compressive strength increased from 22.06 MPa

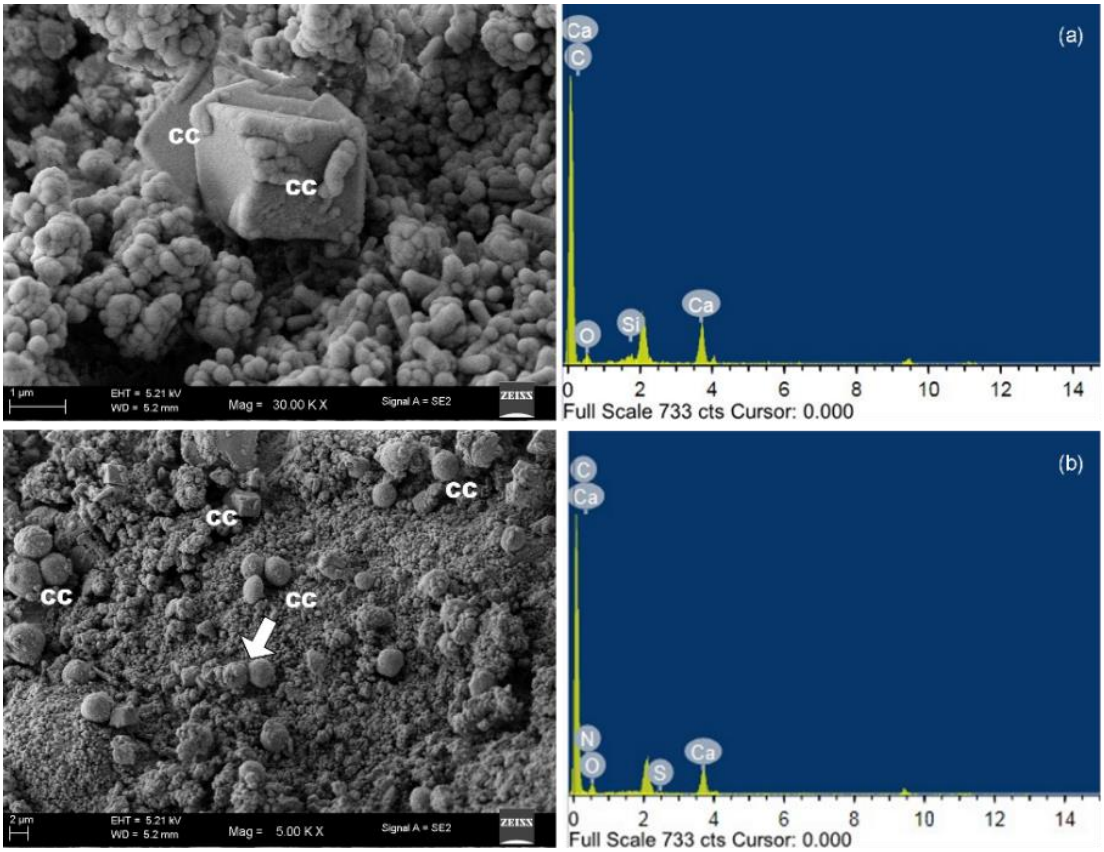


Fig. 4.61 SEM-EDX images representing the $CaCO_3$ crystals (CC) formation on mortar surfaces treated with *S. pevalekii* (a) live cells (b) UV-treated cells

at 7 days to 44.39 MPa at 28 days. The LT specimens observed a 25.54% increase, whereas UVT specimens showed a 15.84% surge in compressive strength after 28 days of curing compared to control specimens. The compressive strength of the LT specimen showed improved strength than the UVT with the curing age. It might be due to the slower physiological activity of UV-treated cell culture than live cells. The photosynthetic reaction by live active cells contributed to the carbonate precipitation by increasing the pH in the microenvironment. In fact, the metabolic active live cells provide more nucleation sites than the dead bacteria since the negative charge on the cell wall is higher and increases their binding capacity. Skevi et al. (2021) described 24% and 35% strength enhancement compared to the control by adding live and dead *B. cohii* bacteria. Likewise, Zhu et al. (2017) reported UV-killed specimens showed higher compressive strength than the live cells. However, Heveran et al. (2020) stated negligible compressive strength differences using *Synechococcus* sp. PCC 7002. Srinivas et al. (2021) reported an improvement in the strength of cement mortar treated with microalgae, *S. elongatus*, and *Spirulina platensis*.

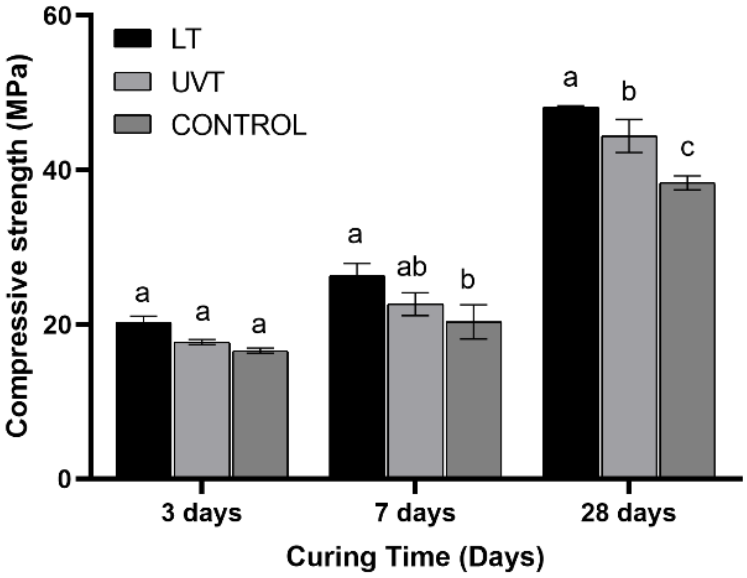


Fig. 4.62 Compressive strength of mortar specimens cured with live and UV-treated *S. pevalekii* cells at 3, 7, and 28 days. Values bearing different letters within the treatment at each time interval are significant at $p<0.05$. Values are mean ± SD (n=3)

4.15.4 Water absorption

Fig. 4.63 represents the cumulative amount of water absorbed per unit cross-sectional area. It was observed that LT and UVT specimens showed lower water absorption than the control specimen. Initially, all the mortar specimens exhibited a rapid rise in water absorption until it became constant in the secondary phase of water absorption. The LT and UVT specimens showed less water absorption than the control specimens. Thus, the cyanobacterial treatment presents an improvement in the durability property of mortar. The low '*k*' value of the surface-treated specimen indicates that bacterial incorporation can significantly improve the permeation properties. At the beginning of the test, water absorption probably results in the rapid filling of large capillary pores near the immersed surface and, finally, a slow rise in the water absorption to more delicate pores far from the submerged surface at the end of testing. Similar results were plotted by Hernández et al. (2016) by incorporating cactus mucilage and marine brown algae extract. Tayebani and Mostofinejad (2019) also reported reduced water absorption due to biological treatment compared to water curing. The sorptivity coefficient '*k*' of water absorption in LT specimens was less than in UVT specimens (Table 4.12).

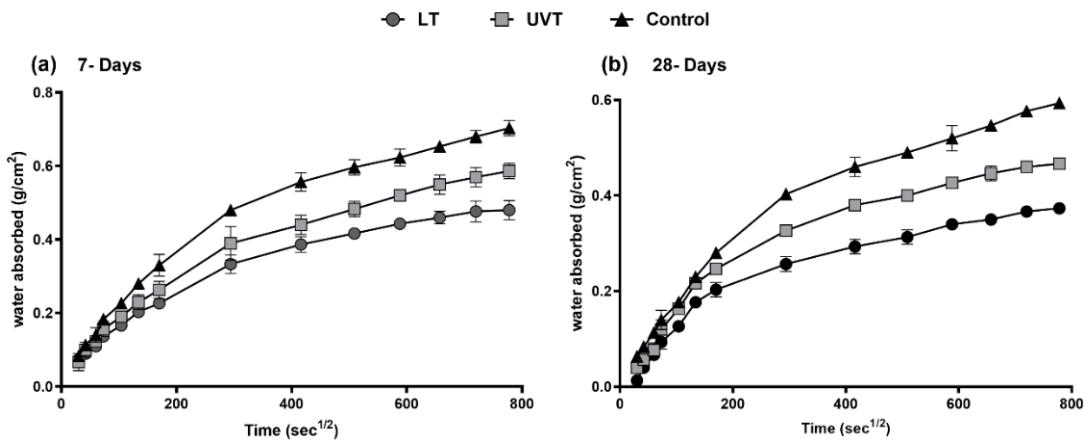


Fig. 4.63 Water absorption of mortar specimens treated with live and UV treated *Synechocystis pevalekii* at (a) 7 days (b) 28 days of curing time. Values are mean ± SD (n=3)

Table 4.12 Sorptivity coefficient different treatments at the age of 7 and 28 days

Specimens	**Sorptivity coefficient (*k*)**	
	7 days	28 days
LT	0.1058 ± 0.00950	0.0702 ± 0.01786
UVT	0.1126 ± 0.01098	0.0922 ± 0.02132
Control	0.1376 ± 0.01423	0.1065 ± 0.02116

4.15.5 Thermogravimetric (TGA) analysis

TGA was conducted for all the specimens at 28 days of curing to confirm the $CaCO_3$ precipitation. The TGA thermograms for LT, UVT, and control specimens are presented in Fig. 4.64a. The TGA results showed immense weight loss of 4.86% in LT specimens and 4.09% in the UVT specimens between 600-800 °C, corresponding to the carbonate weight loss (Fig. 4.64b). However, control displayed only 2.32% weight loss percentage between 600–800 °C. The TGA's steeper peaks support the $CaCO_3$ precipitation by LT and UVT specimens with higher weight loss by LT followed by UVT. Weight loss was comparatively lower in control than LT and UVT specimens. Besides $CaCO_3$ decomposition, another fall with 0.63%, 0.52%, and 0.69% weight loss of $Ca(OH)_2$ was observed 400-450 °C temperature, showing insignificant mass loss due to dehydration of calcium hydroxide (Fig. 4.61b). Along with $CaCO_3$, mortar specimens showed weight loss of calcium hydroxide during TGA, formed due to the hydration of cementitious material during the curing process. The literature shows calcium hydroxide and $CaCO_3$ dehydration occur at 420-540 °C and 500-800 °C (Stuckrath et

al. 2014; Sharma et al. 2017). Thus, this significant drop in $CaCO_3$ dehydration accounts for higher $CaCO_3$ precipitation in bacterial-treated specimens. Therefore, the deposition of $CaCO_3$ can be considered an essential factor in strength enhancement and permeability reduction. The results were in agreement with the reports of other researchers (Pei et al. 2013; Jang et al. 2020).

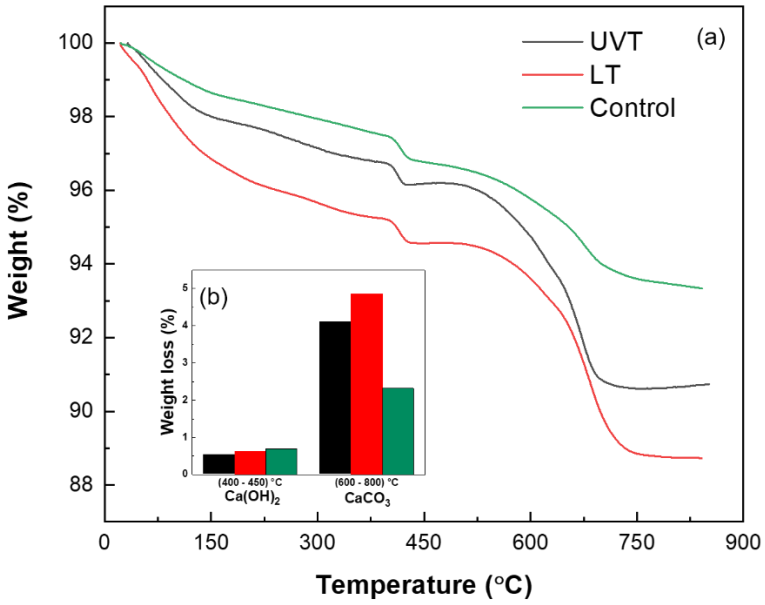


Fig. 4.64 (a) TGA analysis of mortar specimens treated with live and UV-treated *S. pevalekii* cells at 28 days (b) weight loss percentage (%)

4.15.6 Microstructural analysis

The XRD analysis revealed that prominent crystalline quartz (SiO_2) peaks in the control specimen were observed (Fig. 4.65). Among all the peaks shown in the XRD spectra, the calcite polymorph of $CaCO_3$ crystals was dominantly present in LT and UVT specimens, along with the peak of quartz. XRD spectra of LT specimens were observed at 29.4°, 35.9°, 39.4°, 43.3°, and 48.45° corresponding to the 104, 110, 113, 202, and 116 planes of the calcite phase, whereas in UVT, it was observed at 29.4°, 39.4° and 43.3° corresponding to the 10, 110 and 113 planes of the calcite phase (Vu et al. 2020). The diffraction peaks at (2θ) of 27.1°, 39.6° corresponds to 101, 211 planes of vaterite crystals. The presence of calcite peaks approves the crystal formation by *S. pevalekii* cells in the mortar specimens. XRD results were in agreement with the previous study showing precipitation of $CaCO_3$ crystals as a result of bacterial metabolic activity in the harsh environment of the cementitious material (Joshi et al. 2020; Saxena and Tembhurkar 2020; Anand et al. 2022c).

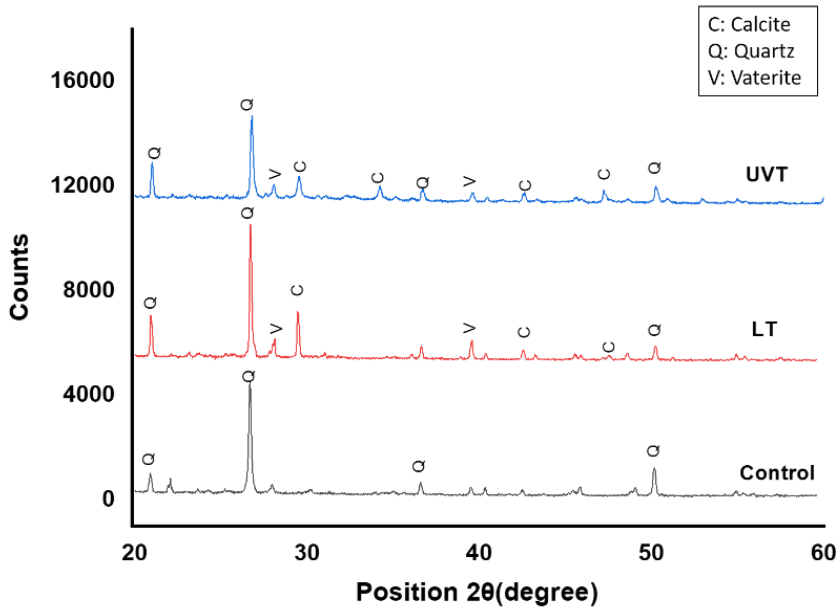


Fig. 4.65 X-ray-diffraction pattern of mortar treated with live treated and UV treated *S. pevalekii* at 28 days

The microstructural analysis of the mortar specimens with UV and live cells and the control specimen treated with water are shown in Fig. 4.66. Fig. 4.66a validates the crystals buildup by UV-treated bacterial cells forming a dense layer of calcite over the mortar surface, which was observed to be tightly packed and in a perfect rhombohedral crystal lattice in a size range of 5 to 10 µm. Likewise, in live treated specimens, the spherical vaterite crystal ranging in size 17-20 µm were observed along with the cubic crystals of 10-15 µm calcite (Fig. 4.66b). Both crystals form is composed of $CaCO_3$, which was confirmed by EDX analysis. Compared to the control, the mineral constituents characterized by EDX analysis clearly show an extensive Ca, O, and C peak in LT and UVT specimens. As observed in EDX analysis, the amount of carbon, oxygen, and calcium formed in the LT sample was 7.25%, 40.93%, and 51.82%, respectively. Similarly, in the EDX analysis of UVT, the amount of carbon, oxygen, and calcium reported was 13.88%, 51.93%, and 33.62%, respectively, which is a comparatively higher amount than the control. Meanwhile, live cells were able to promote both calcite and vaterite precipitation. The precipitation of calcite and vaterite crystals was observed by Chekroun et al. (2004) in the presence of live and UV-treated *Myxococcus xanthus*. The presence of such different morphologies and structures of $CaCO_3$ crystals has been well-defined in previous research. The cubic shape of calcite and the spherical shape of vaterite coexist with the bacterial cell, as Xiao et al. (2010) reported. Different theories have been put forward to illustrate such co-occurrence. Firstly, the vaterite is considered a thermodynamically unstable crystal form, and its nucleation

rate is faster; therefore, slow diffusion of Ca^{2+} and CO_3^{2+} ions can lead to calcite formation (Weiner and Dove 2003). Secondly, the involvement of different organic components of the cell surface provides another nucleation site for biomineralization (Liang et al. 2013). Zhu et al. (2017) reported similar results by treating the specimens with live and UV-killed *Gleocapsa* PCC73106.

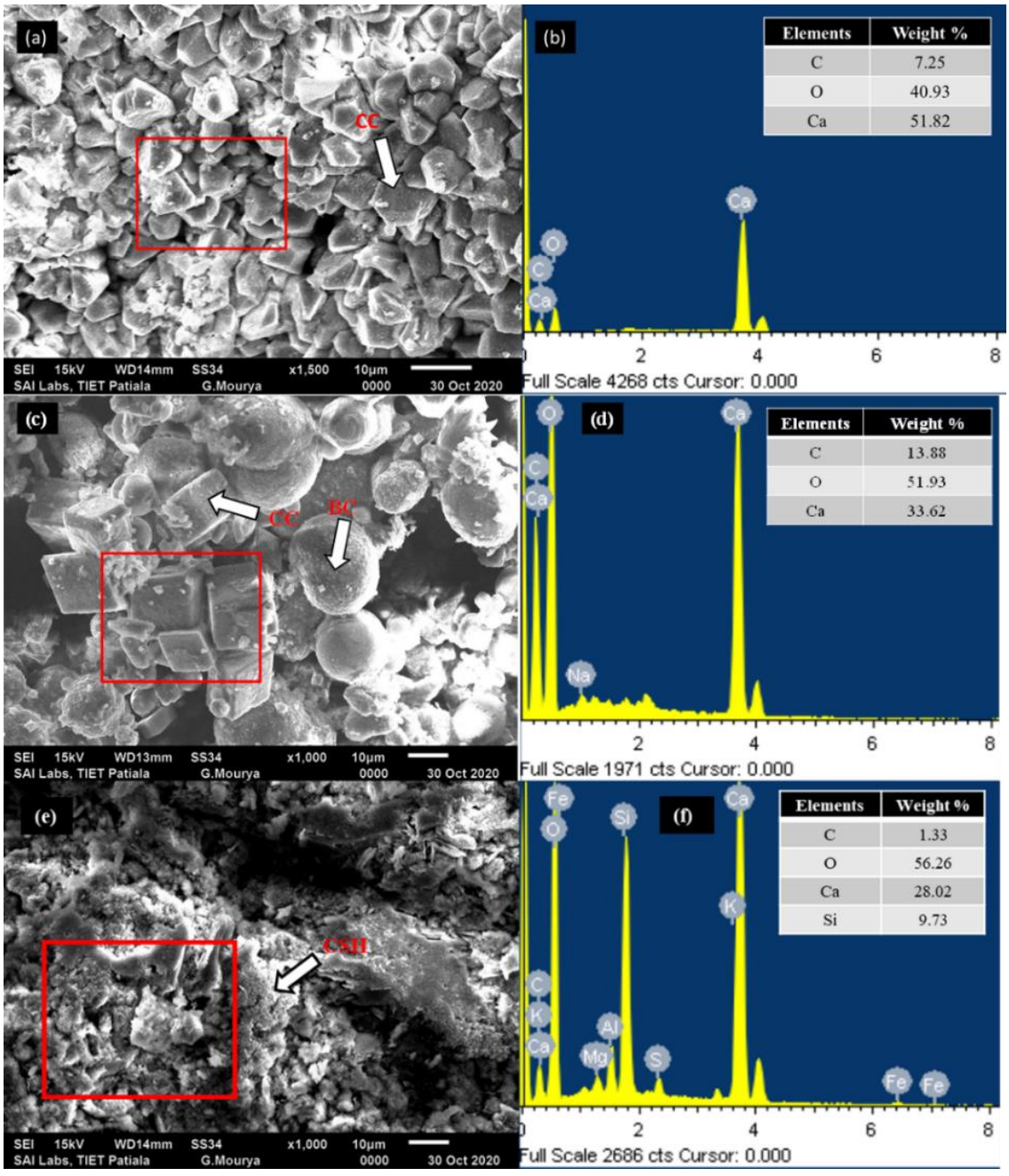


Fig. 4.66 SEM-EDX images represent $CaCO_3$ crystals (CC) in mortar specimens treated with live *S. pevalekii* (B.C.) cells (a, b); UV treated *S. pevalekii* cells (c, d), and control (e, f). The square '□' sign indicates the spot of EDX analysis

4.16 Development of fly ash-based cementitious biogrout incorporating cyanobacteria *Synechocystis pevalekii*

A cementitious biogrout was developed for the remediation of crack in different orientations (horizontal and vertical). Cement grout (CG) is a mix of cement and water in well-defined water-to-binder ratio (w/b). To develop injectable grout, fly ash (FA) was taken as a partial cement replacement to repair the cracks in cementitious structures.

4.16.1 Fresh properties of grout

The influence on the fresh properties of grout mixtures with varying proportions of FA (10% to 50%) and different water and cyanobacterial culture, binder ratios (0.45, 0.47, and 0.50) was investigated using different flowability tests to confirm the injectable property of grout.

4.16.1.1 Marsh cone test

The marsh cone test was conducted within a few seconds after the preparation of the mixture. The time required for an 800 ml grout mixture to flow through the cone is correlated to the viscosity of the cement-based grout, signifying that the longer the flow time, the less is fluidity of the grout mixture. In all six experiment groups of 36 grout mixes, the flow time for the marsh cone test was higher in all the control sets designated as plain grout. With substituting cyanobacterial culture instead of water, the flow time was observed to reduce in culture/binder ratio (c/b) of 0.47 and 0.5. Still, viscosity was detected to be higher in the 0.45 c/b ratio; consequently, flow time was observed to be higher. It might be due to the thickness formed due to the low c/b ratio., The grout mix's viscosity increases upon adding $CaCl_2$ and $NaHCO_3$, reducing the grout mix's flow time through the orifice. Increasing the c/b ratio to 0.47 and 0.5, the flow rate of the grout mixture showed a comparatively less flow time because of a reduction in the viscosity. The decreased flow time of 57s, 53s, 51s, 48s, 45s, and 67s was observed with an increased FA dosage in biogrout with a 0.47 c/b ratio (Table 4.14). Fig. 4.67 shows decreasing trend of the flow time with an increase in the FA dosage (10% – 40%) but a rapid surge in flow time at 50% FA replacement. It is important to understand that FA act as plasticizing material for cement-based grout, improving the flowability of the mixture inside the crack. However, at higher concentrations (50%), the substitution of FA for the surface area of the cement-based grout increases, demanding an increase in w/b or c/b. The statistical analysis showed that FA (0% – 50%) and grout's water/culture to binder ratio (0.45, 0.47, and

0.50) have a significant effect on the flow time of the plain grout as well as biogrout (Table 4.13). Similar results were corroborated by Joshi et al. (2021) using CT5 bacterial culture at 40% FA replacement. Li et al. (2017) also reported a decrease in the flow time by a decrease in the viscosity on increasing the dosage of microfine fly ash (MFA). The optimum percentage of fly ash replacement recommended is 30% - 40%. However, Sha et al. (2018) recommended the optimum percentage of FA as 20%-30% in geotechnical engineering.

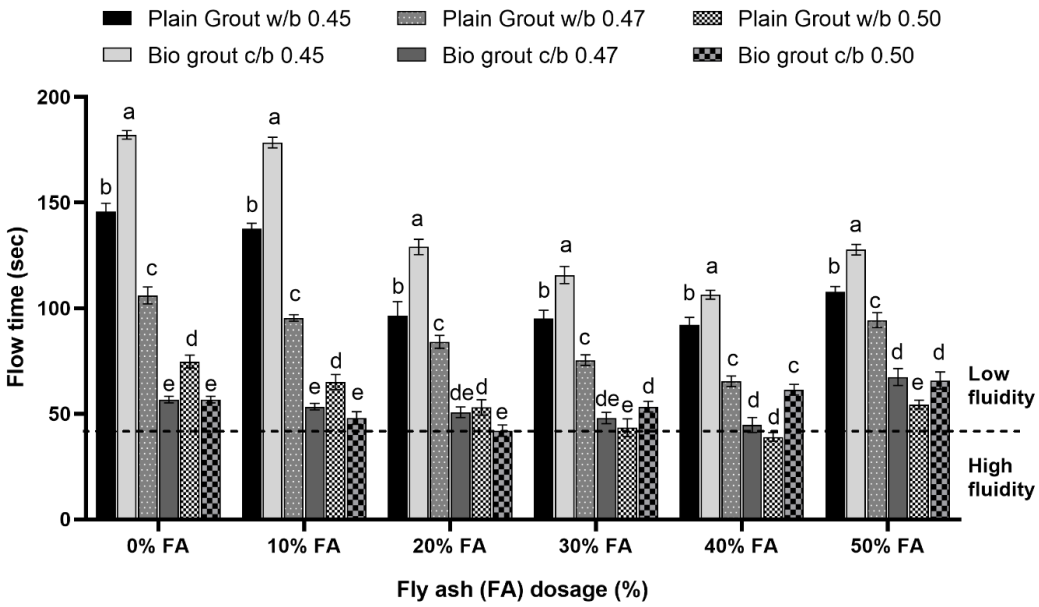


Fig. 4.67 Marsh cone test analysis for fluidity of grout mixtures incorporated with different dosages of fly ash (FA); water/binder (w/b) ratio and culture/binder (c/b) ratio. The dotted line differentiates high and low fluidity for marsh cone test. Values bearing the different letters within the same treatment are significant at $p<0.05$. Values are mean ± SD (n=3)

4.16.1.2 Mini slump test

A miniature slump test is used to examine fresh cementitious paste's workability using a small cone with dimensions of a top diameter of 19 mm, bottom diameter of 38 mm, and height of 57 mm. The spread diameter of the cementitious paste was calculated by lifting the mini-slump cone. Fig. 4.68. illustrates the spread flow diameter of grout mixtures with different w/b and c/b ratios and FA substitutions. As observed, the diameter in the control mix (0% FA) designated as plain grout increased by 49.4% when the w/b ratio increased from 0.45 to 0.5. The spread diameter of the biogrout mixture increased by 46.42% upon increasing the 0.45 to 0.5, which is comparatively lower than the control. This might be because of the increased

thickness of biogrout as calcium chloride, and sodium bicarbonate are added to grout mixture. However, integrating FA with cement in increased quantities (10 to 50%) resulted in a considerable increase in mini-slump flow diameter in all grout mixes, indicating an improvement in fluidity. It significantly improved the flow diameter by 50.54% on the substitution of 40% FA replacement; however, additional FA replacement (50%) lowers the grout spread diameter to 46.87%. Here, FA acts as a lubricating agent because of its smooth texture and spherical particle shape, which enhances the rolling capacity and flowability between the cement particles and cyanobacterial culture, resulting in ball bearing effect reducing the inter-particle friction (Razi et al. 2016; Çınar et al. 2019). The flow diameter of the grout mixture at a c/b ratio 0.47 the diameter observed was 131, 130, 129, 133, 133, and 123 mm compared to plain grout, which showed the flow diameter 111, 111, 114, 117, 122, and 122 mm (Table 4.14). Correspondingly, the flow diameter of the 0.47 c/b ratio grout mixture was in the range of 88 to 140 mm and 98 to 142 mm when the c/b ratio was 0.5. The analysis of variance inferred that enhancement in water/culture binder ratio and FA substitution had a significant effect on the grout mixture (Table 4.13). Çınar et al. (2019) investigated and reported an increase in mini-slump flow with an increase in the dosage concentration of fly ash (5%-25%) and waste marble powder (5%-25%) for cement-based grout.

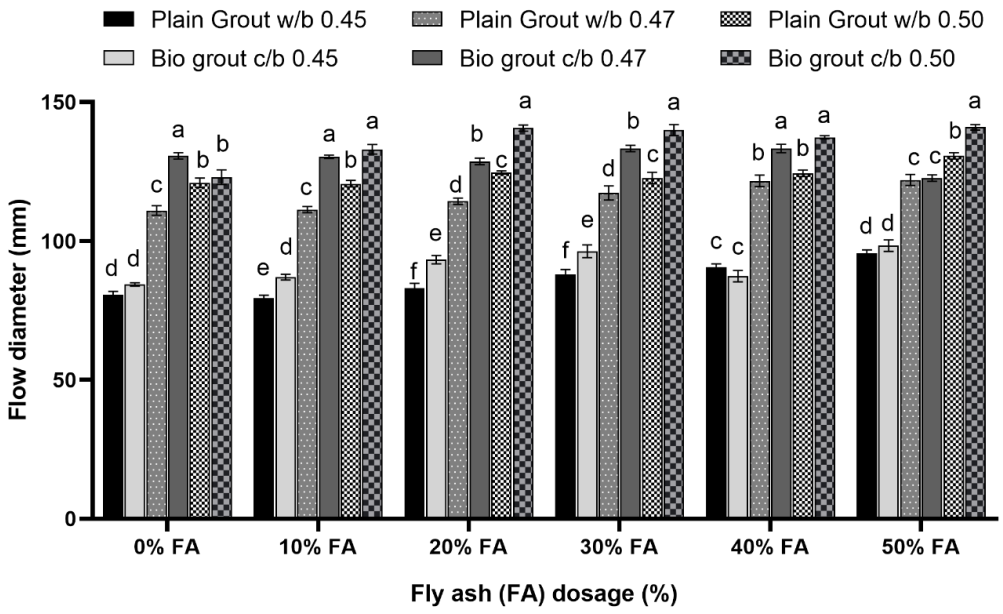


Fig. 4.68 Mini cone test analysis for fluidity of grout mixtures incorporated with different dosages of fly ash (FA); water/binder (w/b) ratio and culture/binder (c/b) ratio. Values bearing the different letters within the same treatment are significant at $p<0.05$. Values are mean ± SD (n=3).

4.16.1.3 Grout bleeding

After six hours of sedimentation with various w/b and c/b ratios (0.45, 0.47, and 0.50), the bleed volume was measured for all the grout mixtures. Fig. 4.69 signifies the increase in percentage bleed of 36 grout mixture with an increase in w/b and c/b ratio; however, grout bleeding decreased with an increase in FA dosage (0% - 50%). The percentage of grout bleeds increased from 3.1% to 4.3% in plain grout as the w/b ratio increased from 0.45 to 0.50. With the increase in FA dosage, the grout bleeding percentage decreased gradually in plain grout from 3.1% to 0.4% with a 0.45 w/b ratio, 3.0% to 1.2% with a w/b ratio of 0.47, and 5.31% to 3.18% with 0.50 w/b ratio. Similar results were recorded for biogrout. For instance, in a c/b ratio of 0.47, the bleeding rate dropped from 3.6% to 0.6% (Table 4.14). The maximum bleed percentage in all six experimental setups was observed in a water and culture/binder ratio of 0.50, followed by 0.47. The lowest grout bleeding (0.2%) was evaluated in 40%, and 50% substituted FA biogrout with a c/b ratio of 0.45, which was considered a minor bleed. Bleed percentage value less than 2% after 3 hours of sedimentation is considered stable for selecting the best grout mixture for geotechnical application (ASTM C940, 2010). Significant variation was observed among the different dosages of FA (0%-50%) and culture/water ratio (0.45, 0.47, and 0.50) of grout on the grout bleeding percentage of the plain and biogrout, as shown in Table 4.13. Vasumithran et al. (2020) also reported an increase in grout bleed with an increase in the w/b ratio. Reduced bleeding of FA-incorporated grouts can be attributed to lessened porosity and improved packing density (Azima and Bundur 2019).

4.16.1.4 Selection of optimum w/b or c/b ratio for grout

The 0.45, 0.47 and 0.50 water or culture to binder ratio (w/b or c/b) and (0% – 50%) fly ash as partial replacement of cement in grout mixes were tested for the fluidity (ASTM C939 2010), mini slump and grout bleeding (ASTM C940 2010). The grout mixes of 0.5 water or culture to binder ratio showed high bleeding at 0% – 50% FA replacement as per the ASTM standard (ASTM C940 2010) and therefore, this grout mix was rejected for further investigation. However, some of the grout mixes prepared by 0.45 and 0.47 w/b or c/b showed good fluidity and low bleeding. Out of these grout mixes (0.45 and 0.47), 0.47 showed higher fluidity with the slump value of 133 mm whereas 0.45 showed maximum slump diameter of 98 mm. As described in Table 4.14, the flow time at 0.45 w/b or c/b ratio was comparatively higher than the 0.47 w/b or c/b ratio (ASTM C939 2010). Since fluidity this is an important parameter for penetrability of biogrout in the depth of crack; therefore 0.47 w/b or c/b ratio of the grout mixes

was selected for the further studies. The selected grout mixes (0.47 w/b or c/b) were further tested for hardened properties with varied replacement of FA.

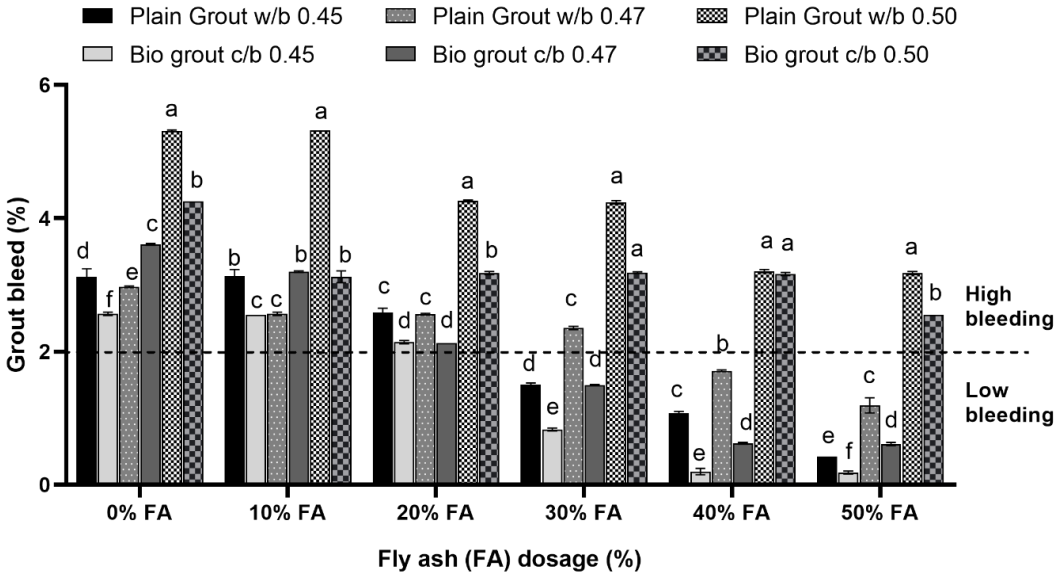


Fig. 4.69 Grout bleeding of grout mixtures incorporated with different dosages of fly ash (FA); water/binder (w/b) ratio and culture/binder (c/b) ratio. The dotted line differentiates low (stable) and high (unstable) grout bleed percentages. Values bearing the different letters within the same treatment are significant at $p<0.05$. Values are mean ± SD (n=3)

Table 4.13 The factorial ANOVA results indicating the effects of different concentrations (0% - 50%) of fly ash (FA) and water/binder (w/b) or culture/binder (c/b) ratio on injectable grout in a crack. The P values < 0.001 indicates the values are highly significant

Variables		**Fly ash (FA)**	**w/b & c/b ratio**	**FA × w/b & c/b ratio**
Marsh Cone test	df	5, 72 P<0.0001	5, 72 P<0.0001	25, 72 P<0.0001
Mini slump test	df	5, 72 P<0.0001	5, 72 P<0.0001	25, 72 P<0.0001
Grout bleed percentage	df	5, 72 P<0.0001	5, 72 P<0.0001	25, 72 P<0.0001
		Fly ash (FA)	**Treatment**	**FA × time**
Slump retention time	df	5,10 P<0.0001	6,12 P<0.0001	30,60 P<0.0001
Initial Setting Time	df	5, 24 P<0.0001	1, 24 P<0.0001	5, 24 P = 0.01
Final Setting Time	df	5, 24 P<0.0001	1, 24 P<0.0001	5, 24 P = 0.5
Compressive strength	df	5, 24 P<0.0001	1, 24 P<0.0001	5, 24 P = 0.13

Table 4.14 Fresh properties (a) Marsh cone, (b) mini-slump cone, and (c) grout bleeding of grout mixtures incorporated with different dosages of fly ash (FA); water/binder (w/b) ratio and culture/binder (c/b) ratio

Grout mixes	w/b	Fresh properties of grout mix						Remarks
		Marsh cone (sec)		Mini slump (mm)		Grout bleeding (%)		
		Plain grout	Bio grout	Plain grout	Bio grout	Plain grout	Bio grout	
0	0.45	146	182	81	84	3.1	2.6	×
10	0.45	138	178	79	87	3.1	2.6	×
20	0.45	96	129	83	93	2.6	2.1	×
30	0.45	95	116	88	96	1.5	0.8	×
40	0.45	92	106	91	87	1.1	0.2	×
50	0.45	108	128	96	98	0.4	0.2	×
0	0.47	106	57	111	131	3.0	3.6	✓
10	0.47	95	53	111	130	2.6	3.2	✓
20	0.47	84	51	114	129	2.6	2.1	✓
30	0.47	75	48	117	133	2.4	1.5	✓
40	0.47	65	45	122	133	1.7	0.6	✓
50	0.47	94	67	122	121	1.2	0.6	✓
0	0.50	75	56	121	123	5.3	4.3	×
10	0.50	65	48	121	133	5.3	3.1	×
20	0.50	53	42	125	141	4.2	3.2	×
30	0.50	43	53	123	140	4.2	3.2	×
40	0.50	39	61	124	137	3.2	3.2	×
50	0.50	54	66	131	141	3.2	2.6	×

×: Rejected ✓: Selected

4.16.1.5 Slump flow retention

Fig. 4.70 presents the mini-slump flow diameter of the plain and bio grout with a w/b (and c/b) ratio 0.47. The workability flow retention of plain and bio grout mix was tested at 20-minute intervals till 120 minutes. The initial flow diameter of the control mix (0% FA) of plain and biogrout mix is 111 and 132 mm, indicating that adding cyanobacterial culture and calcifying solution significantly affects the grout's flowability property. The inclusion of FA content from 0 to 50% in cementitious grout (plain and biogrout) showed an increase in the flowability of grout but decreased with progressive time intervals. As shown in Fig. 4.70b, biogrout with 40% partial replacement had an initial slump flow diameter of 145 mm, which declined to 137 mm at 60 minutes and 131 mm at 120 minutes, showing 9.6% decrease in workability retention. On the other hand, plain grout with 40% FA substituted cementitious grout showed 13.1% decline in workability retention of the grout at 120 minutes (Fig. 4.70a). It can be attributed to the fact

that cyanobacteria are spherical, which increases the flowability of biogrout when added to spherical fly ash. Due to fly ash's ball-bearing effect, the inter-particle friction between cyanobacteria, fly ash, and cement is reduced (Çınar et al. 2020). Therefore, the addition of calcifying solution ($CaCl_2$ and $NaHCO_3$) in the presence of cyanobacteria did not retard the flowability of the grout during 120 minutes study. A similar study was carried out by Khalid et al. (2016), Nair et al. (2020), and Kaladharan and Rajabipour (2022).

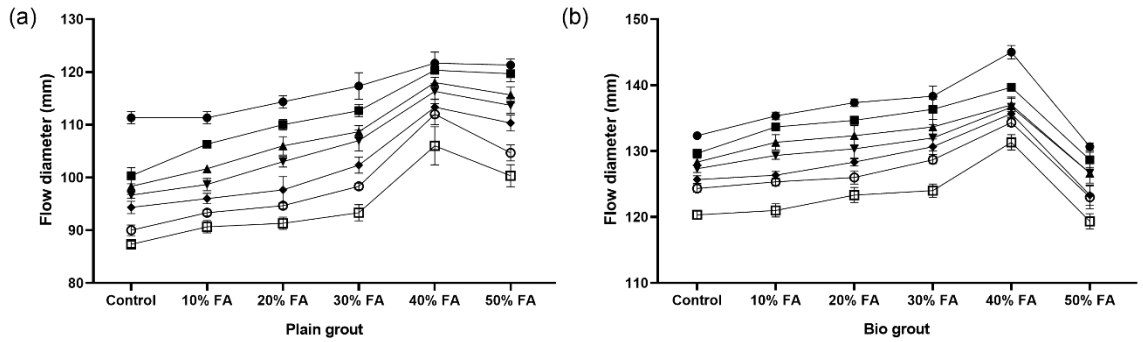


Fig. 4.70 Flow retention diameter of (a) plain grout and (b) biogrout partially replaced with different concentrations of fly ash at different time intervals. Values are mean ± SD (n=3)

4.16.2 Hardened properties of grout

Based on the fresh properties, 0.47 was selected as optimum w/b or c/b. Further, the setting time (initial and final) and compressive strength of the grout mix were studied to determine the optimum FA dosage.

4.16.2.1 Setting time

Using a Vicat apparatus, the setting time of FA amalgamated cement-based biogrout was tested for a w/b and c/b ratio of 0.47. As shown in Fig. 4.71 initial setting time of biogrout prepared by *S pevalekii* cells gradually increased by 50 minutes on replacement of fly ash from 0 to 50%, whereas the final setting time of biogrout increased by 30 minutes. The initial setting of the plain grout increased by 4%, 5%, 12%, and 14% upon increasing the dosage of FA from 20, 30, 40, and 50%, respectively. At the same time, the initial setting time of biogrout increased by 1.8%, 1.8%, 3.7%, 9.4%, and 21.15% upon increasing the dosage of the FA 10, 20, 30, 40, and 50%. The substitution of fly ash in the cementitious mixture increases the initial and final setting time of both biogrout and plain grout, which lowers flowability loss. It accounts for the

fact that as the dosage of FA increases in the grout, the surface area for the attachment of calcium ions (Ca^{2+}) increases, further decreasing the augmentation of the Ca^{2+} in the fresh paste during the primary hydration stage. Because of this, the heat of hydration reduces, increasing the final setting time of the cement-based grout mixture (Yijin et al. 2004; Zhang et al. 2019). Moreover, there is limited time available for transportation and injecting the grout. Therefore, it is crucial to maintain grout hydration. As a result, the initial setting time helps to determine the efficacy of cyanobacterial culture in the grout. Choi et al. (2012) also attributed the decrease in temperature to an increase in the percentage of FA due to the delayed pozzolanic interaction of the fly ash with the hydrating cement's calcium hydroxide. They further added that the higher the percentage of FA, the more decline in the temperature would be observed. Overall, the initial setting time for a biogrout was observed to be higher than the plain grout, which could be explained by the fact of adding cyanobacterial culture along with $CaCl_2$ and $NaHCO_3$ and increasing the concentration of FA (10% - 50%) in the grout. Furthermore, it was noted that the final setting time of FA replaced biogrout and plain grout was attained in less than 90 minutes after reaching the initial setting time. Two-way ANOVA verified that different fly ash dosages significantly affect the setting time of the plain and biogrout along with the water/culture to binder ratio (0.47) (Table 4.13).

4.16.2.2 Effect of fly ash dosage on compressive strength of grouts

The compressive strength of the grout mixture was analyzed for the 0 to 50% FA substitution by keeping the w/b or c/b ratio 0.47. It was noted that at 28 days, the compressive strength of control plain grout increased from 15.8 MPa to 17.0 MPa with an increase in FA dosage up to 40% but declined to 16.1 at 50% dosage. The maximum compressive strength was reported in plain and biogrout mixtures with 40% FA integration From Fig. 4.72. it can be evaluated that replacing *S. pevalekii* culture with water results in strength gain. It was noted that *S. pevalekii* treatment increases the strength of almost all the cyanobacterial grout mixtures compared to the plain control mix. Maximum strength gain was noted in 40% FA incorporated biogrout (19.7 MPa); however, upon further increasing FA dosage, the strength of biogrout declined to 17.2 MPa. The compressive strength for 0%, 10%, 20%, 30%, 40% and 50% biogrout increased by 7.5%, 6.9%, 10%, 7.9%, 15.9% and 6.9%, respectively. The results indicate that overall strength improvement was observed among all the biogrout due to cyanobacterial treatment. It could be due to the calcification by cyanobacterial culture, reducing the pore size and improving the compressive strength of the specimens. Similarly, others researchers have reported

significant improvement in the compressive strength of cementitious material upon curing with the cyanobacterial culture (Zhu et al. 2017). Likewise, Zhang et al. (2020) also reported an increase in cement-based grout compressive strength upon adding (10%-30%) fly ash along with water glass and bentonite. The analysis of variance proved that fly ash variation significantly affects the compressive strength of the grout (Table 4.13).

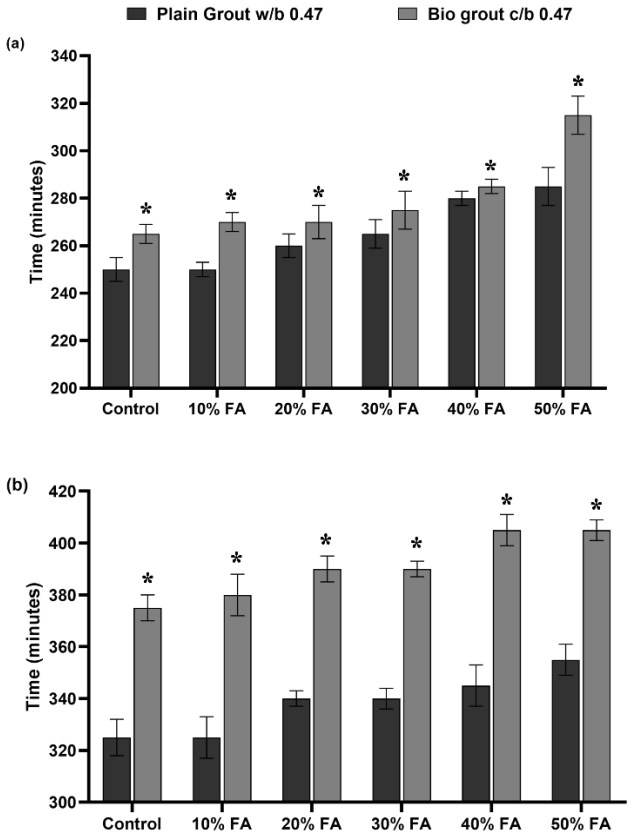


Fig. 4.71 (a) Initial and (b) final setting time of FA (0% – 50%) incorporated plain and biogrout at w/b and c/b ratio 0.47. The asterisk (*) sign indicates values are significant at $p<0.05$ using t-test. Values are mean ± SD (n=3)

4.16.2.3 Selecting the best cement-based biogrout

The best grout mixture with 40% FA substitution and 0.47 culture-to-binder ratio was selected for crack remediation based on the best results obtained from setting time and compressive strength, as presented in Table 6. The strength of the grout depends on the substitution of fly ash and the culture/binder ratio. The flowability test ensures best injectability in the crack vertically and horizontally using a syringe; while strength of grout ensures better mechanical properties of the repaired surface.

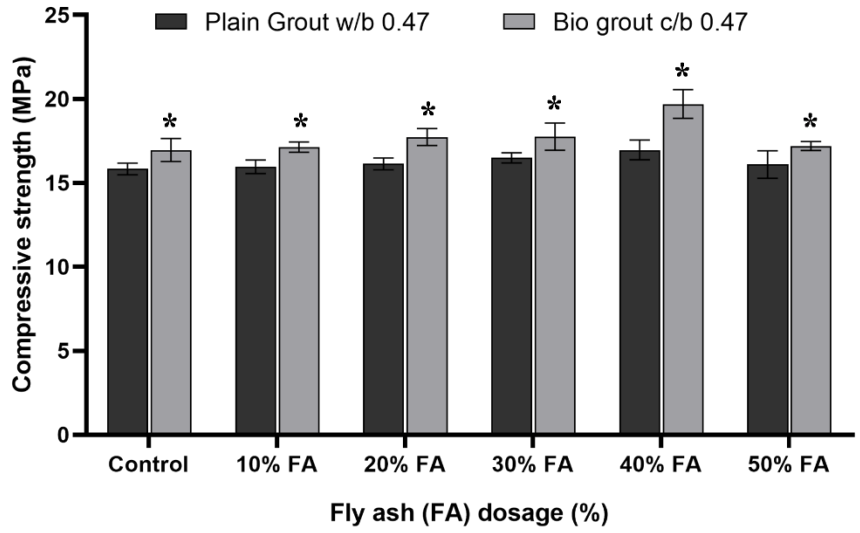


Fig. 4.72 Compressive strength of FA (0% – 50%) incorporated plain and biogrout at w/b and c/b ratio 0.47 after 28 days of curing. The asterisk (*) sign indicates values are significant at $p<0.05$ using t-test. Values are mean ± SD (n=3)

4.16.3 Crack remediation and testing

The pre-cracked concrete specimens (500 × 100 × 100 mm prismatic, 500 × 500 × 500 mm cube and 100 × 50 mm cylindrical specimen) were repaired using two different grout mixtures; plain grout and biogrout. The specimens repaired using 40% FA replaced cement plain grout were categorized as control specimens and were divided on the basis of curing treatment ponding (CPT) and spray (CST), The other group was repaired using 40% FA replaced cement biogrout incorporating *Synechocystis pevalekii* culture (Fig. 4.73). The specimens were subjected to curing treatment using *Synechocystis pevalekii* cell culture supplemented with calcifying solution ($CaCl_2$ + $NaHCO_3$) spray (BST) and ponding treatment (BPT) for 28 days (Fig. 4.74). Once the grout's curing cycle is complete, the flexural strength, compressive strength and water sorptivity of the specimens were assessed. The uncracked specimens (REF) and cracked specimens without treatment (UTC) were taken into account to compare the strength and sorptivity efficiency of the biogrout and plain grout treated specimens.

4.16.3.1 Compressive strength

The compressive strength results for the six different sets of concrete specimens are shown in Fig. 4.75a. The compressive strength of UTC (untreated cracked concrete specimens) without

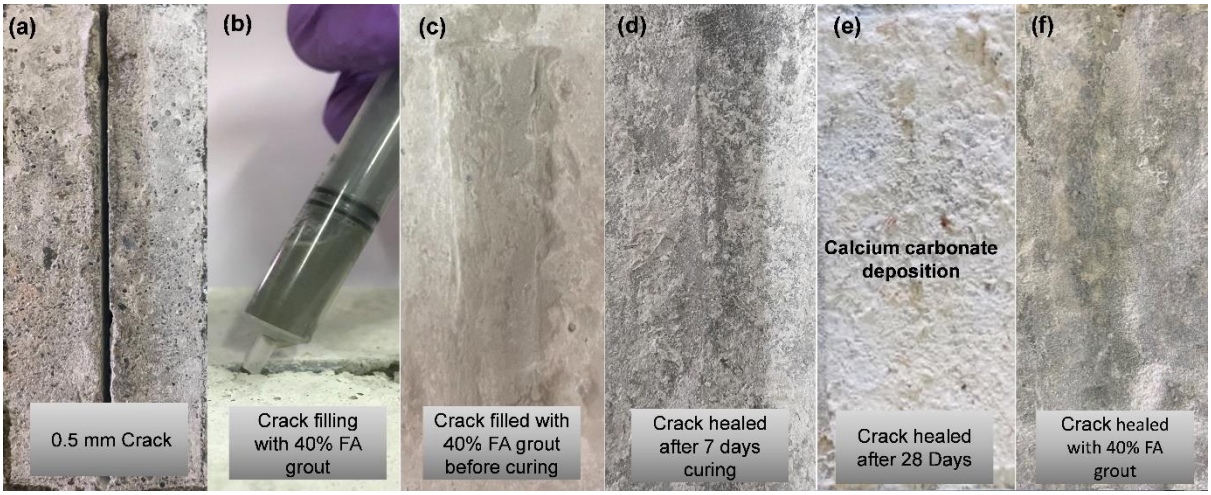


Fig. 4.73 Crack remediation using plain and biogrout (a) cracked specimen (b) injecting grout using 20 ml syringe (c, d) $CaCO_3$ precipitation after 7- and 28-days curing, (e) crack healed area after removal of additional carbonate precipitates

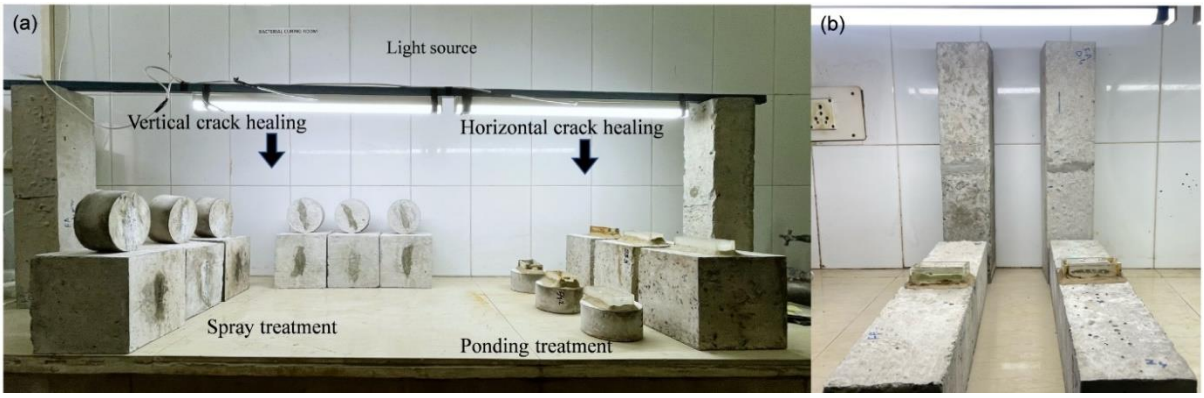


Fig. 4.74 Pictorial representation of curing treatment (spray and ponding)

any grout repairing was 30.8 MPa. The highest compressive strength (41.82 MPa) was observed in biogrout repair with ponding curing treatment (BPT), followed by 38.94 MPa strength in fly ash amended plain grout with ponding treatment (CPT). Compared to UTC, BPT showed a substantial enhancement of 35.78% due to biocalcification by *S. pevalekii* cells in the presence of sodium bicarbonate and calcium chloride, whereas the BST specimen showed the corresponding increase of 23.82%. The compressive strength of the uncracked concrete specimen (designated as REF) was 38.32 MPa. The BPT specimen showed 9.1% improvement in compressive strength than the REF specimen. Therefore, the 40% FA substituted biogrout confirms the improvement in the compressive strength of the concrete specimens by using *S. pevalekii* culture. The statistical analysis depicts a significant improvement in compressive

strength compared to the UTC by the BPT, BST, CPT, and CST. Moreover, the BPT, BST specimens showed more remarkable strength improvement than CPT, and CST specimens. The $CaCO_3$ crystals fill the voids between the FA and cement particles. It is likely to provide additional strength to the repaired specimens. An increase in the calcium and calcite content due to the addition of cyanobacteria could be the main reason for enhancing the concrete's strength. Osman et al. (2021) also conferred similar results using two species, *B. pasteurii*, *B. sphaericus*, and algal, *Dunaliella salina*. Authors further claimed that the significant enhancement of the compressive strength resulted from $CaCO_3$ precipitation upon introducing the algal species. Joshi et al. (2021) reported ponding and spray treatment to be best for bio consolidation of the biogrout prepared by incorporating 40% FA replacement mixed with *Bacillus* culture in the cement grout. Heveran et al. (2020) used *Synechococcus* sp. PCC 7002 to develop living building material (LBM), which has adequate fracture toughness due to $CaCO_3$ precipitation. Another researcher Srinivas et al. (2021) reported efficient crack healing efficiency by two microalgae species, *Synechococcus elongatus* and *Spirulina platensis*.

4.16.3.2 Flexural strength

As shown in Fig. 4.75b, the regain in the flexural strength was observed at 28-day of curing after the specimens were repaired using plain and biogrout. The maximum regain in the flexural strength was observed in BPT (Biogrout treated) specimens, followed by BST, CPT, and CST specimens. The test results of the biogrout and plain grout-treated specimens were compared to the REF (uncracked) and UTC (unrepaired or untreated crack) specimens for better clarification of strength regain. It was observed that the flexural strength for REF and UTC specimens was 4.54 MPa and 3.22 MPa, respectively. The flexural strength recorded after 28-day of curing in BPT, BST, CPT and CST specimens were 4.50 Mpa, 4.11 Mpa, 3.92 Mpa and 3.65 Mpa, respectively. The recovery of strength was evaluated in relation to UTC. The biogrout treated specimens (BPT and BST) showed 28.4% and 27.6% recovery in flexural strength of the concrete specimens. In case of the control specimens; CPT and CST showed only 21.7% and 13.35% recovery of flexural strength. It was observed that BPT and BST specimens outperformed the CPT and CST specimens in strength improvement. It can be due the precipitation of $CaCO_3$ by *S. pevalekii* cells in the presence of sodium bicarbonate and calcium chloride in the biogrout treated specimens, which had further strengthened the grout filling in the crack. It was confirmed using the statistical analysis that BPT, BST, CPT, and CST specimens showed significant recovery in the flexural strength compared to the UTC at a

5% level of significance. Similar results were also corroborated by Xu et al. (2020), Xue et al. (2020) and Kanwal et al. (2022) in self-healing concrete specimens. Feng et al. (2021) also reported 14% recovery in flexural strength in 0.3 mm crack healed specimens at 28 days of curing.

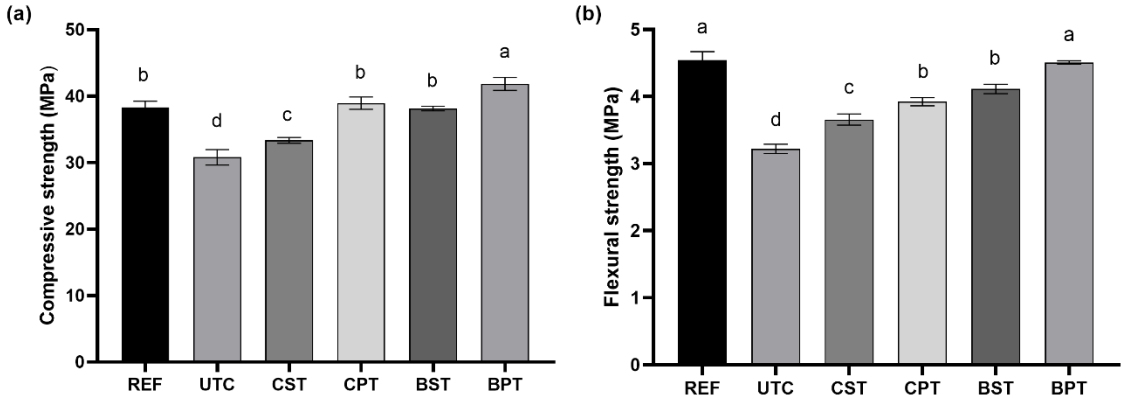


Fig. 4.75 (a) Compressive strength and (b) flexural strength of REF: reference concrete specimen; UTC: untreated concrete; CST: plain (control) grout spray treatment; CPT: Plain (control) grout ponding treatment, BST: biogrout with spray treatment; BPT: biogrout with ponding treatment at 28 days of curing. Values bearing different letters within the treatment are significant at $p<0.05$. Error bars represent standard deviation (n=3)

4.16.3.3 Water tightness

Fig. 4.76 illustrates the effect of MICCP treatment on the collective amount of water absorbed per unit cross-sectional area of the UTC, BPT, BST, CST, CPT, and REF specimen. The BPT specimen showed lower water absorption attributable to calcification in the voids of the FA-incorporated cementitious biogrout. Followed by BPT, the BST specimens showed lower water absorption than REF, CPT, and CST. Compared to all the specimens, UTC showed the highest water absorption with a sorptivity coefficient '*k*' of 0.048. Without any grout healing, the surface area of the UTC specimen for water absorption was more, which enhanced the capillary rise through the specimen. Even though it is reasonable to predict that the presence of an artificial crack in UTC specimens increases the sample's water absorption, comparing the cracked and treated samples' findings to evaluate the performance of plain and biogrout in crack healing quantitatively becomes mandatory. The REF specimens, without any damage, showed lower water absorption than the CPT and CST specimens, possibly due to inefficient repair in

the water-treated specimens. However, the water absorption was comparatively higher in REF than the BPT and BST, clearly indicating the efficiency of bacterial treatment in sealing the cracks. The sorptivity coefficient '*k*' of CPT, CST, and REF was evaluated as 0.035, 0.037, and 0.031, respectively. Compared to this, the sorptivity coefficient of BPT and BST specimens was observed 0.009 and 0.025. Therefore, it can be inferred from the low *k* value that calcification in the cyanobacterial admixed cementitious grout effectively reduced the porosity. The water absorption was observed to be higher during the initial few minutes of six hours of study. It could be because concrete specimens become saturated at a later stage due to water absorption initially. The findings are in harmony with Zhang et al. (2021), who observed that bacterial treatment in the presence of calcium lactate and other nutrients could significantly improve water tightness in crack-healed specimens.

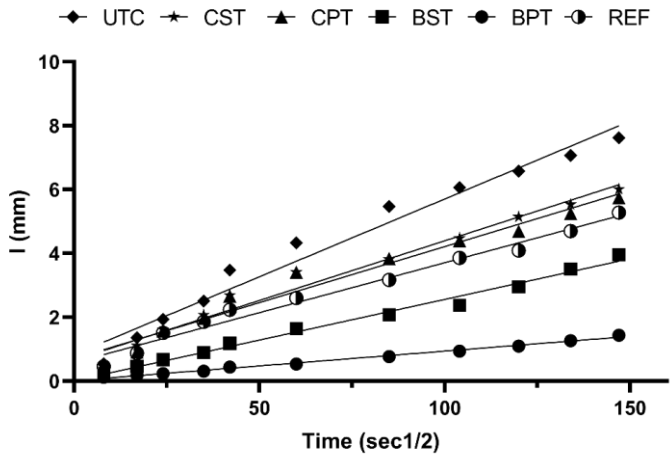


Fig. 4.76 Water sorptivity of concrete specimen after cracks repaired treatment with grouting. UTC: untreated concrete; CST: plain (control) grout spray treatment; CPT: Plain (control) grout ponding treatment, BST: biogrout with spray treatment; BPT: biogrout with ponding; REF: reference concrete specimen at 28 days of curing. All experiments were carried out in triplicate (n=3)

4.16.3.4 Sealing efficiency

The sealing efficiency of the crack-healed specimen was evaluated on the basis of water absorption before and after the 6 hours of the grouting. As shown in Fig. 4.77, the sealing efficiency of crack healed specimens was observed to be 82.23%, 51.53%, 29.60%, and 25.74% in BPT, BST, CPT, and CST specimens, respectively. The REF (uncracked specimen) showed efficiency of 35.18% on the basis of water absorption. The BPT and BST specimens were able to regain and further improve the sealing efficiecny due to $CaCO_3$ precipitation by

cyanobacterial cells. The voids between the FA and cement are filled in by the $CaCO_3$ particles, which densify by the healed region. Therefore, leading to low water absorption by BPT and BST specimens. Thus, it has more sealing efficiency than the CPT, CST, and REF specimens. It was confirmed using the statistical analysis that BPT specimens significantly improved the sealing efficiency compared to the REF, CPT, CST specimens. Similar results were corroborated by Liu et al. (2020) and Wang et al. (2018a) in concrete specimens.

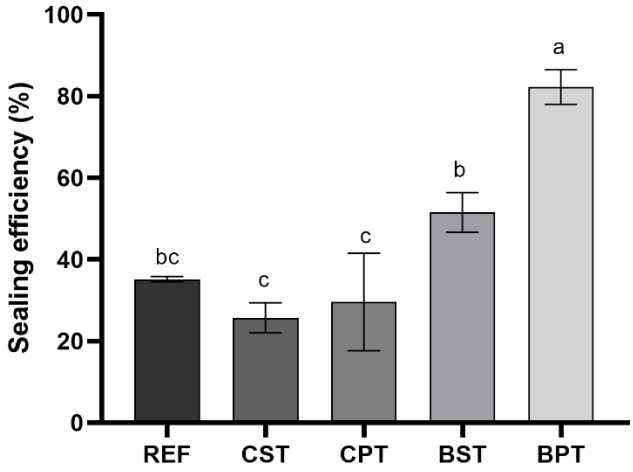


Fig. 4.77 Sealing efficiency of the concrete specimen after cracks repaired treatment with grouting. REF: without crack concrete; CST: plain (control) grout spray treatment; CPT: Plain (control) grout ponding treatment, BST: biogrout with spray treatment; BPT: biogrout with ponding treatment at 28 days of curing. Values bearing different letters within the treatment at each time interval are significant at $p<0.05$. Error bars represent standard deviation (n=3)

4.16.3.5 Microstructural analysis

Biogrout proved to be an effective crack healing remediation due to the bio-deposition of $CaCO_3$. Ponding and spray treatment by *S. pevalekii* cell culture resulted in the precipitation of calcite crystals in the pores of the specimens. It was verified using FESEM-EDS and mapping analysis. Fig. 4.78 confirms the $CaCO_3$ crystal deposition on the upper surface collected 2-10 mm deep from the BPT, BST, CPT, and CST specimens. In FESEM imaging of the BPT specimen, the cluster of stable rhombohedral calcites and the spherical-shaped vaterite crystals were observed. Calcite crystals were estimated to be 3 µm, whereas vaterite crystals was observed to be 3 to 4 µm in size. In BST, the microstructural analysis showed the formation of calcite crystals all over the surface. The spray treatment was equally effective in the precipitation of $CaCO_3$. The size of the calcite crystal formed in BST was in the range of 4 to

4.5 µm. However, no $CaCO_3$ deposition was observed in control samples (Fig. 4.79). The formation of $CaCO_3$ in biogrout specimens was validated using EDS. The bond of Ca, C, and O form the $CaCO_3$. High peaks of calcium, carbon, and oxygen with 38.69, 7.27, 53.61% and 61.01, 2.57, and 36% were observed in BST and BPT specimens, respectively (Fig. 4.80). The $CaCO_3$ precipitation was further verified using a mapping technique for a particular area, as shown in Fig. 4.80. The results were in accordance with the observation of other researchers (Tripathi et al. 2019; Anand et al. 2022b). Previous studies have documented the coexistence of bacterial cells along with $CaCO_3$ crystals with variable shape and structure (Xiao et al. 2010).

4.16.3.6 X-ray powder diffraction (XRD)

X-ray powder diffraction (XRD) results confirmed the presence of calcite crystals at 29.2° with higher intensity in biogrout than in the plain grout specimens (Fig. 4.81). The other peaks of quartz (Q), calcium hydroxide (CH), and calcium silicate hydrates (C-S-H) were also observed in both specimens, which is a widespread occurrence in concrete specimens due to the presence of cement and sand. The visualization of calcite peaks over the surface of the biogrout specimens through microstructural examination validates the fact that MICCP by photoautotrophic cyanobacteria strain plays a significant role in the healing of the cracks by naturally precipitating $CaCO_3$ on the surface and pores of the cementitious biogrout. The CSH gel formed in the specimen results from hydration in the cementitious biogrout. Similar results were reported by Anand et al. (2022c) in crack remediation.

4.16.3.7 Thermogravimetric analysis

To validate the $CaCO_3$ precipitation as a healing agent in crack remediation, TGA was performed after 28 days of curing. Along with $CaCO_3$, concrete specimens also revealed weight loss of calcium hydroxide, instigated during the curing process due to the hydration of cementitious material. Fig.4.82a shows the TGA thermograms for biogrout and plain grout specimens. The significant mass loss of 3.74% of $CaCO_3$ at 600-800 °C, two times more than the plain grout, was noted in the biogrout specimens (Fig. 4.82b). Jadhav et al. (2018) corroborated similar results, reporting a 50 -100 °C peak of evaporation of water and a 560 - 700 °C a peak of $CaCO_3$. Another researcher, Sarkar et al. (2022), demonstrated a 1.8-fold increase in calcite precipitation in cracks remediated using alkali-activated fly ash composites in the presence of bacteria.

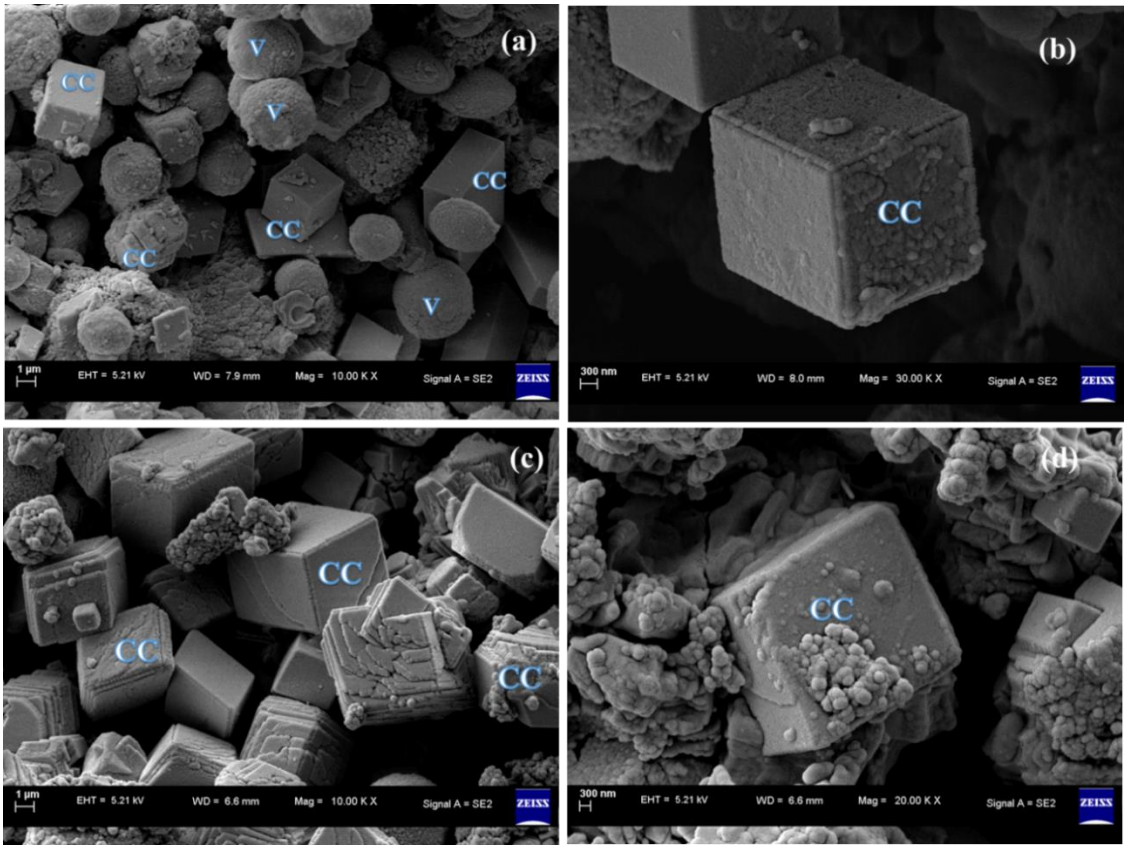


Fig. 4.78 FESEM imaging represents cubic shaped calcite and spherical shaped vaterite (V) $CaCO_3$ (CC) crystals formed in (a, b) biogrout ponding treatment: BPT, (c, d); biogrout spray treatment: BST specimens

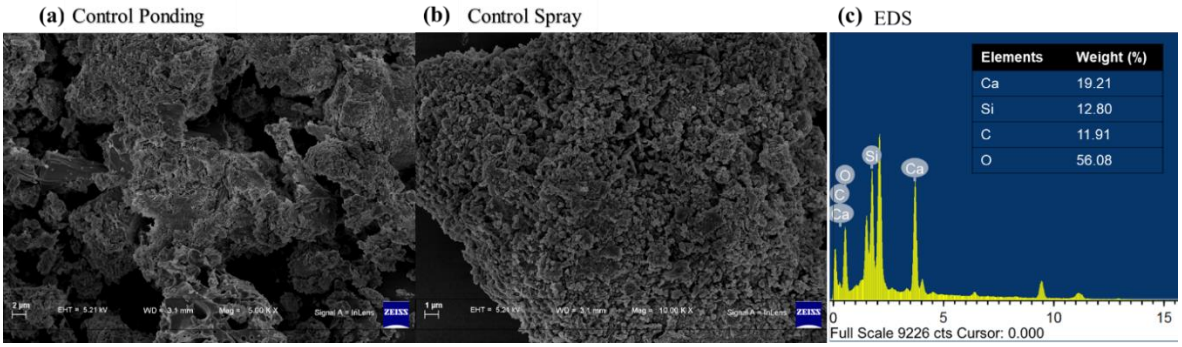


Fig. 4.79 FESEM imaging of (a) Plain ponding grout treatment: CPT, (b) plain spray grout treatment: CST and (c) EDS of control plain grout

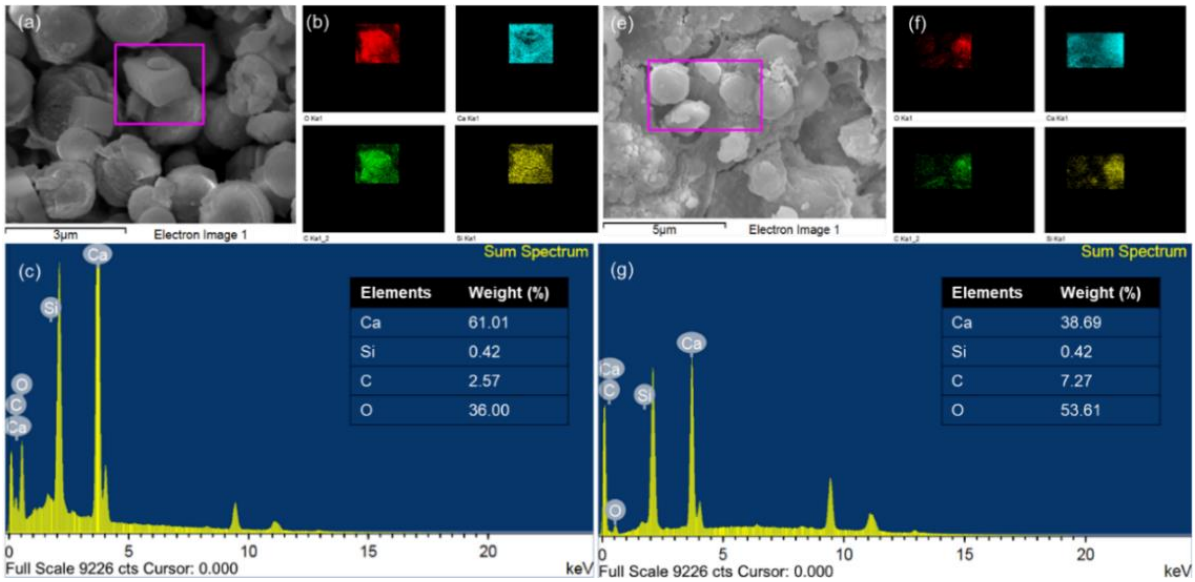


Fig. 4.80 EDS imaging and mapping of (a, b, c) biogrout ponding treatment: BPT, (e, f, g); biogrout spray treatment: BST

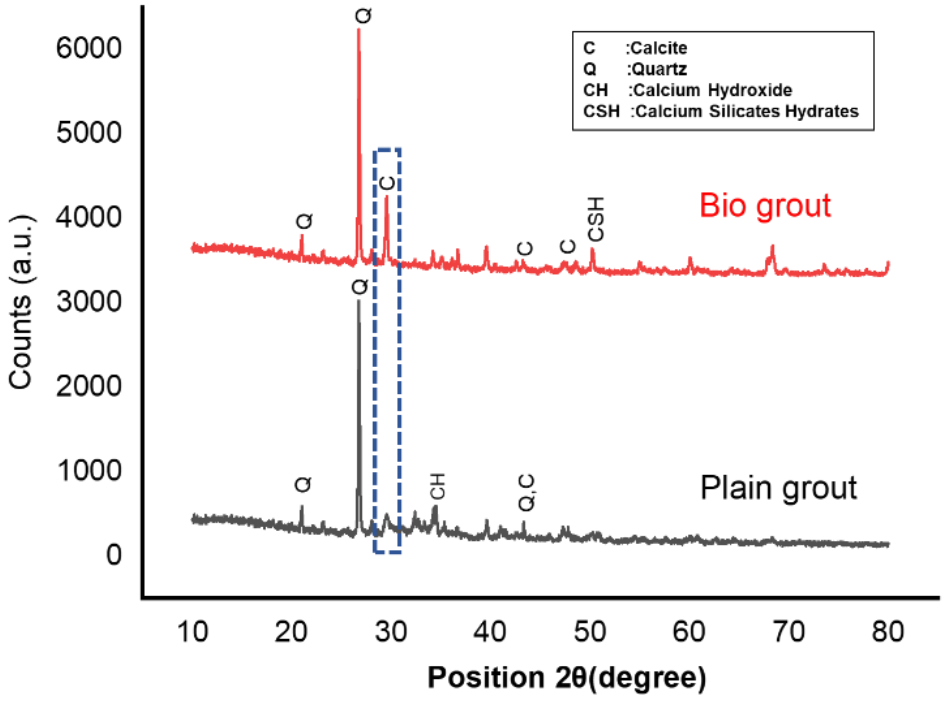


Fig. 4.81 XRD plot of plain and biogrout samples at 28 days of curing

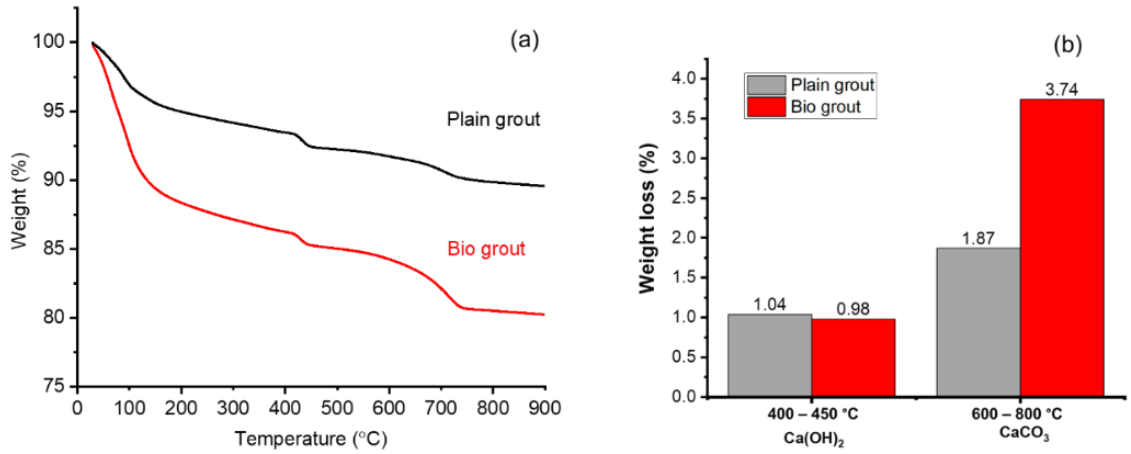


Fig. 4.82 (a) Thermogravimetric analysis (TGA) and (b) weight loss (%) of the plain and biogrout samples at 28 days of curing

4.17 Conclusions

A photoautotrophic *S. pevalekii* is a $CaCO_3$-inducing cyanobacterium that has proved to be an efficient agent for sand consolidation and improving cementitious properties. Cyanobacteria do not release any harmful pollutants into the environment. The cyanobacteria also had a synergistic effect with cement and fly ash. The biogrout was developed by partially replacing cement with fly ash amalgamated with *S. pevalekii* cells, which successfully repaired the cracks with different (horizontal and vertical) orientations. FESEM-EDS, XRD, and TGA verified the $CaCO_3$ precipitation in the mortar and crack-repaired specimens.

4(C) Comparison of strength and permeability properties of concrete by photoautotrophic and heterotrophic bacteria

4.18 Microbial density and $CaCO_3$ precipitation

As shown in Fig. 4.83, microbial growth and the amount of $CaCO_3$ precipitated by *S. pevalekii* and *B. paramycoides* were measured after 24, 48, 72, 96, and 120 hours of incubation. At the end of the experiment, *S. pevalekii* and *B. paramycoides* precipitated 695.7 and 860 mg/100 ml of $CaCO_3$. The $CaCO_3$ precipitation by *B. paramycoides* was 19.1% more than that of *S. pevalekii*. The incubation time was found to have a significant effect on the $CaCO_3$ precipitation. The cell density was evaluated in the NB and BG11 broth in correspondence to the $CaCO_3$ precipitation. The cell density of *S. pevalekii* cells showed an increasing trend during incubation (Fig. 4.83a), whereas *B. paramycoides* cell culture showed a declining trend after 48 hours of incubation (Fig. 4.83b). It might be due to exhaustion of the nutrients in the NB. The photoautotrophic bacteria can survive at low nutrient requirements and have a more extended log phase than the heterotrophic bacteria. The cell density was evaluated by measuring cell numbers and expressing them in log cfu/ml. Initially, 1 $\times 10^6$ cells were inoculated in the medium corresponding to log 6.0 CFU/ml. The *B. paramycoides* increased to 8.5 log CFU/ml after 48 hours of incubation. Then, the biomass of *B. paramycoides* decreased to 7.2 log CFU/mL after 120 hours. Similarly, *S. pevalekii* cells increased to 7.9 log CFU/mL after 120 hours.

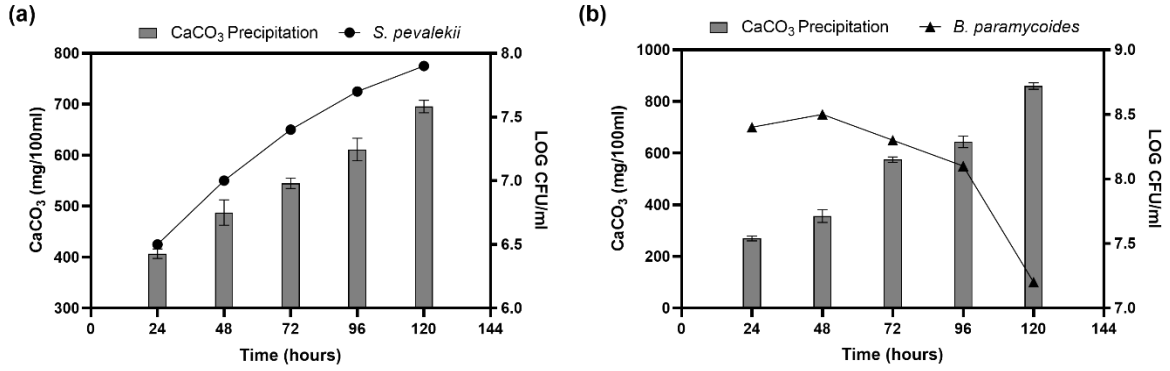


Fig. 4.83 Cell density of microbes and $CaCO_3$ precipitation by (a) *S. pevalekii* and (b) *B. paramycoides* cells during 120 hours of incubation

At the same time, the amount of dissolved calcium in the filtrate was analyzed with increased incubation time using atomic adsorption spectroscopy. The dissolved calcium in the culture

broth decreased with increased incubation time. The amount of dissolved Ca^{2+} ions in NB inoculated with *B. paramycoides* after 24 and 120 hours was 16.9 mM and 1.3 mM, respectively. Meanwhile, the amount of dissolved Ca^{2+} in BG11 broth inoculated with *S. pevalekii* was 20.5 mM and 7.8 mM after 120 hours of incubation (Fig. 4.84). The photoautotrophic cyanobacteria and heterotrophic bacteria efficiently induced the $CaCO_3$ precipitation in solution. The *B. paramycoides* is a ureolytic strain and significantly precipitated more $CaCO_3$ than the *S. pevalekii*. Many external environmental factors can influence $CaCO_3$ precipitation. The $CaCO_3$ precipitation by the *S. pevalekii* strain is due to a phototrophic reaction in comparison to *B. paramycoides*, which is due to urea hydrolysis (Obst et al. 2009; Jansson and Northen 2010; Zhu and Dittrich 2016). The ureolytic reaction is a direct pathway for $CaCO_3$ formation (Wen et al. 2020). At the same time, the photosynthetic response by cyanobacteria can indirectly influence $CaCO_3$ precipitation through EPS production, which serves as a suitable nucleation site for mineralization (Veaudor et al. 2020). Ureolytic reactions occur in the presence of the urease enzyme released during the metabolic activity of the bacteria. Ureolytic bacteria use urea as a nitrogen source, and their enzymatic activity leads to the formation of ammonia and carbonate ions (Dhami et al. 2013b). The binding of calcium ions (Ca^{2+}) with carbonates increases with increasing incubation time until equilibrium was reached. The maximum $CaCO_3$ precipitation by bacterial biomass in the NB supplemented with urea and $CaCl_2$ was observed till 120 hours of incubation. After equilibrium was attained, no $CaCO_3$ precipitation was observed, possibly due to nutrient unavailability. However, cyanobacterial cells can survive longer than heterotrophic bacteria (Yu et al. 2020b). The statistical analysis proved that incubation time significantly affects ($p < 0.05$) the $CaCO_3$ precipitation by *S. pevalekii* and *B. paramycoides* strains. Similar results were also reported in previous studies by various researchers (Helmi et al. 2016; Imran et al. 2019; Li et al. 2021; Leeprasert et al. 2022). Researchers have also reported $CaCO_3$ precipitation induced by *Synechococcus* (Liang et al. 2013), and *Synechocystis* (Han et al. 2013; Han et al. 2017a) in solution at lab scale study.

4.18.1 FESEM analysis

Fig, 4.85 shows FESEM imaging of the $CaCO_3$ crystal in powdered precipitates collected in the filtrate after the $CaCO_3$ experiment. The crystallization was observed to be rhombohedral calcite as formed in both the solutions by *S. pevalekii* and *B. paramycoides*. The crystals formed

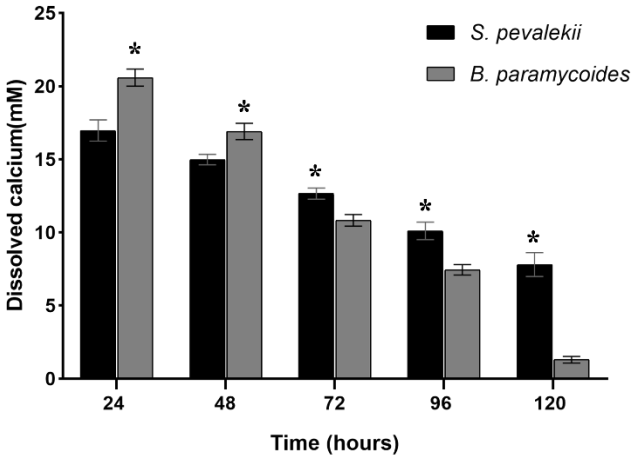


Fig. 4.84 Dissolved calcium (Ca^{2+}) ions in the BG11 and NB broth during $CaCO_3$ precipitation experiment. The asterisk (*) sign indicates values are significant at $p<0.05$ using t-test. Values are mean ± SD (n=3)

in size ranging from 500 nm to 5 µm aggregated to form different structural layer as seen by both the strains. The observation was taken after 120 hours of incubation at respective temperature conditions. The $CaCO_3$ crystallization confirmed the biomineralization efficiency of *S. pevalekii* and *B. paramycoides* microbial strain in controlled laboratory conditions. The formation of biofilm was observed in *S. pevalekii* precipitates. Cyanobacteria have a layer of extracellular polymeric substances (EPS), which can form biofilms. It has been observed that some of the rhombohedral and spherical deposits were closely associated with each other, creating a stacked layer of crystallization, while the remaining ones were randomly distributed throughout the biofilm. Similar findings were also reported by Zhu et al. (2017).

4.18.2 Effect of initial pH on the growth of cyanobacterial and bacterial cells

Fig. 4.86 shows the growth pattern of photoautotrophic and heterotrophic bacteria at different pH (6 - 12) conditions. The most favorable pH range for heterotrophic bacterial growth, as observed, is between 7 and 10, with maximum growth. Meanwhile, the optimum range for photoautotrophic bacteria was between the pH range of 7 and 9. During the heterotrophic growth cycle, the initial concentration of cells during the log phase was approximately 10^1 cells/ml, which increased gradually to ~10^3 cells/ml during the initial log phase after 6 hours of incubation at 37 °C in nutrient broth media. Meanwhile, the lag phase at pH 11-12 is continuous for 6 – 8 hours and then enters the log phase until 18 hours of incubation. On the contrary, the lag phase of *S. pevalekii* cells lasts for 48, which gradually enters the exponential

phase and lasts for 216 hours of the culture period. After that point, the growth of *S. pevalekii* gradually entered the initial stationary phase. Photoautotrophic bacteria have longer shelf life than the heterotrophic bacteria. The lag phase of the photoautotrophic bacteria last longer than the heterotrophic bacteria. Moreover, photoautotrophic bacteria require less nutrients for their growth (Kamennaya et al. 2012). Similar results were also reported by various researchers (Wu et al. 2019; Feng et al. 2021c; Qian et al. 2021).

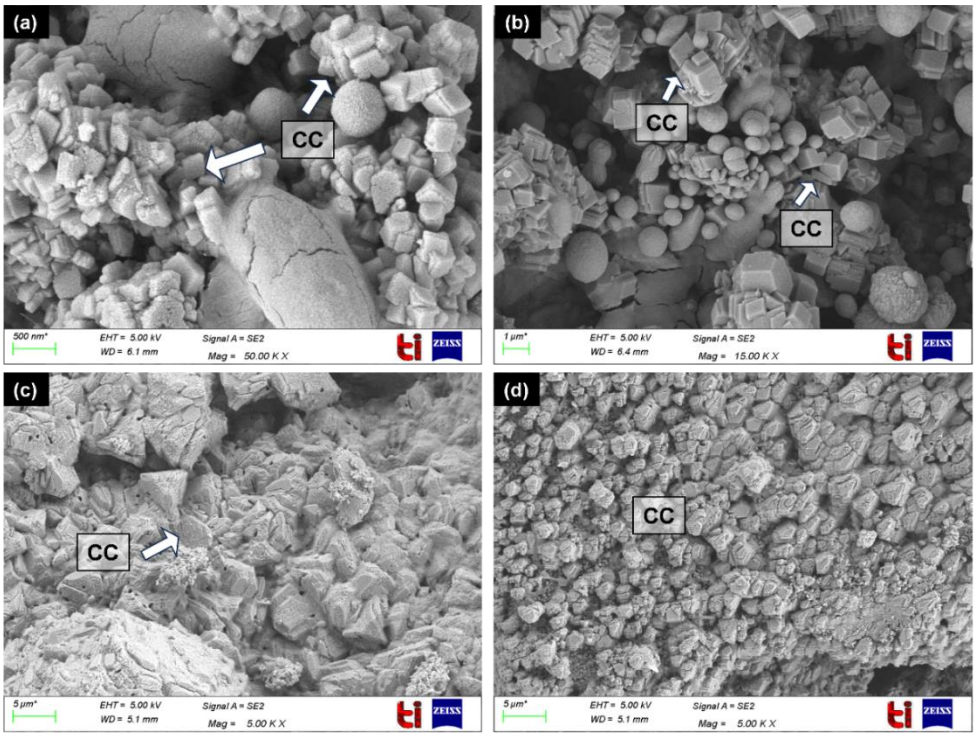


Fig. 4.85 FESEM analysis of $CaCO_3$ (CC) crystals formed by (a, b) *S. pevalekii* and (c, d) *B. paramycoides* after 120 hours

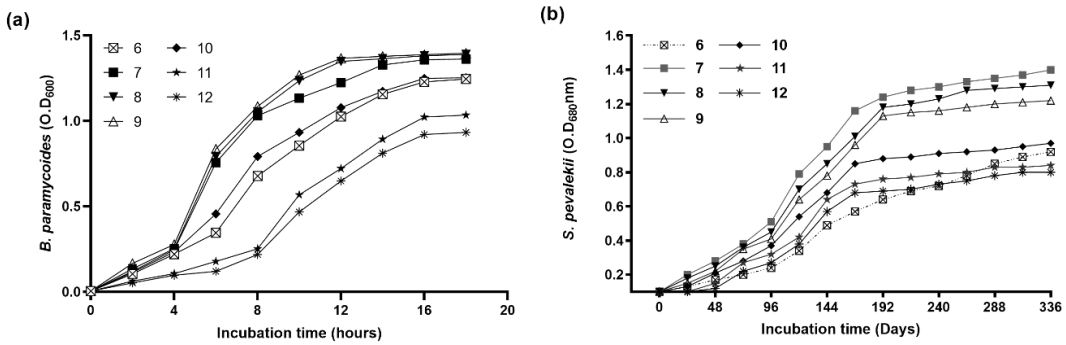


Fig. 4.86 Effect of initial pH (6 – 12) on growth of *B. paramycoides* and *S. pevalekii* cell culture at different time interval

4.18.3 Effect of initial pH on $CaCO_3$ precipitation

The pH affects the growth and $CaCO_3$ precipitation. As shown in Fig. 4.87, the maximum $CaCO_3$ precipitation was observed in nutrient broth inoculated with *B. paramycoides* at pH 9. At pH 9, *S. pevalekii* and *B. paramycoides* cells precipitated 858.3 mg/100 ml and 1025.3 mg/100 ml of $CaCO_3$ after 120 hours, respectively. The $CaCO_3$ precipitation by *S. pevalekii* at pH 10, 11, and 12 was 799.6, 668.3 and 594. 3 mg/100 ml, respectively. Similarly, $CaCO_3$ precipitation by *B. paramycoides* at pH 10, 11, and 12 was 975.6, 952.6, and 897.6 mg/100 ml, respectively. The pH of the medium affects the cell membrane permeability and growth of the bacterial cells, thus affecting the $CaCO_3$ precipitation (Yi et al. 2021). The increase in pH of the medium showed an increase in the $CaCO_3$ precipitation but decreased after the pH rose to 10, 11, and 12. The $CaCO_3$ precipitated at high pH illustrates the efficiency of ureolytic and photoautotrophic bacterial activity in cementitious environments. Similar results were reported by other researchers (Korchef and Touaibi 2020; Baffoe and Ghahremaninezhad 2022; Lv et al. 2022). Xu et al. (2018) documented optimum pH for ureolytic activity is 7 to 9.5. Hu et al. (2015) corroborated the formation of different polymorphs of $CaCO_3$ precipitates with the variation in pH. The precipitation of elements such as magnesium, calcium, and iron in an alkaline environment (pH > 10.4) is likely to occur with the growth of cyanobacteria (Vandamme et al. 2012; Paquette et al. 2022).

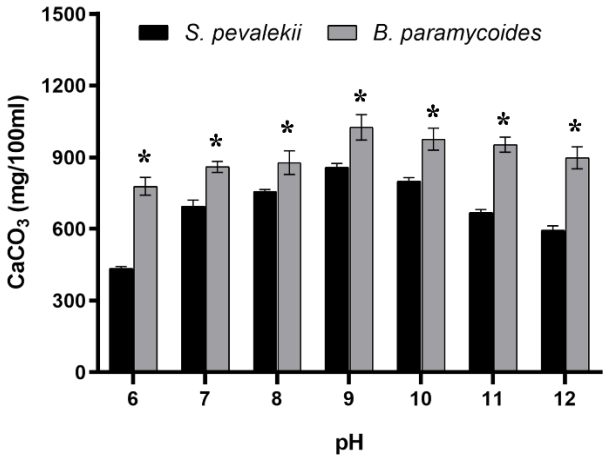


Fig. 4.87 $CaCO_3$ precipitation by *S. pevalekii* and *B. paramycoides* at varied initial pH of BG11 and nutrient broth after 120 hours. The asterisk (*) sign indicates values are significant at $p<0.05$ using a t-test. Values are mean ± SD (n=3)

4.19 Strength and permeability properties

4.19.1 Compressive strength

The strength properties of concrete specimens were tested at 3, 7, and 28 days of curing. Fig. 4.88a shows a significant improvement in compressive strength was observed in *S. pevalekii* (SPC) and *B. paramycoides* (BPC) compared to the control. After 28 days of curing, the compressive strength of SPC and BPC specimens was 43.7 MPa and 44.5 MPa, respectively. At the same time, the control specimens showed 34.5 MPa of compressive strength. The strength of the concrete was significantly higher in samples treated by heterotrophic bacteria. The percentage increase (Δ%) in strength was evaluated compared to the control specimens by both bacteria. The SPC specimens showed a 26.6% improvement in compressive strength compared to the BPC specimens, which showed a 28.9% improvement in the strength properties of concrete (Fig. 4.88b). Comparing both bacteria, *B. paramycoides* cured specimens showed 14.97% more compressive strength than *S. pevalekii* cured specimens after seven days. However, upon further increasing the curing age, i.e., 28 days, the compressive strength of the *S. pevalekii* specimens improved, and the difference in the strength of the BPC and SPC specimens was only 1.8%. In cyanobacteria, the thickening property of the exopolymeric substance (EPS) surrounding the cell increases the bonding mechanism using the adhesion property (Srinivas et al. 2021). With the increase in the curing period, the adhesion property helps the cyanobacterial cells to bind with the cement particles and aggregates. EPS are mainly polysaccharidic in nature. The adhesion of cells to the rigid substrate depends on several parameters, including substrate composition, pH, organic film, cell density, and surface roughness (Costa et al. 2018). Microorganisms adhere to substrates either by generic physico-chemical forces, such as van der Waals and electrostatic forces, or by the specific surface structures of the cell, such as pili, fimbriae, or other appendages (Loosdrecht et al. 1989). The EPS promotes the cyanobacterial cells adhesion to the rough surface and subsequently form $CaCO_3$ above them by attracting the positively charged Ca^{2+} using the negatively charged functional groups such as carboxylate, amine, phosphoryl/phosphodiester, and hydroxyl present on the cell surface (Zhu and Dittrich 2016). Consequently, the $CaCO_3$ particles formed by cyanobacteria act as fillers that plug the interconnected pores in the concrete matrix, reducing the air gap. During ureolytic reaction by heterotrophic bacteria, the urease enzyme acts as a catalyst and initiates the $CaCO_3$ precipitation as bacterial growth enters the log phase. If urea and calcium sources are available, the biomass of bacteria produces the carbonate precipitation that fills up the pores in the concrete (Skevi et al. 2021). The analysis of variance

inferred that incorporating different bacterial treatments and curing periods (3, 7, and 28 days) significantly affected the strength properties of concrete (Table. 4.15). Other researchers reported similar findings upon adding heterotrophic bacteria in cementitious specimens (Skevi et al. 2021; Karthick et al. 2022). In another research carried out by Hernández et al. (2016) and Zhu et al. (2017), the compressive strength of the concrete and mortar specimens was significantly improved by cactus mucilage, marine brown and *Gloeocapsa* PCC73106, algae, respectively

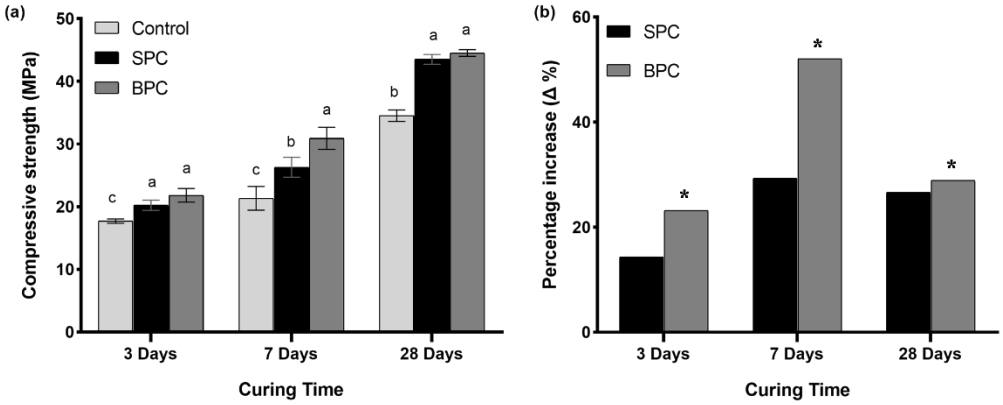


Fig. 4.88 (a) Compressive strength (b) percentage change in compressive strength of concrete specimens at 3, 7, 28 days of curing. Values bearing different letters within the treatment at each time interval are significant at $p<0.05$. The asterisk (*) sign indicates values are significant at $p<0.05$ using a t-test. Error bars represent standard deviation (n=3)

Table 4.15 The ANOVA results indicate the effects of different treatments (*S. pevalekii*, *B. paramycoides*, and control) and time of curing for concrete specimens

Variables	Degree of freedom	Treatment	Time	Interaction (Treatment × Time)
Compressive strength	df	2,18 P < 0.0001	2,18 P < 0.0001	4,18 P = 0.0004
RCPT	df	2,12 P < 0.0001	1,12 P < 0.0001	2,12 P= 0.0016

4.19.2 Relative strength index

The relative strength index (RSI) of different microbial treatment and curing periods was evaluated to validate the SPC and BPC specimen's strength index compared to the control. As shown in Fig. 4.89, the RSI of the SPC specimen increased with an increase in the curing

period. Initially, at 3 days the RSI of the SPC specimen was 1.14 at 3 days which increased to 1.23 and 1.26 at 7 and 28 days of curing period. However, RSI of BPC specimens was 1.23 initially which increased to 1.45 at the 7 days and further decreased to 1.28 at 28 days of curing age. There was significant difference in RSI of SPC and BPC specimen at 7 days which clearly indicates a lesser amount of $CaCO_3$ precipitation in the SPC specimen at 7 days. This could be explained by the fact that ureolytic activity of the heterotrophic bacteria is fast as compared to light dependent pathway of photoautotrophic bacteria. The cells biomass increases with increase in incubation period in curing period of photoautotrophic bacteria which tremendously improves the strength properties of concrete at 28 days. Similar findings were reported by other researchers (Fan et al. 2010; Ghahremani et al. 2023).

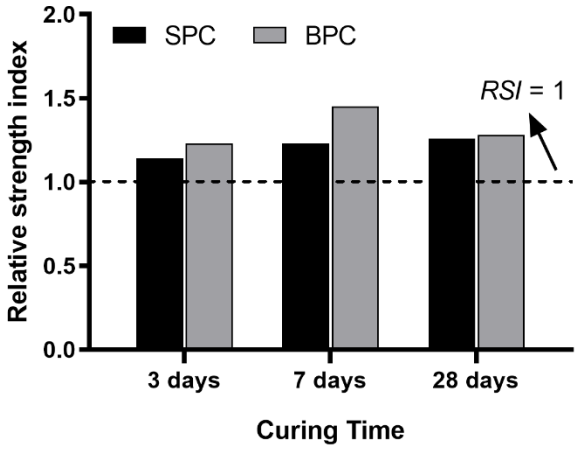


Fig. 4.89 Relative strength index of SPC and BPC specimens at 3, 7 and 28 days of curing

4.19.3 Rapid chloride penetration test (RCPT)

The RCPT of the concrete specimen was tested at 7 and 28 days of curing. The chloride penetration in the concrete samples decreased with an increased curing period. A significant decrease was observed in concrete specimens treated by *S. pevalekii* and *B. paramycoides* bacterial culture. Compared to the control, the BPC specimens treated by heterotrophic bacteria *B. paramycoides* showed minimum penetration among all the groups. Fig. 4.90a represents the current passed through SPC and BPC specimens during the RCPT experiment, which was 1901 and 1440 coulombs (C). As shown in Fig. 4.90b, the test results for BPC specimens showed 27.2% and 57.8% reduction after 7 and 28 days of curing by decreasing chloride ingression during the RCPT experiment, respectively. On the contrary, SPC specimens showed 20.6% and 44.3% reductions in chloride penetration. As per the ASTM C1202 (2012), the

penetrability of chloride ions after 28 days of curing was moderate based on the charge passed through the specimens. This might be due to $CaCO_3$ particles that seal the pores in concrete, making it difficult for water and other particles to infiltrate through concrete pores. However, the charge passed through the control specimen was higher than SPC and BPC specimens. The efficiency of the BPC specimen was initially observed to be equivalent to SPC specimens after seven days of curing. However, upon further increasing the curing period, the chloride ingression was significantly reduced by BPC specimens followed by SPC specimens. The statistical analysis showed that different curing treatments (*S. pevalekii*, *B. paramycoides,* and control) and curing time (7 and 28 days) have a significant effect on the chloride penetration in the cylindrical specimen (Table 4.15). Similar findings were reported by other researchers (Nosouhian et al. 2016; Sadrmomtazi et al. 2018; Wu et al. 2019; Soda and Mini 2022).

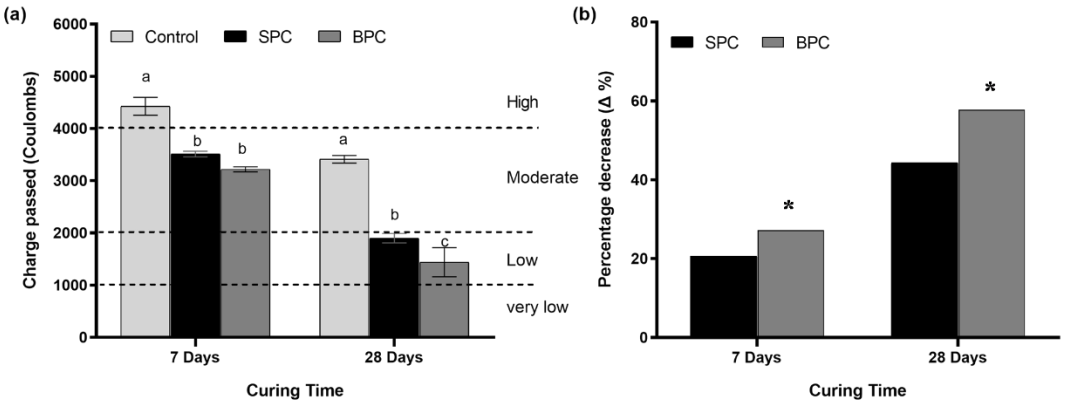


Fig. 4.90 (a) Rapid chloride permeability test (RCPT) (b) percentage change in RCPT at 7, 28 days of curing. Values bearing different letters within the treatment at each time interval are significant at $p<0.05$. The asterisk (*) sign indicates values are significant at $p<0.05$ using t-test. Error bars represent standard deviation (n=3)

4.19.4 Sorptivity test

The water absorption test was carried out at 7 and 28 days of curing. The results were analysed during the rapid absorption phase for initial 6 hours. The results are illustrated in Fig. 4.91a and 4.91b as the average water absorption by 100 mm × 50 mm cylindrical specimens against square root mean of time. The seven days cured SPC and BPC specimens showed cumulative water absorption of 1.3 and 1.2 mm of water after 6 hours of the experiment, respectively (Fig. 4.91a). Compared to which control specimen showed water absorption of 2 mm. It clearly indicates that bacterial treatment significantly affects the water absorption rate compared to the

control. After seven days, the sorptivity coefficient '*k*' of BPC, SPC, and control specimens was observed to be 0.007, 0.008, and 0.011, respectively. After 28 days of curing, the control specimens showed higher water absorption of 1.7 mm, which might be due to the rise of water through capillary pores. However, bacterial curing showed a significant reduction in BPC and SPC specimens. BPC specimens showed 0.94 mm of average water absorption whereas SPC showed 1.2 mm of water absorption at the end of experiment. It might be due to the activity of bacteria that precipitates the $CaCO_3$ particles in the pores of the concrete. As a result, the interconnected capillary pores were blocked, reducing the water's capillary rise in concrete. The sorptivity coefficient '*k*' evaluated for the BPC, SPC, and control specimens was 0.005, 0.007, and 0.01, respectively (Table 4.16). The lower sorptivity coefficient '*k*' for the BPC and SPC specimens proved that ureolytic action and photosynthetic reaction reduce the capillary pores of the specimens. Similar results were reported by Xu et al. (2018), Anand et al. (2022a), and Vaezi et al. (2020) in ureolytic bacteria-based concrete. Zhu et al. (2017) reported reduced water absorption using live and UV-killed cyanobacterial cells in mortar compared to the control specimen

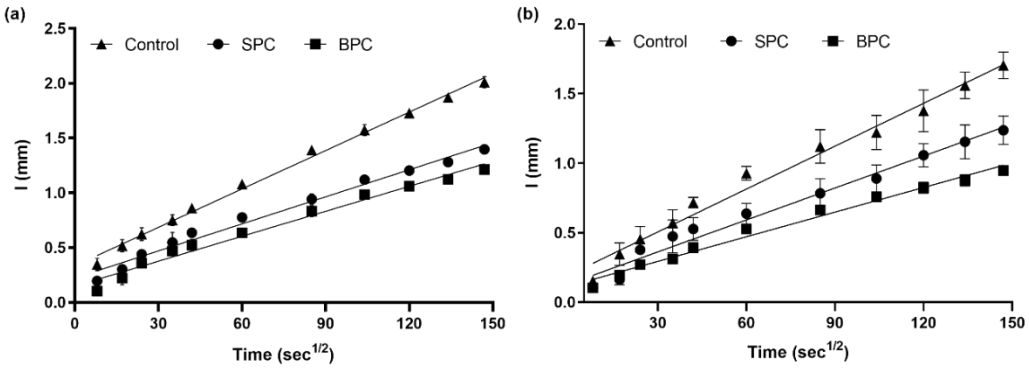


Fig. 4.91 Water absorption concrete specimens treated with *S. pevalekii* (SPC), *B. paramycoides* (BPC) along with the control at (a) 7 days (b) 28 days of curing

Table 4.16 The ANOVA results indicate the effects of different treatments (*S. pevalekii*, *B. paramycoides*, and control) and time of curing on sorptivity for concrete specimens

Variables	Sorptivity coefficient ('*k*')		R^2		P value	Significant
	7 days	28 days	7 days	28 days		
Control	0.01168	0.01207	0.9906	0.9592	P<0.0001	Yes
SPC	0.00823	0.007658	0.9766	0.9415	P<0.0001	Yes
BPC	0.00759	0.005902	0.9715	0.9792	P<0.0001	Yes

4.19.5 Microstructural analysis

Fig. 4.92 shows the structural analysis of $CaCO_3$ precipitation in the concrete sample. The crystals were overlapping, forming a dense layer of calcite in the concrete by *S. pevalekii* and *B. paramycoides*. Whereas, calcite formation was not seen in control (Fig. 4.92a). The crystals were tightly packed and formed perfect rhombohedral crystal lattice in a size range of 0.5 –1 μm in SPC specimens (Fig. 4.92b). Likewise, *B. paramycoides* treated specimens showed rhombohedral crystal formation ranging in size 5 – 10 μm (Fig. 4.92c). The crystals exhibit a variation in sizes of calcite precipitated, which can be attributed to the interaction between nucleation and growth. This interaction is influenced by effects of microbial concentration and cementation media. The small amount of vaterite crystals were also formed. Different theories have been proposed to explain coexistence of two different polymorphs 'calcite and vaterite' together. It is widely acknowledged that vaterite is a thermodynamically unstable crystal form and exhibits a higher nucleation rate compared to other forms of $CaCO_3$ (Weiner and Patricia M. Dove 2003; Xie et al. 2023). The slow diffusion of Ca^{2+} and CO_3^{2+} ions can result in the formation of calcite in the later stage (Xiao et al. 2010). Another possible reason could be involvement of different functional groups of the cell surface that provides nucleation site for biomineralization (Liang et al. 2013). Both crystals precipitates were $CaCO_3$, which was confirmed by EDX and XRD analysis. The mineral constituents characterized by EDX analysis indicates the amount of calcium, oxygen, and carbon formed in SPC and BPC specimens was high as compared to the control which could be due to $CaCO_3$ precipitation. The calcite precipitation by heterotrophic bacteria was also reported by Park et al. (2022b), Qian et al. (2022), and Qin et al. (2021). Similarly, Zhu et al. (2017) and Zhu et al. (2018) demonstrated calcite precipitation by cyanobacterial species Anand et al. (2022b) reported calcite crystallization by *Bacillus megaterium* SS3 in concrete. Previous studies have also demonstrated the presence of $CSH/Ca(OH)_2$ in the microstutucral analysis of concrete (Tahmouresi et al. 2021; Akhtar et al. 2022).

4.19.6 X-ray diffraction (XRD)

The X-ray diffraction analysis confirmed calcite precipitation in the hardened concrete cured using two microbial cultures (*S. pevalekii* and *B. paramycoides*) at 28 days. XRD spectrums of SPC, BPC, and control sample are presented in Fig. 4.93. The prominent peaks observed in the powdered concrete sample are quartz (Q), calcium silicate hydrate (CSH), calcite (C), and vaterite (V). The intensity peak of calcite observed at 29.2° was higher in SPC and BPC

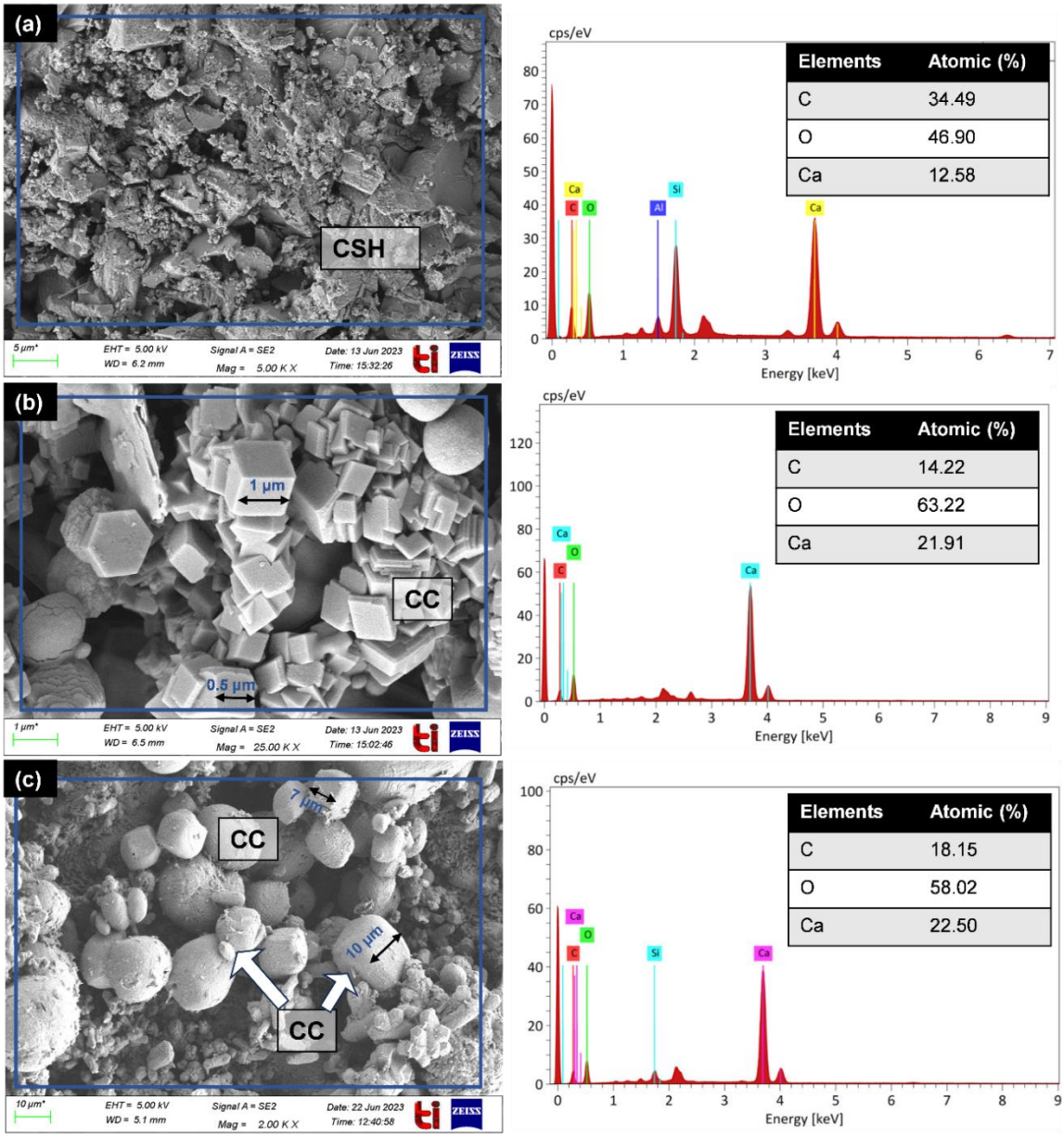


Fig. 4.92 FESEM-EDS of (a) control (b) SPC (c) BPC specimen showing $CaCO_3$ (CC) Crystallization . The square '□' sign indicates the spot for EDS analysis

specimens than in the control. Calcite, aragonite, and vaterite are the three primary polymorphs of $CaCO_3$ crystals, out of which calcite is the most stable form of crystalline (Weiner and Dove 2003; Xiao et al. 2010; Chandra et al. 2023). The microbial activity occurring in concreteresults in calcite crsytallization in the concrete matrix. The weak diffraction peak of vaterite was also seen in the SPC and BPC specimens which is a thermodynamically unstable crystal form with a high nucleation rate. The slow diffusion of carbonates (CO_3^{2-}) and calcium ions (Ca^{2+}) can lead to calcite formation (Weiner and Dove 2003). Both microbial cultures efficiently induced the calcite precipitation in the concrete. It is unclear why different polymorphs of $CaCO_3$ are

formed during microbial biomineralization in concrete. Stuckrath et al. inferred the presence of functional groups, such as sulfhydryl (-SH), amino ($-NH_2$), carboxyl (-COOH), and hydroxyl (-OH) groups, that serve as nucleation sites for binding with Ca^{2+} ions can control the crystal deposition (Stuckrath et al. 2014). Other factors affecting $CaCO_3$ precipitation are calcium ion concentration, dissolved inorganic carbon (DIC) concentration, pH, and the availability of nucleation sites (Tripathi et al. 2019).

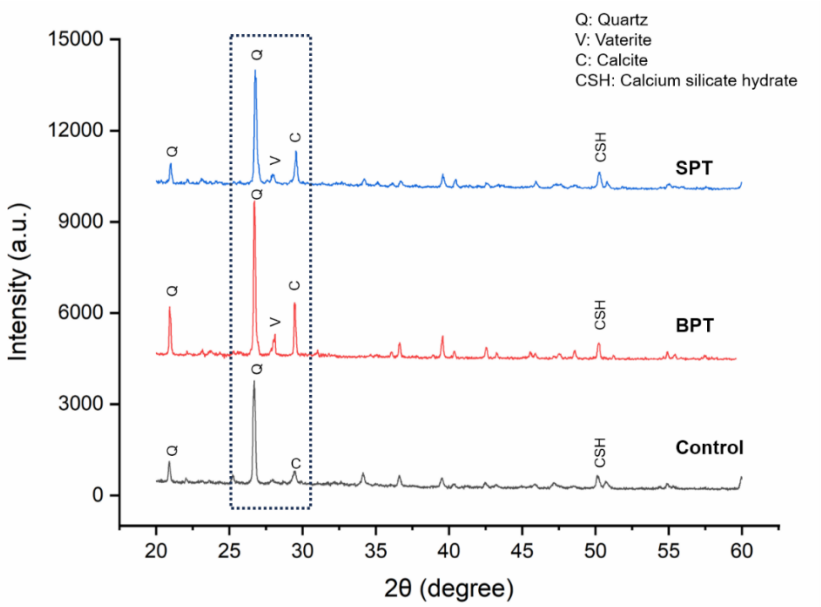


Fig. 4.93 XRD of control, SPC, and BPC concrete specimen

4.19.7 Cost analysis

The cost of the two different MICCP mechanisms consists of the price of the bacterial growth media. Conventional concrete costs approximately Rs.5623/m^3 (68.36 USD/m^3) (Sharma et al. 2023). The MICCP product's theoretical cost depends on the microorganism's price and the nutrients growth media used. The total cost estimated for nutrient broth for heterotrophic bacteria is around Rs 30.93/L (0.37 USD/L). The cyanobacterial nutrient media (BG11 broth, $NaHCO_3$, and $CaCl_2$) cost around Rs 16.21/L (0.19 USD/L). This cost is very near to the bacteria estimated by other studies (Lee and Park 2018; Ribeiro et al. 2020; Verma et al. 2022). The cost analysis demonstrated that the price of microbial concrete incorporating heterotrophic and photoautotrophic is 2.0 and 1.5 times higher than conventional concrete, respectively. Adding photoautotrophic bacteria and BG11 nutrient media reduces the cost by 23.6%. The potential for further cost reduction in the production of bacterial concrete can be done using inexpensive nutrient ingredients, such as corn steep liquor, or lactose mother liquor from the

starch industry (Joshi et al. 2018b). The total cost of the nutrients would be significantly reduced by cheaper source.

4.20 Conclusions

The current investigation elucidates the comparative influence of photoautotrophic and heterotrophic bacteria on $CaCO_3$ precipitation and concrete's strength and permeability properties. There was no significant difference in the compressive strength of SPC and BPC specimens after 28 days. The sorptivity coefficient '*k*' evaluated for the BPC, SPC, and control specimens was 0.005, 0.007, and 0.01 after 28 days, respectively. The charge passed through the SPC and BPC concrete specimen after 28 days was 1901 and 1440 C, respectively. Indeed, ureolytic bacteria exhibited better results in permeability, and $CaCO_3$ induced was higher in the ureolytic bacteria. However, cyanobacteria culture has an advantage over ureolytic bacteria as it has a more prolonged lag phase of growth and reduces the emission of ammonia in an environment, which is a significant concern. Therefore, cyanobacteria can be used instead of ureolytic bacteria, which can be a significant breakthrough as a sustainable, eco-friendly MICCP technique.

4(D)Evaluation of biomineralization on marble surface by heterotrophic and photoautotrophic bacteria

The environment is polluted with many harmful pollutants, chief amongst them are sulfur dioxide (SO_2) and nitrogen dioxide (NO_2). When these pollutants combine with rainwater, they create sulphuric and nitric acids, the pH of which falls within the range of 4 to 6. The current investigation explored the efficiency of heterotrophic and photoautotrophic bacteria for restoration of the lost carbonate layer due to the weathering effect of acid rain on the marble samples.

4.21 Calcification on the marble surface

Fig. 4.94 shows an increase in weight gain of the marble stone with an increase in the deposition of $CaCO_3$ precipitation by ureolytic *B. paramycoides* MD6 and photoautotrophic bacteria *S. pevalekii*. Also, with an increase in the incubation period (7, 14, 21 and 28 days), a significant increase in the $CaCO_3$ deposition on the surface was observed. The *B. paramycoides* treated marble stones showed 0.97, 1.24, and 1.40 g increase in weight gain after 28 days when bacterial concentration was 6×10^3, 6×10^5, and 6×10^7, respectively. At the same time, the *S. pevalekii* cells showed 1.24, 1.67, and 1.94 g increase in the weight gain of the marble stone incubated in cell concentrations 6×10^3, 6×10^5, and 6×10^7, respectively. *S. pevalekii* culture showed more calcification potential than the *B. paramycoides* culture. However, both bacterial strains were efficient in $CaCO_3$ precipitation. The cell concentration has a significant effect on the $CaCO_3$ precipitation. With an increase in the cell number, the uptake of Ca^{2+} ions might have been boosted, which led to the rise in the $CaCO_3$ precipitation on the surface. Comparing the calcite precipitation by two bacteria, *S. pevalekii* culture produced 33% - 35% more $CaCO_3$ precipitation. The statistically analyzed data showed a significant effect of incubation time and cell concentration on the $CaCO_3$ precipitation (Table 4.16). Other researchers reported similar results (Rodriguez-Navarro et al. 2003; Rodriguez-Navarro et al. 2012; Daskalakis et al. 2014).

4.22 Effect of acid solution and biomineralization efficiency on the marble surface

To study the effect of four atmospheric pollutants, we exposed marble stones to acid spray (analogous to acid rain) comprising HNO_3, H_2SO_4, and a mixture of HNO_3/H_2SO_4. The weight loss of the marble stone was noted at 7, 14, and 21 days following the acid spray of four different test groups. After the loss of carbonate granules from the marble stone, the samples were treated using ureolytic bacteria *B. paramycoides* and photoautotrophic *S. pevalekii*

culture. The marble stones were divided into two categories; Biomineralization by *B. paramycoides* (BP) and Biomineralization by *S. pevalekii* (BSP) to study the effect of calcification on the marble.

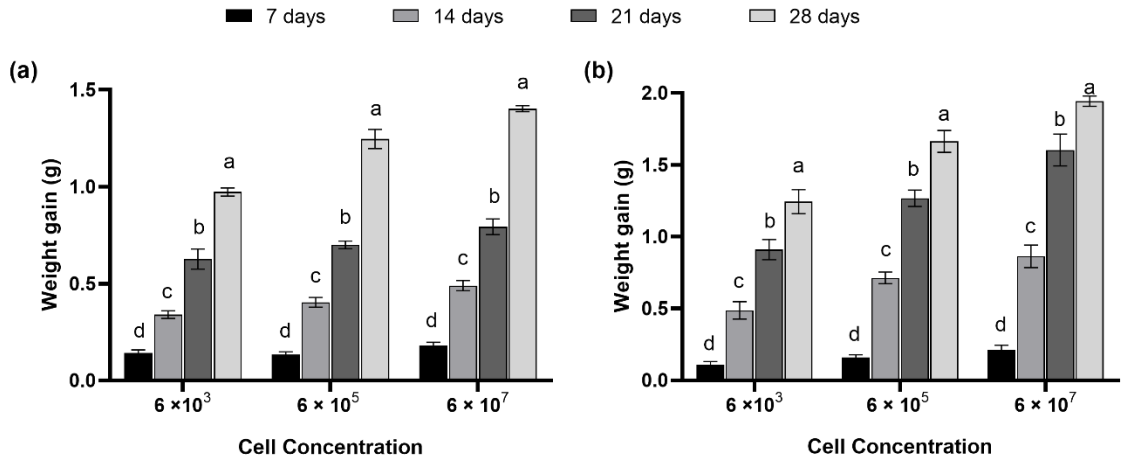


Fig. 4.94 Weight gain of the marble surface due to $CaCO_3$ deposition on the surface by metabolic activity of (a) *B. paramycoides* and (b) *S. pevalekii*. Values bearing different letters within the treatment at each time interval are significant at $p<0.05$. Error bars represents standard deviation (n = 3)

4.22.1 Effect of acid spray on the stone

Fig. 4.95 depicts the weight loss of marble stone due to acid attack of four different acid solutions with continuous spray for 21 days. The weight loss was observed to increase with the acid rain spray time. Initially, after the 7 days, the weight loss was 1.1 g, 1.09 g, 1.2 g, and 1.06 g in Test 1 (HNO_3), Test 2 ($HNO_3 > H_2SO_4$), Test 3 (H_2SO_4) and Test 4 ($H_2SO_4 > HNO_3$), respectively which increased to 3 g, 3.8 g, 3.3 g, and 2.4 g, respectively after 21 days. The weight loss of marble samples was due to granular disintegration of carbonate from the stone. In Test groups 1 and 2, there was no color change, which was noticeable by the human eye. However, the deposition of H^+ ions on the surface was evident. The anticipated outcome of the wet deposition of hydrogen ions on carbonate stone leads to the dissolution of one mole of calcite for every mole of hydrogen ions deposited (Baedecker and Reddy 1993). A major weight loss was observed in the Test 2 group due to the dissolution of the carbonate stone. This phenomenon can be attributed to nitric acid entering the pores of the stone, where it initiates deterioration (Sikiotis and Kirkitsos 1995; Camaiti et al. 2007). When marble stone was

exposed to a sulphuric acid (H_2SO_4) environment, the formation of white crystallization was observed on the surface with a change in stone color from white to brownish-yellow. The texture appeared to be rough and unaffected by further deterioration. The crystallization had to be removed manually at the end of spray damage as this layer was observed to continually deteriorate the surface, causing a change in color and texture. Vazquez et al. (2016) explained that crystallization is due to the presence of calcium in the stone, which forms gypsum crust on the surface when it comes in contact with sulphate (SO_2). However, this crystallization varies greatly depending on the type of stone used and its texture. Similar results were reported by Baedecker and Reddy (1993), Zhu et al. (2015b) and Kumar (2017). The statistical analyzed data revealed acid attack had significant effect on weight loss due to granular removal of carbonate grains from the surface when different concentration of acid spray was used (Table 4.17).

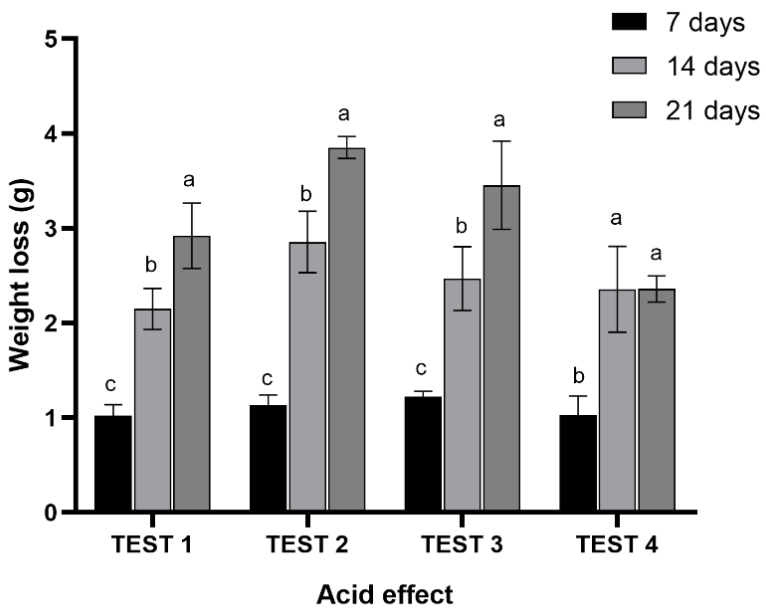


Fig. 4.95 Weight loss of marble stone due to the detrimental effect of acid spray. Values bearing different letters within the treatment at each time interval are significant at $p<0.05$. Error bars represents standard deviation (n = 3)

4.22.2 Restoration by *B. paramycoides* and *S. pevalekii*

The acid-deteriorated marble stones were treated by ureolytic *B. paramycoides* and photosynthetic bacteria *S. pevalekii* by inducing $CaCO_3$ (Fig. 4.96). The $CaCO_3$ precipitates filled the pits created on the surface due to the granular disintegration of grains from the stone.

The surface was replenished by forming a $CaCO_3$ coating on the surface and gaining in the lost weight of the marble. The weight gain was observed to increase with the treatment period. The weight gain in BP samples after ureolytic treatment for 28 days in Test 1, Test 2, Test 3 and Test 4 groups, was 2.05 g, 1.99 g, 1.64 g, and 1.58 g, which corresponds to 2.5%, 2.36%, 2.0% and 1.9% increase in weight, respectively (Fig. 4.97a). Likewise, when marble samples (BSP) were treated by *S. pevalekii* culture, the weight gain was 2.32, 2.92, 3.02, and 2.56 g, corresponding to 2.5%, 3.1%, 3.3%, 2.8% increase in the weight after 28 days (Fig. 4.97b). Two different MICCP techniques were implemented in the current study. However, the results were almost similar concerning the formation of $CaCO_3$ coating with slightly higher precipitation by photosynthetic bacteria. It might be due to the higher surface-to-volume ratio of photosynthetic cyanobacteria than ureolytic bacteria forming a bond on the surface. The bacterial cell wall is a nucleation site for carbonate precipitates (Williams et al. 2017). The calcite deposition filled the voids created on the surface due to acid solution damage. The white calcite deposition formed a coating on the damaged marble surface. This improved the texture and color of the surface, specifically in Test 3 and Test 4 groups where color alteration was observed due to sulfate attack (Fig. 4.98). The immersion technique was adopted in the current investigation for two significant reasons. Firstly, for equal distribution of substrates and Ca^{2+} ions on the surface. Secondly, the constant precipitation in the solution due to moisture and nutrient availability enhances the MICCP treatment. Also, with an increased treatment period, $CaCO_3$ precipitation on the surface improved. However, the experiment was carried out for 28 days, showing significant improvement in the texture and color of the surface. Similar results were reported by De Muynck et al. (2011), who noted a significant improvement in the surface. De Muynck et al. reported a 1.49%, 4.34%, and 4.51% increase in weight because of the catalytic action of *Bacillus sphaericus* LMG 22257, leading to carbonate deposition on the porous stones. In another research by De Muynck et al. (2010) also reported that weight gain was higher with an increase in the treatment period. Rodriguez- et al. (2012) also evaluated the $CaCO_3$ efficiency of *Myxococcus xanthus and Brevundimonas diminuta*. The study's findings revealed that $CaCO_3$ precipitates by bacterial ureolytic action exhibited stable binding with the carbonate stone surfaces. The analysis of variance also corroborated the fact that biomineralization treatment and time had a significant effect on the weight gain of the marble samples (Table 4.17).

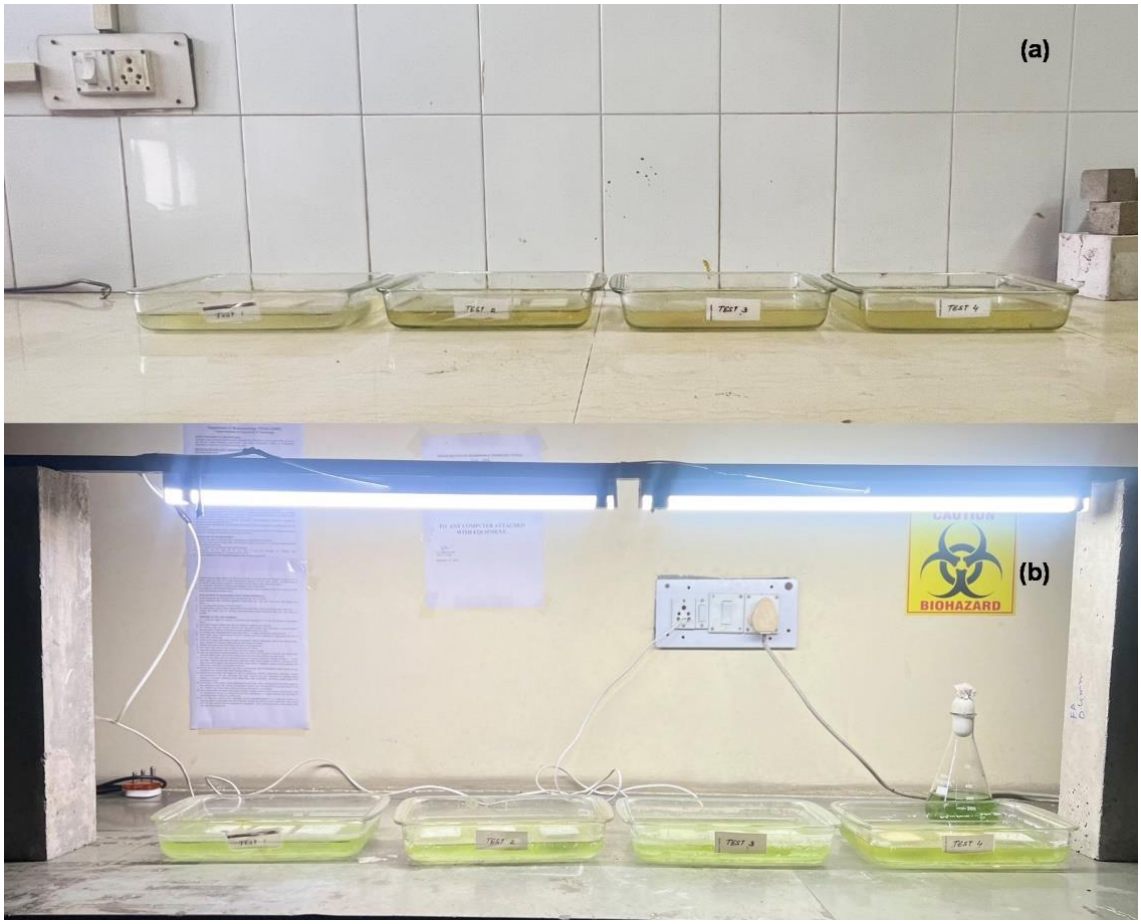


Fig. 4.96 Incubation of acid affected marble samples in (a) heterotrophic and (b) photoautotrophic bacteria

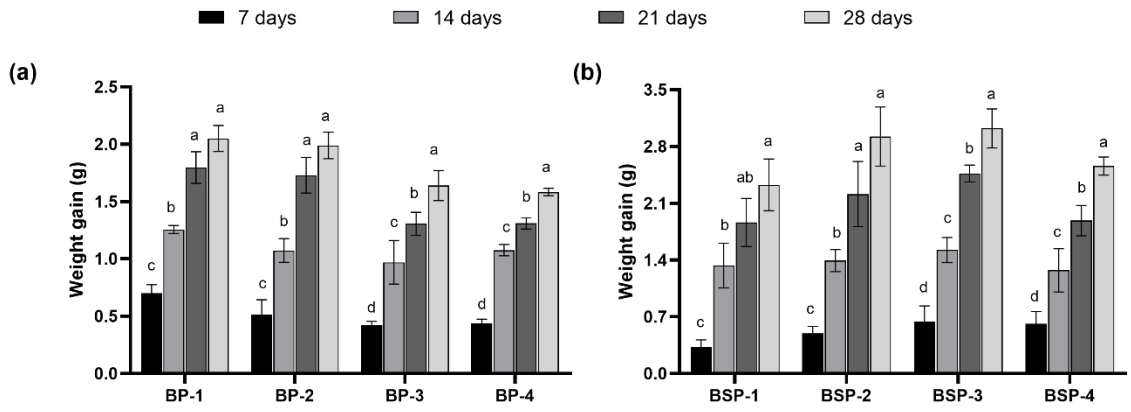


Fig. 4.97 Weight gain due to $CaCO_3$ deposition in (a) BP samples treated by *B. paramycoides* (b) BSP samples treated by *S. pevalekii*. Values bearing different letters within the treatment at each time interval are significant at $p<0.05$. Error bars represents standard deviation (n = 3)

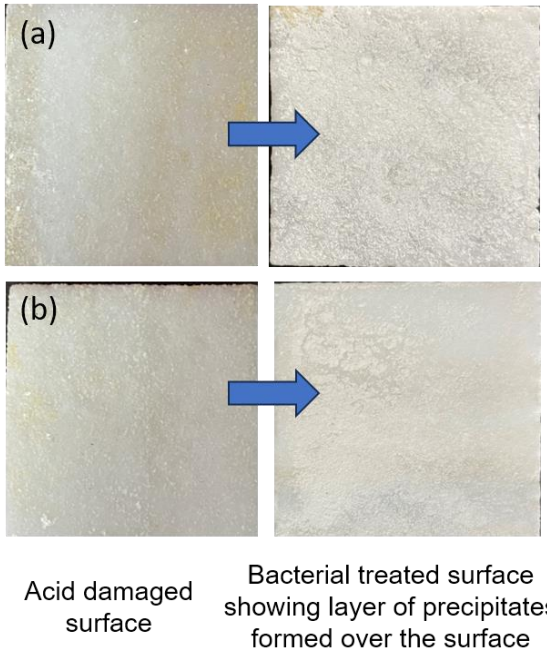


Fig. 4.98 The improvement of color and texture of marble stones after the MICCP treatment (a) *B. paramycoides* (b) *S. pevalekii*

4.22.3 Weight loss due to sonication

Fig. 4.99a and Fig. 4.99b illustrate the weight loss in BP and BSP marble specimens treated by *B. paramycoides* and *S. pevalekii* culture, respectively. The weight loss was due to removing loosely attached $CaCO_3$ precipitates from the surface after the sonication experiment, which was analogous to wind erosion in the environment. The weight loss in BP specimens treated by *B. paramycoides* was 0.082 g, 0.086 g, 0.09 g, and 0.062g in Test 1, Test 2, Test 3, and Test 4, respectively. At the same time, the weight loss in BSP specimens treated by *S. pevalekii* was 0.13 g, 0.11 g, 0.10 g, and 0.09 g in Test 1, Test 2, Test 3, and Test 4, respectively. The overall weight loss percentage was less than 1%, less than the calcite deposition on stone. The $CaCO_3$ crystallization formed by *B. paramycoides* and *S. pevalekii* was resistant to sonication, confirming the firm adhesion and consolidating property of the $CaCO_3$ formed. Based on the weight loss due to sonication, the consolidation effect of calcite precipitated by *B. paramycoides* had a more substantial adhesion property with the surface than the precipitation formed by photoautotrophic bacteria. It might be attributed to the stability of the different crystal polymorphs formed during the bacteria's metabolic activity (Weiner and Dove 2003). Many researchers have studied the consolidation effect of $CaCO_3$ stone by evaluating the weight loss due to sonication. Daskalakis et al. (2015) carried out sonication for 25 minutes

and reported a reduction in weight loss due to the strong bonding of $CaCO_3$ precipitated by *B. pumilus*. According to De Muynck et al. (2010), the amount of $CaCO_3$ precipitated on the surface as an outcome of the deposition process (0.19–1.12 g) was significantly higher than the amount of carbonates loss due to sonication (0.05–0.09 g). Recently, Zhu et al. (2015a) evaluated the adhesion of calcite in concrete cubes and reported only a 4% reduction in weight after the sonication experiment. Zhu and colleagues additionally explained that the $CaCO_3$ precipitated by *Synechococcus* was not removable by scratching the surface with tweezers. The statistically analyzed data showed a significant effect of sonication and the number of cycles leading to the removal of carbonates precipitated by *B. paramycoides* and *S. pevalekii* (Table 4.17).

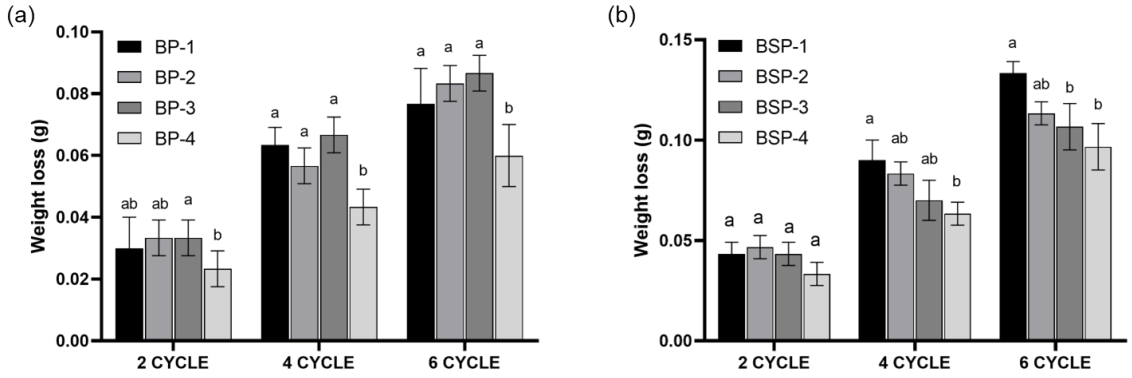


Fig. 4.99 Weight loss of marble samples after sonication treated by (a) *B. paramycoides* and (b) *S. pevalekii*. Values bearing different letters within the treatment at each time interval are significant at $p<0.05$. Error bars represents standard deviation (n = 3)

Table 4.17 The factorial ANOVA analysis indicates the effects of different treatments and curing times for marble samples

Variables			Treatment	Time	Interaction (Treatment×Time)
Acid attack		df	3, 6 P < 0.0001	2, 4 P=0.0010	6, 12 P=0.0010
MICCP treatment	*B. paramycoides*	df	3, 6 P = 0.0083	3, 6 P < 0.0001	9, 18 P = 0.0003
	S. pevalekii	df	3, 6 P < 0.0001	3, 6 P = 0.1138	9, 18 P = 0.1073
Sonication	*B. paramycoides*	df	2, 4 P < 0.0001	3, 6 P = 0.0002	6, 12 P = 0.0082
	S. pevalekii	df	2, 4 P < 0.0001	3, 6 P = 0.0027	6, 12 P = 0.0421

4.22.4 Roughness

Table 4.18 represents the root mean square deviation (RMS; S_q), skewness (S_{sk}) and kurtosis (S_{ku}) of the marble surface analyzed using atomic force microscopy (AFM). The RMS value for control was 20.97 nm (Fig. 4.100). The distribution was negatively skewed indicating the surface had valleys which might be because unpolished marble specimen was used in the current investigation (Mwema et al. 2018). The roughness was observed to increase in the acid affected marble specimens. Fig. 4.101 shows the 2D and 3D topographic images of marble surface affected by different acid solution (HNO_3, HNO_3 > H_2SO_4, H_2SO_4, H_2SO_4 > HNO_3). The intensity band on the right-hand side of 2D image illustrates the depth and height of valleys along the Z axis caused due to weathering of stone after the dissolution of granules by acid spray. Maximum roughness was observed in marble samples treated by nitric acid in Test group 1 and 2. The distribution achieved was negatively skewed in all test groups with maximum skewness in Test 1 (treated by HNO_3). The RMS value for T1, T2, T3, T4 samples was 297.79, 283.74, 183.42, and 183.05 nm. The kurtosis (S_{ku}) measured the sharpness intensity of the peaks. The S_{ku} value more than 3 indicates the surface is spiky whereas if the value is less than 3 the surface is bumpy and if the value is equivalent to 3 the surface is perfectly distributed (Mwema et al. 2018). The microbial treatment by *B. paramycoides* and *S. pevalekii* improved the roughness of the surface. Fig. 4.102 and 4.103 shows the 2D and 3D topographic images of marble samples treated by *B. paramycoides* (BP) and *S. pevalekii* (BSP). The root square deviation was reduced significantly in bacterial treated specimens. The RMS value was reduced by 53.3%, 42.5%, 76.4%, and 77% in BP samples. At the same time, the RMS value was reduced by 53.6%, 52.8%, 49.2%, and 74.2% in BSP samples. The skewness was positively distributed in BP-1, BP-3, BP-4 and BSP-3 samples. Whereas the skewness was negatively skewed in BP-2, BSP1, BSP-2, and BSP-4. It indicates the peaks and valleys which could be due to calcite deposition on the surface filling the pits formed by acid solution spray. The S_{ku} and S_{sk} value for BP samples was 2.2 and 0.69 indicating the symmetrical distribution of analyzed data. The RMS value for BP sample was 43.26 nm depicting the improved surface roughness. Though both microbial strains were efficient in improving the roughness caused by acid, proving it as an efficient technique for improving the topography of the marble surface damaged by acid weathering. Similar work was carried out by Manoudis et al. (2007) using polymer-silica coating on the acid affected marbles. Many researchers have reported significant improvement of limestone structure and monuments using MICCP technique by ureolytic bacteria (De Muynck et al. 2010; Ercole et al. 2010; Jroundi et al. 2012; Erşan et al. 2020).

Table 4.18 Roughness analysis of acid affected, bacterial and cyanobacterial treated marble samples

Parameters		RMS (S_q) (nm)	Skewness (S_{sk})	Kurtosis (S_{ku})
Control	C	20.97 ± 18.01	-0.25	- 0.86
Acid affected marble	T1	297.79 ± 232.09	-0.62	0.7
	T2	283.74 ± 211.86	- 0.11	1.62
	T3	183.42 ± 165.38	- 0.14	- 1.44
	T4	183.05 ± 148.25	- 0.21	- 0.17
Bacterial treated marble	BP-1	138.91 ± 108.23	0.08	0.81
	BP-2	163.91 ± 129.33	- 0.15	0.24
	BP-3	43.26 ± 32.45	0.69	2.2
	BP-4	42.10 ± 33.29	0.04	- 0.02
Cyanobacterial treated marble	BSP-1	138.01 ± 112.82	- 0.52	- 0.46
	BSP-2	133.82 ± 101.16	- 0.24	0.82
	BSP-3	93.16 ± 72.76	0.25	0.19
	BSP-4	108.78 ± 83.47	- 0.14	0.56

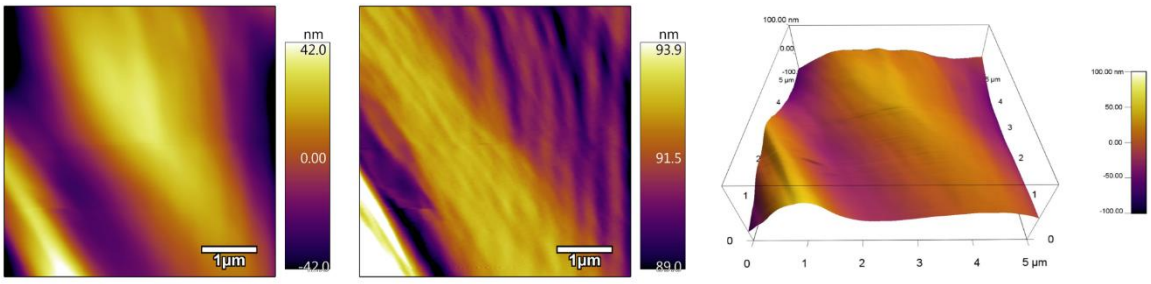


Fig. 4.100 Roughness of the control marble surface without any deterioration and treatment

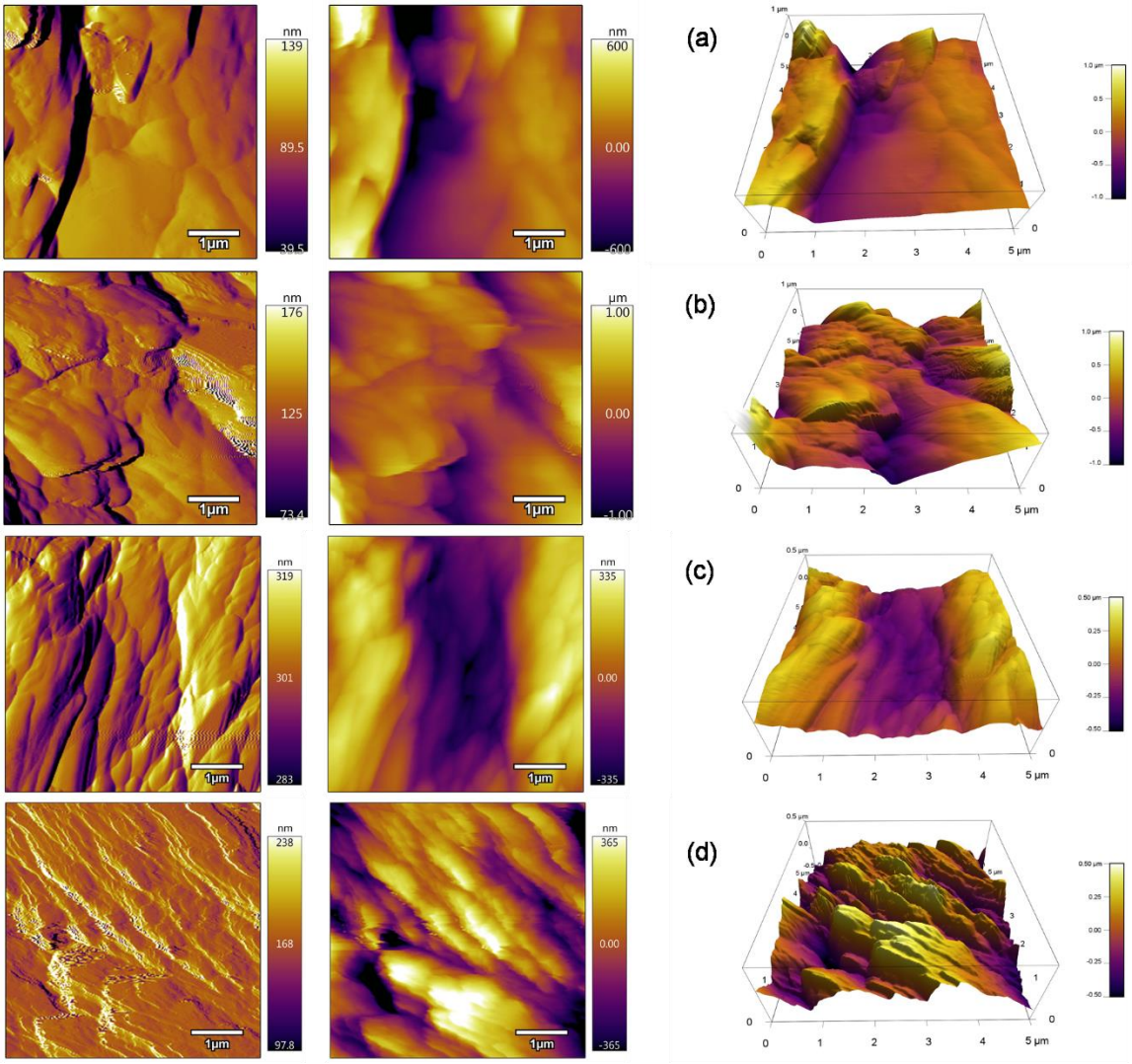


Fig. 4.101 Roughness of marble surface affected by artificial acid rain constituting (a) Test 1 (HNO_3), (b) Test 2 (HNO_3 > H_2SO_4), (c) Test 3 (H_2SO_4) and (d) Test 4 (H_2SO_4 > HNO_3)

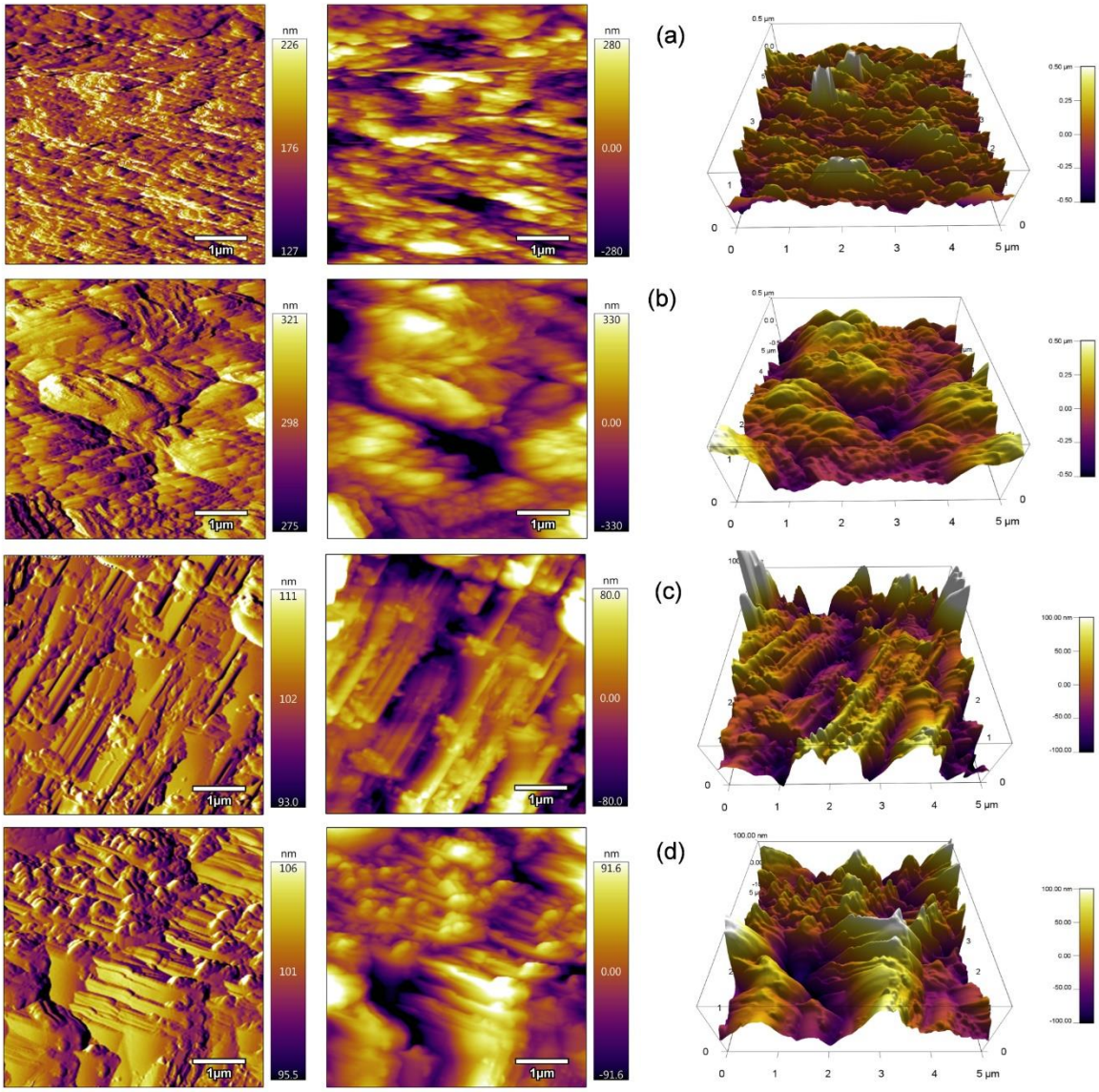


Fig. 4.102 Roughness of marble surface treated by *B. paramycoides* culture (a) Test 1 (HNO_3), (b) Test 2 (HNO_3 > H_2SO_4), (c) Test 3 (H_2SO_4) and (d) Test 4 (H_2SO_4 > HNO_3) using MICCP technique

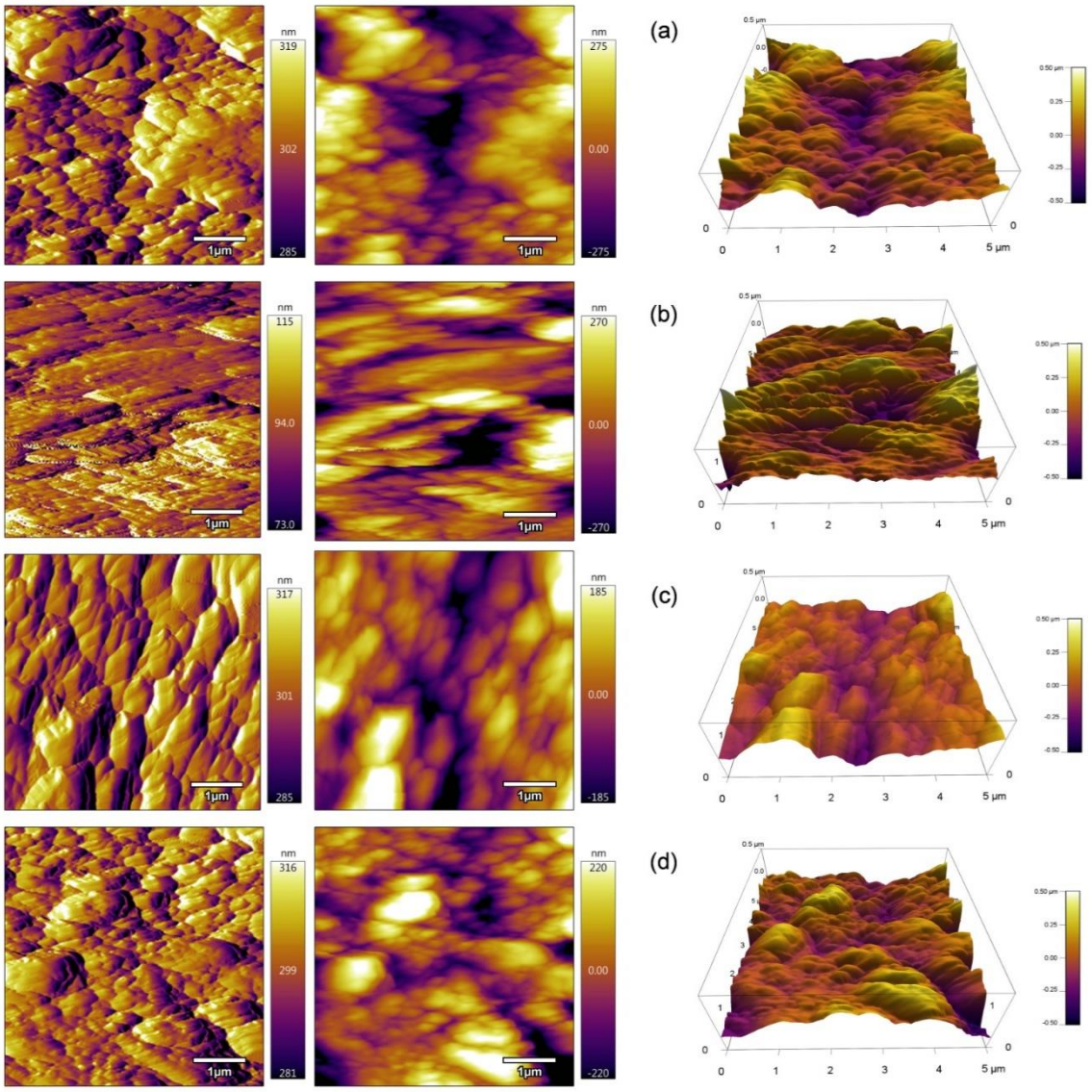


Fig. 4.103 Roughness of marble surface treated by *S. pevalekii* culture (a) Test 1 (HNO_3), (b) Test 2 (HNO_3 > H_2SO_4), (c) Test 3 (H_2SO_4) and (d) Test 4 (H_2SO_4 > HNO_3) using MICCP technique

4.22.5 Visual examination

Fig. 4.104 and Fig. 4.105 shows the microscopically observation of control (before the experiment), acid damaged surface (after the acid attack) and bacterial repaired surface (after the MICCP treatment) by DinoLite microscope. The formation of voids or pits due to granular loss of carbonate from stone was clearly evident in nitric acid damaged surface in Test 1 and Test 2 group (Fig. 4.104b and 4.105b). Whereas, in Test 3 and Test 4 some color alteration

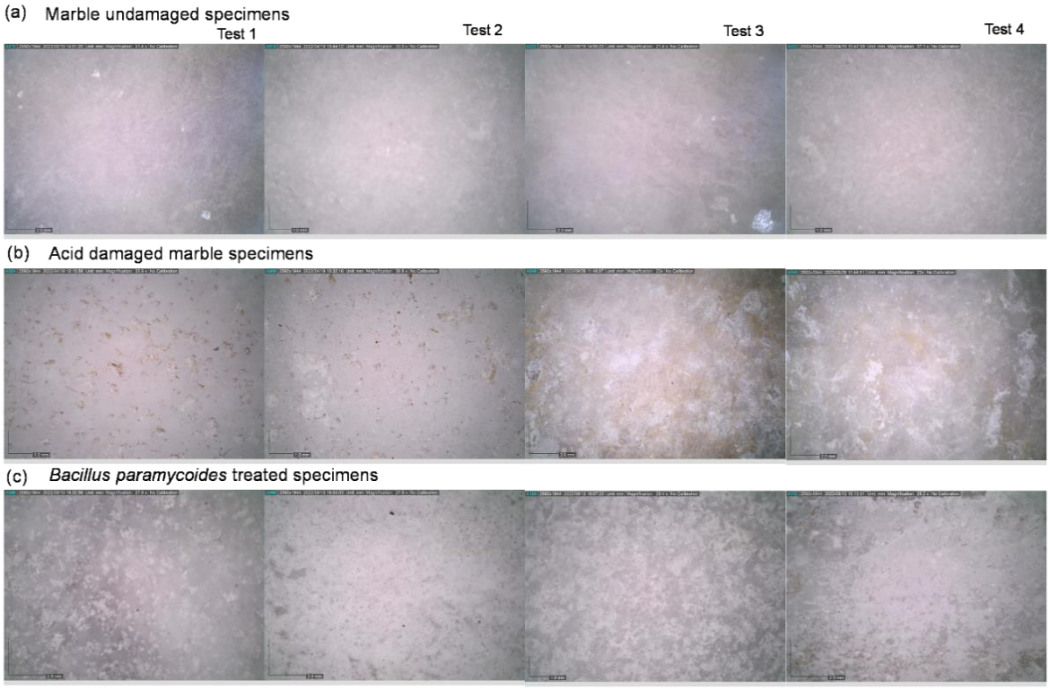


Fig. 4.104 Microscopic observation of marble surface (a) Control; before deterioration (b) marble surface after the different test group of acid attack (analogous to acid rain) (c) microbial (BP) treated surface showing $CaCO_3$ deposition

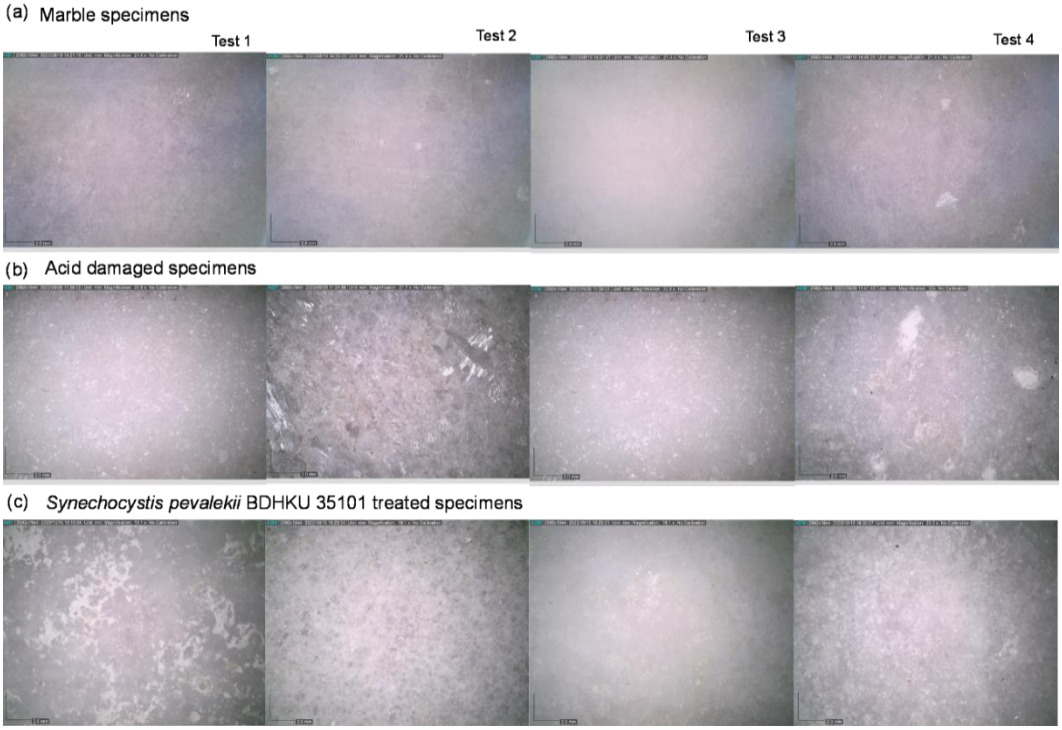


Fig. 4.105 Microscopic observation of marble surface (a) Control; before deterioration (b) marble surface after the different test group of acid attack (analogous to acid rain) (c) microbial (BSP) treated surface showing $CaCO_3$ deposition

along with the roughness on the surface was observed. The formation of crystallization was also observed in Test groups 3 and 4 after exposure to the sulphuric acid rain spray. The damage degraded the surface of its natural color and polish. The MICCP treatment by ureolytic (Fig. 4.104c) and photosynthetic bacteria (Fig. 4.105c) successfully improved the marble surface's texture and color by forming a $CaCO_3$ layer. The voids formed in Test group 1 and 2 were completely healed due to calcite deposition.

4.22.6 FESEM analysis

Fig. 4.106 illustrated the formation of spikes over the surface, describing the weathering of the stone due to granular disintegration in T1, T2, T3, and T4 samples. The lost carbonate granular from the surface was significantly substituted by $CaCO_3$ precipitation by *B. paramycoides* and *S. pevalekii*. A layer of carbonate coating was formed on the surface. Figs. 4.107 and 4.108 show the formation of calcite and vaterite crystallization on the marble surface in BP and BSP samples. The crystals were rhombohedral and spherical with 5-10 μm in size. The crystallization was analyzed for its elemental analysis through EDS, which clearly indicates the presence of C, O, and Ca. Bacteria and archaea can initiate and regulate the formation of carbonate minerals at both the nanometric and micrometric scales (Zhu and Dittrich 2016). Through the production of various metabolic byproducts, such as proteins, polysaccharides, and other extracellular polymeric substances (EPS), as well as the charged groups present within their microbial cell walls, these microorganisms can influence the crystal properties and chemical composition of the minerals by interacting with anions and cations (Robles-Fernández et al. 2022). Similar results were reported by (Minto et al. 2018; Ortega-Villamagua et al. 2020).

4.22.7 Conclusions

In comparing the efficacy of photoautotrophic and heterotrophic bacteria in marble, it was observed that the former demonstrated superior performance by producing a thicker calcite layer on the surface. However, the calcite produced by heterotrophic bacteria was more stable and provide significant consolidation effect on the surface as observed by sonication experiment. The roughness was observed to improve by both microbial strains. The results were confirmed by FESEM-EDS. Therefore, MICCP technique can be used an eco-friendly treatment for acid rain affected marble monuments and buildings.

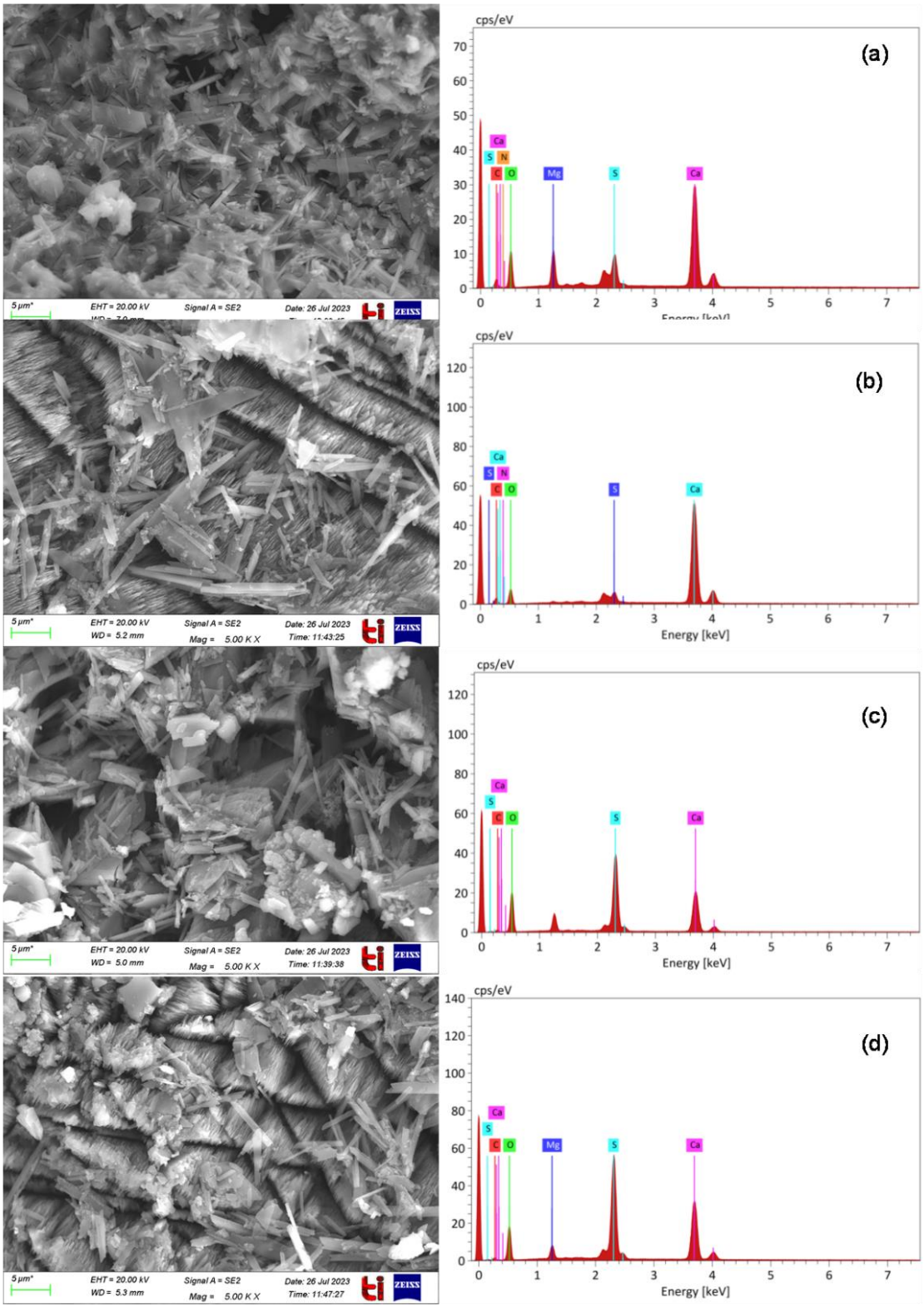


Fig. 4.106 FESEM analysis of the acid affected marble surface (a) Test 1, (b) Test 2, (c) Test 3, (d) Test 4.

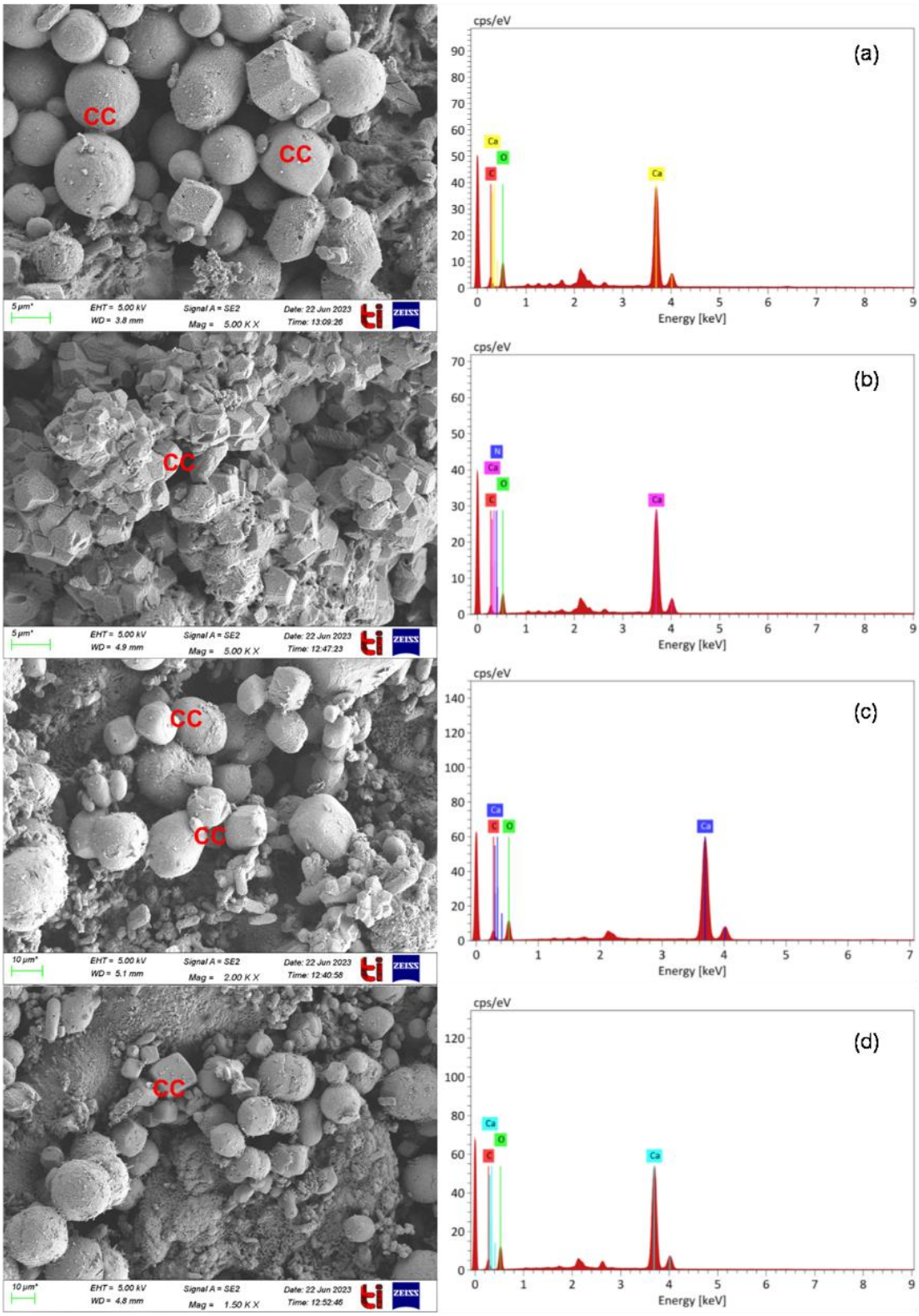


Fig. 4.107 FESEM analysis *B. paramycoides* treated marble surface (a) BP-1, (b) BP-2, (c) BP-3, (d) BP-4

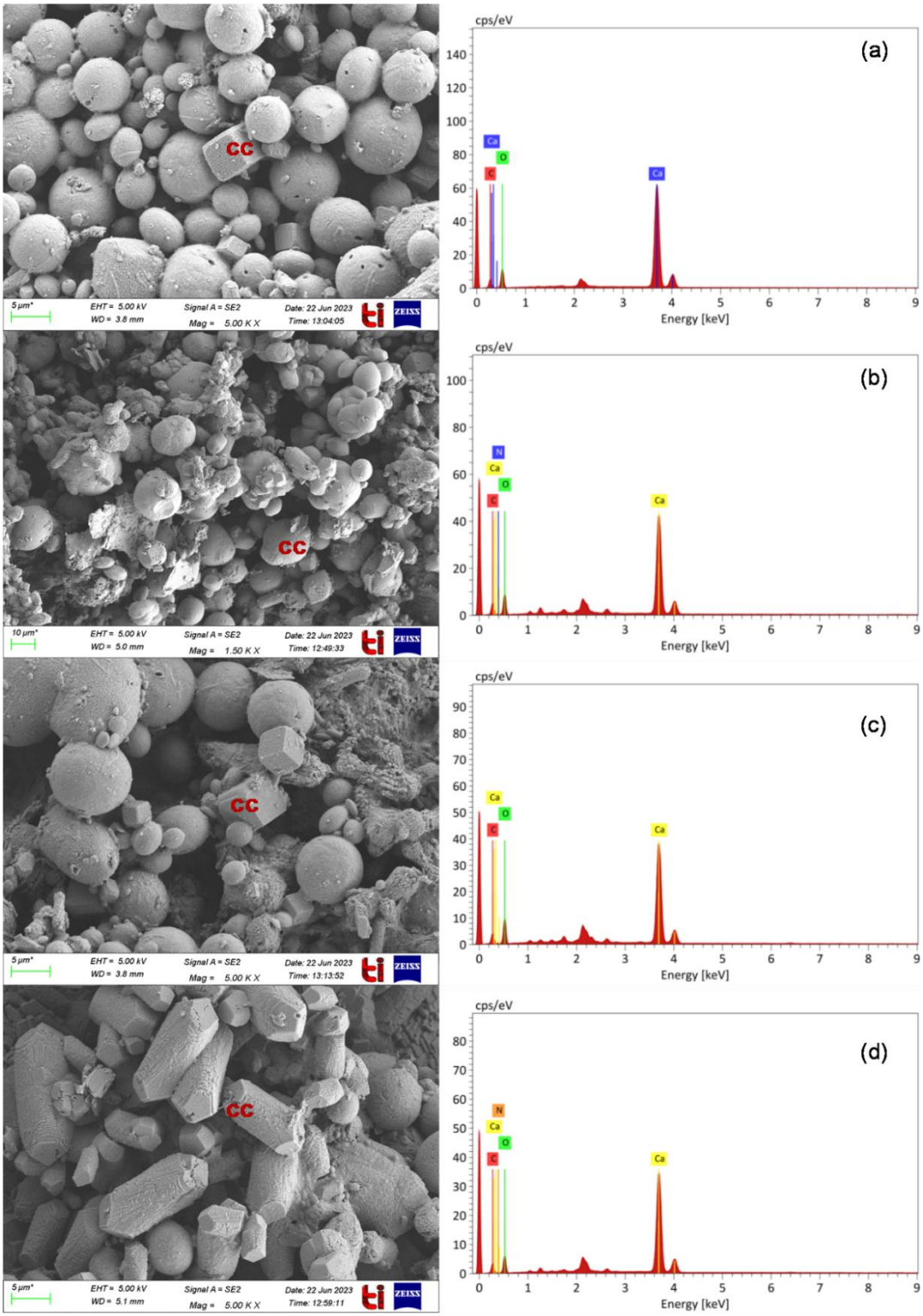


Fig. 4.108 FESEM analysis of the *S. pevalekii* treated marble surface (a) BSP-1, (b) BSP-2, (c) BSP-3, (d) BSP-4

Chapter 5 Summary

MICCP has shown promising results in various engineering applications, as well as repairing cracks in cementitious materials. Many of these studies were performed by heterotrophic bacteria. The objective of the current investigation was to develop better understanding of heterotrophic and photoautotrophic bacteria. The results are summarized into three sections; heterotrophic bacteria, photoautotrophic bacteria and comparison of two bacteria to improve properties of mortar, concrete and marble.

5.1 Heterotrophic bacteria

The present study focused on isolating and characterizing urease-producing bacteria from marble dust and their efficiency in $CaCO_3$ precipitation. The marble dust was collected from a dumping yard in Kishangarh, Rajasthan, India, and isolated 7 urease-producing bacterial isolates. The isolated bacterial strains were able to catalyze the hydrolysis reaction of urea to form ammonia and bicarbonate ions, leading to increased pH in the surrounding environment. This increased pH promotes the formation of hydroxide ions and bicarbonate ions, which in turn promotes $CaCO_3$ precipitation. The bacteria act as a nucleation site for positively charged calcium ions. The study identified the urease-producing bacterial isolates belonged to genus *Bacillus*. These bacteria were identified as *Bacillus cereus* MD1, *Bacillus paranthracis* MD2, *Bacillus paranthracis* MD3, *Bacillus paramycoides* MD4, *Bacillus paramycoides* MD5, *Bacillus paramycoides* MD6 and *Bacillus paramycoides* MD7 based on their 16S rRNA sequence analysis. These bacterial isolates were further studied for their urease activity and $CaCO_3$ precipitation efficiency. The maximum urease activity of 1512 U/ml and $CaCO_3$ precipitation of 1232 mg/100 ml was observed by *B. paramycoides* MD6 strain. The efficiency of $CaCO_3$ precipitated was tested for its consolidation property in sand plugging experiment. The consolidated sand column was further divided into three parts to estimate the $CaCO_3$ content using EDTA titration. The reduction in flow rate was observed in all the bacterial treated sand columns with maximum $CaCO_3$ precipitation was observed in the upper layer of the column. The best results were obtained in sand column treated by MD6 bacterial strain with 42.96 mg/g $CaCO_3$ precipitation. Based on the urease activity, $CaCO_3$ precipitation, and consolidation experiment, the *Bacillus paramycoides* MD6 was selected for further testing. The growth cycle, urease activity and $CaCO_3$ precipitation were significantly influenced by different temperature and pH condition. The optimum temperature for growth of *B. paramycoides* MD6 was 37 °C

and pH range of 7-10. The maximum urease activity of 1126.55 U/ml was recorded at 37 °C. Whereas, the highest urease activity of 1547.8 U/ml was recorded at pH 9 of the solution. $CaCO_3$ precipitated in the broth analyzed using scanning electron microscopy (SEM) were identified as calcite. The sand consolidation experiment was conducted for three different sizes of grains (150 µm, 300 µm, and 600 µm). The flow rate reduced significantly from 7.7 to 2.3 ml/min. Similarly, the flow rate reduced from 7.4 to 2.5 ml/min and 8.6 to 2.6 ml/min in 300 and 600 µm sized sand plugged columns, respectively. The bacterial admixed columns were compact, with maximum $CaCO_3$ precipitation in the upper layer of the sand column. A sand column with a 150 µm grain size had the highest precipitation rate. The 150 µm sand column showed 42.5 mg/g $CaCO_3$ precipitation with 22.5 mg/g in the lower layer. Compared to 150 µm, the other two sand columns showed 24% and 26.8% less calcite precipitation in the upper layer of the sand column. A microstructural analysis (SEM-EDS) proved that rhombohedral $CaCO_3$ precipitation in the voids of sand columns. The crystallization was further confirmed by XRD analysis. The XRD graph showed the highest peak calcite formed at 29.4°, which corresponds to 104 planes of calcite phase.

The cementitious properties (strength and permeability) of concrete specimens were tested for biomineralization efficiency of *B. paramycoides*. The compressive strength of *B. paramycoides* cured (BPC) specimens (150 × 150 × 150 mm cubes) after 28 days was 44.5 MPa. BPC specimens showed a 28.9% improvement in strength property as compared to the control. The chloride penetration of the concrete specimen cured by *B. paramycoides* showed 27.2% and 57.8% reduction in charge passed in BPC specimens after 7 and 28 days of curing, respectively. Similarly, the sorptivity coefficient '*k*' of BPC specimens was observed to be 0.007 and 0.005 at 7 and 28 days, respectively. The sorptivity coefficient '*k*' for the control specimens was 0.011 and 0.01 at 7 and 28 days, respectively. Therefore, ureolytic action by *B. paramycoides* significantly improved concrete's strength and permeation properties.

The current study was further extended to develop metakaolin (MK) as a sustainable carrier material for immobilizing bacterial spores using adsorption technique. The spores of the bacterial strain *B. paramycoides* were prepared in commercially available nutrient broth (NB) media, and industrial waste corn steep liquor (CSL) media. The MK powder was used as a carrier material to immobilize the spores. The biomaterial stored at 25 °C was labeled as NB-25, CSL-25, and at 4 °C was labeled as NB-4 and CSL-4. When NB was used as a nutrient source, the developed biomaterial exhibited a cell count of 7.6 and 7.5 log cfu/g after 180 days

at 4 °C and 25 °C, respectively. Whereas, when CSL was used as a nutrient source, the cell viability of the biomaterial was 7.4 and 7.3 log cfu/g after 180 days of storage at 4 °C and 25 °C, respectively. It was observed that the biomaterial stored at 4 °C proved to be effectively more efficient than the 25 °C for maintaining the spores in the dormant stage for a long period of time. The urease activity and $CaCO_3$ precipitation were evaluated for biomaterial stored at different temperature conditions. The highest urease activity of 738.9 U/ml was recorded after 96 h of incubation at 37 °C in CSL-4, followed by 731 U/ml in NB-4. Similarly, the $CaCO_3$ precipitation by biomaterial stored at 4 °C was observed to be higher as compared to the 25 °C storage. The $CaCO_3$ precipitation by NB-4 and CSL-4 was observed to be 642.4 and 652.4 mg/100 ml after 120 h of incubation at 37 °C and hence further selected for testing concrete properties and crack remediation. Prismatic specimens of 500 × 100 × 100 mm, 150 mm cubes, and 100 (dia) × 200 (height) mm cylindrical concrete specimens were tested. The flexural strength of NB-4 and CSL-4 concrete specimens improved by 17.7% and 19.1% after the specimens were cured in the growth media. Similarly, the compressive strength of the NB-4 and CSL-4 concrete specimens improved by 28.3% and 27.3% at 28 days. The sorptivity coefficient was evaluated for the NB-4 and CSL-4 at 7 and 28 days. The sorptivity coefficients of the NB-4 specimens was 0.006 and 0.002 at 7 and 28 days, respectively. Likewise, the sorptivity coefficient for the CSL-4 specimens was 0.006 and 0.002 at 7 and 28 days, respectively. However, the control specimens showed sorptivity coefficients of 0.01, and 0.008 at 7 and 28 days of curing, respectively, which were comparatively higher than those of the bacterial-treated specimens. The low '*k*' values confirmed that incorporating bacterial spores can significantly improve the permeation properties. Precipitation of $CaCO_3$ crystals was confirmed by FESEM-EDS. The cracked 400 × 100 × 100 mm prismatic specimen consisting of the biomaterial was subjected to a self-healing treatment at room temperature. The crack of approximately 0.5 mm was injected and sprayed with nutrient broth and CSL broth supplemented with 2% urea and 25 mM $CaCl_2$ to activate spores immobilized in the biomaterial. The crack width was measured at different intervals, and images were obtained for visual monitoring using a DinoLite microscope. In the control specimens, no reduction in crack width was observed. The NB-4 specimen showed 98.2% crack healing efficiency after 40 days. Whereas the CSL-4 specimen showed 99.14% crack healing efficiency after 50 days. Water tightness was evaluated based on the amount of water flowing through the crack zone in 20 s until complete crack closure. In NB-4 specimens, a total 13.1 ml of water flowed through the cracked location marked "A, B, C" which declined to 0.9 ml on the 40^{th} day. Similarly, in CSL-4, the water flow reduced from 17.8 ml to 1.6 ml on the 50^{th} day. Based on this, 92.8%

and 88.9% sealing efficiency were evaluated in NB-4 and CSL-4 specimens. The ultrasonic pulse velocity (UPV) was measured at different crack healing percentages to determine the efficiency of MICCP. NB-4 and CSL-4 crack-healed specimens showed a regain in the UPV as compared to the control specimens. The UPV value in NB-4 and CSL-4 specimens was 4049 and 4018 m/s before cracking and 3982 and 3986 m/s after complete crack healing, respectively. Negligible recovery was seen in control. The study demonstrated significant enhancements in self-healing through MICCP, as evidenced by surface crack observations, FESEM-EDS and XRD. A uniform distribution of rhombohedral and spherical shaped crystals was observed in the sample. The crystals were stacked to form a calcite and vaterite layer. In contrast, calcite deposition was not observed in the control specimens. Elemental examination revealed that the healed biocementitious material consisted of four essential elements: carbon (C), oxygen (O), calcium (Ca), and quartz or silica (Si). The formation of calcium carbonate was confirmed by high-intensity peaks of calcite and vaterite at 29.2° and 27.1° in the bioconcrete specimens, respectively.

5.2 Photoautotrophic bacteria

Five cyanobacterial strains, *Aphanocapsa montana* BDU21001, *Aphanothece* species BDHKU 40501, *Gleocapsa* species BDU 40111, *Synechococcus elongatus* BDU14174 and *Synechocystis pevalekii* BDHKU 35101 were procured and tested for $CaCO_3$ precipitation in BG11 broth supplemented with 50 mM sodium bicarbonate ($NaHCO_3$) and 100 mM calcium chloride ($CaCl_2$). The $CaCO_3$ precipitated by *A. montana*, *Aphanothece* sp., *Gleocapsa* sp., *S. elongatus*, and *S. pevalekii* were 475, 439, 534, 604, and 695 mg/100 ml, respectively. *S. pevalekii* was selected for further studies based on its $CaCO_3$ precipitating ability. The $CaCO_3$ precipitation was also tested at different pH (6 - 12) in BG11 medium supplemented with calcifying media (50 mM $NaHCO_3$ and 100 mM $CaCl_2$). $CaCO_3$ precipitation increased with the increase of pH up to 9.0 and thereafter decreased. Maximum $CaCO_3$ precipitation was recorded at pH 9.0 (752 mg/100 ml).

The sand consolidation experiment was carried out using *S. pevalekii*. The sand consolidation experiment was performed using live (LT), and UV treated UVT) cells to determine the binding properties of crystals. The flow rate of the calcifying medium was measured at regular intervals until the flow rate was reduced. The flow rate was estimated to be 16.38, 17.44, and 18.52 ml/min in the experiment set—LT, UVT and C (control), which reduced to 4.10, 6.23 and 16.13 ml/min, respectively. The upper part of the column in LT and UVT was dense and more rigid

than the bottom parts. The maximum $CaCO_3$ content in the upper layer in LT and UVT-treated sand columns was 8.67 and 6.67 mg/g, respectively. The $CaCO_3$ precipitation recorded in the middle part of the LT and UVT columns were 6.43 mg/g, and 5.43 mg/g, respectively. The upper layer of the sand column was analyzed using SEM-EDS and observed dense aggregation of crystals. The crystals were rhombohedral in shape with a size of 5–7 μm. However, no calcite deposition was observed in the control after 14 days of treatments.

Further, the influence of photoautotrophic cyanobacteria on compressive strength, and water absorption properties were tested at 7 and 28 days of curing. The LT specimens observed a 25.54% increase, whereas UVT specimens showed a 15.84% surge in compressive strength after 28 days of curing compared to control specimens. Water absorption decreased significantly in the LT specimens. The low '*k*' value of the surface-treated specimen indicates that bacterial incorporation can significantly improve the permeation properties. The microstructural analysis confirmed rhombohedral calcite crystal formation and the bacterial cells in mortar specimens.

This study was extended to develop an eco-friendly, sustainable grout for crack remediation using *S. pevalekii*. The biogrout was prepared using fly ash as a partial cement replacement in the cementitious grout. The best grout was selected based on the fresh and hardened properties of biogrout. The different dosages of fly ash (0%-50%) by keeping water (or cyanobacterial culture) to binder ratios of 0.45, 0.47, and 0.50 were tested. Based on flowability (marsh cone, mini slump, grout bleeding) results, a 0.47 culture/binder ratio was selected to examine different FA dosages for slump flow retention and hardened properties. The substitution of fly ash in the cementitious mixture increased the initial and final setting time of both biogrout and plain grout. The compressive strength was measured for 50 × 50 × 50 mm cube specimens. The strength was observed to be higher for 40% FA substituted cementitious biogrout which was selected for repairing cracks at the lab scale. Different cracked concrete specimens were repaired by injecting the grout in the crack region and then curing the healed region using ponding and spray treatment for 28 days. The strength and sorptivity coefficient were evaluated for crack-repaired specimens, and the results were compared with uncracked (REF) and untreated (UTC) concrete specimens. The compressive strength of the REF specimens was 38.32 MPa. The highest compressive strength (41.82 MPa) was observed in biogrout repair with *S. pevalekii* ponding curing treatment (BPT), followed by 38.94 MPa strength in fly ash amended plain grout with water ponding treatment (CPT). Similarly, the flexural strength for REF and UTC specimens was 4.54 MPa and 3.22 MPa, respectively. The flexural strength recorded after 28 days of curing by cyanobacterial ponding (BPT) and spray treatment (BST)

was 4.50 and 4.11, respectively. Whereas the control (water) ponding (CPT) and spray treatment (CST) showed 3.92 and 3.65 Mpa, of flexural strength, respectively. The sorptivity coefficient '*k*' of CPT, CST and REF was evaluated as 0.035, 0.037 and 0.031, respectively. Compared to this, the sorptivity coefficient of BPT and BST specimens was observed to be 0.009 and 0.025 after 28 days. Therefore, it can be inferred from the low *k* value that calcification in the cyanobacterial admixed cementitious grout effectively reduced the porosity. The sealing efficiency of the crack-healed specimen was evaluated on the basis of water absorption before and after 6 hours of the grouting. The sealing efficiency of crack-healed specimens was observed to be 35.18%, 82.23%, 51.53%, 29.60%, and 25.74% in REF, BPT, BST, CPT, and CST specimens, respectively. The BPT and BST specimens were able to regain and further improve the sealing efficiency due to $CaCO_3$ precipitation by cyanobacterial cells. The sample was collected from the crack-healed region and analysed for $CaCO_3$ precipitation using FESEM-EDS. The rhombohedral calcite crystals were observed in BPT and BST specimens, whereas no crystallization was observed in the control. The crystallization was further confirmed by XRD and TGA. XRD results confirmed the presence of calcite crystal at 29.2° with high intensity in biogrout than in the plain grout specimens. The significant mass loss of 3.74% of $CaCO_3$ at 600-800 °C was noted in the biogrout specimens, which was two times more than the plain grout. The developed fly ash incorporated biogrout will help as an economical and eco-friendly MICCP technology for the remediation of existing cracks in concrete structures.

5.3 Comparison of strength and permeability properties of concrete by photoautotrophic and heterotrophic bacteria

Concerning the comparative analysis of *S. pevalekii* and *B. paramycoides*, there was no significant difference in the compressive strength of SPC and BPC specimens after 28 days. The compressive strength of SPC and BPC specimens was 43.7 MPa and 44.5 MPa after 28 days of curing, respectively. The relative strength index (RSI) of the SPC and BPC specimen as compared to the control was 1.26 and 1.45 at 28 days of curing period, respectively. The microbial cultures used further improved concrete properties by decreasing the latter's permeability. The sorptivity coefficient '*k*' of SPC and BPC specimens after 28 days was 0.007 and 0.005, respectively. The charge passed through the SPC and BPC concrete specimen after 28 days was 1901 and 1440 coulombs, respectively.

5.4 Evaluation of biomineralization on marble surface by heterotrophic and photoautotrophic bacteria

The biomineralization efficiency of *B. paramycoides* and *S. pevalekii* was tested on the marble surface and continuous weight gain was observed in the marble specimens due to calcite layer binding at the surface. The maximum weight gain was recorded in marble samples treated by 6×10^{-7} cells with 1.40 g and 1.94 g of $CaCO_3$ bound to the surface in *B. paramycoides* and *S. pevalekii* treated samples, respectively. To investigate the influence of acid rain on marble stones, the slabs were categorized into four experimental groups of 3 marble stones with 4 × 4 × 2 cm dimensions. The four groups involve four different concentrations (Test 1 - 4) of acid solutions (analogous to the acid rain) of sulfuric acid (H_2SO_4) and nitric acid (HNO_3). The marble stones were exposed to four acidic solutions (HNO_3, $HNO_3 > H_2SO_4$, H_2SO_4 and $H_2SO_4 > HNO_3$) as spray for three weeks. The weight of all stone samples was measured before and after the experiment. The weight loss in different tests (1 - 4) was 3.0, 3.8, 3.3 and 2.4%, respectively. The samples were further treated by *B. paramycoides* (BP) and *S. pevalekii* (BSP) culture to restore the damage caused by the acid-affected marble. Weight gain was observed in all samples ranging from 1.9 – 2.56%. Whereas the weight gain in *S.* pevalekii treated samples was 2.5, 3.1, 3.3 and 2.8%. The improvement in aesthetic restoration of the surface was observed and visualized using a DinoLite microscope. The adhesion property of the $CaCO_3$ precipitation induced by the bacteria was analyzed using sonication. The percentage loss in weight of marble samples in B (1-4) samples was 0.09, 0.1, 0.1, and 0.07, respectively. Likewise, the weight loss % in BSP (1-4) samples was 0.14, 0.12, 0.12, and 0.11, respectively. It is lower than the weight gained due to biomineralization activity. Thus, proving the efficiency of MICCP in restoring lost marble calcite. It gives an indirect approximation of surface material-substratum adhesion force. The root mean square roughness (RMS) was evaluated for marble samples using atomic force microscopy. The RMS roughness of the marble samples affected by different concentrations of acid HNO_3, $HNO_3 > H_2SO_4$, H_2SO_4 and $H_2SO_4 > HNO_3$ was 297.79, 283.74, 183.42, and 183.05 nm, respectively. The samples were later treated by using *B. paramycoides,* and RMS roughness evaluated for different sets was 138.9, 163.9, 43.26, and 42.1 nm, respectively. The samples treated by *S. pevalekii* showed roughness of 138.01, 133.83, 93.16 and 108.78, respectively. The samples were analyzed using FESEM-EDS, which proved precipitation of calcite and vaterite on the surface of the marble and filled the gaps caused by acid.

5.5 Conclusions and future scope

The current study focused on the potential application of *B. paramycoides* MD6 and *S. pevalekii* BDHKU 35101 in concrete and marble structures. The study suggests that MICCP mechanism of heterotrophic bacteria was more effective in improving the concrete properties than photoautotrophic bacteria. However, the calcite bound to marble surface was observed more in samples treated by photoautotrophic bacteria than heterotrophic bacteria. Comparing the interaction of both microbes, photoautotrophic culture has an advantage over ureolytic bacteria as it reduces the emission of ammonia in an environment which is a major concern.

This study also provided in depth knowledge of direct incorporation of bacteria and immobilization of bacteria in carrier material (metakaolin and fly ash). Indeed, immobilization of spores provided protection to the bacteria during mixing and casting of concrete mix. The results suggest both were effective MICCP techniques for improving the cementitious and marble structural properties. The study also concluded that CSL, an industrial by-product of the starch industry can be used an alternative to NB media, as an inexpensive nutritional source for growth of bacterial cells in the microbial treatment of concrete. It may contribute to the development of cost-effective and environmentally-friendly MICCP technology for field-scale applications in the future.

The promising outcomes of the current study will serve to facilitate the development of this microbial-based approach from the laboratory scale to commercial scale. It is necessary to conduct further research on the effectiveness of MICCP on actual concrete structures and marble monuments. Such studies should focus on minimizing costs and extending the service life of materials. It is important to examine the environmental and social advantages of using MICCP. It would be beneficial to investigate the role of bio-based self-healing mechanisms in varied climatic conditions. Ultimately, the development of specifications and test standards is necessary to evaluate the performance of microbes and self-healing materials in concrete and stone structures. Considering the fact and significant research on microbial self-healing have in the past two decades, it is anticipated that this technology will prove useful in practical application. However, several scientific and technical obstacles must first be overcome.

References

Abdelraouf, AE, Mohammed, TA (2013) Isolation, characterization and application of calcite producing bacteria from urea rich soils. J Adv Sci Eng Res 3:388–399.

Abel-santos E (2015) Endospores, Sporulation and Germination. (Second Edition) In Molecular medical microbiology. Academic Press 163 -178. https://doi.org/10.1016/B978-0-12-397169-2.00009-3

Abouhussien AA, Hassan AAA (2015) Optimizing the durability and service life of self-consolidating concrete containing metakaolin using statistical analysis. Constr Build Mater 76:297–306. https://doi.org/10.1016/j.conbuildmat.2014.12.010

Achal V, Kawasaki S (2016) Biogrout: A novel binding material for soil improvement and concrete repair. Front Microbiol 7:314. https://doi.org/10.3389/FMICB.2016.00314/BIBTEX

Achal V, Mukherjee A, Reddy MS (2010a) Biocalcification by *Sporosarcina pasteurii* using corn steep liquor as the nutrient source. Ind Biotechnol 6:170–174. https://doi.org/10.1089/ind.2010.6.170

Achal V, Mukherjee A, Reddy MS (2010b) Characterization of two urease-producing and calcifying *Bacillus* spp. isolated from cement. J Microbiol Biotechnol 20:1571–1576. https://doi.org/10.4014/jmb.1006.06032

Achal V, Mukherjee A, Reddy MS (2011a) Effect of calcifying bacteria on permeation properties of concrete structures. J Ind Microbiol Biotechnol 38:1229–1234. https://doi.org/10.1007/s10295-010-0901-8

Achal V, Mukherjee A, Reddy MS (2011b) Microbial concrete: Way to enhance the durability of building structures. J Mater Civ Eng 23:730–734. https://doi.org/10.1061/(ASCE)MT.1943-5533.0000159

Achal V, Pan X, Özyurt N (2011c) Improved strength and durability of fly ash-amended concrete by microbial calcite precipitation. Ecol Eng 37:554–559. https://doi.org/10.1016/j.ecoleng.2010.11.009

Adolphe JP, Loubière JF, Paradas J, Soleilhavoup F (1990) Procédé de traitement biologique d'une surface artificielle. European patent 90400G97.

Ahmad SSE, Elmahdy MAR, Elshami AA (2022) Bacterial sustainable concrete for repair and rehabilitation of structural cracks. J Sustain Cem Mater 12:5, 627-646. https://doi.org/10.1080/21650373.2022.2101156

Akhtar JN, Khan RA, Khan RA, Akhtar MN, Nejem JK (2022) Influence of natural zeolite and mineral additive on bacterial self-healing concrete: A Review. Civ Eng J 8:1069–1085. https://doi.org/10.28991/CEJ-2022-08-05-015

Alazhari M, Sharma T, Heath A, Cooper R, Paine K (2018) Application of expanded perlite encapsulated bacteria and growth media for self-healing concrete. Constr Build Mater 160:610–619 . https://doi.org/10.1016/j.conbuildmat.2017.11.086

Aletayeb SM, Jiryaei Sharahi M, Karimi A (2021) Dust stabilization using biological method against wind erosion. Arab J Geosci 14:1551. https://doi.org/10.1007/s12517-021-07775-z

Algaifi AH, Abu Bakar S, Rahman Mohd. Sam A, Ismail M, Razin Zainal Abidin A, Shahir S, Ali Hamood Altowayti W (2020) Insight into the role of microbial calcium carbonate and the factors involved in self-healing concrete. Constr Build Mater 254:119258. https://doi.org/10.1016/j.conbuildmat.2020.119258

Alghamri R, Kanellopoulos A, Al-Tabbaa A (2016) Impregnation and encapsulation of lightweight aggregates for self-healing concrete. Constr Build Mater 124:910–921 . https://doi.org/10.1016/j.conbuildmat.2016.07.143

Ali MF, Mukhtar H, Dufossé L (2023) Microbial calcite induction: a magic that fortifies and heals concrete. Int J Environ Sci Technol 20:1113–1134. https://doi.org/10.1007/s13762-022-03941-2

Altermann W, Kazmierczak J, Oren A, Wright DT (2006) Cyanobacterial calcification and its rock-building potential during 3.5 billion years of Earth history. Geobiology 4:147–166. https://doi.org/10.1111/j.1472-4669.2006.00076.x

Al-Thawadi S, Cord-Ruwisch R (2012) Calcium carbonate crystals formation by ureolytic bacteria isolated from australian soil and sludge. J Adv Sci Eng Res 2:12–26.

Althoey F, Zaid O, Arbili MM, Martínez-García R, Alhamami A, Shah HA, Yosri AM (2023) Physical, strength, durability and microstructural analysis of self-healing concrete: A systematic review. Case Stud Constr Mater 18:e01730. https://doi.org/10.1016/j.cscm.2022.e01730

Amiri A, Azima M, Bundur ZB (2018) Crack remediation in mortar via biomineralization: Effects of chemical admixtures on biogenic calcium carbonate. Constr Build Mater 190:317–325. https://doi.org/10.1016/j.conbuildmat.2018.09.083

Amiri A, Bundur ZB (2016) Application of biogenic calcium carbonate precipitation in developing self-healing cement-based mortar. In 12th International Congress on Advances in Civil Engineering (pp. 21-23).

Amiri A, Bundur ZB (2018) Use of corn-steep liquor as an alternative carbon source for biomineralization in cement-based materials and its impact on performance. Constr Build Mater 165:655–662. https://doi.org/10.1016/j.conbuildmat.2018.01.070

Amjad H, Arsalan Khushnood R, Ali Memon S (2023) Biomimetic robust self-healing of Bacillus Subtilis immobilized through sisal fiber for next-generation concrete infrastructure. Constr Build Mater 368:130299. https://doi.org/10.1016/j.conbuildmat.2023.130299

Anand K, Goyal S, Kaur N, Reddy MS (2022a) Viable FA based bacterial cells as sustainable solution for corrosion prevention in RC structures. Constr Build Mater 365:130056 . https://doi.org/10.2139/ssrn.4138214

Anand K, Goyal S, Reddy MS (2022b) Long-term viable SF immobilized bacterial cells as sustainable solution for crack healing in concrete. Structures 43:1342–1355. https://doi.org/10.1016/j.istruc.2022.07.056

Anand K, Goyal S, Reddy MS (2022c) Crack healing in concrete by microbially induced calcium carbonate precipitation as assessed through electromechanical impedance technique. Eur J Environ Civ Eng 27:1123-1143.

https://doi.org/10.1080/19648189.2022.2075470

Anand K, Goyal S, Reddy MS (2023) Development of field applicable remediation procedure using bio-cementitious grout for concrete cracks in variable orientations. J Build Eng Accepted:106024 . https://doi.org/10.1016/j.jobe.2023.106024

Anbu P, Kang CH, Shin YJ, So JS (2016) Formations of calcium carbonate minerals by bacteria and its multiple applications. Springerplus 5:250. https://doi.org/10.1186/s40064-016-1869-2

Anisuddin, S and Khaleeq, S (2005) Deterioration and rehabilitation of concrete structures in hot and arid regions. In: Khosrowshahi, F (Ed.), 21st Annual ARCOM Conference, 7-9 September 2005, SOAS, University of London. Association of Researchers in Construction Management, 1: 441-51.

Araújo M, Chatrabhuti S, Gurdebeke S, Alderete N, Van Tittelboom K, Raquez JM, Cnudde V, Van Vlierberghe S, De Belie N, Gruyaert E (2018) Poly(methyl methacrylate) capsules as an alternative to the proof-of-concept'' glass capsules used in self-healing concrete. Cem Concr Compos 89:260–271. https://doi.org/10.1016/j.cemconcomp.2018.02.015

Artesani A, Turo F Di, Zucchelli M, Traviglia A (2020) Recent advances in protective coatings for cultural heritage–an overview. Coatings 10:217. doi:10.3390/coatings10030217

Arun G (1989) Conservation and Restoration of Cultural Heritage. Pelagia Res Libr Adv Appl Sci Res 7:159–167

ASTM C1202 (2012) Standard Test Method for Electrical Indication of Concrete's Ability to Resist Chloride Ion Penetration. Am Soc Test Mater Int 1–8. https://doi.org/10.1520/C1202-10.2

ASTM C1437 (2015) Standard Test Method for Flow of Hydraulic Cement Mortar. Am Soc Test Mater Int 6–7.

ASTM C1585 (2013) Standard Test Method for Measurement of Rate of Absorption of Water by Hydraulic Cement Concretes. Am Soc Test Mater Int 41:1–6 . https://doi.org/10.1520/C1585-13.2

ASTM C597 (2016) Pulse Velocity Through Concrete. Am Soc Test Mater Int 04:3–6. https://doi.org/10.1520/C0597-16.2

ASTM C618 (2019) Standard specification for coal fly ash and raw or calcined natural pozzolan for use. Am Soc Test Mater Int 3–6.

ASTM C939 (2010) Standard Test Method for Flow of Grout for Preplaced-Aggregate Concrete (Flow Cone Method). Am Soc Test Mater Int 04:9–11.

ASTM C940 (2010) Standard Test Method for Expansion and Bleeding of Freshly Mixed Grouts for Preplaced-Aggregate Concrete in the Laboratory. Am Soc Test Mater Int 1–3. https://doi.org/10.1520/C0940-10a.2

Azima M, Bundur ZB (2019) Influence of *Sporasarcina pasteurii* cells on rheological properties of cement paste. Constr Build Mater 225:1086–1097 . https://doi.org/10.1016/j.conbuildmat.2019.07.132

Babakhani S, Fahmi A, Katebi H, A. Ouria, A. Majnouni-Toutakhane KG and, Kafil HS Non-sterile corn steep liquor a novel, cost effective and powerful culture media for *Sporosarcina pasteurii* cultivation for sand improvement. J Appl Microbiol 130: 1232–1244. https://doi.org/10.1111/jam.14866

Badogiannis EG, Sfikas IP, Voukia D V., Trezos KG, Tsivilis SG (2015) Durability of metakaolin Self-Compacting Concrete. Constr Build Mater 82:133–141. https://doi.org/10.1016/j.conbuildmat.2015.02.023

Baedecker PA, Reddy MM (1993) The erosion of carbonate stone by acid rain: Laboratory and field investigations. J Chem Educ 70:104–108. https://doi.org/10.1021/ed070p104

Baffoe E, Ghahremaninezhad A (2022) The effect of biomolecules on enzyme-induced calcium carbonate precipitation in cementitious materials. Constr Build Mater 345:128323. https://doi.org/10.1016/j.conbuildmat.2022.128323

Baglioni P, Chelazzi D, Giorgi R, Poggi G (2013) Colloid and materials science for the conservation of cultural heritage: Cleaning, consolidation, and deacidification. Langmuir 29:5110–5122. https://doi.org/10.1021/la304456n

Bai T, Liang Y, Li C, Jiang X, Li Y, Chen A, Wang H, Xu F, Peng C (2022) Application and validation of fly ash based geopolymer mortar as grouting material in porous asphalt concrete. Constr Build Mater 332:127154. https://doi.org/10.1016/j.conbuildmat.2022.127154

Bang SC, Min SH, Bang SS (2011) Application of microbiologically induced soil stabilization technique for dust suppression. Int J Geo-Eng 3:27-37.

Bansal R, Dhami NK, Mukherjee A, Reddy MS (2016) Biocalcification by halophilic bacteria for remediation of concrete structures in marine environment. J Ind Microbiol Biotechnol 43:1497–1505. https://doi.org/10.1007/s10295-016-1835-6

Barbhuiya S, Chow PL, Memon S (2015) Microstructure, hydration and nanomechanical properties of concrete containing metakaolin. Constr Build Mater 95:696–702. https://doi.org/10.1016/j.conbuildmat.2015.07.101

Başaran Bundur Z, Bae S, Kirisits MJ, Ferron RD (2017) Biomineralization in self-healing cement-based materials: Investigating the temporal evolution of microbial metabolic state and material porosity. J Mater Civ Eng 29:04017079. https://doi.org/10.1061/(asce)mt.1943-5533.0001838

Basaran Bundur Z, Kirisits MJ, Ferron RD (2015) Biomineralized cement-based materials: Impact of inoculating vegetative bacterial cells on hydration and strength. Cem Concr Res 67:237–245. https://doi.org/10.1016/j.cemconres.2014.10.002

Basaran Z (2013) Biomineralization in cement based materials: inoculation of vegetative cells.

Bazylinski DA (2003) Biologically controlled mineralization in prokaryotes. Rev Mineral Geochemistry 54:217–247 . https://doi.org/10.2113/0540217

Ben Chekroun K, Rodri C, Teresa Gonza M, Maria Arias J, Cultrone G, Rodri M (2004) Precipitation and growth morphology of calcium carbonate induced by *Myxococcus Xanthus*: Implications for recognition of bacterial carbonates. J Sediment Res 74:1527–1404. https://doi.org/10.1306/050504740868

Benedetti F, Kratter M, Atanasio P, Mura F, Beccaccioli M, Scifo J, Sarcina I di, Tomassetti

MC, Schneider K, Rossi M, Cemmi A, Nigro L, Rinaldi T (2023) Isolation of carbonatogenic bacteria for biorestoration. J Cult Herit 64:282–289. https://doi.org/10.1016/j.culher.2023.10.014

Benzerara K, Skouri-Panet F, Li J, Férard C, Gugger M, Laurent T, Couradeau E, Ragon M, Cosmidis J, Menguy N, Margaret-Oliver I, Tavera R, López-Garćia P, Moreira D (2014) Intracellular Ca-carbonate biomineralization is widespread in cyanobacteria. Proc Natl Acad Sci U S A 111:10933–10938. https://doi.org/10.1073/pnas.1403510111

Bergh JM van der, Miljević B, Šovljanski O, Vučetić S, Markov S, Ranogajec J, Bras A (2020) Preliminary approach to bio-based surface healing of structural repair cement mortars. Constr Build Mater 248:118557. https://doi.org/10.1016/j.conbuildmat.2020.118557

Bhaskar S, Anwar Hossain KM, Lachemi M, Wolfaardt G, Otini Kroukamp M (2017) Effect of self-healing on strength and durability of zeolite-immobilized bacterial cementitious mortar composites. Cem Concr Compos 82:23–33. https://doi.org/10.1016/j.cemconcomp.2017.05.013

Bhutange SP, Latkar M V., Chakrabarti T (2020) Studies on efficacy of biocementation of cement mortar using soil extract. J Clean Prod 274:122687. https://doi.org/10.1016/j.jclepro.2020.122687

Bibi S, Oualha M, Ashfaq MY, Suleiman MT, Zouari N (2018) Isolation, differentiation and biodiversity of ureolytic bacteria of Qatari soil and their potential in microbially induced calcite precipitation (MICP) for soil stabilization. RSC Adv 8:5854–5863. https://doi.org/10.1039/c7ra12758h

BIS: 8112 (2013) Specification for 43 grade ordinary Portland cement. Bur. Indian Stand 17:1-11.

Bishnoi S (2020) RILEM Bookseries Calcined clays for sustainable concrete proceedings of the 3rd international conference on calcined clays for sustainable concrete. Springer Nature 25.

Biswas J, Sharma K, Harris KK, Rajput Y (2013) Biodeterioration agents: Bacterial and fungal diversity dwelling in or on the pre-historic rock-paints of Kabra-pahad, India. Iran J

Microbiol 5:309–314. PMID: 24475341; PMCID: PMC3895572.

Borg RP, Cuenca E, Gastaldo Brac EM, Ferrara L (2017) Crack sealing capacity in chloride-rich environments of mortars containing different cement substitutes and crystalline admixtures. J. Sustain. Cem. 7:141–159. https://doi.org/10.1080/21650373.2017.1411297

Bouabidi ZB, El-Naas MH, Zhang Z (2019) Immobilization of microbial cells for the biotreatment of wastewater: A review. Environ Chem Lett 17:241–257. https://doi.org/10.1007/s10311-018-0795-7

Bras A, Henriques FMA (2009) The influence of the mixing procedures on the optimization of fresh grout properties. Mater Struct Constr 42:1423–1432. https://doi.org/10.1617/s11527-008-9461-z

Bras A, Henriques FMA, Cidade MT (2010) Effect of environmental temperature and fly ash addition in hydraulic lime grout behaviour. Constr Build Mater 24:1511–1517. https://doi.org/10.1016/j.conbuildmat.2010.02.001

Bundeleva IA, Shirokova LS, Pokrovsky OS, Bénézeth P, Ménez B, Gérard E, Balor S (2014) Experimental modeling of calcium carbonate precipitation by cyanobacterium *Gloeocapsa* sp. Chem Geol 374–375:44–60. https://doi.org/10.1016/j.chemgeo.2014.03.007

Burbank MB, Weaver TJ, Williams BC, Crawford RL (2012) Urease Activity of ureolytic bacteria isolated from six soils in which calcite was precipitated by indigenous bacteria. Geomicrobiol J 29:389–395. https://doi.org/10.1080/01490451.2011.575913

Camaiti M, Bugani S, Bernardi E, Morselli L, Matteini M (2007) Effects of atmospheric NOx on biocalcarenite coated with different conservation products. Appl Geochemistry 22:1248–1254. https://doi.org/10.1016/j.apgeochem.2007.03.035

Cappelletti G, Fermo P (2016) Hydrophobic and superhydrophobic coatings for limestone and marble conservation. In Smart Composite Coatings and Membranes (pp. 421-452). Woodhead Publishing. https://doi.org/10.1016/B978-1-78242-283-9.00015-4

Cappelletti G, Fermo P, Camiloni M (2015) Smart hybrid coatings for natural stones

conservation. Prog Org Coatings 78:511–516. https://doi.org/10.1016/j.porgcoat.2014.05.029

Cardoso R, Pedreira R, Duarte Sofia OD, Monteiro GA (2020) About calcium carbonate precipitation on sand biocementation. Eng Geol 282:105726. https://doi.org/10.1016/j.enggeo.2020.105726

Castanier S, Le Métayer-Levrel G, Orial G, Loubière J-F, Perthuisot J-P (2000). Bacterial carbonatogenesis and applications to preservation and restoration of historic property. In: Ciferri, O., Tiano, P., Mastromei, G. (eds) Of Microbes and Art. Springer, Boston, MA. https://doi.org/10.1007/978-1-4615-4239-1_14

Castenholz RW, Wilmotte A, Herdman M, Rippka R, Waterbury JB, Iteman I, Hoffmann L (2001) Phylum BX. Cyanobacteria. In: Bergey's Manual® of Systematic Bacteriology. Springer New York, pp 473–599. https://doi.org/10.1007/978-0-387-21609-6_27

Castro-Alonso MJ, Montañez-Hernandez LE, Sanchez-Muñoz MA, Macias Franco MR, Narayanasamy R, Balagurusamy N (2019) Microbially induced calcium carbonate precipitation (MICP) and its potential in bioconcrete: Microbiological and molecular concepts. Front Mater 6:126. https://doi.org/10.3389/fmats.2019.00126

Celik F, Canakci H (2015) An investigation of rheological properties of cement-based grout mixed with rice husk ash (RHA). Constr Build Mater 91:187–194. https://doi.org/10.1016/j.conbuildmat.2015.05.025

Chandra S, Bhattacharya S, Pandit S, Banerjee S, Roy A, Rai AK (2023) Cyanobacteria as an eco-friendly bioresource for EPS production with crack healing capacity in concrete. Biocatal Agric Biotechnol 54:102909. https://doi.org/10.1016/j.bcab.2023.102909

Charpe AU, Bhutange SP, Latkar M V, Chakrabarti T (2021) Studies on Biocementation of Mortar and Identification of Causative Bacteria. Arab J Sci Eng 46:4563–4576. https://doi.org/10.1007/s13369-020-05040-1

Checinska A, Paszczynski A, Burbank M (2015) *Bacillus* and other spore-forming genera: Variations in responses and mechanisms for survival. Annu Rev Food Sci Technol 6:351–369. https://doi.org/10.1146/annurev-food-030713-092332

Chen H, Qian C, Huang H (2016) Self-healing cementitious materials based on bacteria and nutrients immobilized respectively. Constr Build Mater 126:297–303. https://doi.org/10.1016/j.conbuildmat.2016.09.023

Choi SG, Wang K, Chu J (2016) Properties of biocemented, fiber reinforced sand. Constr Build Mater 120:623–629. https://doi.org/10.1016/j.conbuildmat.2016.05.124

Choi SG, Wang K, Wen Z, Chu J (2017) Mortar crack repair using microbial induced calcite precipitation method. Cem Concr Compos 83:209–221 . https://doi.org/10.1016/j.cemconcomp.2017.07.013

Choi SJ, Lee SS, Monteiro PJM (2012) Effect of fly ash fineness on temperature rise, setting, and strength development of mortar. J Mater Civ Eng 24:499–505. https://doi.org/10.1061/(asce)mt.1943-5533.0000411

Christie G, Setlow P (2020) *Bacillus* spore germination: Knowns, unknowns and what we need to learn. Cell Signal 74:109729. https://doi.org/10.1016/j.cellsig.2020.109729

Chu J, Stabnikov V, Ivanov V (2012) Microbially induced calcium carbonate precipitation on surface or in the bulk of soil. Geomicrobiol J 29:544–549. https://doi.org/10.1080/01490451.2011.592929

Chuo SC, Mohamed SF, Setapar SHM, Ahmad A, Jawaid M, Wani WA, Yaqoob AA, Ibrahim MNM (2020) Insights into the current trends in the utilization of bacteria for microbially induced calcium carbonate precipitation. Materials (Basel) 13:4993. https://doi.org/10.3390/ma13214993

Çınar M, Karpuzcu M, Çanakcı H (2019) Effect of waste marble powder and fly ash on the rheological characteristics of cement based grout. Civ Eng J 5:777–788. https://doi.org/10.28991/cej-2019-03091287

Çınar M, Karpuzcu M, Çanakcı H (2020) The measurement of fresh properties of cement-based grout containing waste marble powder. Meas J Int Meas Confed 150:106833. https://doi.org/10.1016/j.measurement.2019.07.061

Clifton JR (1988) Deterioration of Concrete. In: Beedle, L.S. (eds) Second Century of the

Skyscraper. Springer, Boston, MA (pp. 959-963). https://doi.org/10.1007/978-1-4684-6581-5_81

Costa OYA, Raaijmakers JM, Kuramae EE (2018) Microbial extracellular polymeric substances: Ecological function and impact on soil aggregation. Front Microbiol 9:1636. https://doi.org/10.3389/fmicb.2018.01636

Cox G, James JM, Leggett KEA, Armstrong R, Osborne L (1989) Cyanobacterially deposited speleothems: Subaerial stromatolites. Geomicrobiol J 7:245–252. https://doi.org/10.1080/01490458909377870

Cuccurullo A, Gallipoli D, Bruno AW, Augarde C, Hughes P, La Borderie C (2022) Earth stabilisation via carbonate precipitation by plant-derived urease for building applications. Geomech Energy Environ 30:100230. https://doi.org/10.1016/j.gete.2020.100230

Cui M, Liu Y, Zhang J (2020) Sulfamethoxazole and tetracycline induced alterations in biomass, photosynthesis, lipid productivity, and proteomic expression of *Synechocystis* sp. PCC 6803. Environ Sci Pollut Res 27:30437–30447. https://doi.org/10.1007/s11356-020-09327-6

Daskalakis MI, Magoulas A, Kotoulas G, Katsikis I, Bakolas A, Karageorgis AP, Mavridou A, Doulia D, Rigas F (2014) *Cupriavidus metallidurans* biomineralization ability and its application as a bioconsolidation enhancer for ornamental marble stone. Appl Microbiol Biotechnol 98:6871–6883. https://doi.org/10.1007/s00253-014-5753-0

Daskalakis MI, Rigas F, Bakolas A, Magoulas A, Kotoulas G, Katsikis I, Karageorgis AP, Mavridou A (2015) Vaterite bio-precipitation induced by *Bacillus pumilus* isolated from a solutional cave in Paiania, Athens, Greece. Int Biodeterior Biodegrad 99:73–84. https://doi.org/10.1016/j.ibiod.2014.12.005

Datta S, Christena LR, Rajaram YRS (2013) Enzyme immobilization: an overview on techniques and support materials. 3 Biotech 3:1–9. https://doi.org/10.1007/s13205-012-0071-7

De Belie N (2016) Application of bacteria in concrete: a critical evaluation of the current status. RILEM Tech Lett 1:56. https://doi.org/10.21809/rilemtechlett.2016.14

De Belie N, Gruyaert E, Al-Tabbaa A, Antonaci P, Baera C, Bajare D, Darquennes A, Davies R, Ferrara L, Jefferson T, Litina C, Miljevic B, Otlewska A, Ranogajec J, Roig-Flores M, Paine K, Lukowski P, Serna P, Tulliani JM, Vucetic S, Wang J, Jonkers HM (2018) A Review of Self-Healing Concrete for Damage Management of Structures. Adv Mater Interfaces 5:1800074. https://doi.org/10.1002/admi.201800074

De Belie N, Wang J (2015) Bacteria-based repair and self-healing of concrete. J Sustain Cem Based Mater, 5:35-56. https://doi.org/10.1080/21650373.2015.1077754

De Muynck W, Cox K, Belie N De, Verstraete W (2008) Bacterial carbonate precipitation as an alternative surface treatment for concrete. Constr Build Mater 22:875–885. https://doi.org/10.1016/j.conbuildmat.2006.12.011

De Muynck W, Leuridan S, Van Loo D, Verbeken K, Cnudde V, De Belie N, Verstraete W (2011) Influence of pore structure on the effectiveness of a biogenic carbonate surface treatment for limestone conservation. Appl Environ Microbiol 77:6808–6820. https://doi.org/10.1128/AEM.00219-11

De Muynck W, Verbeken K, De Belie N, Verstraete W (2010) Influence of urea and calcium dosage on the effectiveness of bacterially induced carbonate precipitation on limestone. Ecol Eng 36:99–111. https://doi.org/10.1016/j.ecoleng.2009.03.025

De Wever A, Benzerara K, Coutaud M, Caumes G, Poinsot M, Skouri-Panet F, Laurent T, Duprat E, Gugger M (2019) Evidence of high Ca uptake by cyanobacteria forming intracellular $CaCO_3$ and impact on their growth. Geobiology 17:676–690. https://doi.org/10.1111/gbi.12358

DeJong JT, Mortensen BM, Martinez BC, Nelson DC (2010) Bio-mediated soil improvement. Ecol Eng 36:197–210. https://doi.org/10.1016/j.ecoleng.2008.12.029

Delić D, Stajković-Srbinović O, Buntić A (2022) Hazards and Usability of Coal Fly Ash. In: Saljnikov, E., Mueller, L., Lavrishchev, A., Eulenstein, F. (eds) Advances in understanding soil degradation. Innovations in landscape research. Springer, Cham. https://doi.org/10.1007/978-3-030-85682-3_26

Dhami NK, Reddy MS, Mukherjee A (2013a) *Bacillus megaterium* mediated mineralization of

calcium carbonate as biogenic surface treatment of green building materials. World J Microbiol Biotechnol 29:2397–2406. https://doi.org/10.1007/s11274-013-1408-z

Dhami NK, Reddy MS, Mukherjee A (2014) Synergistic role of bacterial urease and carbonic anhydrase in carbonate mineralization. Appl Biochem Biotechnol 172:2552–2561. https://doi.org/10.1007/s12010-013-0694-0

Dhami NK, Reddy MS, Mukherjee A (2016) Significant indicators for biomineralisation in sand of varying grain sizes. Constr Build Mater 104:198–207. https://doi.org/10.1016/j.conbuildmat.2015.12.023

Dhami NK, Reddy MS, Mukherjee MS (2013b) Biomineralization of calcium carbonates and their engineered applications: A review. Front Microbiol 4:314. https://doi.org/10.3389/fmicb.2013.00314

Dinarvand P, Rashno A (2021) Review of the potential application of bacteria in self-healing and the improving properties of concrete/mortar. J Sustain Cem Mater 11:250–271. https://doi.org/10.1080/21650373.2021.1936268

Dittrich M, Sibler S (2010) Calcium carbonate precipitation by cyanobacterial polysaccharides. Geol Soc Spec Publ 336:51–63. https://doi.org/10.1144/SP336.4

Do TM, Laue J, Mattsson H, Jia Q (2023) Excess pore water pressure generation in fine granular materials under undrained cyclic triaxial loading. Int J Geo-Engineering 14:8. https://doi.org/10.1186/s40703-023-00185-y

Douglas S, Beveridge TJ (1998) Mineral formation by bacteria in natural microbial communities. FEMS Microbiol Ecol 26:79–88. https://doi.org/10.1016/S0168-6496(98)00027-0

Duo L, Kan-liang T, Hui-li Z, Yu-yao W, Kang-yi N, Shi-can Z (2018) Experimental investigation of solidifying desert aeolian sand using microbially induced calcite precipitation. Constr Build Mater 172:251–262. https://doi.org/10.1016/j.conbuildmat.2018.03.255

Dzionek A, Wojcieszyńska D, Guzik U (2016) Natural carriers in bioremediation: A review.

Electron J Biotechnol 23:28–36. https://doi.org/10.1016/j.ejbt.2016.07.003

Ehrlich HL (1999) Microbes as geologic agents: Their role in mineral formation. Geomicrobiol J 16:135–153. https://doi.org/10.1080/014904599270659

El-Diadamony H, Amer AA, Sokkary TM, El-Hoseny S (2018) Hydration and characteristics of metakaolin pozzolanic cement pastes. HBRC J 14:150–158. https://doi.org/10.1016/j.hbrcj.2015.05.005

Elmi F, Etemadifar Z, Emtiazi G (2023) Biosynthesis of calcite nanocrystal by a novel polyextremophile bhargavaea cecembensis-related strain isolated from sandy soil. Microb Ecol 85:698–707. https://doi.org/10.1007/s00248-022-01977-y

Ercole C, Bozzelli P, Altieri F, Cacchio P, Del Gallo M, al VC et (2010) Extracellular polysaccharides (EPS) and capsular polysaccharides (CPS) isolated from calcifying bacteria and their utilization as a limestone consolidant. J Biotechnol 150:211–212. https://doi.org/10.1016/j.jbiotec.2010.09.026

Erşan YÇ, Da Silva FB, Boon N, Verstraete W, De Belie N (2015) Screening of bacteria and concrete compatible protection materials. Constr Build Mater 88:196–203. https://doi.org/10.1016/j.conbuildmat.2015.04.027

Erşan YÇ, Verbruggen H, De Graeve I, Verstraete W, De Belie N, Boon N (2016) Nitrate reducing $CaCO_3$ precipitating bacteria survive in mortar and inhibit steel corrosion. Cem Concr Res 83:19–30. https://doi.org/10.1016/j.cemconres.2016.01.009

Erşan YÇ, Wang J, Fraeye D, Boon N, Belie N De (2020) Surface consolidation of maastricht limestone by means of *Bacillus sphaericus* under varying treatment conditions. J Sustain Cem Mater 32: 04020342. https://doi.org/10.1061/(ASCE)MT.1943-5533.0003447

Estroff LA (2008) Introduction: biomineralization. Chem rev 108: 4329-4331. https://doi.org/10.1021/cr8004789

Fan YF, Hu ZQ, Zhang YZ, Liu JL (2010) Deterioration of compressive property of concrete under simulated acid rain environment. Constr Build Mater 24:1975–1983. https://doi.org/10.1016/j.conbuildmat.2010.04.002

Farajnia A, Shafaat A, Farajnia S, Sartipipour M, Khodadadi Tirkolaei H (2022) The efficiency of ureolytic bacteria isolated from historical adobe structures in the production of bio-bricks. Constr Build Mater 317:125868. https://doi.org/10.1016/j.conbuildmat.2021.125868

Feng C, Zong X, Cui B, Guo H, Zhang W, Zhu J (2022) Application of carrier materials in self-healing cement-based materials based on microbial-induced mineralization. Crystals 12:797. https://doi.org/10.3390/cryst12060797

Feng J, Chen B, Sun W, Wang Y (2021a) Microbial induced calcium carbonate precipitation study using Bacillus subtilis with application to self-healing concrete preparation and characterization. Constr Build Mater 280:122460. https://doi.org/10.1016/j.conbuildmat.2021.122460

Feng J, Chen B, Sun W, Wang Y (2021b) Microbial induced calcium carbonate precipitation study using *Bacillus subtilis* with application to self-healing concrete preparation and characterization. Constr Build Mater 280:122460. https://doi.org/10.1016/j.conbuildmat.2021.122460

Feng J, Chen B, Sun W, Wang Y (2021c) Microbial induced calcium carbonate precipitation study using *Bacillus subtilis* with application to self-healing concrete preparation and characterization. Constr Build Mater 280:122460. https://doi.org/10.1016/j.conbuildmat.2021.122460

Fermo P, Cappelletti G, Cozzi N, Padeletti G, Kaciulis S, Brucale M, Merlini M (2014) Hydrophobizing coatings for cultural heritage. A detailed study of resin/stone surface interaction. Appl Phys A Mater Sci Process 116:341–348. https://doi.org/10.1007/s00339-013-8127-z

Ferris FG, Phoenix V, Fujita Y, Smith RW (2004) Kinetics of calcite precipitation induced by ureolytic bacteria at 10 to 20°C in artificial groundwater. Geochim Cosmochim Acta 68:1701–1710. https://doi.org/10.1016/S0016-7037(03)00503-9

Fitri L, Aulia TB, Fauzi A, Kamil GA (2023) Characterization and screening of urease activity of ureolytic bacteria from landfills soil in Banda Aceh, Indonesia. Biodiversitas 24:910–915. https://doi.org/10.13057/biodiv/d240229

Fronczyk J, Janek M, Szeląg M, Pyzik A, Franus W (2023) Immobilization of (bio-)healing agents for self-healing concrete technology: Does it really ensure long-term performance? Compos Part B Eng 266:110997. https://doi.org/10.1016/j.compositesb.2023.110997

Fujita M, Nakashima K, Achal V, Kawasaki S (2017) Whole-cell evaluation of urease activity of Pararhodobacter sp. isolated from peripheral beachrock. Biochem Eng J 124:1–5 . https://doi.org/10.1016/j.bej.2017.04.004

Gao M, Guo J, Cao H, Wang H, Xiong X, Krastev R, Nie K, Xu H, Liu L (2020a) Immobilized bacteria with pH-response hydrogel for self-healing of concrete. J Environ Manage 261:110225. https://doi.org/10.1016/j.jenvman.2020.110225

Gao M, Guo J, Cao H, Wang H, Xiong X, Krastev R, Nie K, Xu H, Liu L (2020b) Immobilized bacteria with pH-response hydrogel for self-healing of concrete. J Environ Manage 261:110225. https://doi.org/10.1016/j.jenvman.2020.110225

Garg S, Kaur P, Pandit M, Fareeduddin, Kaur G, Kamboj A, Thakur SN (2019) Makrana Marble: a Popular Heritage Stone Resource from NW India. Geoheritage 11:909–925. https://doi.org/10.1007/s12371-018-00343-0

Gaylarde CC, Morton LHG, Loh K, Shirakawa MA (2011) Biodeterioration of external architectural paint films - A review. Int Biodeterior Biodegrad 65:1189–1198. https://doi.org/10.1016/j.ibiod.2011.09.005

Ghahremani G, Bagheri A, Zanganeh H (2023) The effect of size and shape of pores on the prediction model of compressive strength of foamed concrete. Constr Build Mater 371:130720. https://doi.org/10.1016/j.conbuildmat.2023.130720

Gleaton J, Lai Z, Xiao R, Chen Q, Zheng Y (2019) Microalga-induced biocementation of martian regolith simulant: Effects of biogrouting methods and calcium sources. Constr Build Mater 229:116885. https://doi.org/10.1016/j.conbuildmat.2019.116885

Golubic S, Seong-Joo L (1999) Early cyanobacterial fossil record: Preservation, palaeoenvironments and identification. Eur J Phycol 34:339–348. https://doi.org/10.1080/09670269910001736402

Gomez MG, Martinez BC, Dejong JT, Hunt CE, Devlaming LA, Major DW, Dworatzek SM (2015) Field-scale bio-cementation tests to improve sands. Proc Inst Civ Eng Gr Improv 168:206–216. https://doi.org/10.1680/grim.13.00052

González Á, Parraguez A, Corvalán L, Correa N, Castro J, Stuckrath C, González M (2020) Evaluation of portland and pozzolanic cement on the self-healing of mortars with calcium lactate and bacteria. Constr Build Mater 257:119558. https://doi.org/10.1016/j.conbuildmat.2020.119558

Górecka E, Jastrzębska M (2011) Review article: Immobilization techniques and biopolymer carriers. Biotechnol Food Sci 75:65–86.

Gulin LB, Schwantes-Cezario N, Florian M (2021) Viability of *Bacillus subtilis* immobilization using silica gel for self-healing of cement based materials. Int J Adv Eng Res Sci 8:1-10. https://doi.org/10.22161/ijaers.86.1

Gupta S, Kua HW, Pang SD (2018) Healing cement mortar by immobilization of bacteria in biochar: An integrated approach of self-healing and carbon sequestration. Cem Concr Compos 86:238–254. https://doi.org/10.1016/j.cemconcomp.2017.11.015

Gupta S, Pang SD, Kua HW (2017) Autonomous healing in concrete by bio-based healing agents – A review. Constr Build Mater 146:419–428. https://doi.org/10.1016/j.conbuildmat.2017.04.111

Hall TA (1999) BioEdit: a user-friendly biological sequence alignment editor and analysis program for Windows 95/98/NT. In *Nucleic acids symposium series* (Vol. 41, pp. 95-98).

Hamamura N, Olson SH, Ward DM, Inskeep WP (2006) Microbial population dynamics associated with crude-oil biodegradation in diverse soils. Appl Environ Microbiol 72:6316–6324 . https://doi.org/10.1128/AEM.01015-06

Han Z, Meng R, Yan H, Zhao H, Han M, Zhao Y, Sun B, Sun Y, Wang J, Zhuang D, Li W, Lu L (2017a) Calcium carbonate precipitation by *Synechocystis* sp. PCC6803 at different Mg/Ca molar ratios under the laboratory condition. Carbonates and Evaporites 32:561–575. https://doi.org/10.1007/s13146-016-0322-5

Han Z, Yan H, Zhou S, Zhao H, Zhang Y, Zhang N, Yao C, Zhao L, Han C (2013) Precipitation of calcite induced by *Synechocystis* sp. PCC6803. World J Microbiol Biotechnol 29:1801–1811. https://doi.org/10.1007/s11274-013-1341-1

Han Z, Zhao Y, Yan H, Zhao H, Han M, Sun B, Meng R, Zhuang D, Li D, Gao W, Du S, Wang X, Fan K, Hu W, Zhang M (2017b) The Characterization of Intracellular and Extracellular Biomineralization Induced by *Synechocystis* sp. PCC6803 Cultured under Low Mg/Ca Ratios Conditions. Geomicrobiol J 34:362–373. https://doi.org/10.1080/01490451.2016.1197986

Han Z, Zhuang D, Yan H, Zhao H, Sun B, Li D, Sun Y, Hu W, Xuan Q, Chen J, Xiu Y (2017c) Thermogravimetric and kinetic analysis of thermal decomposition characteristics of microbial calcites induced by cyanobacteria *Synechocystis* sp. PCC6803. J Therm Anal Calorim 127:1371–1379. https://doi.org/10.1007/s10973-016-6026-1

Hasan K, Karim A, Islam MT, Ali M Bin, Rahman MT, Rahman MM, Yahaya FM (2023) A review of the mechanical properties and durability of concrete containing recycled seashells as a partial cement replacement. J Mater Cycles Waste Manag 25:3192–3216. https://doi.org/10.1007/s10163-023-01795-5

Haynes H, O'Neill R, Neff M, Kumar Mehta R (2008) Salt weathering distress on concrete exposed to sodium sulfate environment. ACI Mater J 105:35–43. https://doi.org/10.14359/19205

Heidari M, Torabi-Kaveh M, Mohseni H (2017) Assessment of the Effects of Freeze–Thaw and Salt Crystallization Ageing Tests on Anahita Temple Stone, Kangavar, West of Iran. Geotech Geol Eng 35:121–136. https://doi.org/10.1007/s10706-016-0090-y

Heidrich C, Feuerborn H, Weir A (2013) Coal combustion products: a global perspective. 2013 World of Coal Ash (WOCA) Conference. Lexington, KY (Vol. 22, p. 25).

Helmi FM, Elmitwalli HR, Elnagdy SM, El-Hagrassy AF (2016) Calcium carbonate precipitation induced by ureolytic bacteria *Bacillus licheniformis*. Ecol Eng 90:367–371. https://doi.org/10.1016/j.ecoleng.2016.01.044

Hernández EF, De Cano-Barrita PFJ, Torres-Acosta AA (2016) Influence of cactus mucilage

and marine brown algae extract on the compressive strength and durability of concrete. Mater Constr 66: e074. https://doi.org/10.3989/mc.2016.07514

Heveran CM, Williams SL, Qiu J, Artier J, Hubler MH, Cook SM, Cameron JC, Srubar W V. (2020) Biomineralization and Successive Regeneration of Engineered Living Building Materials. Matter 2:481–494. https://doi.org/10.1016/j.matt.2019.11.016

Hu Y Bin, Wolthers M, Wolf-Gladrow DA, Nehrke G (2015) Effect of pH and phosphate on calcium carbonate polymorphs precipitated at near-freezing temperature. Cryst Growth Des 15:1596–1601. https://doi.org/10.1021/cg500829p

Hu Y, Liu W, Zhang Q, Hu X (2022) Investigation on mineralization performance and spore germination conditions of calcium carbonate mineralizing bacteria. Mater Res Express 9:065403. https://doi.org/10.1088/2053-1591/ac7709

Huber B, Hilbig H, Drewes JE, Müller E (2017) Evaluation of concrete corrosion after short- and long-term exposure to chemically and microbially generated sulfuric acid. Cem Concr Res 94:36–48 . https://doi.org/10.1016/j.cemconres.2017.01.005

Hueck HJ (2001) The biodeterioration of materials - An appraisal. Int. Biodeterior. Biodegrad. 48:5–11. https://doi.org/10.1016/S0964-8305(01)00061-0

Hussey MA (2013) Endospore Stain Protocol. Am Soc Microbiol 1–11.

Iijima H, Nakaya Y, Kuwahara A, Hirai MY (2015) Seawater cultivation of freshwater cyanobacterium *Synechocystis* sp. PCC 6803 drastically alters amino acid composition and glycogen metabolism. 6:326. https://doi.org/10.3389/fmicb.2015.00326

Imran M Al, Nakashima K, Evelpidou N, Kawasaki S (2019) Factors affecting the urease activity of native ureolytic bacteria isolated from coastal areas. Geomech Eng 17:421–427. https://doi.org/10.12989/gae.2019.17.5.421

IS 10262 (2019) Indian Standard, Concrete Mix Proportioning – Guidelines (Second Revision). Bur Indian Stand 1–42.

IS 3812: Part 1 (2013) specification (2013) Pulverized Fuel Ash - Specification: Part 1 For Use as Pozzolana in Cement, Cement Mortar and Concrete. Bur Indian Stand 1–12.

IS 383 (2016) Specification for Coarse and Fine Aggregates From Natural Sources for Concrete. Bur. Indian Stand 1–21.

IS 4031 (Part 6) (2005) Methods Of Physical Tests For Hydraulic Cement Part 6 Determination Of Compressive Strength Of Hydraulic Cement Other Than Masonry Cement (First Revision). Bur Indian Stand 1–3.

IS 516 (2021) Hardened Concrete - Methods of Test - Part 1 Testing of Strength of Hardened Concrete -Section 1 Compressive, Flexural and Split Tensile Strength. Bur Indian Stand 1–20.

IS 5513 (1996) Vicat's Apparatus - Specification. Bur Indian Stand 1–12.

Islam MM, Hoque N, Islam M, Ibney Gias I (2022) An experimental study on the strength and crack healing performance of *E. coli* bacteria-induced microbial concrete. Adv Civ Eng 2022:3060230. https://doi.org/10.1155/2022/3060230

Ivanov V, Stabnikov V, Kawasaki S (2019) Ecofriendly calcium phosphate and calcium bicarbonate biogrouts. J Clean Prod 218:328–334. https://doi.org/10.1016/j.jclepro.2019.01.315

Jadhav UU, Lahoti M, Chen Z, Qiu J, Cao B, Yang EH (2018) Viability of bacterial spores and crack healing in bacteria-containing geopolymer. Constr Build Mater 169:716–723. https://doi.org/10.1016/j.conbuildmat.2018.03.039

Jafarnia MS, Khodadad Saryazdi M, Moshtaghioun SM (2020) Use of bacteria for repairing cracks and improving properties of concrete containing limestone powder and natural zeolite. Constr Build Mater 242:118059. https://doi.org/10.1016/j.conbuildmat.2020.118059

Jan SU, Zada S, Rafiq M, Sajjad W, Khan MA, Hasan F (2022) Calcium carbonate precipitation by cave bacteria isolated from Kashmir Cave, Khyber Pakhtunkhwa, Pakistan. Microscopy Research and Technique 1–12. https://doi.org/10.1002/jemt.24105

Jang I, Son D, Kim W, Park W, Yi C (2020) Effects of spray-dried co-cultured bacteria on cement mortar. Constr Build Mater 243:118206.

https://doi.org/10.1016/j.conbuildmat.2020.118206

Jansson C, Northen T (2010) Calcifying cyanobacteria-the potential of biomineralization for carbon capture and storage. Curr Opin Biotechnol 21:365–371. https://doi.org/10.1016/j.copbio.2010.03.017

Jarwar MA, Buey P, Sanz-montero ME, Dumontet S, Chianese E, Pasquale V (2023) Co-Precipitation of Cd, Cr, Pb, Zn, and carbonates using *Vibrio harveyi* strain isolated from mediterranean seaiment sediment. Minerals 13:627. https://doi.org/10.3390/min13050627

Jiang L, Han Q, Wang W, Zhang Y, Lu W, Li Z (2023) A sugar-coated microbial agent for self-healing cracks in concrete. J Build Eng 66:105890. https://doi.org/10.1016/j.jobe.2023.105890

Jiang L, Jia G, Jiang C, Li Z (2020) Sugar-coated expanded perlite as a bacterial carrier for crack-healing concrete applications. Constr Build Mater 232:117222. https://doi.org/10.1016/j.conbuildmat.2019.117222

Jiang L, Xue X, Zhang W, Yang J, Zhang H, Li Y, Zhang R, Zhang Z, Xu L, Qu J, Song J, Qin J (2015) The investigation of factors affecting the water impermeability of inorganic sodium silicate-based concrete sealers. Constr Build Mater 93:729–736. https://doi.org/10.1016/j.conbuildmat.2015.06.001

Jie P, Zhiming L (2019) Influence of temperature on microbially induced calcium carbonate precipitation for soil treatment. PLoS One 14: e0218396. https://doi.org/10.1371/journal.pone.0218396

Jimenez-Lopez C, Jroundi F, Pascolini C, Rodriguez-Navarro C, Piñar-Larrubia G, Rodriguez-Gallego M, González-Muñoz MT (2008) Consolidation of quarry calcarenite by calcium carbonate precipitation induced by bacteria activated among the microbiota inhabiting the stone. Int Biodeterior Biodegrad 62:352–363. https://doi.org/10.1016/j.ibiod.2008.03.002

Jin Q, Zhou M, Zhu L, Liu H, Zhu F (2022) Microbial growth and calcium carbonate nucleation properties in mineral admixtures. Adv Mater Sci Eng 2022:2177630. https://doi.org/10.1155/2022/2177630

Jongvivatsakul P, Janprasit K, Nuaklong P, Pungrasmi W, Likitlersuang S (2019) Investigation of the crack healing performance in mortar using microbially induced calcium carbonate precipitation (MICP) method. Constr Build Mater 212:737–744. https://doi.org/10.1016/j.conbuildmat.2019.04.035

Jonkers HM, Schlangen HEJG (2007) Crack repair by concrete immobilized bacteria. In Proceedings of the first international conference on self-healing materials. Springer (pp. 1-7).

Jonkers HM, Thijssen A, Muyzer G, Copuroglu O, Schlangen E (2010) Application of bacteria as self-healing agent for the development of sustainable concrete. Ecol Eng 36:230–235. https://doi.org/10.1016/j.ecoleng.2008.12.036

Joshi S, Goyal S, Mukherjee A, Reddy MS (2017) Microbial healing of cracks in concrete: a review. J Ind Microbiol Biotechnol 44:1511–1525. https://doi.org/10.1007/s10295-017-1978-0

Joshi S, Goyal S, Reddy MS (2018a) Influence of nutrient components of media on structural properties of concrete during biocementation. Constr Build Mater 158:601–613. https://doi.org/10.1016/j.conbuildmat.2017.10.055

Joshi S, Goyal S, Reddy MS (2018b) Corn steep liquor as a nutritional source for biocementation and its impact on concrete structural properties. J Ind Microbiol Biotechnol 45:657–667. https://doi.org/10.1007/s10295-018-2050-4

Joshi S, Goyal S, Reddy MS (2020) Influence of biogenic treatment in improving the durability properties of waste amended concrete: A review. Constr Build Mater 263:120170. https://doi.org/10.1016/j.conbuildmat.2020.120170

Joshi S, Goyal S, Reddy MS (2021) Bio-consolidation of cracks with fly ash amended biogrouting in concrete structures. Constr Build Mater 300:124044. https://doi.org/10.1016/j.conbuildmat.2021.124044

Jroundi F, Gómez-Suaga P, Jimenez-Lopez C, González-Muñoz MT, Fernandez-Vivas MA (2012) Stone-isolated carbonatogenic bacteria as inoculants in bioconsolidation treatments for historical limestone. Sci Total Environ 425:89–98.

https://doi.org/10.1016/j.scitotenv.2012.02.059

Jroundi F, Schiro M, Ruiz-Agudo E, Elert K, Martín-Sánchez I, González-Muñoz MT, Rodriguez-Navarro C (2017) Protection and consolidation of stone heritage by self-inoculation with indigenous carbonatogenic bacterial communities. Nat Commun 8:279. https://doi.org/10.1038/s41467-017-00372-3

Justo-Reinoso I, Heath A, Gebhard S, Paine K (2021) Aerobic non-ureolytic bacteria-based self-healing cementitious composites: A comprehensive review. J Build Eng 42:102834. https://doi.org/10.1016/j.jobe.2021.102834

Justo-Reinoso I, Reeksting BJ, Hamley-Bennett C, Heath A, Gebhard S, Paine K (2022) Air-entraining admixtures as a protection method for bacterial spores in self-healing cementitious composites: Healing evaluation of early and later-age cracks. Constr Build Mater 327:126877. https://doi.org/10.1016/j.conbuildmat.2022.126877

Kadapure SA, Kulkarni G, Prakash KB, Kadapure PS (2020) Mechanical and durability performance of sustainable bacteria blended fly ash concrete: an experimental study. Int J Sustain Eng 13:45–53. https://doi.org/10.1080/19397038.2019.1644386

Kaladharan G, Rajabipour F (2022) Evaluation and beneficiation of high sulfur and high alkali fly ashes for use as supplementary cementitious materials in concrete. Constr Build Mater 339:127672. https://doi.org/10.1016/j.conbuildmat.2022.127672

Kalantary F, Moosazadeh R, Tabandeh F, Ganjian N (2022) Bio-cementation of loose sand using *Staphylococcus* sp. IR-103: a field study. Arab J Geosci 15:963. https://doi.org/10.1007/s12517-022-09869-8

Kamennaya NA, Ajo-Franklin CM, Northen T, Jansson C (2012) Cyanobacteria as biocatalysts for carbonate mineralization. Minerals 2:338-364. https://doi.org/10.3390/min2040338

Kan L li, Lv J wei, Duan B bei, Wu M (2019) Self-healing of Engineered Geopolymer Composites prepared by fly ash and metakaolin. Cem Concr Res 125:105895. https://doi.org/10.1016/j.cemconres.2019.105895

Kang CH, So JS (2016) Heavy metal and antibiotic resistance of ureolytic bacteria and their

immobilization of heavy metals. Ecol Eng 97:304-312. https://doi.org/10.1016/j.ecoleng.2016.10.016

Kantro D (1980) Influence of Water-Reducing Admixtures on Properties of Cement Paste-A Miniature Slump Test. Cem Concr Aggregates 2:95. https://doi.org/10.1520/cca10190j

Kantzas A, Stehmeìer L, Marentette DF, Ferris FG, Jha KN, Marentette FM (1992) A Novel Method of Sand Consolidation Through Bacteriogenic Mineral Plugging. Annu Tech Meet 1992. https://doi.org/10.2118/92-46

Kanwal M, Khushnood RA, Khaliq W, Wattoo AG, Shahid T (2022) Synthesis of pyrolytic carbonized bagasse to immobilize *Bacillus subtilis*; application in healing micro-cracks and fracture properties of concrete. Cem Concr Compos 126:104334. https://doi.org/10.1016/j.cemconcomp.2021.104334

Kappaun K, Piovesan AR, Carlini CR, Ligabue-Braun R (2018) Ureases: Historical aspects, catalytic, and non-catalytic properties - A review. J Adv Res 13:3–17. https://doi.org/10.1016/j.jare.2018.05.010

Karimi N, Mostofinejad D (2020) *Bacillus subtilis* bacteria used in fiber reinforced concrete and their effects on concrete penetrability. Constr Build Mater 230:117051. https://doi.org/10.1016/j.conbuildmat.2019.117051

Karthick DM, Rampradheep GS, Shankar S (2022) Strength and durability performance of modified cement-based concrete incorporated immobilized bacteria. Environ Sci Pollut Res 29:21670–21681. https://doi.org/10.1007/s11356-021-17414-5

Kaur N, Reddy MS, Mukherjee A (2013) Biomineralization of calcium carbonate polymorphs by the bacterial strains isolated from calcareous sites. J Microbiol Biotechnol 23:707–714 . https://doi.org/10.4014/jmb.1212.11087

Kaur NP, Majhi S, Dhami NK, Mukherjee A (2020) Healing fine cracks in concrete with bacterial cement for an advanced non-destructive monitoring. Constr Build Mater 242:118151 . https://doi.org/10.1016/j.conbuildmat.2020.118151

Kaur P, Joshi S, Shinde OA, Sudhakara Reddy M (2021) Utilization of Biomineralized Steel

Slag in Cement Mortar to Improve Its Properties. J Mater Civ Eng 33:04021116. https://doi.org/10.1061/(asce)mt.1943-5533.0003749

Kaur R, Kaur S (2021) Mechanism of bacterial ureolytic calcite precipitation (BUCP) and their Application : Review. 13:327–335

Kaushal V, Najafi M, Love J, Qasim SR (2020) Microbiologically induced deterioration and protection of concrete in municipal sewerage system: Technical review. J Pipeline Syst Eng Pract 11:03119002. https://doi.org/10.1061/(asce)ps.1949-1204.0000424

Kennedy MJ, Reader Lisa M Swierczynski SL, Kennedy M (1994) Historical perspective Preservation records of micro-organisms : evidence of the tenacity of life. Microbiology 140:2513–2529. https://doi.org/10.1099/00221287-140-10-2513

Khadhim HJ, Ebrahim SE, Ammar SH (2019) Isolation and identification of ureolytic bacteria isolated from livestock soil to improve the strength of cement mortar. Eng Technol J 37:24–28. https://doi.org/10.30684/etj.37.3C.3

Khalid AR, Rizwan SA, Hanif U, Hameed MH (2016) Effect of mixing time on flowability and slump retention of self-compacting paste system incorporating various secondary raw materials. Arab J Sci Eng 41:1283–1290. https://doi.org/10.1007/s13369-015-1885-5

Khaliq W, Ehsan MB (2016) Crack healing in concrete using various bio influenced self-healing techniques. Constr Build Mater 102:349–357. https://doi.org/10.1016/j.conbuildmat.2015.11.006

Khambholja DB, Gamit D, Patel H, Kumar P (2022) Isolation and characterisation of urease producing bacteria and their capacity to precipitate calcium carbonate. Def. Life Sci. J 7:89-96. https://doi.org/10.14429/dlsj.7.17279

Khan MBE, Shen L, Dias-da-Costa D (2021) Self-healing behaviour of bio-concrete in submerged and tidal marine environments. Constr Build Mater 277:122332. https://doi.org/10.1016/j.conbuildmat.2021.122332

Khushnood RA, Ali AM, Faraz Bhatti M, Ahmed Khan H (2022) Self-healing fungi concrete using potential strains *Rhizopus oryzae* and *Trichoderma longibrachiatum*. J Build Eng

50:104155. https://doi.org/10.1016/j.jobe.2022.104155

Khushnood RA, Qureshi ZA, Shaheen N, Ali S (2020) Bio-mineralized self-healing recycled aggregate concrete for sustainable infrastructure. Sci Total Environ 703:135007. https://doi.org/10.1016/j.scitotenv.2019.135007

Kim H, Son HM, Seo J, Lee HK (2021) Recent advances in microbial viability and self-healing performance in bacterial-based cementitious materials : A review. Constr Build Mater 274:122094. https://doi.org/10.1016/j.conbuildmat.2020.122094

Kim HJ, Eom HJ, Park C, Jung J, Shin B, Kim W, Chung N, Choi IG, Park W (2015) Calcium carbonate precipitation by *Bacillus* and *Sporosarcina* strains isolated from concrete and analysis of the bacterial community of concrete. J Microbiol Biotechnol 26:540–548. https://doi.org/10.4014/jmb.1511.11008

Knoll AH (2003) Biomineralization and evolutionary history. Rev Mineral Geochemistry 54:329–356. https://doi.org/10.2113/0540329

Korchef A, Touaibi M (2020) Effect of pH and temperature on calcium carbonate precipitation by CO_2 removal from iron-rich water. Water Environ J 34:331–341. https://doi.org/10.1111/wej.12467

Kotelnikova AD, Rogova OB, Karpukhina EA, Solopov AB, Levin IS, Levkina VV, Proskurnin MA, Volkov DS (2022) Assessment of the structure, composition, and agrochemical properties of fly ash and ash-and-slug waste from coal-fired power plants for their possible use as soil ameliorants. J Clean Prod 333:130088. https://doi.org/10.1016/j.jclepro.2021.130088

Kourkoutas Y, Bekatorou A, Banat IM, Marchant R, Koutinas AA (2004) Immobilization technologies and support materials suitable in alcohol beverages production: A review. Food Microbiol 21:377–397. https://doi.org/10.1016/j.fm.2003.10.005

Krajewska B (2018) Urease-aided calcium carbonate mineralization for engineering applications: A review. J Adv Res 13:59–67. https://doi.org/10.1016/j.jare.2017.10.009

Kranz SA, Wolf-Gladrow D, Nehrke G, Langer G, Rost B (2010) Calcium carbonate

precipitation induced by the growth of the marine cyanobacterium *Trichodesmium*. Limnol Oceanogr 55:2563–2569. https://doi.org/10.4319/lo.2010.55.6.2563

Krishna P, Arora A, Reddy MS (2008) An alkaliphilic and xylanolytic strain of actinomycetes *Kocuria* sp. RM1 isolated from extremely alkaline bauxite residue sites. World J Microbiol Biotechnol 24:3079–3085. https://doi.org/10.1007/s11274-008-9801-8

Krishnapriya S, Venkatesh Babu DL, G. PA (2015) Isolation and identification of bacteria to improve the strength of concrete. Microbiol Res 174:48–55. https://doi.org/10.1016/j.micres.2015.03.009

Kua HW, Gupta S, Aday AN, Srubar W V. (2019) Biochar-immobilized bacteria and superabsorbent polymers enable self-healing of fiber-reinforced concrete after multiple damage cycles. Cem Concr Compos 100:35–52. https://doi.org/10.1016/j.cemconcomp.2019.03.017

Kumar S (2017) Acid Rain-The Major Cause of Pollution: Its Causes, Effects and Solution. Int J Appl Chem 13:53–58.

Kumari C, Das B, Jayabalan R, Davis R, Sarkar P (2017) Effect of Nonureolytic Bacteria on Engineering Properties of Cement Mortar. J Mater Civ Eng 29:1–9. https://doi.org/10.1061/(asce)mt.1943-5533.0001828

Kumari D, Pan X, Lee DJ, Achal V (2014) Immobilization of cadmium in soil by microbially induced carbonate precipitation with *Exiguobacterium undae* at low temperature. Int Biodeterior Biodegrad 94:98–102. https://doi.org/10.1016/j.ibiod.2014.07.007

Larosche CJ (2009) Types and causes of cracking in concrete structures. In Failure, distress and repair of concrete structures (pp. 57-83). Woodhead Publishing Limited.

Le Métayer-Levrel G, Castanier S, Orial G, Loubière JF, Perthuisot JP (1999) Applications of bacterial carbonatogenesis to the protection and regeneration of limestones in buildings and historic patrimony. Sediment Geol 126:25–34. https://doi.org/10.1016/S0037-0738(99)00029-9

Lee YS, Park W (2018) Current challenges and future directions for bacterial self-healing

concrete. Appl Microbiol Biotechnol 102:3059–3070. https://doi.org/10.1007/s00253-018-8830-y

Leeprasert L, Chonudomkul D, Boonmak C (2022) Biocalcifying potential of ureolytic bacteria isolated from soil for biocementation and material crack repair. Microorganisms 10:963. https://doi.org/10.3390/microorganisms10050963

Lei B, Li W, Li Z, Wang G, Sun Z (2018) Effect of Cyclic Loading Deterioration on Concrete Durability: Water Absorption, Freeze-Thaw, and Carbonation. J Mater Civ Eng 30: 04018220. https://doi.org/10.1061/(asce)mt.1943-5533.0002450

Li J, Oliver IM, Cam N, Boudier T, Blondeau M, Leroy E, Cosmidis J, Skouri-Panet F, Guigner JM, Férard C, Poinsot M, Moreira D, Lopez-Garcia P, Cassier-Chauvat C, Chauvat F, Benzerara K (2016) Biomineralization patterns of intracellular carbonatogenesis in cyanobacteria: Molecular hypotheses. Minerals 6:10. https://doi.org/10.3390/min6010010

Li M, Do H, Ding Y, Wang Y, Zhao C, Wu D, Zhang C (2022a) The isolation and characterization of *Glutamicibacter* DC1 to induce carbonate precipitation of some heavy metals at low-temperature. Polish J Environ Stud 31:1693–1703. https://doi.org/10.15244/pjoes/142611

Li M, Fu QL, Zhang Q, Achal V, Kawasaki S (2015) Bio-grout based on microbially induced sand solidification by means of asparaginase activity. Sci Rep 5:16128. https://doi.org/10.1038/srep16128

Li P, Qu W (2010) Remediation of historic buildings and patrimony by bacterially induced mineralization. Adv Mater Res 133–134:1253–1258. https://doi.org/10.4028/www.scientific.net/AMR.133-134.1253

Li S, Li Z, Sha F, Zhang Q, Liu R (2017) Investigation of viscous behaviour and strength of microfine-cement-based grout mixed with microfine fly ash and superplasticiser. Adv Cem Res 29:206–215. https://doi.org/10.1680/jadcr.16.00118

Li W, Fishman A, Achal V (2021) Ureolytic bacteria from electronic waste area, their biological robustness against potentially toxic elements and underlying mechanisms. J

Environ Manage 289:112517. https://doi.org/10.1016/j.jenvman.2021.112517

Li W, Hua L, Shi Y, Wang P, Liu Z, Cui D, Sun X (2022b) Influence of metakaolin on the hydration and microstructure evolution of cement paste during the early stage. Appl Clay Sci 229:106674. https://doi.org/10.1016/j.clay.2022.106674

Liang A, Paulo C, Zhu Y, Dittrich M (2013) CaCO3 biomineralization on cyanobacterial surfaces: Insights from experiments with three Synechococcus strains. Colloids Surfaces B Biointerfaces 111:600–608. https://doi.org/10.1016/j.colsurfb.2013.07.012

Liu C, Xu X, Lv Z, Xing L (2020a) Self-healing of concrete cracks by immobilizing microorganisms in recycled aggregate. J Adv Concr Technol 18:168–178. https://doi.org/10.3151/jact.18.168

Liu X jun, Fan J yue, Yu J, Gao X (2021) Solidification of loess using microbial induced carbonate precipitation. J Mt Sci 18:265–274. https://doi.org/10.1007/s11629-020-6154-8

Liu Y hui, Yang P, Ku T, Gao S wen (2020b) Effect of different nanoparticles on the grouting performance of cement-based grouts in dynamic water condition. Constr Build Mater 248:118663. https://doi.org/10.1016/j.conbuildmat.2020.118663

Liu YL, Wang YS, Fang G, Alrefaei Y, Dong B, Xing F (2018) A preliminary study on capsule-based self-healing grouting materials for grouted splice sleeve connection. Constr Build Mater 170:418–423. https://doi.org/10.1016/j.conbuildmat.2018.03.088

Loosdrecht VMCM, Lyklema J, Norde W, Zehnder AJB (1989) Bacterial adhesion: A physicochemical approach. Microb Ecol 17:1–15 . https://doi.org/10.1007/BF02025589

López-Moreno A, Sepúlveda-Sánchez JD, Mercedes Alonso Guzmán EM, Le Borgne S (2014) Calcium carbonate precipitation by heterotrophic bacteria isolated from biofilms formed on deteriorated ignimbrite stones: Influence of calcium on EPS production and biofilm formation by these isolates. Biofouling 30:547–560. https://doi.org/10.1080/08927014.2014.888715

Lors C, Ducasse-Lapeyrusse J, Gagné R, Damidot D (2017) Microbiologically induced

calcium carbonate precipitation to repair microcracks remaining after autogenous healing of mortars. Constr Build Mater 141:461–469. https://doi.org/10.1016/j.conbuildmat.2017.03.026

Lowenstam HA (1981) Minerals formed by weathering. Science 211:1126–1131. https://www.jstor.org/stable/1685216.

Ludwig M, Bryant DA (2011) Transcription profiling of the model cyanobacterium *Synechococcus* sp. Strain PCC 7002 by next-gen (SOLiD^{TM}) sequencing of cDNA. Front Microbiol 2:41. https://doi.org/10.3389/fmicb.2011.00041

Luo M, Qian C, Li R (2015) Factors affecting crack repairing capacity of bacteria-based self-healing concrete. Constr Build Mater 87:1–7. https://doi.org/10.1016/j.conbuildmat.2015.03.117

Lv C, Tang C-S, Zhu C, Li W-Q, Chen T-Y, Zhao L, Pan X-H (2022) Environmental dependence of microbially induced calcium carbonate crystal precipitations: Experimental Evidence and Insights. J Geotech Geoenvironmental Eng 148:04022050. https://doi.org/10.1061/(asce)gt.1943-5606.0002827

Mahawish A, Bouazza A, Gates WP (2019) Unconfined Compressive Strength and Visualization of the Microstructure of Coarse Sand Subjected to Different Biocementation Levels. J Geotech Geoenvironmental Eng 145:04019033. https://doi.org/10.1061/(asce)gt.1943-5606.0002066

Maleki-Kakelar M, Aghaeinejad-Meybodi A, Sanjideh S, Azarhoosh MJ (2022) Cost-effective optimization of bacterial urease activity using a hybrid method based on response surface methodology and artificial neural networks. Environ Process 9:7. https://doi.org/10.1007/s40710-022-00564-0

Malke H (1982) B. D. Davis, R. Dulbecco, H. N. Eisen and H. S. Ginsberg, Microbiology (3rd Edition). 1355 S., ca. 1300 Abb., ca. 150 Tab. Hagerstown 1980. Harper & Row Publishers. DFL 65.00. Z Allg Mikrobiol 22:279–279. https://doi.org/10.1002/jobm.19820220411

Mann S (1993) Molecular tectonics in biomineralization and biomimetic materials chemistry.

Nature 365:499–505. https://doi.org/10.1038/365499a0

Manoudis P, Papadopoulou S, Karapanagiotis I, Tsakalof A, Zuburtikudis I, Panayiotou C (2007) Polymer-Silica nanoparticles composite films as protective coatings for stone-based monuments. J Phys Conf Ser 61:1361–1365. https://doi.org/10.1088/1742-6596/61/1/269

Marín S, Cabestrero O, Demergasso C, Olivares S, Zetola V, Vera M (2021) An indigenous bacterium with enhanced performance of microbially-induced Ca-carbonate biomineralization under extreme alkaline conditions for concrete and soil-improvement industries. Acta Biomater 120:304–317. https://doi.org/10.1016/j.actbio.2020.11.016

Martinez RE, Pokrovsky OS, Schott J, Oelkers EH (2008) Surface charge and zeta-potential of metabolically active and dead cyanobacteria. J Colloid Interface Sci 323:317–325. https://doi.org/10.1016/j.jcis.2008.04.041

Mazzoli R, Giuffrida MG, Pessione E (2018) Back to the past—forever young: cutting-edge biochemical and microbiological tools for cultural heritage conservation. Appl Microbiol Biotechnol 102:6815–6825. https://doi.org/10.1007/s00253-018-9121-3

Mekonnen E, Kebede A, Nigussie A, Kebede G, Tafesse M (2021) Isolation and Characterization of Urease-Producing Soil Bacteria. Int. J. Microbiol. 2021: 8888641. https://doi.org/10.1155/2021/8888641

Membré JM, Leporq B, Vialette M, Mettler E, Perrier L, Thuault D, Zwietering M (2005) Temperature effect on bacterial growth rate: Quantitative microbiology approach including cardinal values and variability estimates to perform growth simulations on/in food. Int J Food Microbiol 100:179–186. https://doi.org/10.1016/j.ijfoodmicro.2004.10.015

Merz-Preiß M, Riding R (1999) Cyanobacterial tufa calcification in two freshwater streams: Ambient environment, chemical thresholds and biological processes. Sediment Geol 126:103–124. https://doi.org/10.1016/S0037-0738(99)00035-4

Minto JM, Tan Q, Lunn RJ, El Mountassir G, Guo H, Cheng X (2018) 'Microbial mortar'-restoration of degraded marble structures with microbially induced carbonate

precipitation. Constr Build Mater 180:44–54. https://doi.org/10.1016/j.conbuildmat.2018.05.200

Mirza J, Mirza MS, Roy V, Saleh K (2002) Basic rheological and mechanical properties of high-volume fly ash grouts. Constr Build Mater 16:353–363. https://doi.org/10.1016/S0950-0618(02)00026-0

Mohamed AM, Khallaf R (2022) Fly Ash Application as Supplementary Cementitious Material : A Review. Materials. 15:2664. https://doi.org/10.3390/ma15072664

Mondal S, Ghosh A (Dey) (2018) Investigation into the optimal bacterial concentration for compressive strength enhancement of microbial concrete. Constr Build Mater 183:202–214. https://doi.org/10.1016/j.conbuildmat.2018.06.176

Mosquera MJ, Pozo J, Esquivias L (2003) Stress during drying of two stone consolidants applied in monumental conservation. J Sol-Gel Sci Technol 26:1227–1231. https://doi.org/10.1023/A:1020776622689

Muhammed AS, Kassim KA, Ahmad K, Zango MU, Chong CS, Makinda J (2021) Influence of multiple treatment cycles on the strength and microstructure of biocemented sandy soil. Int J Environ Sci Technol 18:3427–3440. https://doi.org/10.1007/s13762-020-03073-5

Mutitu KD, Munyao MO, Wachira MJ, Mwirichia R, Thiong'o KJ, Marangu MJ (2019) Effects of biocementation on some properties of cement-based materials incorporating *Bacillus* Species bacteria–a review. J Sustain Cem Mater 8:309–325. https://doi.org/10.1080/21650373.2019.1640141

Mwema FM, Oladijo OP, Sathiaraj TS, Akinlabi ET (2018) Atomic force microscopy analysis of surface topography of pure thin aluminum films. Mater Res Express 5: 046416. https://doi.org/10.1088/2053-1591/aabe1b

Nain N, Surabhi R, Yathish N V., Krishnamurthy V, Deepa T, Tharannum S (2019) Enhancement in strength parameters of concrete by application of *Bacillus* bacteria. Constr Build Mater 202:904–908. https://doi.org/10.1016/j.conbuildmat.2019.01.059

Nair N, Mohammed Haneefa K, Santhanam M, Gettu R (2020) A study on fresh properties of

limestone calcined clay blended cementitious systems. Constr Build Mater 254:119326. https://doi.org/10.1016/j.conbuildmat.2020.119326

Najjar MF, Soliman AM, Nehdi ML (2017) Grouts incorporating supplementary cementitious materials for two-stage concrete. J Mater Civ Eng 29:04016298. https://doi.org/10.1061/(asce)mt.1943-5533.0001841

Nasser AA, Sorour NM, Saafan MA, Abbas RN (2022) Microbially-Induced-Calcite-Precipitation (MICP): A biotechnological approach to enhance the durability of concrete using *Bacillus pasteurii* and *Bacillus sphaericus*. Heliyon 8:e09879. https://doi.org/10.1016/j.heliyon.2022.e09879

Natarajan KR (1995) Kinetic study of the enzyme urease from *Dolichos biflorus*. J Chem Educ 73:556–557. https://doi.org/10.1021/ed072p556

Nathan VK, Vijayan J, Parvathi A (2020) Optimization of urease production by *Bacillus halodurans* PO15: a mangrove bacterium from Poovar mangroves, India. Mar Life Sci Technol 2:194–202. https://doi.org/10.1007/s42995-020-00031-5

Naveed M, Duan J, Uddin S, Suleman M, Hui Y, Li H (2020a) Application of microbially induced calcium carbonate precipitation with urea hydrolysis to improve the mechanical properties of soil. Ecol Eng 153:105885. https://doi.org/10.1016/j.ecoleng.2020.105885

Naveed S, Yu Q, Zhang C, Ge Y (2020b) Extracellular polymeric substances alter cell surface properties, toxicity, and accumulation of arsenic in *Synechocystis* PCC6803. Environ Pollut 261:114233. https://doi.org/10.1016/j.envpol.2020.114233

Nedwell DB (1999) Effect of low temperature on microbial growth: Lowered affinity for substrates limits growth at low temperature. FEMS Microbiol Ecol 30:101–111. https://doi.org/10.1016/S0168-6496(99)00030-6

Nehdi ML, Suleiman AR, Soliman AM (2014) Investigation of concrete exposed to dual sulfate attack. Cem Concr Res 64:42–53. https://doi.org/10.1016/j.cemconres.2014.06.002

Nemati M, Greene EA, Voordouw G (2005) Permeability profile modification using bacterially formed calcium carbonate: Comparison with enzymic option. Process Biochem 40:925–

933. https://doi.org/10.1016/j.procbio.2004.02.019

Nezafat TM, Tajabadi-Ebrahimi M, Esfandi Sarafraz M, Akhavan Sepahi A (2023) Investigation of self-healing properties in concrete with *Bacillus licheniformis* isolated from agricultural soil. J Build Eng 67:106057. https://doi.org/10.1016/j.jobe.2023.106057

Nguyen TH, Ghorbel E, Fares H, Cousture A (2019) Bacterial self-healing of concrete and durability assessment. Cem Concr Compos 104:103340. https://doi.org/10.1016/j.cemconcomp.2019.103340

Ni F, Zhao Y, Hou X, Zhen G, Ni W, Shen X, Tong H (2020) Formation of an organic–inorganic hybrid network structure by in situ polymerization of silicone to protect cultural heritage stonework. J Mater Civ Eng 32:04019322. https://doi.org/10.1061/(asce)mt.1943-5533.0002993

Nimafar M, Hosseini SJ, Akhlaghi A, Samali B, Soltaninia S (2023) Effect of bacterial carbonate precipitation on the durability of concrete specimens exposed to high temperatures. J Mater Civ Eng 35: 04022394. https://doi.org/10.1061/(asce)mt.1943-5533.0004521

NOAA (2022) Carbon dioxide now more than 50 higher than pre-industrial levels. 1–6.

Nosouhian F, Mostofinejad D, Hasheminejad H (2016) Concrete durability improvement in a sulfate environment using bacteria. J Mater Civ Eng 28:1–12. https://doi.org/10.1061/(asce)mt.1943-5533.0001337

Obst M, Dittrich M, Kuehn H (2006) Calcium adsorption and changes of the surface microtopography of cyanobacteria studied by AFM, CFM, and TEM with respect to biogenic calcite nucleation. Geochemistry, Geophys Geosystems 7:Q06011. https://doi.org/10.1029/2005GC001172

Obst M, Wehrli B, Dittrich M (2009) $CaCO_3$ nucleation by cyanobacteria: Laboratory evidence for a passive, surface-induced mechanism. Geobiology 7:324–347. https://doi.org/10.1111/j.1472-4669.2009.00200.x

Oliveira ADT, D'Orey Gaivão Portela Bragança M, Miguel Pinkoski I, Carrera G (2021) The

effect of silica nanocapsules on self-healing concrete. Constr Build Mater 300:124010. https://doi.org/10.1016/j.conbuildmat.2021.124010

Omoregie AI, Khoshdelnezamiha G, Senian N, Ong DEL, Nissom PM (2017) Experimental optimisation of various cultural conditions on urease activity for isolated *Sporosarcina pasteurii* strains and evaluation of their biocement potentials. Ecol Eng 109:65–75. https://doi.org/10.1016/j.ecoleng.2017.09.012

Omoregie AI, Ong DEL, Nissom PM (2019) Assessing ureolytic bacteria with calcifying abilities isolated from limestone caves for biocalcification. Lett Appl Microbiol 68:173–181. https://doi.org/10.1111/lam.13103

Omoregie AI, Senian N, Ye Li P, Hei NL, Leong DOE, Henry Ginjom IR, Nissom PM (2016) Screening for urease-producing bacteria from limestone caves of sarawak. Borneo J Resour Sci Technol 6:37–45. https://doi.org/10.33736/bjrst.213.2016

Onyelowe KC, Kontoni DPN, Ebid AM, Dabbaghi F, Soleymani A, Jahangir H, Nehdi ML (2022) Multi-objective optimization of sustainable concrete containing fly ash based on environmental and mechanical considerations. Buildings 12:948. https://doi.org/10.3390/buildings12070948

Ortega-Villamagua E, Gudiño-Gomezjurado M, Palma-Cando A (2020) Microbiologically induced carbonate precipitation in the restoration and conservation of cultural heritage materials. Molecules 25:5499. https://doi.org/10.3390/molecules25235499

Osman KM, Taher FM, Abd EL-Tawab A, Faried AS (2021) Role of different microorganisms on the mechanical characteristics, self-healing efficiency, and corrosion protection of concrete under different curing conditions. J Build Eng 41:102414. https://doi.org/10.1016/j.jobe.2021.102414

Paine K (2016) Bacteria-based self-healing of concrete: effects of environment, exposure and crack size. Proc RILEM Conf Microorg Mater Interact 1:1-15.

Pan X, Shi C, Jia L, Zhang J, Wu L (2016) Effect of inorganic surface treatment on air permeability of cement-based materials. J Mater Civ Eng 28:04015145. https://doi.org/10.1061/(asce)mt.1943-5533.0001424

Pan X, Shi Z, Shi C, Ling TC, Li N (2017) A review on concrete surface treatment Part I: Types and mechanisms. Constr Build Mater 132:578–590. https://doi.org/10.1016/j.conbuildmat.2016.12.025

Paquette AJ, Vadlamani A, Demirkaya C, Strous M, De la Hoz Siegler H (2022) Nutrient management and medium reuse for cultivation of a cyanobacterial consortium at high pH and alkalinity. Front Bioeng Biotechnol 10:1–15. https://doi.org/10.3389/fbioe.2022.942771

Park G, Kim Y, Ho H, Lee O, Park J, Kim Y, Min K, Heo M, Son H (2022a) Characterization and applicability of novel alkali – tolerant carbonatogenic bacteria as environment-friendly bioconsolidants for management of concrete structures and soil erosion. J Environ Manage 321:115929. https://doi.org/10.1016/j.jenvman.2022.115929

Park M, Park S, Yoo JY, Kim Y, Lee KM, Hwang DY, Son HJ (2022b) Enzyme-mediated biocalcification by a novel alkaliphilic *Bacillus psychrodurans* LC40 and its eco-friendly application as a biosealant for crack healing. Sci Total Environ 802:149841. https://doi.org/10.1016/j.scitotenv.2021.149841

Paulo C, Kenney JPL, Persson P, Dittrich M (2018) Effects of phosphorus in growth media on biomineralization and cell surface properties of marine cyanobacteria *Synechococcus*. Geosci 8:471. https://doi.org/10.3390/geosciences8120471

Pei R, Liu J, Wang S, Yang M (2013) Use of bacterial cell walls to improve the mechanical performance of concrete. Cem Concr Compos 39:122–130. https://doi.org/10.1016/j.cemconcomp.2013.03.024

Pentecost A (1978) Blue-green algae and freshwater carbonate deposits. Proc R Soc London - Biol Sci 200:43–61. https://doi.org/10.1098/rspb.1978.0004

Pentecost A (1984) Effects of sedimentation and light intensity on mat-forming *Oscillatoriaceae* with particular reference to *Microcoleus lyngbyaceus* gomont. Microbiology 130:983–990. https://doi.org/10.1099/00221287-130-4-983

Perito B, Marvasi M, Barabesi C, Mastromei G, Bracci S, Vendrell M, Tiano P (2014) A *Bacillus subtilis* cell fraction (BCF) inducing calcium carbonate precipitation:

Biotechnological perspectives for monumental stone reinforcement. J Cult Herit 15:345–351. https://doi.org/10.1016/j.culher.2013.10.001

Phang IRK, Chan YS, Wong KS, Lau SY (2018) Isolation and characterization of urease-producing bacteria from tropical peat. Biocatal Agric Biotechnol 13:168–175. https://doi.org/10.1016/j.bcab.2017.12.006

Phillips AJ, Gerlach R, Lauchnor E, Mitchell AC, Cunningham AB, Spangler L (2013) Engineered applications of ureolytic biomineralization: A review. Biofouling 29:715–733. https://doi.org/10.1080/08927014.2013.796550

Phua YJ, Røyne A (2018) Bio-cementation through controlled dissolution and recrystallization of calcium carbonate. Constr Build Mater 167:657–668. https://doi.org/10.1016/j.conbuildmat.2018.02.059

Pillay DL, Olalusi OB, Kiliswa MW, Awoyera PO, Kolawole JT, Babafemi AJ (2022) Engineering performance of metakaolin based concrete. Clean Eng Technol 6:100383. https://doi.org/10.1016/j.clet.2021.100383

Piumetti M (2022) Molecular Dynamics and Complexity in Catalysis and Biocatalysis. Mol Dyn Complex Catal Biocatal. https://doi.org/10.1007/978-3-030-88500-7

Pungrasmi W, Intarasoontron J, Jongvivatsakul P, Likitlersuang S (2019) Evaluation of microencapsulation techniques for MICP bacterial spores Applied in Self-Healing Concrete. Sci Rep 9:12484. https://doi.org/10.1038/s41598-019-49002-6

Qian C, Chen H, Ren L, Luo M (2015) Self-healing of early age cracks in cement-based materials by mineralization of carbonic anhydrase microorganism. Front Microbiol 6:1225. https://doi.org/10.3389/fmicb.2015.01225

Qian C, Chen Y, Xue B (2022) Microbial mineralization at the surface layer of cement-based materials and its effect on efflorescence performance. J Build Eng 52:104480. https://doi.org/10.1016/j.jobe.2022.104480

Qian C, Ren X, Rui Y, Wang K (2021) Characteristics of bio-$CaCO_3$ from microbial bio-mineralization with different bacteria species. Biochem Eng J 176:108180.

https://doi.org/10.1016/j.bej.2021.108180

Qin J, Qin Q, Li X, Xue J, Wang R, Zhang Q, Wang P, Guo Z, Gong Y (2021) Urea supply control in microbial carbonate precipitation to effectively fill pores of concrete. Constr Build Mater 310:125123. https://doi.org/10.1016/j.conbuildmat.2021.125123

Qin W, Wang C yu, Ma Y xuan, Shen M juan, Li J, Jiao K, Tay FR, Niu L na (2020) Microbe-mediated extracellular and intracellular mineralization: environmental, industrial, and biotechnological applications. Adv Mater 32:1907833. https://doi.org/10.1002/adma.201907833

Rais MS, Khan RA (2021) Experimental investigation on the strength and durability properties of bacterial self-healing recycled aggregate concrete with mineral admixtures. Constr Build Mater 306:124901. https://doi.org/10.1016/j.conbuildmat.2021.124901

Rajczakowska M, Habermehl-Cwirzen K, Hedlund H, Cwirzen A (2019) Autogenous self-healing: A better solution for concrete. J Mater Civ Eng 31:1–19. https://doi.org/10.1061/(asce)mt.1943-5533.0002764

Ramachandran SK, Ramakrishnan V, Bang SS (2001) Remediation of Concrete Using Micro-organisms. ACI Mater J 98:3–9. doi:10.14359/10154

Ramakrishnan VV GA (2015) Nitrogen Sources and Cycling in the Ecosystem and its Role in Air, Water and Soil Pollution: A Critical Review. J Pollut Eff Control 03:136. https://doi.org/10.4172/2375-4397.1000136

Ranjan P, Soda K, Chakravarthi EK, Mogal A, Mini KM (2022a) Statistical and experimental investigation on self-healing of microcracks in cement mortar by encapsulation of calcite precipitating bacteria into expanded perlite. Constr Build Mater 342:127985. https://doi.org/10.1016/j.conbuildmat.2022.127985

Ranjan P, Soda K, Chakravarthi K, Mini KM (2023) Experimental and statistical investigation on strength and microcracks remediation in cement mortar using expanded vermiculite as a bacterial carrier. J Build Eng 63:105567. https://doi.org/10.1016/j.jobe.2022.105567

Rathakrishnan D, Gopalan AK (2022) Isolation and characterization of halophilic isolates from

Indian salterns and their screening for production of hydrolytic enzymes. Environ Challenges 6:10042 . https://doi.org/10.1016/j.envc.2021.100426

Rauf M, Khaliq W, Khushnood RA, Ahmed I (2020) Comparative performance of different bacteria immobilized in natural fibers for self-healing in concrete. Constr Build Mater 258:119578. https://doi.org/10.1016/j.conbuildmat.2020.119578

Razi PZ, Razak HA, Khalid NHA (2016) Sustainability, eco-point and engineering performance of different workability OPC fly-ash mortar mixes. Materials (Basel) 9:341. https://doi.org/10.3390/ma9050341

Reddy GPV, Murali Krishna B, Tadepalli T, Rathish Kumar P (2020) Image-based deterioration assessment of concrete. Mater Today Proc 32:788–796. https://doi.org/10.1016/j.matpr.2020.03.716

Reyad AM, Mokhtar G (2023) Impact of the immobilized *Bacillus cereus* MG708176 on the characteristics of the bio-based self-healing concrete. Sci Rep 13:500. https://doi.org/10.1038/s41598-023-27640-1

Ribeiro DM, Roncaratti LF, Possa GC, Garcia LC, Cançado LJ, Williams TCR, dos Santos Alves Figueiredo Brasil B (2020) A low-cost approach for *Chlorella sorokiniana* production through combined use of urea, ammonia and nitrate based fertilizers. Bioresour Technol Reports 9:100354 . https://doi.org/10.1016/j.biteb.2019.100354

Rippka R, Deruelles J, Waterbury JB (1979) Generic assignments, strain histories and properties of pure cultures of cyanobacteria. J Gen Microbiol 111:1–61. https://doi.org/10.1099/00221287-111-1-1

Risdanareni P, Wang J, Boon N, De Belie N (2023) Alkali activated lightweight aggregate as bacterial carrier in manufacturing self-healing mortar. Constr Build Mater 368:130375. https://doi.org/10.1016/j.conbuildmat.2023.130375

Rivadeneyra MA, Delgado G, Soriano M, Ramos-Cormenzana A, Delgado R (2000) Precipitation of carbonates by *Nesterenkonia halobia* in liquid media. Chemosphere 41:617–624. https://doi.org/10.1016/S0045-6535(99)00496-8

Robles-Fernández A, Areias C, Daffonchio D, Volker C. Vahrenkamp, Sánchez-Román M (2022) The role of microorganisms in the nucleation of carbonates, environmental implications and applications. Minerals 12:1562. https://doi.org/10.3390/min12121562

Rodriguez-Navarro C, Jroundi F, Gonzalez-Muñoz MT (2015) Stone consolidation by bacterial carbonatogenesis: evaluation of in situ applications. Restor Build Monum 21:9–20. https://doi.org/10.1515/rbm-2015-0002

Rodriguez-Navarro C, Jroundi F, Schiro M, Ruiz-Agudo E, González-Muñoz MT (2012) Influence of substrate mineralogy on bacterial mineralization of calcium carbonate: Implications for stone conservation. Appl Environ Microbiol 78:4017–4029. https://doi.org/10.1128/AEM.07044-11

Rodriguez-Navarro C, Rodriguez-Gallego M, Chekroun K Ben, Gonzalez-Muñoz MT (2003) Conservation of ornamental stone by *Myxococcus xanthus*-induced carbonate biomineralization. Appl Environ Microbiol 69:2182–2193. https://doi.org/10.1128/AEM.69.4.2182-2193.2003

Roger T, Bhakoo M, Zhang Z (2008) Bacterial adhesion and biofilms on surfaces. 18:1049–1056. https://doi.org/10.1016/j.pnsc.2008.04.001

Rouf A, Kanojia V, Naik HR (2017) Cell immobilization: An overview on techniques and its applications in food industry. Int J Chem Stud 5:1817-1824.

Rui Y, Qian C (2021) The regulation mechanism of bacteria on the properties of biominerals. J Cryst Growth 570:126214. https://doi.org/10.1016/j.jcrysgro.2021.126214

S. Bright Singh, Murugan M (2022) Effect of metakaolin on the properties of pervious concrete. Constr Build Mater 346:128476. https://doi.org/10.1016/j.conbuildmat.2022.128476

Sadrmomtazi A, Tahmouresi B, Khoshkbijari RK (2018) Effect of fly ash and silica fume on transition zone, pore structure and permeability of concrete. Mag Concr Res 70:519–532. https://doi.org/10.1680/jmacr.16.00537

Sarkar M, Maiti M, Akbar M, Xu S (2022) Evaluation of the crack-healing performance and

durability of bacteria integrated alkali-activated fly ash composites. J Build Eng 54:104642. https://doi.org/10.1016/j.jobe.2022.104642

Saxena S, Tembhurkar AR (2020) Microbiological induced calcium carbonate process to enhance the properties of cement mortar. Mater Today Proc 21:1350–1354. https://doi.org/10.1016/j.matpr.2020.01.173

Scherer GW (2004) Stress from crystallization of salt. Cem Concr Res 34:1613–1624. https://doi.org/10.1016/j.cemconres.2003.12.034

Schwantes-Cezario N, Medeiros LP, De Oliveira AG, Nakazato G, Katsuko Takayama Kobayashi R, Toralles BM (2017) Bioprecipitation of calcium carbonate induced by *Bacillus subtilis* isolated in Brazil. Int Biodeterior Biodegrad 123:200–205. https://doi.org/10.1016/j.ibiod.2017.06.021

Seifan M, Berenjian A (2019a) Microbially induced calcium carbonate precipitation: a widespread phenomenon in the biological world. Appl Microbiol Biotechnol 103:4693–4708. https://doi.org/10.1007/s00253-019-09861-5

Seifan M, Berenjian A (2020) Bio self-healing nanoconcretes. In *Smart Nanoconcretes and Cement-Based Materials* (pp. 547-558). Elsevier.

Seifan M, Mendoza S, Berenjian A (2020) Mechanical properties and durability performance of fly ash based mortar containing nano- and micro-silica additives. Constr Build Mater 252:119121. https://doi.org/10.1016/j.conbuildmat.2020.119121

Seifan M, Samani AK, Berenjian A (2016a) Bioconcrete: next generation of self-healing concrete. Appl Microbiol Biotechnol 100:2591–2602. https://doi.org/10.1007/s00253-016-7316-z

Seifan M, Samani AK, Berenjian A (2016b) Induced calcium carbonate precipitation using *Bacillus* species. Appl Microbiol Biotechnol 100:9895–9906. https://doi.org/10.1007/s00253-016-7701-7

Seifan M, Samani AK, Berenjian A (2017) New insights into the role of pH and aeration in the bacterial production of calcium carbonate ($CaCO_3$). Appl Microbiol Biotechnol

101:3131–3142 . https://doi.org/10.1007/s00253-017-8109-8

Seifan M, Sarmah AK, Ebrahiminezhad A, Ghasemi Y, Samani AK, Berenjian A (2018) Bio-reinforced self-healing concrete using magnetic iron oxide nanoparticles. Appl Microbiol Biotechnol 102:2167–2178. https://doi.org/10.1007/s00253-018-8782-2

Setlow P (2003) Spore germination. Curr Opin Microbiol 6:550–556. https://doi.org/10.1016/j.mib.2003.10.001

Setlow P, Johnson EA (2019) Spores and their significance. Food microbiology: fundamentals and frontiers. (pp 45-79). ASM Press, Washington, DC https://doi.org/10.1128/9781555818463.ch3

Sha F, Li S, Liu R, Li Z, Zhang Q (2018) Experimental study on performance of cement-based grouts admixed with fly ash, bentonite, superplasticizer and water glass. Constr Build Mater 161:282–291. https://doi.org/10.1016/j.conbuildmat.2017.11.034

Shaheen N, Khushnood RA, Memon SA, Adnan F (2023) Feasibility assessment of newly isolated calcifying bacterial strains in self-healing concrete. Constr Build Mater 362:129662 . https://doi.org/10.1016/j.conbuildmat.2022.129662

Shannag MJ (2002) High-performance cementitious grouts for structural repair. Cem Concr Res 32:803–808. https://doi.org/10.1016/S0008-8846(02)00710-X

Sharma B, Singh A, Joshi S, Reddy MS (2022) Utilization of sandstone waste in cement mortar for sustainable production of building materials through biomineralization. J Sustain Cem Mater 12: 712-720. https://doi.org/10.1080/21650373.2022.2116500

Sharma H, Sharma SK, Ashish DK, Adhikary SK, Singh G (2023) Effect of various bio-deposition treatment techniques on recycled aggregate and recycled aggregate concrete. J Build Eng 66:105868. https://doi.org/10.1016/j.jobe.2023.105868

Sharma M, Satyam N, Reddy KR (2020a) Comparison of improved shear strength of biotreated sand using different ureolytic strains and sterile conditions. Soil Use Manag. 38:771-789. https://doi.org/10.1111/sum.12690

Sharma M, Satyam N, Reddy KR (2020b) Strength Enhancement and Lead Immobilization of

Sand Using Consortia of Bacteria and Blue-Green Algae. J Hazardous, Toxic, Radioact Waste 24:04020049 . https://doi.org/10.1061/(asce)hz.2153-5515.0000548

Sharma M, Satyam N, Reddy KR (2021) Rock-like behavior of biocemented sand treated under non-sterile environment and various treatment conditions. J Rock Mech Geotech Eng 13:705–716. https://doi.org/10.1016/j.jrmge.2020.11.006

Sharma TK, Alazhari M, Heath A, Paine K, Cooper RM (2017) Alkaliphilic *Bacillus* species show potential application in concrete crack repair by virtue of rapid spore production and germination then extracellular calcite formation. J Appl Microbiol 122:1233–1244. https://doi.org/10.1111/jam.13421

Siddique R, Singh K, Kunal P, Singh M, Corinaldesi V, Rajor A (2016) Properties of bacterial rice husk ash concrete. Constr Build Mater 121:112–119 . https://doi.org/10.1016/j.conbuildmat.2016.05.146

Sidiq A, Gravina R, Giustozzi F (2019) Is concrete healing really efficient? A review. Constr Build Mater 205:257–273. https://doi.org/10.1016/j.conbuildmat.2019.02.002

Siegesmund S, Snethlage R (2014) Stone in architecture: Properties, durability: Fifth edition

Sikiotis D, Kirkitsos P (1995) The adverse effects of nitrates on stone monuments. Sci Total Environ 171:173–182. https://doi.org/10.1016/0048-9697(95)04718-8

Silva FB, Boon N, De Belie N, Verstraete W (2015) Industrial application of biological self-healing concrete: Challenges and economical feasibility. J Commer Biotechnol 21:31–38. https://doi.org/10.5912/jcb662

Singh AK, Singh M, Verma N (2017) Extraction, purification, kinetic characterization and immobilization of urease from *Bacillus sphaericus* MTCC 5100. Biocatal Agric Biotechnol 12:341–347 . https://doi.org/10.1016/j.bcab.2017.10.020

Singh H, Gupta R (2020) Cellulose fiber as bacteria-carrier in mortar: Self-healing quantification using UPV. J Build Eng 28:101090. https://doi.org/10.1016/j.jobe.2019.101090

Singh H, Siddique R (2022) Utilization of crushed recycled glass and metakaolin for

development of self-compacting concrete. Constr Build Mater 348:128659. https://doi.org/10.1016/j.conbuildmat.2022.128659

Singh JS, Kumar A, Rai AN, Singh DP (2016) Cyanobacteria: A precious bio-resource in agriculture, ecosystem, and environmental sustainability. Front Microbiol 7:1–19. https://doi.org/10.3389/fmicb.2016.00529

Singh M (2019) Urease activity and deposition of calcium carbonate layers on a 16th century Mughal monument. Curr Sci 116:1840–1849. https://doi.org/10.18520/cs/v116/i11/1840-1849

Sisomphon K, Copuroglu O, Koenders EAB (2012) Self-healing of surface cracks in mortars with expansive additive and crystalline additive. Cem Concr Compos 34:566–574. https://doi.org/10.1016/j.cemconcomp.2012.01.005

Skevi L, Reeksting BJ, Hoffmann TD, Gebhard S, Paine K (2021) Incorporation of bacteria in concrete: The case against MICP as a means for strength improvement. Cem Concr Compos 120:104056. https://doi.org/10.1016/j.cemconcomp.2021.104056

Skinner HCW, Jahren AH (2007) Chapter 8: Biomineralization. Treatise on geochemistry 8:1-69. https://doi.org/10.1016/B0-08-043751-6%2F08128-7

Soda PRK, Chakravarthi EK, Mogal A, Mini KM (2022) Statistical and experimental investigation on self-healing of microcracks in cement mortar by encapsulation of calcite precipitating bacteria into expanded perlite. Constr Build Mater 342:127985. https://doi.org/10.1016/j.conbuildmat.2022.127985

Soda PRK, Mini KM (2022) Performance enhancement and remediation of microcracks in cement mortar by doping calcite-precipitating microorganisms. J Mater Civ Eng 34: 04022035. https://doi.org/10.1061/(asce)mt.1943-5533.0004176

Sohail MG, Disi Z Al, Zouari N, Nuaimi N Al, Kahraman R, Gencturk B, Rodrigues DF, Yildirim Y (2022) Bio self-healing concrete using MICP by an indigenous *Bacillus cereus* strain isolated from Qatari soil. Constr Build Mater 328:126943. https://doi.org/10.1016/j.conbuildmat.2022.126943

Son Y, Min J, Jang I, Yi C, Park W (2022) Development of a novel compressed tablet-based bacterial agent for self-healing cementitious material. Cem Concr Compos 129:104514 . https://doi.org/10.1016/j.cemconcomp.2022.104514

Soysal A, Milla J, King GM, Hassan M, Rupnow T (2020) Evaluating the self-healing efficiency of hydrogel-encapsulated bacteria in concrete. Transp Res Rec 2674:113–123 . https://doi.org/10.1177/0361198120917973

Srinivas M K, Alengaram UJ, Ibrahim S, Phang SM, Vello V, Jun HK, Alnahhal AM (2021) Evaluation of crack healing potential of cement mortar incorporated with blue-green microalgae. J Build Eng 44:102958 . https://doi.org/10.1016/j.jobe.2021.102958

Stabnikov V, Ivanov V, Chu J (2015) Construction Biotechnology: a new area of biotechnological research and applications. World J Microbiol Biotechnol 31:1303–1314. https://doi.org/10.1007/s11274-015-1881-7

Stabnikov V, Jian C, Ivanov V, Li Y (2013) Halotolerant, alkaliphilic urease-producing bacteria from different climate zones and their application for biocementation of sand. World J Microbiol Biotechnol 29:1453–1460. https://doi.org/10.1007/s11274-013-1309-1

Stabnikov V, Naeimi M, Ivanov V, Chu J (2011) Formation of water-impermeable crust on sand surface using biocement. Cem Concr Res 41:1143–1149. https://doi.org/10.1016/j.cemconres.2011.06.017

Stocks-Fischer S, Galinat JK, Bang SS (1999) Microbiological precipitation of $CaCO_3$. Soil Biol Biochem 31:1563–1571. https://doi.org/10.1016/S0038-0717(99)00082-6

Stuckrath C, Serpell R, Valenzuela LM, Lopez M (2014) Quantification of chemical and biological calcium carbonate precipitation: Performance of self-healing in reinforced mortar containing chemical admixtures. Cem Concr Compos 50:10–15. https://doi.org/10.1016/j.cemconcomp.2014.02.005

Su Y, Feng J, Zhan Q, Zhang Y, Qian C (2019) Non-ureolytic microbial self-repairing concrete for low temperature environment. Smart Mater Struct 28:075041. https://doi.org/10.1088/1361-665X/ab2012

Sun X, Miao L, Tong T, Wang C (2019a) Study of the effect of temperature on microbially induced carbonate precipitation. Acta Geotech 14:627–638. https://doi.org/10.1007/s11440-018-0758-y

Sun X, Miao L, Wu L, Chen R (2019b) Improvement of bio-cementation at low temperature based on *Bacillus megaterium*. Appl Microbiol Biotechnol 103: 7191–7202. https://doi.org/10.1007/s00253-019-09986-7

Tahmouresi B, Nemati P, Asadi MA, Saradar A, Mohtasham Moein M (2021) Mechanical strength and microstructure of engineered cementitious composites: A new configuration for direct tensile strength, experimental and numerical analysis. Constr Build Mater 269:121361. https://doi.org/10.1016/j.conbuildmat.2020.121361

Tang CS, Yin L yang, Jiang N jun, Zhu C, Zeng H, Li H, Shi B (2020) Factors affecting the performance of microbial-induced carbonate precipitation (MICP) treated soil: a review. Environ Earth Sci 79:94. https://doi.org/10.1007/s12665-020-8840-9

Tanyildizi H, Ziada M, Uysal M, Doğruöz Güngör N, Coşkun A (2022) Comparison of bacteria-based self-healing methods in metakaolin geopolymer mortars. Case Stud Constr Mater 16: e00895. https://doi.org/10.1016/j.cscm.2022.e00895

Tayebani B, Mostofinejad D (2019) Self-healing bacterial mortar with improved chloride permeability and electrical resistance. Constr Build Mater 208:75–86. https://doi.org/10.1016/j.conbuildmat.2019.02.172

Tezer MM, Bundur ZB (2020) Two-Part Bio-Based Self-Healing Repair Agent for Cement-Based Mortar. Curr Top Trends Durab Build Mater Components - Proc 15th Int Conf Durab Build Mater Components, DBMC 2020:137–144. https://doi.org/10.23967/dbmc.2020.142

Thomas M (2011) The effect of supplementary cementing materials on alkali-silica reaction: A review. Cem Concr Res 41:1224–1231. https://doi.org/10.1016/j.cemconres.2010.11.003

Thompson JB, Ferris FG (1990) Cyanobacterial precipitation of gypsum, calcite, and magnesite from natural alkaline lake water. Geology 18:995–99.

https://doi.org/10.1130/0091-7613(1990)018<0995:CPOGCA>2.3.CO;2

Tiano P, Biagiotti L, Mastromei G (1999) Bacterial bio-mediated calcite precipitation for monumental stones conservation: Methods of evaluation. J Microbiol Methods 36:139–145 . https://doi.org/10.1016/S0167-7012(99)00019-6

Toncheva-Panova T, Pouneva I, Chernev G, Minkova K (2010) Incorporation of *Synechocystis* salina in hybrid matrices. Effect of UV-B radiation on the copper and cadmium biosorption. Biotechnol Biotechnol Equip 24:1946–1949. https://doi.org/10.2478/V10133-010-0068-5

Tripathi E, Anand K, Goyal S, Reddy MS (2019) Bacterial based admixed or spray treatment to improve properties of concrete. Sadhana - Acad Proc Eng Sci 44:19. https://doi.org/10.1007/s12046-018-0999-3

Troiano F, Gulotta D, Balloi A, Polo A, Toniolo L, Lombardi E, Daffonchio D, Sorlini C, Cappitelli F (2013) Successful combination of chemical and biological treatments forthecleaning of stone artworks. Int Biodeterior Biodegrad 85:294–304. https://doi.org/10.1016/j.ibiod.2013.08.011

Tyagi G, Lahoti M, Srivastava A, Patil D (2023) Bioconcrete - Enabled Resilient Construction : a Review. Appl Biochem Biotechnol. https://doi.org/10.1007/s12010-023-04427-8

Tziviloglou E, Wiktor V, Jonkers HM, Schlangen E (2017) Selection of nutrient used in biogenic healing agent for cementitious materials. Front Mater 4:15. https://doi.org/10.3389/fmats.2017.00015

Uma V S, Dineshbabu G, Subramanian G, Uma L, Prabaharan D (2014) Biocalcification mediated remediation of calcium rich ossein effluent by filamentous marine cyanobacteria. J. Bioremed. Biodeg 5:7. https://doi.org/10.4172/2155-6199.1000257

Vaezi M, Zareei SA, Jahadi M (2020) Recycled microbial mortar: Effects of bacterial concentration and calcium lactate content. Constr Build Mater 234:117349. https://doi.org/10.1016/j.conbuildmat.2019.117349

Van Paassen LA, Harkes MP, Van Zwieten GA, Van Der Zon WH, Van Der Star WRL, Van

Loosdrecht MCM (2009) Scale up of BioGrout: A biological ground reinforcement method. Proc 17th Int Conf Soil Mech Geotech Eng Acad Pract Geotech Eng 3:2328–2333 . https://doi.org/10.3233/978-1-60750-031-5-2328

Van Tittelboom K, De Belie N (2013) Self-healing in cementitious materials-a review Materials, 6:2182-2217. https://doi.org/10.3390/ma6062182

Van Tittelboom K, De Belie N, Lehmann F, Grosse CU (2012) Acoustic emission analysis for the quantification of autonomous crack healing in concrete. Constr Build Mater 28:333–341. https://doi.org/10.1016/j.conbuildmat.2011.08.079

Vandamme D, Foubert I, Fraeye I, Meesschaert B, Muylaert K (2012) Flocculation of Chlorella vulgaris induced by high pH: Role of magnesium and calcium and practical implications. Bioresour Technol 105:114–119. https://doi.org/10.1016/j.biortech.2011.11.105

Vardhan K, Goyal S, Siddique R, Singh M (2015) Mechanical properties and microstructural analysis of cement mortar incorporating marble powder as partial replacement of cement. Constr Build Mater 96:615–621. https://doi.org/10.1016/j.conbuildmat.2015.08.071

Vasumithran M, Anand KB, Sathyan D (2020) Effects of fillers on the properties of cement grouts. Constr Build Mater 246:118346. https://doi.org/10.1016/j.conbuildmat.2020.118346

Vazquez P, Carrizo L, Thomachot-Schneider C, Gibeaux S, Alonso FJ (2016) Influence of surface finish and composition on the deterioration of building stones exposed to acid atmospheres. Constr Build Mater 106:392–403. https://doi.org/10.1016/j.conbuildmat.2015.12.125

Veaudor T, Blanc-Garin V, Chenebault C, Diaz-Santos E, Sassi JF, Cassier-Chauvat C, Chauvat F (2020) Recent advances in the photoautotrophic metabolism of cyanobacteria: Biotechnological implications. Life 10:71. https://doi.org/10.3390/life10050071

Verma M, Upreti K, Vats P, Singh S, Singh P, Dev N, Kumar Mishra D, Tiwari B (2022) Experimental Analysis of Geopolymer Concrete: A Sustainable and Economic Concrete Using the Cost Estimation Model. Adv Mater Sci Eng 2022:7488254. https://doi.org/10.1155/2022/7488254

Villa F, Gulotta D, Toniolo L, Borruso L, Cattò C, Cappitelli F (2020) Aesthetic alteration of marble surfaces caused by biofilm formation: Effects of chemical cleaning. Coatings 10:122. https://doi.org/10.3390/coatings10020122

Vincent J, Colin B, Lanneluc I, Sabot R, Turcry P, Mahieux P, Refait P, Jeannin M, Sabl S (2022a) New Biocalcifying Marine Bacterial Strains Isolated from Calcareous Deposits and Immediate Surroundings. Microorganisms. 10:76. https://doi.org/10.3390/microorganisms10010076

Vincent J, Koziorowszki L, Frein A, Lanneluc I, Refait P, Sabl S, Jeannin M (2022b) Bioelectrochemistry Calcareous deposit formation under cathodic polarization and marine biocalcifying bacterial activity. Adv Mater Sci Eng 148:108271. https://doi.org/10.1016/j.bioelechem.2022.108271

Vu HHT, Khan MD, Van Tran T, Quang DV, Dao VD, Lee S, Ahn JW, Jung SH (2020) Use of calcite mud from paper factories in phosphorus treatment. Sustain 12:5982. https://doi.org/10.3390/su12155982

Wakefield RD, Jones MS (1998) An introduction to stone colonizing micro-organisms and biodeterioration of building stone. Q J Eng Geol 31:301–313. https://doi.org/10.1144/GSL.QJEG.1998.031.P4.03

Wang J, Ersan YC, Boon N, De Belie N (2016) Application of microorganisms in concrete: a promising sustainable strategy to improve concrete durability. Appl Microbiol Biotechnol 100:2993–3007 . https://doi.org/10.1007/s00253-016-7370-6

Wang J, Jonkers HM, Boon N, De Belie N (2017) *Bacillus sphaericus* LMG 22257 is physiologically suitable for self-healing concrete. Appl Microbiol Biotechnol 101:5101–5114 . https://doi.org/10.1007/s00253-017-8260-2

Wang J, Mignon A, Snoeck D, Wiktor V, Van Vliergerghe S, Boon N, De Belie N (2015) Application of modified-alginate encapsulated carbonate producing bacteria in concrete: A promising strategy for crack self-healing. Front Microbiol 6:1088. https://doi.org/10.3389/fmicb.2015.01088

Wang J, Mignon A, Trenson G, Van Vlierberghe S, Boon N, De Belie N (2018a) A chitosan

based pH-responsive hydrogel for encapsulation of bacteria for self-sealing concrete. Cem Concr Compos 93:309–322. https://doi.org/10.1016/j.cemconcomp.2018.08.007

Wang J, Mignon A, Trenson G, Van Vlierberghe S, Boon N, De Belie N (2018b) A chitosan based pH-responsive hydrogel for encapsulation of bacteria for self-sealing concrete. Cem Concr Compos 93:309–322. https://doi.org/10.1016/j.cemconcomp.2018.08.007

Wang J, Van Tittelboom K, De Belie N, Verstraete W (2012a) Use of silica gel or polyurethane immobilized bacteria for self-healing concrete. Constr Build Mater 26:532–540. https://doi.org/10.1016/j.conbuildmat.2011.06.054

Wang JY, De Belie N, Verstraete W (2012b) Diatomaceous earth as a protective vehicle for bacteria applied for self-healing concrete. J Ind Microbiol Biotechnol 39:567–577. https://doi.org/10.1007/s10295-011-1037-1

Wang JY, Soens H, Verstraete W, De Belie N (2014) Self-healing concrete by use of microencapsulated bacterial spores. Cem Concr Res 56:139–152. https://doi.org/10.1016/j.cemconres.2013.11.009

Wang L, Ren Z, Wang H, Liang X, Liu S, Ren J, He Y (2022a) Microstructure-property relationships in cement mortar with surface treatment of microbial induced carbonate precipitation. Compos Part B 239:109986. https://doi.org/10.1016/j.compositesb.2022.109986

Wang L, Ren Z, Wang H, Liang X, Liu S, Ren J, He Y, Zhang M (2022b) Microstructure-property relationships in cement mortar with surface treatment of microbial induced carbonate precipitation. Compos Part B Eng 239:109986. https://doi.org/10.1016/j.compositesb.2022.109986

Wang X, Huang Y, Huang Y, Zhang J, Fang C, Yu K, Chen Q, Li T, Han R, Yang Z, Xu P, Liang G, Su D, Ding X, Li D, Han N, Xing F (2019) Laboratory and field study on the performance of microcapsule-based self-healing concrete in tunnel engineering. Constr Build Mater 220:90–101. https://doi.org/10.1016/j.conbuildmat.2019.06.017

Wang X, Li C, He J (2022c) A highly effective strain screened from soil and applied in cementing fine sand based on MICP-bonding technology. J Biotechnol 350:55–66.

https://doi.org/10.1016/j.jbiotec.2022.03.016

Wang X, Xu J, Wang Z, Yao W (2022d) Use of recycled concrete aggregates as carriers for self-healing of concrete cracks by bacteria with high urease activity. Constr Build Mater 337:127581 . https://doi.org/10.1016/j.conbuildmat.2022.127581

Webster A, May E (2006) Bioremediation of weathered-building stone surfaces. Trends Biotechnol 24:255–260. https://doi.org/10.1016/j.tibtech.2006.04.005

Wei S, Cui H, Jiang Z, Liu H, He H, Fang N (2015) Biomineralization processes of calcite induced by bacteria isolated from marine sediments. Brazilian J Microbiol 46:455–464. https://doi.org/10.1590/S1517-838246220140533

Wei T, Yashir N, An F, Imtiaz SA, Li X, Li H (2022) Study on the performance of carbonate-mineralized bacteria combined with eggshell for immobilizing Pb and Cd in water and soil. Environ Sci Pollut Res 29:2924–2935. https://doi.org/10.1007/s11356-021-15138-0

Weiner S, Patricia M. Dove (2003) An Overview of Biomineralization Processes and the Problem of the Vital Effect. Rev Mineral Geochemistry 54:1–29. https://doi.org/10.2113/0540001

Weisburg WG, Barns SM, Pelletier DA, Lane DJ (1991) 16S ribosomal DNA amplification for phylogenetic study. J Bacteriol 173:697–703. https://doi.org/10.1128/jb.173.2.697-703.1991

Wen K, Li Y, Amini F, Li L (2020) Impact of bacteria and urease concentration on precipitation kinetics and crystal morphology of calcium carbonate. Acta Geotech 15:17–27. https://doi.org/10.1007/s11440-019-00899-3

Whiffin VS (2004) Microbial CaCO 3 precipitation for the production of Biocement. Perth: Murdoch University. 20

Whiffin VS, van Paassen LA, Harkes MP (2007) Microbial carbonate precipitation as a soil improvement technique. Geomicrobiol J 24:417–423. https://doi.org/10.1080/01490450701436505

Wiktor V, Jonkers HM (2011) Quantification of crack-healing in novel bacteria-based self-

healing concrete. Cem Concr Compos 33:763–770. https://doi.org/10.1016/j.cemconcomp.2011.03.012

Williams SL, Artier J, Qiu J, Heveran C, Nagarajan A, Hubler M, Cook SM, Cameron JC, Srubar Iii W V (2019) 3 rd International Conference on Bio-Based Building Materials regenerative hydrogel-based microbial mortars: investigation of viability and strength in successive material generations. Acad J Civ Eng 37:238–243. https://doi.org/10.26168/icbbm2019.34

Williams SL, Kirisits MJ, Ferron RD (2017) Influence of concrete-related environmental stressors on biomineralizing bacteria used in self-healing concrete. Constr Build Mater 139:611–618 . https://doi.org/10.1016/j.conbuildmat.2016.09.155

Woodson RD (2009) Causes of distress and deterioration of concrete. Concr Struct 19–29. https://doi.org/10.1016/b978-1-85617-549-4.00003-4

Wu LYL, Soutar AM, Zeng XT (2005) Increasing hydrophobicity of sol-gel hard coatings by chemical and morphological modifications. Surf Coatings Technol 198:420–424. https://doi.org/10.1016/j.surfcoat.2004.10.050

Wu M, Hu X, Zhang Q, Xue D, Zhao Y (2019) Growth environment optimization for inducing bacterial mineralization and its application in concrete healing. Constr Build Mater 209:631–643. https://doi.org/10.1016/j.conbuildmat.2019.03.181

Wu M, Johannesson B, Geiker M (2012) A review: Self-healing in cementitious materials and engineered cementitious composite as a self-healing material. Constr Build Mater 28:571–583. https://doi.org/10.1016/j.conbuildmat.2011.08.086

Wu Y, Tan L, Liu W, Wang B, Wang J, Cai Y, Lin X (2015) Profiling bacterial diversity in a limestone cave of the western Loess Plateau of China. Front Microbiol 6:244. https://doi.org/10.3389/fmicb.2015.00244

Xiao J, Wang Z, Tang Y, Yang S (2010) Biomimetic mineralization of $CaCO_3$ on a phospholipid monolayer: From an amorphous calcium carbonate precursor to calcite via vaterite. Langmuir 26:4977–4983. https://doi.org/10.1021/la903641k

Xiao X, Tan ACY, Unluer C, Yang EH (2023) Development of a functionally graded bacteria capsule for self-healing concrete. Cem Concr Compos 136:104863. https://doi.org/10.1016/j.cemconcomp.2022.104863

Xiao X, Unluer C, Yang E (2022a) Study on the viability of unprotected bacterial spores directly embedded in a reactive magnesia cement matrix for potential crack healing. Constr Build Mater 346:128424. https://doi.org/10.1016/j.conbuildmat.2022.128424

Xiao X, Unluer C, Yang E (2022b) Study on the viability of unprotected bacterial spores directly embedded in a reactive magnesia cement matrix for potential crack healing. Constr Build Mater 346:128424. https://doi.org/10.1016/j.conbuildmat.2022.128424

Xiao Y, Stuedlein AW, Pan Z, Liu H, Matthew Evans T, He X, Lin H, Chu J, van Paassen LA (2020) Toe-Bearing Capacity of Precast Concrete Piles through Biogrouting Improvement. J Geotech Geoenvironmental Eng 146:06020026. https://doi.org/10.1061/(asce)gt.1943-5606.0002404

Xie D, Zhang R, Wang J (2023) The influence of environmental factors and precipitation precursors on enzyme-induced carbonate precipitation (EICP) process and its application on modification of recycled concrete aggregates. J Clean Prod 395:136444. https://doi.org/10.1016/j.jclepro.2023.136444

Xu H, Lian J, Gao M, Fu D, Yan Y (2019a) Self-Healing Concrete Using Rubber Particles to to Immobilize Bacterial Spores. Materials (Basel) 12:2313. https://doi.org/10.3390/ma12142313

Xu H, Peng X, Bai S, Ta K, Yang S, Liu S, Bin Jang H, Guo Z (2019b) Precipitation of calcium carbonate mineral induced by viral lysis of cyanobacteria: Evidence from laboratory experiments. Biogeosciences 16:949–960. https://doi.org/10.5194/bg-16-949-2019

Xu J, Tang Y, Wang X, Wang Z, Yao W (2020) Application of ureolysis-based microbial CaCO3 precipitation in self-healing of concrete and inhibition of reinforcement corrosion. Constr Build Mater 265:120364. https://doi.org/10.1016/j.conbuildmat.2020.120364

Xu J, Wang X (2018) Self-healing of concrete cracks by use of bacteria-containing low alkali cementitious material. Constr Build Mater 167:1–14.

https://doi.org/10.1016/j.conbuildmat.2018.02.020

Xu J, Wang X, Wang B (2018) Biochemical process of ureolysis-based microbial $CaCO_3$ precipitation and its application in self-healing concrete. Appl Microbiol Biotechnol 102:3121–3132 . https://doi.org/10.1007/s00253-018-8779-x

Xue C, Li W, Qu F, Sun Z, Shah SP (2020) Self-healing efficiency and crack closure of smart cementitious composite with crystalline admixture and structural polyurethane. Constr Build Mater 260:119955 . https://doi.org/10.1016/j.conbuildmat.2020.119955

Yang D, Xu G, Duan Y, Dong S (2022) Self-healing cement composites based on bleaching earth immobilized bacteria. J Clean Prod 358:132045. https://doi.org/10.1016/j.jclepro.2022.132045

Yang Y, Chu J, Cao B, Liu H, Cheng L (2020) Biocementation of soil using non-sterile enriched urease-producing bacteria from activated sludge. J Clean Prod 262:121315. https://doi.org/10.1016/j.jclepro.2020.121315

Yao ZT, Xia MS, Sarker PK, Chen T (2014) A review of the alumina recovery from coal fly ash, with a focus in China. Fuel 120:74–85 . https://doi.org/10.1016/j.fuel.2013.12.003

Yazici Ş, Güller C, Ayekin B, Mardani A, Akkaya A (2023) Usability of sustainable materials on bacteria-based self-healing in cementitious systems. J Intell Mater Syst Struct. 34:1998-2019. https://doi.org/10.1177/1045389X231157358

Yi H, Zheng T, Jia Z, Su T, Wang C (2021) Study on the influencing factors and mechanism of calcium carbonate precipitation induced by urease bacteria. J Cryst Growth 564:126113 . https://doi.org/10.1016/j.jcrysgro.2021.126113

Yijin L, Shiqiong Z, Jian Y, Yingli G (2004) The effect of fly ash on the fluidity of cement paste, mortar and concrete. Proc Int Work Sustain Dev Concr Technol 339–345

Yılmazer Polat B, Uysal M (2021) Bacterial crack healing in metakaolin based geopolymer mortars. J Build Eng 39:102291 . https://doi.org/10.1016/j.jobe.2021.102291

Yu J, Zhang M, Li G, Meng J, Leung CKY (2020a) Using nano-silica to improve mechanical and fracture properties of fiber-reinforced high-volume fly ash cement mortar. Constr

Build Mater 239:117853. https://doi.org/10.1016/j.conbuildmat.2019.117853

Yu R, Chai H, Yu Z, Wu X, Liu Y, Shen L, Li J, Ye J, Liu D, Ma T, Gao F, Zeng W (2020b) Behavior and mechanism of cesium biosorption from aqueous solution by living *Synechococcus* PCC7002. Microorganisms 8:491. https://doi.org/10.3390/microorganisms8040491

Yu W, Rao Z, Yuan H, Wei P, Nyarko-Appiah JE, Jiang W (2023) An efficient and environmental friendly strategy for alumina extraction and Fe–Si alloys production from coal fly ash by combining vacuum thermal reduction, alkali dissolving, and magnetic separation. J Clean Prod 408:137129. https://doi.org/10.1016/J.JCLEPRO.2023.137129

Yu Y, You L, Liu D, Hollinshead W, Tang YJ, Zhang F (2013) Development of *Synechocystis* sp. PCC 6803 as a phototrophic cell factory. Mar Drugs 11:2894–2916. https://doi.org/10.3390/md11082894

Yuan H, Zhang Q, Hu X, Wu M, Zhao Y, Feng Y, Shen D (2022) Application of zeolite as a bacterial carrier in the self-healing of cement mortar cracks. Constr Build Mater 331:127324. https://doi.org/10.1016/j.conbuildmat.2022.127324

Zamani M, Nikafshar S, Mousa A, Behnia A (2020) Bacteria encapsulation using synthesized polyurea for self-healing of cement paste. Constr Build Mater 249:118556. https://doi.org/10.1016/j.conbuildmat.2020.118556

Zhang J, Liu Y, Feng T, Zhou M, Zhao L, Zhou A, Li Z (2017) Immobilizing bacteria in expanded perlite for the crack self-healing in concrete. Constr Build Mater 148:610–617. https://doi.org/10.1016/j.conbuildmat.2017.05.021

Zhang L V, Nehdi ML, Suleiman AR, Mehdizadeh M, Gan M, Marani A, Tuyan M (2021a) Crack self-healing in bio-green concrete. Compos Part B 227:109397. https://doi.org/10.1016/j.compositesb.2021.109397

Zhang L V., Suleiman AR, Mehdizadeh Allaf M, Marani A, Tuyan M, Nehdi ML (2022) Crack self-healing in alkali-activated slag composites incorporating immobilized bacteria. Constr Build Mater 326:126842. https://doi.org/10.1016/j.conbuildmat.2022.126842

Zhang S, Qiao WG, Chen PC, Xi K (2019) Rheological and mechanical properties of microfine-cement-based grouts mixed with microfine fly ash, colloidal nanosilica and superplasticizer. Constr Build Mater 212:10–18. https://doi.org/10.1016/j.conbuildmat.2019.03.314

Zhang X, Jin Z, Li M, Qian C (2021b) Effects of carrier on the performance of bacteria-based self-healing concrete. Constr Build Mater 305:124771. https://doi.org/10.1016/j.conbuildmat.2021.124771

Zhang X, Zhan Q, Su Y, Qian C, Shao J, Wang Z (2023) Scale preparation of core–shell bacterial healing agent for concrete and evaluation of shell protection and core mineralization ability. Constr Build Mater 406:133366. https://doi.org/10.1016/j.conbuildmat.2023.133366

Zhang Y, Wang S, Zhang B, Hou D, Li H, Li L, Wang J, Lin C (2020) A preliminary investigation of the properties of potassium magnesium phosphate cement-based grouts mixed with fly ash, water glass and bentonite. Constr Build Mater 237:117501. https://doi.org/10.1016/j.conbuildmat.2019.117501

Zheng T, Qian C (2020) Self-Healing of Later-Age Cracks in Cement-Based Materials by Encapsulation-Based Bacteria. J Mater Civ Eng 32:04020341. https://doi.org/10.1061/(asce)mt.1943-5533.0003437

Zhong Y, Li P, Hao J, Wang X (2020) Bioinspired Self-Healing of Kinetically Inert Hydrogels Mediated by Chemical Nutrient Supply. ACS Appl Mater Interfaces 12:6471–6478. https://doi.org/10.1021/acsami.9b20445

Zhu T, Dittrich M (2016) Carbonate precipitation through microbial activities in natural environment, and their potential in biotechnology: A review. Front Bioeng Biotechnol 4:4. https://doi.org/10.3389/fbioe.2016.00004

Zhu T, Lin Y, Lu X, Dittrich M (2018) Assessment of cyanobacterial species for carbonate precipitation on mortar surface under different conditions. Ecol Eng 120:154–163. https://doi.org/10.1016/j.ecoleng.2018.05.038

Zhu T, Lu X, Dittrich M (2017) Calcification on mortar by live and UV-killed biofilm-forming

cyanobacterial *Gloeocapsa* PCC73106. Constr Build Mater 146:43–53. https://doi.org/10.1016/j.conbuildmat.2017.04.026

Zhu T, Merroun ML, Arhonditsis G, Dittrich M (2021a) Attachment on mortar surfaces by cyanobacterium *Gloeocapsa* PCC 73106 and sequestration of CO_2 by microbially induced calcium carbonate. Microbiology open 10: e1243. https://doi.org/10.1002/mbo3.1243

Zhu T, Paulo C, Merroun ML, Dittrich M (2015a) Potential application of biomineralization by *Synechococcus* PCC8806 for concrete restoration. Ecol Eng 82:459–468. https://doi.org/10.1016/j.ecoleng.2015.05.017

Zhu WK, Mu T, Zhang YK, Duan T, Luo XG (2015b) Coating of microbially produced calcium carbonate onto stone materials. Sci China Technol Sci 58:266–272. https://doi.org/10.1007/s11431-014-5710-2

Zhu X, Mignon A, Nielsen SD, Zieger SE, Koren K, Boon N, De Belie N (2021b) Viability determination of *Bacillus sphaericus* after encapsulation in hydrogel for self-healing concrete via microcalorimetry and in situ oxygen concentration measurements. Cem Concr Compos 119: 104006. https://doi.org/10.1016/j.cemconcomp.2021.104006

Zhu Z, Bassey AP, Huang T, Zhang Y, Ali Khan I, Huang M (2022) The formation, germination, and cold plasma inactivation of bacterial spore. Food Chem Adv 1:100056. https://doi.org/10.1016/j.focha.2022.100056

Appendix I

Bacillus cereus strain MD1 16S ribosomal RNA gene, partial sequence

GenBank: OR673981.1

FASTA Graphics

Go to:

```
LOCUS       OR673981               1452 bp    DNA     linear   BCT 21-OCT-2023
DEFINITION  Bacillus cereus strain MD1 16S ribosomal RNA gene, partial
            sequence.
ACCESSION   OR673981
VERSION     OR673981.1
KEYWORDS    .
SOURCE      Bacillus cereus
  ORGANISM  Bacillus cereus
            Bacteria; Bacillota; Bacilli; Bacillales; Bacillaceae; Bacillus;
            Bacillus cereus group.
REFERENCE   1  (bases 1 to 1452)
  AUTHORS   Sidhu,N. and Reddy,M.S.
  TITLE     Isolation and Characterization of calcifying Bacteria from Marble
            Dust and thier biomineralization efficacy
  JOURNAL   Unpublished
REFERENCE   2  (bases 1 to 1452)
  AUTHORS   Sidhu,N. and Reddy,M.S.
  TITLE     Direct Submission
  JOURNAL   Submitted (16-OCT-2023) Department of Biotechnology, Thapar
            Institute of Engineering & Technology, Bhadson Road, Patiala,
            PUNJAB 147004, India
COMMENT     ##Assembly-Data-START##
            Sequencing Technology :: Sanger dideoxy sequencing
            ##Assembly-Data-END##
FEATURES             Location/Qualifiers
     source          1..1452
                     /organism="Bacillus cereus"
                     /mol_type="genomic DNA"
                     /strain="MD1"
                     /db_xref="taxon:1396"
                     /country="India"
                     /collection_date="Dec-2018"
     rRNA            <1..>1452
                     /product="16S ribosomal RNA"
ORIGIN
        1 cgaaggggat gcttaaacat gcaagtcgag cgaatggatt aagagcttgc tcttatgaag
       61 ttagcggcgg acgggtgagt aacacgtggg taacctgccc ataagactgg gataactccg
      121 ggaaaccggg gctaataccg gataacattt tgaaccgcat ggttcgaaat tgaaaggcgg
      181 cttcggctgt cacttatgga tggacccgcg tcgcattagc tagttggtga ggtaacggct
      241 caccaaggca acgatgcgta gccgacctga gagggtgatc ggccacactg ggactgagac
      301 acggcccaga ctcctacggg aggcagcagt agggaatctt ccgcaatgga cgaaagtctg
      361 acggagcaac gccgcgtgag tgatgaaggc tttcgggtcg taaaactctg ttgttaggga
      421 agaacaagtg ctagttgaat aagctggcac cttgacggta cctaaccaga aagccacggc
      481 taactacgtg ccagcagccg cggtaatacg taggtggcaa gcgttatccg gaattattgg
      541 gcgtaaagcg cgcgcaggtg gtctcttaag tctgatgtga aagcccacgg ctcaaccgtg
      601 gagggtcatt ggaaactggg agacttgagt gcagaagagg aaagtggaat tccatgtgta
      661 gcggtgaaat gcgtagagat atggaggaac accagtggcg aaggcgactt tctggtctgt
      721 aactgacact gaggcgcgaa agcgtgggga gcaaacagga ttagataccc tggtagtcca
      781 cgccgtaaac gatgagtgct aagtgttaga gggtttccgc cctttagtgc tgaagttaac
      841 gcattaagca ctccgcctgg ggagtacggc cgcaaggctg aaactcaaag gaattgacgg
      901 gggcccgcac aagcggtgga gcatgtggtt taattcgaag caacgcgaag aaccttacca
      961 ggtcttgaca tcctctgaaa accctagaga tagggcttct ccttcgggag cagagtgaca
     1021 ggtggtgcat ggttgtcgtc agctcgtgtc gtgagatgtt gggttaagtc ccgcaacgag
     1081 cgcaaccctt gatcttagtt gccatcatta agttgggcac tctaaggtga ctgccggtga
     1141 caaaccggag gaaggtgggg atgacgtcaa atcatcatgc cccttatgac ctgggctaca
     1201 cacgtgctac aatggacggt acaaagagct gcaagaccgc gaggtggagc taatctcata
     1261 aaaccgttct cagttcggat tgtaggctgc aactcgccta catgaagctg gaatcgctag
     1321 taatcgcgga tcagcatgcc gcggtgaata cgttcccggg ccttgtacac accgcccgtc
     1381 acaccacgag agtttgtaac acccgaagtc ggtggggtaa ccttttggag ccagccgcct
     1441 taagggtcct tg
//
```

Bacillus paranthracis strain MD2 16S ribosomal RNA gene, partial sequence

GenBank: OR673982.1

FASTA Graphics

Go to:

```
LOCUS       OR673982                1471 bp    DNA     linear   BCT 21-OCT-2023
DEFINITION  Bacillus paranthracis strain MD2 16S ribosomal RNA gene, partial
            sequence.
ACCESSION   OR673982
VERSION     OR673982.1
KEYWORDS    .
SOURCE      Bacillus paranthracis
  ORGANISM  Bacillus paranthracis
            Bacteria; Bacillota; Bacilli; Bacillales; Bacillaceae; Bacillus;
            Bacillus cereus group.
REFERENCE   1  (bases 1 to 1471)
  AUTHORS   Sidhu,N. and Reddy,M.S.
  TITLE     Isolation and Characterization of calcifying Bacteria from Marble
            Dust and thier biomineralization efficacy
  JOURNAL   Unpublished
REFERENCE   2  (bases 1 to 1471)
  AUTHORS   Sidhu,N. and Reddy,M.S.
  TITLE     Direct Submission
  JOURNAL   Submitted (16-OCT-2023) Department of Biotechnology, Thapar
            Institute of Engineering & Technology, Bhadson Road, Patiala,
            PUNJAB 147004, India
COMMENT     ##Assembly-Data-START##
            Sequencing Technology :: Sanger dideoxy sequencing
            ##Assembly-Data-END##
FEATURES             Location/Qualifiers
     source          1..1471
                     /organism="Bacillus paranthracis"
                     /mol_type="genomic DNA"
                     /strain="MD2"
                     /db_xref="taxon:2026186"
                     /country="India"
                     /collection_date="Dec-2018"
     rRNA            <1..>1471
                     /product="16S ribosomal RNA"
ORIGIN
        1 gctcaggatg aacgctggcg gcgtgcctaa tacatgcaac gtcgagcaga atggattaag
       61 cagcttgctc ttatgaagtt agcggcggac gggtgagtaa cacgtgggta acctgcccat
      121 aagactggga taactccggg aaaccggggc taataccgga taacattttg aaccgcatgg
      181 ttcgaaattg aaaggcggct tcggctgtca cttatggatg gacccgcgtc gcattagcta
      241 gttggtgagg taacggctca ccaaggcaac gatgcgtagc cgacctgaga gggtgatcgg
      301 ccacactggg actgagacac ggcccagact cctacgggag gcagcagtag ggaatcttcc
      361 gcaatggacg aaagtctgac ggagcaacgc cgcgtgagtg atgaaggctt tcgggtcgta
      421 aaactctgtt gttagggaag aacaagtgct agttgaataa gctggcacct tgacggtacc
      481 taaccagaaa gccacggcta actacgtgcc agcagccgcg gtaatacgta ggtggcaagc
      541 gttatccgga attattgggc gtaaagcgcg cgcaggtggt ttcttaagtc tgatgtgaaa
      601 gcccacggct caaccgtgga gggtcattgg aaactgggag acttgagtgc agaagaggaa
      661 agtggaattc catgtgtagc ggtgaaatgc gtagagatat ggaggaacac cagtggcgaa
      721 ggcgactttc tggtctgtaa ctgacactga ggcgcgaaag cgtggggagc aaacaggatt
      781 agataccctg gtagtccacg ccgtaaacga tgagtgctaa gtgttagagg gtttccgccc
      841 tttagtgctg aagttaacgc attaagcact ccgcctgggg agtacggccg caaggctgaa
      901 actcaaagga attgacgggg gcccgcacaa gcggtggagc atgtggttta attcgaagca
      961 acgcgaagaa ccttaccagg tcttgacatc ctctgacaac cctagagata gggcttctcc
     1021 ttcgggagca gagtgacagg tggtgcatgg ttgtcgtcag ctcgtgtcgt gagatgttgg
     1081 gttaagtccc gcaacgagcg caacccttga tcttagttgc catcattaag ttgggcactc
     1141 taaggtgact gccggtgaca aaccggagga aggtggggat gacgtcaaat catcatgccc
     1201 cttatgacct gggctacaca cgtgctacaa tggacggtac aaagagctgc aagaccgcga
     1261 ggtggagcta atctcataaa accgttctca gttcggattg taggctgcaa ctcgcctaca
     1321 tgaagctgga atcgctagta atcgcggatc agcatgccgc ggtgaatacg ttcccgggcc
     1381 ttgtacacac cgcccgtcac accacgagag tttgtaacat ccgcgaagtc ggtggggcca
     1441 ccttttggaa ccaagccgcc cttaagtggg a
//
```

Bacillus paranthracis strain MD3 16S ribosomal RNA gene, partial sequence

GenBank: OR673983.1

FASTA Graphics

Go to:

```
LOCUS       OR673983               1468 bp    DNA     linear   BCT 21-OCT-2023
DEFINITION  Bacillus paranthracis strain MD3 16S ribosomal RNA gene, partial
            sequence.
ACCESSION   OR673983
VERSION     OR673983.1
KEYWORDS    .
SOURCE      Bacillus paranthracis
  ORGANISM  Bacillus paranthracis
            Bacteria; Bacillota; Bacilli; Bacillales; Bacillaceae; Bacillus;
            Bacillus cereus group.
REFERENCE   1  (bases 1 to 1468)
  AUTHORS   Sidhu,N. and Reddy,M.S.
  TITLE     Isolation and Characterization of calcifying Bacteria from Marble
            Dust and thier biomineralization efficacy
  JOURNAL   Unpublished
REFERENCE   2  (bases 1 to 1468)
  AUTHORS   Sidhu,N. and Reddy,M.S.
  TITLE     Direct Submission
  JOURNAL   Submitted (16-OCT-2023) Department of Biotechnology, Thapar
            Institute of Engineering & Technology, Bhadson Road, Patiala,
            PUNJAB 147004, India
COMMENT     ##Assembly-Data-START##
            Sequencing Technology :: Sanger dideoxy sequencing
            ##Assembly-Data-END##
FEATURES             Location/Qualifiers
     source          1..1468
                     /organism="Bacillus paranthracis"
                     /mol_type="genomic DNA"
                     /strain="MD3"
                     /db_xref="taxon:2026186"
                     /country="India"
                     /collection_date="Dec-2018"
     rRNA            <1..>1468
                     /product="16S ribosomal RNA"
ORIGIN
        1 ccgggggggaa tgctaatact tgcaacgtcg agcgaatgga ttaagagctt gctcttatga
       61 agttagcggc ggacgggtga gtaacacgtg ggtaacctgc ccataagact gggataactc
      121 cgggaaaccg gggctaatac cggataacat tttgaaccgc atggttcgaa attgaaaggc
      181 ggcttcggct gtcacttatg gatggacccg cgtcgcatta gctagttggt gaggtaacgg
      241 ctcaccaagg caacgatgcg tagccgacct gagagggtga tcggccacac tgggactgag
      301 acacggccca gactcctacg ggaggcagca gtagggaatc ttccgcaatg gacgaaagtc
      361 tgacggagca acgccgcgtg agtgatgaag gctttcgggt cgtaaaactc tgttgttagg
      421 gaagaacaag tgctagttga ataagctggc accttgacgg tacctaacca gaaagccacg
      481 gctaactacg tgccagcagc cgcggtaata cgtaggtggc aagcgttatc cggaattatt
      541 gggcgtaaag cgcgcgcagg tggtttctta agtctgatgt gaaagcccac ggctcaaccg
      601 tggagggtca ttggaaactg ggagacttga gtgcagaaga ggaaagtgga attccatgtg
      661 tagcggtgaa atgcgtagag atatggagga acaccagtgg cgaaggcgac tttctggtct
      721 gtaactgaca ctgaggcgcg aaagcgtggg gagcaaacag gattagatac cctggtagtc
      781 cacgccgtaa acgatgagtg ctaagtgtta gagggtttcc gccctttagt gctgaagtta
      841 acgcattaag cactccgcct ggggagtacg gccgcaaggc tgaaactcaa aggaattgac
      901 gggggcccgc acaagcggtg gagcatgtgg tttaattcga agcaacgcga agaaccttac
      961 caggtcttga catcctctga caaccctaga gatagggctt ctccttcggg agcagagtga
     1021 caggtggtgc atggttgtcg tcagctcgtg tcgtgagatg ttgggttaag tcccgcaacg
     1081 agcgcaaccc ttgatcttag ttgccatcat taagttgggc actctaaggt gactgccggt
     1141 gacaaaccgg aggaaggtgg ggatgacgtc aaatcatcat gccccttatg acctgggcta
     1201 cacacgtgct acaatggacg gtacaaagag ctgcaagacc gcgaggtgga gctaatctca
     1261 taaaaccgtt ctcagttcgg attgtaggct gcaactcgcc tacatgaagc tggaatcgct
     1321 agtaatcgcg gatcagcatg ccgcggtgaa tacgttcccg ggccttgtac acaccgcccg
     1381 tcacaccacg agagtttgta acatcccgaa tcggtggggt aacctttgg aacccacccg
     1441 ccaaaggggg aacaaagaat ggggtgaa
//
```

Bacillus paramycoides strain MD4 16S ribosomal RNA gene, partial sequence

GenBank: OR673984.1

FASTA Graphics

Go to:

```
LOCUS       OR673984                1460 bp    DNA     linear   BCT 21-OCT-2023
DEFINITION  Bacillus paramycoides strain MD4 16S ribosomal RNA gene, partial
            sequence.
ACCESSION   OR673984
VERSION     OR673984.1
KEYWORDS    .
SOURCE      Bacillus paramycoides
  ORGANISM  Bacillus paramycoides
            Bacteria; Bacillota; Bacilli; Bacillales; Bacillaceae; Bacillus;
            Bacillus cereus group.
REFERENCE   1  (bases 1 to 1460)
  AUTHORS   Sidhu,N. and Reddy,M.S.
  TITLE     Isolation and Characterization of calcifying Bacteria from Marble
            Dust and thier biomineralization efficacy
  JOURNAL   Unpublished
REFERENCE   2  (bases 1 to 1460)
  AUTHORS   Sidhu,N. and Reddy,M.S.
  TITLE     Direct Submission
  JOURNAL   Submitted (16-OCT-2023) Department of Biotechnology, Thapar
            Institute of Engineering & Technology, Bhadson Road, Patiala,
            PUNJAB 147004, India
COMMENT     ##Assembly-Data-START##
            Sequencing Technology :: Sanger dideoxy sequencing
            ##Assembly-Data-END##
FEATURES             Location/Qualifiers
     source          1..1460
                     /organism="Bacillus paramycoides"
                     /mol_type="genomic DNA"
                     /strain="MD4"
                     /db_xref="taxon:2026194"
                     /country="India"
                     /collection_date="Dec-2018"
     rRNA            <1..>1460
                     /product="16S ribosomal RNA"
ORIGIN
        1 gggggcctа atacatgcaa gtcgagcgaa tggattaaga gcttgctctt atgaagttag
       61 cggcggacgg gtgagtaaca cgtgggtaac ctgcccataa gactgggata actccgggaa
      121 accggggcta ataccggata acattttgaa ccgcatggtt cgaaattgaa aggcggcttc
      181 ggctgtcact tatggatgga cccgcgtcgc attagctagt tggtgaggta acggctcacc
      241 aaggcaacga tgcgtagccg acctgagagg gtgatcggcc acactgggac tgagacacgg
      301 cccagactcc tacgggaggc agcagtaggg aatcttccgc aatggacgaa agtctgacgg
      361 agcaacgccg cgtgagtgat gaaggctttc gggtcgtaaa actctgttgt tagggaagaa
      421 caagtgctag ttgaataagc tggcaccttg acggtaccta accagaaagc cacggctaac
      481 tacgtgccag cagccgcggt aatacgtagg tggcaagcgt tatccggaat tattgggcgt
      541 aaagcgcgcg caggtggttt cttaagtctg atgtgaaagc ccacggctca accgtggagg
      601 gtcattggaa actgggagac ttgagtgcag aagaggaaag tggaattcca tgtgtagcgg
      661 tgaaatgcgt agagatatgg aggaacacca gtggcgaagg cgactttctg gtctgtaact
      721 gacactgagg cgcgaaagcg tggggagcaa acaggattag ataccctggt agtccacgcc
      781 gtaaacgatg agtgctaagt gttagagggt ttccgccctt tagtgctgaa gttaacgcat
      841 taagcactcc gcctggggag tacggccgca aggctgaaac tcaaaggaat tgacgggggc
      901 ccgcacaagc ggtggagcat gtggtttaat tcgaagcaac gcgaagaacc ttaccaggtc
      961 ttgacatcct ctgacaaccc tagagatagg gcttctcctt cgggagcaga gtgacaggtg
     1021 gtgcatggtt gtcgtcagct cgtgtcgtga gatgttgggt taagtcccgc aacgagcgca
     1081 acccttgatc ttagttgcca tcattaagtt gggcactcta aggtgactgc cggtgacaaa
     1141 ccggaggaag gtggggatga cgtcaaatca tcatgcccct tatgacctgg gctacacacg
     1201 tgctacaatg gacggtacaa agagctgcaa gaccgcgagg tggagctaat ctcataaaac
     1261 cgttctcagt tcggattgta ggctgcaact cgcctacatg aagctggaat cgctagtaat
     1321 cgcggatcag catgccgcgg tgaatacgtt cccgggcctt gtacacaccg cccgtcacac
     1381 cacgagagtt tgtaacaccc gaagtcggtg gggtaacctt ttggagccag ccgcctaagg
     1441 tgggacagat gattggggtg
//
```

Bacillus paramycoides strain MD6 16S ribosomal RNA gene, partial sequence

GenBank: OR673986.1

FASTA Graphics

Go to:

```
LOCUS       OR673986                1440 bp    DNA     linear   BCT 21-OCT-2023
DEFINITION  Bacillus paramycoides strain MD6 16S ribosomal RNA gene, partial
            sequence.
ACCESSION   OR673986
VERSION     OR673986.1
KEYWORDS    .
SOURCE      Bacillus paramycoides
  ORGANISM  Bacillus paramycoides
            Bacteria; Bacillota; Bacilli; Bacillales; Bacillaceae; Bacillus;
            Bacillus cereus group.
REFERENCE   1  (bases 1 to 1440)
  AUTHORS   Sidhu,N. and Reddy,M.S.
  TITLE     Isolation and Characterization of calcifying Bacteria from Marble
            Dust and thier biomineralization efficacy
  JOURNAL   Unpublished
REFERENCE   2  (bases 1 to 1440)
  AUTHORS   Sidhu,N. and Reddy,M.S.
  TITLE     Direct Submission
  JOURNAL   Submitted (16-OCT-2023) Department of Biotechnology, Thapar
            Institute of Engineering & Technology, Bhadson Road, Patiala,
            PUNJAB 147004, India
COMMENT     ##Assembly-Data-START##
            Sequencing Technology :: Sanger dideoxy sequencing
            ##Assembly-Data-END##
FEATURES             Location/Qualifiers
     source          1..1440
                     /organism="Bacillus paramycoides"
                     /mol_type="genomic DNA"
                     /strain="MD6"
                     /db_xref="taxon:2026194"
                     /country="India"
                     /collection_date="Dec-2018"
     rRNA            <1..>1440
                     /product="16S ribosomal RNA"
ORIGIN
        1 atgcaacgtg cgagcgaatg gattaagagc ttgctcttat gaagttagcg gcggacgggt
       61 gagtaacacg tgggtaacct gcccataaga ctgggataac tccgggaaac cggggctaat
      121 accggataac attttgaacc gcatggttcg aaattgaaag gcggcttcgg ctgtcactta
      181 tggatggacc cgcgtcgcat tagctagttg gtgaggtaac ggctcaccaa ggcaacgatg
      241 cgtagccgac ctgagagggt gatcggccac actgggactg agacacggcc cagactccta
      301 cgggaggcag cagtagggaa tcttccgcaa tggacgaaag tctgacggag caacgccgcg
      361 tgagtgatga aggctttcgg gtcgtaaaac tctgttgtta gggaagaaca agtgctagtt
      421 gaataagctg gcaccttgac ggtacctaac cagaaagcca cggctaacta cgtgccagca
      481 gccgcggtaa tacgtaggtg gcaagcgtta tccggaatta ttgggcgtaa agcgcgcgca
      541 ggtggtttct taagtctgat gtgaaagccc acggctcaac cgtggagggt cattggaaac
      601 tgggagactt gagtgcagaa gaggaaagtg gaattccatg tgtagcggtg aaatgcgtag
      661 agatatggag gaacaccagt ggcgaaggcg actttctggt ctgtaactga cactgaggcg
      721 cgaaagcgtg gggagcaaac aggattagat accctggtag tccacgccgt aaacgatgag
      781 tgctaagtgt tagagggttt ccgcccttta gtgctgaagt taacgcatta agcactccgc
      841 ctggggagta cggccgcaag gctgaaactc aaaggaattg acgggggccc gcacaagcgg
      901 tggagcatgt ggtttaattc gaagcaacgc gaagaacctt accaggtctt gacatcctct
      961 gacaacccta gagatagggc ttctccttcg ggagcagagt gacaggtggt gcatggttgt
     1021 cgtcagctcg tgtcgtgaga tgttgggtta agtcccgcaa cgagcgcaac ccttgatctt
     1081 agttgccatc attaagttgg gcactctaag gtgactgccg gtgacaaacc ggaggaaggt
     1141 ggggatgacg tcaaatcatc atgcccctta tgacctgggc tacacacgtg ctacaatgga
     1201 cggtacaaag agctgcaaga ccgcgaggtg gagctaatct cataaaaccg ttctcagttc
     1261 ggattgtagg ctgcaactcg cctacatgaa gctggaatcg ctagtaatcg cggatcagca
     1321 tgccgcggtg aatacgttcc cgggccttgt acacaccgcc cgtcacacca cgagagtttg
     1381 taacatcccg aagtcgcgtg gggtaacctt tggagccagc cgcctaaggg gacagaaggg
//
```

Bacillus paramycoides strain MD7 16S ribosomal RNA gene, partial sequence

GenBank: OR673987.1

FASTA Graphics

Go to:

```
LOCUS       OR673987               1450 bp    DNA     linear   BCT 21-OCT-2023
DEFINITION  Bacillus paramycoides strain MD7 16S ribosomal RNA gene, partial
            sequence.
ACCESSION   OR673987
VERSION     OR673987.1
KEYWORDS    .
SOURCE      Bacillus paramycoides
  ORGANISM  Bacillus paramycoides
            Bacteria; Bacillota; Bacilli; Bacillales; Bacillaceae; Bacillus;
            Bacillus cereus group.
REFERENCE   1  (bases 1 to 1450)
  AUTHORS   Sidhu,N. and Reddy,M.S.
  TITLE     Isolation and Characterization of calcifying Bacteria from Marble
            Dust and thier biomineralization efficacy
  JOURNAL   Unpublished
REFERENCE   2  (bases 1 to 1450)
  AUTHORS   Sidhu,N. and Reddy,M.S.
  TITLE     Direct Submission
  JOURNAL   Submitted (16-OCT-2023) Department of Biotechnology, Thapar
            Institute of Engineering & Technology, Bhadson Road, Patiala,
            PUNJAB 147004, India
COMMENT     ##Assembly-Data-START##
            Sequencing Technology :: Sanger dideoxy sequencing
            ##Assembly-Data-END##
FEATURES             Location/Qualifiers
     source          1..1450
                     /organism="Bacillus paramycoides"
                     /mol_type="genomic DNA"
                     /strain="MD7"
                     /db_xref="taxon:2026194"
                     /country="India"
                     /collection_date="Dec-2018"
     rRNA            <1..>1450
                     /product="16S ribosomal RNA"
ORIGIN
        1 tgcctaatac atgcaacgtc gagcgaatgg attaagcagc ttgctcttat gaagttagcg
       61 gcggacgggt gagtaacacg tgggtaacct gcccataaga ctgggataac tccgggaaac
      121 cggggctaat accggataac attttgaacc gcatggttcg aaattgaaag gcggcttcgg
      181 ctgtcactta tggatggacc cgcgtcgcat tagctagttg gtgaggtaac ggctcaccaa
      241 ggcaacgatg cgtagccgac ctgagagggt gatcggccac actgggactg agacacggcc
      301 cagactccta cgggaggcaa tcttccgcaa tggacgaaag tctgacggag caacgccgcg
      361 tgagtgatga aggctttcgg gtcgtaaaac tctgttgtta gggaagaaca agtgctagtt
      421 gaataagctg gcaccttgac ggtacctaac cagaaagcca cggctaacta cgtgccagca
      481 gccgcggtaa tacgtaggtg gcaagcgtta tccggaatta ttgggcgtaa agcgcgcgca
      541 ggtggtttct taagtctgat gtgaaagccc acggctcaac cgtggagggt cattggaaac
      601 tgggagactt gagtgcagaa gaggaaagtg gaattccatg tgtagcggtg aaatgcgtag
      661 agatatggag gaacaccagt ggcgaaggcg actttctggt ctgtaactga cactgaggcg
      721 cgaaagcgtg gggagcaaac aggattagat accctggtag tccacgccgt aaacgatgag
      781 tgctaagtgt tagagggttt ccgcccttta gtgctgaagt taacgcatta agcactccgc
      841 ctggggagta cggccgcaag gctgaaactc aaaggaattg acgggggccc gcacaagcgg
      901 tggagcatgt ggtttaattc gaagcaacgc gaagaacctt accaggtctt gacatcctct
      961 gacaacccta gagatagggc ttctccttcg ggagcagagt gacaggtggt gcatggttgt
     1021 cgtcagctcg tgtcgtgaga tgttgggtta agtcccgcaa cgagcgcaac ccttgatctt
     1081 agttgccatc attaagttgg gcactctaag gtgactgccg gtgacaaacc ggaggaaggt
     1141 ggggatgacg tcaaatcatc atgcccctta tgacctgggc tacacacgtg ctacaatgga
     1201 cggtacaaag agctgcaaga ccgcgaggtg gagctaatct cataaaaccg ttctcagttc
     1261 ggattgtagg ctgcaactcg cctacatgaa gctggaatcg ctagtaatcg cggatcagca
     1321 tgccgcggtg aatacgttcc cgggccttgt acacaccgcc cgtcacacca cgagagtttg
     1381 taacatcccg aagtcgcgtg gggtaacctc ttggacccag ccgcctaagg tgggacagat
     1441 gattggggtg
//
```

AMB Express

ORIGINAL ARTICLE

Open Access

Biomineralization of cyanobacteria *Synechocystis pevalekii* improves the durability properties of cement mortar

Navneet Sidhu[1], Shweta Goyal[2] and M. Sudhakara Reddy[1*]

Abstract

Microbially induced calcium carbonate precipitation (MICCP) is considered a novel eco-friendly technique to enhance the structural properties of cementitious-based material. Maximum studies have emphasized using ureolytic bacteria to improve the durability properties of building structures. In this study, the role of photoautotrophic bacteria *Synechocystis pevalekii* BDHKU 35101 has been investigated for calcium carbonate precipitation in sand consolidation, and enhancing mechanical and permeability properties of cement mortar. Both live and UV-treated *S. pevalekii* cells were used to treat the mortar specimens, and the results were compared with the control. The compressive strength of mortar specimens was significantly enhanced by 25.54% and 15.84% with live and UV-treated *S. pevalekii* cells at 28-day of curing. Water absorption levels were significantly reduced in bacterial-treated mortar specimens compared to control at 7 and 28-day curing. Calcium carbonate precipitation was higher in live-treated cells than in UV-treated *S. pevalekii* cells. Calcium carbonate precipitation by *S. pevalekii* cells was confirmed with SEM-EDS, XRD, and TGA analysis. These results suggest that *S. pevalekii* can serve as a low-cost and environment friendly MICCP technology to improve the durability properties of cementitious materials.

Keypoints

- Cyanobacterial *Synechocystis pevalekii* cells induced calcification on cement mortar.
- Both live and UV-treated cells increased the compressive strength and reduced the water absorption.
- Biomineralization by *S. pevalekii* serves as a low-cost and eco-friendly MICCP technology.

Keywords: Cyanobacteria, *Synechocystis pevalekii*, Calcium carbonate precipitation, Sand consolidation, Compressive strength, Water absorption, Mortar

Introduction

Microbially induced calcium carbonate precipitation (MICCP) is a biochemical process caused by microorganisms, resulting in calcium carbonate as a product. For the last two decades, this process has drawn significant attention from scientific researchers in the area of environment, biotechnology, and civil engineering because of its eco-efficiency over the expensive chemical treatments for concrete repair and restoration (Dhami et al. 2013). The most studied technique in these processes is ureolysis by heterotrophic bacteria due to its high calcium carbonate precipitating ability (Dhami et al. 2013). Ureolytic bacteria can induce calcium carbonate by accumulating a urease enzyme that utilizes urea as a substrate

*Correspondence: msreddy@thapar.edu

[1] Department of Biotechnology, Thapar Institute of Engineering & Technology, Patiala 147004, Punjab, India
Full list of author information is available at the end of the article

Springer Open

© The Author(s) 2022. **Open Access** This article is licensed under a Creative Commons Attribution 4.0 International License, which permits use, sharing, adaptation, distribution and reproduction in any medium or format, as long as you give appropriate credit to the original author(s) and the source, provide a link to the Creative Commons licence, and indicate if changes were made. The images or other third party material in this article are included in the article's Creative Commons licence, unless indicated otherwise in a credit line to the material. If material is not included in the article's Creative Commons licence and your intended use is not permitted by statutory regulation or exceeds the permitted use, you will need to obtain permission directly from the copyright holder. To view a copy of this licence, visit http://creativecommons.org/licenses/by/4.0/.

and calcium as a source for mineralization. However, one of the significant setbacks in ureolysis is the release of ammonia gas, a harmful air pollutant with a pungent smell. The ammonia formation results in nitrogen oxide releasing into the atmosphere, producing a foul odor (De Muynck et al. 2010). Moreover, excess ammonium in the concrete increases the risk of salt damage by converting it into nitric acid (Seifan et al. 2016). Scientists are hence, continuously looking for another alternative to overcome this drawback. The use of phototrophic bacteria can serve as a potential source alternative to heterotrophic bacteria in enhancing the durability properties of building structures.

Recently, an eco-efficient approach involving photoautotrophic bacteria has gained attention in utilizing them in improving the durability properties of building materials (Zhu et al. 2017, 2018). Unlike ureolytic bacteria, photoautotrophic bacteria use carbon dioxide and sunlight as energy instead of urea and produce carbonate crystals. Photoautotrophic bacteria such as cyanobacteria can induce carbonate precipitation in aquatic and terrestrial environments (Douglas and Beveridge 2006; Dittrich and Sibler 2010; Kranz et al. 2010). Therefore, the utilization of cyanobacteria for the biomineralization process in cementitious structures has attracted many researchers (Zhu et al. 2017, 2018).

Phylogenetically cyanobacteria are diverse and found in moist soil, marine or freshwater, extreme habitats like hot springs, hypersaline water, and deserts. The most distinctive characteristic of cyanobacteria is its ability to survive in a minimum requirement of light, carbon dioxide (CO_2), and water (Singh et al. 2016). Due to the exchange process of HCO_3^- /OH^- ions across the cell membrane during CO_2 fixation, the pH increases, creating an alkaline microenvironment that favors the carbonate precipitation (Han et al. 2013). The photosynthetic reaction of cyanobacteria is catalyzed by RUBISCO-carboxylase and carbonic anhydrase enzymes. The CO_2 enters the cyanobacterial cell through the HCO_3^-/Na^+ symporter, which is further converted to HCO_3^-. In the carbon concentration mechanism (CCM.), HCO_3^- in the cytosol is carried to the carboxysome and converted into CO_2 through carbonic anhydrase activity (Eq. 1). As a result, the OH^- is released across the cell membrane, increasing the pH of the cell exterior (Kamennaya et al. 2012).

$$CO_2 + H_2O \leftrightarrow H^+ + HCO_3^- \quad (1)$$

Calcium carbonate precipitation is an extracellular process that occurs either in exopolysaccharide sheath (EPS) or in the proteinaceous surface layer (S-layer), which are surrounding the cells (Han et al. 2013). Consumption of H^+ ions due to carbonic anhydrase activity increases alkalinization at EPS or S-layer. The EPS layer acts as a nucleation site for calcium carbonate binding. The calcium carbonate precipitation proceeds by following reactions.

$$Ca^{2+} + 2HCO_3^- \leftrightarrow CaCO_3 + CO_2 + H_2O \quad (2)$$

$$Ca^{2+} + CO_3^{2-} \leftrightarrow CaCO_3 \quad (3)$$

Precipitation of calcium carbonate by cyanobacteria such as *Oscillatoria* sp., *Synechococcus* sp., and *Synechocystis* sp., has been reported under laboratory conditions (Gnanasekaran 2014; Han et al. 2017; Paulo et al. 2018). Recently, the carbonate precipitation on cementitious structures by cyanobacteria has also been reported. Researchers reported the carbonate precipitation on the surface of cement mortar by cyanobacterial species such as *Gloeocapsa* sp. and *Synechococcus* sp. (Zhu et al. 2017, 2018; Srinivas et al. 2021) investigated the crack healing of cement mortar by using two microalgal species, *Synechococcus elongatus* and *Spirulina platensis*. Their results suggest that both the species can heal the cracks and improve the durability properties of the cement mortar with maximum potential by *S. platensis*. Though these studies show the potential use of phototrophic bacteria for crack healing and improvement of durability properties, the application of algae is still in the process of development, and more research needs to be done.

The present study was aimed to investigate the biomineralization potential of cyanobacteria, *Synechocystis pevalekii* isolated from the marine ecosystem. The biocalcification potential of *S. pevalekii* was studied by conducting experiments in laboratory conditions. The strength and permeability properties of cement mortar were investigated by treating them with live- and UV killed cells of *S. pevalekii*. The morphology of calcium carbonate crystals formed was determined using by scanning electron microscope (S.E.M.) and physio-chemical analysis by Energy-dispersive X-ray spectroscopy (EDX), X-Ray Diffraction (XRD), and Thermogravimetric analysis (TGA).

Materials and methods

Bacterial strain and cultivation conditions

The cyanobacterial strain, *Synechocystis pevalekii* BDHKU 35,101, isolated from the marine ecosystem (Bhuvaneshwari et al. 2017), was procured from the National Facility for Marine Cyanobacteria, Bharathidasan University Tiruchirappalli, Tamil Nadu, India. *Synechocystis pevalekii* cells are spherical, without individual mucilage envelope. The *S. pevalekii* cells were grown in BG 11 medium (Rippka et al. 1979), which has the following ingredients (g/l): $NaNO_3$ 1.5 g, K_2HPO_4 0.04 g,

$MgSO_4 \cdot 7H_2O$ 0.075 g, $CaCl_2 \cdot 2H_2O$ 0.036 g, Citric acid 0.006 g, Ferric ammonium citrate 0.006 g, EDTA (disodium salt) 0.001 g, Na_2CO_3 0.02 g, Trace metal mix A5 1.0 ml. (H_3BO_3 2.86 g, $MnCl_2 \cdot 4H_2O$ 1.81 g, $ZnSO_4 \cdot 7H_2O$ 0.222 g, $NaMoO_4 \cdot 2H_2O$ 0.39 g, $CuSO_4 \cdot 5H_2O$ 0.079 g, $Co(NO_3)_2 \cdot H_2O$ 49.4)

Sand consolidation

The sand consolidation experiment was performed using live (LT), and UV treated UVT) cells to determine the binding property of crystals. For UV treatment, *S. pevalekii* cell suspension was exposed to UV light for 1 h. For the sand column, locally available clean, dry, well-graded, natural river sand was used. The sand was sieved through 0.3 mm mesh and autoclaved to remove the indigenous microflora (Hamamura et al. 2006). The LT and UVT cells were taken and resuspended in 25 ml sterilized calcification media and prepared as shown in Table 1. For the preparation of sand columns, the slurry of sand keeping the moisture content of 25% was filled into a plastic tube (height 7.6 cm; diameter 3.8 cm) (Fig. 1). The bottom portion of each column was wrapped with Whatman filter paper. A burette was attached at the top of the plastic column to drop calcification media at a constant amount through the column. The control sets were made similar without the bacterial cells, while other specimens had the bacterial inoculum mixed. Outline for the experimental setup and calcifying solution used are presented in Table 1. All the columns were fed with 25 ml calcification media twice with a 12-h duration at room temperature for 14 days. The effluent was collected from the bottom of the sand columns in the beaker at regular intervals of 0, 2, 4, 6, 8, 10, 12, and 14 days to estimate the flow rate and pH to assess the activity of cyanobacterial

Table 1 Sand consolidation experiment set-up with different calcifying media

Groups	Composition of sand column	Calcifying media
Live cells (LT)	Sand (0.3 mm) + bacterial cells + $CaCl_2$ + $NaHCO_3$	Bacterial cells + $CaCl_2$ (100mM) + $NaHCO_3$ (50 mM)
UV treated cells (UVT)	Sand (0.3 mm) + bacterial cells + $CaCl_2$ + $NaHCO_3$	Bacterial cells + $CaCl_2$ (100mM) + $NaHCO_3$ (50 mM)
Control	Sand (0.3 mm) + deionized water	Deionized water

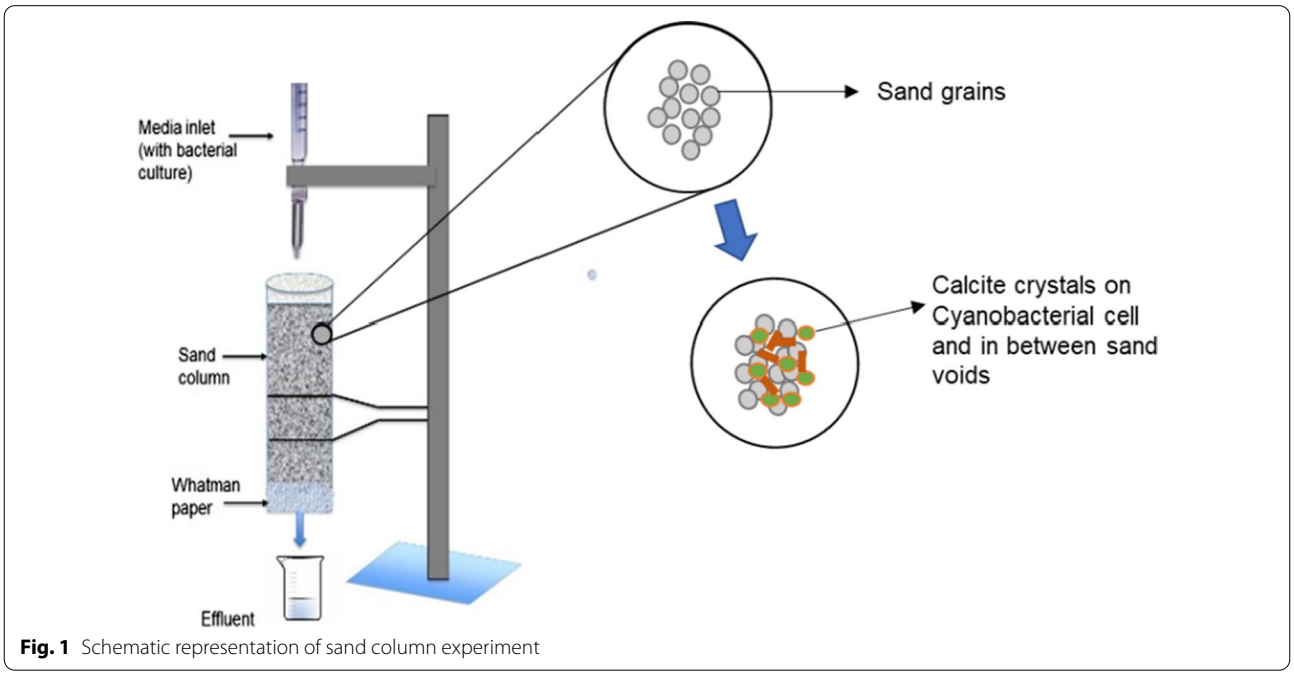


Fig. 1 Schematic representation of sand column experiment

cells within the sand columns. The sand column was opened on day-15, and the consolidated sand column was dried in an oven at 70 °C for 24 h. Samples were digested in 1.0 M hydrochloric acid at 40 °C under continuous stirring and were divided into three layers to estimate the amount of precipitation in each layer using the EDTA titration method (Stocks-Fischer et al. 1999). A small sample of upper consolidated sand layer was taken further for microstructural analysis (SEM-EDS).

Experiments with mortar specimens

Mortar cubes of $70.6 \times 70.6 \times 70.6$ mm were cast using an ordinary Portland cement (43 Grade) according to the IS: 8112 (2013). Locally available natural river sand was used as fine aggregate corroborative to Zone II (IS: 383 2016). Cement mortar mix was prepared by using cement:sand in the ratio of 1:3 (w/w) and water to cement ratio (w/c) of 0.47 as per IS: 4031 (2005). To cast bacterial-treated mortars, both live and UV-treated *S. pevalekii* (4×10^8 cells/ml) culture was used instead of water. The bacterial culture to cement ratio was also maintained at 0.47. Freshly mixed ingredients at the plastic stage were immediately transferred into iron moulds in the casting room at room temperature of 27 ± 2 °C. After 24 h, the specimens were demolded and cured till the testing age. Different treatments, materials used, and the method of curing are mentioned in Table 2. The mortar specimens were divided into three groups. The first group was subjected to live *S. pevalekii* cells, the second group with UV treated culture, and the third group without bacterial treatment. All the mortar specimens were cured for 3-, 7-, and 28-day with their respective medium as mentioned in Table 2. Bacterial-treated specimens were initially submerged in live, and UV killed culture for 24 h and then in BG11 medium with 50 mM $NaHCO_3$ and 100 mM $CaCl_2$ in a plastic container at room temperature of 30 ± 2 °C for different curing periods. All specimens were exposed to a light intensity of 1200 lux for 12 h and kept under darkness for 12 h. For 28-day curing specimens, the cubes were incubated in culture for 24 h at the beginning of every week and then transferred to BG11 medium with 50 mM $NaHCO_3$ and 100 mM $CaCl_2$. At the end of the experiment, mortar specimens were dried at 72 °C for 24 h and analyzed for various parameters.

Testing procedures

The compressive strength was measured with an automatic compression testing machine. A sorptivity test was performed based on the RILEM 25 P.E.M. (II-6) as described in Achal et al. (2011b). Thermogravimetric analysis (TGA) was performed to determine calcium carbonate precipitation in mortar specimens. Briefly, the sample was broken, crushed, and powdered into homogenous particle sizes, and 20 mg of mortar powder was taken in a TGA holder and increased the temperature constantly up to 850 °C with a heating rate of 10 °C/min. Nitrogen (10 ml/min) was used as a purge gas, and the loss of weight (%) of the sample during heating was plotted against temperature (°C). The weight loss in the temperature range of 550–750 °C corresponds to $CaCO_3$ decomposition. Scanning electron microscopy (SEM) (ZEISS EVO 50) was performed for the samples at 28-day, and the elemental composition of microstructural crystals was identified with energy-dispersive X-ray spectroscopy (EDX.). Samples were finely polished and gold-coated with a sputter coating. X-ray diffraction (XRD) was performed using Bruker D8 X-ray diffractometer with a Cu anode (40 kV and 30 mA) and scanning from 20° to 60° at a 2θ angle.

Statistical analysis

All the experiments were performed in triplicates. Data were analyzed by analysis of variance, and the significant differences among the means values were compared by Tukey's test at $P < 0.05$. GraphPad Prism 5.1 software was used for analyzing the data.

Results

Sand consolidation

To study the binding property of the calcium carbonate precipitated by *S. pevalekii* cells, the sand consolidation experiment was performed with both LT and UVT cells of *S. pevalekii*. The sand column was continuously fed with BG11 nutrient media as mentioned in Table 1 for 14

Table 2 Outline of different sets of mortar specimens and mechanism of curing treatment

Specimens	Material used	Mechanism of curing
Control	Cement:sand: 1:3; water/cement ratio 0.47	Water curing for 3,7 and 28 days
LT	Cement:sand: 1:3; live *S. pevalekii* culture/cement ratio 0.47	Curing for 3,7 and 28[a] days in BG11 medium supplied with 100 mM $CaCl_2$, 50 mM $NaHCO_3$.
UVT	Cement:sand: 1:3; UV-treated *S. pevalekii* culture/cement ratio 0.47	Curing for 3,7 and 28[a] days in BG11 medium supplied with 100 mM $CaCl_2$, 50 mM $NaHCO_3$

[a] Mortar cubes were incubated in culture for 24 h. at the beginning of every week and then transferred to medium

days. The sand columns were opened, and a solid cylindrical consolidated sand column was observed in cyanobacterial injected columns. The flow rate of the calcifying medium was measured at regular intervals till 14 days of consolidation. The flow rates of *S. pevalekii* treated columns and the control columns were almost the same initially. There was a 12.9% reduction in the control column flow rate after 14 days, which shows a marginal change in the control column's structures due to the flow. However, the flow rate declined significantly in the LT and UVT columns, indicating that MICCP is causing gradual constraint of the flow channels. The flow rate was almost obstructed at the end of the 12th day. Initially, on the 0-day, the flow rate was estimated to be 16.38, 17.44, and 18.52 ml/min in experiment set—LT, UVT and C (control). The flow rate on the 14th day in the experiment set LT and UVT was 4.10 and 6.23 ml/min, respectively. Bacterial columns showed a maximum 40.2% reduction in the flow rate on the 4th day of study, increasing to 74.90% on the 14th day (Fig. 2a).

The change in pH of the effluent collected at the bottom of the injected calcifying medium was monitored at 0, 2, 4, 6, 8, 10, 12, and 14 days of the experiment. The pH of the effluent was in the range of 7.3–7.5 for LT while 7.6–7.8 for UVT at the end of the 14 days (Fig. 2b). Conversely, the pH of the effluent from control columns remained the same throughout the experiment, i.e., pH 8.1.

The LT column resulted in complete consolidation of sand compared to control without bacteria (Fig. 3a). Sand columns treated with live cells were more compact and firm than UVT columns. Partial binding formed in UVT experimental setup, where about two-thirds of the sand was consolidated (Fig. 3b). There were clumps of sand on the top in UVT, whereas in control, the sand came out as it is without any consolidation (Fig. 3c). The consolidated sand column was further divided into three parts to estimate the calcium carbonate content. The upper part of the column in LT and UVT was dense and harder than the bottom parts. Figure 3d depicts the decreasing trend of calcium carbonate formation in the three layers of the sand column in LT and UVT columns. The maximum calcium carbonate content in the upper layer was

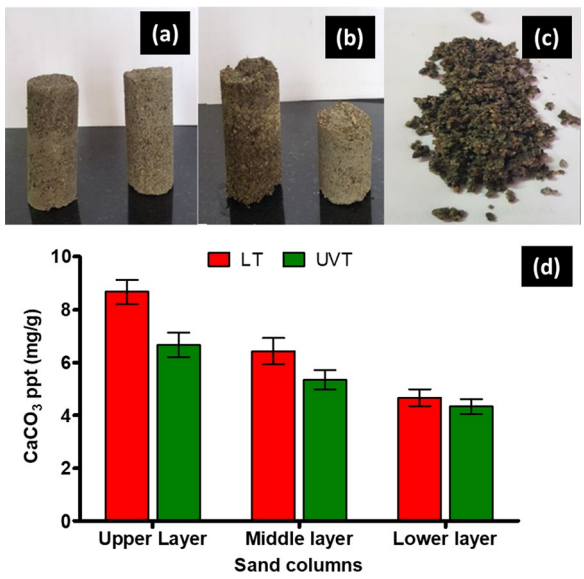


Fig. 3 Sand columns consolidated by **a** live (LT) *S. pevalekii* cells, **b** UV treated (UVT) *S. pevalekii* cells, **c** control, and **d** calcium carbonate precipitation in three different layers of sand columns

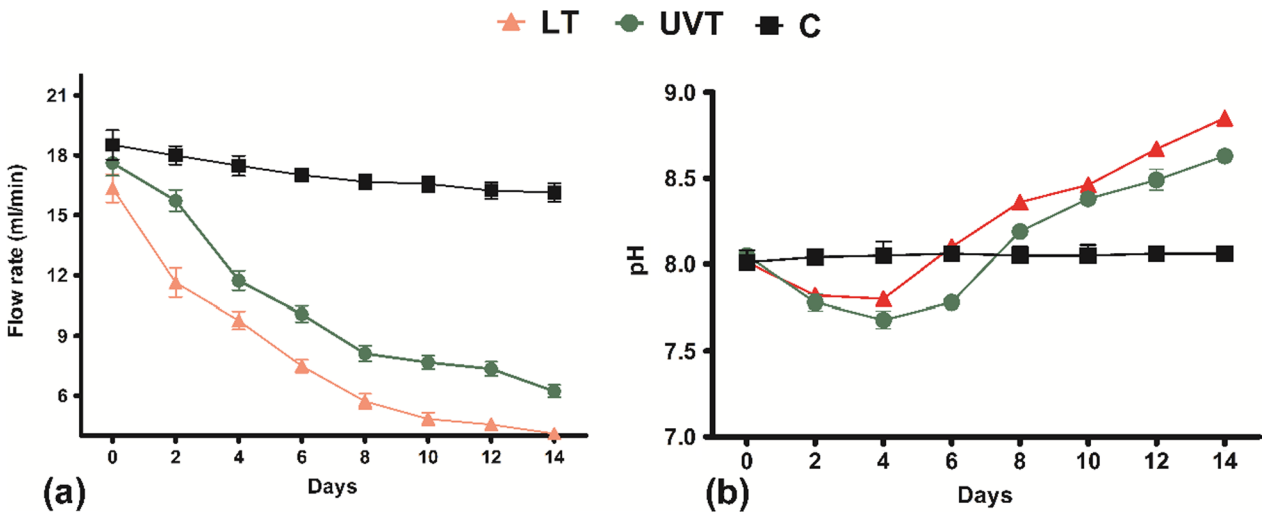


Fig. 2 Estimation of **a** the flow rate of the calcifying solution **b** pH of the effluent solution injected through sand columns till 14 days

8.67 mg/g in LT treated column, and it was 6.67 mg/g in UVT column. The calcium carbonate precipitation in the middle part of sand columns was recorded as 6.43 mg/g, and 5.43 mg/g, respectively in LT and UVT columns.

The upper layer of the sand column was analyzed using SEM-EDS to confirm the calcium carbonate precipitation. Figure 4a and b gives clear confirmation of calcite formation in LT sand column. The precipitation was observed to be dense and bonded to form an aggregation of crystals. Similarly, in Fig. 4d, the staircase of crystals were formed in UVT sand column, which might be due to the accumulation of thick layers of calcite precipitates. The crystals were rhombohedral in shape with a size of 5–7 µm (Fig. 4e). However, no calcite deposition was observed in the control after 14 days of treatments. The precipitated crystal was established to be calcium carbonate polymorph by the elemental analysis of the whole area using energy dispersive spectroscopy (EDS). Figure 4c and f confirm the chemical composition of calcite to be carbon, oxygen, calcium, and silica, which shows the presence of sand particles. These results suggest that *S. pevalekii* cells can precipitate $CaCO_3$ crystals within the voids of the sand column.

Compressive strength

The compressive strength of the mortar specimens was done at different testing ages to study the influence of LT and UVT cells on the cement matrix. The LT and UVT specimens showed improvement in compressive strength, which is attributed to the deposition of $CaCO_3$ within the pores of the cement-sand matrix. As shown in Fig. 5, the compressive strength of LT specimens increased from 26.28 MPa at 7-day to 48.11 MPa at 28-day. A similar trend was recorded with UVT specimens, where the compressive strength increased from 22.06 MPa at 7-day to 44.39 MPa at 28-day. The LT specimens observed a 25.54% increase, whereas UVT specimens showed a

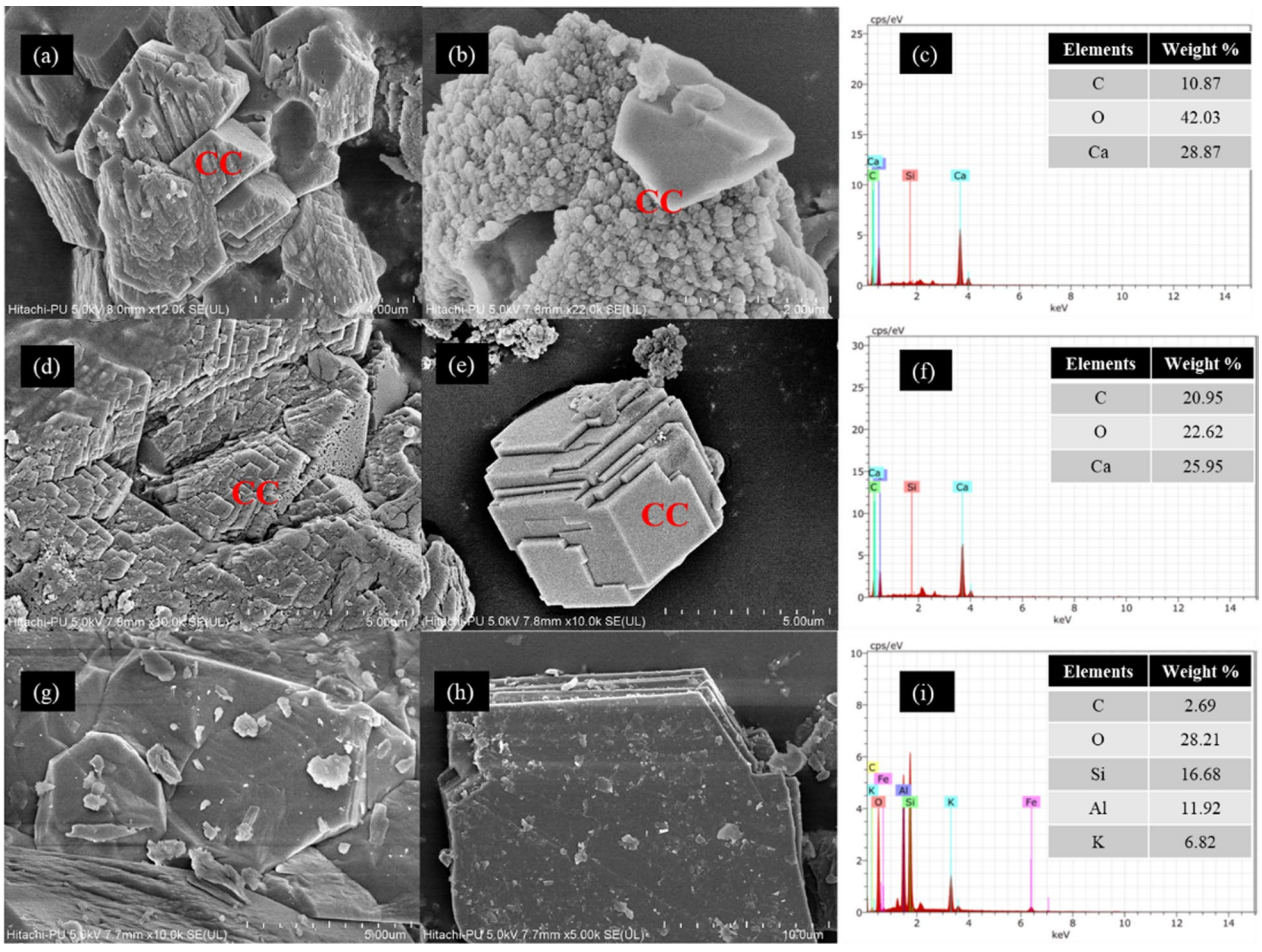


Fig. 4 SEM-EDX images represent $CaCO_3$ crystals (CC) precipitated on upper layer of sand column treated with live (LT) *Synechocystis pevalekii* cells (**a**, **b**), UV treated (UVT) *S. pevalekii* cells (**d**, **e**), and control (**g**, **h**). EDS analysis (**c**, **f**, **i**) was conducted on the whole area

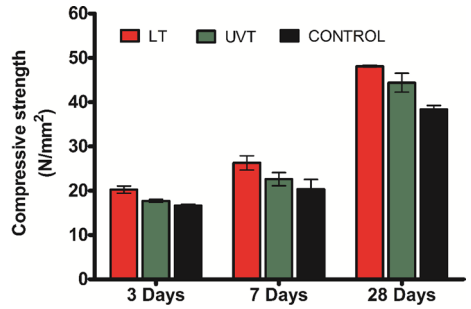


Fig. 5 Compressive strength of mortar specimens cured with live (LT) and UV treated (UVT) *S. pevalekii* cells at the age of 3-, 7-, and 28-day

15.84% surge in compressive strength after 28 days of curing compared to control specimens.

Water absorption

A water absorption test was performed to determine the water absorption rate by capillary action. The graph representing the cumulative amount of water absorbed per unit cross-sectional area is presented in Fig. 6. The LT and UVT specimens showed lower water absorption, while it was higher in the control specimen. The water absorption was observed to be decreased by 1.5 times in LT specimens with respect to the control after 144 h. Initially, all the mortar specimens exhibited a rapid rise in water absorption until it became constant in the secondary phase of water absorption.

Thermogravimetric analysis

Thermogravimetric analysis (TGA) was conducted for all the specimens at 28-day of curing to confirm the calcium carbonate precipitation. The TGA thermograms for LT, UVT, and control specimens are presented in Fig. 7a. The TGA results showed immense weight loss of 4.86% in LT specimens and 4.09% in the UVT specimens between 600 and 800 °C, corresponding to the carbonate weight loss (Fig. 7a). However, control displayed only 2.32% weight loss percentage between 600 and 800 °C. The TGA's steeper peaks support the calcium carbonate precipitation by LT and UVT specimens with higher weight loss by LT followed by UVT. Weight loss was comparatively lower in control than LT and UVT specimens. Besides $CaCO_3$ decomposition, another fall with 0.63%, 0.52%, and 0.69% weight loss of $Ca(OH)_2$ was observed 400–450 °C temperature, showing insignificant mass loss due to dehydration of calcium hydroxide (Fig. 7b).

Microstructural analysis

The XRD analysis revealed that the control specimen's prominent crystalline peaks of quartz (SiO_2) were observed (Fig. 7c). Among all the peaks revealed in the XRD spectra, the calcite polymorph of $CaCO_3$ crystals was dominantly present in LT and UVT specimens along with the peak of quartz. XRD spectra of LT specimens were observed at 29.4°, 35.9°, 39.4°, 43.3°, and 48.45° corresponding to the 104, 110, 113, 202, and 116 planes of the calcite phase, whereas in UVT it was observed at 29.4°, 39.4° and 43.3° corresponding to the 10, 110 and 113 planes of the calcite phase (Vu et al. 2020). The diffraction peaks located at (2θ) of 27.1°, 39.6° corresponds to 101, 211 planes of vaterite crystals. The presence of calcite peaks approves the crystal formation by *S. pevalekii* cells in the mortar specimens.

The microstructural analysis of the mortar specimens with LT, UVT, and control specimen are shown in Fig. 8. Figure 8a validates the crystals buildup by UV treated bacterial cells forming a dense layer of calcite over the mortar surface, which was observed to be tightly packed

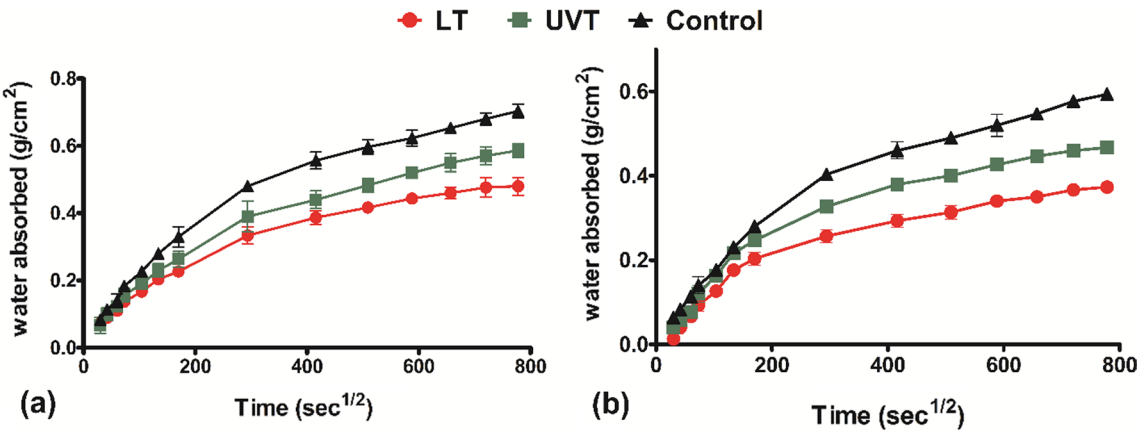


Fig. 6 Water absorption of mortar specimens treated with live (LT) and UV treated (UVT) *Synechocystis pevalekii* at **a** 7-day, and **b** 28-day of curing

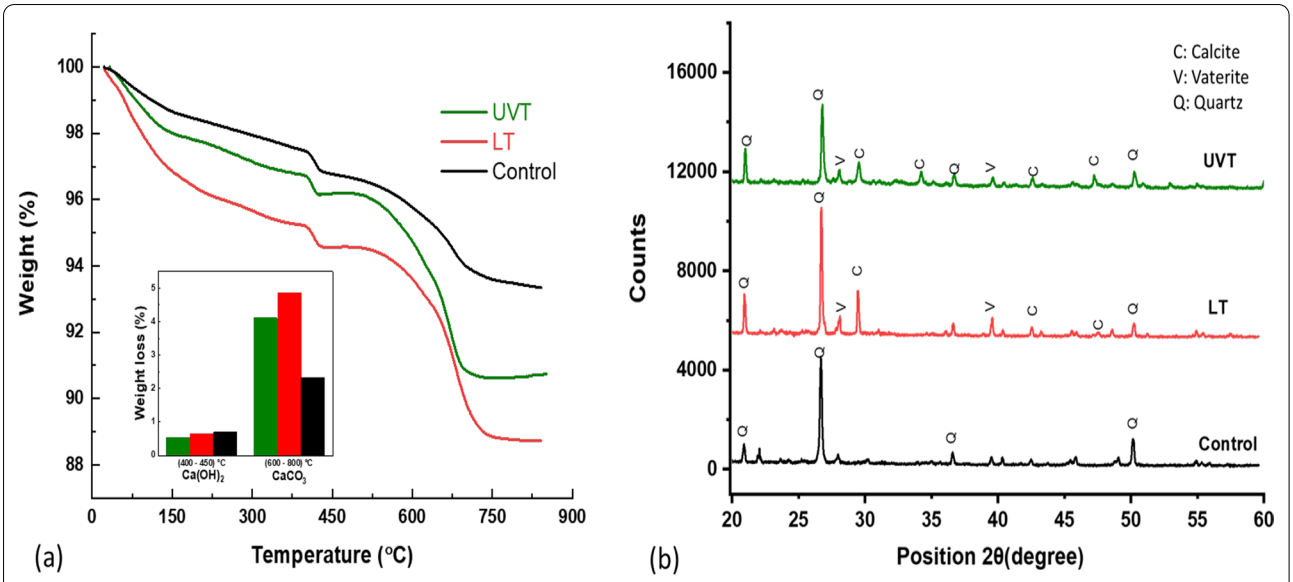


Fig. 7 TGA (**a**), and XRD pattern (**b**) of mortar specimens treated with live (LT) and UV treated (UVT) *Synechocystis pevalekii* cells at 28-day of curing

and in a perfect rhombohedral crystal lattice in a size range of 5–10 µm. Likewise, in live treated specimens, the spherical crystal of vaterite ranging in size 17–20 µm were observed along with the cubic crystals of 10–15 µm calcite (Fig. 8b). Both crystals form calcium carbonate, which was confirmed by EDX analysis. The mineral constituents characterized by EDX analysis clearly show a large Ca, O, C peak in LT and UVT specimens compared to the control. As observed in EDX analysis, the amount of carbon, oxygen, and calcium formed in the LT sample was 7.25%, 40.93%, and 51.82%, respectively. Similarly, in the EDX analysis of UVT, the amount of carbon, oxygen, and calcium reported was 13.88%, 51.93%, and 33.62%, respectively, which is a comparatively higher amount than the control.

Discussion

Sand consolidation by *S. pevalekii*

Calcium carbonate precipitation by *S. pevalekii* cells plugs the pores between the sand particles. The reduction in the flow rate in LT and UVT treated columns is primarily because of the enclosed biomass and carbonates deposition. The carbonate biominerals reduce the pore size between the sand particles, clogging the flow of calcifying material. The pH of the effluent from the control and the bacterial treated columns showed significant variance so that it can be considered an indicator of the activity of MICCP. Therefore, it can be considered that the most functional element in the calcifying solution is calcium chloride along with sodium bicarbonate which acts as a catalyst for precipitation. Dejong et al. (2010) has reiterated that $CaCO_3$ precipitation is an imperative aspect in the distribution of crystals between the sand voids to form bonding between the particles. Sodium bicarbonate used in these columns acts as a catalyst to initiate the formation of calcium carbonate by bacterial cells. Comparatively, minimum calcite content was observed in the bottom part of the columns attributing that growth of *S. pevalekii* cells was promoted in the upper layer of the column due to exposure to the light source and aeration. The results correlated with Dhami et al. (2016), who studied sand consolidation using different grain sizes (0.2, 0.5, and 1.0 mm). They reported an 88% decrease in the flow rate in all bacterial inoculated columns and only a 5% reduction in the control. The effluent pH of bacterial columns was reported to be in the range of 8.5–8.9, whereas the control columns had a pH below 8.1. A similar trend was reported by Achal et al. (2011a), where a decrease in the flow rate and 33% calcite content in the top layer of a sand column. Yang et al. (2020) also reported sand consolidation using urease-producing bacteria. The percentage of calcite precipitated in different layers of the column was in concordance with previous studies (Mahawish et al. 2019; Sharma et al. 2020, 2021).

Experiment on mortar

The compressive strength of the LT specimen showed improved strength than the UVT with the curing age. This might be due to the slower physiological activity of UV-treated cell culture than live cells. Although UV-treated cells are linked to form stronger adhering

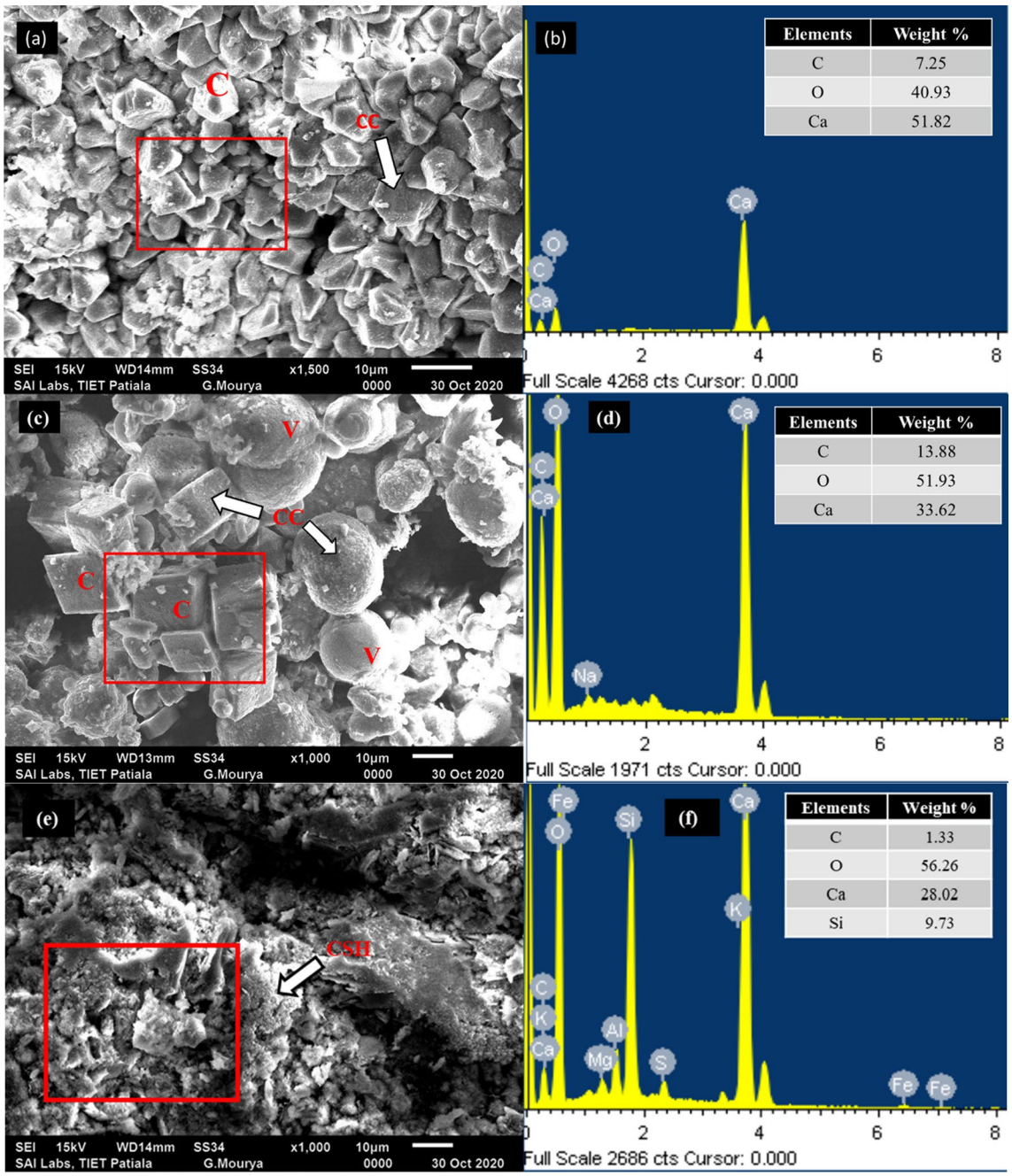


Fig. 8 SEM-EDX images represent precipitation of rhombohedral calcite (C) and spherical vaterite (V) $CaCO_3$ crystals (CC) in mortar specimens treated with live (LT) *Synechocystis pevalekii* cells (**a**, **b**); UV treated (UVT) *S. pevalekii* cells (**c**, **d**), and control (**e**, **f**). Square '□' sign indicates the spot of EDX analysis

to the mortar surface than live cells, live cells actively utilize nutritional media and grow within the medium (Zhu et al. 2018). The photosynthetic reaction by live active cells contributed to the carbonate precipitation by increasing the pH in the microenvironment. In fact, the metabolic active live cells provide more nucleation sites than the dead bacteria since the negative charge on the cell wall is higher and increases their binding capacity (Skevi et al. 2021; Pei et al. 2013) claimed that the live, and dead bacteria have a negligible effect on strength improvement even if nutrient media is provided. On the contrary, Skevi et al. (2021) described 24% and 35%

strength enhancement compared to the control by adding live and dead *Bacillus cohii* bacteria. Likewise, Zhu et al. (2017) reported UV-killed specimens showed higher compressive strength than the live cells. However, Heveran et al. (2020) stated negligible compressive strength differences using *Synechococcus* sp. PCC 7002. Srinivas et al. (2021) reported the improvement of the strength of cement mortar treated with microalgae, *Synechococcus elongatus* and *Spirulina platensis*.

The low '*k*' value of the surface-treated specimen indicates that bacterial incorporation can significantly improve the permeation properties. In the beginning, the water absorption test probably results in the rapid filling of large capillary pores near the immersed surface and, finally, a slow rise in the water absorption at the end of testing to more delicate pores far from the submerged surface. Similar results were plotted by Hernández et al. (2016) by incorporating cactus mucilage and marine brown algae extract. Tayebani and Mostofinejad (2019) also reported a reduction in water absorption due to biological treatment compared to water curing.

Along with calcium carbonate, mortar specimens showed weight loss of calcium hydroxide during TGA, formed due to the hydration of cementitious material during the curing process. According to the literature, calcium hydroxide and calcium carbonate dehydration occur at 420–540 °C and 500–800 °C (Stuckrath et al. 2014; Sharma et al. 2017). Thus, this significant drop in calcium carbonate dehydration accounts for higher $CaCO_3$ precipitation in bacterial-treated specimens. Therefore, the deposition of calcium carbonate can be considered as an important factor in strength enhancement and permeability reduction. The results were in agreement with the reports of other researchers (Pei et al. 2013; Jang et al. 2020). XRD results are in corroboration with the previous studies showing precipitation of calcium carbonate crystals due to bacterial metabolic activities in the cementitious material (Joshi et al. 2020; Saxena and Tembhurkar 2020).

Our study suggests that incorporating live and UV-treated cyanobacterial cells successfully induced calcium carbonate precipitation in the cementitious environment. It is important to consider that UV treated cells retain the cellular membrane as UV radiations are observed by only purines and pyrimidines of nucleic acid. In heat-killed or autoclaved culture, cell lysis occurs, thus destroying the organic framework of the cell membrane (Malke 1982). Therefore, it is conceivable that besides the slow metabolism of the cell, heterogenous nucleation is promoted by a negative charge on the cell wall, which leads to calcite precipitation in UV-treated cells. At the same time, live cells were able to promote both calcite and vaterite precipitation. The precipitation of calcite and vaterite crystals was observed by Chekroun et al. (2004) in the presence of live and UV-treated *Myxococcus xanthus*. Previous research has well defined the presence of such different morphology and structure of calcium carbonate crystals. The cubic shape of calcite and the spherical shape of vaterite coexist along with the bacterial cell, as reported by Xiao et al. (2010). Different theories have been put forward to illustrate such co-occurrence. Firstly, the vaterite is considered a thermodynamically unstable crystal form, and its nucleation rate is faster; therefore, slow diffusion of Ca^{2+} and CO_3^{2+} ions can lead to calcite formation (Weiner and Dove 2003). Secondly, the involvement of different organic components of the cell surface provides another nucleation site for biomineralization (Liang et al. 2013; Zhu et al. 2017) reported similar results by treating the specimens with live and UV-killed *Gleocapsa* PCC73106.

In conclusion, calcium carbonate precipitation by *S. pevalekii* cells improved the mortar's compressive strength and permeation properties in LT and UVT treated specimens compared to control. The compressive strength significantly increased in LT specimens compared to UVT specimens. The microstructural analysis confirmed rhombohedral calcite crystal formation and the bacterial cells in mortar specimens. Thermogravimetric analysis showed a more significant mass loss of carbonate in LT specimens in between 600 and 800 °C than in UVT specimens. Present study results suggest that MICCP by using *S. pevalekii* serves as a low-cost and environment-friendly MICCP technology.

Acknowledgements
We thank the Thapar Institute of Engineering & Technology for facilities.

Author contributions
NS experimental, data analysis, original draft writing SG experimental methodology design, supervison. MSR conceptualization, experimental methodology design, supervision and final editing. All authors read and approved the final manuscript.

Funding
This work was funded by the Department of Biotechnology, Ministry of Science and Technology, Govt. of India, under the research Grant No. BT/PR27190/BCE/8/1428/2017.

Availability of data and materials
Data and materials available on request from the corresponding authors.

Declarations

Ethics approval and consent to participate
Not applicable.

Consent for publication
All authors agree to submit this manuscript for publication.

Competing interests
Authors have no competing interests to declare.

Author details
[1]Department of Biotechnology, Thapar Institute of Engineering & Technology, Patiala 147004, Punjab, India. [2]Department of Civil Engineering, Thapar Institute of Engineering & Technology, Patiala 147004, Punjab, India.

Received: 8 May 2022 Accepted: 11 May 2022
Published online: 19 May 2022

References

Achal V, Mukherjee A, Reddy MS (2011a) Effect of calcifying bacteria on permeation properties of concrete structures. J Ind Microbiol Biotechnol 38:1229–1234. https://doi.org/10.1007/s10295-010-0901-8

Achal V, Mukherjee A, Sudhakara Reddy M (2011b) Microbial concrete: way to enhance the durability of building structures. J Mater Civ Eng 23:730–734. DOI: https://doi.org/10.1061/(ASCE)MT.1943-5533.0000159

Bhuvaneshwari T, Shylajanaciyar M, Prakasam PA, Ezhilmaran K, Karthick L, Subramanian G, Uma L, Prabaharan D (2017) Polyphasic analysis for elucidating the taxonomic position of selected unicellular marine *Cyanobacteria* from Indian and Hong Kong coast. Phytotaxa 307:263–277. https://doi.org/10.11646/phytotaxa.307.4.4

Chekroun KB, Rodri C, Teresa Gonza M, Maria Arias J, Cultrone G, Rodri M (2004) Precipitation and growth morphology of calcium carbonate induced by *Myxococcus xanthus*: implications for recognition of bacterial carbonates. J Sediment Res 74:1527–1404

De Muynck W, Verbeken K, De Belie N, Verstraete W (2010) Influence of urea and calcium dosage on the effectiveness of bacterially induced carbonate precipitation on limestone. Ecol Eng 36:99–111. https://doi.org/10.1016/j.ecoleng.2009.03.025

DeJong JT, Mortensen BM, Martinez BC, Nelson DC (2010) Bio-mediated soil improvement. Ecol Eng 36:197–210. https://doi.org/10.1016/j.ecoleng.2008.12.029

Dhami NK, Reddy MS, Mukherjee MS (2013) Biomineralization of calcium carbonates and their engineered applications: a review. Front Microbiol 4:1–13. https://doi.org/10.3389/fmicb.2013.00314

Dhami NK, Reddy MS, Mukherjee A (2016) Significant indicators for biomineralisation in sand of varying grain sizes. Constr Build Mater 104:198–207. https://doi.org/10.1016/j.conbuildmat.2015.12.023

Dittrich M, Sibler S (2010) Calcium carbonate precipitation by cyanobacterial polysaccharides. Geol Soc Spec Publ 336:51–63. https://doi.org/10.1144/SP336.4

Douglas S, Beveridge TJ (2006) Mineral formation by bacteria in natural microbial communities. FEMS Microbiol Ecol 26:79–88. https://doi.org/10.1111/j.1574-6941.1998.tb00494.x

Gnanasekaran DVS (2014) Biocalcification mediated remediation of calcium rich Ossein effluent by filamentous marine cyanobacteria. J Bioremediat Biodegrad. https://doi.org/10.4172/2155-6199.1000257

Hamamura N, Olson SH, Ward DM, Inskeep WP (2006) Microbial population dynamics associated with crude-oil biodegradation in diverse soils. Appl Environ Microbiol 72:6316–6324. https://doi.org/10.1128/AEM.01015-06

Han Z, Yan H, Zhou S, Zhao H, Zhang Y, Zhang N, Yao C, Zhao L, Han C (2013) Precipitation of calcite induced by *Synechocystis* sp. PCC6803. World J Microbiol Biotechnol 29:1801–1811. https://doi.org/10.1007/s11274-013-1341-1

Han Z, Zhao Y, Yan H, Zhao H, Han M, Sun B, Meng R, Zhuang D, Li D, Gao W, Du S, Wang X, Fan K, Hu W, Zhang M (2017) The characterization of intracellular and extracellular biomineralization induced by *Synechocystis* sp. PCC6803 cultured under low Mg/Ca ratios conditions. Geomicrobiol J 34:362–373. https://doi.org/10.1080/01490451.2016.1197986

Hernández EF, De Cano-Barrita PFJ, Torres-Acosta AA (2016) Influence of cactus mucilage and marine brown algae extract on the compressive strength and durability of concrete. Mater Constr. https://doi.org/10.3989/mc.2016.07514

Heveran CM, Williams SL, Qiu J, Artier J, Hubler MH, Cook SM, Cameron JC, Srubar WV (2020) Biomineralization and successive regeneration of engineered living building materials. Matter 2:481–494. https://doi.org/10.1016/j.matt.2019.11.016

IS: 4031 (2005) (Part 6) Methods of physical tests for hydraulic cement part 6 determination of compressive strength of hydraulic cement other than masonry cement (first revision). Bur. Indian Stand. New Delhi-110002

IS : 8112 (2013) Indian standard specification for 43 grade ordinary Portland cement, Bur. Indian Stand. New Delhi-110002

IS : 383 (2016) Indian standard specification for coarse and fine aggregates from natural sources for concrete, Bur. Indian Stand. New Delhi-110002

Jang I, Son D, Kim W, Park W, Yi C (2020) Effects of spray-dried co-cultured bacteria on cement mortar. Constr Build Mater 243:118206. https://doi.org/10.1016/j.conbuildmat.2020.118206

Joshi S, Goyal S, Sudhakara Reddy M (2020) Influence of biogenic treatment in improving the durability properties of waste amended concrete: a review. Constr Build Mater. https://doi.org/10.1016/j.conbuildmat.2020.120170

Kamennaya NA, Ajo-Franklin CM, Northen T, Jansson C (2012) Cyanobacteria as biocatalysts for carbonate mineralization. Minerals 2:338–364. https://doi.org/10.3390/min2040338

Kranz SA, Wolf-Gladrow D, Nehrke G, Langer G, Rost B (2010) Calcium carbonate precipitation induced by the growth of the marine cyanobacterium *Trichodesmium*. Limnol Oceanogr 55:2563–2569. https://doi.org/10.4319/lo.2010.55.6.2563

Liang A, Paulo C, Zhu Y, Dittrich M (2013) $CaCO_3$ biomineralization on cyanobacterial surfaces: insights from experiments with three *Synechococcus* strains. Colloids Surf B Biointerfaces 111:600–608. https://doi.org/10.1016/j.colsurfb.2013.07.012

Mahawish A, Bouazza A, Gates WP (2019) Unconfined compressive strength and visualization of the microstructure of coarse sand subjected to different biocementation levels. J Geotech Geoenvironmental Eng 145:04019033. https://doi.org/10.1061/(asce)gt.1943-5606.0002066

Malke H (1982) B. D. Davis, R. Dulbecco, H. N. Eisen and H. S. Ginsberg, microbiology (3rd edition). 1355 S., ca. 1300 Abb., ca. 150 Tab. Hagerstown 1980. Harper & Row Publishers. DFL 65.00. Z Allg Mikrobiol 22:279–279. https://doi.org/10.1002/JOBM.19820220411

Paulo C, Kenney JPL, Persson P, Dittrich M (2018) Effects of phosphorus in growth media on biomineralization and cell surface properties of marine cyanobacteria *Synechococcus*. Geoscience. https://doi.org/10.3390/geosciences8120471

Pei R, Liu J, Wang S, Yang M (2013) Use of bacterial cell walls to improve the mechanical performance of concrete. Cem Concr Compos 39:122–130. https://doi.org/10.1016/j.cemconcomp.2013.03.024

Rippka R, Deruelles J, Waterbury JB (1979) Generic assignments, strain histories and properties of pure cultures of cyanobacteria. J Gen Microbiol 111:1–61. https://doi.org/10.1099/00221287-111-1-1

Saxena S, Tembhurkar AR (2020) Microbiological induced calcium carbonate process to enhance the properties of cement mortar. Mater Today Proc 21:1350–1354. https://doi.org/10.1016/j.matpr.2020.01.173

Seifan M, Samani AK, Berenjian A (2016) Bioconcrete: next generation of self-healing concrete. Appl Microbiol Biotechnol 100:2591–2602. https://doi.org/10.1007/s00253-016-7316-z

Sharma TK, Alazhari M, Heath A, Paine K, Cooper RM (2017) Alkaliphilic *Bacillus* species show potential application in concrete crack repair by virtue of rapid spore production and germination then extracellular calcite formation. J Appl Microbiol 122:1233–1244. https://doi.org/10.1111/jam.13421

Sharma M, Satyam N, Reddy KR (2020) Strength enhancement and lead immobilization of sand using consortia of bacteria and blue-green algae. J Hazard Toxic Radioact Waste 24:04020049. https://doi.org/10.1061/(asce)hz.2153-5515.0000548

Sharma M, Satyam N, Reddy KR (2021) Rock-like behavior of biocemented sand treated under non-sterile environment and various treatment conditions. J Rock Mech Geotech Eng 13:705–716. https://doi.org/10.1016/j.jrmge.2020.11.006

Singh JS, Kumar A, Rai AN, Singh DP (2016) Cyanobacteria: a precious bioresource in agriculture, ecosystem, and environmental sustainability. Front Microbiol 7:1–19. https://doi.org/10.3389/fmicb.2016.00529

Skevi L, Reeksting BJ, Hoffmann TD, Gebhard S, Paine K (2021) Incorporation of bacteria in concrete: the case against MICP as a means for strength improvement. Cem Concr Compos 120:104056. https://doi.org/10.1016/j.cemconcomp.2021.104056

Srinivas MK, Alengaram UJ, Ibrahim S, Phang SM, Vello V, Jun HK, Alnahhal AM (2021) Evaluation of crack healing potential of cement mortar incorporated with blue-green microalgae. J Build Eng 44:102958. https://doi.org/10.1016/j.jobe.2021.102958

Stocks-Fischer S, Galinat JK, Bang SS (1999) Microbiological precipitation of $CaCO_3$. Soil Biol Biochem 31:1563–1571. https://doi.org/10.1016/S0038-0717(99)00082-6

Stuckrath C, Serpell R, Valenzuela LM, Lopez M (2014) Quantification of chemical and biological calcium carbonate precipitation: performance of self-healing in reinforced mortar containing chemical admixtures. Cem Concr Compos 50:10–15. https://doi.org/10.1016/j.cemconcomp.2014.02.005

Tayebani B, Mostofinejad D (2019) Self-healing bacterial mortar with improved chloride permeability and electrical resistance. Constr Build Mater 208:75–86. https://doi.org/10.1016/j.conbuildmat.2019.02.172

Vu HHT, Khan MD, Van Tran T, Quang DV, Dao VD, Lee S, Ahn JW, Jung SH (2020) Use of calcite mud from paper factories in phosphorus treatment. Sustain 12:1–13. https://doi.org/10.3390/su12155982

Weiner S, Dove PM (2003) An overview of biomineralization processes and the problem of the vital effect. Rev Mineral Geochem 54:1–29. https://doi.org/10.2113/0540001

Xiao J, Wang Z, Tang Y, Yang S (2010) Biomimetic mineralization of $CaCO_3$ on a phospholipid monolayer: from an amorphous calcium carbonate precursor to calcite via vaterite. Langmuir 26:4977–4983. https://doi.org/10.1021/la903641k

Yang Y, Chu J, Cao B, Liu H, Cheng L (2020) Biocementation of soil using non-sterile enriched urease-producing bacteria from activated sludge. J Clean Prod 262:121315. https://doi.org/10.1016/j.jclepro.2020.121315

Zhu T, Lu X, Dittrich M (2017) Calcification on mortar by live and UV-killed biofilm-forming cyanobacterial *Gloeocapsa* PCC73106. Constr Build Mater 146:43–53. https://doi.org/10.1016/j.conbuildmat.2017.04.026

Zhu T, Lin Y, Lu X, Dittrich M (2018) Assessment of cyanobacterial species for carbonate precipitation on mortar surface under different conditions. Ecol Eng 120:154–163. https://doi.org/10.1016/j.ecoleng.2018.05.038

Publisher's note

Springer Nature remains neutral with regard to jurisdictional claims in published maps and institutional affiliations.

Submit your manuscript to a SpringerOpen journal and benefit from:

- ► Convenient online submission
- ► Rigorous peer review
- ► Open access: articles freely available online
- ► High visibility within the field
- ► Retaining the copyright to your article

Submit your next manuscript at ► springeropen.com



Journal of Sustainable Cement-Based Materials

ISSN: (Print) (Online) Journal homepage: https://www.tandfonline.com/loi/tscm20

Self-healing by biocomposite containing metakaolin immobilized bacterial spores in concrete using low-cost corn steep liquor media

Navneet Sidhu, Shweta Goyal & M. Sudhakara Reddy

To cite this article: Navneet Sidhu, Shweta Goyal & M. Sudhakara Reddy (2023): Self-healing by biocomposite containing metakaolin immobilized bacterial spores in concrete using low-cost corn steep liquor media, Journal of Sustainable Cement-Based Materials, DOI: 10.1080/21650373.2023.2224805

To link to this article: https://doi.org/10.1080/21650373.2023.2224805

Published online: 22 Jun 2023.

Submit your article to this journal

View related articles

View Crossmark data

Full Terms & Conditions of access and use can be found at
https://www.tandfonline.com/action/journalInformation?journalCode=tscm20

Journal of Sustainable Cement-Based Materials, 2023
http://dx.doi.org/10.1080/21650373.2023.2224805

Taylor & Francis
Taylor & Francis Group
Check for updates

Self-healing by biocomposite containing metakaolin immobilized bacterial spores in concrete using low-cost corn steep liquor media

Navneet Sidhu[a], Shweta Goyal[b] and M. Sudhakara Reddy[a]*

[a]*Department of Biotechnology, Thapar Institute of Engineering and Technology, Patiala, Punjab, India;* [b]*Department of Civil Engineering, Thapar Institute of Engineering and Technology, Patiala, Punjab, India*

The present study aimed to develop a biocomposite constituting metakaolin as a suitable carrier material for immobilizing bacterial spores. The biocomposite was stored at 4 °C and 25 °C and showed a sustainable shelf-life of bacterial spores during the storage period of 180 days. Biocomposite was assessed for urease activity and calcium carbonate precipitation in corn steep liquor (CSL) as the growth medium. Significant improvements in strength and permeation were observed at 7 and 28 days of testing in concrete added with biocomposite. The study was extended to test the self-healing capabilities of biocomposite in prismatic specimens using CSL medium. Crack healing showed significant improvement in ultrasonic pulse velocity, indicating progressive healing of the crack, and the repaired surface was examined by water tightness. The precipitated minerals were assessed by scanning electron microscopy and X-ray diffraction. The CSL can be used as low-cost growth media, eventually decreasing the cost of self-healing concrete.

Keywords: Metakaolin; Bacterial spores; Self-healing; CSL; Crack width; flexural strength; water tightness; Ultrasonic pulse velocity

1. Introduction

The occurrence of cracks during the service life of the building is a major concern as it allows access to harmful aggressive ions, which contributes to the premature failure of concrete structures [1,2]. Therefore, it is imperative to repair the damage immediately to ensure the structure's safety and extend its service life. Conventionally, cracks are repaired using chemical-based sealants (synthetic epoxides, polyurethane, epoxy resins, acrylics, and waxes). These sealants actively control undesirable penetration but limit the application due to low heat resistivity and unsustainability [3]. Moreover, it requires continuous maintenance and inspection, making it expensive and laborious [4].

Self-healing cracks *via* microbial-induced calcium carbonate precipitation (MICCP) have shown remarkable results in the recent decade [5–7]. It is a sustainable and promising technique that utilizes the bacterial ability to precipitate stable crystal polymorphs of calcium carbonate ($CaCO_3$) [8,9]. The MICCP can operate independently and seal the cracks regardless of its location. Most of the studies reported the self-healing capabilities of freshly prepared bacterial carrier materials in concrete [10]. There is an extensive need to develop a higher shelf-life bacterial product for upscaling the MICCP technique. Also, the viability of the bacteria is highly important and it is majorly influenced by the toxicity of immobilized carrier materials to bacterial cells, the cell entrapping properties of the material, the availability of bio-agents to bacterial cells, etc. [11,12]. The bacterial survival determination inside the protective carrier is crucial to understand the bacteria's metabolic behaviour [13,14]. Researchers suggested that a suitable carrier material should be non-toxic (safe for the environment and the immobilized element), stable, affordable, and readily available [15]. Also, it is best to use a carrier material synergistic with concrete.

Previously, researchers have reported various carrier materials such as hydrogels [13, 16,17], polyurea microcapsules [18], alginate [19], biochar [20], nanoplates [21], low-weight aggregates [22,23], and silica gel [24–26] as potential carrier materials for MICCP. Some of the above-mentioned carrier materials have a detrimental effect on the strength properties of the concrete [27]. Moreover, gel-based carrier materials such as hydrogel have high-water absorption capacity, which can affect the cement's hydration [28,29]. Additionally, it is unclear how long these bacteria-based carrier materials will remain stable inside the concrete. Therefore, it is preferable to explore concrete-compatible carrier materials that can easily bond with bacteria and improve the self-healing properties of concrete.

In recent studies, metakaolin (MK) has shown engineering benefits in construction industries and is abundantly available. It is a primary industrial by-product containing siliceous aluminous resources exhibiting high pozzolanic activity [30]. It is proven to be successful supplementary cementitious material (SCM) in concrete [31–33]. The micronized size distribution of MK in the concrete mixture promotes early hydration. Metakaolin can react with the free lime (calcium hydroxide) produced by cement hydration to form additional calcium silicate hydrates,

*Corresponding author. Email: msreddy@thapar.edu

© 2023 Informa UK Limited, trading as Taylor & Francis Group

making it an efficient carrier material for MICCP [34]. Metakaolin decreases fluidity through the material, thus enhancing durability and reducing chloride ion diffusion [35], and improving the cement matrix's pore structure [36].

Moreover, using spores instead of freshly inoculated culture using a porous adsorption material will ensure the viability of the biomaterial for a longer duration [37]. Spores are more resistant to heat, radiation, and other chemicals and can survive for several years [38,39]. This makes spores a better bioagent for microbial-induced calcium carbonate precipitation (MICCP). Bacterial spores are formed of thick proteinaceous coats, peptidoglycan cortex, Ca^{2+} ions, dipicolinic acid (DPA), and dehydrated spore core [40]. Spores become active when cracks appear, owing to the ingress of moisture and oxygen in the cracked area [41,42]. The bacterial endospores can withstand the concrete mix's highly alkaline pH during the concrete's cast and drying. Spores can endure high mechanical compressive stresses during concrete curing [43]. Different strategies, such as encapsulation and immobilization, protect spores during concrete mixing as they become dense because of cement hydration reactions [18, 44,45]. The spores are able to induce growth as soon as they receive favourable conditions of growth (desired temperature, moisture, and nutrients that can stimulate germination and overcome the dormancy period of spores). The germination rate of bacterial spores can range from a few minutes to several hours depending on the specific conditions provided. Nutrients (amino acids, sugar) binds to the inner membrane and rehydrates the spore core. Ca^{2+} - DPA (dipicolinic acid) is released from the spore core stimulating germination [46,47]. When spores germinate and vegetative cells start actively growing, they can produce extracellular enzymes, such as urease and carbonic anhydrase due to the metabolic activity of bacteria.

The laboratory-grade nutrient medium used for bacterial or spore cultivation constitutes yeast extract and peptone, which are expensive commercial products [48]. Therefore, implementing MICCP to field scale can be difficult as it will increase the total production cost. Achal et al. have reported lactose mother liquor (LML) and corn steep liquor (CSL) for the growth of bacteria and the cost-effectiveness of the MICCP technique [49,50]. CSL is a low-cost peptone alternative, high in protein, vitamins, minerals, and other growth stimulants [51]. Also, the CSL is proven to enhance the strength and permeability properties of concrete [48, 52]. The study was further extended to examine the growth and self-healing mechanism of spores immobilized in MK by CSL media supplemented with urea and calcium chloride ($CaCl_2$).

In the present investigation, the mineral-based metakaolin material was used as carrier material to immobilize the spores using an adsorption technique. Spores incorporated metakaolin (MK) biocomposite was prepared under aseptic conditions and stored at 4 °C and 25 °C for 180 days. The viability of the biocomposite was studied for a storage period of 180 days. After 180 days, the biocomposite was tested for urease enzyme activity and calcium carbonate precipitation. During casting, the developed biocomposite was immobilized in 500 × 100 × 100 mm prisms, 150 mm cubes, and 100 × 200 mm cylindrical specimens. These specimens were tested for flexural strength, compressive strength, and sorptivity tests at 7 and 28 days of curing. Crack remediation was evaluated for 400 × 100 × 100 mm prism specimens.

The crack healing was evaluated for the ultrasonic pulse velocity (UPV), crack width reduction and water tightness test till the complete crack closure. The precipitating materials were analysed for calcium carbonate precipitation using field-emission surface electron microscopy (FESEM), energy dispersive spectroscopy (EDS) and X-ray diffraction (XRD).

2. Materials and methods

2.1. Bacterial culture and media

The ureolytic bacterial strain MD6 isolated from marble dust was used in this study. Marble dust powder was collected from a marble dumping yard in Kishangarh, Rajasthan, India. The highest urease-producing bacterial isolate, MD6 was selected for further studies and was identified as *Bacillus paramycoides* based on the 16S rRNA sequence analysis by using EzBioCloud database. Corn steep liquor (CSL) was procured from M/s Gulshan Polyols Ltd. Delhi, India. The chemical composition of CSL contains 2.5% reducing sugar, 25.8% lactic acid, 48% crude proteins, 0.4% fats, and 7.6% minerals 7.6% on a dry basis with a pH of 4.0. The bacterial culture was grown in 1.5% CSL medium at 37 °C with agitation at 120 rpm. The pH of the CSL medium was adjusted to 7.5 ± 0.2 using 0.1 mM NaOH solution before autoclaving.

2.2. Materials used

Commercially available ordinary Portland cement (O.P.C.) − 43 grade confirming the Indian Standard (I.S.) [53] was used in this study. Locally available well-graded river sand confirming Zone II as per IS383 − 1970 with a specific gravity of 2.66 was used as fine aggregates [54]. Coarse aggregates of 10 and 20 mm in size with a specific gravity of 2.72 and 2.63, respectively, were used in the current study [54]. The Metakaolin (MK) was obtained from a private vendor. The chemical properties of the MK and O.P.C. − 43 used in the experiment are listed in Table 1.

2.3. Spore preparation and development of metakaolin based biocomposite

To prepare *B. paramycoides* (MD6) spores, the bacterial strain was inoculated in nutrient-deficient (0.3%) CSL broth media (CSL 3 ml/L, $NaHCO_3$ 2.12 g/L, and urea 10 g/L), as according to the method described in Pungrasmi et al. [55]. The culture flask was incubated at $28\,°C \pm 2\,°C$ in an incubator shaker at 100 rpm for seven days. After the incubation period, the culture was exposed to heat shock in a water bath at 80 °C for 10 min to

stimulate spore formation, followed by cold shock for ten minutes by placing the culture flask in crushed ice. The bacterial spores were collected after centrifugation at 5000 rpm for 10 min. The pellet was washed with 0.85% saline to remove any additional CSL medium and was suspended in distilled water. The spore concentration was evaluated using the colony-forming unit (CFU) count.

A concentration of 5.2×10^{-5} spores was uniformly mixed in the MK powder under aseptic conditions to immobilize the bacterial spores . MK powder was used as a carrier material to immobilize the spores. A moisture content of 20% was maintained in the MK material to uniformly mix the spores in the biocomposite [56]. The spore-infused bio-composite was freeze-dried at −20 °C, followed by lyophilization at −55 °C to remove moisture and immobilize the spores in MK powder. A schematic representation of bacterial spore formation and immobilization in MK for the development of biocomposites is shown in Figure 1.

2.4. Storage and viability test

The spore-immobilized MK material, labelled as a biocomposite, was stored in sterile Petri dishes at 25 °C and 4 °C. Viability tests were conducted at regular intervals of seven days during storage. One gram of the sample was weighed from each stored Petri plate and suspended in 9 ml of a 0.85% saline in test tube. Dilutions were made to 10^{-8} by transferring 1 ml of the dilution from each test tube. The efficiency of immobilized spores in the MK carrier material was determined using the CFU count. One hundred microliters of the aliquot were spread on nutrient agar plates using a sterilized spreader. Nutrient agar plates were incubated at 37 °C for 24 – 48 h. The colony-forming units per gram were expressed by determining the log value of the colonies that appeared on nutrient agar plates.

Table 1. Chemical composition of the Metakaolin and the ordinary Portland cement (43 grade).

Composition (%)	Metakaolin	Cement
SiO_2	52.2	21.3
CaO	0.21	63.2
Fe_2O_3	1.53	2.5
Al_2O_3	44.5	7.3
MgO	0.32	1.52
K_2O	0.45	0.54
Na_2O	0.16	0.27
SO_3	0.05	2.42
TiO_2	1.48	0.37

2.5. Urease activity and calcium carbonate precipitation

The urease activity of the stored biocomposite at 4 °C and 25 °C was evaluated after 180 days. The urease activity was carried out in CSL broth supplemented with 2% urea and 1% of biocomposite. Urease activity was measured every 24 h using a phenol-hypochlorite assay, as described by Natarajan [57]. The experiment was carried out in triplicate. In the second set of experiments, the calcium carbonate precipitated by the developed biocomposite was measured by weighing the amount of $CaCO_3$ precipitated in the nutrient broth supplemented with 1% biocomposite, 2% urea, and 25 mM calcium chloride ($CaCl_2$). $CaCO_3$ was collected on Whatman filter paper after 24-hour intervals. The precipitates from each flask were room-dried for 6 h and lyophilized to determine the amount of powdered calcium carbonate collected on the Whatman filter paper. The stored biocomposite that performed best in the viability test, urease assay, and calcium carbonate precipitation was used as a potential self-healing biocomposite for concrete testing.

2.6. Preparation of concrete specimens

To investigate the effect of the biocomposite on the concrete properties, the specimens were cast using the biocomposite stored at 4 °C (selected based on viability and urease activity tests). Prismatic specimens of $500 \times 100 \times 100$ mm, 150 mm cubes, and 100 mm (diameter) × 200 mm (height)

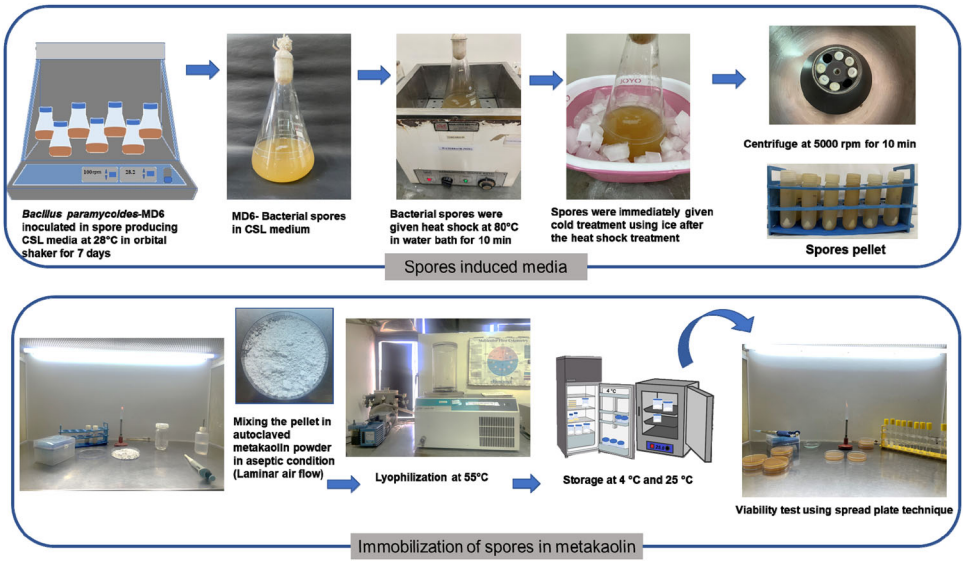


Figure 1. Schematic illustration of *Bacillus paramycoides*- MD6 spores' development and storage after the immobilization in metakaolin (MK) material by lyophilization technique.

Table 2. Mix proportion of the concrete specimens.

Specimens	Mix proportion (kg/m^3) Cement	Sand	Metakaolin bio-composite	Coarse aggregate 10 mm	Coarse aggregate 20 mm	Water/nutrient growth medium
Control	396	722	–	770	513	186
Biocomposite	396	722	7.94**	770	513	186*

*CSL growth medium is composed of CSL broth (1.3% w/v), Urea (2% w/v) and 25 mM Calcium chloride.
**Metakaolin biocomposite stored at 4 °C & 180 days storage age.

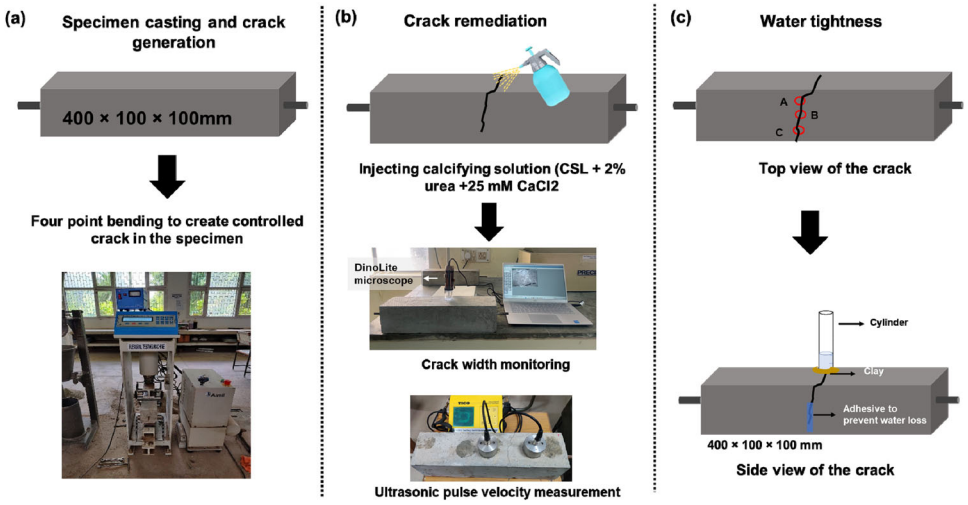


Figure 2. (a) Four-point bending failure to generate the controlled crack (b) crack remediation and monitoring (c) water tightness test; top view of the specimen marked with three different locations of the water flow test on the specimens and side view of the setup of the water flow test with measuring cylinder adhesively attached to the specimen.

Table 3. Summary of the specimen used and test carried out.

Specimen	Testing age (days)	Experiment test	Dimensions
Prismatic	7, 28	Flexural	500 × 100 × 100
Cube	7, 28	Compressive	150 × 150 × 150
Cylinder	7, 28	Sorptivity	100 (dia) × 50 (ht)
Reinforced prismatic	Till complete healing	Visual crack healing	400 × 100 × 100

cylindrical concrete specimens were cast using cement, sand, and coarse aggregate in the proportion of 1:1.82:3.24 (by weight) and 0.47 water-to-cement ratio (w/c), as given in Table 2. The 2% biocomposite stored at 4 °C was added as supplementary material during the mixing of the concrete constituents. Similarly, for crack remediation, prismatic specimens were cast using the same mix proportions, as mentioned above. Reinforced concrete (RC) specimens with dimensions of 400 mm × 100 mm × 100 mm were prepared by embedding a 12 mm rebar at the centre and cured for 28 days. To generate cracks, the prepared RC specimens were subjected to four-point bending failure, as per BIS:516 [58], to attain a crack width of approximately 0.5 mm (Figure 2a). Trials were conducted to achieve a crack width of 0.5 mm.

2.7. Concrete testing

Prismatic specimens with dimensions of 500 × 100 × 100 mm and 150 mm cubes were tested for flexural and compressive strengths at 7 and 28 days of curing, as per the BIS 516 – 1959 standard [58]. Cylindrical specimens of 100 × 50 mm were tested for water absorption according to the ASTM standard [59] at 7 and 28 days of curing. All experiments were performed in triplicate. The details of the concrete specimens are presented in Table 3.

2.8. Crack remediation and monitoring

The cracked prism specimen consisting of the biocomposite was subjected to a self-healing treatment at room temperature. Initially, the cracked region was injected with CSL growth medium supplemented with 2% urea and 25 mM calcium chloride ($CaCl_2$) so that nutrients could reach the depth of the crack (Figure 2b). CSL growth medium was injected using a 20 ml syringe four times a day to activate the spores immobilized in the biocomposite. Later, the spray treatment was repeated daily until complete healing of the cracked region was achieved. The

ultrasonic pulse velocity (UPV) was measured as per ASTM C597 – 02 standard at different crack healing percentages to determine the efficiency of MICCP [60]. The UPV value was estimated by placing the transducer and receiver at a 100 mm distance from the crack as shown in Figure 2b. Three readings were taken at different time intervals.

Water tightness was examined at 0, 14, 28 and 50 days of crack remediation [61]. For this experiment, three different regions were marked as A, B, and C on the crack region to determine the amount of water flowing through the crack (Figure 2c). The flow rate was estimated based on the amount of water flowing through the crack in 20 s. A 50 ml measuring cylinder was adhesively attached with the help of clay to the surface to avoid water leakage. The experiments were conducted until the cracks were completely closed. Crack-sealing efficiency was evaluated based on the amount of water flowing through the defined crack region. The crack-sealing efficiency was evaluated using Equation 1 [62].

$$\text{Sealing efficiency } (\%) = \frac{\text{W.F.}_{\cdot i} - \text{W.F.}_{\cdot t}}{\text{W.F.}_{\cdot i}} \times 100 \quad \text{Eq. (1)}$$

Where WF_i is the initial water flow and WF_t is the final water flow in the crack at different time intervals.

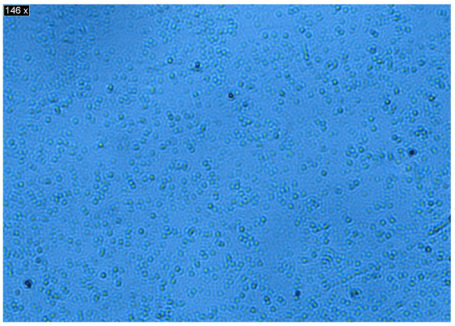


Figure 3. Green-coloured *Bacillus paramycoides* - MD6 spores with an intact outer coating.

2.9. Visual monitoring of crack closure

During the crack remediation process, the reduction in the crack width was periodically monitored using a DinoLite microscope. To better understand crack closure using MICCP, the crack width along the defined length was measured during the healing process. The average of the multiple readings for a particular duration was recorded. The crack-healing efficiency was evaluated according to the equation (Equation 2) [63].

$$\text{Crack healing efficiency } (\%) = \frac{\text{C.W.}_{\cdot i} - \text{C.W.}_{\cdot t}}{\text{C.W.}_{\cdot i}} \times 100 \quad \text{Eq. (2)}$$

CW_i is the initial crack width and CW_t is the crack width at different time intervals.

2.10. Microstructural analysis

To analyse the calcium carbonate precipitation in the bacterial-cured specimen after 28 days of curing, the samples were analysed for FESEM (field emission scanning electron microscopy (FESEM). Energy-dispersive spectroscopy (EDS) was performed to confirm the elemental composition of the precipitate in the concrete. The samples were gold-coated, polished, and coated with carbon to disperse extra charges. X-ray diffraction (XRD) scanning was performed on the powdered concrete samples from 20° to 60° at 2θ angles with a Cu anode (40 kV and 30 mA) using a Bruker D8 X-ray diffractometer.

2.12. Statistical analysis

All experiments were performed in triplicate. Data were analysed using analysis of variance, and significant differences among the means were compared using Tukey's test ($p < 0.05$). All analyses were performed using GraphPad Prism (version 9.3.0) software.

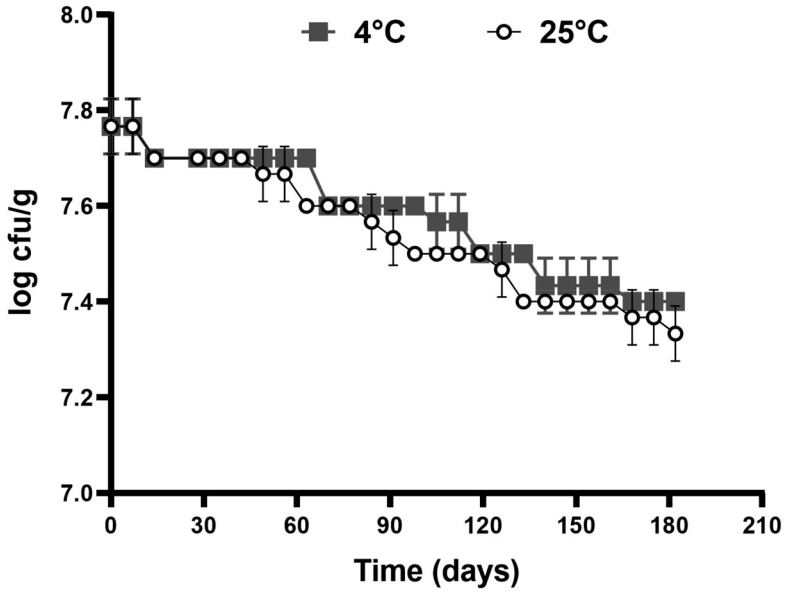


Figure 4. Bacterial cell count (log cfu/g) of developed biocomposite stored at 4 °C and 25 °C in the Petri plate.

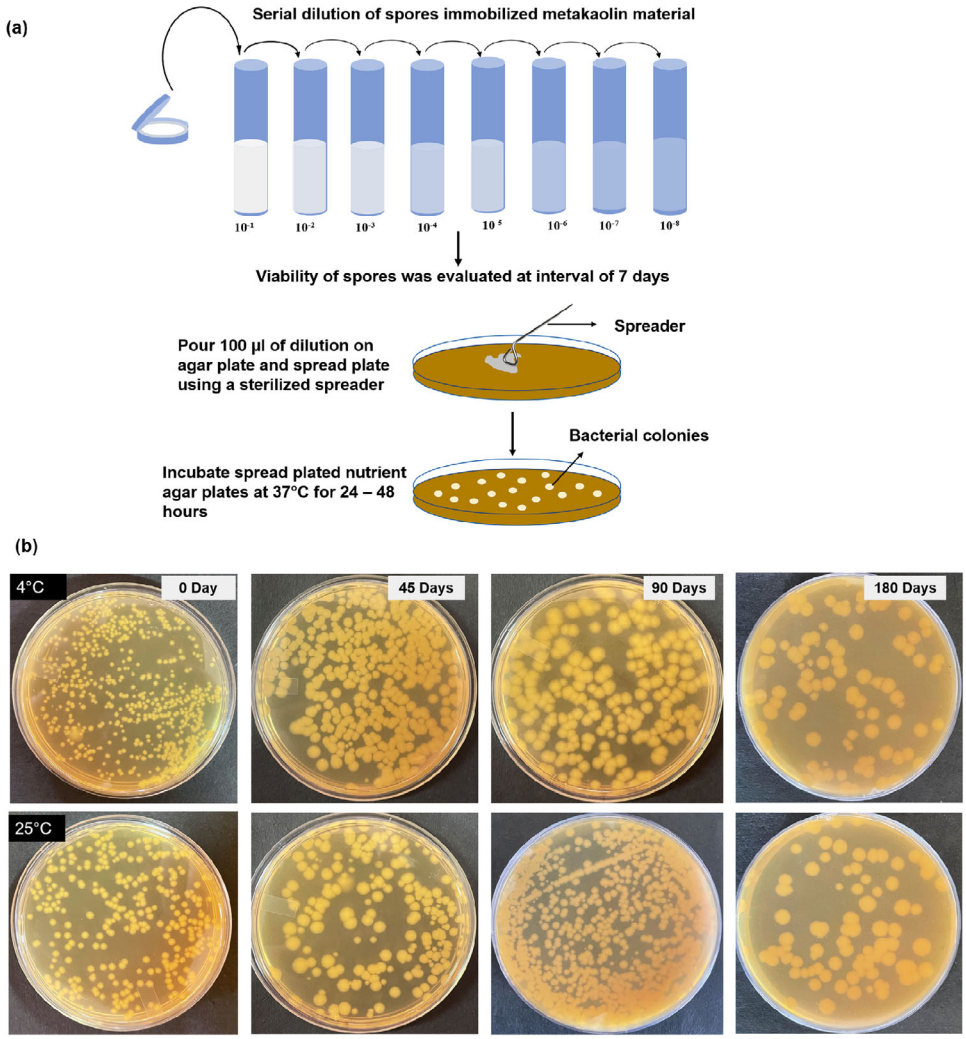


Figure 5. (a) Pictorial representation of serial dilution technique (b) corn steep liquor (CSL) agar plates showing spore viability of developed biocomposite stored at 4 °C and 25 °C for 180 days (26 weeks).

3. Results and discussion

3.1. Viability of biocomposite

Bacterial spores are dormant and have a hard shell known as a spore coat around the cell wall, which helps them to endure harsh environmental conditions such as high temperatures, freezing, and desiccation [64]. The formation of spores was identified by the Schaeffer-Fulton endospore staining method [65]. The spores had green coloured core with intact outer coating as seen under the compound microscope (Figure 3). The use of spores for immobilization ensures the survivability of bacteria after their addition to concrete. The survival of spores immobilized in metakaolin material (biocomposite) was evaluated every 7 days for up to 180 days of storage using the plate count method. Figure 4 shows the viability results evaluated in terms of log colony-forming units per gram (CFU/g). It was observed that for the first 42 days of storage at 25 °C, the developed biocomposite had a consistent cell count of 7.7 log cfu/g. The biocomposite stored at 4 °C maintained the same viability until 63 days of storage. After 91 days of storage at 4 °C and 25 °C, cell viability of the biocomposite was 7.6 and 7.5 log cfu/g, which declined to 7.4 and 7.3 log cfu/g after 180 days of storage. It was observed that the biocomposite stored at 4 °C proved to be more efficient than the 25 °C for maintaining the spores in dormant stage for long period of time. However, it is important to note here that the biocomposite stored at 25 °C was also successful in the maintenance of the immobilized spores during storage with a cell concentration of 7.3 log cfu/g after 180 days. Therefore, it can be inferred that spores stored at different temperatures (25 °C and 4 °C) were able to break the dormant stage and activate the vegetative stage as moisture and nutrients were provided. Figure 5 represents the formation of colony on the solid agar plates depicting the viability of the biocomposite for a storage period of 180 days. The immobilization approach enables bacteria to adhere to the carrier substance, protecting it within the concrete environment for an extended amount of time without any loss of viability. These results are also in agreement with those reported by other researchers [13, 66]. Anand et al. reported the effective survivability of freshly incorporated bacterial cells in fly ash and silica fume after 180 d of storage [4, 56]. Son et al. reported an initial concentration of $2.0 \pm 0.5 \times 10^6$ cfu spores in microcrystalline cellulose tablets [67]. Xiao et al. reported a decline in the concentration of viable spores stored in an alkaline solution at 25 °C

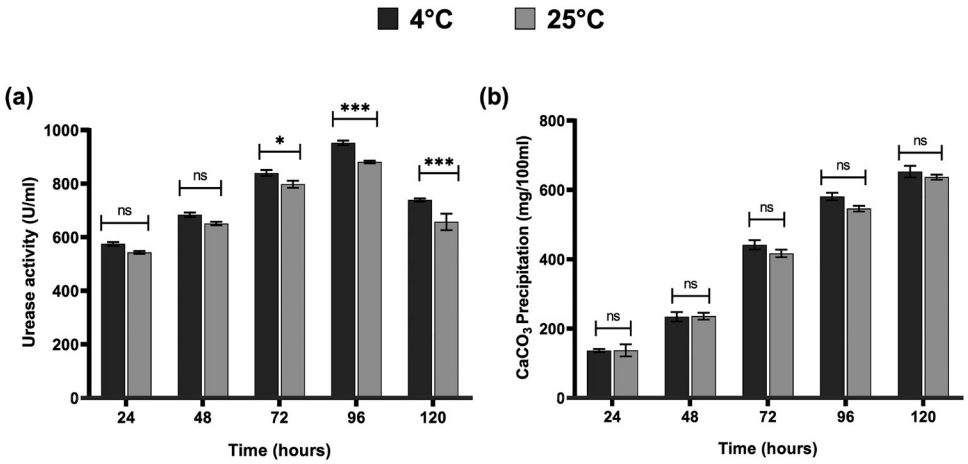


Figure 6. (a) Urease activity and (b) calcium carbonate precipitation of developed biocomposite stored at 4 °C and 25 °C for 180 days.

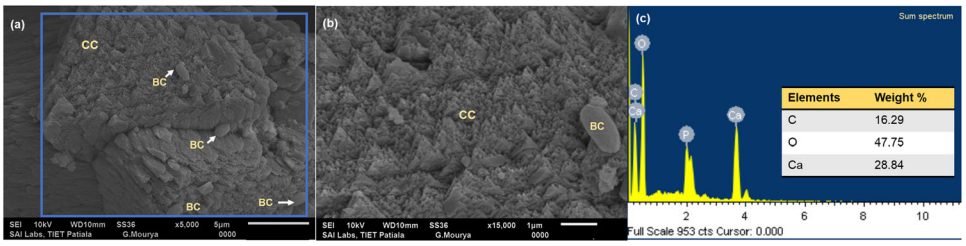


Figure 7. (a, b) S.E.M. analysis of precipitates formed in CSL broth supplemented with 2% urea and 25 mM calcium carbonate. The 'B.C.' represents the 'bacterial cell' and 'CC' represents calcium carbonate precipitation. (c) EDS spectrum marked square '□' shows elemental deposition of the calcium carbonate.

for 30 days [68]. Joshi et al. also reported the utilization of CSL as an alternative nutritional source as efficient as commercial nutrient growth media for the growth of ureolytic bacteria [48].

3.2. *Urease activity and calcium carbonate precipitation*

The amount of urease enzyme that hydrolyses one mole of urea per minute is referred to as one unit of urease. After 180 days of storage at 4 °C and 25 °C, spores immobilized in the biocomposite were tested for urease activity and $CaCO_3$ precipitation. Figure 6a shows the enzyme activity of the bacterial spores produced under favourable conditions. The urease activity showed an increasing trend for the biocomposite stored till 96 h of incubation and a significant loss of the urease activity was observed upon further incubation due to exhaustion of the nutrients. Maximum urease activity of 951.75 U/ml was recorded in the biocomposite stored at 4 °C after 96 h of incubation after which the urease activity declined to 738.95 U/ml at 120 h. The maximum urease activity evaluated by the biocomposite stored at 25 °C was 880.44 U/ml. Similar results were observed by Maleki-Kakelar et al. [68], Achal et al. [69]and Babakhani et al. [70] using CSL as the nutrient growth medium.

The survival of spores during the storage period affects the viability and metabolic activity of bacteria immobilized in the biocomposite. Even after 180 days of storage, the retention in the urease assay proved that spores immobilized in the biocomposite were able to germinate if favourable conditions are provided. During the urease activity, the pH of the medium increases, which creates an alkaline environment adjacent to the bacterial cells for calcium carbonate precipitation [71]. When urea is broken down by the urease enzyme, carbonate ions are produced as a by-product. These carbonate ions then interact with the calcium around the bacterial cell to produce calcium carbonate precipitations [8]. Figure 6b shows the amount of calcium carbonate precipitated by the spore-based biocomposite incubated at 37 °C after 180 days of storage. The experiment was carried out in triplicate, and at each 24-hour interval, the 100 ml flask was taken out to measure the amount of calcium carbonate precipitated. The study was carried out for 120 h, and it was found that the biocomposite stored at 4 °C resulted in 652.43 mg/100 ml. Calcium carbonate precipitation recorded at 4 °C stored spores was 135.77, 233.79, 441.25, 580.67 and 652.43 mg/100 ml at 24, 48, 72, 96, and 120 h, respectively. Similarly, $CaCO_3$ precipitation at 25 °C stored spores was 136.7, 235.67, 416.60, 545.92 and 636.42 mg/ml at 24, 48, 72, 96, and 120 h, respectively. The precipitation ability of the biocomposite proved that spores were able to maintain their shelf life during storage to induce MICCP in the CSL solution. Zamani et al. confirmed the germination of bacterial spores encapsulated in a polyurea polymer and the precipitation of calcium carbonate using FESEM [18]. Other researchers

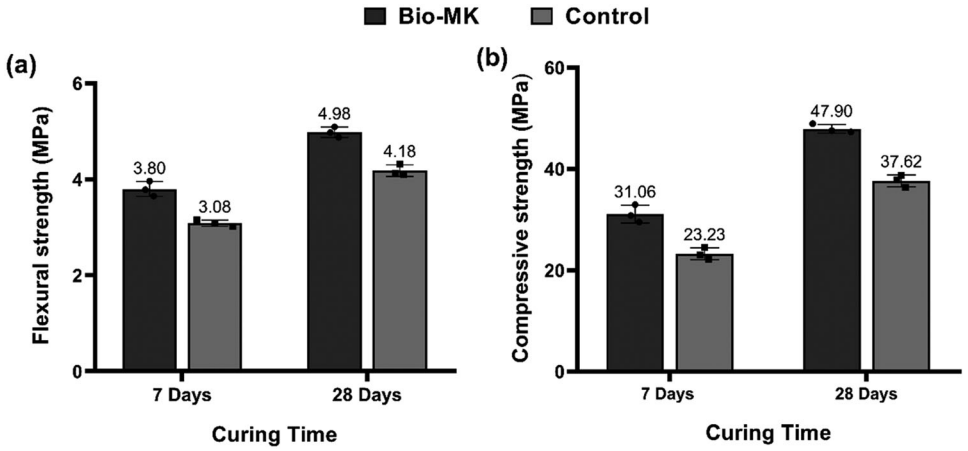


Figure 8. (a) Flexural and (b) compressive strength of bioconcrete and control specimens at the age of 7 and 28 days.

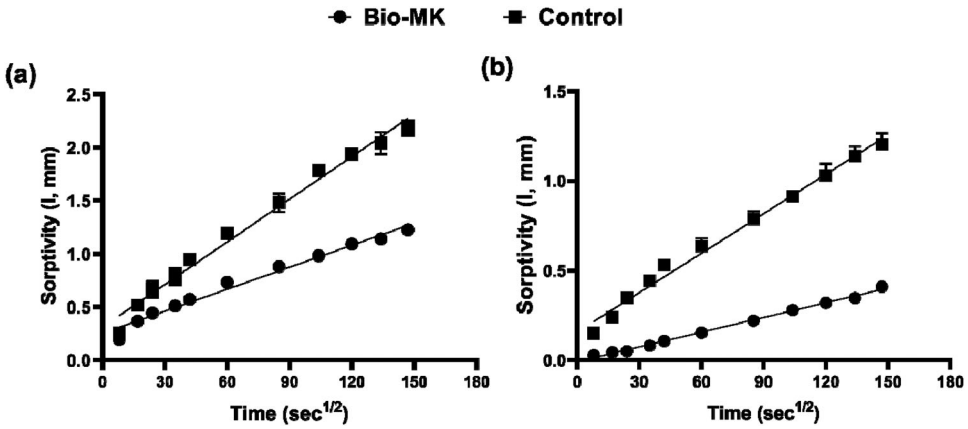


Figure 9. Water absorption by bioconcrete and control specimen at the age of (a) 7 and (b) 28 days.

have reported MICCP using spores immobilized on different carrier materials [19, 72,73].

Figure 7a and b shows the S.E.M. analysis of the calcium carbonate crystals (CC) in the powdered sample collected from the CSL broth using the filtration method. The calcium carbonate precipitation was observed to be forming a staircase kind of layers over one another depicting the abundance of the $CaCO_3$ precipitation by the bacteria. The presence of bacterial cells was also detected in the calcium carbonate precipitates. The EDS analysis confirmed the deposition of calcium carbonate in the form of carbon, oxygen and calcium as shown in Figure 7c. Similar results were presented by Joshi et al. [48] by using CSL as a nutritional source for calcium carbonate precipitation.

3.3. *Strength properties of biocementitious concrete*

Figure 8 shows the (a) flexural and (b) compressive strength results of the concrete specimens incorporated with 2% of biocomposite after 7 and 28 d. The specimens were cured in CSL broth supplemented with 2% urea and 25 mM $CaCl_2$ and control specimens were cured in tap water. The flexural strength of the biocomposite incorporated specimens (labelled as Bio -MK) increased by 19.13% after the specimens were cured in the growth media. Similarly, at 28 d, the compressive strength of the biocomposite incorporated specimens improved by 27.32%. This proves that biocomposite actively increased the strength properties of the concrete. Spores immobilized in the biocomposite survive the harsh conditions of the concrete environment and led to the densification of the concrete matrix by precipitating calcium carbonate in the pores of the specimens. The flexural and compressive strength of control is 4.18 MPa and 37.6 MPa after 28 d curing. Whereas the flexural and compressive strength of Bio - MK is 4.98 and 47.9 MPa. The addition of biocomposite has significantly improved strength properties. It is important to note that no additional bacterial culture was inoculated into the curing medium during the curing. The direct incorporation of urea and calcium chloride without bacteria in cementitious material has retarding effect on the hydration process of concrete [74–77]. However, in this study, the spores immobilized in MK served as an inoculum for bacterial growth, and the bacteria grew when they were given nutrients and moisture. Also, using yeast extract (as media) without any bacteria inoculum decelerates the concrete's strength [52]. However, when bacteria are added together with urea and calcium chloride, it forms calcium carbonate and enhances the strength of concrete [78]. Similar results were confined by Bhutange et al. [79]. Researchers have reported an improvement in flexural and compressive strength by immobilizing bacterial spores in different carrier materials such as zeolite [37], metakaolin-based geopolymers [80],

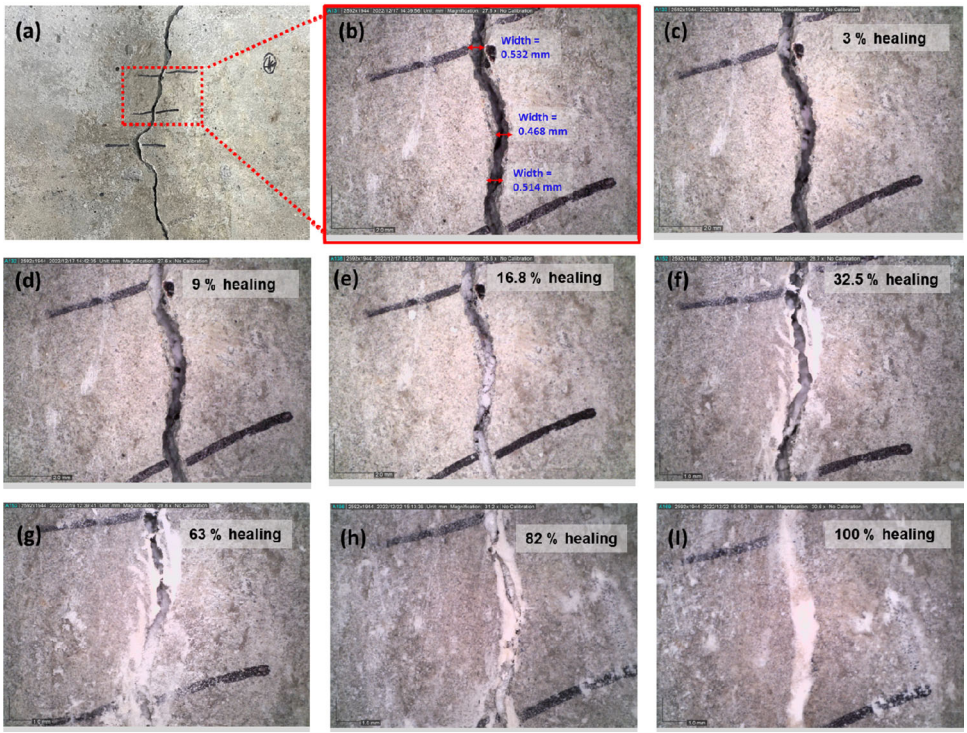


Figure 10. Self-healing of crack by biocomposite in concrete specimens at different healing percentage taken using DinoLite microscope.

and calcium alginate beads [81]. Gao et al. reported a 10.28% increase in compressive strength and a 13.79% increase in flexural strength with the addition of hydrogel beads containing immobilized bacterial spores. In addition, metakaolin is considered a good supplementary cementitious material because it has a high silica content and is reported to increase the strength properties of concrete owing to the early stage of hydration [82,83]. Moreover, the utilization of the CSL as a nutrient medium does not change the chemical characteristics of concrete [48]. The improvement in strength properties of mortar was observed with the addition of CSL as nutrient growth media [52, 69].

3.4. Sorptivity test

Figure 9a and b shows the amount of water absorbed per unit cross-sectional area of the concrete specimen at 7 and 28 d. The bioconcrete specimens prepared using biocomposite (labelled as Bio -MK) were more efficient in controlling the amount of water absorption than the control specimens. The experiment was conducted for 6 h. The cumulative water absorbed at the end of the experiment by 7 days cured control and Bio - MK cylindrical specimens was 2.18 and 1.22 mm, respectively. However, 28 days cured specimens showed reduced water absorption. The water absorption by the control and Bio – MK specimens was 1.20 and 0.41 mm, respectively. This low water absorption rate in biocomposite concrete proves that bacteria calcification in the pores of the concrete matrix. Bacterial cells form calcium carbonate crystals, enhancing the concrete's strength and water permeability. The outcome can be evaluated based on the biotreated specimen's sorptivity coefficient '*k*.' The sorptivity coefficients of the Bio - MK specimens were 0.006 and 0.002 at 7 and 28 d, respectively. However, the control specimens showed sorptivity coefficients of 0.01, and 0.007 at 7 and 28 days of curing, respectively, which were comparatively higher than those of the Bio - MK specimens. The Bio- MK specimens' low '*k*' values confirmed that bacterial spores' incorporation could significantly improve the permeation properties. According to the literature, adding metakaolin to a specimen improves the permeation properties of concrete [84,85]. Similar results were also reported by Pillay et al. on the partial replacement of metakaolin in concrete [83].

3.5. Crack remediation by biocomposite

Two groups of specimens (Bio - MK, and control) were monitored for the complete duration of crack healing. The control specimens were sprayed with water without adding calcifying solution (2% urea and 25 mM $CaCl_2$). Bio – MK specimens were initially subjected to an injection-based treatment of growth media supplemented with calcifying solution (2% urea and 25 mM $CaCl_2$) for five days to activate the endospores and their biomineralization activity at adjacent boundaries of the crack. After which, the spray curing with nutrients and the calcifying solution was employed up to the complete healing. $CaCO_3$ precipitation was not seen in the control specimen. The visual examination of crack healing was monitored, and the crack width was calculated using Eq 1. The UPV and water tightness were studied at different healing durations. Upon complete healing, the healing particles inside the crack were identified using FESEM-EDX and XRD.

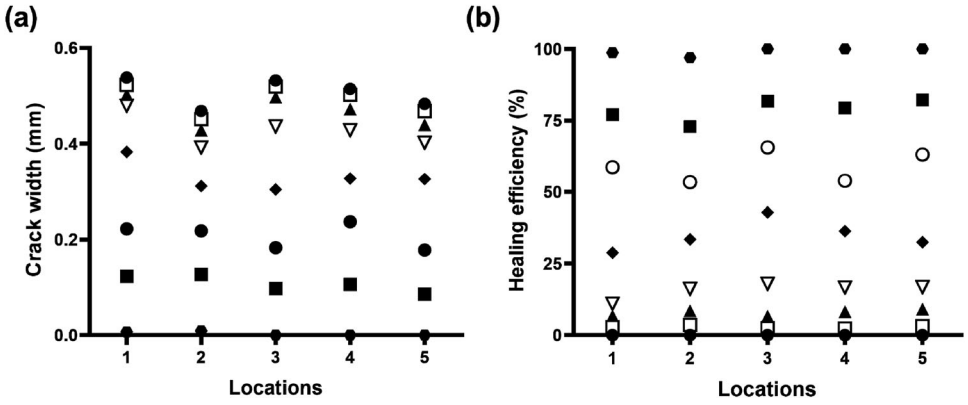


Figure 11. (a) Measurement of crack width at different intervals of time (0 – 50 days) (b) healing efficiency (%) based on the reduction of crack width at 0, 7, 14, 21, 28, 35, 42 and 50 days.

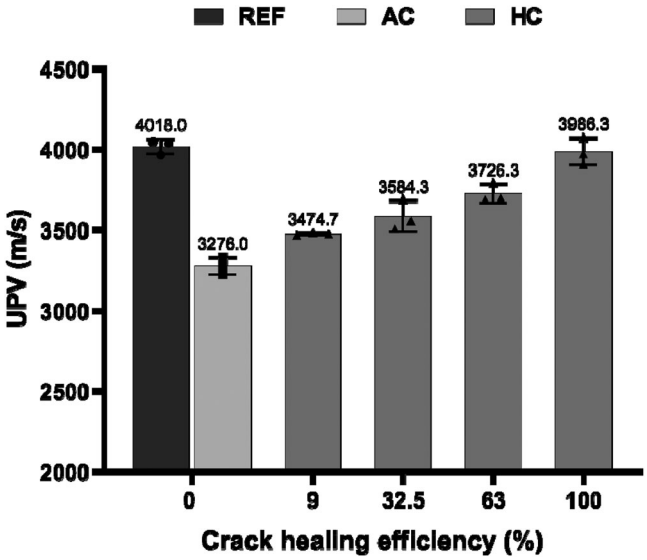


Figure 12. Ultrasonic pulse velocity (UPV) of Bio – MK Concrete crack specimens at different healing percentages of crack (0, 9, 32.5, 63 and 100%).

Initially, the precipitation was only visible on the edges of the crack in Bio – MK specimen. A microscopic image was taken using a DinoLite microscope, showing the deposition of calcium carbonate crystals at the depth of the cracked area (Figure 10). The presence of urea and calcium chloride in the growth medium facilitated ureolytic biochemical reactions in the cracked region promoting the bio-mediated calcium carbonate precipitation. Crack closure was monitored by measuring the reduction in the crack width at five different locations in the concrete specimens. Measurements were taken using a DinoLite microscope. Initially, crack widths of 0.538 mm, 0.468 mm, 0.532 mm, 0.514 mm and 0.483 mm were measured at five locations in the crack region. After the continuous treatment using the CSL medium into the crack region, white carbonate precipitates were observed on the walls of the cracked region after seven days. On the 14th day, visible detection of calcium carbonate was observed, with a reduction in the crack width to 0.502 mm, 0.428 mm, 0.497 mm, 0.472 mm and 0.439 mm. Over a period of 50 days of curing, the crack width at location A decreased from 0.538 to 0. 007 mm, with a crack-healing efficiency of 98.7% (Figure 11a and b). Similarly, at location B, the crack width decreased from 0.468 mm to 0.009 mm, exhibiting a crack-healing efficiency of 97%. At the same time, locations C, D, and E showed healing efficiencies of 100% (Figure 12b). Statistical analysis using one-way ANOVA proved that the crack width was significantly reduced in the 50 days duration at a 5% level of significance. Whilst, no precipitation was seen in control specimens. Specimens incorporated with biocomposite showed autonomous healing of crack width in the range of 0.450- and 0.550-mm. Similar results were corroborated using bacteria immobilized on different carrier materials, such as expanded glass granules [86], hydrogels [17], and rubber particles [87]. Kanwar et al. documented crack healing of 500 μm and 800 μm widths with 100% and 68% crack-sealing efficiency, respectively [88]. Wang et al. reported 84% crack healing ratio with 99% recovery of the compressive strength and water tightness in concrete specimens incorporated with

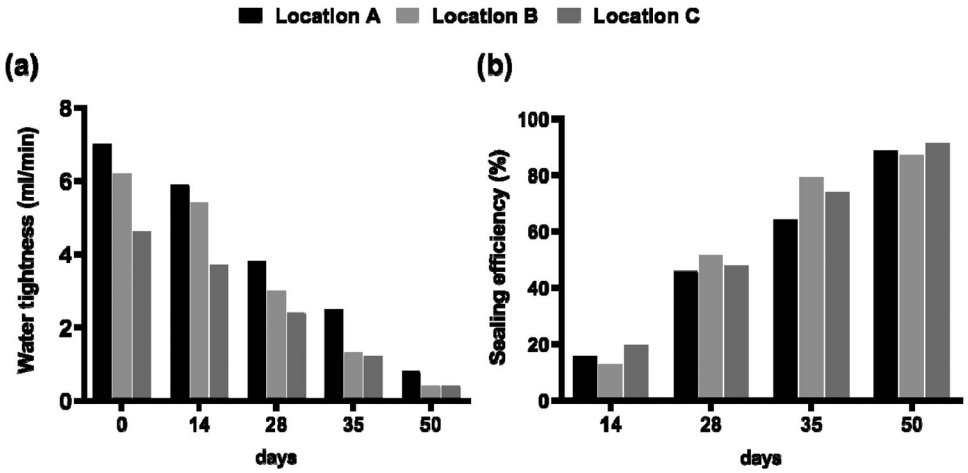


Figure 13. (a)Water tightness and (b) crack sealing efficiency of bacterial treated (*B paramycoides* – MD6) Concrete crack specimens at 0-, 14-, 28, 35- and 50 days curing time.

bacteria immobilized recycled concrete aggregates [89]. Xu et al. reported 100% crack healing with 417 µm crack closure using a low-alkali cementitious material [39]. Anand et al. reported 0.5 mm crack healing in 45 days using bacteria immobilized in silica fume as a carrier material [56]. Previously reported studies have shown that carrier materials have significantly maintained microbial mineralization activity and improved the crack self-healing efficiency [90,91]. Even, the CSL has been proven to be an effective nutrient growth medium for crack healing by Amiri et al. [92,93].

3.6. Regain in ultrasonic pulse velocity (UPV)

Figure 12 shows the UPV measured for a reference specimen (REF) without any cracks, specimens after cracking (A.C.), and specimens with healed cracks (H.C.). The UPV was found to be 4018 m/s in the REF specimen. Also, the UPV was acquired on the cracked prismatic specimen (A.C.) and was recorded to be 3276 m/s. To monitor the healing process, UPV was acquired till the complete healing. The regain in UPV measurement ensured the in-depth healing of cracks due to calcium carbonate precipitation by the bacteria. At 9%, 32.5%, and 63% of crack healing the UPV values were observed to be 3474.7, 3584.3 and 3726.3 m/s. On the complete crack closure, the UPV value was observed to be closer to the reference specimens. This clearly indicates that the crack was 100% healed and was successful in the restoration of the crack region. Moreover, this increase in pulse velocity confirmed the deposition of calcium carbonate at the depth of the crack. Negligible recovery was seen in control, UPV results for which were not included with bacterial healing. Statistical analysis confirmed a significant improvement at the 5% significance level. Other researchers have also reported the recovery of UPV during the healing process [84, 88, 94].

3.7. Water tightness

Water tightness was evaluated based on the amount of water flowing through the crack zone in 20 s until complete crack closure. Different locations were marked as A, B, and C on the specimens to determine the amount of water flowing through the different regions of the crack. The crack widths and depths varied at these locations. At regular intervals, the amount of water flowing through the cylinder fixed at these locations was measured, as described by Kaur et al. [61]. The amounts of water flowing through the crack region initially and during the healing period are shown in Figure 13a. It was observed that initially, 7 ml/20 sec of water flowed through the cracked location A which declined to 5.9 ml/20 sec to 0.8 ml/20 sec at 14 and 50 days, respectively. Similarly, at other locations B the amount of water flowing through the crack region decreased from 6.2 ml/20 sec to 0.4 ml/20 sec at 50 days. As the calcium carbonate precipitates healed the crack, the amount of free water flowing through the crack decreased. The water flow varied at each location, which might be due to variations in crack depth and width.

The crack sealing efficiency percentage was calculated as the amount of free water flowing through the crack zone initially and during the crack healing period. As shown in Figure 13b, the crack-sealing efficiency at location A increased from 15.7% at day 14^{th} to 88.57% on day 50^{th}. Similarly, in locations B and C, 87.09% and 91.3% of sealing efficiency based on the water flow test were estimated at the end of the experiment. Similar results were also reported by Kaur et al. [61]. Likewise, Wang et al. reported an 81–90% water flow reduction in hydrogel-incorporated concrete specimens [11].

3.8. Microstructural characterization

The sample collected from a depth of 10 mm in the healed region was assessed using FESEM and EDS for the biomineralization application of the bacteria. As shown in Figure 14a uniform distribution of rhombohedral and vaterite crystals was observed in the sample. The crystals were stacked to form a calcite layer. The rhombohedral crystals were in the range of 3 - 8 µm in size, whereas the vaterite crystals were in the range of 5 – 7 µm in size. In control, the concrete sample from the cracked area was broken and taken for FESEM-EDS analysis. As seen in Figure 14c and d no calcite crystal deposition was seen.

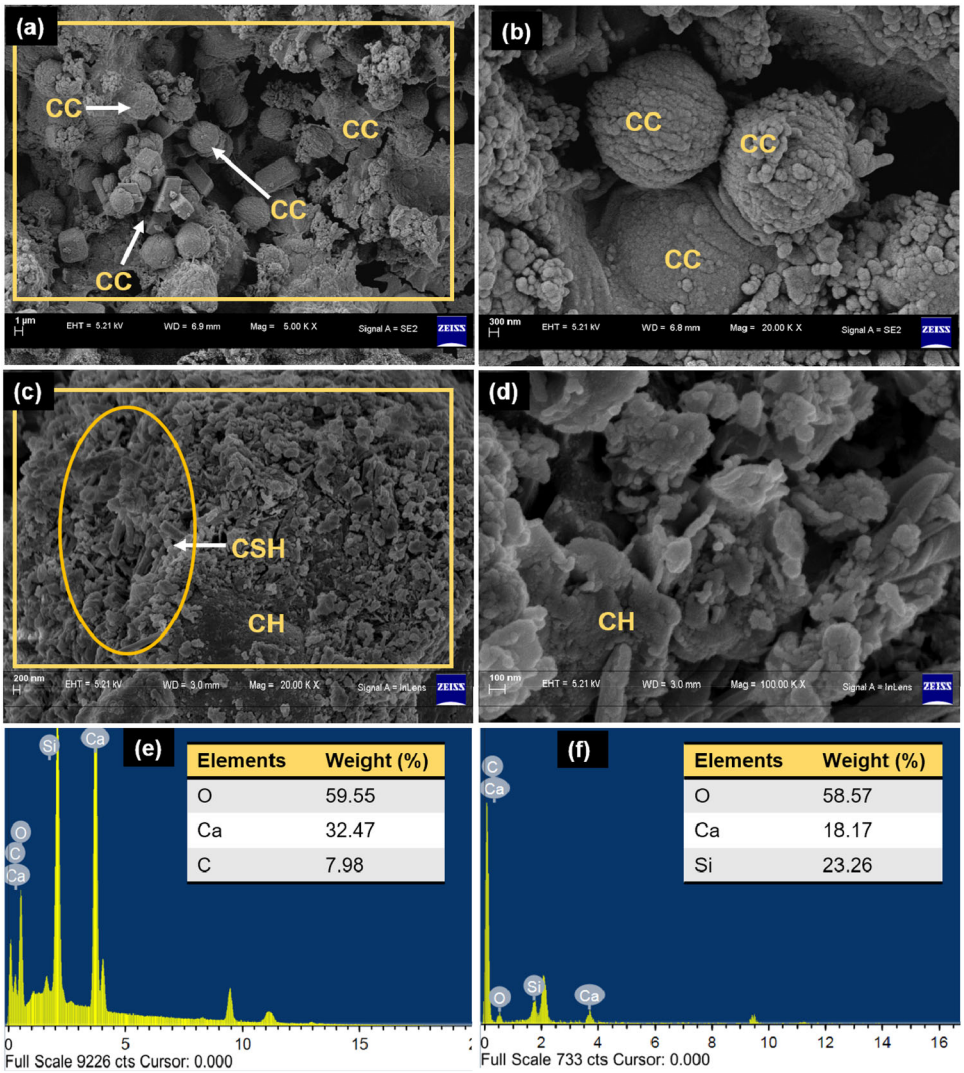


Figure 14. FESEM of the (a, b) crack healed Bio – MK concrete specimens (c, d) control (e, f) EDS spectrum marked '□' represents elemental deposition of the calcium carbonate.

To confirm elemental deposition both the samples were also analysed for EDS. The elemental analysis of the healed precipitates in Bio -MK showed that the crystals formed were composed of calcium carbonate. Elemental examination revealed that the healed biocementitious material consisted of four essential elements: carbon (C), oxygen (O), and calcium (Ca) at 7.98, 59.55, and 32.47 weight percentage ratio (Figure 14e). whereas, silicon (Si), oxygen (O), and calcium (Ca) at 23.26, 58.57, and 18.17 weight percentage ratio was observed in control (Figure 14f). The percentage formation of calcium was observed to be more in Bio-MK which marks the fact there is some bacterial activity going on in Bio-MK specimens leading to calcite formation. Anand et al. corroborated similar calcium carbonate deposition results from a healed region [4]. The existence of calcium carbonate crystals with such diverse forms and structures has been extensively established in literature studies [95,96]. Sidhu et al. also reported the occurrence of the spherical shape of vaterite and the cubic shape of calcite [97]. The results were also in agreement with Achal et al. [69], and Babakhani et al. [70].

Furthermore, the crystalline morphology was verified using X-ray diffraction (XRD). As shown in Figure 15, high-intensity calcite peaks were observed at 29.2°, 39.5°Corresponding to crystallography planes of 104, 113 of calcite. Another X-ray diffraction peak located at (2θ) = 27.5°, corresponds to the 101 planes of the vaterite crystals. The presence of calcite and vaterite peaks confirms that the healed material is calcium carbonate precipitate, which was induced by the immobilized spores in the metakaolin material. Other peaks of quartz (Q), calcium hydroxide (CH), and calcium silicate hydrates (CSH) were also observed in the sample. These peaks were also observed in control concrete specimens. The intensity of the calcite peak in Bio-MK specimen was high as compared to the control. Similar results have been reported by other researchers by introducing bacterial interactions into the cementitious environment [7, 97,98].

3.9. *Autonomous crack healing*

Based on the above-mentioned results and discussion, the current study reports autonomous (microbial) self-healing of the crack using metakaolin (MK) immobilized

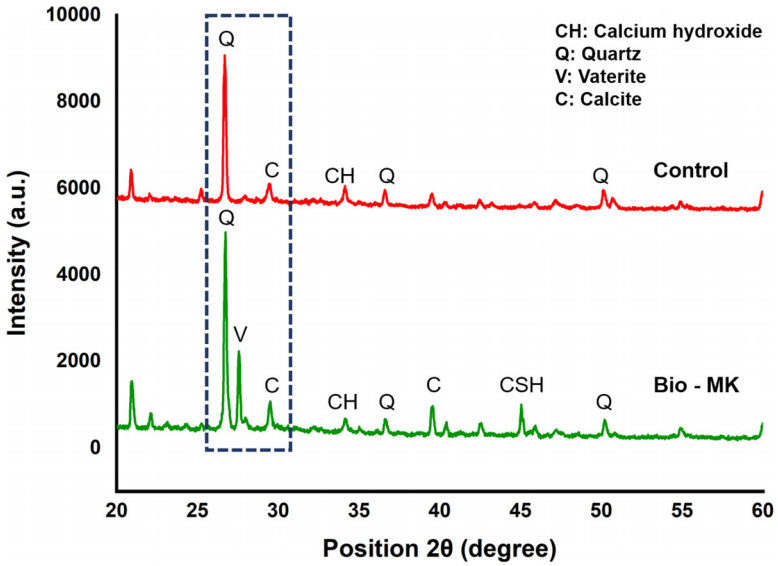


Figure 15. XRD pattern of bio – MK and control specimens.

B. paramycoides spores. In the context of mineralization in concrete, calcium ions can play a significant role. However, it's important to clarify the source of these calcium ions during autogenous and autonomous crack healing. During the hydration process of cement, calcium ions are released, contributing to the formation of calcium hydroxide (CH) and calcium silicate hydrate (C-S-H) gel, the primary binding agent in concrete [99]. During autonomous healing, the presence of bacteria results in higher pH value compared to the control mixture, likely due to urea hydrolysis [72]. The negative charge of bacterial cell wall attracts positively charged Ca^{2+} ions and acts as a nucleation site for $CaCO_3$ precipitation. In terms of mineralization in concrete, both the free Ca^{2+}ions released during cement hydration and those from calcium chloride can contribute to the formation of additional minerals, such as calcium carbonate ($CaCO_3$) [100]. However, when externally provided calcium chloride dissolves in water, it releases calcium ions (Ca^{2+}) that can participate in the MICCP. In addition to autonomous healing, researchers have documented effective autogenous self-healing of cracks up to 0.200 mm in width as a result of cement hydration and carbonation of hydrated products [101–104]. However, autonomous crack healing requires an external trigger to activate the MICCP process [105]. Researchers have reported autonomous crack healing of 0.100 – 1 mm by the addition of bacteria along with a calcifying solution (urea and calcium chloride) for effective biomineralization [106–108]. The study demonstrated significant enhancements in self-healing through microbial-induced calcium carbonate precipitation (MICCP), as evidenced by surface crack observations, FESEM-EDS and XRD. Results were confirmed using XRD spectra in comparison to the control, Bio-MK specimens have high peaks of vaterite and calcite along with CH and CSH. It proves the calcite content in Bio-MK specimens were high which might be due to bacterial activity. Moreover, strength and permeability experiments were tested for the biocomposite and control which showed significant improvement in Bio-MK specimens. Therefore, both the free calcium ions released during cement hydration and those provided by calcium chloride can be involved in the mineralization process.

4. Conclusions

The present study investigated the viability and crack-healing efficiency of *B. paramycoides* spores immobilized in metakaolin (biocomposite). The spores immobilized in metakaolin are viable up to 180 days and improved the compressive and flexural strengths of uncracked specimens by 27.3% and 19.1%, respectively. The sorptivity coefficient '*k*' significantly reduced in Bio-MK specimens compared to the control. The biocomposite-added concrete specimens were able to heal a crack of approximately 500 µm with a crack healing efficiency of 99.14%, which was confirmed by regain in the ultrasonic pulse velocity. These results suggest that developed metakaolin biocomposite could be a potential source along with CSL to heal the cracks of concrete specimens.

Funding

This work was supported by Department of Biotechnology, Ministry of Science and Technology, India.

ORCID

Shweta Goyal http://orcid.org/0000-0002-4427-7787
M. Sudhakara Reddy http://orcid.org/0000-0002-9743-4993

Data availability statement

Some or all data, models, or code that support the findings of this study are available from the corresponding author upon reasonable request

Disclosure statement

No potential conflict of interest was reported by the authors.

Acknowledgments

The authors are thankful to the Department of Biotechnology, Ministry of Science and Technology, Govt. of India, for providing the research grant under BT/PR27190/BCE/8/1428/2017.

References

[1] Guo T, Weng X, Liu C, et al. Evaluation of the bonding and fatigue properties of an innovative rapid repair structure for concrete pavement. Constr Build Mater. 2020;235:117484. doi:10.1016/j.conbuildmat.2019.117484.

[2] Song X, Song X, Liu H, et al. Cement-Based repair materials and the interface with concrete substrates: characterization, evaluation and improvement. Polymers (Basel). 2022;14(7):1485. doi:10.3390/polym14071485.

[3] Dhiman NK, Sidhu N, Agnihotri S, et al. Role of nanomaterials in protecting building materials from degradation and deterioration. Biodegrad Biodeterior Nanoscale. 2022:405–475. https://doi.org/10.1016/B978-0-12-823970-4.00024-5.

[4] Anand K, Goyal S, Reddy MS. Crack healing in concrete by microbially induced calcium carbonate precipitation as assessed through electromechanical impedance technique. Eur J Environ Civ Eng. 2023;27(3):1123–1143. doi:10.1080/19648189.2022.2075470.

[5] Achal V, Mukerjee A, Sudhakara Reddy M. Biogenic treatment improves the durability and remediates the cracks of concrete structures. Constr Build Mater. 2013;48:1–5. doi:10.1016/j.conbuildmat.2013.06.061.

[6] Skevi L, Reeksting BJ, Hoffmann TD, et al. Incorporation of bacteria in concrete: the case against MICP as a means for strength improvement. Cem Concr Compos. 2021;120:104056. doi:10.1016/j.cemconcomp.2021.104056.

[7] Ahmad SSE, Elmahdy M, ELShami AA, et al. Bacterial sustainable concrete for repair and rehabilitation of structural cracks. J Sustain Cem Mater. 2023;12(5):627–646. doi:10.1080/21650373.2022.2101156.

[8] Dhami NK, Reddy MS, Mukherjee MS. Biomineralization of calcium carbonates and their engineered applications: a review. Front Microbiol. 2013;4:1–13. doi:10.3389/fmicb.2013.00314.

[9] Mutitu KD, Munyao MO, Wachira MJ, et al. Effects of biocementation on some properties of cement-based materials incorporating bacillus species bacteria–a review. J Sustain Cem Mater. 2019;8(5):309–325. doi:10.1080/21650373.2019.1640141.

[10] Dinarvand P, Rashno A. Review of the potential application of bacteria in self-healing and the improving properties of concrete/mortar. J Sustain Cem Mater. 2022;11(4):250–271. doi:10.1080/21650373.2021.1936268.

[11] Wang J, Mignon A, Trenson G, et al. A chitosan based pH-responsive hydrogel for encapsulation of bacteria for self-sealing concrete. Cem Concr Compos. 2018;93:309–322. doi:10.1016/j.cemconcomp.2018.08.007.

[12] De Belie N, Wang J. Bacteria-based repair and self-healing of concrete. Bacteria-Based Repair and Self-Healing of Concrete. 2016;5(1–2):35–56. doi:10.1080/2165037320151077754.

[13] Zhu X, Mignon A, Nielsen SD, et al. Viability determination of Bacillus sphaericus after encapsulation in hydrogel for self-healing concrete via microcalorimetry and in situ oxygen concentration measurements. Cem Concr Compos. 2021;104006.

[14] Sharma B, Singh A, Joshi S, et al. Utilization of sandstone waste in cement mortar for sustainable production of building materials through biomineralization. J Sustain Cem Mater. 2023;12(6):712–720. doi:10.1080/21650373.2022.2116500.

[15] Dzionek A, Wojcieszyńska D, Guzik U. Natural carriers in bioremediation: a review. Electron J Biotechnol. 2016;23:28–36. doi:10.1016/j.ejbt.2016.07.003.

[16] Wang JY, Soens H, Verstraete W, et al. Self-healing concrete by use of microencapsulated bacterial spores. Cem Concr Res. 2014;56:139–152. doi:10.1016/j.cemconres.2013.11.009.

[17] Gao M, Guo J, Cao H, et al. Immobilized bacteria with pH-response hydrogel for self-healing of concrete. J Environ Manage. 2020;261:110225. doi:10.1016/j.jenvman.2020.110225.

[18] Zamani M, Nikafshar S, Mousa A, et al. Bacteria encapsulation using synthesized polyurea for self-healing of cement paste. Constr Build Mater. 2020;249:118556. doi:10.1016/j.conbuildmat.2020.118556.

[19] Wang J, Ersan YC, Boon N, et al. Application of microorganisms in concrete: a promising sustainable strategy to improve concrete durability. Appl Microbiol Biotechnol. 2016;100(7):2993–3007. doi:10.1007/s00253-016-7370-6.

[20] Gupta S, Kua HW, Pang SD. Healing cement mortar by immobilization of bacteria in biochar: an integrated approach of self-healing and carbon sequestration. Cem Concr Compos. 2018;86:238–254. doi:10.1016/j.cemconcomp.2017.11.015.

[21] Khaliq W, Ehsan MB. Crack healing in concrete using various bio influenced self-healing techniques. Constr Build Mater. 2016;102:349–357. doi:10.1016/j.conbuildmat.2015.11.006.

[22] Wang L, Ren Z, Wang H, et al. Microstructure-property relationships in cement mortar with surface treatment of microbial induced carbonate precipitation. Compos Part B. 2022;239:109986. doi:10.1016/j.compositesb.2022.109986.

[23] Alghamri R, Kanellopoulos A, Al-Tabbaa A. Impregnation and encapsulation of lightweight aggregates for self-healing concrete. Constr Build Mater. 2016;124:910–921. doi:10.1016/j.conbuildmat.2016.07.143.

[24] Apolinário de Oliveira T, D'Orey Gaivão Portela Bragança M, Miguel Pinkoski I, et al. The effect of silica nanocapsules on self-healing concrete. Constr Build Mater. 2021;300:124010.

[25] Gulin LB, Schwantes-Cezario N, Florian M. Viability of Bacillus subtilis immobilization using silica gel for self-healing of cement based materials. IJAERS. 2021;8:001–010. doi:10.22161/ijaers.86.1.

[26] Wang J, Van Tittelboom K, De Belie N, et al. Use of silica gel or polyurethane immobilized bacteria for self-healing concrete. Constr Build Mater. 2012;26(1):532–540. doi:10.1016/j.conbuildmat.2011.06.054.

[27] Yuan H, Zhang Q, Hu X, et al. Application of zeolite as a bacterial carrier in the self-healing of cement mortar cracks. Constr Build Mater. 2022;331:127324. doi:10.1016/j.conbuildmat.2022.127324.

[28] Zheng T, Qian C. Self-Healing of Later-Age cracks in cement-based materials by encapsulation-based

bacteria. J Mater Civ Eng. 2020;32(11):1–10. doi:10.1061/(ASCE)MT.1943-5533.0003437.
[29] Zhang J, Liu Y, Feng T, et al. Immobilizing bacteria in expanded perlite for the crack self-healing in concrete. Constr Build Mater. 2017;148:610–617. doi:10.1016/j.conbuildmat.2017.05.021.
[30] Li W, Hua L, Shi Y, et al. Influence of metakaolin on the hydration and microstructure evolution of cement paste during the early stage. Appl Clay Sci. 2022;229:106674. doi:10.1016/j.clay.2022.106674.
[31] Bright Singh S, Murugan M. Effect of metakaolin on the properties of pervious concrete. Constr Build Mater. 2022;346:128476. doi:10.1016/j.conbuildmat.2022.128476.
[32] Bishnoi S. RILEM Bookseries Calcined Clays for Sustainable Concrete Proceedings of the 3rd International Conference on Calcined Clays for Sustainable Concrete. 2020. http://www.springer.com/series/8781.
[33] Rais MS, Khan RA. Experimental investigation on the strength and durability properties of bacterial self-healing recycled aggregate concrete with mineral admixtures. Constr Build Mater. 2021;306:124901. doi:10.1016/j.conbuildmat.2021.124901.
[34] El-Diadamony H, Amer AA, Sokkary TM, et al. Hydration and characteristics of metakaolin pozzolanic cement pastes. HBRC J. 2018;14(2):150–158. doi:10.1016/j.hbrcj.2015.05.005.
[35] Badogiannis EG, Sfikas IP, Voukia DV, et al. Durability of metakaolin Self-Compacting concrete. Constr Build Mater. 2015;82:133–141. doi:10.1016/j.conbuildmat.2015.02.023.
[36] Singh H, Siddique R. Utilization of crushed recycled glass and metakaolin for development of self-compacting concrete. Constr Build Mater. 2022;348:128659. doi:10.1016/j.conbuildmat.2022.128659.
[37] Bhaskar S, Anwar Hossain KM, Lachemi M, et al. Effect of self-healing on strength and durability of zeolite-immobilized bacterial cementitious mortar composites. Cem Concr Compos. 2017;82:23–33. doi:10.1016/j.cemconcomp.2017.05.013.
[38] Kennedy MJ, Reader Lisa M, Swierczynski SL, et al. Historical perspective preservation records of microorganisms : evidence of the tenacity of life. Microbiology. 1994;140(10):2513–2529. doi:10.1099/00221287-140-10-2513.
[39] Xu J, Wang X. Self-healing of concrete cracks by use of bacteria-containing low alkali cementitious material. Constr Build Mater. 2018;167:1–14. doi:10.1016/j.conbuildmat.2018.02.020.
[40] Abel-Santos E. Endospores, Sporulation and Germination. Molecular Medical Microbiology, Academic Press,2015, pp 163–178. doi:10.1016/B978-0-12-397169-2.00009-3.
[41] Lee YS, Park W. Current challenges and future directions for bacterial self-healing concrete. Appl Microbiol Biotechnol. 2018;102(7):3059–3070. doi:10.1007/s00253-018-8830-y.
[42] Sharma TK, Alazhari M, Heath A, et al. Alkaliphilic bacillus species show potential application in concrete crack repair by virtue of rapid spore production and germination then extracellular calcite formation. J Appl Microbiol. 2017;122(5):1233–1244. doi:10.1111/jam.13421.
[43] Jonkers HM, Thijssen A, Muyzer G, et al. Application of bacteria as self-healing agent for the development of sustainable concrete. Ecol Eng. 2010;36(2):230–235. doi:10.1016/j.ecoleng.2008.12.036.
[44] Silva FB, Boon N, De Belie N, et al. Industrial application of biological self-healing concrete: challenges and economical feasibility. J Commer Biotechnol. 2015;21:31–38.
[45] Justo-Reinoso I, Reeksting BJ, Hamley-Bennett C, et al. Air-entraining admixtures as a protection method for bacterial spores in self-healing cementitious composites: healing evaluation of early and later-age cracks. Constr Build Mater. 2022;327:126877. doi:10.1016/j.conbuildmat.2022.126877.
[46] Setlow P. Spore germination. Curr Opin Microbiol. 2003;6(6):550–556. doi:10.1016/j.mib.2003.10.001.
[47] Christie G, Setlow P. Bacillus spore germination: knowns, unknowns and what we need to learn. Cell Signal. 2020;74:109729. doi:10.1016/j.cellsig.2020.109729.
[48] Joshi S, Goyal S, Reddy MS. Corn steep liquor as a nutritional source for biocementation and its impact on concrete structural properties. J Ind Microbiol Biotechnol. 2018;45(8):657–667. doi:10.1007/s10295-018-2050-4.
[49] Achal V, Mukherjee A, Reddy MS. Effect of calcifying bacteria on permeation properties of concrete structures. J Ind Microbiol Biotechnol. 2011;38(9):1229–1234. doi:10.1007/s10295-010-0901-8.
[50] Achal V, Mukherjee A, Basu PC, et al. Lactose mother liquor as an alternative nutrient source for microbial concrete production by *Sporosarcina pasteurii*. J Ind Microbiol Biotechnol. 2009;36(3):433–438. doi:10.1007/s10295-008-0514-7.
[51] Cuzman OA, Wittig L, Abancéns FJR, et al. Bacterial "masons" at work with wastes for producing eco-cement. IJESD. 2015;6(10):767–774. doi:10.7763/IJESD.2015.V6.696.
[52] Amiri A, Bundur ZB. Use of corn-steep liquor as an alternative carbon source for biomineralization in cement-based materials and its impact on performance. Constr Build Mater. 2018;165:655–662. doi:10.1016/j.conbuildmat.2018.01.070.
[53] Bureau of Indian Standard (BIS). Is: 8112 – 1989, specification for 43 grade ordinary Portland cement. Bur Indian Stand Delhi. 2013;17:1–11.
[54] IS:383. Indian standard specification for coarse and fine aggregates from natural sources for concrete. Bureau of Indian Standards, New Delhi, 2016;1–21.
[55] Pungrasmi W, Intarasoontron J, Jongvivatsakul P, et al. Evaluation of microencapsulation techniques for MICP bacterial spores applied in self-healing concrete. Sci Rep. 2019;9(1):10. doi:10.1038/s41598-019-49002-6.
[56] Anand K, Goyal S, Reddy MS. Long-term viable SF immobilized bacterial cells as sustainable solution for crack healing in concrete. Structures. 2022;43:1342–1355. doi:10.1016/j.istruc.2022.07.056.
[57] Natarajan KR. Kinetic study of the enzyme urease from Dolichos biflorus. J Chem Educ. 1995;72(6):556–557. doi:10.1021/ed072p556.
[58] IS 516:2014. Method of tests for strength of concrete. IS 516 - 1959 (reaffirmed 2004). New Delhi: Bureau of Indian Standards; 2004.
[59] ASTM C1585-13. Standard test method for measurement of rate of absorption of water by hydraulic cement concretes. ASTM Int. 2013;41:1–6.
[60] American Society for Testing and Material. ASTM C 597-02, standard test method for pulse velocity through concrete. United States Am Soc Test Mater. 2003;4:3–6.
[61] Kaur NP, Majhi S, Dhami NK, et al. Healing fine cracks in concrete with bacterial cement for an advanced non-destructive monitoring. Constr Build Mater. 2020;242:118151. doi:10.1016/j.conbuildmat.2020.118151.

[62] Liu Y h, Yang P, Ku T, et al. Effect of different nanoparticles on the grouting performance of cement-based grouts in dynamic water condition. Constr Build Mater. 2020;248:118663. doi:10.1016/j.conbuildmat.2020.118663.
[63] González Á, Parraguez A, Corvalán L, et al. Evaluation of Portland and pozzolanic cement on the self-healing of mortars with calcium lactate and bacteria. Constr Build Mater. 2020;257:1–11.
[64] Checinska A, Paszczynski A, Burbank M. Bacillus and other spore-forming genera: variations in responses and mechanisms for survival. Annu Rev Food Sci Technol. 2015;6:351–369. doi:10.1146/annurev-food-030713-092332.
[65] Hussey MA, Zayaitz A. Endospore stain protocol. Am Soc Microbiol 2007;8:1–11.
[66] Yang D, Xu G, Duan Y, et al. Self-healing cement composites based on bleaching earth immobilized bacteria. J Clean Prod. 2022;358:132045. doi:10.1016/j.jclepro.2022.132045.
[67] Son Y, Min J, Jang I, et al. Development of a novel compressed tablet-based bacterial agent for self-healing cementitious material. Cem Concr Compos. 2022;129:104514. doi:10.1016/j.cemconcomp.2022.104514.
[68] Maleki-Kakelar M, Aghaeinejad-Meybodi A, Sanjideh S, et al. Cost-effective optimization of bacterial urease activity using a hybrid method based on response surface methodology and artificial neural networks. Environ Process. 2022;9(1):7. doi:10.1007/s40710-022-00564-0.
[69] Achal V, Mukherjee A, Reddy MS. Biocalcification by Sporosarcina pasteurii using corn steep liquor as the nutrient source. Ind Biotechnol. 2010;6(3):170–174. doi:10.1089/ind.2010.6.170.
[70] Babakhani S, Fahmi A, Katebi H, et al. – Babakhani - Non-sterile corn steep liquor a novel, cost effective and powerful culture media for *Sporosarcina pasteurii* cultivation for sand improvement. J Appl Microbiol. 2021;130(4):1232–1244. doi:10.1111/jam.14866.
[71] Achal V, Mukherjee A, Sudhakara Reddy M. Characterization of two urease-producing and calcifying Bacillus spp. isolated from cement. J Microbiol Biotechnol. 2010;20(11):1571–1576. doi:10.4014/jmb.1006.06032.
[72] Xiao X, Unluer C, Yang E. Study on the viability of unprotected bacterial spores directly embedded in a reactive magnesia cement matrix for potential crack healing. Constr Build Mater. 2022;346:128424. doi:10.1016/j.conbuildmat.2022.128424.
[73] Wang J, Jonkers HM, Boon N, et al. *Bacillus sphaericus* LMG 22257 is physiologically suitable for self-healing concrete. Appl Microbiol Biotechnol. 2017;101(12):5101–5114. doi:10.1007/s00253-017-8260-2.
[74] Başaran Bundur Z, Bae S, Kirisits MJ, et al. Biomineralization in self-healing cement-based materials: investigating the temporal evolution of microbial metabolic state and material porosity. J Mater Civ Eng. 2017;29(8):04017079. doi:10.1061/(ASCE)MT.1943-5533.0001838.
[75] Erşan YÇ, Da Silva FB, Boon N, et al. Screening of bacteria and concrete compatible protection materials. Constr Build Mater. 2015;88:196–203. doi:10.1016/j.conbuildmat.2015.04.027.
[76] Anand K, Goyal S, Reddy MS. Development of field applicable remediation procedure using bio-cementitious grout for concrete cracks in variable orientations. J Build Eng. 2023;67:106024. doi:10.1016/j.jobe.2023.106024.
[77] Joshi S, Goyal S, Reddy MS. Influence of nutrient components of media on structural properties of concrete during biocementation. Constr Build Mater. 2018;158:601–613. doi:10.1016/j.conbuildmat.2017.10.055.
[78] Yazici Ş, Güller C, Ayekin B, et al. Usability of sustainable materials on bacteria-based self-healing in cementitious systems. J Intell Mater Syst Struct. 2023. doi:10.1177/1045389X231157358.
[79] Bhutange SP, Latkar MV, Chakrabarti T. Influence of direct urease source incorporation on mechanical properties of concrete. Constr Build Mater. 2021;301:124116. doi:10.1016/j.conbuildmat.2021.124116.
[80] Yılmazer Polat B, Uysal M. Bacterial crack healing in metakaolin based geopolymer mortars. J Build Eng. 2021;39:102291. doi:10.1016/j.jobe.2021.102291.
[81] Soysal A, Milla J, King GM, et al. Evaluating the self-healing efficiency of hydrogel-encapsulated bacteria in concrete. Transp Res Rec. 2020;2674(6):113–123. doi:10.1177/0361198120917973.
[82] Barbhuiya S, Chow PL, Memon S. Microstructure, hydration and nanomechanical properties of concrete containing metakaolin. Constr Build Mater. 2015;95:696–702. doi:10.1016/j.conbuildmat.2015.07.101.
[83] Pillay DL, Olalusi OB, Kiliswa MW, et al. Engineering performance of metakaolin based concrete. Clean Eng Technol. 2022;6:100383. doi:10.1016/j.clet.2021.100383.
[84] Tanyildizi H, Ziada M, Uysal M, et al. Comparison of bacteria-based self-healing methods in metakaolin geopolymer mortars. Case Stud Constr Mater. 2022;16:e00895.
[85] Abouhussien AA, Hassan AAA. Optimizing the durability and service life of self-consolidating concrete containing metakaolin using statistical analysis. Constr Build Mater. 2015;76:297–306. doi:10.1016/j.conbuildmat.2014.12.010.
[86] Zhang LV, Suleiman AR, Mehdizadeh Allaf M, et al. Crack self-healing in alkali-activated slag composites incorporating immobilized bacteria. Constr Build Mater. 2022;326:126842. doi:10.1016/j.conbuildmat.2022.126842.
[87] Xu H, Lian J, Gao M, et al. Self-healing concrete using rubber particles to to immobilize bacterial spores. Materials (Basel). 2019;12(14):2313. doi:10.3390/ma12142313.
[88] Kanwal M, Khushnood RA, Khaliq W, et al. Synthesis of pyrolytic carbonized bagasse to immobilize *Bacillus subtilis*; application in healing microcracks and fracture properties of concrete. Cem Concr Compos. 2022;126:104334. doi:10.1016/j.cemconcomp.2021.104334.
[89] Wang X, Xu J, Wang Z, et al. Use of recycled concrete aggregates as carriers for self-healing of concrete cracks by bacteria with high urease activity. Constr Build Mater. 2022;337:127581. doi:10.1016/j.conbuildmat.2022.127581.
[90] Feng C, Zong X, Cui B, et al. Application of carrier materials in self-healing cement-based materials based on microbial-induced mineralization. Crystals. 2022;12(6):797. doi:10.3390/cryst12060797.
[91] Borg RP, Cuenca E, Gastaldo Brac EM, et al. Crack sealing capacity in chloride-rich environments of mortars containing different cement substitutes and crystalline admixtures. J Sustain Cem Based Mater. 2018;7(3):141–159. https://www.tandfonline.com/doi/abs/10.1080/21650373.2017.1411297. doi:10.1080/21650373207320171411297.
[92] Amiri A, Azima M, Bundur ZB. Crack remediation in mortar via biomineralization: effects of chemical admixtures on biogenic calcium carbonate. Constr Build Mater. 2018;190:317–325. doi:10.1016/j.conbuildmat.2018.09.083.

[93] Amiri A, Basaran Z. Application of biogenic calcium carbonate precipitation in developing self-healing cementbased mortar. 12th International Congress on Advances in Civil Engineering, 2016: 21–23.
[94] Soda PRK, Chakravarthi EK, Mogal A, et al. Statistical and experimental investigation on self-healing of microcracks in cement mortar by encapsulation of calcite precipitating bacteria into expanded perlite. Constr Build Mater. 2022;342:127985. doi:10.1016/j.conbuildmat.2022.127985.
[95] Ben Chekroun K, Rodri C, Teresa Gonza M, et al. Precipitation and growth morphology of calcium carbonate induced by Myxococcus Xanthus: implications for recognition of bacterial carbonates. J Sediment Res. 2004;74:1527.
[96] Xiao J, Wang Z, Tang Y, et al. Biomimetic mineralization of $CaCO_3$ on a phospholipid monolayer: from an amorphous calcium carbonate precursor to calcite via vaterite. Langmuir. 2010;26(7):4977–4983. doi:10.1021/la903641k.
[97] Sidhu N, Goyal S, Reddy MS. Biomineralization of cyanobacteria *Synechocystis pevalekii* improves the durability properties of cement mortar. AMB Expr. 2022;12(1):59. doi:10.1186/s13568-022-01403-z.
[98] Wen K, Li Y, Amini F, et al. Impact of bacteria and urease concentration on precipitation kinetics and crystal morphology of calcium carbonate. Acta Geotech. 2020;15(1):17–27. doi:10.1007/s11440-019-00899-3.
[99] Akhtar JN, Khan RA, Khan RA, et al. Influence of natural zeolite and mineral additive on bacterial self-healing concrete: a review. Civ Eng J. 2022;8(5):1069–1085. doi:10.28991/CEJ-2022-08-05-015.
[100] Basaran Bundur Z, Kirisits MJ, Ferron RD. Biomineralized cement-based materials: impact of inoculating vegetative bacterial cells on hydration and strength. Cem Concr Res 2015; 67: 237–245. doi:10.1016/j.cemconres.2014.10.002.
[101] Rajczakowska M, Habermehl-Cwirzen K, Hedlund H, et al. Autogenous self-healing: a better solution for concrete. J. Mater. Civ. Eng. 2019;31(9):1–19. doi:10.1061/(ASCE)MT.1943-5533.0002764.
[102] Amer Algaifi H, Abu Bakar S, Rahman Mohd. Sam A, et al. Insight into the role of microbial calcium carbonate and the factors involved in self-healing concrete. Constr Build Mater. 2020;254:119258. doi:10.1016/j.conbuildmat.2020.119258.
[103] Seifan M, Samani AK, Berenjian A. Bioconcrete: next generation of self-healing concrete. Appl Microbiol Biotechnol. 2016;100(6):2591–2602. doi:10.1007/s00253-016-7316-z.
[104] Althoey F, Zaid O, Arbili MM, et al. Physical, strength, durability and microstructural analysis of self-healing concrete: a systematic review. Case Stud Constr Mater. 2023;18:e01730. doi:10.1016/j.cscm.2022.e01730.
[105] Islam S, Bhat G. Progress and challenges in self-healing composite materials. Mater Adv. 2021;2(6):1896–1926. doi:10.1039/D0MA00873G.
[106] Zhang LV, Nehdi ML, Suleiman AR, et al. Crack self-healing in bio-green concrete. Compos Part B Eng. 2021;227:109397. doi:10.1016/j.compositesb.2021.109397.
[107] Aytekin B, Mardani A, Yazıcı Ş. State-of-art review of bacteria-based self-healing concrete: biomineralization process, crack healing, and mechanical properties. Constr Build Mater. 2023;378:131198.
[108] Jiang L, Jia G, Jiang C, et al. Sugar-coated expanded perlite as a bacterial carrier for crack-healing concrete applications. Constr Build Mater. 2020;232:117222. doi:10.1016/j.conbuildmat.2019.117222.

Structures 55 (2023) 1144–1158

Contents lists available at ScienceDirect

Structures

journal homepage: www.elsevier.com/locate/structures

Healing of cracks in concrete by using bacterial spores immobilized in metakaolin

Navneet Sidhu [a], Shweta Goyal [b], M. Sudhakara Reddy [a,*]

[a] Department of Biotechnology, Thapar Institute of Engineering & Technology, Patiala 147004, Punjab, India
[b] Department of Civil Engineering, Thapar Institute of Engineering & Technology, Patiala 147004, Punjab, India

ARTICLE INFO

Keywords:
Metakaolin
Bacterial spores
Crack width
Flexural strength
Water tightness
Compressive strength

ABSTRACT

Microbial-induced self-healing of micro cracks is an economical and effective biotechnological approach in concrete structures. The current study explores metakaolin as a suitable carrier material for immobilizing bacterial spores using adsorption technique. The developed biomaterial was stored at 4 °C and 25 °C for 180 days and showed sustainable shelf life of the bacterial spores. The biomaterial stored at 4 °C added as supplementary material during the casting of concrete significantly improved the compressive and flexural strength of concrete at 7 and 28 days. The sorptivity coefficient was 0.006 and 0.002 at 7 and 28 days, respectively, which was comparatively lower than the control. Further, the self-healing capabilities of biomaterial were investigated for approximately 0.5 mm crack in 400 × 100 × 100 mm prismatic specimens. During the crack healing period, the ultrasonic pulse velocity (UPV) was observed to improve by 21.7 % compared to the cracked specimens. The crack was completely healed with 98.2 % healing efficiency. During the healing of crack, the water tightness of the repaired surface was 92.8% efficient verifying reduction in water flow upon complete healing. At the end of testing, the precipitated mineral was assessed by field emission scanning electron microscopy and X-ray diffraction. The developed metakaolin based biomaterial can be used as self-healing supplementary cementitious material.

1. Introduction

Owing to rapid urbanization, the construction industry has grown its investment in constructing new buildings, long-term maintenance, and repairing existing concrete structures [1]. Damage from cracking makes concrete structures less durable and unusable in the long term [2,3]. Hence, it is imperative to repair the damage to restore the safety of structures and extend their service life [4]. Traditionally, cracks are repaired using chemical-based sealants (synthetic epoxides, polyurethane, epoxy resins, acrylics, and waxes), requiring continuous maintenance and inspection, which is expensive and laborious [5]. Such treatments negatively affect the environment and reduce the aesthetic value of concrete structures. In addition, cracks in extensive infrastructure such as roads, buildings, and tunnels in continuous use may not be able to repair the cracks in the afflicted areas owing to the functional area's challenges [6]. The visual detection of major and minor cracks is necessary for engineers to repair. There are minor cracks beyond detection inside the structure, which are crucial to restoring as if left unrepaired, which will affect the structure's durability [7].

Self-healing is an effective crack-repair approach that incorporates bacteria when preparing fresh concrete. Concrete possesses harsh conditions, and alkaliphilic/alkali-tolerant spore-forming strains should be utilized because of the alkaline environment inside the concrete and the need for long-lasting healing agents [8,9]. Spores are more resistant to heat, radiation, and other chemicals [10,11]. This makes spores a better bioagent for microbial-induced calcium carbonate precipitation (MICCP) than freshly prepared cultures. Spores become active when cracks appear, owing to the ingress of moisture and oxygen in the cracked area [12,13]. The bacterial endospores have ability to withstand the highly alkaline pH of the concrete mix during the casting and drying of concrete. Spores can endure high mechanical compressive stresses during concrete curing [14]. Bacterial spores are made up of dehydrated spore cores, peptidoglycan cortex, Ca^{2+} ions, and dipicolinic acid (DPA) [15]. The spores are able to induce growth as soon as they receive favourable conditions of growth (desired temperature, moisture, and nutrients that can stimulate germination and overcome the dormancy period of spores). The germination rate of bacterial spores can range from a few minutes to several hours depending on the specific conditions

* Corresponding author.at: Department of Biotechnology, Thapar Institute of Engineering & Technology, Patiala 147 004, Punjab, India.
E-mail address: msreddy@thapar.edu (M. Sudhakara Reddy).

https://doi.org/10.1016/j.istruc.2023.06.097
Received 25 January 2023; Received in revised form 16 June 2023; Accepted 20 June 2023
Available online 27 June 2023
2352-0124/© 2023 Institution of Structural Engineers. Published by Elsevier Ltd. All rights reserved.

provided. Nutrients (amino acids, sugar) binds to the inner membrane and rehydrates the spore core. Ca^{2+} - DPA (dipicolinic acid) is released from the spore core stimulating germination [16,17]. When spores germinate and vegetative cells start actively growing, they can produce extracellular enzymes, such as urease and carbonic anhydrase due to the metabolic activity of bacteria [18]. Different strategies, such as encapsulation and immobilization, protect spores during concrete mixing as they become dense because of cement hydration reactions [19–21]. Previously, researchers have reported various carrier materials such as hydrogels [8,22,23], polyurea microcapsules [21], alginate [24], biochar [25], nanoplates [26], low-weight aggregates [27,28], and silica gel [29–31] as potential carrier materials for MICCP. However, these carrier materials are considered to have poor compatibility with concrete. Carrier materials without bacterial inoculum can have a negative or zero impact on the mechanical properties of concrete because of their low density and hardness [32]. The high-water absorption capacity of the carrier material can affect the hydration of the cement. Gel-based carrier materials involve a difficult preparation process with increased production cost [33,34]. In addition, the shelf-life of bacteria-based carrier materials for longer durations is not well-defined. The freshly prepared bacterial culture was used for developing carrier-based self-healing materials, which limits the application of MICCP in the field owing to the availability of resources. Therefore, it is crucial to explore concrete-compatible carrier materials with high mineralization capabilities that can easily bond with bacteria and improve the self-healing properties of concrete.

In recent studies, metakaolin (MK) has shown remarkable results as supplementary cementitious materials in construction industries [35–37]. MK is an industrial by product containing siliceous aluminous resource exhibiting high pozzolanic activity [38]. The micronized size distribution of MK in the concrete mixture has improved the cement matrix's pore structure [39]. It can react with the free lime (calcium hydroxide) produced by cement hydration to form additional calcium silicate hydrates [40]. Metakaolin decreases fluidity through the material, thus enhancing durability and reducing chloride ion diffusion [41]. Metakaolin is white coloured, soft and chemically inert material [42]. The immobilization of spores using a porous adsorption material will ensure the viability of the biomaterial for a longer duration [43]. Other researchers such as Zhang et al. employed expanded perlite and clay as self-healing carrier materials in concrete and reported the maximum healing of 0.51 mm and 0.37 mm crack width, respectively [34]. Zheng et al. reported 0.35 mm crack healing using low-alkali sulphoaluminate cement as a carrier to protect spores in a mortar [44]. Due to the different properties of various carriers, the results may vary in different studies. Self-healing cement-based materials require intensive research into developing more practical carrier materials.

In the present investigation, the spores-infused metakaolin (MK) material was prepared under aseptic conditions and stored under refrigerated (4 °C) and ambient (25 °C) requirements for 180 days. The material's viability to induce spore activation was studied for a storage period of 180 days. After 180 days, the 2% spore-infused MK biomaterial stored at 4 °C was used to cast 500 × 100 × 100 mm prisms, 150 mm cubes, and 100 × 200 mm cylindrical specimens. The flexural strength, compressive strength, and sorptivity tests were performed after 7 and 28 days of curing. Crack remediation was evaluated for 400 × 100 × 100 mm prism specimens. The concrete specimens were analysed for calcium carbonate precipitation using field-emission surface electron microscopy (FESEM), energy dispersive spectroscopy (EDS), and X-ray diffraction (XRD).

2. Materials and methods

2.1. Bacterial culture

The urease-producing bacterial strain *Bacillus paramycoides* MSR1 used in this study was isolated from marble dust collected from a marble dumping yard in Kishangarh, Rajasthan, India. The bacterial strain was identified as *B. paramycoides* based on 16S rRNA sequencing EzBioCloud database. The bacteria was grown in nutrient broth (Hi Media, India) at 37 °C with shaking at 120 rpm.

Table 1
Chemical composition of the Metakaolin and the ordinary portland cement (43 grade).

Composition (%)	Metakaolin	Cement
SiO_2	52.2	21.3
CaO	0.21	63.2
Fe_2O_3	1.53	2.5
Al_2O_3	44.5	7.3
MgO	0.32	1.52
K_2O	0.45	0.54
Na_2O	0.16	0.27
SO_3	0.05	2.42
TiO_2	1.48	0.37

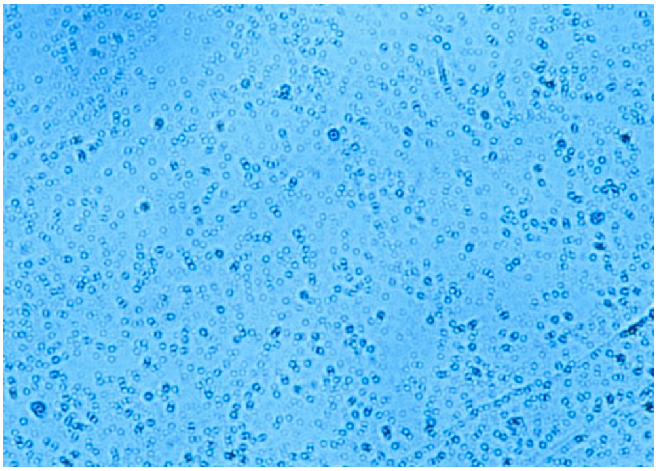


Fig. 1. *Bacillus paramycoides* spores showing intact outer coating.

2.2. Materials used

Commercially available ordinary Portland cement (OPC) – 43 grade confirming the Indian Standard [45] was used in this study. Locally available well-graded river sand confirming Zone II as per IS383 – 1970 with a specific gravity of 2.66 was used as fine aggregates [46]. Coarse aggregates of 10 mm and 20 mm in size with specific gravity of 2.72 and 2.63, respectively, were used in the current study [46]. The Metakaolin (MK) used was obtained from a private vendor. The chemical properties of MK and OPC – 43 used in the experiment are listed in Table 1.

2.3. Spore preparation and development of metakaolin based biomaterial

To prepare the spores of the bacterial strain *B. paramycoides*, modified nutrient broth media (Nutrient broth 3 g/L, $NaHCO_3$ 2.12 g/L, and urea, 10 g/L) was used as reported by Pungrasmi et al. [18]. After inoculation, the culture flask was incubated at 30 °C in an incubator shaker at 100 rpm agitation for seven days. After seven days, the culture was exposed to to heat shock at 80 °C for 10 min to stimulate the spore formation, followed by cold shock for 10 min by placing the culture flask in crushed ice. The spores were collected after centrifuging the medium at 5000 rpm for 10 min. The pellet was washed with 0.85% saline to remove additional nutrient medium and suspended in distilled water. The spores' intactness was tested by subjecting the cells to endospore staining using Malachite green staining. The spores were visualized using the compound microscope. As shown in Fig. 1 the spores show circular shaped morphology and the dark blue-purple staining of the

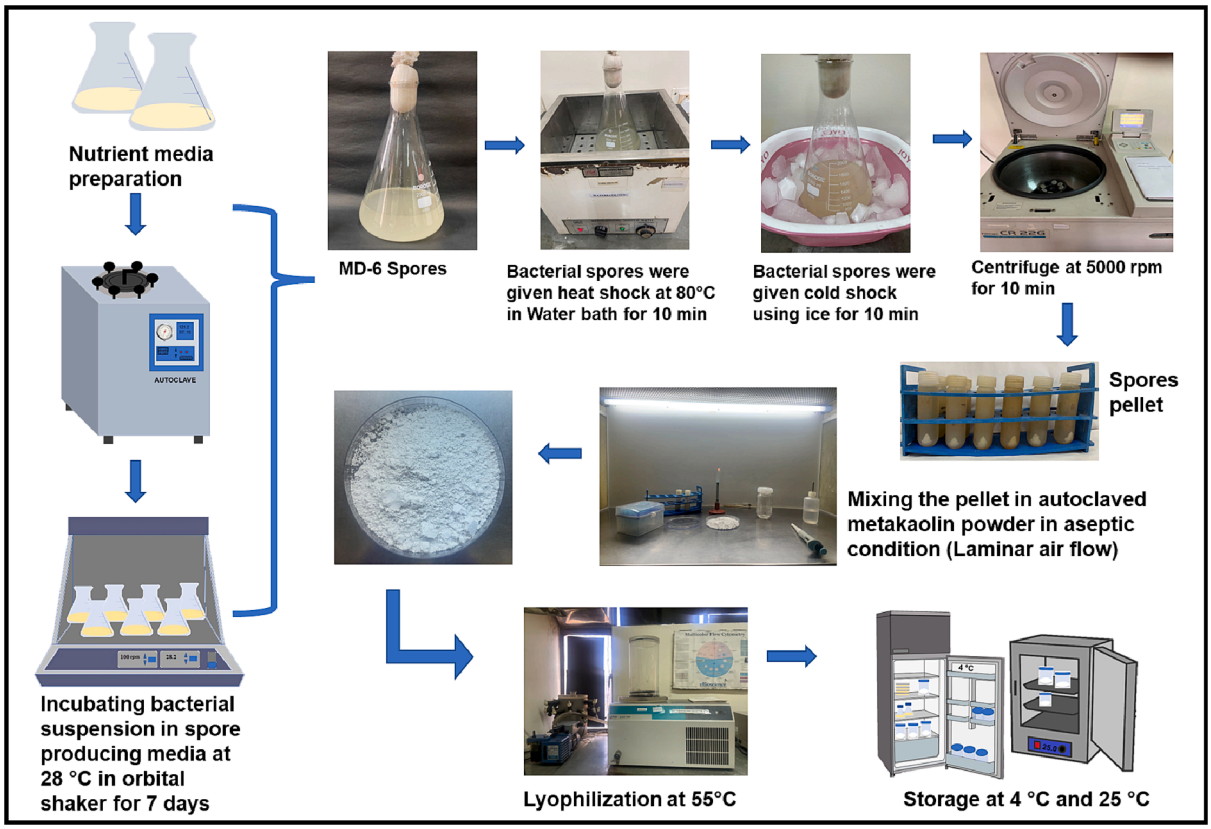


Fig. 2. Schematic illustration of *Bacillus paramycoides* spores' development and storage after the immobilization in metakaolin (MK) material by lyophilization technique.

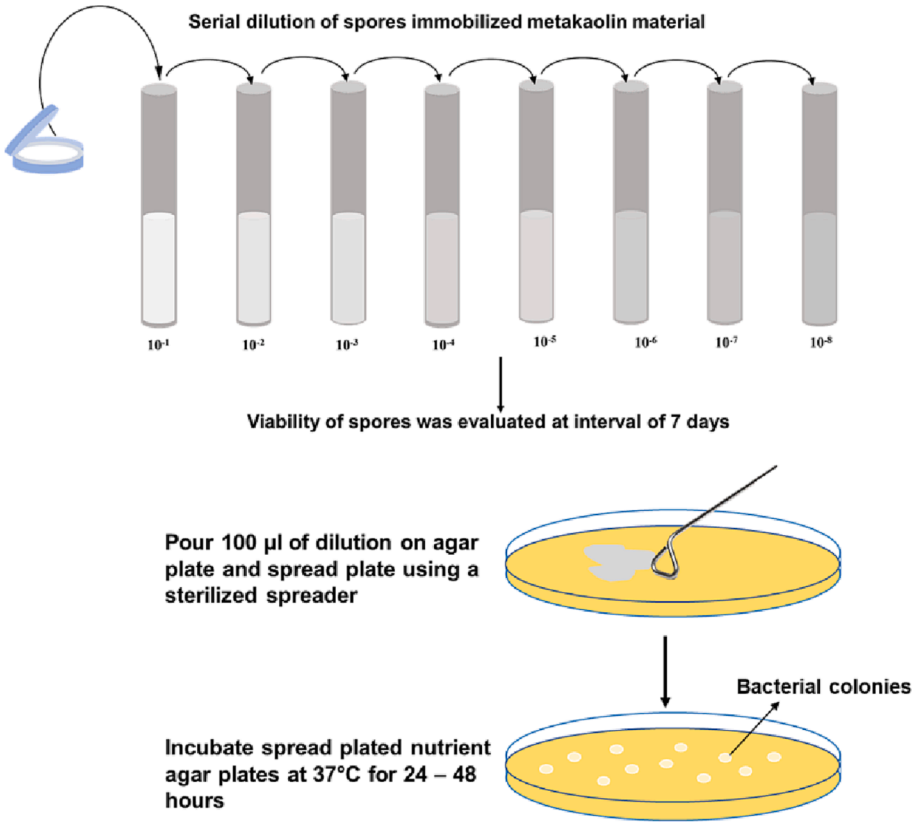


Fig. 3. Schematic representation of the serial dilution technique and nutrient agar plates showing spore viability after 24 h of incubation at 37 °C.

outer coating expected for integral cell walls. The spore concentration was evaluated using the colony-forming unit (CFU) count.

To immobilize the bacterial spores in MK, it is important to mix spore suspension gently and maintain a longer contact time between spores and metakaolin during mixing time. A concentration of 5.2×10^{-5} spores was uniformly mixed in the MK powder under aseptic conditions. MK powder was used as a carrier material to immobilize the spores. A moisture content of 20% was maintained in the MK material to uniformly mix the spores in the biomaterial [47]. The moisture content should be sufficient for the spores to adhere to the metakaolin particles. To immobilize the spores with MK, the mixture was allowed to stay for a few hours. This period allows the spores to interact with the metakaolin particles and establish an immobilization matrix by forming a strong interlinking bond with the metakaolin particles. After development, the mixture can be dried under controlled conditions, such as a lyophilizer to remove excess moisture. The drying ensures the stability and viability of spores for a longer duration. The spore-infused biomaterial was freeze-dried at −20 °C, followed by lyophilization at −55 °C to remove moisture and immobilize the spores in metakaolin powder. A schematic representation of bacterial spore formation and immobilization in MK for the development of biomaterials is shown in Fig. 2.

2.4. Storage and viability test

The spore-immobilized MK material, labelled as biomaterial, was stored in sterile Petri dishes at 25 °C and 4 °C. Viability tests were conducted at regular intervals of seven days during storage. One gram of the sample was weighed from each stored petri plate and suspended in 9 ml of a 0.85% saline test tube. Furthermore, the dilutions were made up to 10^{-8} by transferring 1 ml of the dilution from each test tube, as shown in Fig. 3. The efficiency of immobilized spores in the MK carrier material was determined using the CFU count. One hundred microliters of the aliquot were spread on nutrient agar plates using a sterilized spreader. Nutrient agar plates were incubated at 37 °C for 24 – 48 h. The colony forming units per gram were expressed by determining the log value of the colonies that appeared on the nutrient agar plates.

2.5. Urease activity and calcium carbonate precipitation

Urease activity is defined as the activity of the enzyme to convert urea to ammonia and form hydroxide ions, resulting in an increase in the pH of the medium and creating an alkaline environment surrounding the bacterial cell. As a result of urease activity, the calcium ions present around the cell wall of the bacteria combine with carbonate ions, resulting in the formation of calcium carbonate around the bacterial cell. To evaluate the urease activity of the stored biomaterial, 1% of the biomaterial inoculum was incubated in a nutrient broth supplemented with 2% urea. The experiment was performed in triplicate, and the flasks were incubated at 37 °C for 120 h. Urease activity was examined every 24 h using the phenol-hypochlorite assay, as described by Natarajan [48].

In the second set of experiments, the calcium carbonate precipitated by the developed biomaterial was measured by weighing the amount of $CaCO_3$ precipitated in the nutrient broth supplemented with 1% biomaterial, 2% urea, and 25 mM calcium chloride. $CaCO_3$ was collected on Whatman filter paper after 24 h interval. The precipitates from each flask were room-dried for 6 h and then lyophilized to weigh the amount of powdered calcium carbonate collected on a Whatman filter paper. The stored biomaterial that performed the best in the viability test, urease assay, and calcium carbonate precipitation was used as a potential self-healing biomaterial for concrete testing.

2.6. Preparation of concrete specimens

To investigate the effect of the biomaterial on the concrete properties, the specimens were cast using the biomaterial stored at 4 °C (selected on the basis of the viability and urease activity tests). Prismatic specimens of 500 × 100 × 100 mm, 150 mm cubes, and 100 (dia) × 200 (height) mm cylindrical concrete specimens were cast using cement, sand, and coarse aggregate in the proportion of 1:1.82:3.24 (by weight) and 0.47 water-to-cement ratio (w/c), as given in Table 2. The 2% biomaterial stored at 4 °C was added as supplementary material during the mixing of the concrete constituents. Similarly, for crack remediation, the prismatic specimens were cast using the same mix proportion, as mentioned above. Reinforced concrete (RC) specimens with dimensions of 400 mm × 100 mm × 100 mm were prepared by embedding a 12 mm rebar at the centre and curing for 28 days. To generate cracks, the prepared RC specimens were subjected to four-point bending failure as

Table 2
Mix proportion of the concrete specimens.

Mix proportion (kg/m^3) Specimens	Cement	Sand	Metakaolin biomaterial	Coarse aggregate		Water/ nutrient growth medium
				10 mm	20 mm	
Control	396	722	–	770	513	186
Biomaterial	396	722	7.94**	770	513	186*

*Nutrient growth medium is composed of nutrient broth (1.3 % w/v), Urea (2 % w/v) and 25 mM Calcium chloride. **metakaolin biomaterial stored at 4 °C & 180 days storage age.

Table 3
Summary of the specimen used and tests carried out.

Specimen	Testing age (days)	Experiment test	Dimensions
Prismatic	7, 28	Flexural	500 × 100 × 100
Cube	7, 28	Compressive	150 × 150 × 150
Cylinder	7, 28	Sorptivity	100 (dia) × 50 (ht)
Reinforced prismatic	Till complete healing	Visual crack healing	400 × 100 × 100

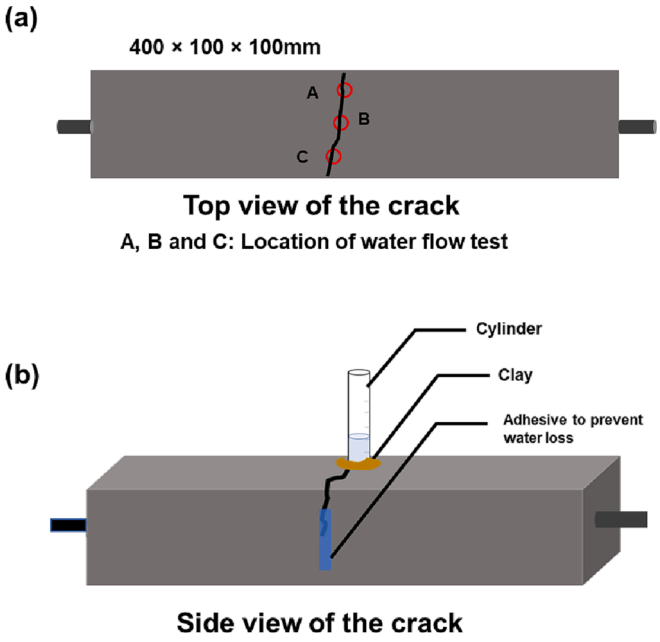


Fig. 4. (a) top view of the specimen marked with three different locations of the water flow test on the specimens (b) side view of the setup of the water flow test with measuring cylinder adhesively attached to the specimen.

per BIS:516 to attain a crack width of approximately 0.5 mm [49]. Trials were conducted to achieve a crack width of 0.5 mm.

2.7. Concrete testing

The 500 × 100 × 100 mm prismatic specimens and 150 mm cubes were tested for flexure and compressive strength at 7 and 28 days of curing, as per the IS 516 – 1959 standard [49]. Cylindrical specimens of 100 × 50 mm were tested for the water absorption test according to the ASTM standard [50] at 7 and 28 days of curing. All experiments were performed in triplicates. The details of the concrete specimens are presented in Table 3.

2.8. Crack remediation and monitoring

The cracked 400 × 100 × 100 mm prismatic specimen consisting of the biomaterial was subjected to a self-healing treatment at room temperature. The cracked region was injected and sprayed with nutrient growth medium (NBUC) supplemented with 2 % urea and 25 mM calcium chloride ($CaCl_2$) to activate spores immobilized in the biomaterial (Fig. 4b). $CaCl_2$ used in the present investigation was 25 mM (3.67 g/L) which is within the permissible limits and do not affect the rebar [51]. NBUC media was sprayed four times a day at two hours intervals till complete healing of the cracked region. The ultrasonic pulse velocity (UPV) was measured as per ASTM C597 − 02 standard at 0, 14, 28, and 40 days of crack repair to determine the efficiency of MICCP treatment for crack repair [52]. Water tightness was examined at 0, 14, 28, and 40 days of crack remediation [53]. The three different regions were marked as A, B, and C on the crack region to test the amount of water flowing through the crack (Fig. 4c). The flow rate was estimated based on the amount of water flowing through the crack within 20 s. A 50 ml measuring cylinder was adhesively attached with the help of clay to the surface to avoid water leakage. The experiment was conducted until the cracks were completely closed. Crack-sealing efficiency was evaluated based on the amount of water flowing through the defined crack region. The crack-sealing efficiency was evaluated using Eq. (1).

$$Sealing\ efficiency(\%) = \frac{WF_i - WF_i}{WF_i} \times 100 \quad (1)$$

Where, WF_i represents initial water flow and WF_t represents water flow at time 't'.

2.9. Visual monitoring of crack closure

During the crack remediation process, the reduction in crack width was periodically monitored using a DinoLite microscope. To better understand crack closure by MICCP, the crack width along the defined length was taken during the healing process. The average of the multiple readings for a particular duration was recorded. Crack-healing efficiency was evaluated as per the equation (Eq. (2) [54].

$$Crack\ healing\ efficiency(\%) = \frac{CW_i - CW_i}{CW_i} \times 100 \quad (2)$$

CW_i is the initial crack width, and CW_t is the crack width at different time intervals.

2.10. Microstructural analysis

To analyse the calcium carbonate precipitation in the bacterial-cured specimen after 28 days of curing, the samples were analysed for FESEM (field emission scanning electron microscopy (FESEM). Energy dispersive spectroscopy (EDS) was performed to confirm the elemental composition of the precipitate in the concrete. The samples were gold-coated, polished, and coated with carbon to disperse the extra charge. X-ray diffraction (XRD) scanning was performed on the powdered concrete samples from 20° to 60° at 2θ angles with a Cu anode (40 kV and 30 mA) using a Bruker D8 X-ray diffractometer.

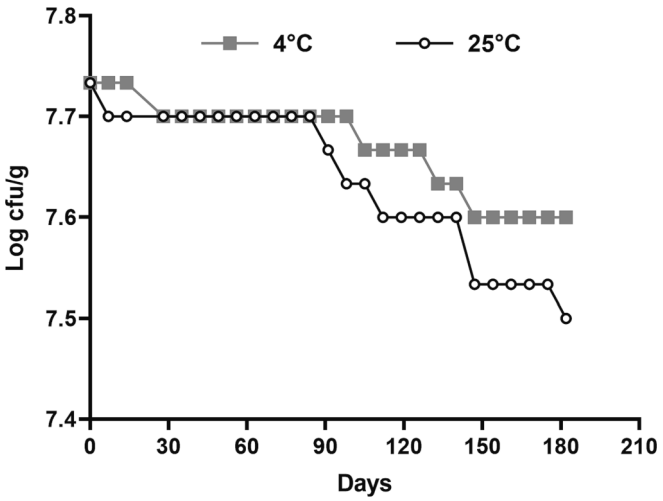


Fig. 5. Bacterial cell count (log cfu/g) of developed biomaterial stored at 4 °C and 25 °C in the petri dish.

2.11. Statistical analysis

All experiments were performed in triplicate. The data were analysed using analysis of variance, and significant differences among the means were compared using Tukey's test ($p < 0.05$). All analyses were performed using GraphPad Prism (version 9.3.0) software.

3. Results and discussion

3.1. Viability of biomaterial during storage

At an interval of 7 days, the viability of the developed biomaterial (spores immobilized in metakaolin materials) was assessed for up to 180 days of storage. The main goal was to use the bacterial cell count method to determine the survivability of bacterial spores immobilized in the produced metakaolin material, and the results are shown in terms of log colony forming units per gram (CFU/g). The developed biomaterial exhibited a constant cell count of 7.7 log cfu/g for the initial 84 days of storage at 4 °C and 25 °C, proving stability of immobilized spores in metakaolin material. Cell viability was reduced to 7.6 log cfu/g at 25 °C after 91 days of storage, as shown in Fig. 5. Comparing the two storage temperatures, the biomaterial stored at 4 °C was more efficient during the storage period. At 180 days, the biomaterial stored at 4 °C and 25 °C showed 7.6 log cfu/g, and 7.5 log cfu/g bacterial cell count, respectively. In general, both storage temperatures were efficient in maintaining the viability of spores in metakaolin (Fig. 6). The spores can remain dormant for many years and become active once they receive moisture and oxygen [20]. The immobilization technique helps the bacteria to bond with the carrier material, protecting it within the concrete environment without any deterioration in its viability. Similar results were observed by Anand et al. [47,55] and Son et al. [56]. The research carried out by Jonkers reported that expanded clay particles-maintained spores' viability for six months [57]. Researchers have also reported the incorporation of several other carrier materials into the concrete matrix, including recycled concrete aggregates [58], hydrogel [23,59], polyurethane [31,60], and microcapsules [8].

3.2. Urease activity and calcium carbonate precipitation

The urease activity and calcium carbonate precipitation were evaluated for the spores immobilized in metakaolin biomaterial stored at

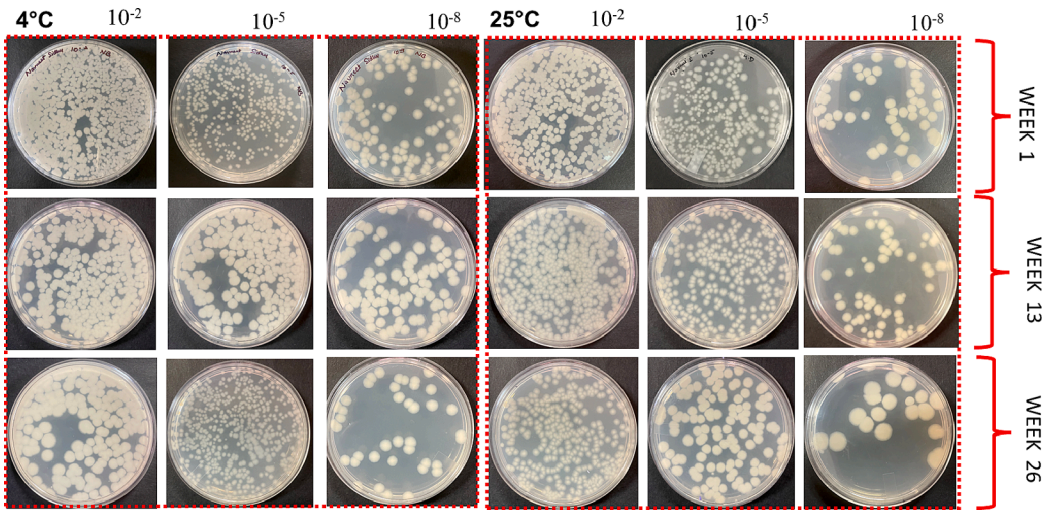


Fig. 6. Pictorial representation of bacterial cells on the nutrient agar Petri plates of developed biomaterial stored at 4 °C and 25 °C for 180 days (26 weeks).

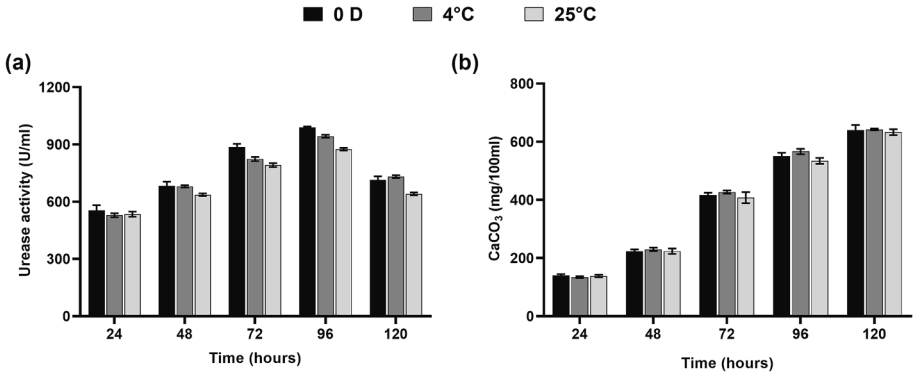


Fig. 7. (a) Urease activity and (b) calcium carbonate precipitation of developed biomaterial before storage at 0 day and after storage at 4 °C and 25 °C for 180 days.

4 °C and 25 °C after 180 days. The results were compared with the urease activity of biomaterial observed before storage at 4 °C and 25 °C. It was observed that the biomaterial when inoculated in nutrient broth supplemented with 2 % urea, the spores were able to germinate and increase the concentration of bacteria in the nutrient broth due to the availability of the nutrients and oxygen. During the 120 h incubation the urease activity was measured at each 24 h intervals. It was observed that urease activity showed increasing trend till the 96 h (Fig. 7). The urease

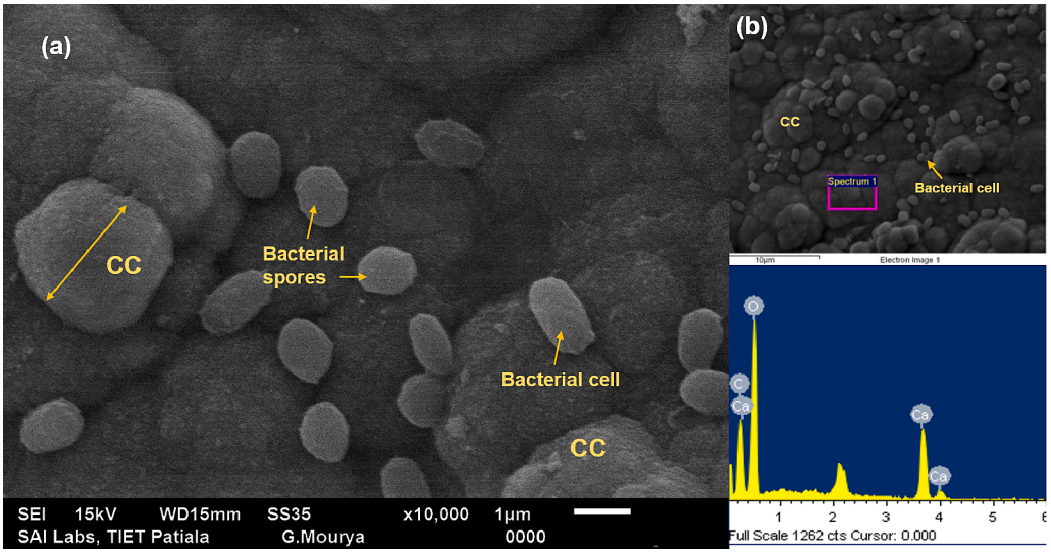


Fig. 8. (a) SEM analysis of filtered calcium carbonate showing rhombohedral calcium carbonate crystal (CC) along with the presence of rod-shaped bacterial cells (b) EDS showing elemental deposition of the calcium carbonate.

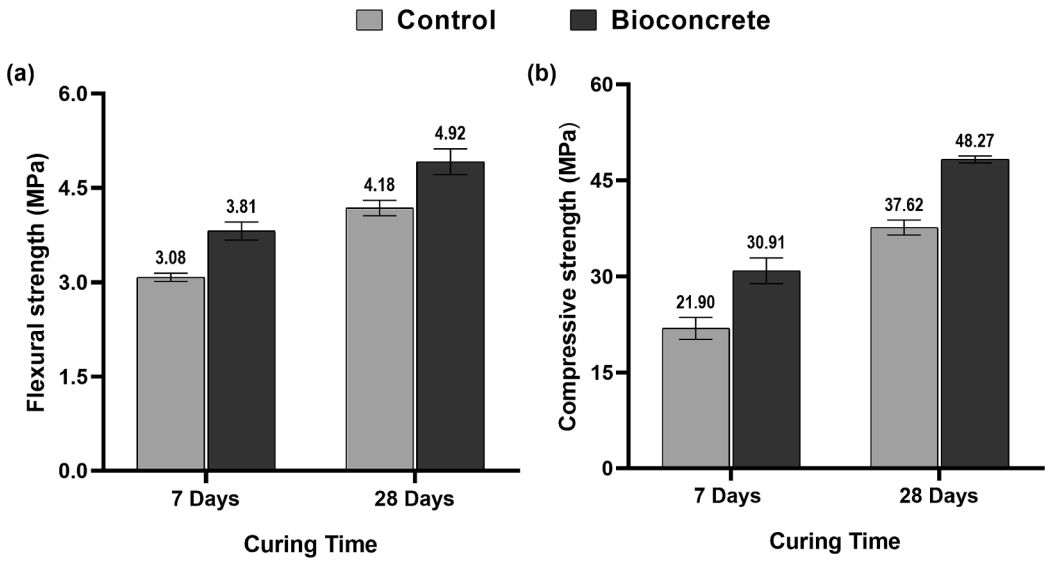


Fig. 9. Flexural and compressive strength of bioconcrete and control specimens at the age of 7 and 28 days.

activity of spores before storage was 989.4 U/ml at 96 h of incubation. The biomaterial stored at 4 °C and 25 °C were both equally efficient to exhibit urease activity after the storage. However, it was observed that urease activity by biomaterial stored at 4 °C showed comparatively higher urease activity than the product stored at 25 °C. At 4 °C, the maximum enzyme activity (942.93 U/ml) was recorded at 96 h incubation, after which a significant drop-in urease activity to 731.03 U/ml was observed at 120 h. Whereas, the biomaterial stored at 25 °C showed 874.8 U/ml urease activity after 96 h of incubation. The capability of the spores to show metabolic activity after 180 days of storage, proved metakaolin is an efficient carrier material for immobilization of the spores.

The catalytic ability of the urease enzyme to decompose urea leads to a yield of carbonate ions, which further react with the calcium surrounding the bacterial cell to form calcium carbonate precipitates in the medium. Fig. 7 shows the amount of calcium carbonate precipitated by the spore-based biomaterial incubated at 37 °C after 180 days of storage. The experiment was carried out in triplicate, and at each 24 h interval, the 100 ml flask was evaluated for the amount of calcium carbonate precipitated. The study was conducted for 120 h, and it was found that the biomaterial stored at 4 °C resulted in 2.5% more $CaCO_3$ precipitation than that at 25 °C, which was non-significant difference based on the different temperature conditions. Calcium carbonate precipitation by biomaterial before storage was 139.6, 223.6, 416.6, 550.8, and 640.4 mg/100 ml at 24, 48, 72, 96, and 120 h, respectively. After storage of 180 days, calcium carbonate precipitation recorded at 4 °C was 134.4, 229.8, 427.2, 566.5, 642.4 mg/100 ml at 24, 48, 72, 96, and 120 h, respectively. Similarly, $CaCO_3$ precipitation at 25 °C was 138.12, 223.7, 407.64, 533.9 and 633.03 mg/100 ml at 24, 48, 72, 96, and 120 h, respectively. The precipitation ability of the biomaterial proved that spores were able to maintain their shelf life during storage to induce MICCP in the nutrient broth solution. The protective shells of the endospores prevent bacterial cells from dying during nutrient deficiency, allowing them to preserve their long shelf lives. Spores form strong resistance to dryness and severe conditions in their surroundings [10,61]. Zamani et al. confirmed the germination of bacterial spores encapsulated in a polyurea polymer and precipitation of calcium carbonate using FESEM [21]. Other researchers have reported MICCP using spores immobilized on different carrier materials [24,62,63].

The calcium carbonate collected on the filter paper was confirmed by scanning electron microscopy (SEM). Fig. 8 shows the occurrence of calcium carbonate crystals (CC) and bacterial cells in the powdered sample collected from the nutrient broth using the filtration method. The calcium carbonate crystals observed were 3–4 μm in size and the bacterial cells were 1 μm in size. The elemental analysis using EDS proved the presence of weight percentage of calcium, carbon, and oxygen 14.89%, 20.11%, 66% in the precipitated powder respectively.

3.3. Strength properties of biocementitious concrete

Fig. 9. shows the flexural and compressive strength results of the concrete specimens after 7 and 28 d of curing in growth media (nutrient broth supplemented with 2% urea and 25 mM calcium chloride) and tap water. After seven days, the flexural and compressive strengths of the bioconcrete increased by 19.14 % and 29.12 %, respectively, after the specimens were cured in the growth broth. The immobilized spores in the specimens germinated upon exposure to nutrient growth media, water, and oxygen. It should be mentioned that during the curing treatment, no additional bacterial culture was inoculated into the curing medium. The inclusion of urea and calcium chloride in cementitious materials without bacteria has a retarding effect on the concrete's hydration process [4,64–66]. However, in this research, the spores immobilized in MK acted as a source for bacterial growth, and the bacteria thrived when provided with nutrients and moisture. Also, using yeast extract (as media) without any bacteria inoculum decelerates the concrete's strength [67]. On the other hand, when bacteria are added together with urea and calcium chloride, it leads to the formation of calcium carbonate and improves the strength of the concrete [68]. At 28 d, the flexural and compressive strengths was improved by 14.9 % and 22.08 %, respectively, compared to those of the control samples. Overall, significant improvements in the strength properties of concrete were observed owing to the application of spores immobilized in metakaolin. This proves that spores survive the harsh conditions of the concrete environment and lead to the densification of the concrete matrix by precipitating calcium carbonate in the pores of the specimens. Previously, researchers reported an improvement in flexural and compressive strength by immobilizing bacterial spores in different carrier materials such as zeolite [43], metakaolin-based geopolymers [69], and calcium alginate beads [70]. Gao et al. reported a 10.28% increase in compressive strength and a 13.79% increase in flexural strength with the addition of hydrogel beads containing immobilized bacterial spores. In addition, metakaolin is considered a good supplementary cementitious material because it has a high silica content and is reported to increase the strength properties of concrete owing to the early stage of hydration [71,72].

The microstructural analysis of the bioconcrete and control specimen

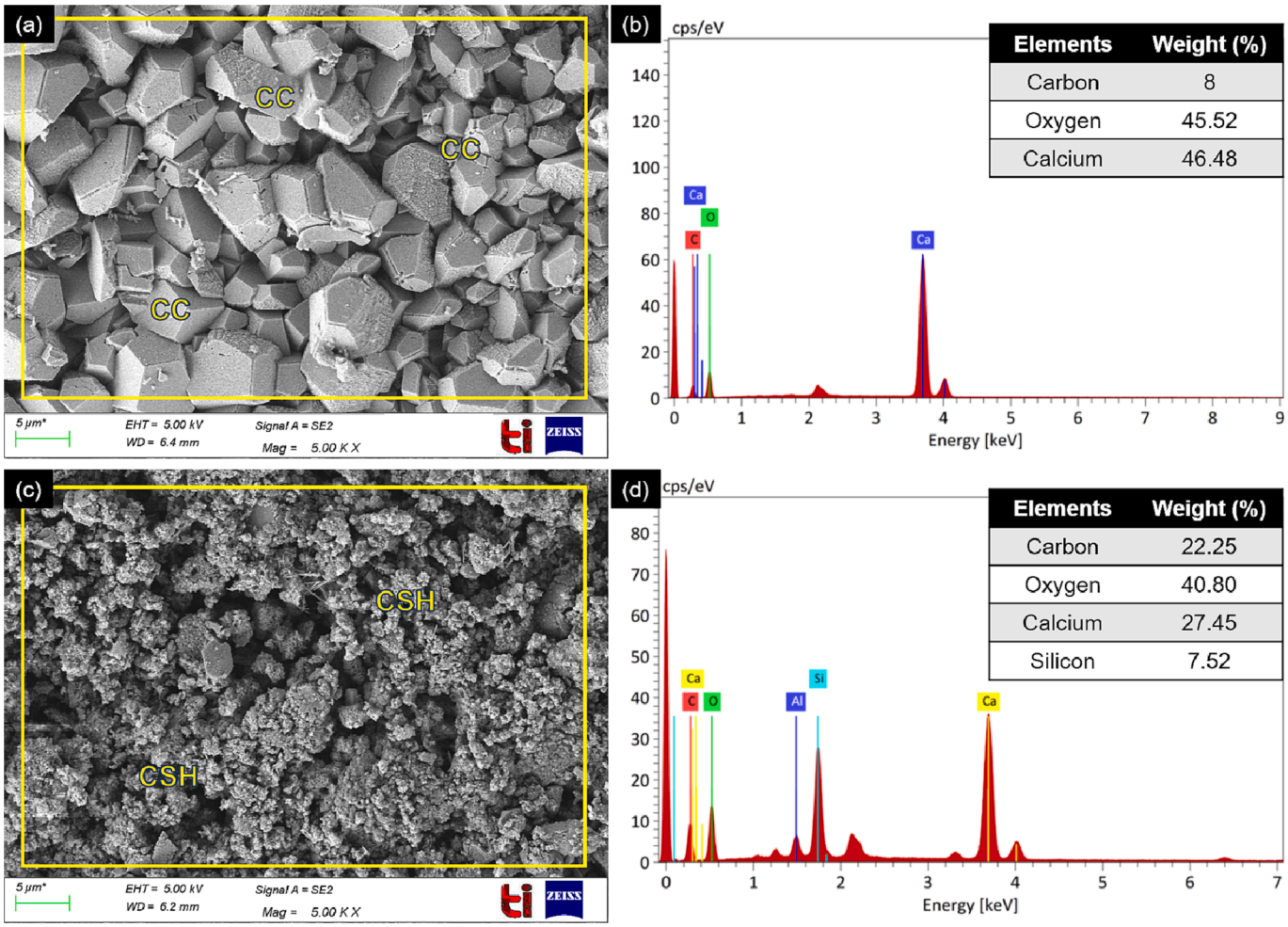


Fig. 10. FESEM-EDS of (a, b) bioconcrete and (c, d) control specimen at 28 days of curing. The '□' marked depicts the spot of EDS analysis.

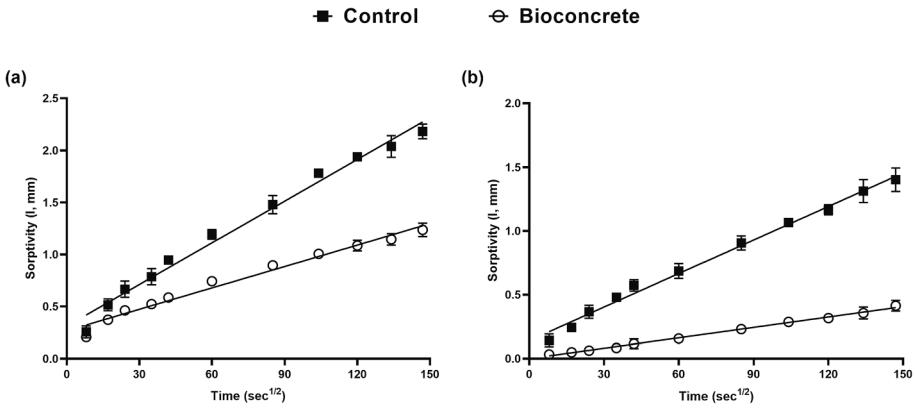


Fig. 11. Water absorption by bioconcrete and control specimen at the age of a) 7 and b) 28 days.

at the age of 28 days of curing clearly shows the formation of calcium carbonate crystals in the pores of the concrete specimens. The crystals were stacked over one another indicating the high concentration of calcite formed (Fig. 10). However, calcite precipitation was not seen in the control sample proving biomaterial stability and biomineralization efficiency in the concrete. The results were confirmed using an EDS. The weight percentage elemental deposition shows 46.48 %, 45.52 %, and 8 % of calcium, oxygen and carbon in the bioconcrete specimen (Fig. 10b). Whereas, in control, 27.45 %, 40.80 %, and 22.25 % formation of calcium, oxygen and carbon in the concrete specimen (Fig. 10d).

3.4. Sorptivity test

Fig. 11 shows the amount of water absorbed per unit cross-sectional area of the concrete specimen at 7 and 28 d. The bioconcrete specimens were more efficient than control specimens. At 5 min immersion, the bioconcrete specimens cured at 7 and 28 days, absorbed 0.20 and 0.05 mm of water whereas control samples absorbed 0.25 and 0.14 mm of water using a capillary action, respectively. The experiment was conducted for 6 h. The cumulative water absorbed at the end of the experiment by the bioconcrete specimens was 1.23 and 0.41 mm at 7

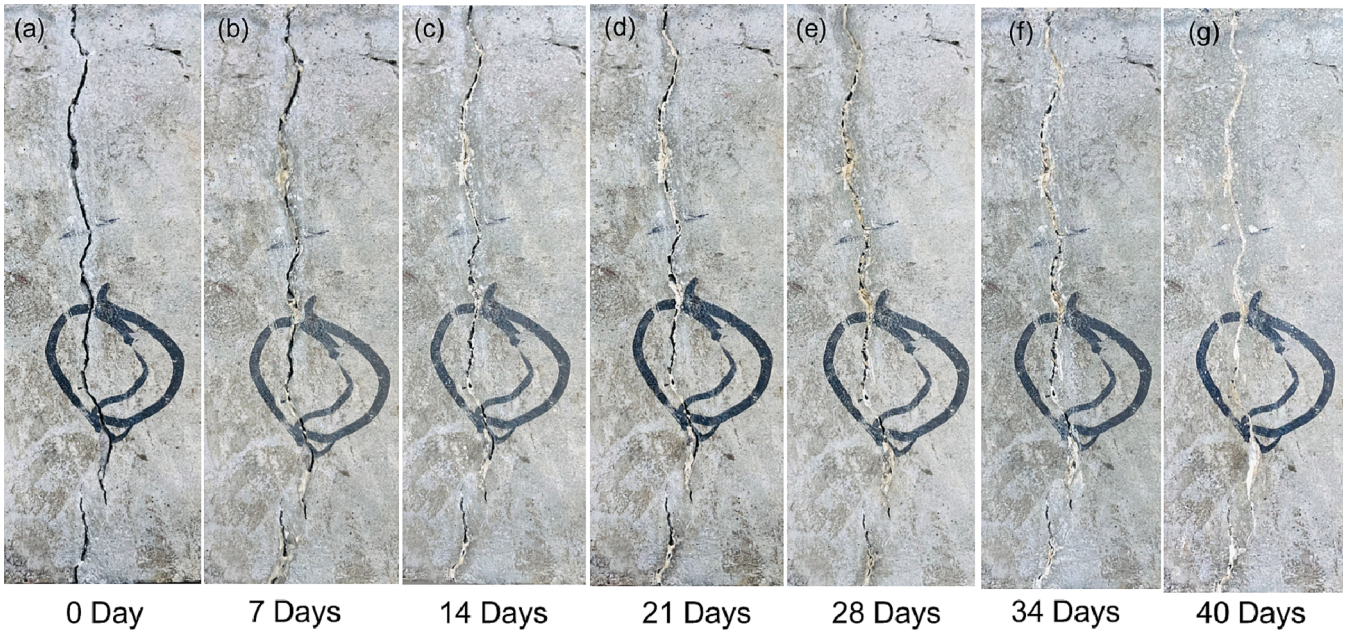


Fig. 12. Self-healing by biomaterials in concrete specimens at 0, 7, 14, 21, 28, 34- and 40-days of crack healing.

and 28 days, respectively. Overall, the bioconcrete specimens exhibited 40.9 % less water than the control specimens after 28 days. This low water absorption rate in bioconcrete proves that bacterial spores immobilized in metakaolin material were able to break the dormant stage and become active, which led to calcification in the pores of the concrete matrix. Bacterial cells form calcium carbonate crystals, which enhance the strength and water permeability of the concrete. The outcome of which can be evaluated on the basis of the sorptivity coefficient '*k*' of biotreated specimen. The sorptivity coefficients of the bioconcrete specimens were 0.006 and 0.002 at 7 and 28 d, respectively. However, the control specimens showed sorptivity coefficients of 0.01, and 0.008 at 7 and 28 days of curing, respectively, which were

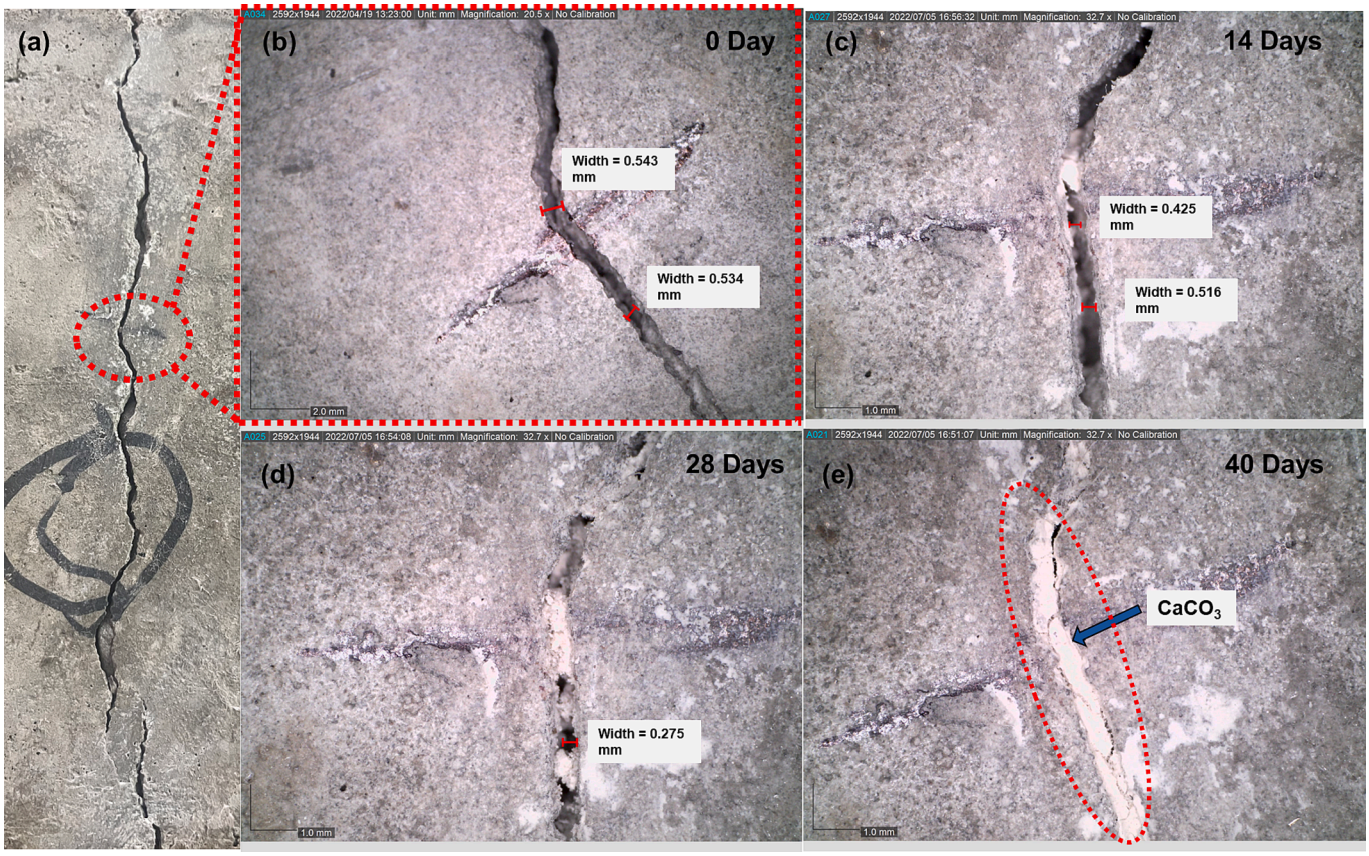


Fig. 13. Self-healing of crack by metakaolin immobilized bacterial (*B. paramycoides*) spores in concrete specimens at 0-, 12-, 24 and 40-days curing time taken using DinoLite microscope.

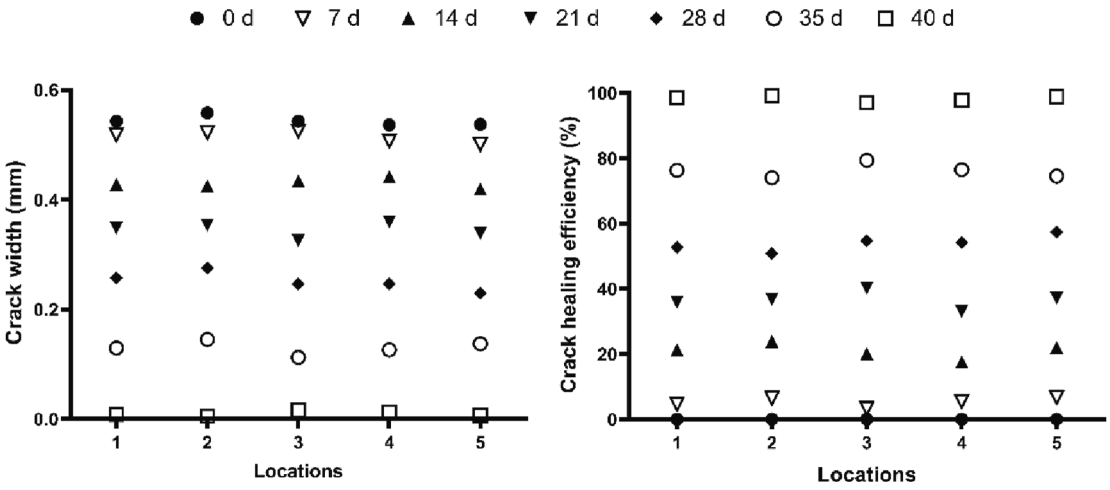


Fig. 14. (a) Evaluation of crack width due to self-healing application by *B. paramycoides* spores immobilized in metakaolin incorporated concrete crack specimens (b) sealing efficiency (%) based on the reduction of crack width at 0, 7, 14, 21, 28, 35, 40 days.

comparatively higher than those of the bioconcrete specimens. The low '*k*' values of the bioconcrete specimens verified that the permeation properties could be significantly improved by bacterial incorporation. According to the literature, the addition of metakaolin to a specimen improves the permeation properties of concrete [73,74]. Similar results were also reported by Pillay et al. on the partial replacement of metakaolin in concrete [72].

4. Crack remediation by *B. Paramycoides* immobilized spores

The concrete specimens were monitored for crack healing at room temperature. Two different groups of specimens, the bioconcrete and control, were closely monitored for crack healing. Crack healing in the concrete was visually monitored at regular intervals using a DinoLite microscope. The cracked region in the 400 × 100 × 100 mm bioconcrete specimen started showing the precipitation of calcium carbonate after seven days. Twenty millilitres of nutrient growth medium (NBUC) supplemented with urea (2%) and calcium chloride (25 mM) were injected into the crack region of the bioconcrete specimens four times a day to maintain moisture for bacterial activity. However, the control specimens were injected only with water. The crack width was measured at different intervals and images were obtained for visual monitoring. In the control specimens, no reduction in crack width was observed. There was no visual detection of any calcification in the control specimens, which explains why the presence of calcium carbonate in the bioconcrete specimens was due to the metabolic function of the spores immobilized in metakaolin. In the bioconcrete specimens, the cracks completely healed after 40 days (Fig. 12). A microscopic image was taken using a DinoLite microscope, showing the deposition of calcium carbonate crystals at the depth of the cracked area, as shown in Fig. 13. It can be stated that the bacterial spores were able to break the dormant endospore stage and become active owing to the availability of moisture and nutrients. The presence of urea and calcium chloride in the nutrient growth medium facilitated bio-mediated calcium carbonate precipitation because of the ureolytic biochemical reactions in the cracked region. Therefore, voids were filled in the concrete specimens. The crack width was monitored for crack closure until the crack was completely closed, and the crack-healing efficiency was calculated based on the crack-width reduction. Water tightness and sealing efficiency were calculated using a water flow test.

Crack closure was monitored by measuring the reduction in the crack width at five different locations in the concrete specimens. Measurements were taken using a DinoLite microscope. Initially, crack widths of 0.543 mm, 0.558 mm, 0.533 mm, 0.516 mm, and 0.537 mm were measured at five locations in the crack region. After the continuous injection of the NBUC medium into the crack region, slight white carbonate precipitates were observed on the walls of the cracked region after eight days. On the 14th day, visible detection of calcium carbonate was observed, with a reduction in the crack width to 0.428, 0.425, 0.434, 0.442, and 0.419 mm. It is worth mentioning here that no additional bacterial culture was inoculated in the nutrient growth medium used for spray treatment. Over a period of 40 days, the crack width at location A decreased from 0.543 to 0. 008 mm, with a crack-healing efficiency of 98.5% (Fig. 14a and14b). Similarly, at location B, the crack width decreased from 0.558 mm to 0.005 mm, exhibiting a crack-healing efficiency of 99.1%. At the same time, locations C, D, and E showed healing efficiencies of 97.05, 97.76 and 98.88%, respectively (Fig. 14b). Statistical analysis using two-way ANOVA proved that the crack width was significantly reduced in the 40-d duration at a 5% level of significance. Whereas in the control specimen water was sprayed and no noticeable calcium carbonate precipitation was seen. The crack width of 0.52 mm was wider for autogenous healing to occur. Specimens incorporated with biomaterial showed autonomous healing of 0.53 mm crack width. Anand et al. reported 0.5 mm crack healing in 45 days using bacteria immobilized in silica fume as a carrier material [47]. Authors further documented no sign of healing in control specimen by using nutrients, urea and calcium chloride on the control cracked specimen. Similar results were corroborated using bacteria immobilized on different carrier materials, such as expanded glass granules [75], hydrogels [23], and rubber particles [76]. Kanwar et al. documented crack healing of 500 μm and 800 μm widths with 100% and 68% crack-sealing efficiency, respectively [77]. Wang et al. reported 84 % crack healing ratio with 99% recovery of the compressive strength and water tightness in concrete specimens incorporated with bacteria immobilized recycled concrete aggregates. Xu et al. [11] reported 100% crack healing with 417 μm crack closure using a low-alkali cementitious material. Previously reported studies have showed that carrier materials have significantly maintained microbial mineralization activity and improved the crack self-healing efficiency [78].

4.1. Water tightness

Water tightness was evaluated based on the amount of water flowing through the crack zone in 20 s until complete crack closure. Different locations were marked as A, B, and C on the specimens to determine the amount of water flowing through the different regions of the crack. The crack widths and depths varied at these locations. At regular intervals, the amount of water flowing through the cylinder fixed at these locations was measured, as described by Kaur et al. [53]. The amounts of water flowing through the crack region initially and during the healing

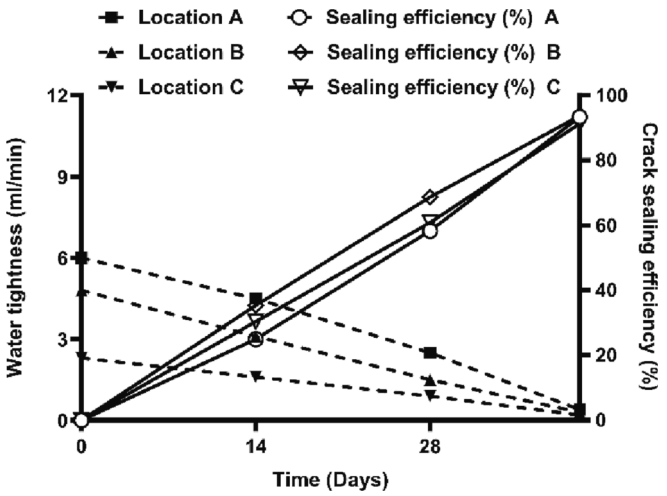


Fig. 15. Water tightness and crack sealing efficiency of bacterial treated (*B. paramycoides*) Concrete crack specimens at 0-, 12-, 24, and 40-days curing time.

period are shown in Fig. 15. It was observed that initially, 6 ml/20 sec of water flowed through the cracked location A which declined to 4.5 ml/20 sec to 0.4 ml/20 sec at 14 and 40 days, respectively. Similarly, at other locations B the amount of water flowing through the crack region decreased from 4.8 ml/20 sec to 0.3 ml/20 sec at 40 days. As the calcium carbonate precipitates filled the empty space in the crack region, the amount of free water flowing through the crack decreased, indicating that the crack area healed because of bacterial biomineralization. The water flow varied at each location, which might be due to variations in crack depth and width. Similarly, in control specimen the rate of water flow remained constant during the experiment. Initially, the amount of water flowing through the cracked locations A, B, and C was 4.6 ml/20 sec, 5.4 ml/20 sec and 3.2 ml/20 sec. There was a negligible difference each time. The average rate of water flow was 4.4 ml/20 sec after 40 days of the experiment.

The crack-sealing efficiency percentage was calculated as the amount of water flowing through the crack zone initially and after crack closure. As shown in Fig. 15, the crack-sealing efficiency at location A increased from 25 % to 93.34 % on day 40. In comparison to location A, 93.75 and 91.3 % of healing was noted at locations B and C. On average, 92.8 % of the area was healed by bacterial spores immobilized in the metakaolin incorporated into the concrete. A similar work was carried out by Wang et al., who reported an 81–90 % water flow reduction in hydrogel-incorporated concrete specimens.

4.2. Ultrasonic pulse velocity (UPV)

The UPV was measured for a reference specimen without a crack in bioconcrete (Bioc.REF) specimens and in control (Cont.REF) specimens. The UPV was noted after crack (AC) formation and until the complete closure of the crack by healing. A maximum pulse velocity of 4049 m/s was observed in the Bioc.REF specimens, which decreased by 19.14 % after cracking of the specimens. The UPV value showed a regain in pulse velocity after the plugging of cracks by calcium carbonate precipitation, formed as a result of bacterial metabolic activity in the bioconcrete specimen. The healing of the crack over a period of 40 days led to 98.2 % closure of the crack width, which eventually resulted in the recovery of the pulse velocity. The UPV was evaluated at intervals of 14, 28, and 40 days of crack healing, as shown in Fig. 16. The increase in pulse velocity confirmed the deposition of calcium carbonate at the depth of the crack. On 14th, 28th, and 40th days of crack healing, the UPV values was observed to be increase by 6.4 %, 11.5%, and 21.7 % compared to the after cracking in bioconcrete specimens, respectively. The UPV value envaulted at complete healing of the crack was observed to be 3982 m/s. The Statistical analysis confirmed a significant improvement in UPV upon crack healing in biomaterial added concrete at the 5% significance level. At the same time, the UPV for Cont.REF without biomaterial incorporation was 3159 ± 36 m/s before cracking which showed 0.7% increase in the pulse velocity after 40 days of the healing period. Therefore, autogenous healing of 0.5 mm crack width was excluded. Other researchers have also reported the recovery of UPV during the autonomous healing process [73,77,79].

4.3. Microstructural characterization

The sample collected from a depth of 10 mm in the healed region was visualized using FESEM and EDS for the biomineralization application of the bacteria. As shown in Fig. 17, a uniform distribution of rhombohedral and vaterite crystals was observed in the sample. The crystals were stacked to form a calcite layer. In contrast, calcite deposition was not observed in the control specimens (Fig. 17c). The rhombohedral crystals were 10–12 μM in size, whereas the vaterite crystals were 5 – 8 μM in

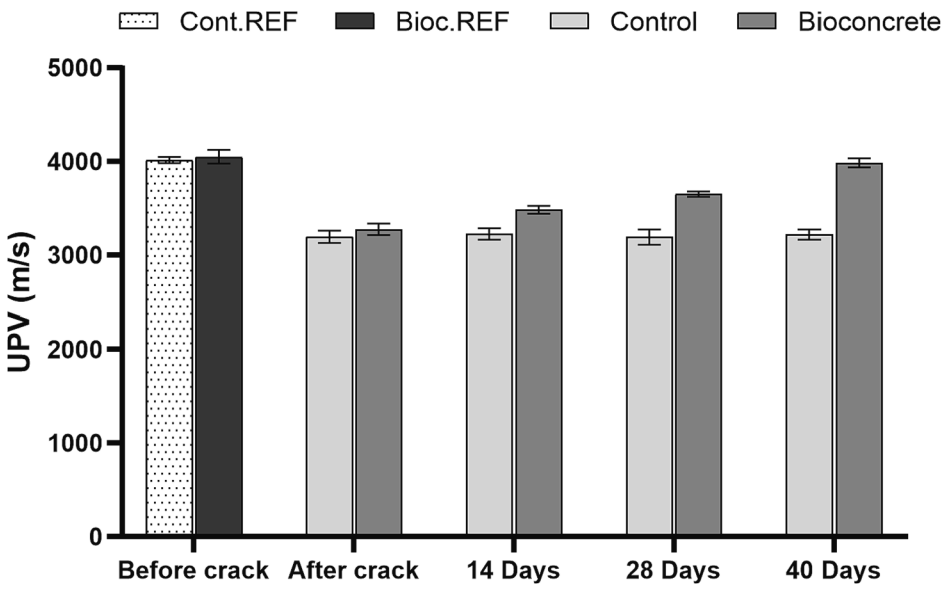


Fig. 16. UPV of bioconcrete and control concrete specimens at different healing times.

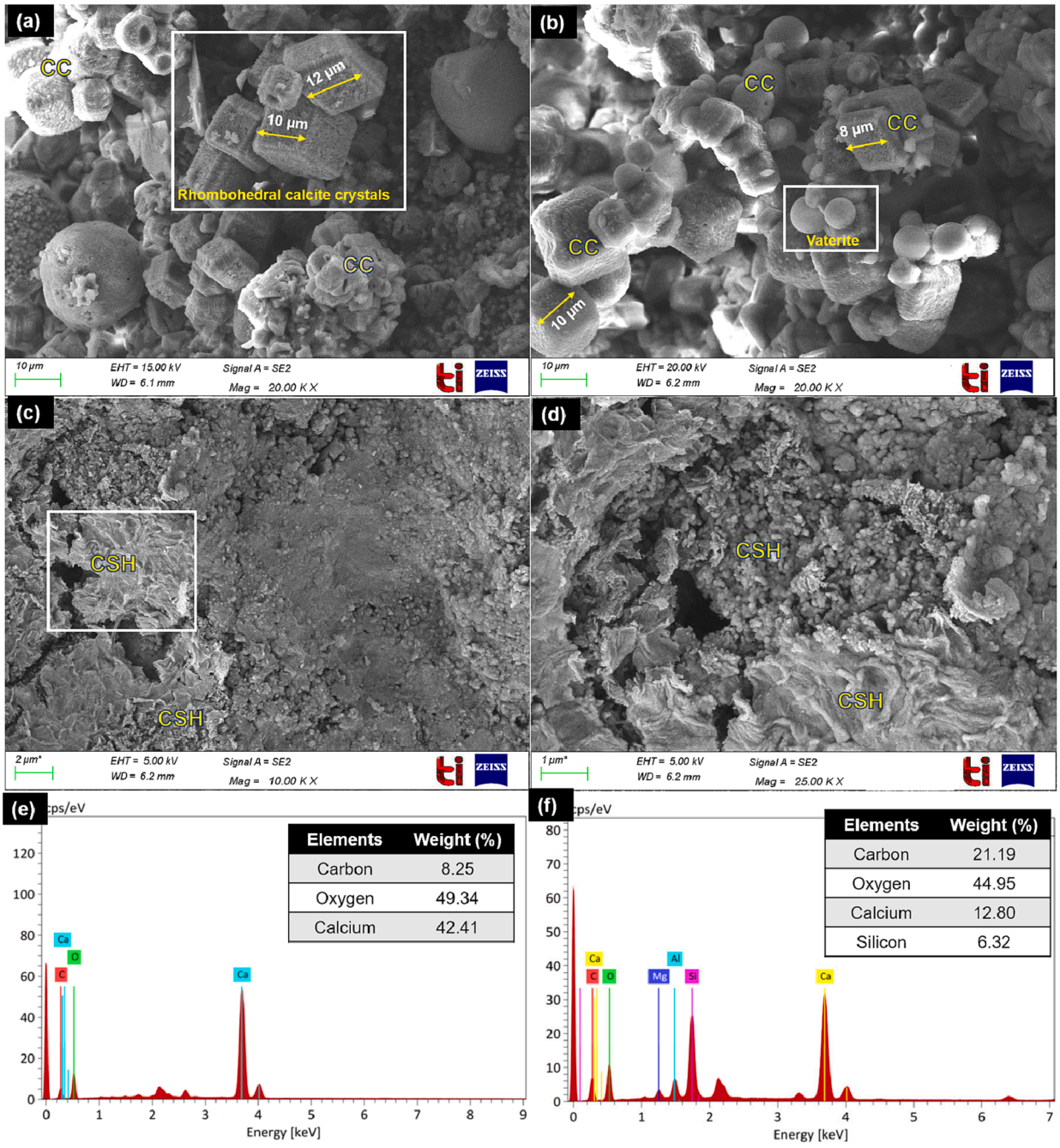


Fig. 17. (a, b) FESEM of the biomaterial added concrete specimens depicting rhombohedral crystal precipitation in healed crack region (c, d) control specimen (e) EDS showing elemental deposition of the calcium carbonate in the healed crack region (f) EDS of the control specimen The '□' marked depicts the spot of EDS analysis.

size. Elemental analysis of the healed precipitates showed that the crystals formed were composed of calcium carbonate. Elemental examination revealed that the healed biocementitious material consisted of four essential elements: carbon (C), oxygen (O), calcium (Ca), and quartz or silica (Si) at 17.42, 53.77, 28.69, and 0.11 wt% ratio. Anand et al. corroborated similar calcium carbonate deposition results from a healed region [55].

Furthermore, the interaction between the cementitious material and biomineralization components was analysed using X-ray diffraction (XRD). An XRD analysis was performed to verify the presence of calcite in the bioconcrete specimens. As shown in Fig. 18, a high-intensity calcite peak was observed at 29.2°, corresponding to 104 planes of calcite. Another X-ray diffraction peak located at (2θ) = 27.1° corresponds to the 101 planes of the vaterite crystals. The presence of calcite peaks confirms that the healed material is calcium carbonate precipitate, which was induced by the immobilized spores in the metakaolin material. Other peaks of quartz (Q), and calcium silicate hydrates (CSH) were also observed in the sample. These peaks were also observed in the control concrete specimens. Similar results have been reported by other researchers by introducing bacterial interactions into the cementitious environment [23,80].

5. Conclusions

The current study reports autonomous (microbial) crack healing of concrete specimens incorporated with *B. paramycoides* spores

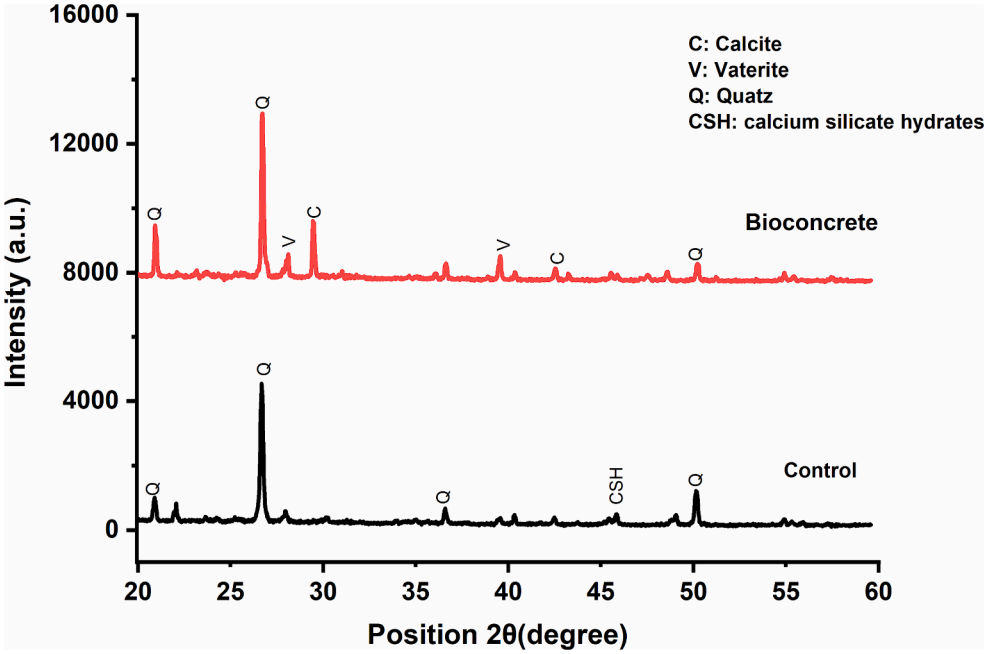


Fig. 18. XRD pattern of bioconcrete and control specimens.

immobilized in metakaolin (MK) by providing nutrients supplemented with 2 % urea and 25 mM $CaCl_2$ upon cracking. The carrier-based biomaterial was developed using an immobilization technique via adsorption technique followed by lyophilization. The biomaterial was stored at 4 and 25 °C for 180 days and showed efficient viability, urease activity, and calcium carbonate precipitation after 180 d of storage. Based on efficiency, the biomaterial stored at 4 °C was used as a supplementary material to improve cementitious properties. The following inferences were drawn from this study:

1. The biomaterial stored at 4 °C showed 7.21 % and 1.6 % higher urease activity and calcium carbonate precipitation, respectively, than those stored at 25 °C.
2. The compressive and flexural strengths were improved by 22.08 % and 14.9 %, respectively, compared to the control sample at the age of 28 days.
3. The sorptivity coefficients of the bioconcrete and control specimens were 0.002 and 0.008, respectively, at 28 d of curing, indicating a reduction in the permeability of the concrete.
4. Using the MICCP technique, the biomaterial-added concrete specimens were able to heal cracks of approximately 500 μm with a crack healing efficiency of 98.2%.
5. Water tightness improved 92.8% crack-sealing efficiency with a reduction in water flow at three different locations of the crack.
6. The ultrasonic pulse velocity of the sample increased during the healing and complete closure of the crack.
7. FESEM-EDS and XRD analyses confirmed the precipitation of calcium carbonate in the cracked region of the concrete specimens.

The study findings proved that spore immobilized in metakaolin could survive in harsh condition of concrete and presents a promising role in the development of concrete that can repair cracks brought on by severe loading.

CRediT authorship contribution statement

Navneet Sidhu: Conceptualization, Investigation, Methodology, Data curation, Validation, Writing – original draft. **Shweta Goyal:** Conceptualization, Methodology, Supervision, Project administration, Resources, Writing – review & editing. **M. Sudhakara Reddy:** Conceptualization, Methodology, Supervision, Project administration, Resources, Writing – review & editing.

Declaration of Competing Interest

The authors declare that they have no known competing financial interests or personal relationships that could have appeared to influence the work reported in this paper.

Acknowledgements

The authors are thankful to the Department of Biotechnology, Ministry of Science and Technology, Govt. of India, for providing the research grant under BT/PR27190/BCE/8/1428/2017.

References:

[1] Danish A, Mosaberpanah MA. Influence of cenospheres and fly ash on the mechanical and durability properties of high-performance cement mortar under different curing regimes. Constr Build Mater 2021;279:122458. https://doi.org/10.1016/j.conbuildmat.2021.122458.
[2] Guo T, Weng X, Liu C, Yu Q, Zhang C, Li Y. Evaluation of the bonding and fatigue properties of an innovative rapid repair structure for concrete pavement. Constr Build Mater 2020;235:11748. https://doi.org/10.1016/j.conbuildmat.2019.117484.
[3] Song X, Song X, Liu H, Huang H, Anvarovna KG, Ugli NAD, et al. Cement-Based Repair Materials and the Interface with Concrete Substrates: Characterization, Evaluation and Improvement. Polymers (Basel) 2022;14:1485. https://doi.org/10.3390/polym14071485.
[4] Anand K, Goyal S, Reddy MS. Development of field applicable remediation procedure using bio-cementitious grout for concrete cracks in variable orientations. J Build Eng 2023;67:106024. https://doi.org/10.1016/j.jobe.2023.106024.
[5] Dhiman NK, Sidhu N, Agnihotri S, Mukherjee A, Reddy MS. Role of nanomaterials in protecting building materials from degradation and deterioration. Biodegrad Biodeterior Nanoscale 2022:405–75. https://doi.org/10.1016/B978-0-12-823970-4.00024-5.
[6] Xu J, Wang X, Wang B. Biochemical process of ureolysis-based microbial $CaCO_3$ precipitation and its application in self-healing concrete. Appl Microbiol Biotechnol 2018;102:3121–32. https://doi.org/10.1007/s00253-018-8779-x.
[7] Rong H, Wei G, Ma G, Zhang Y, Zheng X, Zhang L, et al. Influence of bacterial concentration on crack self-healing of cement-based materials. Constr Build Mater 2020;244:118372. https://doi.org/10.1016/j.conbuildmat.2020.118372.
[8] Wang JY, Soens H, Verstraete W, De Belie N. Self-healing concrete by use of microencapsulated bacterial spores. Cem Concr Res 2014;56:139–52. https://doi.org/10.1016/j.cemconres.2013.11.009.

[9] Liu C, Xu X, Lv Z, Xing L. Self-healing of concrete cracks by immobilizing microorganisms in recycled aggregate. J Adv Concr Technol 2020;18:168–78. https://doi.org/10.3151/jact.18.168.

[10] Kennedy MJ, Reader SL, Swierczynski LM. Historical perspective Preservation records of micro-organisms : evidence of the tenacity of life. Microbiol 1994;140: 2513–29. https://doi.org/10.1099/00221287-140-10-2513.

[11] Xu J, Wang X. Self-healing of concrete cracks by use of bacteria-containing low alkali cementitious material. Constr Build Mater 2018;167:1–14. https://doi.org/10.1016/j.conbuildmat.2018.02.020.

[12] Lee YS, Park W. Current challenges and future directions for bacterial self-healing concrete. Appl Microbiol Biotechnol 2018;102:3059–70. https://doi.org/10.1007/s00253-018-8830-y.

[13] Sharma TK, Alazhari M, Heath A, Paine K, Cooper RM. Alkaliphilic *Bacillus* species show potential application in concrete crack repair by virtue of rapid spore production and germination then extracellular calcite formation. J Appl Microbiol 2017;122:1233–44. https://doi.org/10.1111/jam.13421.

[14] Jonkers HM, Thijssen A, Muyzer G, Copuroglu O, Schlangen E. Application of bacteria as self-healing agent for the development of sustainable concrete. Ecol Eng 2010;36:230–5. https://doi.org/10.1016/j.ecoleng.2008.12.036.

[15] Abel-santos E. Endospores , Sporulation and Germination. Mol Med Microbiol (Second Edition) 2015; 163 -178. doi.org/10.1016/B978-0-12-397169-2.00009-3.

[16] Setlow P. Spore germination. Curr Opin Microbiol 2003;6:550–6. https://doi.org/10.1016/j.mib.2003.10.001.

[17] Christie G, Setlow P. *Bacillus* spore germination: Knowns, unknowns and what we need to learn. Cell Signal 2020;74:109729. https://doi.org/10.1016/j.cellsig.2020.109729.

[18] Pungrasmi W, Intarasoontron J, Jongvivatsakul P, Likitlersuang S. Evaluation of Microencapsulation Techniques for MICP Bacterial Spores Applied in Self-Healing Concrete. Sci Rep 2019;9:1–10. https://doi.org/10.1038/s41598-019-49002-6.

[19] Silva FB, Boon N, De Belie N, Verstraete W. Industrial application of biological self-healing concrete: Challenges and economical feasibility. J Commer Biotechnol 2015;21:31–8. https://doi.org/10.5912/jcb662.

[20] Justo-Reinoso I, Reeksting BJ, Hamley-Bennett C, Heath A, Gebhard S, Paine K. Air-entraining admixtures as a protection method for bacterial spores in self-healing cementitious composites: Healing evaluation of early and later-age cracks. Constr Build Mater 2022;327:126877. https://doi.org/10.1016/j.conbuildmat.2022.126877.

[21] Zamani M, Nikafshar S, Mousa A, Behnia A. Bacteria encapsulation using synthesized polyurea for self-healing of cement paste. Constr Build Mater 2020; 249:118556. https://doi.org/10.1016/j.conbuildmat.2020.118556.

[22] Zhu X, Mignon A, Nielsen SD, Zieger SE, Koren K, Boon N, et al. Viability determination of Bacillus sphaericus after encapsulation in hydrogel for self-healing concrete via microcalorimetry and in situ oxygen concentration measurements. Cem Concr Compos 2021;119:104006. https://doi.org/10.1016/j.cemconcomp.2021.104006.

[23] Gao M, Guo J, Cao H, Wang H, Xiong X, Krastev R, et al. Immobilized bacteria with pH-response hydrogel for self-healing of concrete. J Environ Manage 2020;261: 110225. https://doi.org/10.1016/j.jenvman.2020.110225.

[24] Wang J, Ersan YC, Boon N, De Belie N. Application of microorganisms in concrete: a promising sustainable strategy to improve concrete durability. Appl Microbiol Biotechnol 2016;100:2993–3007. https://doi.org/10.1007/s00253-016-7370-6.

[25] Gupta S, Kua HW, Pang SD. Healing cement mortar by immobilization of bacteria in biochar: An integrated approach of self-healing and carbon sequestration. Cem Concr Compos 2018;86:238–54. https://doi.org/10.1016/j.cemconcomp.2017.11.015.

[26] Khaliq W, Ehsan MB. Crack healing in concrete using various bio influenced self-healing techniques. Constr Build Mater 2016;102:349–57. https://doi.org/10.1016/j.conbuildmat.2015.11.006.

[27] Wang Lu, Ren Z, Wang H, Liang X, Liu S, Ren J, et al. Microstructure-property relationships in cement mortar with surface treatment of microbial induced carbonate precipitation. Compos Part B Eng 2022;239:109986. https://doi.org/10.1016/j.compositesb.2022.109986.

[28] Alghamri R, Kanellopoulos A, Al-Tabbaa A. Impregnation and encapsulation of lightweight aggregates for self-healing concrete. Constr Build Mater 2016;124: 910–21. https://doi.org/10.1016/j.conbuildmat.2016.07.143.

[29] Apolinário de Oliveira T., D'Orey Gaivão Portela Bragança M., Miguel Pinkoski I., Carrera G. The effect of silica nanocapsules on self-healing concrete. Constr Build Mater 2021;300:124010.doi.org/10.1016/j.conbuildmat.2021.124010.

[30] Gulin LB, Schwantes-Cezario N, Florian M. Viability of *Bacillus* subtilis immobilization using silica gel for self-healing of cement based materials. Int J Adv Eng Res Sci 2021;8:001–10. https://doi.org/10.22161/ijaers.86.1.

[31] Wang J, Van Tittelboom K, De Belie N, Verstraete W. Use of silica gel or polyurethane immobilized bacteria for self-healing concrete. Constr Build Mater 2012;26:532–40. https://doi.org/10.1016/j.conbuildmat.2011.06.054.

[32] Yuan H, Zhang Q, Hu X, Wu M, Zhao Y, Feng Y, et al. Application of zeolite as a bacterial carrier in the self-healing of cement mortar cracks. Constr Build Mater 2022;331:127324. https://doi.org/10.1016/j.conbuildmat.2022.127324.

[33] Zheng T, Qian C. Self-Healing of Later-Age Cracks in Cement-Based Materials by Encapsulation-Based Bacteria. J Mater Civ Eng 2020;32:1–10. https://doi.org/10.1061/(asce)mt.1943-5533.0003437.

[34] Zhang J, Liu Y, Feng T, Zhou M, Zhao L, Zhou A, et al. Immobilizing bacteria in expanded perlite for the crack self-healing in concrete. Constr Build Mater 2017; 148:610–7. https://doi.org/10.1016/j.conbuildmat.2017.05.021.

[35] Singh SB, Murugan M. Effect of metakaolin on the properties of pervious concrete. Constr Build Mater 2022;346:128476. https://doi.org/10.1016/j.conbuildmat.2022.128476.

[36] Bishnoi S. RILEM Bookseries Calcined Clays for Sustainable Concrete Proceedings of the 3rd International Conference on Calcined Clays for Sustainable Concrete. 2020.

[37] Rais MS, Khan RA. Experimental investigation on the strength and durability properties of bacterial self-healing recycled aggregate concrete with mineral admixtures. Constr Build Mater 2021;306:124901. https://doi.org/10.1016/j.conbuildmat.2021.124901.

[38] Li W, Hua L, Shi Y, Wang P, Liu Z, Cui D, et al. Influence of metakaolin on the hydration and microstructure evolution of cement paste during the early stage. Appl Clay Sci 2022;229:106674. https://doi.org/10.1016/j.clay.2022.106674.

[39] Singh H, Siddique R. Utilization of crushed recycled glass and metakaolin for development of self-compacting concrete. Constr Build Mater 2022;348:128659. https://doi.org/10.1016/j.conbuildmat.2022.128659.

[40] El-Diadamony H, Amer AA, Sokkary TM, El-Hoseny S. Hydration and characteristics of metakaolin pozzolanic cement pastes. HBRC J 2018;14:150–8. https://doi.org/10.1016/j.hbrcj.2015.05.005.

[41] Badogiannis EG, Sfikas IP, Voukia DV, Trezos KG, Tsivilis SG. Durability of metakaolin Self-Compacting Concrete. Constr Build Mater 2015;82:133–41. https://doi.org/10.1016/j.conbuildmat.2015.02.023.

[42] Rashad AM. Metakaolin as cementitious material: History, scours, production and composition-A comprehensive overview. Constr Build Mater 2013;41:303–18. https://doi.org/10.1016/j.conbuildmat.2012.12.001.

[43] Bhaskar S, Anwar Hossain KM, Lachemi M, Wolfaardt G, Otini KM. Effect of self-healing on strength and durability of zeolite-immobilized bacterial cementitious mortar composites. Cem Concr Compos 2017;82:23–33. https://doi.org/10.1016/j.cemconcomp.2017.05.013.

[44] Zheng T, Su Y, Qian C, Zhou H. Low alkali sulpho-aluminate cement encapsulated microbial spores for self-healing cement-based materials. Biochem Eng J 2020;163: 107756. https://doi.org/10.1016/j.bej.2020.107756.

[45] BIS 8112 – 1989. Specification for 43 grade ordinary Portland cement. Bur Indian Stand, New Delhi. 2013;17:1–11.

[46] BIS 383 - 1970. Indian standard specification for coarse and fine aggregates from natural sources for concrete. Bur Indian Stand, New Delhi, 2016;1–21.

[47] Anand K, Goyal S, Reddy MS. Long-term viable SF immobilized bacterial cells as sustainable solution for crack healing in concrete. Structures 2022;43:1342–55. https://doi.org/10.1016/j.istruc.2022.07.056.

[48] Natarajan KR. Kinetic study of the enzyme urease from Dolichos biflorus. J Chem Educ 1995;73:556–7. https://doi.org/10.1021/ed072p556.

[49] IS 516 -1959. Method of tests for strength of concrete. Bur Indian Stand. New Delhi 2004:1–30.

[50] ASTM. C1585–13. Standard Test Method for Measurement of Rate of Absorption of Water by Hydraulic Cement Concretes. ASTM Int 2013;41:1–6. https://doi.org/10.1520/C1585-13.2.

[51] Paine K. Bacteria-based self-healing of concrete: effects of environment, exposure and crack size. Proc RILEM Conf Microorg Mater Interact 2016: 1-15.

[52] ASTM C 597-02. Standard test Method For Pulse Velocity Through Concrete. Am Soc Test Mater 2003;04:3–6.

[53] Kaur NP, Majhi S, Dhami NK, Mukherjee A. Healing fine cracks in concrete with bacterial cement for an advanced non-destructive monitoring. Constr Build Mater 2020;242:118151. https://doi.org/10.1016/j.conbuildmat.2020.118151.

[54] González Á, Parraguez A, Corvalán L, Correa N, Castro J, Stuckrath C, et al. Evaluation of Portland and Pozzolanic cement on the self-healing of mortars with calcium lactate and bacteria. Constr Build Mater 2020;257:1–11. https://doi.org/10.1016/j.conbuildmat.2020.119558.

[55] Anand K, Goyal S, Reddy MS. Crack healing in concrete by microbially induced calcium carbonate precipitation as assessed through electromechanical impedance technique. Eur J Environ Civ Eng 2023;27:1123–43. https://doi.org/10.1080/19648189.2022.2075470.

[56] Son Y, Min J, Jang I, Yi C, Park W. Development of a novel compressed tablet-based bacterial agent for self-healing cementitious material. Cem Concr Compos 2022;129:104514. https://doi.org/10.1016/j.cemconcomp.2022.104514.

[57] Jonkers HM. Bacteria-based self-healing concrete In-Genium 2021:84–93.

[58] Wang X, Xu J, Wang Z, Yao W. Use of recycled concrete aggregates as carriers for self-healing of concrete cracks by bacteria with high urease activity. Constr Build Mater 2022;337:127581. https://doi.org/10.1016/j.conbuildmat.2022.127581.

[59] Wang J, Mignon A, Snoeck D, Wiktor V, Van Vliergerghe S, Boon N, et al. Application of modified-alginate encapsulated carbonate producing bacteria in concrete: A promising strategy for crack self-healing. Front Microbiol 2015;6:1–14. https://doi.org/10.3389/fmicb.2015.01088.

[60] Bang SS, Galinat JK, Ramakrishnan V. Calcite precipitation induced by polyurethane-immobilized *Bacillus pasteurii*. Enzyme Microb Technol 2001;28: 404–9. https://doi.org/10.1016/S0141-0229(00)00348-3.

[61] Zhu Z, Bassey AP, Huang T, Zhang Y, Ali Khan I, Huang M. The formation, germination, and cold plasma inactivation of bacterial spore. Food Chem Adv 2022;1:100056. https://doi.org/10.1016/j.focha.2022.100056.

[62] Xiao X, Unluer C, Yang E. Study on the viability of unprotected bacterial spores directly embedded in a reactive magnesia cement matrix for potential crack healing. Constr Build Mater 2022;346:128424. https://doi.org/10.1016/j.conbuildmat.2022.128424.

[63] Wang J, Jonkers HM, Boon N, De Belie N. *Bacillus sphaericus* LMG 22257 is physiologically suitable for self-healing concrete. Appl Microbiol Biotechnol 2017; 101:5101–14. https://doi.org/10.1007/s00253-017-8260-2.

[64] Başaran Bundur Z, Bae S, Kirisits MJ, Ferron RD. Biomineralization in Self-Healing Cement-Based Materials: Investigating the Temporal Evolution of Microbial Metabolic State and Material Porosity. J Mater Civ Eng 2017;29:04017079. https://doi.org/10.1061/(asce)mt.1943-5533.0001838.

[65] Erşan YÇ, Da Silva FB, Boon N, Verstraete W, De Belie N. Screening of bacteria and concrete compatible protection materials. Constr Build Mater 2015;88:196–203. https://doi.org/10.1016/j.conbuildmat.2015.04.027.
[66] Joshi S, Goyal S, Reddy MS. Influence of nutrient components of media on structural properties of concrete during biocementation. Constr Build Mater 2018; 158:601–13. https://doi.org/10.1016/j.conbuildmat.2017.10.055.
[67] Amiri A, Bundur ZB. Use of corn-steep liquor as an alternative carbon source for biomineralization in cement-based materials and its impact on performance. Constr Build Mater 2018;165:655–62. https://doi.org/10.1016/j.conbuildmat.2018.01.070.
[68] Yazici Ş, Güller C, Ayekin B, Mardani A, Akkaya A. Usability of sustainable materials on bacteria-based self-healing in cementitious systems. J Intell Mater Syst Struct 2023. https://doi.org/10.1177/1045389X231157358.
[69] Yılmazer Polat B, Uysal M. Bacterial crack healing in metakaolin based geopolymer mortars. J Build Eng 2021;39:102291. https://doi.org/10.1016/j.jobe.2021.102291.
[70] Soysal A, Milla J, King GM, Hassan M, Rupnow T. Evaluating the Self-Healing Efficiency of Hydrogel-Encapsulated Bacteria in Concrete. Transp Res Rec 2020; 2674:113–23. https://doi.org/10.1177/0361198120917973.
[71] Barbhuiya S, Chow PL, Memon S. Microstructure, hydration and nanomechanical properties of concrete containing metakaolin. Constr Build Mater 2015;95: 696–702. https://doi.org/10.1016/j.conbuildmat.2015.07.101.
[72] Pillay DL, Olalusi OB, Kiliswa MW, Awoyera PO, Kolawole JT, Babafemi AJ. Engineering performance of metakaolin based concrete. Clean Eng Technol 2022;6: 100383. https://doi.org/10.1016/j.clet.2021.100383.
[73] Tanyildizi H, Ziada M, Uysal M, Doğruöz Güngör N, Coşkun A. Comparison of bacteria-based self-healing methods in metakaolin geopolymer mortars. Case Stud Constr Mater 2022;16:e00895. https://doi.org/10.1016/j.cscm.2022.e00895.
[74] Abouhussien AA, Hassan AAA. Optimizing the durability and service life of self-consolidating concrete containing metakaolin using statistical analysis. Constr Build Mater 2015;76:297–306. https://doi.org/10.1016/j.conbuildmat.2014.12.010.
[75] Zhang LV, Suleiman AR, Mehdizadeh Allaf M, Marani A, Tuyan M, Nehdi ML. Crack self-healing in alkali-activated slag composites incorporating immobilized bacteria. Constr Build Mater 2022;326:126842. https://doi.org/10.1016/j.conbuildmat.2022.126842.
[76] Xu H, Lian J, Gao M, Fu D, Yan Y. Self-Healing Concrete Using Rubber Particles to to Immobilize Bacterial Spores. Materials (Basel) 2019;12:2313. https://doi.org/10.3390/ma12142313.
[77] Kanwal M, Khushnood RA, Khaliq W, Wattoo AG, Shahid T. Synthesis of pyrolytic carbonized bagasse to immobilize Bacillus subtilis; application in healing micro-cracks and fracture properties of concrete. Cem Concr Compos 2022;126:104334. https://doi.org/10.1016/j.cemconcomp.2021.104334.
[78] Feng C, Zong X, Cui B, Guo H, Zhang W, Zhu J. Application of Carrier Materials in Self-Healing Cement-Based Materials Based on Microbial-Induced Mineralization. Crystals 2022:12: 797. https://doi.org/10.3390/cryst12060797.
[79] Ranjan P, Soda K, Chakravarthi EK, Mogal A, Mini KM. Statistical and experimental investigation on self-healing of microcracks in cement mortar by encapsulation of calcite precipitating bacteria into expanded perlite. Constr Build Mater 2022;342: 127985. https://doi.org/10.1016/j.conbuildmat.2022.127985.
[80] Sidhu N, Goyal S, Reddy MS. Biomineralization of cyanobacteria *Synechocystis pevalekii* improves the durability properties of cement mortar. AMB Express 2022; 12:59. https://doi.org/10.1186/s13568-022-01403-z.

Check for updates

ASCE

Crack Bioremediation in Concrete by Photoautotrophic Cyanobacteria through Fly Ash–Based Cementitious Biogrout

Navneet Sidhu[1]; Shweta Goyal[2]; and M. Sudhakara Reddy[3]

Downloaded from ascelibrary.org by Indian Institute Of Technology Delhi on 11/27/23. Copyright ASCE. For personal use only; all rights reserved.

Abstract: Microbially induced calcium carbonate precipitation (MICCP) is widely employed in various engineering applications, including repairing cracks in cementitious materials. Many of these studies were performed using heterotrophic bacteria that utilize urea and releases harmful foul-smelling environmental pollutant. Cyanobacteria have emerged as potential substitutes for heterotrophic bacteria to overcome this concern. This study used photosynthetic cyanobacteria *Synechocystis pevalekii* to develop an ecofriendly and sustainable grout for crack remediation in concrete. To improve the fluidity characteristics of the grout, fly ash was incorporated as a partial cement replacement in the cementitious grout. The cementitious grouts were tested for fresh properties at different dosages of fly ash (0%–50%) by keeping water (or bacterial culture) to binder ratios of 0.45, 0.47, and 0.50. Based on flowability results, a 0.47 culture/binder ratio was selected to examine different FA dosages for hardened properties. A 40% FA substituted cementitious biogrout was selected for repairing cracks at the lab scale. Different cracked concrete specimens were repaired and cured using ponding and spray treatment for 28 days. At the end of the experiment, a significant improvement in strength and permeability was recorded in biogrout-remediated cracked specimens. The sample was collected from healed cracked region to confirm the healing mineral using field emission surface electron microscope (FESEM), energy dispersive spectroscopy (EDS), X-ray diffraction (XRD), and thermogravimetric analysis (TGA). The developed fly ash incorporated biogrout will help as an economical and ecofriendly MICCP technology for the remediation of existing cracks in the concrete structures. **DOI: 10.1061/JMCEE7.MTENG-16301.** *© 2023 American Society of Civil Engineers.*

Author keywords: *Synechocystis pevalekii*; Crack repair; Concrete; Fly ash; Biomineralization; Compressive strength; Flexural strength; Sorptivity test; Biogrout.

Introduction

Cracks make concrete structures more vulnerable to a significant risk of premature failure due to the penetration of harmful gases and liquid through major and minor cracks (Van Tittelboom et al. 2010). The primary concern is the crack width in the range of 0.5–1.0 mm (Choi et al. 2017; Joshi et al. 2021; Luo et al. 2015). Therefore, developing an early-stage preventative mechanism to repair the crack damage and enhance concrete buildings' service life becomes imperative. There are different methodologies reported in recent years in which the cracks of width ranging from 0.1 to 0.3 mm were repaired using self-healing through biomineralization (Osman et al. 2021; Zhang et al. 2017). Many conventional sealants, such as epoxy resins, polyurethane, acrylics, and waxes, are used to repair the cracks. Though they effectively reduce porosity and plug the crack, such additives are susceptible to deterioration due to their low heat resistance, unsustainability, poorer weather resistance, moisture sensitivity, and are expensive (Dhami et al. 2013; Dhiman et al. 2022). Even autogenous self-healing of minor cracks is possible with a high binder content mixture (Sierra Beltran and Jonkers 2015). In this case the presence of humidity in the immediate environment, the composition of the concrete matrix, and the amount of unhydrated cement present will have a significant role in autogenous healing (Wang et al. 2014). Whereas the self-healing procedures are suitable for smaller crack widths, larger crack widths of 0.5 mm or higher can be efficiently remediated using injectable cementitious grout (Jiang et al. 2020; Wang et al. 2016). In this study, the flowability and strength test for different grout mixture was done to develop a sustainable and cost-effective grout mixture for repairing the cracks in existing concrete structures.

Grouting is the most extensively used injection technique in civil and geotechnical engineering through fluidized material for remediation of distresses of various forms (soil grouting, crack injection, and hole filling in concrete buildings) (Vasumithran et al. 2020). It is important to study the fresh properties of different admixtures before it is applied as cement-based grout for the remediation of concrete structures. The water-to-cement (w/c) ratio is essential in enhancing the flowability and permeability of grout, varying from 0.4 to −2, which further significantly impacts the grout strength (Çınar et al. 2020). Adding different types of mineral additives like rice husk ash, fly ash, silica fume, metakaolin, and cement kiln dust into cement admixed grout at different concentrations changes the fresh properties of grout significantly (Joshi et al. 2021). The incorporation of mineral additives in preparation of the cement grout reduces the overall cost and improves the fluidity and

[1]Ph.D. Scholar, Dept. of Biotechnology, Thapar Institute of Engineering and Technology, Patiala, Punjab 147004, India. ORCID: https://orcid.org/0009-0006-6283-3165. Email: nsidhu_17@thapar.edu

[2]Professor, Dept. of Civil Engineering, Thapar Institute of Engineering and Technology, Patiala, Punjab 147004, India. Email: shweta@thapar.edu

[3]Professor, Dept. of Biotechnology, Thapar Institute of Engineering and Technology, Patiala, Punjab 147004, India (corresponding author). ORCID: https://orcid.org/0000-0002-9743-4993. Email: msreddy@thapar.edu

Note. This manuscript was submitted on January 12, 2023; approved on July 18, 2023; published online on November 24, 2023. Discussion period open until April 24, 2024; separate discussions must be submitted for individual papers. This paper is part of the ***Journal of Materials in Civil Engineering***, © ASCE, ISSN 0899-1561.

long-lasting capacity. Concerning the environmental issues related to fly ash and other additives, it is essential to understand that it is industrial by-product and provides no risk in the utilization of the grout preparation (Celik and Canakci 2015). Worldwide fly ash production is estimated to exceed 900 million tons annually (Delić et al. 2022; Heidrich et al. 2013; Onyelowe et al. 2022). Of these, only 53.5% of the fly ash is utilized as replacement material in cement, brick production, and road construction (Kotelnikova et al. 2022; Onyelowe et al. 2022). Many studies are available in the literature for partial replacement of cement to fly ash (Bai et al. 2022; Li et al. 2022; Sha et al. 2018; Zhang et al. 2020), but limited studies are available for crack repair using fly ash-substituted grout.

With an aim of developing sustainable and efficient grout calcium carbonate producing bacteria can be employed. Microbial-facilitated bioremediation is considered as an ecoefficient and cost-effective technique that significantly increases strength and dilatancy and reduces hydraulic conductivity (Xiao et al. 2020). This technique can also be further extended to form sustainable cement-based biogrout (CBG). Microorganisms promote the precipitation of calcium carbonate, filling the voids and making them more compact and denser. Gleaton et al. (2019) differentiated biogrout into two diverse mechanisms; injection biogrout and premixed biogrout. In injection based biogrout, the microbial calcifying culture is supplemented through ponding or spray after repairing the crack with the normal grout, whereas in the premixed, the microorganisms are added in the grout itself. To effectively develop sustainable bacterial grout as a repair mechanism, it should possess long-term durability, sufficient compressive strength, and low permeability (Achal and Kawasaki 2016; Ivanov et al. 2019). Therefore, water separation, hardening, and flowability are essential measures to be investigated. The most studied microorganisms implicated in the MICCP are photosynthetic microorganisms and urease-producing bacteria. The major drawback of using the latter is releasing ammonia gas, a harmful foul-smelling pollutant (Ivanov et al. 2019). As an alternative, photosynthetic bacteria are recognized as a safe ecological source for MICCP, utilizing light and carbon dioxide as energy sources. It offers a self-sustaining approach for carbon capture and sequestration, resulting in carbonate minerals forming. In cyanobacterial photosynthesis, HCO_3^-/OH^- ions exchange occurs across the cell membrane, resulting in increase in pH (Sidhu et al. 2022). The photosynthetic reaction is catalyzed by RUBISCO-carboxylase and carbonic anhydrase enzymes. The CO_2 enters the cyanobacterial cell through the $HCO_3^-/Na+$ symporter, which is further converted to HCO_3^-. In the carbon concentration mechanism (CCM), HCO_3^- in the cytosol is carried to the carboxysome and converted into CO_2 through carbonic anhydrase activity [Eq. (1)]. As a result, the OH^- is released across the cell membrane, increasing the pH of the cell exterior (Kamennaya et al. 2012). In some cases, cells are able to store excessive Ca^{2+}, precipitate calcium carbonate inside or transport it outside of the cell wall (Waditee et al. 2004). The $CaCO_3$ precipitation reaction proceeds as shown in Eqs. (2) and (3)

$$CO_2 + H_2O \leftrightarrow H^+ + HCO_3^- \quad (1)$$

$$Ca^{2+} + 2HCO^{3-} \leftrightarrow CaCO_3 + CO_2 + H_2O \quad (2)$$

$$Ca^{2+} + CO_3^{2-} \leftrightarrow CaCO_3 \quad (3)$$

Photosynthetic cyanobacterial species such as *Synechocystis* is proven to induce calcium carbonate precipitation under the influence of temperature, light and carbon dioxide in the environment (Han et al. 2013, 2017a). The *Synechocystis* can favourably grow in an alkaline medium and in various unfavourable conditions like low temperature, hyperosmotic stress, and salt stress (Kamennaya et al. 2012; Yu et al. 2013). *Synechocystis* can maintain long-term viability in harsh conditions of the concrete environment (Sidhu et al. 2022; Zhu et al. 2018). Therefore, *Synechocystis* can improve calcium carbonate precipitation by functioning as a better economic and environmental alternative for ureolytic bacteria.

Research Significance

To the authors' best knowledge, this is the first study on developing the ecofriendly biogrout incorporating *Synechocystis pevalekii* BDHKU 35101 and fly ash (FA) as a partial replacement. The key characteristic of present investigation is use of photoautotrophic bacteria which utilizes only natural source of light as energy source. The main aim of the present investigation is to use the photoautotrophic bacteria, *Synechocystis pevalekii* culture to develop the fly ash incorporated biogrout for crack remediation in concrete. The fresh properties (flowability and grout bleeding) of the cement-based grouts were evaluated to determine the optimal water-to-binder ratio (0.45, 0.47, and 0.50) at various fly ash dosages (0%–50% FA). Further, the selected water to binder ratio was evaluated for the hardened properties (setting time and compressive strength) of the grout. Based upon the above-mentioned test, the biogrout was selected for the crack remediation in the concrete specimens. The repaired cracks were cured using ponding and spray treatment for 28 days. At the end of experiment, the healed specimens were examined for the compressive test, flexural test and sorptivity test. The microstructural analysis (FESEM-EDS, XRD), and thermogravimetric (TGA) analysis were performed for the crack-healed concrete specimens.

Experiment Materials

Biological Culture and Materials Used

The photoautotrophic cyanobacterial strain, *Synechocystis pevalekii* BDHKU 35101 procured from the National Facility for Marine Cyanobacteria, Bharathidasan University Tiruchirappalli, Tamil Nadu, India, was used in this study (Bhuvaneshwari et al. 2017). The culture was grown and maintained in BG11 medium at 25°C ± 2°C with the illumination light of 1,200 lux for a photoperiod of 12:12 h (light:dark) at 100 rpm shaking conditions (Sidhu et al. 2022).

The commercially available ordinary portland cement (OPC, 43 grade) corroborative to Indian standard [BIS: 8112 (BIS 2013)] was used. For the cement replacement, fly ash of class F obtained from Rajpura Thermal Plant, Punjab, India, was used. The chemical composition and specific gravity of OPC and FA are presented in Table 1. It can be inferred from table that the alumina percentage is 40.3%. It is a bituminous coal that has generally high content of alumina (Yao et al. 2014). As per ASTM C618 (ASTM 2019) and IS 3812 (Part 1) (IS 2003) standard Class F fly ash has silicon dioxide (SiO_2), aluminum oxide (Al_2O_3), iron oxide (Fe_2O_3) more than 70% of total amount. Many studies are available in literature that reports utilization of fly ash rich in alumina (Achal et al. 2011; Yu et al. 2020; Joshi et al. 2021). Recently, Yu et al. (2023) reported 53.5% of Al_2O_3 is fly ash obtained from thermal power station in central Inner Mongolia of China. Locally available natural well-graded river sand confirming to Zone II as per Indian standard [IS:383 (IS 2016)] was used as fine aggregates. The specific gravity of fine aggregate used was 2.65, and water absorption was 1.5%. The 20 mm and 10 mm particle size of coarse aggregates with specific gravity and water absorption of 2.63 and 1.40%, and 2.65

Downloaded from ascelibrary.org by Indian Institute Of Technology Delhi on 11/27/23. Copyright ASCE. For personal use only; all rights reserved.

Table 1. Chemical composition and specific gravity of ordinary portland cement (Grade 43) and fly ash (FA)

Chemical composition (%)	OPC	FA (Class F)
Calcium oxide (CaO)	65.9	0.5
Silicon dioxide (SiO_2)	21.5	57.2
Aluminum oxide (Al_2O_3)	5.3	40.3
Iron oxide (Fe_2O_3)	3.1	1.0
Sulfur trioxide (SO_3)	1.6	—
Potassium oxide (K_2O)	0.9	0.3
Magnesium oxide (MgO)	0.6	0.1
Sodium oxide (Na_2O)	0.5	0.3
Loss of ignition (LOI)	—	0.7
Specific gravity	3.18	2.33

and 1.43%, respectively, were used. Both fine aggregate and coarse aggregate used in casting confirm the Indian standards [IS:383 (IS 2016)].

Experiment Methods

Calcium Carbonate Precipitation and pH Dynamic

The *Synechocystios pevalekii* BDHKU 35101 cells (OD_{680}–1.0) were inoculated into 250 mL Erlenmeyer flask containing 90 mL of BG11 medium supplemented with 4 mM sodium bicarbonate ($NaHCO_3$) and 25 mM calcium chloride ($CaCl_2$). The flask was incubated at room temperature of 25°C ± 2°C constantly shaken at 110 rpm under illumination of 1,200 lux for photoperiod of 12:12 h (light: dark). The concentration of calcium chloride is within the range of other studies of MICCP (Zhu et al. 2017). All samples were prepared in the triplicate flask. Sample aliquots were filtered through a 0.2 mm cellulose nitrate membrane at 0, 2, 4, 6, 8, 10, 12, 24, 48, 72, 96, 120, 144, 168, 196 h to evaluate the dissolved calcium (Ca^{2+}) and amount of $CaCO_3$ precipitated by EDTA titration method. The pH of the solution was monitored for initial few hours (un pH becomes constant) of the incubation.

Grout Mixture Design

In the present investigation, water-based cement grout, designated as plain grout, and bio-based cement grout, denoted as biogrout, were prepared. The cement grout mixture consists of different ratios of fly ash (0%–50%) by the total cement mass. The water/binder (w/b) and culture/binder (c/b) are important parameters that have a notable outcome on the fresh and hardened properties of the grout mixtures. Therefore, three different w/b and c/b ratio (0.45, 0.47 and 0.50) were used. In total, 36 grout mixtures were designed to study the impact of different fly ash dosages (0%–50%), w/b, and c/b ratios on the properties of cement grout. The 36-grout mixture dosages with respective c/b and w/b ratios were prepared as mentioned in Table 2. The *S. pevalekii* cell suspension was prepared by growing the cell culture at 25°C ± 2°C until it obtained the optical density (OD_{680}) of 1.0. To prepare the biogrout mixture, the water was replaced with *S. pevalekii* cell suspension supplemented with calcium chloride (100 mM) and sodium bicarbonate (25 mM) to the grout mixture.

The grout mixes containing cement without any FA incorporation are designated as control grout. The Hobart-type laboratory mixer (AIMIL India, New Delhi, India) was used to prepare the cement-based fly ash grout. As described by Joshi et al. (2021) a standard procedure was followed for mixing the grout.

Table 2. Outline of composition used in the development of 1,200 g plain (water) and biogrout (*Synechocystis pevalekii* culture) containing a different dosage of FA and cement

S. No.	Cement (g)	Fly ash (g)	*S. pevalekii* culture/water (g)	w/b or c/b	FA (%)
1	1,200	0	540	0.45	0
2	1,080	120	540	0.45	10
3	960	240	540	0.45	20
4	840	360	540	0.45	30
5	720	480	540	0.45	40
6	600	600	540	0.45	50
7	1,200	0	564	0.47	0
8	1,080	120	564	0.47	10
9	960	240	564	0.47	20
10	840	360	564	0.47	30
11	720	480	564	0.47	40
12	600	600	564	0.47	50
13	1,200	0	600	0.50	0
14	1,080	120	600	0.50	10
15	960	240	600	0.50	20
16	840	360	600	0.50	30
17	720	480	600	0.50	40
18	600	600	600	0.50	50

Fresh Properties of Grout Mixture

The cement slurry prepared in the laboratory mixture for grout was immediately used within 5–8 min for different flowability tests. To study the workability and fluidity of cement grout mixture, the marsh cone's flow time, the minislump test, grout bleeding, and setting time were tested (Fig. 1). The Marsh cone flow test was performed to test the grout mixture's flow characteristics as per ASTM C939 (ASTM 2010c). As shown in Fig. 2. after preparing the grout mixture in the laboratory mixer, the experiments were conducted immediately within 5–8 min of preparation. The cementitious grout mix was poured into a metallic V-shaped funnel (capacity of 1,500 cm^3) with a secure vent at the end of the funnel, which is 50 mm long by 4.7 mm in diameter. The outflow time required for 800 mL of grout mix to drift out through the orifice was noted as the flow time. The miniature slump test was done to evaluate the bio-based cement grout's working efficiency by measuring the grout's flow diameter upon lifting the minislump cone. The dimensions of the slump cone were similar to those suggested by Kantro (1980). The accumulation of water above the grout surface is called grout bleeding. Excessive bleeding can devitalize the grout strength by increasing porosity and compromising its durability. The bleeding test was conducted according to the ASTM:C940 (ASTM 2010b). Based on the flowability test, grout mixes with low workability or unmanageable segregation were not selected for further testing.

Slump Flow Retention

To determine the effect of $CaCl_2$ and FA, flow retention time was tested as per ASTM C1437 (ASTM 2015) method described by Kaladharan and Rajabipour (2022) for the grout mixes with maximum workability. The experiment was carried out for plain (without cyanobacterial culture, $CaCl_2$ and $NaHCO_3$) and biogrout (with cyanobacterial culture, $CaCl_2$ and $NaHCO_3$) mixtures at 0.47 w/b and c/b ratio. The flow diameter using minislump cone was determined at a 20-min gap of up to 120 min after the grout mix first come in contact with water. The mixtures were kept in a closed container after the preparation to prevent loss of water due to evaporation. The mixture was remixed for 2 min at 120 rpm before

Downloaded from ascelibrary.org by Indian Institute Of Technology Delhi on 11/27/23. Copyright ASCE. For personal use only; all rights reserved.

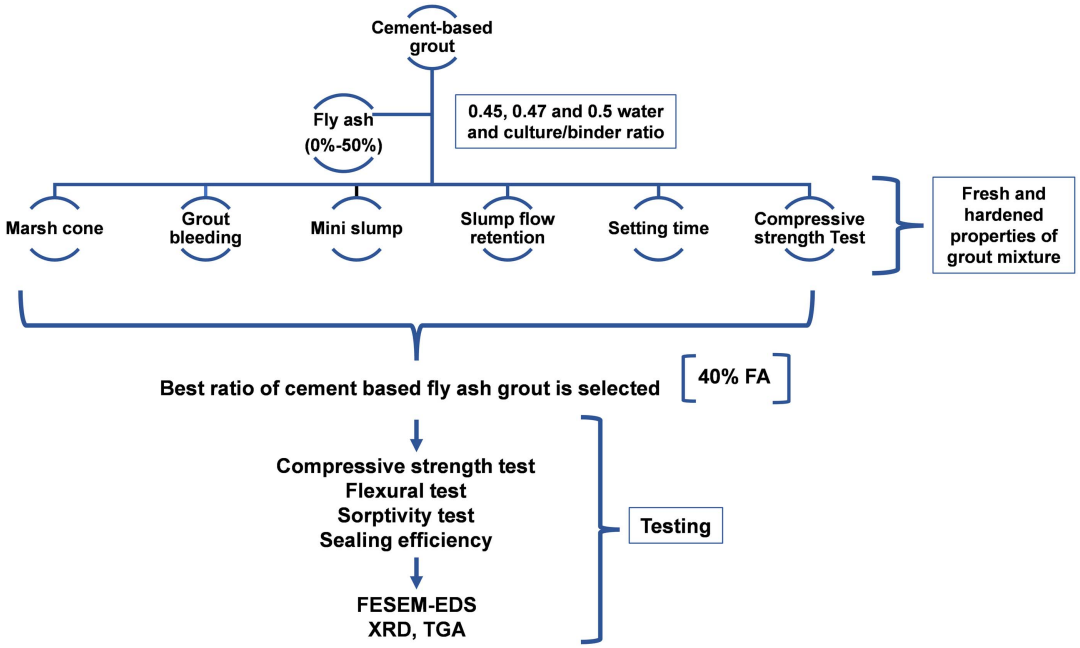


Fig. 1. Outline of different techniques used in the development of biogrout incorporating fly ash (0%–50%) and w/b or c/b (0.45, 0.47, and 0.50) for vertical and horizontal oriented crack remediation.

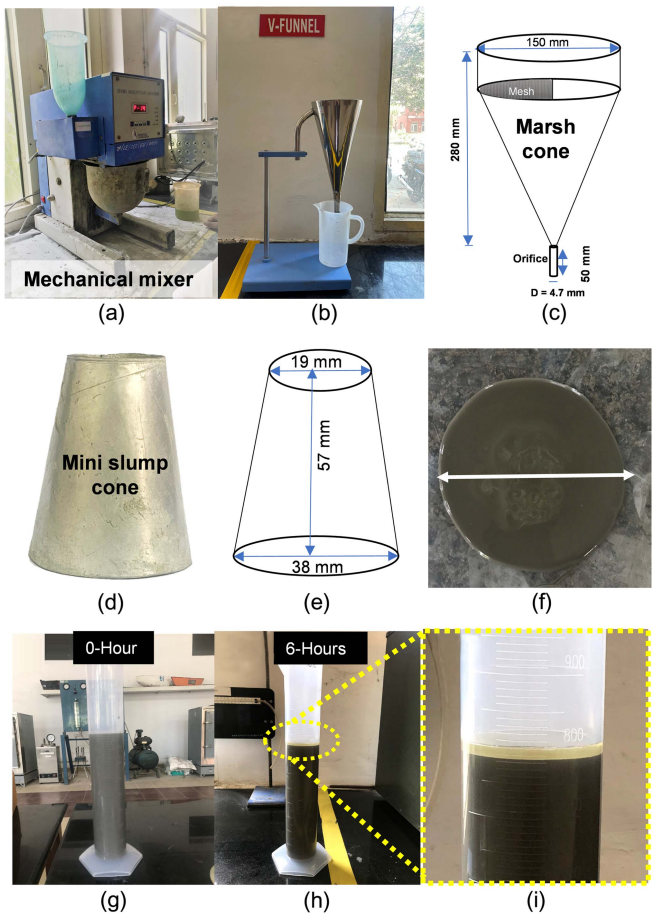


Fig. 2. Study the fresh properties of grout using: (a) mechanical mixer; (b and c) Marsh cone test funnel, and metallic funnel dimensions; (d and e) miniature slump cone and dimensions; (f) flow diameter of fly ash (FA) replaced grout; (g) grout bleeding test at 0 h; (h) grout bleeding test at 6 h; and (i) square shape shows enlarged image grout bleed at 6 h.

each test. Flow diameter of biogrout at each interval was measured by lifting the cone.

Hardened Properties of Grout Mixes

For measurement of setting time and compressive strength, the grout mix of different ratios of FA (0–50) % were used as replacement of cement using 0.47 of c/b and w/b ratio. The initial and final setting time for selected biogrout and plain grout was measured by conducting Vicat needle tests (IS: 4031 (Part 6) (IS 2005). The cube specimens $50 \times 50 \times 50$ mm^3 was cast and demolded after 24 h according to ASTM standard [ASTM:C942 (ASTM 2010a)]. Cube specimens prepared with water grout mixes were designated as plain grout and were cured in water. The cubes prepared with cyanobacterial grout mixes were cured in *S. pevalekii* suspension containing 100 mM $CaCl_2$ (w/v) and 25 mM $NaHCO_3$.

Crack-Embedded Concrete Specimens

To investigate the crack remediation in concrete specimens, prismatic specimens of $500 \times 100 \times 100$ mm^3 for flexural strength, concrete cubes of $150 \times 150 \times 150$ mm^3 (for compressive strength testing) and cylindrical specimens (for water tightness testing) 100 (diameter) $\times$ 50 mm^2 (height) were cast with 0.5 mm width embedded crack. Prismatic and cube specimens were prepared using iron mold of specific dimensions, whereas for cylindrical specimens' polyvinyl chloride (PVC) mold of 100 (diameter) $\times$ 50 (height) mm^2 was used. The lower part of mold was closed with hard board sheet cut with 102 mm diameter to completely cover the lower part of the mold. The mold before adding concrete mix was wrapped with tape to prevent leakage of the mix. Similar protocol was adopted by Joshi et al. (2021) and Anand et al. (2023). The concrete mix was prepared using cement: sand: coarse aggregate in 1:1.82:3.24 (w/w), and the water-to-cement ratio was kept at 0.5. To create an artificial crack, 0.5 mm steel plate was inserted in the concrete specimen, penetrating up to 20 mm immediately

Downloaded from ascelibrary.org by Indian Institute Of Technology Delhi on 11/27/23. Copyright ASCE. For personal use only; all rights reserved.

after pouring the concrete mix. The specimens were monitored until the initial setting of concrete, after which the steel plate was removed carefully such that the concrete surrounding the crack remained uninterrupted and unbroken. All the specimens were kept at room temperature of 27°C ± 2°C for 24 h until demolding. Later, all the specimens were cured in water for up to 28 days.

Crack Remediation with Bio-Based Cement Grout

After curing, crack-damaged concrete specimens were restored using 40% FA amended biogrout. The crack repair technique was divided into two different approaches; horizontal and vertical oriented healing (Fig. 3). In the first approach, the specimens were placed such that crack was in a horizontal position, whereas in another approach, the specimens were positioned vertically. The orientation has been selected on the basis of lab-scale study and field requirement. Though at lab scale, both treatment; horizontal (ponding) and vertical (spray) are feasible. However, in certain circumstances specifically in field, vertical injection treatment would be more applicable than the horizontal treatment. In both methods, the biogrout and plain grout were injected using a 20 mL syringe. Before injection, the cracked surface was thoroughly wetted to mitigate the moisture absorption during grouting. The direction of injection was from one direction to other. In vertical orientation, the crack was filled from bottom to top to uniformly fill the grout in cracked region. Once the biogrout and plain grout were injected horizontally and vertically, the specimens were left uninterrupted for 24 h to harden. Biogrout repaired specimens were cured by *S. pevalekii* cells suspended in calcifying solution (100 Mm $CaCl_2$ and 25 Mm $NaHCO_3$) by ponding (horizontal healing) and spray treatment (vertical healing). Control specimens were cured using water both by ponding and spray treatment. The specimens were divided into three different categories. First, as control uncracked concrete specimen, secondly, plain grout without any cyanobacterial suspension both placed horizontally and vertically. Third, biogrout repaired specimens with horizontal and vertical healing, as presented in Table 3. All the specimens were placed under the artificial light source of 1200 lux for a photoperiod of 12:12 h (light:dark). In the present investigation, atmospheric CO_2

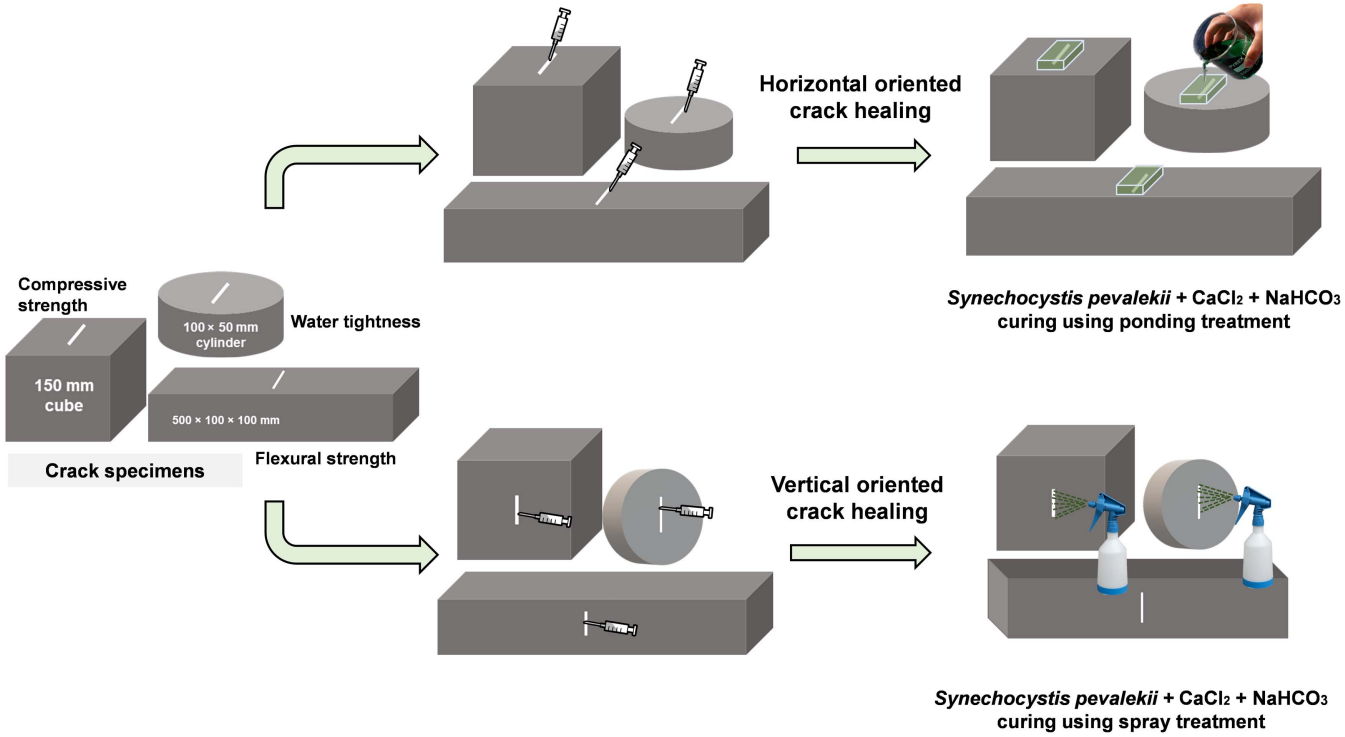


Fig. 3. Graphical representation of the vertical and horizontal oriented crack remediation using *Synechocystis pevalekii* cell culture supplemented with calcifying solution ($CaCl_2 + NaHCO_3$).

Table 3. Outline of different sets of repairing techniques using FA amalgamated cement-based grout specimens and mechanism of curing

Label	Specimens	Grouting material	W/b or C/b ratio	Curing method (28 days)
UTC	Untreated cracked concrete	Without grouting	Without grouting	Water curing
REF	Uncracked concrete	Without grouting	Without grouting	Water curing
CST	Plain grout—control spray treatment	FA (40%) cement (60%)	W/b ratio = 0.47	Water curing (spray-on repaired crack thrice a day)
CPT	Plain grout—control ponding treatment	FA (40%) cement (60%)	W/b ratio = 0.47	Water curing of the repaired area with ponding
BST	Biogrout—spray treatment	FA (40%) cement (60%)	C/b ratio = 0.47	*S. pevalekii* culture (BG11 medium + 100 mM $CaCl_2$ + 25 mM $NaHCO_3$) spray curing thrice a day
BPT	Biogrout—ponding treatment	FA (40%) cement (60%)	C/b ratio = 0.47	Ponding with *S. pevalekii* culture (BG11 medium + 100 mM $CaCl_2$ + 25 mM $NaHCO_3$)

Downloaded from ascelibrary.org by Indian Institute Of Technology Delhi on 11/27/23. Copyright ASCE. For personal use only; all rights reserved.

was taken into account for the experiment. As per Stein (2022) and Shi et al. (2020) concentration of atmospheric carbon dioxide (CO_2) in air is in range of 410–421 ppm. Concrete specimens $500 \times 100 \times 100$ mm^3 and 150 mm cube was tested for flexural and compressive strength as per the Indian standards [IS 516:2014 (IS 2004)]. Concrete cylindrical specimen 100 (diameter) × 50 (height) mm^2 was tested for evaluating the water tightness ASTM C1585 (ASTM 2013). However, the modification was done for testing the water tightness, only crack repaired (70×30) mm^2 region of the 100 (diameter) × 50 (height) mm^2 cylindrical specimen was exposed for water absorption test. The rest of the area was covered with the epoxy sealant. The sealing efficiency of the crack-healed specimens using plain and biogrout was evaluated for 70 (length) × 30 (width) mm^2 area cylinder specimens by calculating the water absorption at 6 h using the equation [Eq. (4)] as described by Liu et al. (2020)

$$SE(\%) = \frac{Q_0 - Q_g}{Q_0} \times 100 \quad (4)$$

where SE represents the sealing efficiency of grout, Q_0 is designated as initial water absorption before grouting, and Q_g = water absorption after grouting.

Microstructural Analysis

The crystals' morphology, characterization, and size were identified using a field emission scanning electron microscope (FESEM). To further elaborate on the elemental composition of the crystals, the energy dispersive spectroscopy (EDS) was done at 28 days, for which a small piece of the sample was collected from the biogrout and plain grout specimens after curing the crack-healed grouted specimens at 28 days. To analyze the crystal composition and identification, the XRD was performed using powdered samples collected from the biogrout and plain grout samples.

Statistical Analysis

All the experiments were performed in triplicates. The data were analyzed by analysis of variance, and significant differences among the means were compared by the Tukey test $p < 0.05$. All the analyses were performed using GraphPad Prism (version 9.2.0) software.

Results and Discussion

Calcium Carbonate Precipitation and pH Dynamic

Biomineralization is a result of the photosynthetic activity of cyanobacteria in the presence of carbon dioxide (CO_2) and light. The calcium carbonate ($CaCO_3$) precipitation showed an increasing trend until 196 h of study. The precipitation recorded in the controlled laboratory conditions initially at 2 h interval was 77, 132.67, 180, 214, 252.34, 283.67, and 311 mg/mL (Fig. 4). After 24 h the precipitation in the BG11 medium was increased to 406.7 mg/mL. The precipitation was constantly occurring in the flask by *S. pevalekii* BDHKU 35101 strain during 196 h of study due to a phototrophic reaction. Cyanobacteria used calcium chloride provided in the medium as the source of calcium and formed carbonate ions using illumination light source. Simultaneously, the amount of calcium removal from the medium was evaluated based on the presence of calcium ions in the supernatant extracted at different

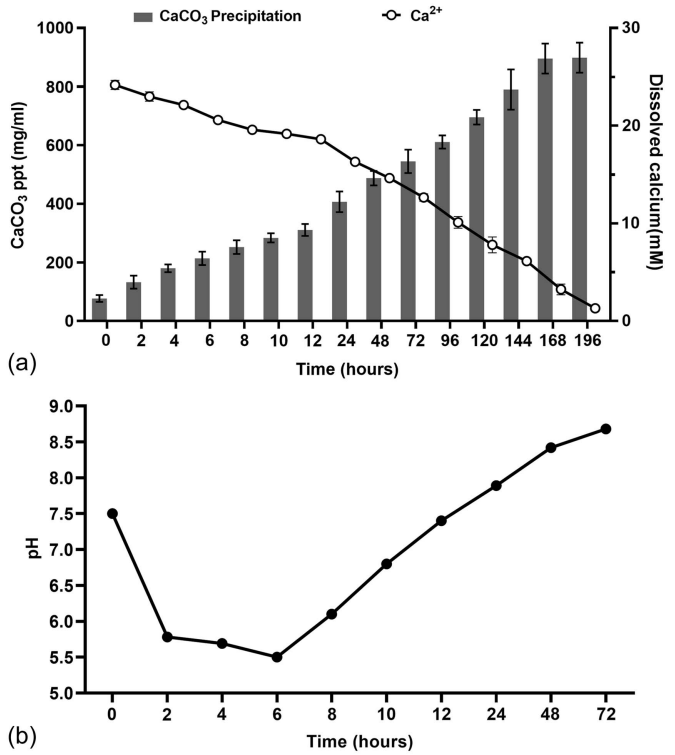


Fig. 4. (a) Calcium carbonate precipitated and amount of Ca^{2+} ions present in the BG11 medium due to the photosynthetic reaction by *S. pevalekii* BDHKU 35101; and (b) change in pH of the medium until 72 h of incubation at 25°C ± 0.2°C.

interval of time. As observed in Fig. 4, the amount of soluble Ca^{2+} ions in the medium decreased with the calcium carbonate precipitation. At 24 h, the BG11 medium flask incubated at 25°C ± 0.2°C showed 7.7 mM of the calcium removal from the medium due to the binding of calcium with bicarbonates (HCO^{3-}) in the media to form calcium carbonate; the calcium ions present in the medium were less than 1.5 mM even after 196 h of the study.

Calcification in the flask under illumination was directly concurred with a small increase in pH that occurred after 8 h of sampling period. Initially, pH was 7.5 ± 0.2 which dropped sharply to 5.78, after injecting $CaCl_2$, this may be due to the change of speciation in the solution. Calcium chloride when added to the media it absorbs hydroxide and leaves free protons behind. This lowers the pH of the media. The photosynthetic metabolism of the cyanobacterial strains was directly responsible for the alkalinization of the experimental microenvironment because the pH did not increase in any of the control samples. pH of the medium was monitored for 72 h. Slight increase in pH of the medium was observed from 5.50 after 6 h to 6.10 after 8 h (Fig. 4). pH increased in the cultural flask under laboratory conditions with white color precipitation observable in the flask. Sudden surge in the pH after the fall of pH was observed due to exchange of HCO^{3-}/H^+ across the cell membrane (Miller and Colman 1980). During photosynthesis, CO_2 is synthesized to form organic matter and bicarbonate is converted to form CO_2 and OH^- (also called CO_2 concentration mechanism). The OH^- is then released into the solution which increases the pH of the medium (Zhu and Dittrich 2016). Precipitation of calcium carbonate in solution was confirmed by the EDTA titration. Zhu et al. (2018) also reported drop in the pH from 8 to 30 h in BG 11 medium due to $CaCO_3$ precipitation by *Synechocystis* sp. These

Downloaded from ascelibrary.org by Indian Institute Of Technology Delhi on 11/27/23. Copyright ASCE. For personal use only; all rights reserved.

results were in accordance with the finding of Han et al. (2013) who reported maximum carbonate precipitation at pH 10 and 100 mg/1 Ca^{2+} concentration by *Synechocystis sp*. PCC6803. Similar results were documented by (Han et al. 2017b; Liang et al. 2013; Novitsky 1981; Obst et al. 2009).

Fresh Properties of Grout Mixes

Cement grout (CG) is a mix of cement and water in well-defined water-to-binder ratio (w/b). To develop injectable grout, fly ash (FA) is taken as a partial cement replacement to repair the cracks in cementitious structures. The influence on the fresh properties of grout mixtures with varying proportions of FA (10%–50%) and different water and cyanobacterial culture, binder ratios (0.45, 0.47, and 0.50) was investigated using different flowability tests to confirm the injectable property of grout.

Marsh Cone Test

The Marsh cone test was conducted within a few seconds after the preparation of the mixture. The time required for an 800 mL grout mixture to flow through the cone is correlated to the viscosity of the cement-based grout, signifying that the longer the flow time, the less is fluidity of the grout mixture. In all six experiment groups of 36 grout mixes, the flow time for the marsh cone test was higher in all the control sets designated as plain grout. With substituting cyanobacterial culture instead of water, the flow time was observed to reduce in culture/binder ratio (c/b) of 0.47 and 0.5. Still, viscosity was detected to be higher in the 0.45 c/b ratio; consequently, flow time was observed to be higher. It might be due to the thickness formed due to the low c/b ratio. The viscosity of the grout mixes increases upon the addition of $CaCl_2$ and $NaHCO_3$, reducing the grout mix's flow time through the orifice. Increasing the c/b ratio to 0.47 and 0.5, the flow rate of the grout mixture showed a comparative less flow time because of a reduction in the viscosity. The decreased flow time of 57, 53, 51, 48, 45, and 67 s was observed with an increased FA dosage in biogrout with a 0.47 c/b ratio. Fig. 5(a) shows decreasing trend of the flow time with an increase in the FA dosage (10%–40%) but a rapid surge in flow time at 50% FA replacement. It is important to understand that FA act as plasticizing material for cement-based grout, improving the flowability of the mixture inside the crack. However, at higher concentrations (50%), the substitution of FA for the surface area of the cement-based grout increases, demanding an increase in w/b or c/b. The statistical analysis showed that FA (0%–50%) and grout's water/culture to binder ratio (0.45, 0.47, and 0.50) have a significant effect on the flow time of the plain grout and biogrout (Table 4). Similar results were corroborated by Joshi et al. using CT5 bacterial culture at 40% FA replacement (Joshi et al. 2021). Li et al. (2017) also reported a decrease in the flow time by a decrease in the viscosity on increasing the dosage of microfine fly ash (MFA). The optimum percentage of fly ash replacement recommended is 30%–40% (Li et al. 2017). However, Sha et al. (2018) recommended the optimum percentage of FA as 20%–30% in geotechnical engineering.

Minislump Test

A miniature slump test is used to examine fresh cementitious paste's workability using a small cone with dimensions of a top diameter of 19 mm, bottom diameter of 38 mm, and height of 57 mm. The spread diameter of the cementitious paste was calculated by lifting the minislump cone. Fig. 5(b) illustrates the spread flow diameter of grout mixtures with different w/b and c/b ratios and FA substitutions. As observed, the diameter in the control mix (0% FA) designated as plain grout increased by 49.4% when the w/b ratio increased from 0.45 to 0.5. The spread diameter of the biogrout mixture increased by 46.42% upon increasing the 0.45–0.5, which is comparatively lower than the control grout. This might be because of the increased thickness of biogrout as calcium chloride, and sodium bicarbonate are added to grout mixture. However, integrating FA with cement in increased quantities (10%–50%) resulted in a considerable increase in minislump flow diameter in all grout mixes, indicating an improvement in fluidity. It significantly improved the flow diameter by 50.54% on the substitution of 40% FA replacement; however, additional FA replacement (50%) lowers the grout spread diameter to 46.87%. Here, FA acts as a lubricating agent because of its smooth texture and spherical particle shape, which enhances the rolling capacity and flowability between the cement particles and cyanobacterial culture, resulting in ball bearing effect reducing the inter-particle friction (Çınar et al. 2019; Razi et al. 2016). The flow diameter of the grout mixture at a c/b ratio 0.47 the diameter observed was 131, 130, 129, 133, 133, and 123 mm compared with plain grout, which showed the flow diameter 111, 111, 114, 117, 122, and 122 mm. Correspondingly, the flow diameter of the 0.47 c/b ratio grout mixture was in the range of 88–140 mm and 98–142 mm when the c/b ratio was 0.5. The analysis of variance inferred that enhancement in water/culture binder ratio and FA substitution had a significant effect on the grout mixture (Table 4). Çinar et al. (2019) investigated and reported an increase in minislump flow with an increase in the dosage concentration of fly ash (5%–25%) and waste marble powder (5%–25%) for cement-based grout.

Grout Bleeding

After 6 h of sedimentation with various w/b and c/b ratios (0.45, 0.47, and 0.50), the bleed volume was measured for all the grout mixtures. Fig. 5(c) signifies the increase in percentage bleed of 36 grout mixture with an increase in w/b and c/b ratio; however, grout bleeding decreased with an increase in FA dosage (0%–50%). The percentage of grout bleeds increased from 3.1% to 4.3% in plain grout as the w/b ratio increased from 0.45 to 0.50. With the increase in FA dosage, the grout bleeding percentage decreased gradually in plain grout from 3.1% to 0.4% with a 0.45 w/b ratio, 3.0%–1.2% with a w/b ratio of 0.47, and 5.31%–3.18% with 0.50 w/b ratio. Similar results were recorded for biogrout. For instance, in a c/b ratio of 0.47, the bleeding rate dropped from 3.6% to 0.6%. The maximum bleed percentage in all six experimental setups was observed in a water and culture/binder ratio of 0.50, followed by 0.47. The lowest grout bleeding (0.2%) was evaluated in 40%, and 50% substituted FA biogrout with a c/b ratio of 0.45, which was considered a minor bleed. Bleed percentage value less than 2% after 3 h of sedimentation is considered stable for selecting the best grout mixture for geotechnical application [ASTM C940 (ASTM 2010b)]. Significant variation was observed among the different dosages of FA (0%–50%) and culture/water ratio (0.45, 0.47, and 0.50) of grout on the grout bleeding percentage of the plain and biogrout, as shown in Table 4. Vasumithran et al. (2020) also reported an increase in grout bleed with an increase in the w/b ratio. Reduced bleeding of FA-incorporated grouts can be attributed to lessened porosity and improved packing density (Azima and Bundur 2019).

The 0.45, 0.47, and 0.50 water or culture to binder ratio (w/b or c/b) and (0%–50%) fly ash as partial replacement of cement in grout mixes were tested for the fluidity [ASTM C939 (ASTM 2010c)], minislump and grout bleeding [ASTM:C940 (ASTM 2010b)]. The grout mixes of 0.5 water or culture to binder ratio showed high bleeding at 0%–50% FA replacement as per the ASTM

Downloaded from ascelibrary.org by Indian Institute Of Technology Delhi on 11/27/23. Copyright ASCE. For personal use only; all rights reserved.

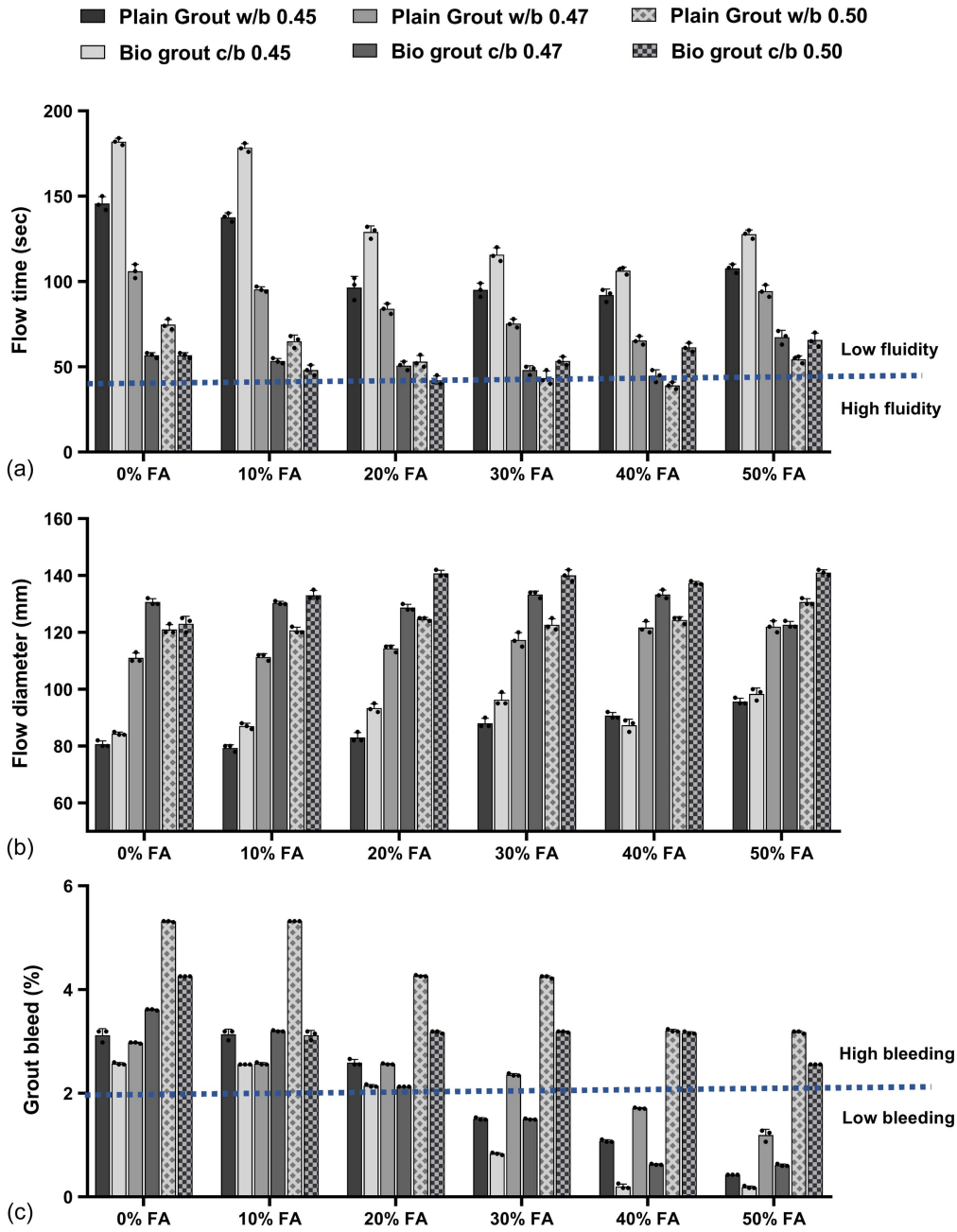


Fig. 5. Fresh properties of grout: (a) Marsh cone; (b) minislump cone; and (c) grout bleeding test analysis of fluidity of grout mixtures incorporated with different dosages of fly ash (FA); water/binder (w/b) ratio and culture/binder (c/b) ratio. The line differentiates high and low fluidity for Marsh cone test and low (stable) and high (unstable) grout bleed percentages. Individual data points are shown in each bar. Error bars represents standard deviation (n = 3).

standard [ASTM:C940 (ASTM 2010b)] and therefore, this grout mix was rejected for further investigation. However, some of the grout mixes prepared by 0.45 and 0.47 w/b or c/b showed good fluidity and low bleeding. Out of these grout mixes (0.45 and 0.47), 0.47 showed higher fluidity with the slump value of 133 mm, whereas 0.45 showed maximum slump diameter of 98 mm. As described in Table 4, the flow time at 0.45 w/b or c/b ratio was comparatively higher than the 0.47 w/b or c/b ratio [ASTM C939 (ASTM 2010c)]. Because fluidity is an important parameter for the penetrability of biogrout in the depth of crack; therefore, 0.47 w/b or c/b ratio of the grout mixes was selected for the further studies. The selected grout mixes (0.47 w/b or c/b) were further tested for flow retention and hardened properties with varied replacement of FA.

Slump Flow Retention

Fig. 6 presents the minislump flow diameter of the plain and biogrout with w/b (and c/b) ratio of 0.47. The workability flow retention of plain and biogrout mix was tested at 20-min intervals until 120 min. Initial flow diameter of the control mix (0% FA) of plain and biogrout mix is 111 and 132 mm, indicating that the addition of cyanobacterial culture along with the calcifying solution significantly affects the grout's flowability property. Inclusion of FA

Downloaded from ascelibrary.org by Indian Institute Of Technology Delhi on 11/27/23. Copyright ASCE. For personal use only; all rights reserved.

Table 4. Fresh properties Marsh cone, minislump cone, and grout bleeding of grout mixtures incorporated with different dosages of fly ash (FA); water/binder (w/b) ratio; and culture/binder (c/b) ratio

		Fresh properties of grout mix						
		Marsh cone (s)		Minislump (mm)		Grout bleeding (%)		
Grout mixes	w/b	Plain grout	Biogrout	Plain grout	Biogrout	Plain grout	Biogrout	Remarks
0	0.45	146	182	81	84	3.1	2.6	Rejected
10	0.45	138	178	79	87	3.1	2.6	Rejected
20	0.45	96	129	83	93	2.6	2.1	Rejected
30	0.45	95	116	88	96	1.5	0.8	Rejected
40	0.45	92	106	91	87	1.1	0.2	Rejected
50	0.45	108	128	96	98	0.4	0.2	Rejected
0	0.47	106	57	111	131	3.0	3.6	Selected
10	0.47	95	53	111	130	2.6	3.2	Selected
20	0.47	84	51	114	129	2.6	2.1	Selected
30	0.47	75	48	117	133	2.4	1.5	Selected
40	0.47	65	45	122	133	1.7	0.6	Selected
50	0.47	94	67	122	121	1.2	0.6	Selected
0	0.50	75	56	121	123	5.3	4.3	Rejected
10	0.50	65	48	121	133	5.3	3.1	Rejected
20	0.50	53	42	125	141	4.2	3.2	Rejected
30	0.50	43	53	123	140	4.2	3.2	Rejected
40	0.50	39	61	124	137	3.2	3.2	Rejected
50	0.50	54	66	131	141	3.2	2.6	Rejected

content from 0% to 50% in cementitious grout (plain and biogrout) showed increase in flowability of grout but decreased with progressive time interval. As shown in Fig. 6(b), biogrout with 40% partial replacement, had initial slump flow diameter of 145 mm which declined to 137 mm at 60 min and 131 mm at 120 min showing 9.6% decrease in workability retention. On the other hand, plain grout with 40% FA substituted cementitious grout showed 13.1% decline in workability retention of the grout at 120 min [Fig. 6(a)]. This can be attributed to the fact that cyanobacteria are in spherical shape which increases the flowability of biogrout when added along with spherical shaped fly ash. Due to the ball bearing effect of fly ash the interparticle friction between cyanobacteria, fly ash and cement are reduced (Çınar et al. 2019). Therefore, the addition of calcifying solution ($CaCl_2$ and $NaHCO_3$) in the presence of cyanobacteria did not retard the flowability of the grout during 120 min study. Similar study was carried out by (Kaladharan and Rajabipour 2022; Khalid et al. 2016; Nair et al. 2020).

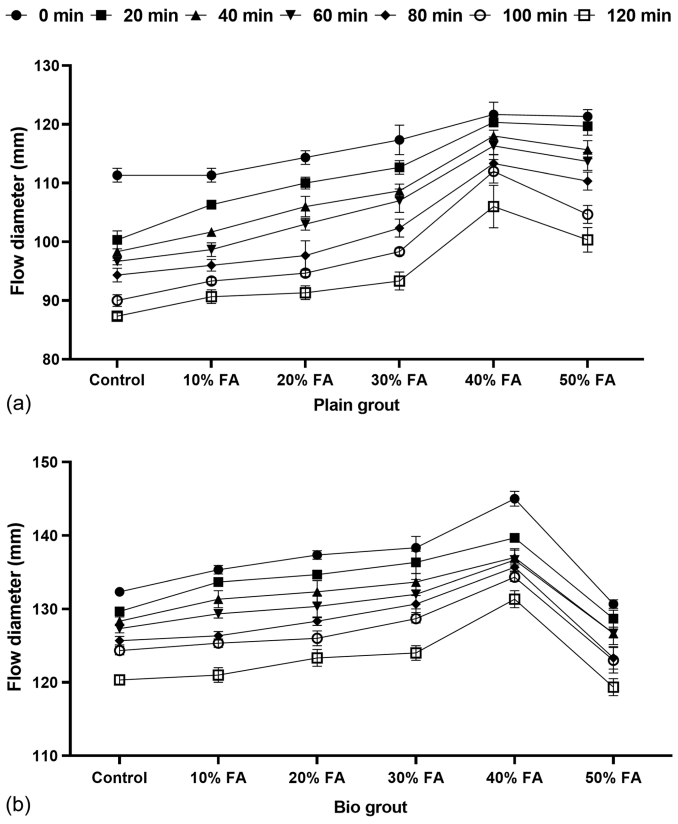


Fig. 6. Flow retention diameter of: (a) plain grout; and (b) biogrout partially replaced with different concentrations of fly ash at different time intervals.

Setting Time

Using a Vicat apparatus, the setting time of FA amalgamated cement-based biogrout was tested for a w/b and c/b ratio of 0.47. As shown in Fig. 7 initial setting time of biogrout prepared by *S pevalekii* cells gradually increased by 50 min on replacement of fly ash from 0% to 50%, whereas the final setting time of biogrout increased by 30 min. The initial setting of the plain grout increased by 4%, 5%, 12%, and 14% upon increasing the dosage of FA from 20%, 30%, 40%, and 50%, respectively. At the same time, the initial setting time of biogrout increased by 1.8%, 1.8%, 3.7%, 9.4%, and 21.15% upon increasing the dosage of the FA 10%, 20%, 30%, 40%, and 50%. The substitution of fly ash in the cementitious mixture increases the initial and final setting time of both biogrout and plain grout, which encourages lowers flowability loss. This accounts for the fact that as the dosage of FA increases in the grout, the surface area for the attachment of calcium ions (Ca^{2+}) increases which further declines the augmentation of the Ca^{2+} in the fresh paste during the primary stage of hydration. Because of this, the heat of hydration decreases, resulting in an increase in the final setting time of the cement-based grout mixture (Yijin et al. 2004; Zhang et al. 2019). Moreover, there is limited time available for transportation and injecting the grout; therefore, it is crucial to maintain grout hydration. As a result, the initial

Downloaded from ascelibrary.org by Indian Institute Of Technology Delhi on 11/27/23. Copyright ASCE. For personal use only; all rights reserved.

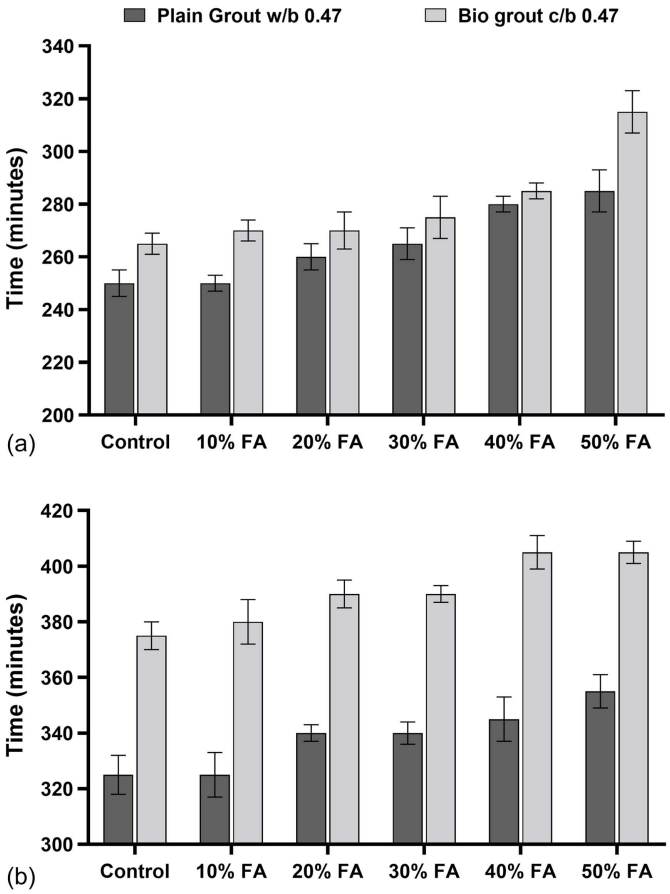


Fig. 7. (a) Initial; and (b) final setting time of FA (0%–50%) incorporated plain and biogrout at w/b and c/b ratio 0.47.

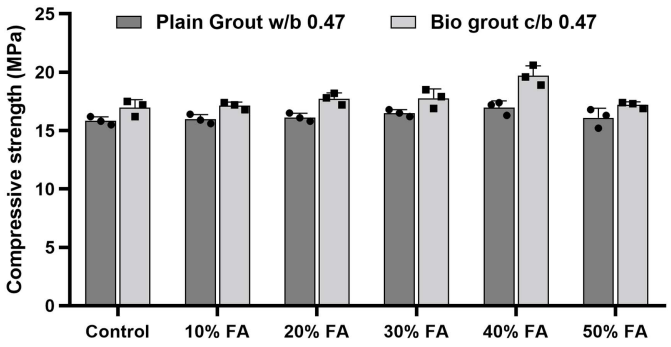


Fig. 8. Compressive strength of FA (0%–50%) incorporated plain and biogrout at w/b and c/b ratio 0.47 after 28 days of curing. Individual data points are shown in each bar. Error bars represents standard deviation (n = 3).

setting time helps to determine the efficacy of cyanobacterial culture in the grout. Choi et al. (2012) also attributed the decrease in temperature to an increase in the percentage of FA due to delayed pozzolanic interaction of the fly ash with the hydrating cement's calcium hydroxide. They further added that the more the percentage of FA, the more decline in the temperature would be observed. Overall, the initial setting time for a biogrout was observed to be higher than the plain grout, which could be explained by the fact of adding cyanobacterial culture along with $CaCl_2$ and $NaHCO_3$ and increasing the concentration of FA (10%–50%) in the grout.

Furthermore, it was noted that the final setting time of FA replaced biogrout and plain grout was attained in less than 90 min after reaching the initial setting time. Two-way ANOVA verified that different fly ash dosage significantly affects the setting time of the plain and biogrout along with the water/culture to binder ratio (0.47).

Effect of Fly Ash Dosage on Compressive Strength of Grouts

The compressive strength of the grout mixture was analyzed for the 0%–50% FA substitution by keeping the w/b or c/b ratio 0.47. It was noted that at 28 days, the compressive strength of control plain grout increased from 15.8 to 17.0 MPa with an increase in FA dosage up to 40% but declined to 16.1 at 50% dosage (Fig. 8). The maximum compressive strength was reported in plain and biogrout mixtures with 40% FA integration.

From Fig. 8. it is evaluated that replacing *S. pevalekii* culture with water results in strength gain. It was noted that *S. pevalekii* treatment increases the strength of almost all the cyanobacterial grout mixtures compared with the plain control mix. Maximum strength gain was noted in 40% FA incorporated biogrout (19.7 MPa); however, upon further increasing FA dosage, the strength of biogrout declined to 17.2 MPa. The compressive strength for 0%, 10%, 20%, 30%, 40%, and 50% biogrout increased by 7.5%, 6.9%, 10%, 7.9%, 15.9%, and 6.9%, respectively. The results indicate that overall strength improvement was observed among all the biogrout due to cyanobacterial treatment. It could be due to the calcification by cyanobacterial culture, reducing the pore size and improving the compressive strength of the specimens. Similarly, others researchers have reported significant improvement in the compressive strength of cementitious material upon curing with the cyanobacterial culture (Sidhu et al. 2022; Zhu et al. 2017). Likewise, Zhang et al. (2020) also reported an increase in cement-based grout compressive strength upon adding (10%–30%) fly ash along with water glass and bentonite. The analysis of variance proved that fly ash variation significantly affects the compressive strength of the grout (Table 5).

Selecting the Best Cement-Based Biogrout

The best grout mixture with 40% FA substitution and 0.47 culture to binder ratio was selected for crack remediation based on the best results obtained from setting time and compressive strength as presented in Table 6. The strength of the grout depends on the substitution of fly ash and the culture/binder ratio. The flowability test ensures best injectability in the crack vertically and horizontally using a syringe; whereas strength of grout ensures better mechanical properties of the repaired surface.

Crack Remediation and Testing

The pre-cracked concrete specimens ($500 \times 100 \times 100$ mm^3 prismatic, $500 \times 500 \times 500$ mm^3 cube, and 100×50 mm^2 cylindrical specimen) were repaired using two different grout mixtures—plain grout and biogrout. The specimens repaired using 40% FA replaced cement plain grout were categorized as control specimens and were divided on the basis of curing treatment ponding (CPT) and spray (CST). The other group was repaired using 40% FA replaced cement biogrout incorporating *Synechocystis pevalekii* culture (Fig. 9). The specimens were subjected to curing treatment using *Synechocystis pevalekii* cell culture supplemented with calcifying solution ($CaCl_2 + NaHCO_3$) spray (BST) and ponding treatment (BPT) for

Downloaded from ascelibrary.org by Indian Institute Of Technology Delhi on 11/27/23. Copyright ASCE. For personal use only; all rights reserved.

Table 5. The factorial ANOVA results indicating the effects of different concentrations (0%–50%) of fly ash (FA) and water/binder (w/b) or culture/binder (c/b) ratio on injectable grout in a crack

Variables	Degree of freedom	Fly ash (FA)	w/b and c/b ratio	FA × w/b and c/b ratio
Marsh cone test	df	5, 72 $p < 0.0001$	5, 72 $p < 0.0001$	25, 72 $p < 0.0001$
Minislump test	df	5, 72 $p < 0.0001$	5, 72 $p < 0.0001$	25, 72 $p < 0.0001$
Grout bleed percentage	df	5, 72 $p < 0.0001$	5, 72 $p < 0.0001$	25, 72 $p < 0.0001$
Initial setting time	df	5, 24 $p < 0.0001$	1, 25 $p < 0.0001$	5, 25 $p = 0.01$
Final setting time	df	5, 24 $p < 0.0001$	1, 25 $p < 0.0001$	5, 25 ns
Compressive strength	df	5, 24 $p < 0.0001$	1, 25 $p < 0.0001$	5, 25 ns

Note: The p values <0.001 indicate the values are highly statistically significant; df = degree of freedom; and ns = non significant.

Table 6. Hardened properties (setting time and compressive strength) of the 0.47 w/b and c/b grout mix at different dosage of fly ash (0%–50%)

		Hardened properties						
		Initial setting time (min)		Final setting time (min)		Compressive strength (MPa)		
Grout mixes	w/b	Plain grout	Biogrout	Plain grout	Biogrout	Plain grout	Biogrout	Remarks
0	0.47	250	265	325	375	15.83	17.0	Rejected
10	0.47	250	270	325	380	15.97	17.1	Rejected
20	0.47	260	270	340	390	16.13	17.7	Rejected
30	0.47	265	275	340	390	16.50	17.8	Rejected
40	0.47	280	285	345	405	16.97	19.7	Selected
50	0.47	285	315	355	405	16.10	17.2	Rejected

28 days (Fig. 9). Once the grout's curing cycle is complete, the flexural strength, compressive strength and water sorptivity of the specimens were assessed. The uncracked specimens (REF) and cracked specimens without treatment (UTC) were taken into account to compare the strength and sorptivity efficiency of the biogrout and plain grout treated specimens.

Compressive Strength

The compressive strength results for the six different sets of concrete specimens are shown in Fig. 10(a). The compressive strength of UTC (untreated cracked concrete specimens) without any grout repairing was 30.8 MPa. The highest compressive strength (41.82 MPa) was observed in biogrout repair with ponding curing treatment (BPT), followed by 38.94 MPa strength in fly ash amended plain grout with ponding treatment (CPT). Compared with UTC, BPT showed a substantial enhancement of 35.78% due to biocalcification by *S. pevalekii* cells in the presence of sodium bicarbonate and calcium chloride; whereas the BST specimen showed the corresponding increase of 23.82%. The compressive strength of the uncracked concrete specimen (designated as REF) was 38.32 MPa. The BPT specimen showed 9.1% improvement in compressive strength than the REF specimen. Therefore, the 40% FA substituted biogrout confirms the improvement in the compressive strength of the concrete specimens by using *S. pevalekii* culture. The statistical analysis depicts a significant improvement in compressive strength compared with the UTC by the BPT, BST, CPT, and CST. Moreover, the BPT and BST specimens showed more remarkable strength improvement than CPT and CST specimens. The $CaCO_3$ crystals fill the voids between the FA and cement particles. It is likely to provide additional strength to the repaired specimens.

An increase in the calcium and calcite content due to the addition of cyanobacteria could be the main reason for enhancing the concrete's strength. Osman et al. (2021) also conferred similar results using two different species, *Bacillus pasteurii*, *B. sphaericus*, and algal species *Dunaliella salina.* The authors further claimed that the significant enhancement of the compressive strength resulted from $CaCO_3$ precipitation upon introducing the algal species. Joshi et al. (2021) reported ponding and spray treatment to be best for bioconsolidation of the biogrout prepared by incorporating 40% FA replacement mixed with *Bacillus* culture in the cement grout. Heveran et al. (2020) used *Synechococcus* sp. PCC 7002 to develop living building material (LBM), which has adequate fracture toughness due to calcium carbonate precipitation. Another researcher Srinivas et al. (2021) reported efficient crack healing efficiency by two microalgae species, namely, *Synechococcus elongatus* and *Spirulina platensis*.

Flexural Strength

As shown in Fig. 10(b), the regain in the flexural strength was observed at 28-day of curing after the specimens were repaired

Downloaded from ascelibrary.org by Indian Institute Of Technology Delhi on 11/27/23. Copyright ASCE. For personal use only; all rights reserved.



Fig. 9. Crack remediation using plain and biogrout: (a) cracked specimen; (b) injecting grout using 20 mL syringe; (c) repaired crack before curing; (d and e) calcium carbonate precipitation after 7 and 28 days of curing; (f) crack healed area after removal of additional carbonate precipitates; and (g and h) pictorial representation of curing treatment (spray and ponding).

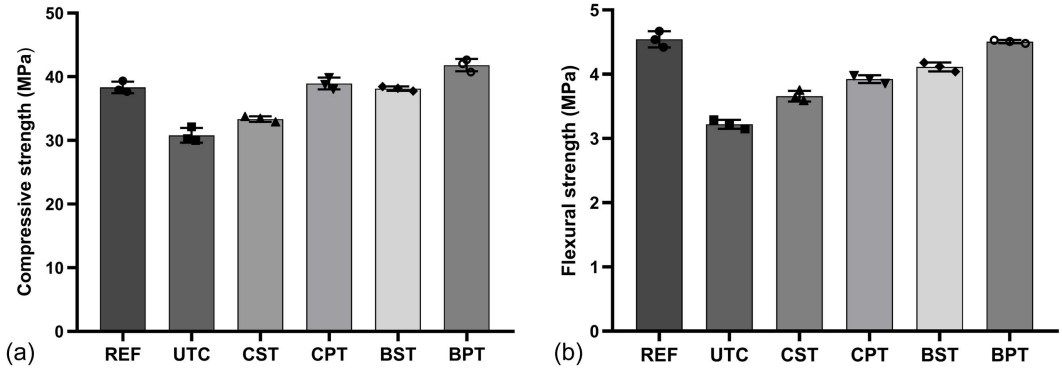


Fig. 10. (a) Compressive strength; and (b) flexural strength of REF: reference concrete specimen; UTC: untreated concrete; CST: plain (control) grout spray treatment; CPT: plain (control) grout ponding treatment; BST: biogrout with spray treatment; and BPT: biogrout with ponding treatment at 28 days of curing. Individual data points are shown in each bar. Error bars represent standard deviation (n = 3).

using plain and biogrout. The maximum regain in the flexural strength was observed in BPT (Biogrout treated) specimens, followed by BST, CPT, and CST specimens. The test results of the biogrout and plain grout-treated specimens were compared with the REF (uncracked) and UTC (unrepaired or untreated crack) specimens for better clarification of strength regain. It was observed that the flexural strength for REF and UTC specimens was 4.54 and 3.22 MPa, respectively. The flexural strength recorded

Downloaded from ascelibrary.org by Indian Institute Of Technology Delhi on 11/27/23. Copyright ASCE. For personal use only; all rights reserved.

after 28-day of curing in BPT, BST, CPT and CST specimens were 4.50, 4.11, 3.92, and 3.65 Mpa, respectively. The recovery of strength was evaluated in relation to UTC. The biogrout treated specimens (BPT and BST) showed 28.4% and 27.6% recovery in flexural strength of the concrete specimens. In case of the control specimens; CPT and CST showed only 21.7% and 13.35% recovery of flexural strength, respectively. It was observed that BPT and BST specimens outperformed the CPT and CST specimens in strength improvement. It can be due the precipitation of calcium carbonate by *S. pevalekii* cells in the presence of sodium bicarbonate and calcium chloride in the biogrout treated specimens, which had further strengthened the grout filling in the crack. It was confirmed using the statistical analysis that BPT, BST, CPT, and CST specimens showed significant recovery in the flexural strength with the UTC at a 5% level of significance. Similar results were also corroborated by Xu et al. (2020), Xue et al. (2020), and Kanwal et al. (2022) in self-healing concrete specimens. Feng et al. (2021) also reported 14% recovery in flexural strength in 0.3 mm crack healed specimens at 28 days of curing.

Water Tightness

Fig. 11 illustrates the effect of MICCP treatment on the collective amount of water absorbed per unit cross-sectional area of the UTC, BPT, BST, CST, CPT, and REF specimen. The BPT specimen showed the lower water absorption attributable to calcification in the voids of the FA incorporated cementitious biogrout. Followed by BPT, the BST specimens showed lower water absorption than REF, CPT and CST. In comparison to all the specimens, UTC was observed to show the highest water absorption with a sorptivity coefficient k of 0.048. In untreated UTC specimens, more surface area due to crack was exposed which led to higher water absorption through the test area of the specimen. Even though it is reasonable to predict that the presence of an artificial crack in UTC specimens increases the sample's water absorption, it becomes mandatory to compare the cracked and treated samples' findings to evaluate the performance of plain and biogrout in crack healing quantitatively. The REF specimens without any damage showed lower water absorption than the CPT and CST specimens which might be due to inefficient repair in the water treated specimens. However, the water absorption was comparatively higher in REF than the BPT and BST, clearly indicating efficiency of bacterial treatment in sealing the cracks.

The sorptivity coefficient k of CPT, CST, and REF was evaluated as 0.035, 0.037, and 0.031, respectively. with this the sorptivity coefficient of BPT and BST specimens was observed 0.009 and 0.025. Therefore, it is inferred from the low k value that calcification in the cyanobacterial admixed cementitious grout effectively reduced the porosity. It was observed that the rate of water absorption was higher during the initial few minutes of 6 h of study which could be due to capillary action of fine pores to actively absorb the water. This phase is also called rapid absorption phase. After the rapid phase, water continues to transport during secondary phase (starts after 1 day) into gel pores, which is primarily controlled by the mechanism of diffusion [Lee 2014; ASTM C1585: 2013 (ASTM 2013); Yang et al. 2019)]. The findings are in harmony with Zhang et al. (2021) who observed that bacterial treatment in the presence of calcium lactate and other nutrients could significantly improve water tightness in crack-healed specimens.

Sealing Efficiency

The sealing efficiency of the crack-healed specimen was evaluated on the basis of water absorption before and after the 6 h of the grouting. As shown in Fig. 12, the sealing efficiency of crack healed specimens was observed to be 82.23%, 51.53%, 29.60%, and 25.74% in BPT, BST, CPT, and CST specimens, respectively. The REF (uncracked specimen) showed efficiency of 35.18% on the basis of water absorption. The BPT and BST specimens were

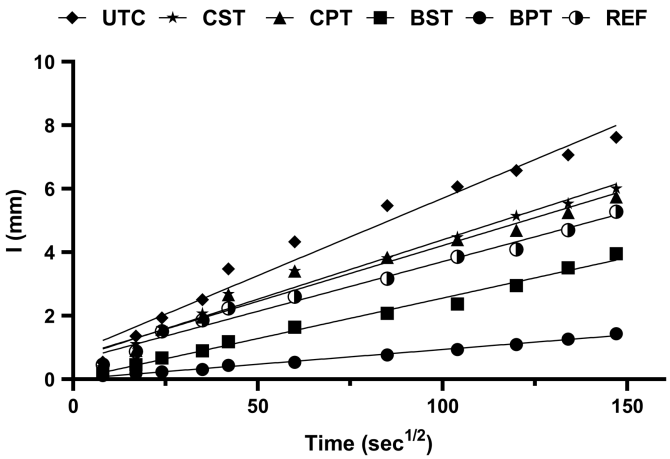


Fig. 11. Water sorptivity of concrete specimen after cracks repaired treatment with grouting. UTC: untreated concrete; CST: plain (control) grout spray treatment; CPT: plain (control) grout ponding treatment; BST: biogrout with spray treatment; BPT: biogrout with ponding; and REF: reference concrete specimen at 28 days of curing. All experiments were carried out in triplicate (n = 3).

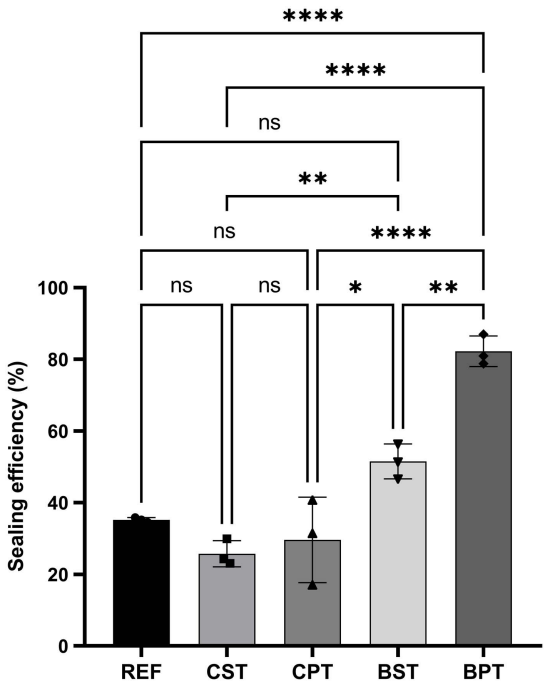


Fig. 12. Sealing efficiency of the concrete specimen after cracks repaired treatment with grouting. REF: without crack concrete; CST: plain (control) grout spray treatment; CPT: plain (control) grout ponding treatment, BST: biogrout with spray treatment; BPT: biogrout with ponding treatment at 28 days of curing. Individual data points are shown in each bar. Error bars represent standard deviation (n = 3). The star sign (*) indicates the statistical analysis at $p < 0.05$.

Downloaded from ascelibrary.org by Indian Institute Of Technology Delhi on 11/27/23. Copyright ASCE. For personal use only; all rights reserved.

able to regain and further improve the sealing efficiecny due to calcium carbonate precipitation by cyanobacterial cells. The voids between the FA and cement are filled in by the $CaCO_3$ particles which densify in the healed region, therefore, leading to low water absorption by BPT and BST specimens. Thus, more sealing efficiency than the CPT, CST, and REF specimens. It was confirmed using the statistical analyis that BPT specimens were able to significantly improve the sealing efficiency compared with the REF, CPT, CST specimens. Similar results were corroborated by Liu et al. (2020) and Wang et al. (2018) in concrete specimens.

In the current investigation, cyanobacteria were recognized as an efficient microorganism to remediate the cracks using an eco-friendly technique over the commonly used ureolysis approach for calcification because there is no release of harmful pollutants like ammonia. Moreover, it is economical as it uses light energy for biomineralization.

Microstructural Analysis

Biogrout proved to be an effective crack healing remediation due to the biodeposition of $CaCO_3$. Ponding and spray treatment by *S. pevalekii* cell culture resulted in the precipitation of calcite crystals in the pores of the specimens. It was verified using FESEM (field emission scanning electron microscopy), EDS (energy-dispersive X-ray spectroscopy), and mapping analysis. Fig. 13 confirms the calcium carbonate crystal deposition on the upper surface collected 2–10 mm deep from the BPT, and BST specimens. In FESEM imaging of the BPT specimen, the cluster of stable rhombohedral calcites and the spherical-shaped vaterite crystals were observed. Calcite crystals were estimated to be 3 μm, whereas vaterite crystals was observed to be 3–4 μm in size. In BST, the microstructural analysis showed the formation of calcite crystals all over the surface. The spray treatment was equally effective in the precipitation of calcium carbonate. The size of the calcite crystal formed in BST was in the range of 4–4.5 μm. However, no calcium carbonate deposition was observed in control samples (Fig. 14). The formation of calcium carbonate in biogrout specimens was validated using EDS. High peaks of calcium, carbon, and oxygen with 38.69, 7.27, 53.61 % and 61.01, 2.57, and 36 % were observed in BST and BPT specimens, respectively (Fig. 15). The calcium carbonate precipitation was further verified using a mapping technique for a particular area, as shown in Fig. 14. The bond of Ca, C, and O form the $CaCO_3$. The results were in accordance with the observation of other researchers (Anand et al. 2022b; Tripathi et al. 2019). Previous studies have documented the coexistence of bacterial cells along with calcium carbonate crystals with variable shape and structure (Xiao et al. 2010).

X-ray powder diffraction (XRD) results confirmed the presence of calcite crystal at 29.2° with high intensity in biogrout than in the plain grout specimens (Fig. 16). The other peaks of quartz (Q), calcium hydroxide (CH), and calcium silicate hydrates (C-S-H) were also observed in both the specimens, which is a very common occurrence in concrete specimens due to the presence of cement and sand. The visualization of calcite peaks over the surface of the biogrout specimens through microstructural examination validates the fact that MICCP by photoautotrophic cyanobacteria strain plays a significant role in the healing of the cracks by naturally precipitating calcium carbonate on the surface and pores of

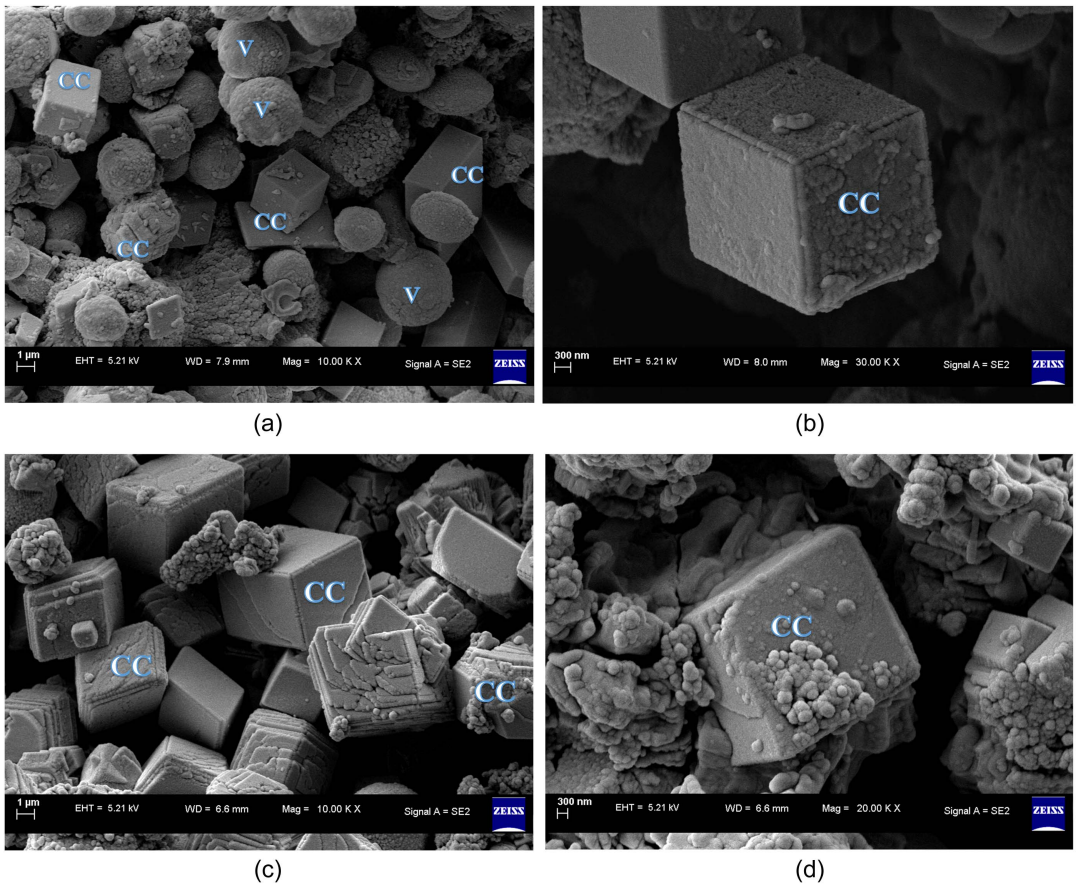


Fig. 13. FESEM imaging represents cubic shaped calcite and spherical shaped vaterite (V) calcium carbonate (CC) crystals formed in: (a and b) biogrout ponding treatment: BPT; (c and d) biogrout spray treatment: BST specimens.

Downloaded from ascelibrary.org by Indian Institute Of Technology Delhi on 11/27/23. Copyright ASCE. For personal use only; all rights reserved.

Downloaded from ascelibrary.org by Indian Institute Of Technology Delhi on 11/27/23. Copyright ASCE. For personal use only; all rights reserved.

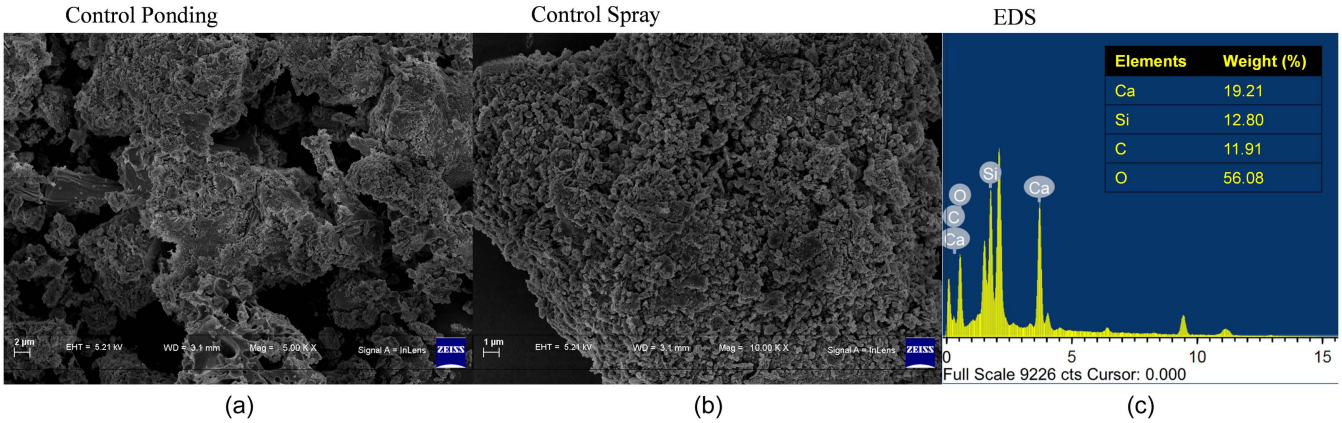


Fig. 14. FESEM imaging of: (a) plain ponding grout treatment: CPT; (b) plain spray grout treatment: CST; and (c) EDS of control plain grout.

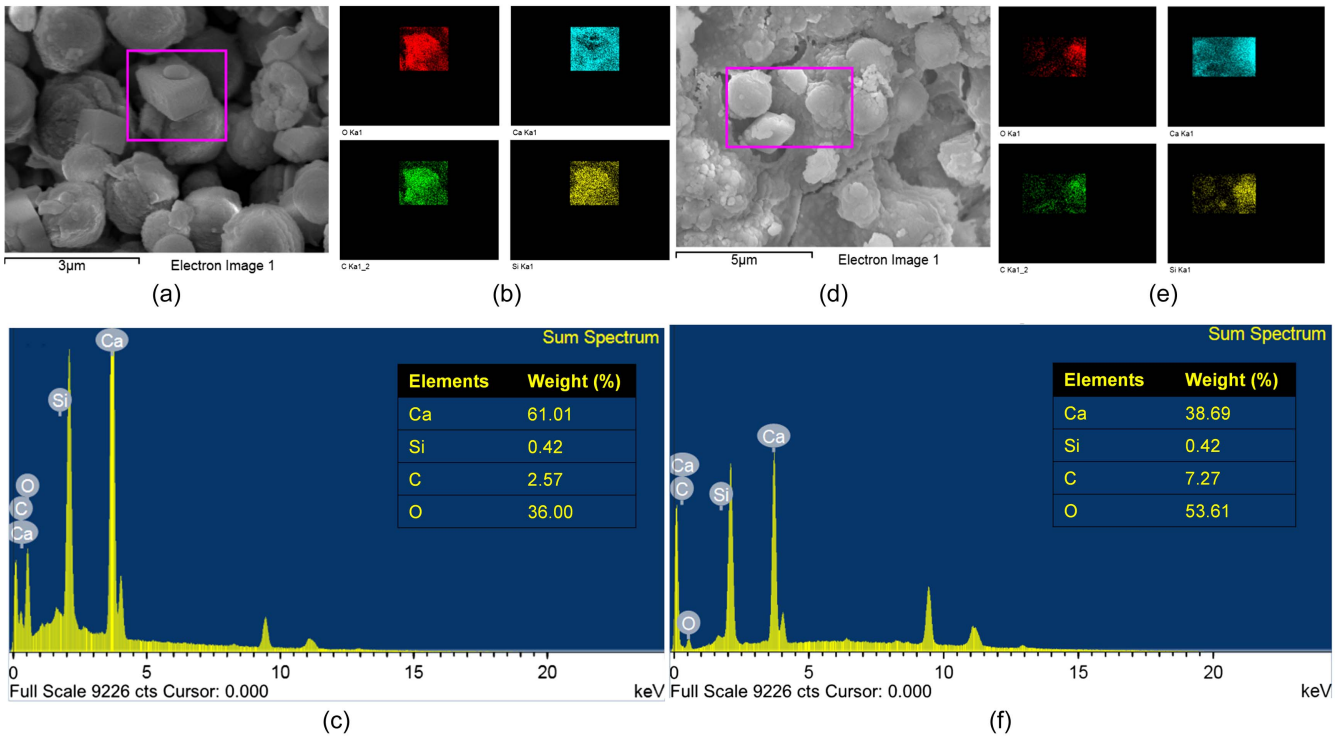


Fig. 15. EDS imaging and mapping of: (a–c) biogrout ponding treatment: BPT; and (d–f) biogrout spray treatment: BST.

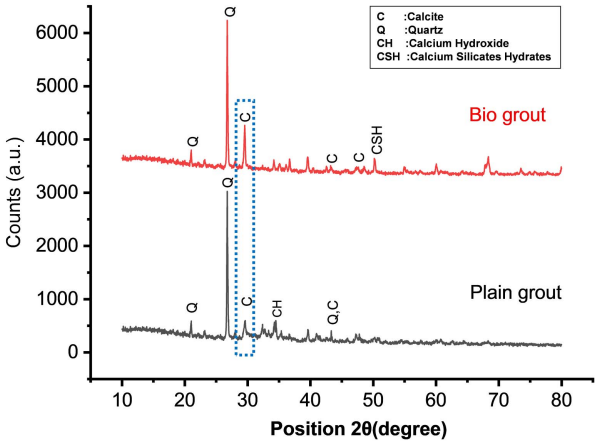


Fig. 16. XRD plot of plain and biogrout samples at 28 days of curing.

the cementitious biogrout. The CSH gel formed in the specimen results from hydration in the cementitious biogrout. Similar results were reported by Anand and his coworkers in crack remediation (Anand et al. 2022a).

Thermogravimetric Analysis

To validate the calcium carbonate precipitation as a healing agent in crack remediation, TGA was performed after 28 days of curing. Along with calcium carbonate, concrete specimens also revealed weight loss of calcium hydroxide, instigated during the curing process due to the hydration of cementitious material. Fig. 17(a) shows the TGA thermograms for biogrout and plain grout specimens. The significant mass loss of 3.74% of calcium carbonate at 600°C–800°C was noted in the biogrout specimens, which was two times more than the plain grout [Fig. 17(b)]. Jadhav et al. (2018) corroborated similar results, reporting a 50°C–100°C peak of evaporation

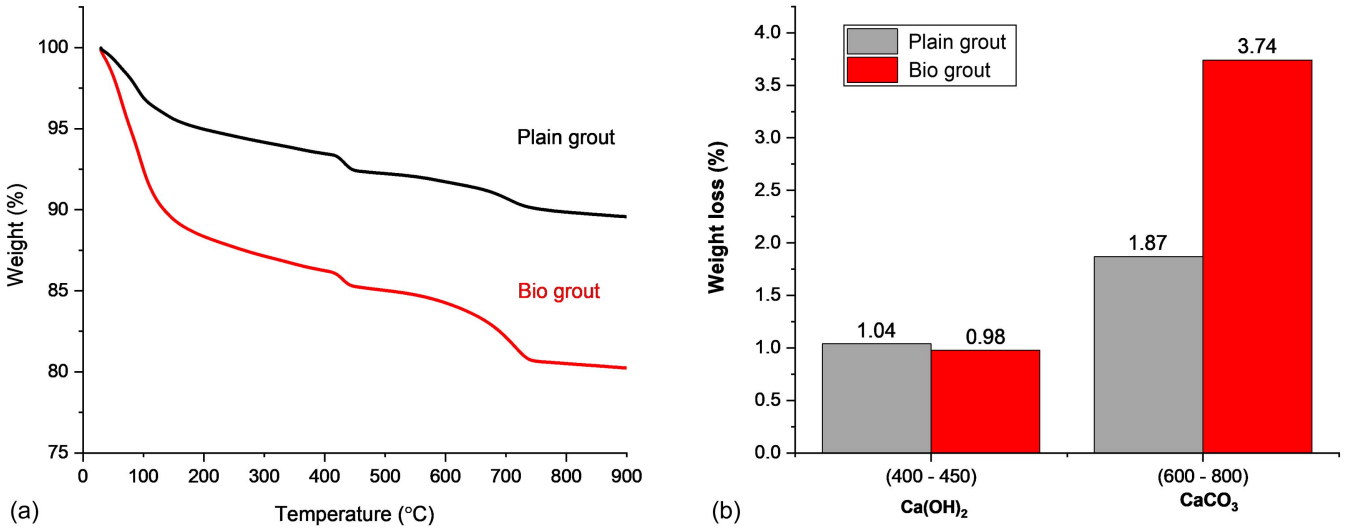


Fig. 17. (a) Thermogravimetric analysis (TGA); and (b) weight loss (%) of the plain and biogrout samples at 28 days of curing.

of water and a 560°C–700°C a peak of calcium carbonate. Another researcher, Sarkar et al. (2022), demonstrated a 1.8-fold increase in calcite precipitation in cracks remediated using alkali-activated fly ash composites in the presence of bacteria.

Conclusions

The present investigation introduces the role of photoautotrophic cyanobacteria *S. pevalekii* BDHKU 35101for horizontal and vertical oriented crack healing using biogrout. The two different cement-based grout mixtures, biogrout, and control (plain) grout, were compared with differentiate the role of MICCP in crack repair. Based on the flowability test, the workability and injectability of the grout with different dosage of FA (0%–50%) and c/b, w/b (0.45, 047, and 0.50) were studied to select the optimal concentration of FA and the c/b ratio. The following conclusions were drawn from the study:

1. Flow time, flow diameter, grout bleeding percentage, and flow retention with time showed best results with c/b and w/b ratios 0.47 with 40% substitution of FA cement-based biogrout.
2. Initial and final setting times of 40% FA biogrout was observed to be 4 h 45 min and 6 h 45 min, respectively.
3. The maximum compressive strength was observed by a grout mixture prepared using a 0.47 c/b ratio substituted with 40% FA in the cement-based grout. Therefore, it was further selected the crack remediation and testing.
4. The biogrout treated specimens (BPT and BST) showed higher compressive and flexural strength than the controlled specimens (CPT, CST, REF, and UTC).
5. Permeability of the biogrout specimens was lower than plain grout, which proves precipitation in the pores of biogrout blocks the passage of water through the voids.
6. The sealing efficiency of the BPT and BST' specimens improved significantly compared with REF, CPT, and CST specimens.
7. Microstructural analysis (FESEM-EDS, XRD) and TGA verified the calcite precipitation after 28 days of curing in biogrout specimens.

Data Availability Statement

All data, models, and code generated or used during the study are included in the published article.

Acknowledgments

The authors are thankful to the Department of Biotechnology, Ministry of Science and Technology, Govt. of India, for providing the research grant under BT/PR27190/BCE/8/1428/2017.

References

Achal, V., and S. Kawasaki. 2016. "Biogrout: A novel binding material for soil improvement and concrete repair." *Front. Microbiol.* 7 (MAR): 314. https://doi.org/10.3389/FMICB.2016.00314/BIBTEX.

Achal, V., X. Pan, and N. Özyurt. 2011. "Improved strength and durability of fly ash-amended concrete by microbial calcite precipitation." *Ecol. Eng.* 37 (4): 554–559. https://doi.org/10.1016/j.ecoleng.2010.11.009.

Anand, K., S. Goyal, and M. S. Reddy. 2022a. "Crack healing in concrete by microbially induced calcium carbonate precipitation as assessed through electromechanical impedance technique." *Eur. J. Environ. Civ. Eng.* 0 (0): 1–21. https://doi.org/10.1080/19648189.2022.2075470.

Anand, K., S. Goyal, and M. S. Reddy. 2022b. "Long-term viable SF immobilized bacterial cells as sustainable solution for crack healing in concrete." In Vol. 43 of *Structures*, 1342–1355. Amsterdam, Netherlands: Elsevier. https://doi.org/10.1016/j.istruc.2022.07.056.

Anand, K., S. Goyal, and M. S. Reddy. 2023. "Development of field applicable remediation procedure using bio-cementitious grout for concrete cracks in variable orientations." *J. Build. Eng.* 67 (May): 106024. https://doi.org/10.1016/j.jobe.2023.106024.

ASTM. 2010a. *Standard test method for compressive strength of grouts for preplaced-aggregate concrete in the laboratory.* ASTM:C942-10. West Conshohocken, PA: ASTM.

ASTM. 2015. *Standard test method for flow of hydraulic cement mortar.* ASTM C1437. West Conshohocken, PA: ASTM.

ASTM. 2010b. *Standard test method for expansion and bleeding of freshly mixed grouts for preplaced-aggregate concrete in the laboratory.* ASTM:C940-10a. West Conshohocken, PA: ASTM.

ASTM. 2010c. *Standard test method for flow of grout for preplaced-aggregate concrete (flow cone method).* ASTM C939. West Conshohocken, PA: ASTM.

ASTM. 2013. *Standard test method for measurement of rate of absorption of water by hydraulic cement concretes.* ASTM C1585-13. West Conshohocken, PA: ASTM.

ASTM. 2019. *Standard specification for coal fly ash and raw or calcined natural pozzolan for use.* ASTM C618. West Conshohocken, PA: ASTM.

Downloaded from ascelibrary.org by Indian Institute Of Technology Delhi on 11/27/23. Copyright ASCE. For personal use only; all rights reserved.

Downloaded from ascelibrary.org by Indian Institute Of Technology Delhi on 11/27/23. Copyright ASCE. For personal use only; all rights reserved.

Azima, M., and Z. B. Bundur. 2019. "Influence of *Sporasarcina pasteurii* cells on rheological properties of cement paste." *Constr. Build. Mater.* 225 (Nov): 1086–1097. https://doi.org/10.1016/j.conbuildmat.2019.07.132.

Bai, T., Y. Liang, C. Li, X. Jiang, Y. Li, A. Chen, H. Wang, F. Xu, and C. Peng. 2022. "Application and validation of fly ash based geopolymer mortar as grouting material in porous asphalt concrete." *Constr. Build. Mater.* 332 (Nov): 127154. https://doi.org/10.1016/j.conbuildmat.2022.127154.

Bhuvaneshwari, T., M. Shylajanaciyar, P. A. Prakasam, K. Ezhilmaran, L. Karthick, G. Subramanian, L. Uma, and D. Prabaharan. 2017. "Polyphasic analysis for elucidating the taxonomic position of selected unicellular marine cyanobacteria from Indian and Hong Kong coast." *Phytotaxa* 307 (4): 263–277. https://doi.org/10.11646/phytotaxa.307.4.4.

BIS (Bureau of Indian Standards). 2013. *Specification for 43 grade ordinary portland cement by Bureau of Indian Standards*. BIS: 8112. New Delhi, India: BIS.

Celik, F., and H. Canakci. 2015. "An investigation of rheological properties of cement-based grout mixed with rice husk ash (RHA)." *Constr. Build. Mater.* 91 (Aug): 187–194. https://doi.org/10.1016/j.conbuildmat.2015.05.025.

Choi, S. G., K. Wang, Z. Wen, and J. Chu. 2017. "Mortar crack repair using microbial induced calcite precipitation method." *Cem. Concr. Compos.* 83 (Oct): 209–221. https://doi.org/10.1016/j.cemconcomp.2017.07.013.

Choi, S. J., S. S. Lee, and P. J. M. Monteiro. 2012. "Effect of fly ash fineness on temperature rise, setting, and strength development of mortar." *J. Mater. Civ. Eng.* 24 (5): 499–505. https://doi.org/10.1061/(ASCE)MT.1943-5533.0000411.

Çınar, M., M. Karpuzcu, and H. Çanakcı. 2019. "Effect of waste marble powder and fly ash on the rheological characteristics of cement based grout." *Civ. Eng. J.* 5 (4): 777–788. https://doi.org/10.28991/cej-2019-03091287.

Çınar, M., M. Karpuzcu, and H. Çanakcı. 2020. "The measurement of fresh properties of cement-based grout containing waste marble powder." *Meas. J. Int. Meas. Confederation* 150 (Jan): 106833. https://doi.org/10.1016/j.measurement.2019.07.061.

Delić, D., O. Stajković-Srbinović, and A. Buntić. 2022. "Hazards and usability of coal fly ash." In *Advances in understanding soil degradation*, 571–608. Cham, Switzerland: Springer. https://doi.org/10.1007/978-3-030-85682-3_26.

Dhami, N. K., M. S. Reddy, and M. S. Mukherjee. 2013. "Biomineralization of calcium carbonates and their engineered applications: A review." *Front. Microbiol.* 4 (Oct): 1–13. https://doi.org/10.3389/fmicb.2013.00314.

Dhiman, N. K., N. Sidhu, S. Agnihotri, A. Mukherjee, and M. S. Reddy. 2022. "Role of nanomaterials in protecting building materials from degradation and deterioration." In *Biodegradation and biodeterioration at the nanoscale*, 405–475. Amsterdam, Netherlands: Elsevier. https://doi.org/10.1016/B978-0-12-823970-4.00024-5.

Feng, J., B. Chen, W. Sun, and Y. Wang. 2021. "Microbial induced calcium carbonate precipitation study using *Bacillus subtilis* with application to self-healing concrete preparation and characterization." *Constr. Build. Mater.* 280 (Jun): 122460. https://doi.org/10.1016/j.conbuildmat.2021.122460.

Gleaton, J., Z. Lai, R. Xiao, Q. Chen, and Y. Zheng. 2019. "Microalga-induced biocementation of Martian regolith simulant: Effects of biogrouting methods and calcium sources." *Constr. Build. Mater.* 229 (Dec): 116885. https://doi.org/10.1016/j.conbuildmat.2019.116885.

Han, Z., et al. 2017a. "The characterization of intracellular and extracellular biomineralization induced by *Synechocystis sp*. PCC6803 cultured under low Mg/Ca ratios conditions." *Geomicrobiol. J.* 34 (4): 362–373. https://doi.org/10.1080/01490451.2016.1197986.

Han, Z., et al. 2017b. "Thermogravimetric and kinetic analysis of thermal decomposition characteristics of microbial calcites induced by cyanobacteria Synechocystis sp. PCC6803." *J. Therm. Anal. Calorim.* 127 (2): 1371–1379. https://doi.org/10.1007/s10973-016-6026-1.

Han, Z., H. Yan, S. Zhou, H. Zhao, Y. Zhang, N. Zhang, C. Yao, L. Zhao, and C. Han. 2013. "Precipitation of calcite induced by *Synechocystis sp*. PCC6803." *World J. Microbiol. Biotechnol.* 29 (10): 1801–1811. https://doi.org/10.1007/s11274-013-1341-1.

Heidrich, C., H. Feuerborn, and A. Weir. 2013. "Coal combustion products: A global perspective." In *VGB PowerTech.* 12: 46–52.

Heveran, C. M., S. L. Williams, J. Qiu, J. Artier, M. H. Hubler, S. M. Cook, J. C. Cameron, and W. V. Srubar. 2020. "Biomineralization and successive regeneration of engineered living building materials." *Matter* 2 (2): 481–494. https://doi.org/10.1016/j.matt.2019.11.016.

IS (Indian Standard). 2003. *Pulverized fuel ash—Specification. Part 1: For use as Pozzolana in cement, cement mortar and concrete (second revision)*. IS: 3812 (Part-1). New Delhi, India: IS.

IS (Indian Standard). 2004. *Method of tests for strength of concrete*. IS 516:2014. New Delhi, India: IS.

IS (Indian Standard). 2005. *Methods of physical tests for hydraulic cement part 6 determination of compressive strength of hydraulic cement other than masonry cement (first revision)*. IS: 4031 (Part 6). New Delhi, India: IS.

IS (Indian Standard). 2016. *Coarse fine aggregates concrete specification*. IS:383. New Delhi, India: IS.

Ivanov, V., V. Stabnikov, and S. Kawasaki. 2019. "Ecofriendly calcium phosphate and calcium bicarbonate biogrouts." *J. Cleaner Prod.* 218 (May): 328–334. https://doi.org/10.1016/j.jclepro.2019.01.315.

Jadhav, U. U., M. Lahoti, Z. Chen, J. Qiu, B. Cao, and E. H. Yang. 2018. "Viability of bacterial spores and crack healing in bacteria-containing geopolymer." *Constr. Build. Mater.* 169 (Apr): 716–723. https://doi.org/10.1016/j.conbuildmat.2018.03.039.

Jiang, L., G. Jia, C. Jiang, and Z. Li. 2020. "Sugar-coated expanded perlite as a bacterial carrier for crack-healing concrete applications." *Constr. Build. Mater.* 232 (Jan): 117222. https://doi.org/10.1016/j.conbuildmat.2019.117222.

Joshi, S., S. Goyal, and M. Sudhakara Reddy. 2021. "Bio-consolidation of cracks with fly ash amended biogrouting in concrete structures." *Constr. Build. Mater.* 300 (Sep): 124044. https://doi.org/10.1016/j.conbuildmat.2021.124044.

Kaladharan, G., and F. Rajabipour. 2022. "Evaluation and beneficiation of high sulfur and high alkali fly ashes for use as supplementary cementitious materials in concrete." *Constr. Build. Mater.* 339 (Jan): 127672. https://doi.org/10.1016/j.conbuildmat.2022.127672.

Kamennaya, N. A., C. M. Ajo-Franklin, T. Northen, and C. Jansson. 2012. "Cyanobacteria as biocatalysts for carbonate mineralization." *Minerals* 2 (4): 338–364. https://doi.org/10.3390/min2040338.

Kantro, D. 1980. "Influence of water-reducing admixtures on properties of cement paste—A miniature slump test." *Cem. Concr. Aggregates* 2 (2): 95. https://doi.org/10.1520/CCA10190J.

Kanwal, M., R. A. Khushnood, W. Khaliq, A. G. Wattoo, and T. Shahid. 2022. "Synthesis of pyrolytic carbonized bagasse to immobilize *Bacillus subtilis*; application in healing micro-cracks and fracture properties of concrete." *Cem. Concr. Compos.* 126 (Oct): 104334. https://doi.org/10.1016/j.cemconcomp.2021.104334.

Khalid, A. R., S. A. Rizwan, U. Hanif, and M. H. Hameed. 2016. "Effect of mixing time on flowability and slump retention of self-compacting paste system incorporating various secondary raw materials." *Arab. J. Sci. Eng.* 41 (4): 1283–1290. https://doi.org/10.1007/s13369-015-1885-5.

Kotelnikova, A. D., O. B. Rogova, E. A. Karpukhina, A. B. Solopov, I. S. Levin, V. V. Levkina, M. A. Proskurnin, and D. S. Volkov. 2022. "Assessment of the structure, composition, and agrochemical properties of fly ash and ash-and-slug waste from coal-fired power plants for their possible use as soil ameliorants." *J. Cleaner Prod.* 333 (Nov): 130088. https://doi.org/10.1016/j.jclepro.2021.130088.

Lee, N. 2014. "Use of sorptivity as a guide to concrete durability performance." *Mater. Sci.* 1–9.

Li, G., C. Zhou, W. Ahmad, K. I. Usanova, M. Karelina, A. M. Mohamed, and R. Khallaf. 2022. "Fly ash application as supplementary cementitious material: A review." *Materials* 15: 2664. https://doi.org/10.3390/ma15072664.

Li, S., Z. Li, F. Sha, Q. Zhang, and R. Liu. 2017. "Investigation of viscous behaviour and strength of microfine-cement-based grout mixed with microfine fly ash and superplasticiser." *Adv. Cem. Res.* 29 (5): 206–215. https://doi.org/10.1680/jadcr.16.00118.

Liang, A., C. Paulo, Y. Zhu, and M. Dittrich. 2013. "$CaCO_3$ biomineralization on cyanobacterial surfaces: Insights from experiments with three *Synechococcus* strains." *Colloids Surf., B* 111 (Nov): 600–608. https://doi.org/10.1016/j.colsurfb.2013.07.012.

Liu, Y. H., P. Yang, T. Ku, and S. W. Gao. 2020. "Effect of different nanoparticles on the grouting performance of cement-based grouts in dynamic water condition." *Constr. Build. Mater.* 248 (Jul): 118663. https://doi.org/10.1016/j.conbuildmat.2020.118663.

Luo, M., C. X. Qian, and R. Y. Li. 2015. "Factors affecting crack repairing capacity of bacteria-based self-healing concrete." *Constr. Build. Mater.* 87 (Jul): 1–7. https://doi.org/10.1016/j.conbuildmat.2015.03.117.

Miller, A. G., and B. Colman. 1980. "Evidence for HCO_3–Transport by the blue-green alga (Cyanobacterium) *Coccochloris peniocystis*." *Plant Physiol.* 65 (2): 397–402. https://doi.org/10.1104/pp.65.2.397.

Nair, N., K. Mohammed Haneefa, M. Santhanam, and R. Gettu. 2020. "A study on fresh properties of limestone calcined clay blended cementitious systems." *Constr. Build. Mater.* 254 (Sep): 119326. https://doi.org/10.1016/j.conbuildmat.2020.119326.

Novitsky, J. A. 1981. "Calcium carbonate precipitation by marine bacteria." *Geomicrobiol. J.* 2 (4): 375–388. https://doi.org/10.1080/01490458109377775.

Obst, M., B. Wehrli, and M. Dittrich. 2009. "$CaCO_3$ nucleation by cyanobacteria: Laboratory evidence for a passive, surface-induced mechanism." *Geobiology* 7 (3): 324–347. https://doi.org/10.1111/j.1472-4669.2009.00200.x.

Onyelowe, K. C., D. P. N. Kontoni, A. M. Ebid, F. Dabbaghi, A. Soleymani, H. Jahangir, and M. L. Nehdi. 2022. "Multi-objective optimization of sustainable concrete containing fly ash based on environmental and mechanical considerations." *Buildings* 12 (7): 948. https://doi.org/10.3390/buildings12070948.

Osman, K. M., F. M. Taher, A. Abd EL-Tawab, and A. S. Faried. 2021. "Role of different microorganisms on the mechanical characteristics, self-healing efficiency, and corrosion protection of concrete under different curing conditions." *J. Build. Eng.* 41 (Sep): 102414. https://doi.org/10.1016/j.jobe.2021.102414.

Razi, P. Z., H. A. Razak, and N. H. A. Khalid. 2016. "Sustainability, ecopoint and engineering performance of different workability OPC fly-ash mortar mixes." *Materials* 9 (5): 341. https://doi.org/10.3390/ma9050341.

Sarkar, M., M. Maiti, M. Akbar, and S. Xu. 2022. "Evaluation of the crack-healing performance and durability of bacteria integrated alkali-activated fly ash composites." *J. Build. Eng.* 54 (Jan): 104642. https://doi.org/10.1016/j.jobe.2022.104642.

Sha, F., S. Li, R. Liu, Z. Li, and Q. Zhang. 2018. "Experimental study on performance of cement-based grouts admixed with fly ash, bentonite, superplasticizer and water glass." *Constr. Build. Mater.* 161 (Feb): 282–291. https://doi.org/10.1016/j.conbuildmat.2017.11.034.

Shi, X., H. Xiao, H. Azarabadi, J. Song, X. Wu, X. Chen, and K. S. Lackner. 2020. "Sorbents for the direct capture of CO_2 from ambient air." *Angew. Chem. Int. Ed.* 59 (18): 6984–7006. https://doi.org/10.1002/anie.201906756.

Sidhu, N., S. Goyal, and M. S. Reddy. 2022. "Biomineralization of cyanobacteria *Synechocystis pevalekii* improves the durability properties of cement mortar." In *AMB express*. Berlin: Springer. https://doi.org/10.1186/s13568-022-01403-z.

Sierra Beltran, M. G., and H. M. Jonkers. 2015. "Crack self-healing technology based on bacteria." *J. Ceram. Process. Res.* 16 (S1): s33–s39.

Srinivas, M. K., U. J. Alengaram, S. Ibrahim, S. M. Phang, V. Vello, H. K. Jun, and A. M. Alnahhal. 2021. "Evaluation of crack healing potential of cement mortar incorporated with blue-green microalgae." *J. Build. Eng.* 44 (Dec): 102958. https://doi.org/10.1016/j.jobe.2021.102958.

Stein, T. 2022. "Carbon dioxide now more than 50% higher than pre-industrial levels." NOAA. Accessed June 3, 2022. https://www.noaa.gov/news-release/carbon-dioxide-now-more-than-50-higher-than-pre-industrial-levels.

Tripathi, E., K. Anand, S. Goyal, and M. S. Reddy. 2019. "Bacterial based admixed or spray treatment to improve properties of concrete." *Sadhana* 44 (1): 1–8. https://doi.org/10.1007/s12046-018-0999-3.

Van Tittelboom, K., N. De Belie, W. De Muynck, and W. Verstraete. 2010. "Use of bacteria to repair cracks in concrete." *Cem. Concr. Res.* 40 (1): 157–166. https://doi.org/10.1016/j.cemconres.2009.08.025.

Vasumithran, M., K. B. Anand, and D. Sathyan. 2020. "Effects of fillers on the properties of cement grouts." *Constr. Build. Mater.* 246 (Jun): 118346. https://doi.org/10.1016/j.conbuildmat.2020.118346.

Waditee, R., G. S. Hossain, Y. Tanaka, T. Nakamura, M. Shikata, J. Takano, T. Takabe, and T. Takabe. 2004. "Isolation and functional characterization of Ca^{2+}/H^+ antiporters from cyanobacteria." *J. Biol. Chem.* 279 (6): 4330–4338. https://doi.org/10.1074/jbc.M310282200.

Wang, J., A. Mignon, G. Trenson, S. Van Vlierberghe, N. Boon, and N. De Belie. 2018. "A chitosan-based pH-responsive hydrogel for encapsulation of bacteria for self-sealing concrete." *Cem. Concr. Compos.* 93 (May): 309–322. https://doi.org/10.1016/j.cemconcomp.2018.08.007.

Wang, J. Y., H. Soens, W. Verstraete, and N. De Belie. 2014. "Self-healing concrete by use of microencapsulated bacterial spores." *Cem. Concr. Res.* 56 (Feb): 139–152. https://doi.org/10.1016/j.cemconres.2013.11.009.

Wang, K., Z. Wen, and S. Choi. 2016. *Development of an ecofriendly, cost-effective biogrout for concrete crack repair.* Tech Rep. Ames, IA: Iowa State Univ.

Xiao, J., Z. Wang, Y. Tang, and S. Yang. 2010. "Biomimetic mineralization of $CaCO_3$ on a phospholipid monolayer: From an amorphous calcium carbonate precursor to calcite via vaterite." *Langmuir* 26 (7): 4977–4983. https://doi.org/10.1021/la903641k.

Xiao, Y., A. W. Stuedlein, Z. Pan, H. Liu, T. Matthew Evans, X. He, H. Lin, J. Chu, and L. A. van Paassen. 2020. "Toe-bearing capacity of precast concrete piles through biogrouting improvement." *J. Geotech. Geoenviron. Eng.* 146 (12): 06020026. https://doi.org/10.1061/(asce)gt.1943-5606.0002404.

Xu, J., Y. Tang, X. Wang, Z. Wang, and W. Yao. 2020. "Application of ureolysis-based microbial $CaCO_3$ precipitation in self-healing of concrete and inhibition of reinforcement corrosion." *Constr. Build. Mater.* 265 (Dec): 120364. https://doi.org/10.1016/j.conbuildmat.2020.120364.

Xue, C., W. Li, F. Qu, Z. Sun, and S. P. Shah. 2020. "Self-healing efficiency and crack closure of smart cementitious composite with crystalline admixture and structural polyurethane." *Constr. Build. Mater.* 260 (Nov): 119955. https://doi.org/10.1016/j.conbuildmat.2020.119955.

Yang, L., D. Gao, Y. Zhang, J. Tang, and Y. Li. 2019. "Relationship between sorptivity and capillary coefficient for water absorption of cement-based materials: Theory analysis and experiment." *R. Soc. Open Sci.* 6 (6): 190112. https://doi.org/10.1098/rsos.190112.

Yao, Z. T., M. S. Xia, P. K. Sarker, and T. Z. Chen. 2014. "A review of the alumina recovery from coal fly ash, with a focus in China." *Fuel* 120 (Mar): 74–85. https://doi.org/10.1016/j.fuel.2013.12.003.

Yijin, L., Z. Shiqiong, Y. Jian, and G. Yingli. 2004. "The effect of fly ash on the fluidity of cement paste, mortar and concrete." In *Proc., Int. Workshop on Sustainable Development and Concrete Technology*, 339–345. Ames, IA: Iowa State Univ.

Yu, J., M. Zhang, G. Li, J. Meng, and C. K. Leung. 2020. "Using nano-silica to improve mechanical and fracture properties of fibre-reinforced high-volume fly ash cement mortar." *Constr. Build. Mater.* 239 (Jun): 117853. https://doi.org/10.1016/j.conbuildmat.2019.117853.

Yu, W., Z. Rao, H. Yuan, P. Wei, J. E. Nyarko-Appiah, and W. Jiang. 2023. "An efficient and environmental friendly strategy for alumina extraction and Fe–Si alloys production from coal fly ash by combining vacuum thermal reduction, alkali dissolving, and magnetic separation." *J. Cleaner Prod.* 408 (Jul): 137129. https://doi.org/10.1016/j.jclepro.2023.137129.

Yu, Y., L. You, D. Liu, W. Hollinshead, Y. J. Tang, and F. Zhang. 2013. "Development of *Synechocystis sp.* PCC 6803 as a phototrophic cell factory." *Mar. Drugs* 11 (8): 2894–2916. https://doi.org/10.3390/md11082894.

Zhang, J., B. Mai, T. Cai, J. Luo, W. Wu, B. Liu, N. Han, F. Xing, and X. Deng. 2017. "Optimization of a binary concrete crack self-healing system containing bacteria and oxygen." *Materials* 10 (2): 116. https://doi.org/10.3390/ma10020116.

Zhang, L. V., M. L. Nehdi, A. R. Suleiman, M. Mehdizadeh, M. Gan, A. Marani, and M. Tuyan. 2021. "Crack self-healing in bio-green

Downloaded from ascelibrary.org by Indian Institute Of Technology Delhi on 11/27/23. Copyright ASCE. For personal use only; all rights reserved.

concrete." *Composites, Part B* 227 (Sept): 109397. https://doi.org/10.1016/j.compositesb.2021.109397.

Zhang, S., W. G. Qiao, P. C. Chen, and K. Xi. 2019. "Rheological and mechanical properties of microfine-cement-based grouts mixed with microfine fly ash, colloidal nanosilica and superplasticizer." *Constr. Build. Mater.* 212 (Jul): 10–18. https://doi.org/10.1016/j.conbuildmat.2019.03.314.

Zhang, Y., S. Wang, B. Zhang, D. Hou, H. Li, L. Li, J. Wang, and C. Lin. 2020. "A preliminary investigation of the properties of potassium magnesium phosphate cement-based grouts mixed with fly ash, water glass and bentonite." *Constr. Build. Mater.* 237 (Mar): 117501. https://doi.org/10.1016/j.conbuildmat.2019.117501.

Zhu, T., and M. Dittrich. 2016. "Carbonate precipitation through microbial activities in natural environment, and their potential in biotechnology: A review." *Front. Bioeng. Biotechnol.* 4: 4. https://doi.org/10.3389/fbioe.2016.00004.

Zhu, T., Y. Lin, X. Lu, and M. Dittrich. 2018. "Assessment of cyanobacterial species for carbonate precipitation on mortar surface under different conditions." *Ecol. Eng.* 120 (May): 154–163. https://doi.org/10.1016/j.ecoleng.2018.05.038.

Zhu, T., X. Lu, and M. Dittrich. 2017. "Calcification on mortar by live and UV-killed biofilm-forming cyanobacterial Gloeocapsa PCC73106." *Constr. Build. Mater.* 146 (Aug): 43–53. https://doi.org/10.1016/j.conbuildmat.2017.04.026.

Downloaded from ascelibrary.org by Indian Institute Of Technology Delhi on 11/27/23. Copyright ASCE. For personal use only; all rights reserved.

Journal of Building Engineering 82 (2024) 108190



Contents lists available at ScienceDirect

Journal of Building Engineering

journal homepage: www.elsevier.com/locate/jobe



Comparative study of heterotrophic and photoautotrophic bacteria on strength and permeability properties of concrete

Navneet Sidhu [a], Shweta Goyal [b], M. Sudhakara Reddy [a,*]

[a] Department of Biotechnology, Thapar Institute of Engineering & Technology, Patiala 147004, Punjab, India
[b] Department of Civil Engineering, Thapar Institute of Engineering & Technology, Patiala 147004, Punjab, India

ARTICLE INFO

Keywords:
Cyanobacteria
Synechocystis pevalekii
Bacillus paramycoides
Compressive strength
Sorptivity test
RCPT

ABSTRACT

The incorporation of bacterial biomass to cementitious materials improves the strength and permeability properties by altering the pore structure. Previous studies report significant improvement in the strength properties of concrete by using ureolytic bacteria. However, several challenges limit its application in the field, and one such limitation is the release of ammonia gas, a harmful foul-smelling pollutant. In some studies, cyanobacteria are being used as an alternative to heterotrophic bacteria. The present study compares the effect of the addition of heterotrophic bacteria, *Bacillus paramycoides,* and phototrophic bacteria, *Synechocystis pevalekii* BDHKU 35101, on the strength and permeability properties of concrete. The specimens treated with *S. pevalekii* (SPC) and *B. paramycoides* (BPC) improved the compressive strength significantly compared to the control, however, a marginal difference (1.8 %) was observed between the SPC and BPC specimens. The charge passed through SPC and BPC specimens during the rapid chloride permeability test was 1901 and 1440 coulombs, respectively after 28 days of curing. The water absorption reduced after 28 days with 0.007 and 0.005 sorptivity coefficients of SPC and BPC specimens, respectively. The $CaCO_3$ crystallization in SPC and BPC specimens was confirmed using a field emission scanning electron microscope (FESEM) and energy dispersive X-ray spectroscopy (EDS). The peaks of calcite and vaterite were observed in X-ray diffraction (XRD). This study affirms that both *B. paramycoides* and *S. pevalekii* significantly improved the strength and permeability properties of concrete. However, photoautotrophic cyanobacteria do not release harmful pollutants and also sequester atmospheric CO_2 during calcification and can serve as potential substitute/alternative for ureolytic bacteria.

1. Introduction

Concrete is the most used construction material globally because of its climate resilience [1]. It offers a variety of benefits in terms of adaptability and durability. Due to rapid urbanization, the construction industry faces a sustainability crisis because of the excessive use of chemical and polluting materials to improve concrete strength and durability [2]. The extensive use of conventional water repellents like silane and siloxane and chemical-based sealants (synthetic epoxides, polyurethane, epoxy resins, acrylics, and waxes) on cement-based materials presents a significant environmental hazard owing to their inability to break down naturally [3,4]. Another economical and environmentally safe approach is employing calcite-producing microorganisms to facilitate microbial cementation. Microbial-induced carbonate precipitation (MICP) is an eco-efficient substitute for conventional cement binder methods [5]. MICP

* Corresponding author.
E-mail address: msreddy@thapar.edu (M.S. Reddy).

https://doi.org/10.1016/j.jobe.2023.108190
Received 24 August 2023; Received in revised form 10 November 2023; Accepted 20 November 2023
Available online 23 November 2023
2352-7102/© 2023 Elsevier Ltd. All rights reserved.

requires less mechanical energy and has a low or zero carbon footprint, contributing to developing cost-effective processes with environmental benefits [6]. A variety of microorganisms (photoautotrophic, heterotrophic, and sulphate-reducing bacteria) are capable of calcium carbonate ($CaCO_3$) precipitation [7,8]. Most of the MICP research focused on applying heterotrophic bacteria in concrete due to the fast reaction rate and high efficiency for $CaCO_3$ precipitation. $CaCO_3$ precipitation by heterotrophic bacteria involves the degradation of urea to form carbonic acid and ammonia [9]. The carbonic acid (H_2CO_3) further equilibrates in water to form ammonia (NH_4^+), carbonate (CO_3^{2-}), and hydroxide ions (OH^-). Hydroxide ions lead to the alkalinization of the solutions. In the presence of calcium ions, 1 mol of carbonate precipitates to form 1 mol of calcium carbonate (Fig. 1). Previous studies demonstrated improved cementitious properties by using different ureolytic and non-ureolytic strains of bacteria. Many *Bacillus* species precipitate $CaCO_3$ mineralization by non-ureolytic pathways. Tziviloglou et al. isolated alkali-resistant *Bacillus cohnii* and *Bacillus alkalinitrilicus* from alkaline natural lakes and reported improvement in the cementitious properties of mortar [10]. Jang et al. reported reduced sorptivity and $CaCO_3$ precipitation by non-ureolytic alkali-tolerant (*L. boronitolerans* YS11) and alkaliphilic (*B. alkaliphilus* AK13) bacteria in mortar [11]. Many ureolytic strains such as *Bacillus sphaericus* [12–14] *Bacillus pasteurii* [15–18], *Bacillus megaterium* [19–22], *Bacillus alkalinitrilicus* [23], *Bacillus subtilis* [24,25], *Bacillus paramycoides* [26] and *Bacillus pseudofirmus* [27,28] improve the durability and permeability properties of concrete. The major drawback is the release of ammonia (foul-smelling pollutant) which results in nitrogen oxide (NO_x) emission into the atmosphere, causing health and environmental concerns [29,30]. Therefore, the researchers are looking for alternative strains that do not pollute the environment and improve the properties of concrete. One such group of microorganisms are cyanobacteria which use light energy and carbon dioxide to precipitate calcium carbonate [31,32].

Microorganisms, especially cyanobacteria, secrete exopolymeric substances (EPS), a complex mixture of polysaccharides, proteins, nucleic acids, and other chemical substances. It generates a slimy matrix around bacterial cells and is essential for biofilm develop-

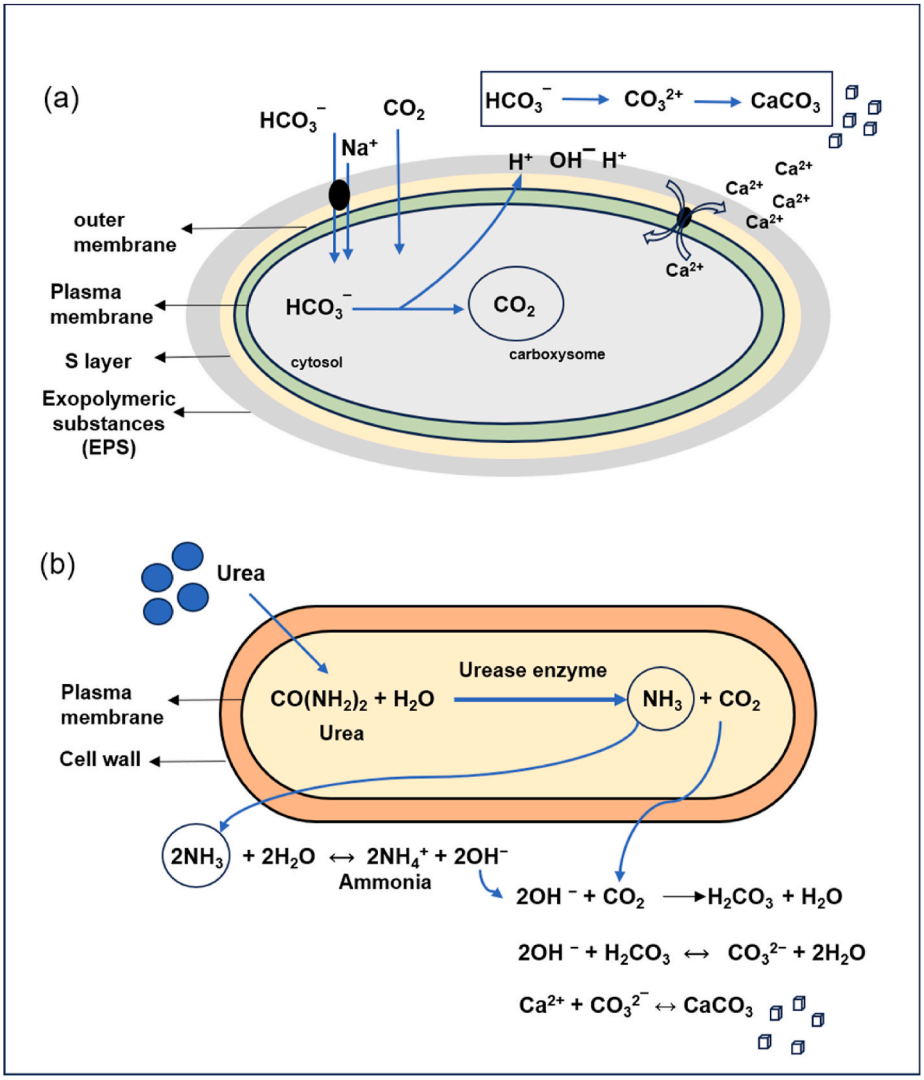


Fig. 1. Biochemical reaction of calcium carbonate precipitation in a) photoautotrophic cyanobacteria and b) heterotrophic bacterial cell.

ment. When cyanobacteria are injected and allowed to grow in concrete, they create EPS, which can interact with the cementitious matrix. Cyanobacteria carry out oxygenic photosynthesis, converting carbon dioxide (CO_2) to organic matter. The calcification activity in cyanobacteria is a non-obligate process that is influenced by exopolymeric substances (EPS) layer, photosynthetic activity, carbon concentrating mechanism (CCM), and environmental factors. Among these, CCM is an integral part of the calcification [33]. This calcification process occurs in the EPS layer outside the cell wall. The alkaline pH is maintained in the EPS layer due to the carbonic anhydrase activity in the carboxysome. In this mechanism, the CO_2 is transported through the plasma membrane to the cytosol by bicarbonate (HCO_3^-) and sodium (Na^+) symports. Cytosolic bicarbonate is further converted to carbon dioxide by carbonic anhydrase activity [31]. Then CO_2 reacts with water to form carbonic acid (H_2CO_3), which dissociates to form bicarbonate (HCO_3^-) and release hydrogen ions (H^+) (Eqs. (1)–(3)). This phenomenon leads to the alkalinization of the cell surface by an increase in the pH [31,34]. The alkalization shifts the bicarbonate equilibrium and increases the carbonate (CO_3^{2-}) concentration on the cell's outer membrane (Eq. (3)).

$$CO_2 + H_2O \leftrightarrow H_2CO_3 \tag{1}$$

$$H_2CO_3 \leftrightarrow HCO_3^- + H^+ \tag{2}$$

$$HCO_3^- \leftrightarrow CO_3^{2-} + H^+ \tag{3}$$

When a calcium source is available, the calcium ions (Ca^{2+}) are transported to the cell surface by Ca^{2+}/H^+ antiporter/or are attracted by negatively charged groups in the cell wall [35]. Bacterial and cyanobacterial cells have various functional groups, such as sulfhydryl (-SH), amino (-NH_2), carboxyl (-COOH), and hydroxyl (-OH) groups, which serve as nucleation sites for binding with Ca^{2+} ions in solution and increase the $CaCO_3$ precipitation presumably in the EPS and S layer surrounding the cell (Eqs. (4) and (5)) [36].

$$Ca^{2+} + 2HCO_3^- \leftrightarrow CaCO_3 + CO_2 + H_2O \tag{4}$$

$$Ca^{2+} + CO_3^{2-} \leftrightarrow CaCO_3 \tag{5}$$

Many cyanobacterial species, such as *Oscillatoria* sp., *Synechococcus* sp., and *Synechocystis* sp., are reported to precipitate $CaCO_3$ [37–39]. Zhu et al. [40], and Obst et al. [35] reported that the mortar cubes treated with cyanobacterial strain under illumination and darkness did not differ significantly in $CaCO_3$ precipitation, and both were comparable to that of the control. Cyanobacteria has the ability to adapt to low-light or dark conditions. Cyanobacterial cells can use even minimal ambient light to perform photosynthesis, utilizing chlorophyll and other pigments to capture photons and convert them into chemical energy [34]. Cyanobacteria also store energy in the form of glycogen or other storage polysaccharides during the periods of light [40]. These reserves can be used to sustain their metabolic processes when light is scarce. The dead intact cells containing plasma membrane and outermost S-layer macromolecules with carboxylate amine, and hydroxyl functions, have been proposed to effectively generate a net negative surface charge as a function of increasing pH [41]. Two microalgal species, *Synechococcus elongatus* and *Spirulina platensis* were used to heal the cracks, in a mortar [42]. These studies present the potential use of cyanobacteria for improving cementitious properties. However, the application of $CaCO_3$ precipitation by cyanobacteria is still in the process of development, and more research needs to be done before its application in the field.

The present investigation mainly focuses on the comparative analysis of photoautotrophic and heterotrophic bacteria in improving the mechanical and permeability properties of concrete. The microstructural analysis of concrete specimens was performed using field emission scanning electron microscope (FESEM) and energy dispersive X-ray spectroscopy (EDS), and X-ray diffraction (XRD) to confirm the $CaCO_3$ precipitation. An attempt has also been made to analyse the economics of both the processes.

2. Materials and methodology

2.1. Biological culture

The study used two strains, photoautotrophic bacteria, *Synechocystis pevalekii* BDHKU 35101 and the other ureolytic bacteria, *Bacillus paramycoides* MD6, with different modes of nutrition. *S. pevalekii* BDHKU 35101 was obtained from the National Facility for Marine Cyanobacteria at Bharathidasan University Tiruchirappalli, Tamil Nadu, India [43]. This strain was cultivated and maintained in blue-green algae (BG11) broth under controlled conditions of 25 ± 2 °C, with the illumination of 1200 lux for 12 h of light followed by 12 h of dark under shaking conditions at 110 rpm [31]. *B. paramycoides*, a heterotrophic strain, was isolated from marble dust collected from a marble dumping yard in Kishangarh, Rajasthan, India. The *B. paramycoides* was grown in nutrient broth (Hi media, India) and incubated at 37 °C under shaking conditions at 120 rpm.

2.2. Materials

The study used commercially available ordinary Portland cement (OPC) - 43 grade, as per the Indian standard [44]. As fine aggregates, locally sourced natural well-graded river sand was used, meeting the requirements of Zone II according to the Indian standard [45]. The fine aggregate had a specific gravity of 2.62 and a water absorption rate of 1.3%. Coarse aggregates with particle sizes of 20 mm and 10 mm were used, having specific gravities of 2.61 and 2.63, and water absorption rates of 1.38% and 1.42%, respectively [46]. The use of a combination of two different coarse aggregate sizes was done to achieve maximum particle density in the concrete mix. Smaller aggregates (10 mm in this case) fill the gaps between the larger aggregates (20 mm), leading to a denser mixture. The fine and coarse aggregates used in the casting process complied with the Indian standards [45].

2.3. Microbial growth cycle

The cyanobacterial strains *S. pevalekii* BDHKU 35101 was inoculated in autoclaved BG11 broth and incubated at 25 ± 2 °C and under shaking conditions (110 rpm) with 12 h light and 12 h dark cycle. *B. paramycoides* was inoculated in autoclaved nutrient broth (NB) and incubated at 37 °C. The initial inoculum dose was maintained same (Optical density of 0.05) for both the bacteria. The growth was monitored by spectrophotometric measurement at 680 nm for *S. pevalekii and* 600 nm for *B. paramycoides* with regular intervals of time.

2.4. Microbial density and calcium carbonate precipitation

The *S. pevalekii* cells with an optical density of 0.5 at 680 nm were introduced in BG11 broth supplemented with 50 mM sodium bicarbonate ($NaHCO_3$) and 100 mM calcium chloride ($CaCl_2$). The flasks were then placed on a rotating shaker in a temperature-controlled incubator at 25 ± 2 °C under the constant shaking of 110 rpm. Illumination was provided at an intensity of 1200 lux, with a photoperiod of 12 h of light followed by 12 h of dark. The concentration of $CaCl_2$ used is within the range of concentrations employed in other studies on microbially induced calcium carbonate precipitation (MICCP) [47,48]. At the same time, overnight grown *B. paramycoides* with an optical density of 0.5 was inoculated in the nutrient broth supplemented with 2% urea and 25 mM $CaCl_2$. Triplicate flasks were prepared for each sample. The *S. pevalekii* growth was monitored by spectrophotometric measurement at O.D. of 680 nm and direct cell counting by haemocytometer at regular intervals of time. Similarly, for *B. paramycoides* the cells were plated on Nutrient Agar medium and counted the bacterial colonies and expressed in log colony forming units (log cfu/ml) at specific time intervals (24, 48, 72, 96, and 120 h). At the same time, the sample was collected and filtered through a 0.45 μm cellulose nitrate membrane to measure the quantity of $CaCO_3$ precipitated. The precipitates were washed twice with deionised water and lyophilized for FESEM analysis. The filtered solution was analysed for dissolved calcium (Ca^{2+}) ions using atomic absorption spectroscopy (AAS) experiment.

2.5. Effect of initial pH on $CaCO_3$ precipitation

The $CaCO_3$ precipitation was noted at different pH (6, 7, 8, 9, 10, 11 and 12) conditions by inoculating the *S. pevalekii* and *B. paramycoides* culture in BG11 broth and nutrient broth, respectively. The pH of the BG11 broth and nutrient broth was adjusted prior to autoclaving by sodium hydroxide (NaOH) and hydrochloride acid (HCl). The BG11 broth was supplemented with 50 mM $NaHCO_3$ and 100 mM $CaCl_2$. Whereas the nutrient broth was supplemented with 2 % urea and 25 mM $CaCl_2$. After 120 h, the broth was collected and filtered through a 0.45 μm cellulose nitrate membrane. The precipitates were washed twice with deionised water and dried in lyophilizer. The weight of $CaCO_3$ precipitates collected was measured.

2.6. Strength and permeability of concrete specimens

Prismatic specimens of 150 mm cubes and 100 (dia) × 200 (height) mm cylindrical concrete specimens were cast using cement,

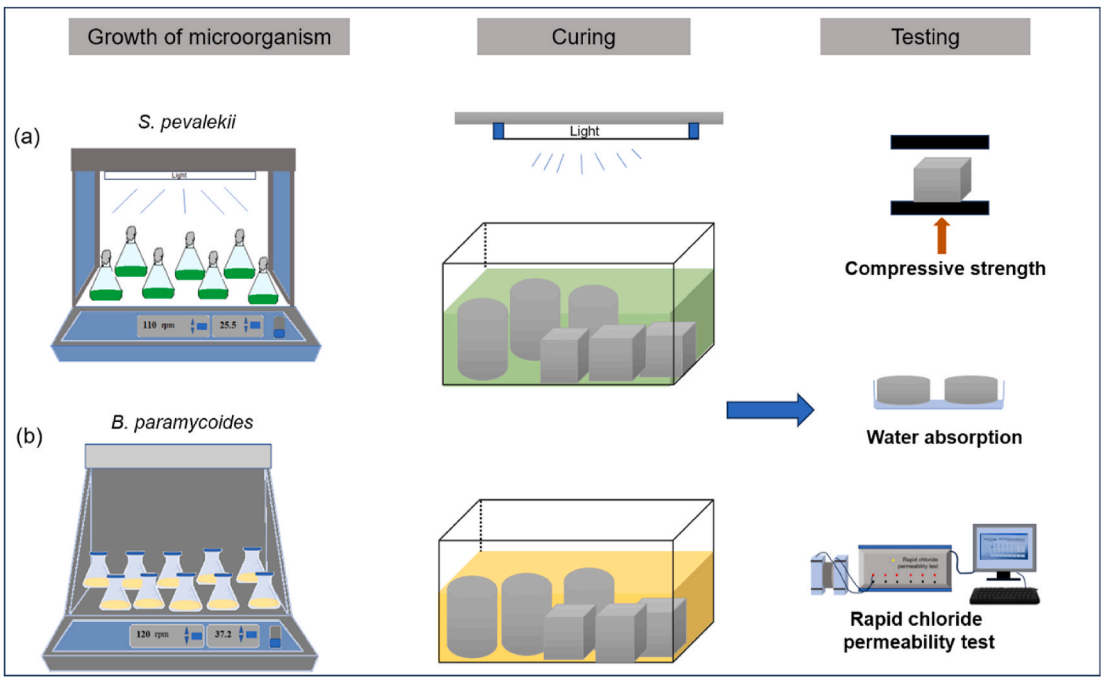


Fig. 2. The experimental setup for photoautotrophic bacteria *Synechocystis pevalekii* and heterotrophic bacteria *Bacillus paramycoides* for strength and permeability improvement in concrete.

sand, and coarse aggregate in the proportion of 1:1.82:3.24 (by weight) and 0.47 water-to-cement ratio (w/c) [46]. The culture of *B. paramycoides* (OD – 0.5) and *S. pevalekii* (OD – 0.5) was incorporated in the concrete mix along with the respective nutrients during the cast. The nutrition media used for *B. paramycoides* was nutrient broth (NB) along with 2% urea and 25 mM $CaCl_2$. Whereas for *S. pevalekii* culture, BG11 broth with 100 mM $CaCl_2$ and 50 mM $NaHCO_3$. The specimens were cured with respective bacterial culture and nutrient media as shown in Fig. 2. The control was prepared and cured in tap water. A detailed summary of the experimental set up is mentioned in Table 1. The 150 × 150 × 150 mm cubes were cast and tested for compressive strength, as per the Indian standards [49]. The compression test was carried at an age of 3, 7 and 28 days of curing, using the COMPTEST 3000 automatic compression testing machine (AIMIL India Ltd, New Delhi). A Relative strength index (RSI) was evaluated based on the compressive strength of the SPC and BPC specimen. Relative strength index (RSI) analysis is defined as the ratio between the compressive strength of microbes admixed (SPC and BPC) and normal concrete (control) [50]. Test specimens of 100 (dia) × 200 (ht) mm dimensions were cast for rapid chloride permeability (RCPT) and sorptivity coefficient. The 100 × 200 mm specimens were sliced into 100 (dia) × 50 (ht) mm size for testing the RCPT [51] and sorptivity experiment [52] as per the ASTM standard. For sorptivity test, the amount of water absorbed per unit cross-sectional area was calculated for each time interval at 60 s, 5, 10, 20, 30, 60 min, and every hour up to a maximum of 6 h. The RCPT test was performed to determine its resistance to chloride ion penetration. This test method involves saturating the concrete specimens and monitoring the amount of electrical current that passes through a concrete sample over a period of 6 h. The total charge passed (in terms of coulombs) is directly proportional to the electrical conductance of the concrete and a measure of its chloride penetrability. The results were expressed in the coulombs measuring the amount of current passed at 30-min intervals for 6 h.

2.7. Microstructural analysis

To determine the crystallization in concrete by bacterial treatment, the small chunk of concrete sample was taken for the microstructural investigation. Samples were sputter-coated with gold after being carefully polished. The FESEM-EDS was performed to determine the elements that make up microstructural crystals. X-ray diffraction (XRD) was carried out to identify the minerals and crystal formation in the sample. The Bruker D8 X-ray diffractometer was used to conduct the X-ray diffraction (XRD), which involved scanning from 20 to 60° at a two-theta angle with Cu anode (40 kV and 30 mA).

2.8. Cost analysis

The economic analysis of the biocalcification process by both the bacteria were analysed by considering the cost of various components in the media. This information was then used to compare the cost of utilizing the two different microbial (*S. pevalekii* and *B. paramycoides*) cultures in the calcification process.

2.9. Statistical analysis

All the experiments were performed in triplicates. Data were analysed by analysis of variance, and the means were compared using Tukey's test at $P < 0.05$. using the GraphPad Prism 8.0.1 software.

3. Results and discussion

3.1. Microbial growth cycle

Fig. 3 illustrates the cyanobacterial and bacterial density at different time intervals. Variation in cell density was observed in both photoautotrophic and heterotrophic bacteria. The exponential growth of *S. pevalekii* started from after 48 h and lasted until the 288 h of the culture period. Later, *S. pevalekii* growth gradually entered the initial stationary phase. The lag phase of the growth kinetics corresponds to a low concentration of bacterial cells ($\sim 10^1$ cells/ml), whereas the initial-log phase of growth kinetics corresponds to the concentration of $\sim 10^3$ cells/ml. The highest concentration of live, active cells was observed during the late log phase or early stationary phase of growth, which is equivalent to the optical density of 2.02. The lag phase for heterotrophic bacteria, *B. paramycoides* retained for 4 h after which it enters into the log phase. The cells grow exponentially during the log phase increasing the concentration of cells ($\sim 10^6$ cells/ml). After 10 h, the bacterial cycle enters the stationary phase which corresponds to an optical density of 1.27. Similar reports were reported by Foster et al. [53]and Sahoo et al. [54].

3.2. Microbial density and calcium carbonate precipitation

As shown in Fig. 4, microbial growth and amount of $CaCO_3$ precipitated by *S. pevalekii* and *B. paramycoides* was measured after 24,

Table 1
Outline of the different mix design of the experiment and curing treatment.

Specimens	Material used	Curing
Control	Cement: sand: coarse aggregates Water/cement = 0.47	Water curing
BPC[a]	Cement: sand: coarse aggregates culture/cement = 0.47 2 % urea +25 mM $CaCl_2$	Submersion in *B. paramycoides* culture supplemented with 2% urea and 25 mM $CaCl_2$
SPC[a]	Cement: sand: coarse aggregates culture/cement = 0.47 50 mM $NaHCO_3$ + 100 mM $CaCl_2$	Submersion in *S. pevalekii* culture supplemented with 50 mM $NaHCO_3$ and 100 mM $CaCl_2$

[a] The curing medium was replenished every seven days with respective media and inoculated with the freshly prepared culture.

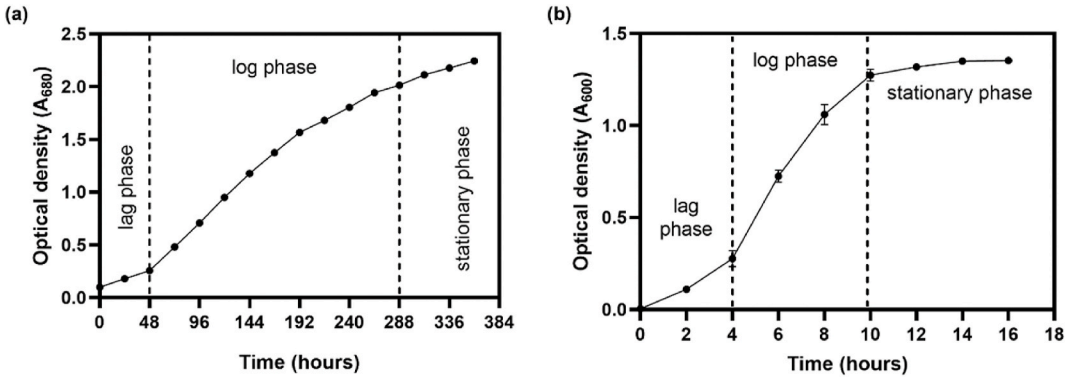


Fig. 3. Growth curve of (a) *S. pevalekii* and (b) *B. paramycoides* cell culture marked by different phases such as lag phase, log phase, and stationary phase at different time interval.

48, 72, 96, and 120 h of incubation. At the end of the experiment, *S. pevalekii* and *B. paramycoides* precipitated 695.7 and 860 mg/100 ml of $CaCO_3$. The $CaCO_3$ precipitation by *B. paramycoides* was 19.1% more than the cyanobacterial strain, *S. pevalekii*. The incubation time was found to have a significant effect on the $CaCO_3$ precipitation. The cell density was evaluated in the NB and BG11 broth in correspondence to the $CaCO_3$ precipitated. The cell density of *S. pevalekii* cells showed an increasing trend during the incubation period (Fig. 4a) whereas *B. paramycoides* cell culture showed a declining trend after 48 h of incubation (Fig. 4b). This might be due to exhaustion of the nutrients in the NB. The photoautotrophic bacteria can survive at low nutrient requirement and has longer log phase than the heterotrophic bacteria. The cell density was evaluated by measuring cell numbers and expressing them in log cfu/ml. Initially, 1×10^6 cells were inoculated in the medium which corresponds to log 6.0 CFU/ml. The *B. paramycoides* increased to 8.5 log CFU/ml after 48 h of incubation. Then, the biomass of *B. paramycoides* decreased to 7.2 log CFU/mL after 120 h. Similarly, *S. pevalekii* cells increased to 7.9 log CFU/mL after 120 h.

At similar time, the amount of dissolved calcium in the filtrate was analysed with the increase in incubation time using atomic adsorption spectroscopy (Fig. 5). The dissolved calcium in the culture broth decreased with an increase in the incubation time. The amount of dissolved Ca^{2+} ions in NB inoculated with *B. paramycoides* after 24 and 120 h was 16.9 mM and 1.3 mM, respectively. Whereas the amount of dissolved Ca^{2+} in BG11 broth inoculated *S. pevalekii* was 20.5 mM and 7.8 mM after 120 h of incubation. The photoautotrophic cyanobacteria and heterotrophic bacteria efficiently induced the $CaCO_3$ precipitation in solution. The *B. paramycoides* is a ureolytic strain and significantly precipitated more $CaCO_3$ than the *S. pevalekii*. Many external environmental factors can influence $CaCO_3$ precipitation. The $CaCO_3$ precipitation by the *S. pevalekii* strain is due to a phototrophic reaction in comparison to *B. paramycoides*, which is due to urea hydrolysis [8,33,35]. The ureolytic reaction is a direct pathway for calcium carbonate formation [55]. At the same time, the photosynthetic response by cyanobacteria can indirectly influence calcium carbonate precipitation through EPS production, which serves as a suitable nucleation site for mineralization [56]. Ureolytic reactions occur in the presence of the urease enzyme released during the metabolic activity of the bacteria. Ureolytic bacteria can use urea as a nitrogen source, and their enzymatic activity leads to the formation of ammonia and carbonate ions [57]. The binding of calcium ions (Ca^{2+}) with carbonates increases with increasing incubation time until equilibrium is reached. The maximum $CaCO_3$ precipitation by bacterial biomass in the NB supplemented with urea and $CaCl_2$ was observed till 120 h of incubation. After the equilibrium is attained, no $CaCO_3$ precipitation was observed, which might be due to the unavailability of nutrients. However, cyanobacterial cells can survive for a long time compared to heterotrophic bacteria [58]. The statistical analysis proved that incubation time significantly affects ($p < 0.001$) the $CaCO_3$ precipitation by *S. pevalekii* and *B. paramycoides* strains. Similar results were reported in the previous studies [59–62]. Researchers have also reported calcium carbonate precipitation induced by *Synechococcus* [63], and *Synechocystis* [39,64] in

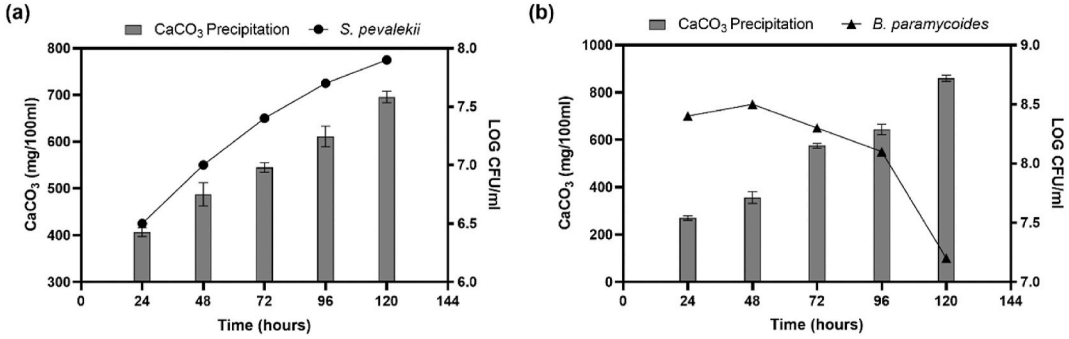


Fig. 4. Cell density of microbes and calcium carbonate ($CaCO_3$) precipitation by (a) *S. pevalekii* and (b) *B. paramycoides* cells during 120 h incubation.

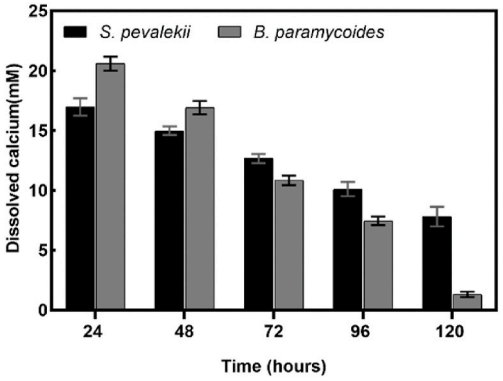


Fig. 5. Dissolved calcium (Ca^{2+}) ions in the BG11 and NB broth during $CaCO_3$ precipitation experiment.

solution at lab scale study.

3.3. FESEM analysis

Fig. 6 shows FESEM imaging of the calcium carbonate crystal in powdered precipitates collected in the filtrate after the calcium carbonate experiment. The crystallization was observed to be rhombohedral calcite as formed in both the solutions by *S. pevalekii* and *B. paramycoides*. The crystals formed in size ranging from 500 nm to 5 μm aggregated to form different structural layers as seen by both strains. The observation was taken after 120 h of incubation at respective temperature conditions. The $CaCO_3$ crystallization confirmed the biomineralization efficiency of *S. pevalekii* and *B. paramycoides* in controlled laboratory conditions. The formation of biofilm was observed in *S. pevalekii* precipitates. Cyanobacteria have a layer of exopolymeric substances (EPS), which can form biofilms. It has been observed that some of the rhombohedral and spherical precipitates were closely associated with each other forming a stacked layer of crystallization, while the remaining ones were randomly distributed throughout the biofilm. Similar findings were reported by Zhu et al. [47].

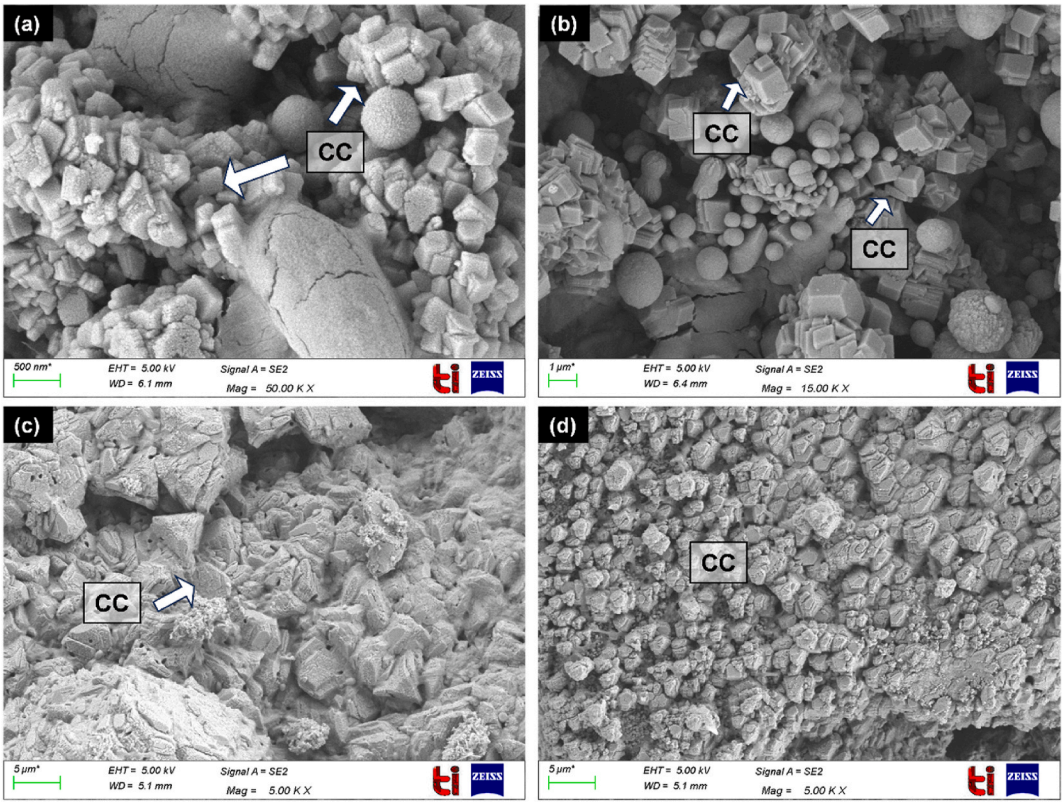


Fig. 6. FESEM analysis of calcium carbonate crystallization formed by (a, b) *S. pevalekii* and (c, d) *B. paramycoides* after 120 h.

3.4. Effect of initial pH on $CaCO_3$ precipitation

The pH affects the growth and $CaCO_3$ precipitation. As shown in Fig. 7, the maximum $CaCO_3$ precipitation was observed in nutrient broth inoculated with *B. paramycoides* at pH 9. At pH 9, the *S. pevalekii* and *B. paramycoides* precipitated 858.3 mg/100 ml and 1025.3 mg/100 ml of $CaCO_3$ after 120 h, respectively. The $CaCO_3$ precipitation by *S. pevalekii* at pH 10, 11, and 12 was 799.6, 668.3 and 594.3 mg/100 ml, respectively. Similarly, $CaCO_3$ precipitation by *B. paramycoides* at pH 10, 11, and 12 was 975.6, 952.6, and 897.6 mg/100 ml, respectively. The pH of the medium affects the cell membrane permeability and growth of the bacterial cells, thus affecting the $CaCO_3$ precipitation [65]. The increase in pH of the medium showed an increase in the $CaCO_3$ precipitation but decreased after the pH rose to 10, 11, and 12. The $CaCO_3$ precipitated at high pH illustrates the efficiency of ureolytic and photoautotrophic bacteria activity in cementitious environments. Whether ureolytic or photoautotrophic, both are efficient $CaCO_3$ precipitating microorganisms. Similar results were reported by other researchers [66–68]. Xu et al. documented optimum pH for ureolytic activity is 7–9.5 [69]. Hu et al. corroborated the formation of different polymorphs of calcium carbonate precipitates with the variation in pH [70]. The precipitation of elements such as magnesium, calcium and iron Fe in an alkaline environment (pH > 10.4) is likely to occur with the growth of cyanobacteria [71,72].

3.5. Compressive strength

The strength properties of concrete specimens were tested at 3, 7, and 28 days of curing. Fig. 8a shows a significant improvement in compressive strength was observed in *S. pevalekii* cured specimens (SPC) and *B. paramycoides* cured specimens (BPC) compared to the control. After 28 days of curing, the compressive strength of SPC and BPC specimens was 43.7 MPa and 44.5 MPa, respectively. At the same time, the control specimens showed 34.5 MPa of compressive strength. The strength of the concrete was significantly higher in samples treated by heterotrophic bacteria. The percentage increase (Δ%) in strength was evaluated compared to the control specimens by both strains. The SPC specimens showed a 26.6% improvement in compressive strength compared to which BPC specimens showed a 28.9% improvement in the strength properties of concrete (Fig. 8b). Comparing both strains, *B. paramycoides* cured specimens showed 14.97% more compressive strength than *S. pevalekii* cured specimens after seven days. However, upon further increasing the curing age, i.e., 28 days, the compressive strength of the *S. pevalekii* specimens improved, and the difference in the strength of the BPC and SPC specimens was only 1.8%. In cyanobacteria, the thickening property of the exopolymeric substance (EPS) surrounding the cell increases the bonding mechanism using the adhesion property [42]. With the increase in the curing period, the adhesion property helps the cyanobacterial cells to bind with the cement particles and aggregates. EPS mainly consists of proteins and polysaccharides. The adhesion of cells to the hard substrate depends on several parameters, including substrate composition, pH, organic film, cell density and surface roughness [73]. Microorganisms adhere to substrates either by generic physical–chemical forces, such as van der Waals and electrostatic forces, or by the specific surface structures of the cell, such as pili, fimbriae, or other appendages [74]. The EPS promotes the cyanobacterial cells adhesion to the rough surface, and subsequently form calcium carbonate above them by attracting the positively charged Ca^{2+} using the negatively charged functional groups such as carboxylate, amine, phosphoryl/phosphodiester and hydroxyl present on the cell surface [8]. Consequently, the calcium carbonate particles formed by cyanobacteria act as fillers that plug the interconnected pores in the concrete matrix, reducing the air gap. During ureolytic reaction by heterotrophic bacteria urease enzyme acts as a catalyst and initiates the $CaCO_3$ precipitation as bacterial growth enters the log phase. If urea and calcium sources are available, the biomass of bacteria produces the carbonate precipitation that fills up the pores in the concrete [75,76]. The analysis of variance inferred that the incorporation of different bacterial treatments and curing periods (3, 7 and 28 days) had a significant effect on the strength properties of concrete (Table 2). Similar findings were reported by other researchers upon the addition of heterotrophic bacteria in cementitious specimens [26,75,77]. In another research carried out by Hernández et al. and Zhu et al. the compressive strength of the concrete and mortar specimens was significantly improved by cactus mucilage, marine brown and *Gloeocapsa* PCC73106, algae, respectively [47,78].

3.6. Relative strength index

As shown in Fig. 9 the RSI of the SPC specimen increased with an increase in curing period. Initially, at 3 days the relative strength

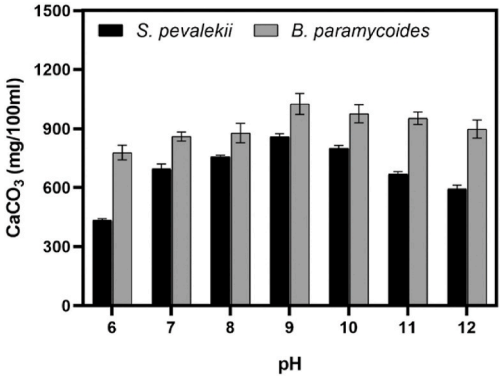


Fig. 7. Calcium carbonate precipitation by *S. pevalekii* and *B. paramycoides* at varied initial pH of BG11 and nutrient broth after 120 h.

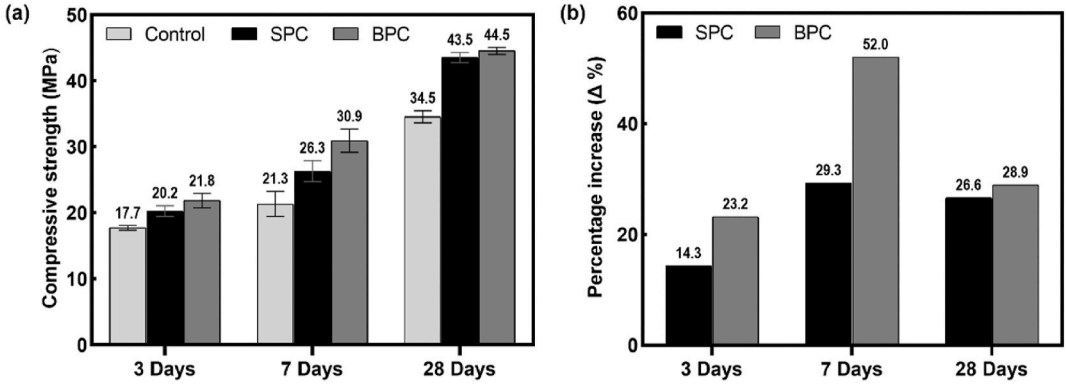


Fig. 8. (a) Compressive strength (b) percentage change in compressive strength at 3, 7, 28 days of curing.

Table 2
The factorial ANOVA results indicate the effects of different treatments (*S. pevalekii*, *B. paramycoides*, and control) and time of curing for concrete specimens.

Variables		Treatment	Time	Interaction (Specimens × Time)
Compressive strength	df	2,18	2,18	4,18
		$P < 0.0001$	$P < 0.0001$	$P = 0.0004$
RCPT	df	2,12	1,12	2,12
		$P < 0.0001$	$P < 0.0001$	$P = 0.0016$

index (RSI) of the SPC specimen was 1.14, which increased to 1.23 and 1.26 at 7 and 28 days of curing period, respectively. However, RSI of BPC specimens was 1.23 at 3 days, which increased to 1.45 at 7 days and decreased to 1.28 at 28 days of curing. There was a significant difference in the RSI of SPC and BPC specimens at 7 days which clearly indicates a lesser amount of $CaCO_3$ precipitation in the SPC specimen at 7 days. This could be explained by the fact that ureolytic activity of the heterotrophic bacteria is fast as compared to light-dependent pathway of photoautotrophic bacteria. The cell biomass increased with increase in incubation period in curing period of photoautotrophic bacteria which tremendously improved the strength properties of concrete at 28 days. Similar findings were reported by other researchers [79,80].

3.7. Rapid chloride penetration test (RCPT)

The RCPT of the concrete specimen was tested at 7 and 28 days of curing. The chloride penetration in the concrete samples decreased with an increased curing period. A significant decrease was observed in concrete specimens treated by *S. pevalekii* and *B. paramycoides* bacterial culture. Compared to the control, the BPC specimens treated by heterotrophic strain *B. paramycoides* showed minimum penetration among all the groups. Fig. 10a represents the current passed through SPC and BPC specimens during the RCPT experiment, which was 1901 and 1440 coulombs (C). As shown in Fig. 10b, the test results for BPC specimens showed 27.2% and 57.8% reduction after 7 and 28 days of curing by decreasing chloride ingression during the RCPT experiment, respectively. On the contrary, SPC specimens showed 20.6 % and 44.3% reductions in chloride penetration. As per the ASTM standard C1202, the penetrability of chloride ions after 28 days of curing was moderate based on the charge passed through the specimens [51]. This might be due to $CaCO_3$ particles that seal the pores in concrete, making it difficult for water and other particles to infiltrate through concrete

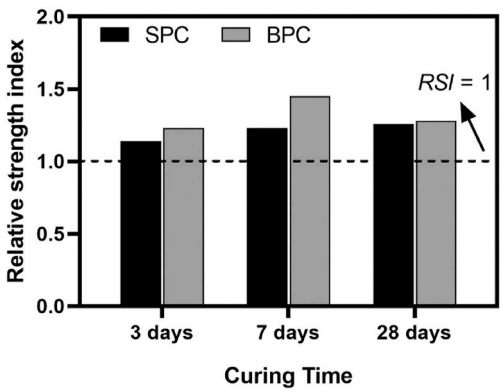


Fig. 9. Relative strength index of SPC and BPC specimens at 3, 7 and 28 days of curing.

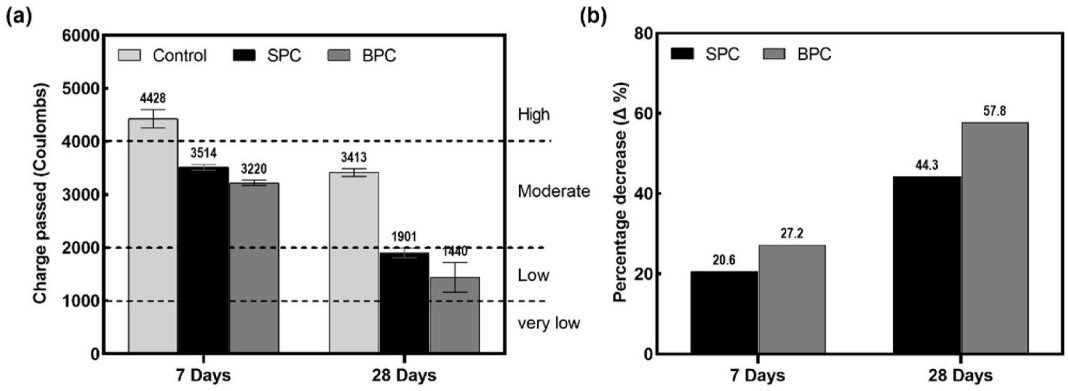


Fig. 10. (a) Rapid chloride permeability test (RCPT) (b) percentage change in RCPT at 7, 28 days of curing.

pores. However, the charge passed through the control specimen was higher than SPC and BPC specimens. The efficiency of the BPC specimen was initially observed to be equivalent to SPC specimens after seven days of curing. However, upon further increasing the curing period, the chloride ingression was significantly reduced by BPC specimens followed by SPC specimens. The statistical analysis showed that different curing treatments (*S. pevalekii*, *B. paramycoides,* and control) and curing time (7 and 28 days) have a significant effect on the chloride penetration in the cylindrical specimen (Table 2.). Similar findings were reported by other researchers [81–84].

3.8. Sorptivity test

The water absorption test was carried out at 7 and 28 days of curing. The results were analysed during the rapid absorption phase for initial 6 h. The results are illustrated in Fig. 11a and b as the average water absorption by 100 mm × 50 mm cylindrical specimens against square root mean of time. The seven days cured SPC and BPC specimens showed cumulative water absorption of 1.3 and 1.2 mm of water after 6 h of the experiment, respectively (Fig. 11a). Compared to which control specimen showed water absorption of 2 mm. It clearly indicates that bacterial treatment significantly affects the water absorption rate compared to the control. After seven days, the sorptivity coefficient '*k*' of BPC, SPC, and control specimens was observed to be 0.007, 0.008, and 0.011, respectively. After 28 days of curing, the control specimens showed higher water absorption of 1.7 mm, which might be due to the rise of water through capillary pores. However, bacterial curing showed a significant reduction in BPC and SPC specimens. BPC specimens showed 0.94 mm of average water absorption whereas SPC showed 1.2 mm of water absorption at the end of experiment. It might be due to the activity of bacteria that precipitates the $CaCO_3$ particles in the pores of the concrete. As a result, the interconnected capillary pores were blocked, reducing the water's capillary rise in concrete. The sorptivity coefficient '*k*' evaluated for the BPC, SPC, and control specimens was 0.005, 0.007, and 0.01, respectively (Table 3). The lower sorptivity coefficient '*k*' for the BPC and SPC specimens proved that ureolytic action and photosynthetic reaction reduce the capillary pores of the specimens. Similar results were reported by Xu et al. [69], Anand et al. [22], and Vaezi et al. [85] in ureolytic bacteria-based concrete. Sidhu et al. reported reduced water absorption using live and UV-killed cyanobacterial cells in mortar compared to the control specimen [47].

3.9. Microstructural analysis

Fig. 12 shows the structural analysis of calcium carbonate precipitation in the concrete sample. The crystals were overlapping, forming a dense layer of calcite in the concrete by *S. pevalekii* and *B. paramycoides*. Whereas, calcite formation was not seen in control (Fig. 12a). The crystals were tightly packed and formed perfect rhombohedral crystal lattice in a size range of 0.5–1 μm in SPC specimens (Fig. 12b). Likewise, *B. paramycoides* treated specimens showed rhombohedral crystal formation ranging in size 5–10 μm

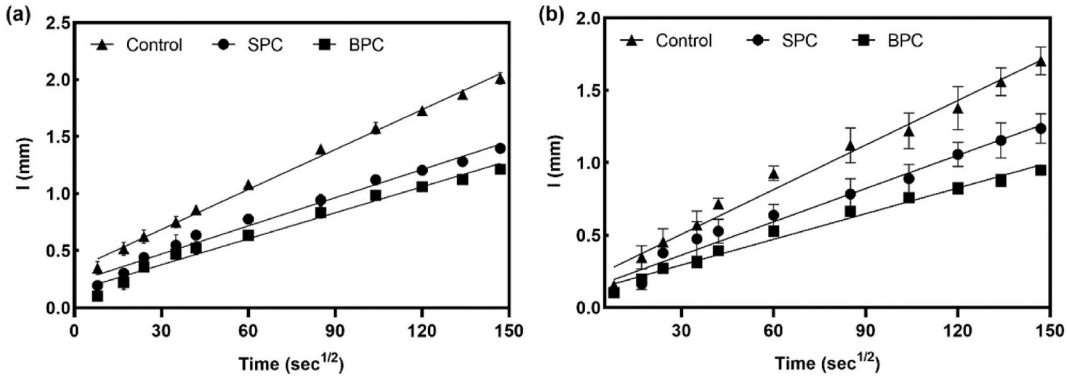


Fig. 11. Water absorption concrete specimens treated with *S. pevalekii* (SPC), *B. paramycoides* (BPC) along with the control at (a) 7 days (b) 28 days of curing.

Table 3
The factorial ANOVA results indicate the effects of different treatments (*S. pevalekii*, *B. paramycoides*, and control) and time of curing for concrete specimens.

variables	Sorptivity coefficient 'k'		R^2			
	7 days	28 days	7 days	28 days	P value	Significant
Control	0.01168	0.01207	0.9906	0.9592	$P < 0.0001$	Yes
SPC	0.00823	0.007658	0.9766	0.9415	$P < 0.0001$	Yes
BPC	0.00759	0.005902	0.9715	0.9792	$P < 0.0001$	Yes

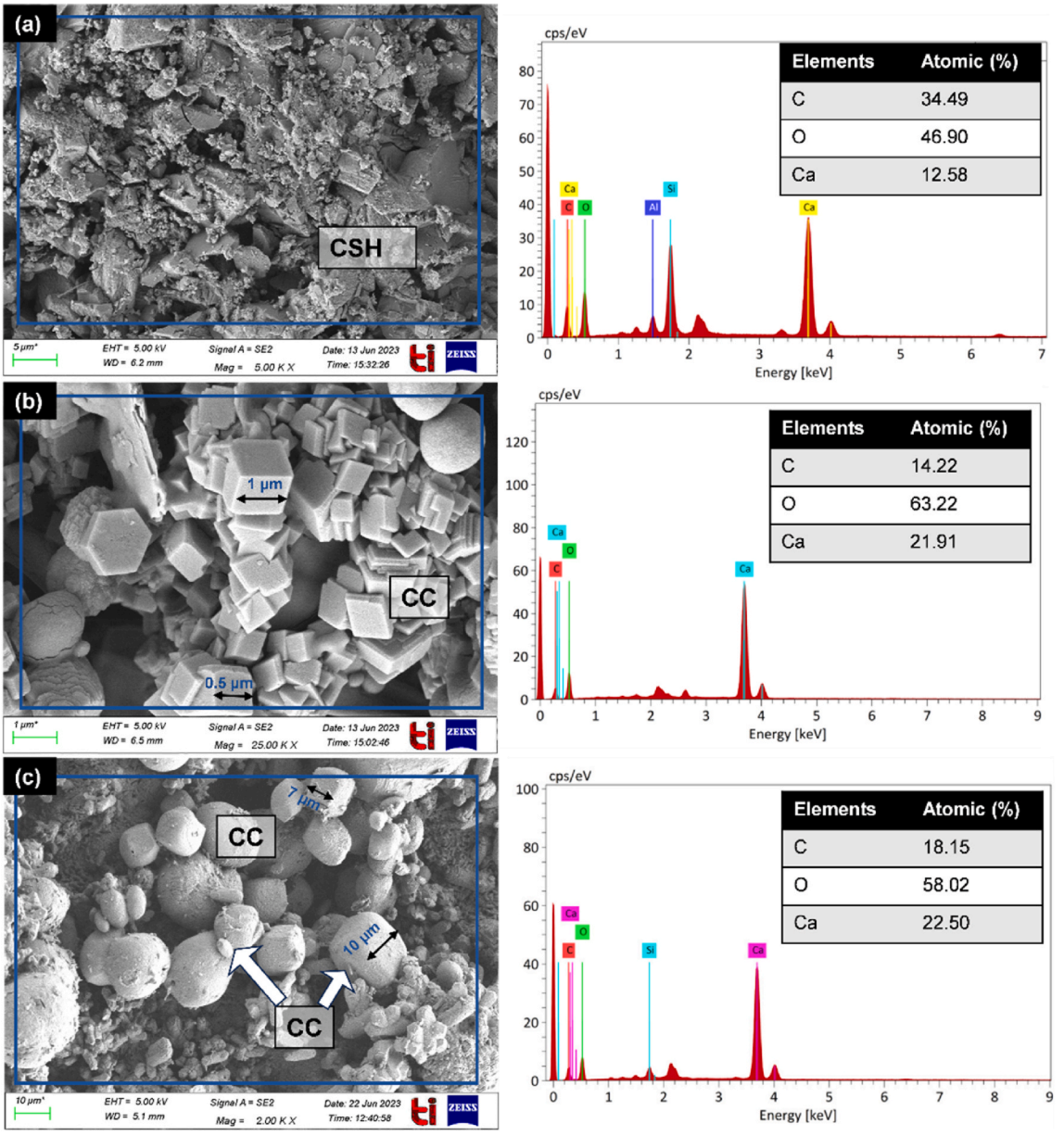


Fig. 12. FESEM-EDS of (a) control (b) SPC (c) BPC specimen. The square '□' sign indicates the spot for EDS analysis.

(Fig. 12c). The crystals exhibited a variation in sizes of calcite precipitated, which can be attributed to the interaction between nucleation and growth. This interaction is influenced by the effects of microbial concentration and cementation media. A small amount of vaterite crystals were also formed. Different theories have been proposed to explain the coexistence of two different polymorphs 'calcite and vaterite' together. It is widely acknowledged that vaterite is a thermodynamically unstable crystal form and exhibits a higher nucleation rate compared to other forms of calcium carbonate [86,87]. The slow diffusion of Ca^{2+} and CO_3^{2+} ions can result in

the formation of calcite in the later stage [88]. Another possible reason could be involvement of different functional groups of the cell surface that provides nucleation site for biomineralization [63]. Both crystals precipitates were calcium carbonate, which was confirmed by EDX and XRD analysis. The mineral constituents characterized by EDX analysis indicates the amount of calcium, oxygen, and carbon formed in SPC and BPC specimens was high as compared to the control which could be due to calcium carbonate precipitation. The calcite precipitation by heterotrophic bacteria was also reported by Park et al. [89], Qian et al. [90], and Qin et al. [91]. Similarly, Zhu et al. demonstrated calcite precipitation by cyanobacterial species [47,92]. Anand et al. reported calcite crystallization by *Bacillus megaterium* SS3 in concrete [93]. Previous studies have also demonstrated the presence of CSH/$Ca(OH)_2$ in the microstructural analysis of concrete [94,95].

3.10. XRD

The X-ray diffraction analysis confirmed calcite precipitation in the hardened concrete cured using two microbial cultures (*S. pevalekii* and *B. paramycoides*) at 28 days. XRD spectrums of SPC, BPC, and control sample are presented in Fig. 13. The prominent peaks observed in the powdered concrete sample are quartz (Q), calcium silicate hydrate (CSH), calcite (C), and vaterite (V). The intensity peak of calcite observed at 29.2° was higher in SPC and BPC specimens than in the control. Calcite, aragonite, and vaterite are the three primary polymorphs of calcium carbonate crystals, out of which calcite is the most stable form of crystalline [86,88,96]. The microbial activity occurring in concrete results in calcite crsytallization in the concrete matrix. The weak diffraction peak of vaterite was also seen in the SPC and BPC specimens which is a thermodynamically unstable crystal form with a high nucleation rate. The slow diffusion of carbonates (CO_3^{2-}) and calcium ions (Ca^{2+}) can lead to calcite formation [86]. Both microbial cultures efficiently induced the calcite precipitation in the concrete. It is unclear why different polymorphs of calcium carbonate are formed during microbial $CaCO_3$ mineralization in concrete. Stuckrath et al. inferred the presence of functional groups, such as sulfhydryl (-SH), amino (-NH_2), carboxyl (-COOH), and hydroxyl (-OH) groups, that serve as nucleation sites for binding with Ca^{2+} ions can control the crystal deposition [97]. Other factors affecting $CaCO_3$ precipitation are calcium ion concentration, dissolved inorganic carbon (DIC) concentration, pH, and the availability of nucleation sites [98].

3.11. Cost analysis

The total cost of the two different MICP mechanism consists of the price of the bacterial growth media. The price of conventional concrete is approximately Rs.5623/m^3 (68.36 USD/m^3) [99]. The theoretical cost of the MICP product depends on the price of the microorganism and the nutrients growth media used. The total cost estimated for nutrient broth for heterotrophic bacteria is about Rs 30.93/L (0.37 USD/L), while it was Rs 16.21/L (0.19 USD/L) for cyanobacterial nutrient media (BG11 broth). This cost is very much near to the cost of bacteria estimated by other studies [100–102]. The cost analysis demonstrated that the price of microbial concrete incorporating heterotrophic and photoautotrophic is 2.0 and 1.5 times higher than the price of conventional concrete, respectively. The potential for further cost reduction in the production of bacterial concrete can be done using inexpensive nutrient ingredients, such as corn steep liquor a waste from starch industry [103], or lactose mother liquor (from dairy industry) [104].

4. Conclusions

The current investigation elucidates the efficiency of $CaCO_3$ precipitation by photoautotrophic and heterotrophic bacteria and its impact on concrete's strength and permeability properties. The $CaCO_3$ precipitation pathway varied in both microbial cultures because of their different metabolic activities. Concerning the comparative analysis of *S. pevalekii* and *B. paramycoides*, there was no significant difference in the compressive strength of SPC and BPC specimens after 28 days. The microbial cultures used further improved concrete properties by decreasing the latter's permeability. The sorptivity coefficient '*k*' of SPC and BPC specimens after 28 days was 0.007 and 0.005, respectively. The charge passed through the SPC and BPC concrete specimen after 28 days was 1901 and 1440 coulombs, respectively. These findings suggest MICP mechanism of heterotrophic bacteria was more effective in improving the concrete properties than the MICP mechanism of photoautotrophic bacteria. Comparing the interaction of bacteria with cementitious material,

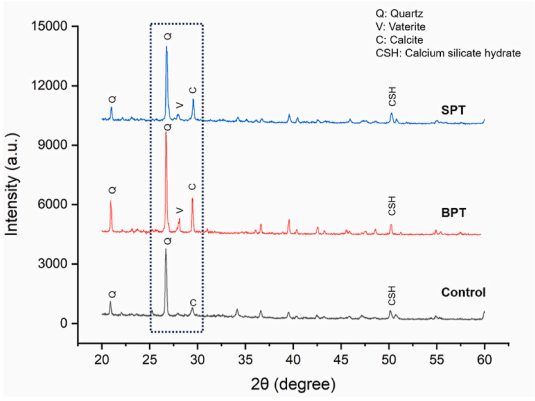


Fig. 13. XRD of control, SPC, and BPC concrete specimen.

photoautotrophic culture has an advantage over ureolytic bacteria as it reduces the emission of ammonia in an environment which is a major concern.

CrediT authorship contribution statement

Navneet Sidhu: Investigation, Methodology, Data Curation, Data Analysis, Validation, Writing Original Draft. **Shweta Goyal**: Conceptualization, Methodology, Supervision, Project Administration, Resources, Writing - Review & Editing. **M. Sudhakara Reddy**: Conceptualization, Methodology, Supervision, Project Administration, Resources, Writing - Review & Editing.

Declaration of competing interest

The authors declare that they have no known competing financial interests or personal relationships that could have appeared to influence the work reported in this paper.

Data availability

Data will be made available on request.

Acknowledgments

The authors are thankful to the Department of Biotechnology, Ministry of Science and Technology, Govt. of India, for providing the research grant under BT/PR27190/BCE/8/1428/2017.

References

[1] S.A. Miller, F.C. Moore, Climate and health damages from global concrete production, Nat. Clim. Change 10 (2020) 439–443, https://doi.org/10.1038/s41558-020-0733-0.
[2] L.S. Wong, Microbial cementation of ureolytic bacteria from the genus *Bacillus*: a review of the bacterial application on cement-based materials for cleaner production, J. Clean. Prod. 93 (2015) 5–17, https://doi.org/10.1016/j.jclepro.2015.01.019.
[3] N.K. Dhiman, N. Sidhu, S. Agnihotri, A. Mukherjee, M.S. Reddy, Role of nanomaterials in protecting building materials from degradation and deterioration, Biodegrad. Biodeterior. Nanoscale (2022) 405–475, https://doi.org/10.1016/B978-0-12-823970-4.00024-5.
[4] S.P. Bhutange, M.V. Latkar, Microbially induced calcium carbonate precipitation in construction materials, J. Mater. Civil Eng. 32 (2020) 1–12, https://doi.org/10.1061/(asce)mt.1943-5533.0003141.
[5] A.I. Omoregie, K. Muda, O.O. Ojuri, C.Y. Hong, F.M. Pauzi, N.S.B.A. Ali, The global research trend on microbially induced carbonate precipitation during 2001–2021: a bibliometric review, Environ. Sci. Pollut. Res. 29 (2022) 89899–89922, https://doi.org/10.1007/s11356-022-24046-w.
[6] A.S. Muhammed, K.A. Kassim, K. Ahmad, M.U. Zango, C.S. Chong, J. Makinda, Influence of multiple treatment cycles on the strength and microstructure of biocemented sandy soil, Int. J. Environ. Sci. Technol. 18 (2021) 3427–3440, https://doi.org/10.1007/s13762-020-03073-5.
[7] M.F. Ali, H. Mukhtar, L. Dufossé, Microbial calcite induction: a magic that fortifies and heals concrete, Int. J. Environ. Sci. Technol. 20 (2023) 1113–1134, https://doi.org/10.1007/s13762-022-03941-2.
[8] T. Zhu, M. Dittrich, Carbonate precipitation through microbial activities in natural environment, and their potential in biotechnology: a review, Front. Bioeng. Biotechnol. 4 (2016) 4, https://doi.org/10.3389/fbioe.2016.00004.
[9] A. Cuccurullo, D. Gallipoli, A.W. Bruno, C. Augarde, P. Hughes, C. La Borderie, Earth stabilisation via carbonate precipitation by plant-derived urease for building applications, Geomech. Energy Environ. 30 (2022), 100230, https://doi.org/10.1016/j.gete.2020.100230.
[10] E. Tziviloglou, V. Wiktor, H.M. Jonkers, E. Schlangen, Selection of nutrient used in biogenic healing agent for cementitious materials, Front. Mater. 4 (2017) 15, https://doi.org/10.3389/fmats.2017.00015.
[11] Jang, D. Son, W. Kim, W. Park, C. Yi, Effects of spray-dried co-cultured bacteria on cement mortar, Construct. Build. Mater. 243 (2020), 118206, https://doi.org/10.1016/j.conbuildmat.2020.118206.
[12] J. Wang, H.M. Jonkers, N. Boon, N. De Belie, *Bacillus sphaericus* LMG 22257 is physiologically suitable for self-healing concrete, Appl. Microbiol. Biotechnol. 101 (2017) 5101–5114, https://doi.org/10.1007/s00253-017-8260-2.
[13] A.A. Nasser, N.M. Sorour, M.A. Saafan, R.N. Abbas, Microbially-Induced-Calcite-Precipitation (MICP): a biotechnological approach to enhance the durability of concrete using *Bacillus pasteurii* and *Bacillus sphaericus*, Heliyon 8 (2022), e09879, https://doi.org/10.1016/j.heliyon.2022.e09879.
[14] P. Jongvivatsakul, K. Janprasit, P. Nuaklong, W. Pungrasmi, S. Likitlersuang, Investigation of the crack healing performance in mortar using microbially induced calcium carbonate precipitation (MICP) method, Construct. Build. Mater. 212 (2019) 737–744, https://doi.org/10.1016/j.conbuildmat.2019.04.035.
[15] P. Kaur, S. Joshi, O.A. Shinde, M. Sudhakara Reddy, Utilization of biomineralized steel slag in cement mortar to improve its properties, J. Mater. Civil Eng. 33 (2021), 04021116, https://doi.org/10.1061/(asce)mt.1943-5533.0003749.
[16] L.V. Zhang, A.R. Suleiman, M. Mehdizadeh Allaf, A. Marani, M. Tuyan, M.L. Nehdi, Crack self-healing in alkali-activated slag composites incorporating immobilized bacteria, Construct. Build. Mater. 326 (2022), 126842, https://doi.org/10.1016/j.conbuildmat.2022.126842.
[17] A.I. Omoregie, D.E.L. Ong, P.M. Nissom, Assessing ureolytic bacteria with calcifying abilities isolated from limestone caves for biocalcification, Lett. Appl. Microbiol. 68 (2019) 173–181, https://doi.org/10.1111/lam.13103.
[18] V. Achal, A. Mukherjee, M.S. Reddy, Biocalcification by *Sporosarcina pasteurii* using corn steep liquor as the nutrient source, Ind. Biotechnol. 6 (2010) 170–174, https://doi.org/10.1089/ind.2010.6.170.
[19] N. Nain, R. Surabhi, N.V. Yathish, V. Krishnamurthy, T. Deepa, S. Tharannum, Enhancement in strength parameters of concrete by application of *Bacillus* bacteria, Construct. Build. Mater. 202 (2019) 904–908, https://doi.org/10.1016/j.conbuildmat.2019.01.059.
[20] N.K. Dhami, M.S. Reddy, A. Mukherjee, *Bacillus megaterium* mediated mineralization of calcium carbonate as biogenic surface treatment of green building materials, World J. Microbiol. Biotechnol. 29 (2013) 2397–2406, https://doi.org/10.1007/s11274-013-1408-z.
[21] X. Sun, L. Miao, L. Wu, R. Chen, Improvement of bio-cementation at low temperature based on Bacillus megaterium, Appl. Microbiol. Biotechnol. 103 (2019) 7191–7202.
[22] K. Anand, S. Goyal, N. Kaur, M.S. Reddy, Viable FA based bacterial cells as sustainable solution for corrosion prevention in RC structures, Construct. Build. Mater. 365 (2022), 130056, https://doi.org/10.2139/ssrn.4138214.
[23] V. Wiktor, H.M. Jonkers, Quantification of crack-healing in novel bacteria-based self-healing concrete, Cem. Concr. Compos. 33 (2011) 763–770, https://doi.org/10.1016/j.cemconcomp.2011.03.012.
[24] N. Karimi, D. Mostofinejad, *Bacillus subtilis* bacteria used in fiber reinforced concrete and their effects on concrete penetrability, Construct. Build. Mater. 230 (2020), 117051, https://doi.org/10.1016/j.conbuildmat.2019.117051.

[25] J. Feng, B. Chen, W. Sun, Y. Wang, Microbial induced calcium carbonate precipitation study using *Bacillus subtilis* with application to self-healing concrete preparation and characterization, Construct. Build. Mater. 280 (2021), 122460, https://doi.org/10.1016/j.conbuildmat.2021.122460.

[26] N. Sidhu, S. Goyal, M.S. Reddy, Self-healing by biocomposite containing metakaolin immobilized bacterial spores in concrete using low-cost corn steep liquor media, J. Sustain. Cem. Mater. 12 (2023) 1430–1446, https://doi.org/10.1080/21650373.2023.2224805.

[27] Á. González, A. Parraguez, L. Corvalán, N. Correa, J. Castro, C. Stuckrath, M. González, Evaluation of Portland and Pozzolanic cement on the self-healing of mortars with calcium lactate and bacteria, Construct. Build. Mater. 257 (2020), 119558, https://doi.org/10.1016/j.conbuildmat.2020.119558.

[28] M. Zamani, S. Nikafshar, A. Mousa, A. Behnia, Bacteria encapsulation using synthesized polyurea for self-healing of cement paste, Construct. Build. Mater. 249 (2020), 118556, https://doi.org/10.1016/j.conbuildmat.2020.118556.

[29] G.A. Ramakrishnan VV, Nitrogen sources and cycling in the ecosystem and its role in air, water and soil pollution: a Critical Review, J. Pollut. Eff. Control. 3 (2015) 136, https://doi.org/10.4172/2375-4397.1000136.

[30] Justo-Reinoso, A. Heath, S. Gebhard, K. Paine, Aerobic non-ureolytic bacteria-based self-healing cementitious composites: a comprehensive review, J. Build. Eng. 5 (2021), 035006, https://doi.org/10.1016/j.jobe.2021.102834.

[31] N. Sidhu, S. Goyal, M.S. Reddy, Biomineralization of cyanobacteria *Synechocystis pevalekii* improves the durability properties of cement mortar, Amb. Express 12 (2022) 59, https://doi.org/10.1186/s13568-022-01403-z.

[32] T. Zhu, C. Paulo, M.L. Merroun, M. Dittrich, Potential application of biomineralization by *Synechococcus* PCC8806 for concrete restoration, Ecol. Eng. 82 (2015) 459–468, https://doi.org/10.1016/j.ecoleng.2015.05.017.

[33] C. Jansson, T. Northen, Calcifying cyanobacteria-the potential of biomineralization for carbon capture and storage, Curr. Opin. Biotechnol. 21 (2010) 365–371, https://doi.org/10.1016/j.copbio.2010.03.017.

[34] N.A. Kamennaya, C.M. Ajo-Franklin, T. Northen, C. Jansson, Cyanobacteria as biocatalysts for carbonate mineralization, Minerals 2 (2012) 338–364, https://doi.org/10.3390/min2040338.

[35] M. Obst, B. Wehrli, M. Dittrich, $CaCO_3$ nucleation by cyanobacteria: laboratory evidence for a passive, surface-induced mechanism, Geobiology 7 (2009) 324–347, https://doi.org/10.1111/j.1472-4669.2009.00200.x.

[36] H. Deng, X.M. Wang, C. Du, X.C. Shen, F.Z. Cui, Combined effect of ion concentration and functional groups on surface chemistry modulated $CaCO_3$ crystallization, CrystEngComm 14 (2012) 6647–6653, https://doi.org/10.1039/c2ce25731a.

[37] V.S. Gnanasekaran D, Biocalcification mediated remediation of calcium rich ossein effluent by filamentous marine cyanobacteria, J. Biorem. Biodegrad. 5 (2014) 257, https://doi.org/10.4172/2155-6199.1000257.

[38] S.A. Miller, A. Horvath, P.J.M. Monteiro, Impacts of booming concrete production on water resources worldwide, Nat. Sustain. 1 (2018) 69–76, https://doi.org/10.1038/s41893-017-0009-5.

[39] Z. Han, R. Meng, H. Yan, H. Zhao, M. Han, Y. Zhao, B. Sun, Y. Sun, J. Wang, D. Zhuang, W. Li, L. Lu, Calcium carbonate precipitation by *Synechocystis* sp. PCC6803 at different Mg/Ca molar ratios under the laboratory condition, Carbonates Evaporites 32 (2017) 561–575, https://doi.org/10.1007/s13146-016-0322-5.

[40] T. Zhu, X. Lu, M. Dittrich, Calcification on mortar by live and UV-killed biofilm-forming cyanobacterial *Gloeocapsa* PCC73106, Construct. Build. Mater. 146 (2017) 43–53, https://doi.org/10.1016/j.conbuildmat.2017.04.026.

[41] Kromkamp, Formation and functional significance of storage products in cyanobacteria, N. Z. J. Mar. Freshw. Res. 21 (1987) 457–465, https://doi.org/10.1080/00288330.1987.9516241.

[42] R.E. Martinez, O.S. Pokrovsky, J. Schott, E.H. Oelkers, Surface charge and zeta-potential of metabolically active and dead cyanobacteria, J. Colloid Interface Sci. 323 (2008) 317–325, https://doi.org/10.1016/j.jcis.2008.04.041.

[43] M. Srinivas, U.J. Alengaram, S. Ibrahim, S.M. Phang, V. Vello, H.K. Jun, A.M. Alnahhal, Evaluation of crack healing potential of cement mortar incorporated with blue-green microalgae, J. Build. Eng. 44 (2021), 102958, https://doi.org/10.1016/j.jobe.2021.102958.

[44] T. Bhuvaneshwari, M. Shylajanaciyar, P.A. Prakasam, K. Ezhilmaran, L. Karthick, G. Subramanian, L. Uma, D. Prabaharan, Polyphasic analysis for elucidating the taxonomic position of selected unicellular marine cyanobacteria from indian and Hong Kong coast, Phytotaxa 307 (2017) 263–277, https://doi.org/10.11646/phytotaxa.307.4.4.

[45] IS 8112, Specification for 43 grade ordinary Portland cement, Bur. Indian Stand. 17 (2013) 1–11.

[46] IS 383, Specification for Coarse and Fine Aggregates from Natural Sources for Concrete, Bur. Indian Stand., 2016, pp. 1–24.

[47] IS 10262, Indian Standard, Concrete Mix Proportioning – Guidelines (Second Revision), Bureau of Indian Stand, 2019, pp. 1–42.

[48] K. Paine, Bacteria-based self-healing concrete: effects of environment, exposure and crack size, in: Proceedings of the RILEM Conference on Microorganisms-Cementitious Materials Interactions vol. 1, RILEM Publications SARL, Paris, France, 2016, pp. 1–15.

[49] IS 516, Method of Tests for Strength of Concrete, Bur. Indian Stand., 2004, pp. 1–30.

[50] F. Chen, K. Wu, L. Ren, J. X, H. Zheng, Internal curing effect and compressive strength calculation of recycled clay brick aggregate concrete, Materials 12 (2019) 1815, https://doi.org/10.3390/ma12111815.

[51] ASTM C1202, Standard test method for electrical indication of concrete's ability to resist chloride ion penetration, Am. Soc. Test. Mater. Int. (2012) 1–8, https://doi.org/10.1520/C1202-10.2.

[52] ASTM C1585, Standard test method for measurement of rate of absorption of water by hydraulic cement concretes, Am. Soc. Test. Mater. Int. 41 (2013) 1–6, https://doi.org/10.1520/C1585-13.2.

[53] J.S. Foster, A.K. Singh, L.J. Rothschild, L.A. Sherman, Growth-phase dependent differential gene expression in *Synechocystis* sp. strain PCC 6803 and regulation by a group 2 sigma factor, Arch. Microbiol. 187 (2007) 265–279, https://doi.org/10.1007/s00203-006-0193-6.

[54] K.K. Sahoo, M. Arakha, P. Sarkar, D.P. Robin, S. Jha, Enhancement of properties of recycled coarse aggregate concrete using bacteria, Int. J. Smart Nano Mater. 7 (2016) 22–38, https://doi.org/10.1080/19475411.2016.1152322.

[55] K. Wen, Y. Li, F. Amini, L. Li, Impact of bacteria and urease concentration on precipitation kinetics and crystal morphology of calcium carbonate, Acta Geotech. 15 (2020) 17–27, https://doi.org/10.1007/s11440-019-00899-3.

[56] T. Veaudor, V. Blanc-Garin, C. Chenebault, E. Diaz-Santos, J.F. Sassi, C. Cassier-Chauvat, F. Chauvat, Recent advances in the photoautotrophic metabolism of cyanobacteria: biotechnological implications, Life 10 (2020) 17, https://doi.org/10.3390/life10050071.

[57] N.K. Dhami, M.S. Reddy, M.S. Mukherjee, Biomineralization of calcium carbonates and their engineered applications: a review, Front. Microbiol. 4 (2013) 314, https://doi.org/10.3389/fmicb.2013.00314.

[58] R. Yu, H. Chai, Z. Yu, X. Wu, Y. Liu, L. Shen, J. Li, J. Ye, D. Liu, T. Ma, F. Gao, W. Zeng, Behavior and mechanism of cesium biosorption from aqueous solution by living *Synechococcus* PCC7002, Microorganisms 8 (2020) 491, https://doi.org/10.3390/microorganisms8040491.

[59] F.M. Helmi, H.R. Elmitwalli, S.M. Elnagdy, A.F. El-Hagrassy, Calcium carbonate precipitation induced by ureolytic bacteria *Bacillus licheniformis*, Ecol. Eng. 90 (2016) 367–371, https://doi.org/10.1016/j.ecoleng.2016.01.044.

[60] Leeprasert, D. Chonudomkul, C. Boonmak, Biocalcifying potential of ureolytic bacteria isolated from soil for biocementation and material crack repair, Microorganisms 10 (2022) 963, https://doi.org/10.3390/microorganisms10050963.

[61] Al Imran, K. Nakashima, N. Evelpidou, S. Kawasaki, Factors affecting the urease activity of native ureolytic bacteria isolated from coastal areas, Geomech. Eng. 17 (2019) 421–427, https://doi.org/10.12989/gae.2019.17.5.421.

[62] W. Li, A. Fishman, V. Achal, Ureolytic bacteria from electronic waste area, their biological robustness against potentially toxic elements and underlying mechanisms, J. Environ. Manag. 289 (2021), 112517, https://doi.org/10.1016/j.jenvman.2021.112517.

[63] A. Liang, C. Paulo, Y. Zhu, M. Dittrich, $CaCO_3$ biomineralization on cyanobacterial surfaces: insights from experiments with three *Synechococcus* strains, Colloids Surf., B 111 (2013) 600–608, https://doi.org/10.1016/j.colsurfb.2013.07.012.

[64] Z. Han, H. Yan, S. Zhou, H. Zhao, Y. Zhang, N. Zhang, C. Yao, L. Zhao, C. Han, Precipitation of calcite induced by *Synechocystis* sp. PCC6803, World J. Microbiol. Biotechnol. 29 (2013) 1801–1811, https://doi.org/10.1007/s11274-013-1341-1.

[65] H. Yi, T. Zheng, Z. Jia, T. Su, C. Wang, Study on the influencing factors and mechanism of calcium carbonate precipitation induced by urease bacteria, J. Cryst. Growth 564 (2021), 126113, https://doi.org/10.1016/j.jcrysgro.2021.126113.

[66] A. Korchef, M. Touaibi, Effect of pH and temperature on calcium carbonate precipitation by CO_2 removal from iron-rich water, Water Environ. J. 34 (2020) 331–341, https://doi.org/10.1111/wej.12467.

[67] E. Baffoe, A. Ghahremaninezhad, The effect of biomolecules on enzyme-induced calcium carbonate precipitation in cementitious materials, Construct. Build. Mater. 345 (2022), 128323, https://doi.org/10.1016/j.conbuildmat.2022.128323.

[68] C. Lv, C.-S. Tang, C. Zhu, W.-Q. Li, T.-Y. Chen, L. Zhao, X.-H. Pan, Environmental dependence of microbially induced calcium carbonate crystal precipitations: experimental evidence and insights, J. Geotech. Geoenviron. Eng. 148 (2022), 04022050, https://doi.org/10.1061/(asce)gt.1943-5606.0002827.

[69] J. Xu, X. Wang, B. Wang, Biochemical process of ureolysis-based microbial $CaCO_3$ precipitation and its application in self-healing concrete, Appl. Microbiol. Biotechnol. 102 (2018) 3121–3132, https://doi.org/10.1007/s00253-018-8779-x.

[70] Y. Bin Hu, M. Wolthers, D.A. Wolf-Gladrow, G. Nehrke, Effect of pH and phosphate on calcium carbonate polymorphs precipitated at near-freezing temperature, Cryst. Growth Des. 15 (2015) 1596–1601, https://doi.org/10.1021/cg500829p.

[71] D. Vandamme, I. Foubert, I. Fraeye, B. Meesschaert, K. Muylaert, Flocculation of *Chlorella vulgaris* induced by high pH: role of magnesium and calcium and practical implications, Bioresour. Technol. 105 (2012) 114–119, https://doi.org/10.1016/j.biortech.2011.11.105.

[72] A.J. Paquette, A. Vadlamani, C. Demirkaya, M. Strous, H. De la Hoz Siegler, Nutrient management and medium reuse for cultivation of a cyanobacterial consortium at high pH and alkalinity, Front. Bioeng. Biotechnol. 10 (2022), 942771, https://doi.org/10.3389/fbioe.2022.942771.

[73] O.Y.A. Costa, J.M. Raaijmakers, E.E. Kuramae, Microbial extracellular polymeric substances: ecological function and impact on soil aggregation, Front. Microbiol. 9 (2018) 1636, https://doi.org/10.3389/fmicb.2018.01636.

[74] M.C.M. van Loosdrecht, J. Lyklema, W. Norde, A.J.B. Zehnder, Bacterial adhesion: a physicochemical approach, Microb. Ecol. 17 (1989) 1–15, https://doi.org/10.1007/BF02025589.

[75] L. Skevi, B.J. Reeksting, T.D. Hoffmann, S. Gebhard, K. Paine, Incorporation of bacteria in concrete: the case against MICP as a means for strength improvement, Cem. Concr. Compos. 120 (2021), 104056, https://doi.org/10.1016/j.cemconcomp.2021.104056.

[76] Sidhu, S. Goyal, M.S. Reddy, Healing of cracks in concrete by using bacterial spores immobilized in metakaolin, Structures 55 (2023) 1144–1158, https://doi.org/10.1016/j.istruc.2023.06.097.

[77] M. Dhivakar Karthick, G.S. Rampradheep, S. Shankar, Strength and durability performance of modified cement-based concrete incorporated immobilized bacteria, Environ. Sci. Pollut. Res. 29 (2022) 21670–21681, https://doi.org/10.1007/s11356-021-17414-5.

[78] E.F. Hernández, P.F.J. De Cano-Barrita, A.A. Torres-Acosta, Influence of cactus mucilage and marine brown algae extract on the compressive strength and durability of concrete, Mater. Construcción 66 (2016) e074, https://doi.org/10.3989/mc.2016.07514.

[79] G. Ghahremani, A. Bagheri, H. Zanganeh, The effect of size and shape of pores on the prediction model of compressive strength of foamed concrete, Construct. Build. Mater. 371 (2023), 130720, https://doi.org/10.1016/j.conbuildmat.2023.130720.

[80] Y.F. Fan, Z.Q. Hu, Y.Z. Zhang, J.L. Liu, Deterioration of compressive property of concrete under simulated acid rain environment, Construct. Build. Mater. 24 (2010) 1975–1983, https://doi.org/10.1016/j.conbuildmat.2010.04.002.

[81] F. Nosouhian, D. Mostofinejad, H. Hasheminejad, Concrete durability improvement in a sulfate environment using bacteria, J. Mater. Civ. Eng. 28 (2016), 04015064, https://doi.org/10.1061/(asce)mt.1943-5533.0001337.

[82] M. Wu, X. Hu, Q. Zhang, D. Xue, Y. Zhao, Growth environment optimization for inducing bacterial mineralization and its application in concrete healing, Construct. Build. Mater. 209 (2019) 631–643, https://doi.org/10.1016/j.conbuildmat.2019.03.181.

[83] P.R.K. Soda, M.K. M, Performance enhancement and remediation of microcracks in cement mortar by doping calcite-precipitating microorganisms, J. Mater. Civ. Eng. 34 (2022), 04022035, https://doi.org/10.1061/(asce)mt.1943-5533.0004176.

[84] A. Sadrmomtazi, B. Tahmouresi, R.K. Khoshkbijari, Effect of fly ash and silica fume on transition zone, pore structure and permeability of concrete, Mag. Concr. Res. 70 (2018) 519–532, https://doi.org/10.1680/jmacr.16.00537.

[85] M. Vaezi, S.A. Zareei, M. Jahadi, Recycled microbial mortar: effects of bacterial concentration and calcium lactate content, Construct. Build. Mater. 234 (2020), 117349, https://doi.org/10.1016/j.conbuildmat.2019.117349.

[86] S. Weiner, An overview of biomineralization processes and the problem of the vital effect, Rev. Mineral. Geochem. 54 (2003) 1–29, https://doi.org/10.2113/0540001.

[87] D. Xie, R. Zhang, J. Wang, The influence of environmental factors and precipitation precursors on enzyme-induced carbonate precipitation (EICP) process and its application on modification of recycled concrete aggregates, J. Clean. Prod. 395 (2023), 136444, https://doi.org/10.1016/j.jclepro.2023.136444.

[88] J. Xiao, Z. Wang, Y. Tang, S. Yang, Biomimetic mineralization of $CaCO_3$ on a phospholipid monolayer: from an amorphous calcium carbonate precursor to calcite via vaterite, Langmuir 26 (2010) 4977–4983, https://doi.org/10.1021/la903641k.

[89] M. Park, S. Park, J.Y. Yoo, Y. Kim, K.M. Lee, D.Y. Hwang, H.J. Son, Enzyme-mediated biocalcification by a novel alkaliphilic *Bacillus psychrodurans* LC40 and its eco-friendly application as a biosealant for crack healing, Sci. Total Environ. 802 (2022), 149841, https://doi.org/10.1016/j.scitotenv.2021.149841.

[90] C. Qian, Y. Chen, B. Xue, Microbial mineralization at the surface layer of cement-based materials and its effect on efflorescence performance, J. Build. Eng. 52 (2022), 104480, https://doi.org/10.1016/j.jobe.2022.104480.

[91] J. Qin, Q. Qin, X. Li, J. Xue, R. Wang, Q. Zhang, P. Wang, Z. Guo, Y. Gong, Urea supply control in microbial carbonate precipitation to effectively fill pores of concrete, Construct. Build. Mater. 310 (2021), 125123, https://doi.org/10.1016/j.conbuildmat.2021.125123.

[92] T. Zhu, Y. Lin, X. Lu, M. Dittrich, Assessment of cyanobacterial species for carbonate precipitation on mortar surface under different conditions, Ecol. Eng. 120 (2018) 154–163, https://doi.org/10.1016/j.ecoleng.2018.05.038.

[93] K. Anand, S. Goyal, M.S. Reddy, Long-term viable SF immobilized bacterial cells as sustainable solution for crack healing in concrete, Structures 43 (2022) 1342–1355, https://doi.org/10.1016/j.istruc.2022.07.056.

[94] B. Tahmouresi, P. Nemati, M.A. Asadi, A. Saradar, M. Mohtasham Moein, Mechanical strength and microstructure of engineered cementitious composites: a new configuration for direct tensile strength, experimental and numerical analysis, Construct. Build. Mater. 269 (2021), 121361, https://doi.org/10.1016/j.conbuildmat.2020.121361.

[95] J.N. Akhtar, R.A. Khan, R.A. Khan, M.N. Akhtar, J.K. Nejem, Influence of natural zeolite and mineral additive on bacterial self-healing concrete: a Review, Civil Eng. J. 8 (2022) 1069–1085, https://doi.org/10.28991/CEJ-2022-08-05-015.

[96] S. Chandra, S. Bhattacharya, S. Pandit, S. Banerjee, A. Roy, A.K. Rai, Cyanobacteria as an eco-friendly bioresource for EPS production with crack healing capacity in concrete, Biocatal. Agric. Biotechnol. 54 (2023), 102909, https://doi.org/10.1016/j.bcab.2023.102909.

[97] C. Stuckrath, R. Serpell, L.M. Valenzuela, M. Lopez, Quantification of chemical and biological calcium carbonate precipitation: performance of self-healing in reinforced mortar containing chemical admixtures, Cem. Concr. Compos. 50 (2014) 10–15, https://doi.org/10.1016/j.cemconcomp.2014.02.005.

[98] E. Tripathi, K. Anand, S. Goyal, M.S. Reddy, Bacterial based admixed or spray treatment to improve properties of concrete, Sadhana - Acad. Proc. Eng. Sci. 44 (2019) 19, https://doi.org/10.1007/s12046-018-0999-3.

[99] H. Sharma, S.K. Sharma, D.K. Ashish, S.K. Adhikary, G. Singh, Effect of various bio-deposition treatment techniques on recycled aggregate and recycled aggregate concrete, J. Build. Eng. 66 (2023), 105868, https://doi.org/10.1016/j.jobe.2023.105868.

[100] Y.S. Lee, W. Park, Current challenges and future directions for bacterial self-healing concrete, Appl. Microbiol. Biotechnol. 102 (2018) 3059–3070, https://doi.org/10.1007/s00253-018-8830-y.

[101] M. Verma, K. Upreti, P. Vats, S. Singh, P. Singh, N. Dev, D. Kumar Mishra, B. Tiwari, Experimental analysis of geopolymer concrete: a sustainable and economic concrete using the cost estimation model, Adv. Mater. Sci. Eng. 2022 (2022), 7488254, https://doi.org/10.1155/2022/7488254.

[102] D.M. Ribeiro, L.F. Roncaratti, G.C. Possa, L.C. Garcia, L.J. Cançado, T.C.R. Williams, B. dos Santos Alves, Figueiredo Brasil, A low-cost approach for *Chlorella sorokiniana* production through combined use of urea, ammonia and nitrate based fertilizers, Bioresour. Technol. Rep. 9 (2020), 100354, https://doi.org/10.1016/j.biteb.2019.100354.

[103] S. Joshi, S. Goyal, M.S. Reddy, Corn steep liquor as a nutritional source for biocementation and its impact on concrete structural properties, J. Ind. Microbiol. Biotechnol. 45 (2018) 657–667, https://doi.org/10.1007/s10295-018-2050-4.

[104] V. Achal, A. Mukherjee, P.C. Basu, M.S. Reddy, Lactose mother liquor as an alternative nutrient source for microbial concrete production by *Sporosarcina pasteurii*, J. Ind. Microbiol. Biotechnol. 36 (2009) 433–438, https://doi.org/10.1007/s10295-008-0514-7.